

# **Parametric Studies on the Cavity Micro-Bioreactor via Computational Fluid Dynamics Simulations**

By

Wei Leng Tan

A thesis submitted in fulfilment of the requirements for the award of  
Master by Engineering Science (Research) of the Department of  
Mechanical and Aerospace Engineering

October 2008

# Statement of Originality

---

I declare that this thesis contains no material which has been accepted for the award of any other degree or diploma in any university or other institution and affirms that to the best of the candidate's knowledge the thesis contains no material previously published or written by another person, except where due reference is made in the text of the thesis.

---

Wei Leng Tan

October 2008

# Summary

---

There is much research still needed to improve the outcomes from culturing embryos using *in-vitro* techniques, as they are still not comparable to natural, *in-vivo* embryo cultivation. Recent studies have found that growing embryos in a specially formulated “niche environment”, in effect mimicking that experienced by *in-vivo* embryos, could improve the overall culture efficiency. With this motivation, this thesis examines a new bioreactor design that incorporates the concept of the “niche environment”. This is termed the micro-bioreactor. This is accomplished by conducting parameter studies to examine the effect of the fluid dynamics and bioreactor geometry on factors contributing to the performance of the micro-bioreactor.

Eight parameters are chosen to cover four aspects of the physical and functional features of the micro-bioreactor: cavity dimensions, perfusion of culture medium, embryo growth and scaling-up of embryo production. The studies are carried out numerically, modelling the flow and transport of solutes. They focus on quantifying and analysing the effect on the immediate solute and flow environment experienced by the embryo as control parameters are varied. The solute transport processes modelled are the uptake of oxygen as the embryo develops and the production of lactate, which is a waste product during growth.

The parameter studies that examined the dimensions of the cavity reveal that modifications to the cavity size and opening have a strong influence on the fluid flow and solute transport around the embryo. Amongst all the modifications applied, changing the cavity aspect ratio has the largest effect on the fluid flow and the solute transport. However, it must be noted that the influence of changing the cavity aspect ratio and width weakens when these two parameters are increased past certain critical values. This appears to be a key parameter, which can be used to adjust embryo shear stress on, and solute transport to/from, the embryo.

The parametric studies that examined the perfusion of the culture medium discover that changing the inflow rate is preferred over changing the height of the culture medium in adjusting the shear stress experienced by the embryo. Likewise, changing the inflow rate is also effective in altering the solute concentration on the embryo surface when the flow is advection dominant. If the flow is diffusion dominant, the influence of the inflow rate becomes insignificant.

The study that investigated the effects induced by changes in solute exchange rates and embryo size during embryo growth indicated that for the flow regime examined, the lactate concentration at the embryo is directly proportional to the lactate production rate; the oxygen concentration at the embryo is inversely proportional to the uptake rate; and the shear stress experienced by the embryo is inversely proportional to embryo size. These changes to the solute production and consumption rates during the embryo development have a profound influence on solute concentrations. On the contrary, the change of embryo size has a lesser impact on the shear stress.

The parametric studies that investigated the scale-up of embryo production reveal that placing more embryos in the same cavity and adding more cavities to the micro-bioreactor incur an unwanted side effect of different distributions of solute concentration and shear stress amongst the embryos. However, the differences in the global measures of these characteristics were not large. The approach of adding more cavities appears preferable over placing more embryos in the same cavity as it is found to lessen the effect. Also, it is found that the spacing between the cavities noticeably influences the solute transport and fluid flow in both cavities, where a decrease in the spacing increases the solute concentration and shear stress experienced by the embryo.

Regardless of which parameter is being varied, the distribution of the solutes from the top of the embryo to the bottom is similar. Lactate levels are large at the base while oxygen levels are low there. The shear stress on embryo surface is predominantly influenced by the flow recirculations in the cavity and the strong channel flow across the cavity opening. The location of the peak shear stress corresponds well with the locations where these flow features impinge on the embryo surface.

To conclude, the parameter studies provide guidelines in defining some of the dimensions and operational settings for the micro-bioreactor by providing quantitative predictions as parameters are varied. Ideally, this work would have feed into a parallel experimental program, which was the original plan; however, experiments were delayed. That would have allowed feedback between the numerical and experimental programs allowing optimisation of the bioreactor operation. Future work includes improving the numerical model employed in the parameter studies, especially the oxygen uptake/lactate production models, and extensions such as examining cavities with porous bottoms, which may allow more uniform solute distributions around the embryo.

# Acknowledgement

---

Firstly, I would like to express my gratitude to both my supervisors: Professor Mark Thompson and Professor Kerry Hourigan for their continuous guidance and supervision throughout the candidature, for their valuable support and insight in overcoming the obstacles and refining the research, as well as for their efforts in proof reading this manuscript. I would also like to thank Dr. George Thouas for his assistance and advice on embryo culture and his effort in proof reading the literature review on embryo culture. I would like to acknowledge the financial support from the Monash International Overseas Postgraduate Research Scholarship (MIPRS), the Australian Postgraduate Award (APA), the Monash Graduate Scholarship (MGS) and the Monash Departmental Scholarship (MDS).

Secondly, I would like to thank all my friends and colleagues Ying Hao, Joine, Allen, Alan, Soon and many more who supported me during the candidature and shared many of the memorable and humorous office moments with me.

Lastly, I would like to dedicate this work to my family (mum, dad and Jitt), Ee Hui and her family: Thank you for your constant support, guidance and love all along during the difficult times in the candidature. And I also want to thank Hermitzu and Brandy – my hermits which has accompanied me through many nights of thesis writing.

# Publication Relating to Thesis

---

Tan, W. L., Thouas, G. A., Thompson, M. C. and Hourigan, K. (2007). “Computational fluid dynamics investigation of a cavity micro-bioreactor”. Proceeding of the 16<sup>th</sup> Australasian Fluid Mechanics Conference, Gold Coast, Queensland, Australia.

# Nomenclature

---

<b><u>Symbol</u></b>	<b><u>Explanation</u></b>
$\mu$	Viscosity of culture medium
$A$	Surface area of a discretised cell
AR	Cavity aspect ratio
$B$	Cavity width
$B^*$	Normalized cavity width
BC	Boundary condition
$C$	Normalized solute concentration
$C$	Solute concentration
$C_{ref}$	Default solute concentration
CFD	Computational fluid dynamics
$D$	Cavity depth
$D_{embryo}$	Embryo diameter
$D_f$	Culture medium height
$D_f^*$	Normalized culture medium height
$D_{solute}$	Diffusivity of the solute within the culture medium
$Kn$	Knudsen number
$L$	Characteristic length of flow system / Length of cavity
$L_s$	Cavity spacing
$L_s^*$	Normalized cavity spacing
$Ma$	Mach number
$P$	Normalized pressure term
$p^*$	Initial normalized general pressure term
$p'$	Normalized correction pressure term
$Pe$	Peclet number
$Pe_{lactate}$	Peclet number for lactate
$Pe_{oxygen}$	Peclet number for oxygen
$R_0$	Normalized radius of cylinder inside cavity (Galaktionov <i>et al</i> 1999)

<b><u>Symbol</u></b>	<b><u>Explanation</u></b>
$Re$	Reynolds number
$S$	Normalized source or sink of solute
$Sc$	Schmidt number
$Sc_{lactate}$	Schmidt number for lactate
$Sc_{oxygen}$	Schmidt number for oxygen
$S_{lac}$	Lactate exchange rate
$S_{oxy}$	Oxygen exchange rate
$S_{\Phi}$	Source or sink of $\Phi$
$U$	Average velocity of fluid flow
$\mathbf{U}$	Normalized fluid velocity vector
$\mathbf{u}$	Fluid velocity vector
$\mathbf{u}^*$	Initial normalized velocity
$V$	Inflow rate of culture medium (defined at inlet)
$x, y, z$	Cartesian coordinates in a flow system
$\Gamma$	General diffusion coefficient
$P$	Density of culture medium
$\tau$	Normalized shear stress
$\tau$	Shear stress
$\tau_{ref}$	Default shear stress
$\Phi$	General flow variable
$\Phi_{face}$	Value of $\Phi$ at a cell surface

# Contents

---

<b>1.0 INTRODUCTION .....</b>	<b>1</b>
<b>2.0 LITERATURE REVIEW .....</b>	<b>4</b>
2.1 EMBRYO CULTURE SYSTEMS .....	6
2.1.1 <i>Overview of Pre-implantation Embryo Development</i> .....	6
2.1.2 <i>Background and Significance of Embryo Culture</i> .....	9
2.1.3 <i>Embryo Culture Media</i> .....	12
2.1.4 <i>Physical and Environmental Conditions of Embryo Culture</i> .....	15
2.1.4.1 Somatic Cell Support.....	15
2.1.4.2 Extended Culture Periods .....	16
2.1.4.3 Ratio of Embryos to Medium Volume .....	17
2.1.4.4 The Gas Phase.....	18
2.1.4.5 Temperature Regulation and Light Conditions.....	19
2.1.4.6 Osmotic Pressure of Culture Medium .....	20
2.1.4.7 Incubator Containment .....	21
2.1.4.8 The Embryo Culture Vessel.....	21
2.2 MODIFICATION OF EMBRYO CULTURE VESSELS .....	24
2.2.1 <i>Perfused Vessels</i> .....	24
2.2.2 <i>Culture Vessels with Microcavities</i> .....	26
2.2.3 <i>Perfused Microfluidic Vessels</i> .....	29
2.3 FLUID FLOW IN MICROFLUIDIC SYSTEMS .....	33
2.3.1 <i>Highly Viscous Flow</i> .....	33
2.3.2 <i>Diffusion Dominance</i> .....	34
2.3.3 <i>Large Surface Area to Volume Ratio</i> .....	35
2.3.4 <i>Rarefaction Effects</i> .....	37
2.4 PROPOSED NEW MICRO-BIOREACTOR DESIGN .....	40
2.4.1 <i>Evaluation of Micro-Bioreactor Design</i> .....	41
2.4.2 <i>Motivation for Parametric Studies</i> .....	42
2.4.3 <i>Overview of Numerical Modelling</i> .....	44
2.4.3.1 Analytical Model Approximations .....	44
2.4.3.2 Discrete Fluid Modelling.....	45
2.4.3.3 Continuum Fluid Modelling .....	47
2.4.3.4 Selection of Numerical Method for Parametric Studies .....	49
2.5 CONCLUSIONS .....	50
<b>3.0 METHODOLOGY.....</b>	<b>51</b>
3.1 PHYSICAL MODEL.....	52
3.2 MATHEMATICAL MODEL .....	56
3.3 NUMERICAL MODEL .....	60
3.3.1 <i>Finite Volume Method and Spatial Discretisation</i> .....	61
3.3.2 <i>The Computational Grid</i> .....	64
3.3.3 <i>Boundary Conditions</i> .....	69
3.3.4 <i>Convergence Criteria</i> .....	72
3.4 MODEL VALIDATIONS .....	75

3.4.1	<i>Grid Resolution Studies</i>	75
3.4.1.1	2D Grid Resolution Study	76
3.4.1.2	3D Grid Resolution Study	82
3.4.2	<i>Validation of Fluid Flow Modelling</i>	84
3.4.2.1	Model Validation on 2D Model	84
3.4.2.2	Model Validation on 3D Model	87
3.4.3	<i>Validation of Solute Transport Modelling</i>	91
3.5	CONCLUSION	98
<b>4.0</b>	<b>TWO-DIMENSIONAL PARAMETRIC STUDIES</b>	<b>99</b>
4.1	DEFAULT SETUP OF THE TWO-DIMENSIONAL MICRO-BIOREACTOR	100
4.2	CAVITY ASPECT RATIO PARAMETRIC STUDY	101
4.2.1	<i>Problem Setup</i>	101
4.2.2	<i>Flow Structures in the Cavity</i>	104
4.2.3	<i>Solute Concentration Changes with AR</i>	107
4.2.4	<i>Solute Distribution around the Embryo</i>	109
4.2.5	<i>Implications for Solute Transport</i>	114
4.2.6	<i>Embryo Surface Shear Stress Changes with AR</i>	114
4.2.7	<i>Local Shear Stress Distribution on Embryo Surface</i>	116
4.2.8	<i>Implications for Shear Stress Changes</i>	120
4.2.9	<i>Conclusion and Summary</i>	120
4.3	CULTURE MEDIUM INFLOW RATE PARAMETRIC STUDY	122
4.3.1	<i>Problem Setup</i>	122
4.3.2	<i>Peclet Number: Relevance in Solute Transport</i>	124
4.3.3	<i>Particle Trajectories in the Cavity</i>	125
4.3.4	<i>Changes in Solute Transport</i>	127
4.3.5	<i>Implication for Solute Transport</i>	134
4.3.6	<i>Changes in Embryo Shear Stress</i>	135
4.3.7	<i>Implications for Shear Stress Changes and Summary</i>	139
4.4	CULTURE MEDIUM HEIGHT PARAMETRIC STUDY	140
4.4.1	<i>Problem Setup</i>	140
4.4.2	<i>Solute Concentration Changes with Culture Medium Height</i>	142
4.4.3	<i>Solute Distribution around the Embryo</i>	148
4.4.4	<i>Implication for Solute Transport</i>	152
4.4.5	<i>Shear Stress Changes with Culture Medium Height</i>	152
4.4.6	<i>Implication for Shear Stress Changes</i>	158
4.4.7	<i>Conclusion and Summary</i>	158
4.5	EMBRYO GROWTH PARAMETRIC STUDY	160
4.5.1	<i>Problem Setup</i>	160
4.5.2	<i>Embryo Growth at Different Stages</i>	161
4.5.3	<i>Establishment of Governing Factors</i>	164
4.5.4	<i>Variation of Solutes Concentration</i>	172
4.5.5	<i>Solutes Distribution around the Embryo</i>	176
4.5.6	<i>Implication for Solute Transport</i>	183
4.5.7	<i>Variation of Shear Stress</i>	183
4.5.8	<i>Shear Stress Distribution on the Embryo</i>	187
4.5.9	<i>Implications for Shear Stress Changes</i>	189
4.5.10	<i>Conclusions and Summary</i>	189
4.6	MULTIPLE CAVITIES PARAMETRIC STUDY	191
4.6.1	<i>Problem Setup</i>	192
4.6.2	<i>Cavity Spacing: Flow Structure Variation</i>	194
4.6.3	<i>Cavity Spacing: Change of Solute Concentration</i>	198

4.6.4	<i>Cavity Spacing: Solute Distribution around the Embryo</i> .....	201
4.6.5	<i>Multiple Cavity Interaction: Changes of Solute Concentration</i> .....	208
4.6.6	<i>Multiple Cavity Interaction: Solute Distribution around the Embryo</i> .....	210
4.6.7	<i>Implication for Solute Transport</i> .....	212
4.6.8	<i>Cavity Spacing: Changes to Shear Stress</i> .....	213
4.6.9	<i>Cavity Spacing: Shear Stress Distribution on the Embryo</i> .....	215
4.6.10	<i>Multiple Cavity Interaction: Change of Shear Stress</i> .....	218
4.6.11	<i>Multiple Cavity Interaction: Shear Stress Distribution on the Embryo</i> .....	221
4.6.12	<i>Implication for Shear Stress Changes</i> .....	221
4.6.13	<i>Conclusions and Summary</i> .....	222
4.7	FINAL COMMENTS .....	223
<b>5.0</b>	<b>THREE-DIMENSIONAL PARAMETRIC STUDIES</b> .....	<b>224</b>
5.1	DEFAULT SCENARIO ON THREE-DIMENSIONAL MICRO-BIOREACTOR .....	225
5.2	CAVITY WIDTH PARAMETRIC STUDY .....	226
5.2.1	<i>Problem Setup</i> .....	227
5.2.2	<i>Solute Concentration Changes</i> .....	228
5.2.3	<i>Solute Distribution on the Embryo</i> .....	233
5.2.4	<i>Implication for Solute Transport</i> .....	238
5.2.5	<i>Shear Stress Changes</i> .....	239
5.2.6	<i>Shear Stress Distribution on the Embryo</i> .....	243
5.2.7	<i>Implication for Shear Stress Changes</i> .....	248
5.2.8	<i>Comparison of 2D Model against 3D Model</i> .....	248
5.2.9	<i>Conclusion and Summary</i> .....	255
5.3	CAVITY SHAPE PARAMETRIC STUDY .....	257
5.3.1	<i>Problem Setup</i> .....	257
5.3.2	<i>Comparison of Overall Solute Concentration</i> .....	262
5.3.3	<i>Comparison of Solute Distribution</i> .....	268
5.3.4	<i>Comparison of Overall Shear Stress</i> .....	274
5.3.5	<i>Comparison of Shear Stress Distribution</i> .....	278
5.3.6	<i>Implication for Solute Transport and Shear Stress Changes</i> .....	282
5.3.7	<i>Conclusion and Summary</i> .....	283
5.4	MULTIPLE EMBRYOS PARAMETRIC STUDY .....	285
5.4.1	<i>Problem Setup</i> .....	285
5.4.2	<i>Comparison of Overall Solutes Concentration</i> .....	288
5.4.3	<i>Solutes Distributions on the Embryos</i> .....	296
5.4.4	<i>Comparison of Overall Shear Stress</i> .....	300
5.4.5	<i>Shear Stress Distribution on Embryos</i> .....	306
5.4.6	<i>Implications for Solute Transport and Shear Stress Changes</i> .....	309
5.4.7	<i>Conclusion and Summary</i> .....	310
5.5	EXPLANATION ON THE SMALL VARIATION OF OXYGEN CONCENTRATION .....	312
<b>6.0</b>	<b>CONCLUSIONS</b> .....	<b>314</b>
6.1	RELEVANCE OF THE PARAMETRIC STUDIES .....	315
6.1.1	<i>Cavity Dimensions</i> .....	315
6.1.2	<i>Perfusion of Culture Medium</i> .....	323
6.1.3	<i>Embryo Growth</i> .....	329
6.1.4	<i>Scaling up Embryo Production</i> .....	334
6.2	LIMITATION OF NUMERICAL MODEL .....	343
6.2.1	<i>Inadequacy of Model Capability, Validation and Optimisation</i> .....	343
6.2.2	<i>Assumptions on Culture Medium</i> .....	345

6.2.3	<i>Assumptions on Boundary Conditions of the Model</i> .....	346
6.3	CONCLUDING REMARKS.....	348
<b>7.0</b>	<b>FUTURE WORK</b> .....	<b>349</b>

---



# 1.0 Introduction

---

Embryo culture has been used as an important practical method in experimental embryology and assisted reproduction for several decades since the dawn of twentieth century (Biggers 1987). The method is important to embryology in enabling an understanding of embryo growth, improving transgenic techniques and increasing the rate of success of embryo production in animal breeding as an adjunct to *in-vitro* fertilization (IVF) (Gor and Lucassen 1993). The method is also pivotal to human IVF programs. However, while embryo culture has been optimized greatly in recent times, it has not reached its maximum potential. Cleavage rates and viability of preimplantation mammalian embryos are found to be reduced by *in-vitro* culture (Streffer, Van Beuningen *et al.* 1980; Harlow and Quinn 1982). Also, the viability of embryos produced by assisted reproduction techniques that include *in-vitro* embryo culture is relatively less than the viability of *in-vivo* derived embryos (Glasgow, Zeringue *et al.* 2001; Raty, Walters *et al.* 2004). For these reasons, much work has been undertaken to increase the efficiency of the *in-vitro* embryo culture, mainly by improving culture techniques, formulating better culture media, and to a lesser extent, by enhancing the design of bioreactors so as to modify the physical culture environment used to cultivate the embryos (Glasgow, Zeringue *et al.* 2001; Raty, Walters *et al.* 2004).

The vessels used in embryo culture, or bioreactors, have remained relatively under-developed compared to embryo culture techniques and culture media (Beebe, Wheeler *et al.* 2002). Therefore, there remains a substantial demand for further research into improving design and function for embryo culture bioreactors. Some modifications of existing static culture systems have included examples such as the Well-of-the-Well (WOW) culture system by Vajita *et al.* (Vajita, Peura *et al.* 2000), the Glass Oviduct (GO) culture system by Thouas *et al.* (Thouas, Jones *et al.* 2003) and new microchannel culture systems that utilize microfluidic concepts (Glasgow, Zeringue *et al.* 2001; Suh, Phadke *et al.* 2003; Raty, Walters *et al.* 2004). All of these systems show promising results as alternative embryo culture systems.

With the same aim of improving the culture vessel in mind, a new bioreactor design termed the *cavity micro-bioreactor* is proposed. Its key feature is to include the promising concept of microfluidics and the concept of a “niche environment” into the bioreactor design. The idea of this “niche environment” is inspired by the recurring theme in living tissues of local cavity environments that house small sub-populations of cells such as stem cells (Fuchs, Tumber *et al.* 2004). Apart from the recent work done on the GO and WOW culture systems, the hypothesis that the “niche environment” is beneficial to embryo growth is also supported by the findings of Lane and Gardner (Lane and Gardner 1992). They found that by simply decreasing the incubation volume and thereby reducing the size of the controlling environment, the localised concentration of the embryotrophic growth factors around the embryo is increased and this improves the embryo growth.

Investigating the feasibility of this new bioreactor design forms the first step of realizing this bioreactor concept for laboratory and clinical usage. The investigation begins with conducting parametric studies to examine effects of changing some of the design parameters of the micro-bioreactor. Using the findings gained from these studies, the prototype of the micro-bioreactor will be constructed; flow and embryo growth experiments will then be carried out to determine the feasibility and competency of the micro-bioreactor.

Due to the large amount of work needed for the entire feasibility investigation, this thesis only covers the work done in conducting parametric studies to examine the bioreactor design. The parameters are studied numerically via computational fluid dynamics (CFD) simulations. As a precursor to the actual study, the CFD modelling of the fluid flow and solute transport are initially tested and validated. Several design parameters which cover the aspects of cavity dimensions, perfusion of culture medium, embryo growth and embryo production scale up are examined numerically to determine how they may influence the localised environment of the embryo. Findings gained from these studies are hoped to provide an understanding of how controllable parameters affect embryo development. Ultimately, it is hoped that these findings will help to

optimize and improve actual laboratory and clinical bioreactors that may emanate from this work.

The thesis is organized as follows:

- Chapter 2 reviews embryo culture and past developments on bioreactors. It also reviews the development of microfluidic devices and numerical methods suitable to examine microfluidic flows.
- Chapter 3 explains the numerical model employed to simulate the fluid flow and solute transport in the bioreactor. It also covers the validations undertaken to ascertain the suitability of the numerical model.
- Chapter 4 and 5, respectively, report on the findings from the two-dimensional and three-dimensional parametric studies. Specifically, the findings from the simulations are interpreted and discussed for their implications to bioreactor design.
- Chapter 6 concludes the thesis by comparing the major findings from all the parametric studies and relates them to the objective of the thesis. It also discusses the limitations of the numerical model.
- Chapter 7 presents some recommendations for future work.

## 2.0 Literature Review

---

The broad aim of this project is to examine and optimize fluid dynamics related aspects of bioreactors for culturing embryos. Part of the motivation for this is to address the growing need to improve embryo growth and development in an artificial environment, generally called an *in-vitro* environment. As is indicated below, the overall efficiency of *in-vitro* embryo culture is still low compared to natural *in-vivo* (inside the female reproductive tract) embryo culture. While considerable research has already been undertaken to improve this situation, most of these efforts have been centred on non-fluid dynamical aspects: such as refining the culture media, developing better culturing techniques and optimizing the culture environment parameters. There have been fewer attempts to examine bioreactor designs that hold the embryo in place while the culture process takes place. By developing a bioreactor that specifically suits *in-vitro* embryo growth, it is believed that a higher overall culture efficiency can be obtained, adding to the improvements obtained from better culture media and techniques.

This chapter begins with an overview of embryo culture, its relation to assisted reproduction techniques and various approaches taken to raise the success rate of cultivation. This emphasizes the importance of embryo culture, indicates the state-of-the-art, and importantly draws attention to the drawbacks of current bioreactor designs to provide an optimum environment for embryo growth. After this, the focus narrows to two concepts: fluid perfusion and the “niche environment”. This is because previous research has indicated that a larger number of surviving blastocysts (an early stage of the developing embryo) and better embryo quality have been obtained when these factors have been employed in the culturing procedures. By further evaluating some of this previous work, a better understanding of the benefits and drawbacks of these factors can be appreciated. This leads naturally to the concept of a *cavity micro-bioreactor*, the bioreactor design that forms the basis of this study.

In short, this chapter aims to:

- Establish the importance of embryo culture methodology, and justify the need for rationally designed culture technology, such as special-purpose bioreactor designs.
- Examine fluid perfusion and the idea of a “niche environment” as important factors that may be utilized to possibly improve embryo growth and survival rates.

## 2.1 Embryo Culture Systems

This literature review begins by providing some background to *in-vitro* culture of pre-implantation mammalian embryos, the first phase of embryo development, between fertilization and implantation into the womb. General aspects of culture methodologies and biological requirements, relationships with other aspects of assisted reproduction technology (ART) research, and relevant discoveries to date are reviewed. Particular attention is drawn to physical aspects of embryo culture, since the emergence of the method (Biggers 1987). Ultimately, by reviewing the development of embryo culture systems, and identifying the need for more optimal artificial culture environments, this section indicates the current lack of research into improving embryo bioreactors and justifies the need to remedy this situation.

### 2.1.1 Overview of Pre-implantation Embryo Development

*In-vitro*<sup>1</sup> embryo culture is the method of growing embryos in an artificial medium outside the body. Naturally, it is a technique that requires considerable attention to the biochemical and physical environment, since deficiencies can compromise performance, as will be seen in the later reviews. Categorized as a specialized form of tissue culture, mammalian embryo culture was reported to be first conducted as early the 1890s by Heape (Heape 1891) in his rabbit embryo transfer experiment. Since then it has grown to be of great importance in experimental and clinical embryology. The development of embryo culture has been very active, having been applied to assisted reproduction and as a research method for various species such as rodents, livestock and non-human primates (Wright and O' Fallon 1987). Much of the work on embryo culture formed the basis of *in-vitro* fertilization (IVF) in humans for the treatment of infertility. In brief, generally pre-implantation embryos are cultured by placing them in a culture vessel such as a petri-dish, multi-well plate or a test tube filled with the appropriate culture media and they are then allowed them to grow with minimal disturbance. In order to prevent the evaporation of the culture media (as this would alter its volume and chemical properties such as pH and dissolved gas composition), the surface of the culture media is commonly covered with an oil layer. The entire culture vessel setup is

---

<sup>1</sup> the words *in-vitro* literally translates from latin into “in glass”, and nowadays pertains to cultivation of cells in an artificial environment outside the living body

located in an incubator, which provides a constant temperature and humidity suitable for embryo growth.

The early development of the mammalian embryo (Figure 2.1) has been described in detail by Dawson (Dawson 1990). In summary, the embryo undergoes several morphological changes from the 1-cell stage to the blastocyst stage, and these stages remain the same when embryos are cultivated *in-vitro*. After the fusion of the germ cell (gamete) derived from the male (sperm) and the female (oocyte) to form a fertilized oocyte (zygote or 1-cell embryo), the embryo then begins symmetrical cleavage divisions to form two, four and eight daughter cells, corresponding to the 2-cell, 4-cell and 8-cell stages respectively. These divided cells are contained in close contact within a spherical membrane shell called the zona pellucida. The dividing embryo then begins the process of compaction at the subsequent morula stage, where the embryonic cells begin to adhere to each other. About one third of these cells are pushed to one side to form the inner cell mass (ICM) that will eventually form the newborn foetus in the womb. The remaining cells are distributed close to the surface of the zona pellucida to form the trophoblast cell layer. The latter will eventually form the placental tissues and membranes that contain the foetus, interfacing with the maternal blood supply for nutritional support of gestation. As can be seen from Figure 2.1, at the morula stage the compacting embryo develops a fluid-filled cavity called the blastocoel, formed from within the embryo, which enables expansion of the blastocyst. Upon completion of cavitation and full expansion of the blastocyst, the zona pellucida thins and degenerates, allowing the blastocyst to escape or “hatch”, a step immediately preceding interaction with the uterine tissue *in-vivo*.

The overall framework of *in-vitro* embryo cultivation is aimed at adequately supporting the early embryonic growth stages described above. The general culture process is as follows. After formation of a zygote, either by *in-vitro* fertilization or embryo collection from a female mammal (except for humans, where this technique is banned), the embryo is incubated and allowed to develop in a specially formulated nutrient solution, maintained under defined physiological conditions. Upon reaching the desired growth stage, the embryo may then be transferred back into the uterus of the female for further growth *in-utero*, depending on whether the embryo is used for experimental research, or

for assisted conception. Embryos nowadays can generally be grown *in-vitro* from any stage between zygote and blastocyst, however, there are specific stages at which growth can arrest or “block”. In these cases, embryonic cell division ceases and the embryo subsequently deteriorates and dies. This appears to be mainly caused by genetic factors and/or incorrect nutrient supply. This process is also species specific, with examples such as mouse and hamster embryos that arrest at the 2-cell stage (Bavister 1987) in contrast to rabbit embryos which do not exhibit this growth arrest (Kane 1987). Further discussion of developmental arrest in relation to culture methodology appears in Section 2.1.2 of this chapter.

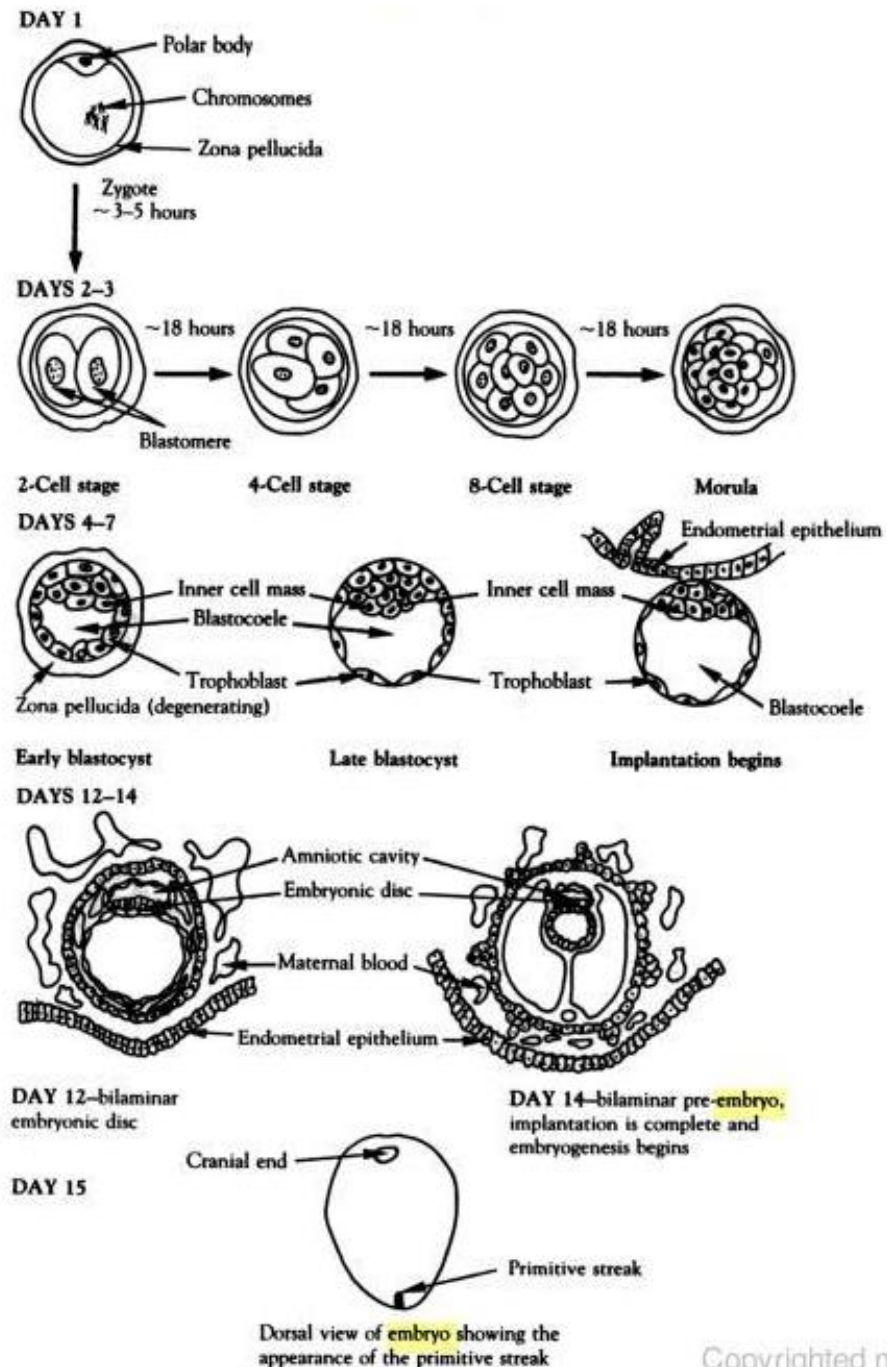


Figure 2.1: Diagram showing the general stages occurring in the maturation of a human embryo from its formation on day 1 to the final form at day 15 (Dawson 1990).

### 2.1.2 Background and Significance of Embryo Culture

Significant research into the methodology and application of embryo culture is demonstrated by numerous progressive reviews of the method, and has been motivated by its experimental and clinical relevance (Brinster 1969), (Biggers 1987), (Bavister 1995), (Wood and Trounson 1999), (Bongso and Gardner 1999). Despite significant

progress in the optimisation of aspects of the approach, these authors have highlighted the need for continued research and further incremental improvements, especially in areas such as physical culture conditions that have been largely unexplored.

Along with IVF and embryo transfer, embryo culture is one of the key procedures in clinical ART, as mentioned by Dawson in her review on the scientific aspects of human embryo research (Dawson 1990). Safe and controlled *in-vitro* culture conditions are required for successful human embryo development, which is often compromised in infertile couples. The ability to manipulate embryos at this stage within a laboratory is also important for genetic testing of embryos prior to implantation (Dawson 1990; Wood and Trounson 1999). This technique allows one to detect if a certain embryo has genetic abnormalities, to reduce the likelihood of abortions and birth defects.

In animal models, embryo culture allows direct access to all stages of the pre-implantation period of mammalian embryo development, allowing detailed investigation of physiological and metabolic processes. Mammalian embryos are therefore useful models for research toward understanding human embryo development. It is not possible to measure such quantities without extracting the embryo from the reproductive organ and disturbing its normal growth (Bongso and Gardner 1999). The development of mouse embryos *in-vitro*, for example, is often used to determine the toxicity of culture solutions and conditions used in clinical IVF (see chapter 11 of Trounson and Gardner, under 1-cell assay).

Most recently, embryo culture has driven research in other areas such as stem cell research, where embryo culture is the sole means of obtaining human embryonic stem cells (Thomson, Itskovitz-Eldor et al. 1998; O' Shea 1999). As discussed by various authors (Pera, Reubinoff *et al.* 2000; Lovell-Badge 2001), research on stem cells promises to introduce new directions in medical research, such as new ways to treat diseases and physiological injuries via tissue regeneration, repair of genetic disorders, and new methods to approach drug discoveries and testing. Hence, the continuous development of embryo culture is vital to ensure progress of this important cell culture based research.

While it has been reported that embryos from many species are able to be cultured *in-vitro*, the success rate, in terms of the percentage of successful births and the quality of embryos produced, is still not entirely comparable to that of naturally produced embryos. Many investigations have been conducted to find out the reasons for this difference, and to improve the culture conditions with the ultimate goal of increasing the success rate to approach that of *in-vivo* performance. In his review of embryo cultivation trends Bavister has drawn up a historical time line that categorizes the development of embryo culture into four periods (Bavister 1995):

- *The pioneering period* (up to 1960s): This covers the period of fundamental discoveries that show it is possible to culture embryos outside the reproductive tract. The development of complex but ill-defined culture media specifically to support the growth of mammalian embryo also began in this period.
- *The classic period* (1960s to 1970s): This is a highly productive research period where many discoveries were made in understanding the physiological and metabolic requirements of different embryos. Many culture medium formulations, which include both simple and complex formulations, were devised and examined to find out the optimal choice to culture the embryos. Many of the discoveries were made in culturing mouse and rabbit embryos, although the successful culture of embryos from other species such as cow, pig and human were also demonstrated.
- *The latent period* (1970s to 1990s): In this period, progress was comparatively slow since most embryo cultures other than those of the mouse experienced blocks to development as mentioned previously. A variety of methods were devised to try to overcome these blocks, such as utilizing various types of simple defined culture media or modifications to the environment surrounding the embryo, but not much success was achieved.
- *The renaissance period* (1990s to current): This period starts with intensified attempts to overcome the developmental blocks. Success was achieved in culturing embryos of various species up to the later blastocyst stage. In the process of understanding these developmental blocks, more information regarding the metabolic and nutrient requirements of the embryo were gained. Various types of simple, chemically defined culture media were developed to

better support embryo growth. A new culture technique termed co-culture that provides high culture success rate was also developed.

Apart from the early initial discoveries on the possibility of successful embryo cultivation outside the living body, most of the breakthroughs subsequently arose from efforts to overcome the blocks to development of embryo growth. Depending on species, these developmental blocks inhibit embryo growth from progressing to the stage allowing transplantation back into the reproductive tract. For example, until 1995, no-one had been able to cultivate a hamster embryo pass the 2-cell stage, regardless of whether the embryo had been formed by *in-vivo* or *in-vitro* fertilization (Bavister 1987).

### **2.1.3 Embryo Culture Media**

As indicated above much of the advancement in embryo culture has been driven by research on refining the culture medium, or more specifically, determining the right medium composition to promote optimal embryo development. This is well reflected by the numerous reviews on the state-of-the-art of culture medium optimisation (Brinster 1969; Biggers 1987; Bavister 1995; Gardner and Lane 1999). It has been found that varying the composition of key factors such as serum and carbohydrates can dramatically influence whether an embryo is able to overcome the blocks to development. Incremental changes in the amounts of certain chemicals in a medium can have a profound impact on the mortality of the embryo. Early culture media consisted of naturally occurring protein extracts like blood plasma or egg white. Some media were supplemented with minerals that were thought to aid embryo growth. While these components did improve ongoing embryo survival, the cultivation efficiency was still relatively poor, as mentioned in the review on early embryo culture by Brinster (Brinster 1969), with progressive improvements over time (Biggers 1987). From the classic period onwards, two types of culture media were devised; simple solutions (containing only salts and carbohydrates) and complex solutions (containing added nutrient supplements and vitamins). The rationale to improve embryo growth was the same, but simple media tended to be more chemically defined, so were chemically safer but not necessarily optimal in a biological sense.

Complex culture media contain a long list of chemical components including amino acids, vitamins and trace minerals, usually supplemented with 5% to 20% serum or other protein sources. While designed to support the growth of somatic cells in culture, complex media has been used to culture a variety of embryos since the classic period, and is still being employed for embryo culture research today. There are however two main drawbacks of complex media. Firstly, it is believed that these solutions may contain a range of components that are potentially detrimental to embryo development; such as inappropriate levels of carbohydrates that inhibit the growth of mouse embryos past the 2-cell stage (Brinster 1965; Biggers, Whittingham et al. 1967; Sakkas, Urner *et al.* 1993; Quinn 1995). This is compounded by the difficulty of resolving whether specific components are toxic in the presence of other components. Secondly, the addition of serum, which is a medium that originates from the blood clotting process, may harm the embryo, as well as mask the effect of toxic components in the medium. This view opposes the hypothesis that serum compensates for the essential components that are missing from the composition of the culture media, but is supported by the findings of various researchers that suggest serum may be one of the factors that inhibit embryo growth (John and Kiessling 1988; Maurer 1992; Gardner 1994; Bavister 1995). The exception appears to be its use for bovine embryos, which consume large amounts of serum protein as a nutrient, much like somatic cells do (Eckert, Pugh *et al.* 1998). Apart from that, each batch of serum is chemically different, even if it comes from the same species. The inclusion of serum prevents the standardization of culture conditions and thereby means that embryo culture studies may be not repeatable. Nevertheless, complex media remain in use today, because of the need to provide as many beneficial nutrients as possible, at correct levels for embryos. (Blood) serum has mostly been superseded by more purified versions such as serum albumin. Also, more recently identified problems such as degradation of amino acids into toxic ammonium (Gardner and Lane 1993) has been solved by replacement with more stable amino acids (Biggers, McGinnis *et al.* 2004).

Due to the difficulties associated with complex culture media, simple media have been devised, especially to minimize the possibility of unknown and undesirable effects, and complex interactions between the components. Simple culture media mainly consist of simple salt solutions with added energy substrates (concentrations adjusted) to support

the growth of certain embryo types (Gardner and Lane 1999). While still generally inadequate to support embryo growth at an acceptable rate, many studies regarding the metabolic requirements of the embryos (Biggers and Stern 1973; Rizzino 1987; Wright and O' Fallon 1987; Gardner 1998) have helped to define suitable concentration of nutrients and composition of other chemicals such as amino acids so that the resulting simple media can provide improved embryo growth. On the other hand, it must also be noted that this type of culture medium has classically included serum in its composition, so it has inherited similar drawbacks of the complex culture medium of variability of batches related to variability of growth outcomes. Bavister in his review (Bavister 1995) reported several attempts to compare the performance of the simple and complex culture medium to gauge the supposed improvement of the simple culture medium. No fruitful outcomes have been obtained as the results were found to be inconsistent. It is strongly believed that it was the inclusion of serum that was a major cause of this inconsistency, leading to widespread support for its replacement as one of the media components (Maurer 1992; Gardner 1994; Bavister 1995).

Recently, there has been considerable attention drawn to the development of sequential culture media such as "G1/G2" media and "Universal IVF" media. These media support the changing nutrient and energy needs throughout embryo growth from the 1-cell stage to the blastocyst stage. As emphasized by Gardner (Gardner 1998), the embryo has very different physiology throughout its growth and associated with this is the change in the nutrient requirements, and subsequently, the change in energy metabolism. For example, for mouse embryos, the main energy source for it prior to compaction (from from the 1-cell to 8-cell stage) are pyruvate, lactate and amino acids; while after compaction (morula to blastocyst stage), an increase in glucose uptake and utilization has been reported. Perhaps paradoxically, it is noted that glucose is actually inhibitory to embryo growth prior to the compaction process; however, it becomes an important energy substrate after the compaction. Favourable outcomes found by various researchers (Gardner and Sakkas 1993; Pinyopummintr and Bavister 1995; Fong and Bongso 1998; Van Langendonck, Demylle *et al.* 2001) using these two-stage or sequential culture media further support their use in embryo culture. Nevertheless the debate continues, as some researchers have not been able to find experimental evidence to support the need for sequential media (Biggers, McGinnis *et al.* 2005). Despite continuing debate,

embryo culture media mostly remain as a complex solutions, consisting of defined levels and types of energy substrates, stable amino acids, vitamins, growth factors, metal chelating agents, osmotic stabilizers and some kind of serum replacement (Gardner 2008).

#### **2.1.4 Physical and Environmental Conditions of Embryo Culture**

Compared to the modification of culture medium formulation, relatively less effort has been expended to optimize physical and environmental aspects, which can also strongly affect the success rate of embryo cultivation. Most of these investigations centre on finding out the optimal conditions to culture an embryo in a common static (unmixed or unperfused) culture system. Both physical and biochemical components of the culture system work together, as occurs *in-vivo*, where embryos are subjected (changing) fluid environments with specific biochemical and physical properties. The following subsections highlight some important considerations, leading up to a review of culture vessels and microfluidic containment.

##### **2.1.4.1 Somatic Cell Support**

Co-culture is a technique for cultivation of embryos in the presence of somatic cells such as epithelial cells, where basically embryos are placed on the surface of a cell “feeder” layer, The key rationale is that the somatic support cells replicate the type of biological environment within the reproductive tract, which is essentially a fluid environment created by cell monolayers. As indicated by Bongso *et al.* (Bongso, Sakkas *et al.* 1999) in his review of the co-culture technique, during the latent period where the advancement of embryo culture research was less progressive due to difficulties in overcoming embryo developmental blocks, the co-culture method showed promising results in overcoming these blocks. This quickly raised the popularity of the method and many researchers developed this technique further (Biggers, Gwatkin *et al.* 1962; Heyman, Menezo *et al.* 1987; Sakkas and Trounson 1990; Lai, Stein *et al.* 1992). However, there are still some negative aspects that held back the wider acceptance of this technique. Firstly, while it provides a possible means of obtaining a higher culture success rate, additional effort is required to culture and maintain the somatic feeder cells in addition to the embryo itself. This raises the cost and time to perform embryo culture. Secondly, due to the presence of cell types other than the embryo, the selection of the

culture medium to maintain the growth and function of both cell types becomes complicated, as the culture medium needs to be nutritionally suitable for both, rather than just the somatic cells (Bongso, Sakkas *et al.* 1999). Another drawback is that the use of these somatic helper cells may inadvertently pass viral infections to the embryo (Marsh 1994). Furthermore, it is impractical and time consuming to screen each batch of feeder cells prior to cultivation. This in particular poses a potentially serious health concern if one plans to co-culture embryos for clinical use. In general, while a feeder layer essentially functions to produce factors in the culture medium, these factors represent a relatively undefined mixture of beneficial and toxic factors. Feeder layers also remove essential nutrients from the medium that may be necessary for the embryos themselves. It is much more practical, as emphasized by Bavister in his review on the topic of co-culture (Bavister 1995), to try to understand how co-culture improves conventional culture, and then apply this understanding to create better defined culture media (this ensured the repeatability of the culture process), to suit the changing needs of the embryo.

#### **2.1.4.2 Extended Culture Periods**

The second main culture technique concerns the revised procedure of culturing the embryo up to the blastocyst stage before transplantation back to the female reproductive tract, referred to as “extended culture”. Human embryos are commonly transferred at the 4-cell or 8-cell stage (Gardner and Lane 1997) to enable time for embryos at this earlier stage to adjust to the internal environment of the womb before compaction and blastocyst formation. Recently, extended culture has been more widely applied clinically, based on its extensive usage in animal models (Jones, Trounson *et al.* 1998).

There are three main advantages to extending the time of culture of embryos *in-vitro*:

1. It is found that the growth of the embryo is synchronized with its location in the reproductive tract during the normal *in-vivo* condition. Prior to compaction, the embryo at its 1-cell to morula stage travels from the ovaries across the fallopian tube and ampulla region. After compaction, the embryo at the blastocyst stage would have been transferred to the uterus and be implanted to the uterus surface for further growth. By transferring the *in-vitro* cultivated embryo at the

blastocyst stage instead of earlier stage, it is believed that such synchronization with the normal *in-vivo* condition will increase the growth success rate.

2. By extending the *in-vitro* culture period up to the blastocyst stage, one can identify those with the best developmental potential (for example: faster development rate and normality under microscopy examination). This would also in theory raise the success rate of the embryo transfer.
3. One can run diagnostic tests to examine the embryo for genetic anomalies, and screen for genetic disease, as the embryo when reaching the blastocyst would have activated its genetic material. At present, embryos are tested at the 6-8 cell stage (Handyside 1998) but without the extended culture there would be no way of telling if the sampled embryo has been damaged and therefore unable to continue to grow.

There are various studies that demonstrate the effectiveness of extended culture of embryos (Buster, Bustillo *et al.* 1985; Huisman, Alberda *et al.* 1994; Olivennes, Hazout *et al.* 1994; Scholtes and Zeilmaker 1996), confirming the gaining popularity of this procedure. The current shortfall of it is that it depends on the capability of the *in-vitro* culture system to produce a normal embryo at the blastocyst stage, although new methods of testing embryos at this stage are emerging, to ensure the safety and wider usage of this method. It remains important to continue to investigate how to successfully culture embryos up to the blastocyst stage, and how improvements in culture conditions and technology can progress this method. Blastocyst culture is more successful, but practically is not always preferable to culture to the early cleavage stages, mainly because of strains on laboratory time and resources and its inadequacy for small groups of human embryos of which less than half normally form blastocysts.

#### **2.1.4.3 Ratio of Embryos to Medium Volume**

Another important but largely overlooked idea for improving the culture technique lies in modifying the culture volume and the density of embryos. As mentioned in the reviews by Bavister (Bavister 1995) and Gardner (Gardner and Lane 1997) under this topic, many researchers had conducted studies on several species and demonstrated the benefits of increasing the embryo per culture medium ratio: either by decreasing the culture volume or increasing the numbers of embryo per fixed volume of the culture

medium (Wiley, Yanami *et al.* 1986; Paria and Dey 1990). A systematic study by Lane (Lane and Gardner 1992) on varying the culture volume and embryo density also verified these beneficial outcomes. It is hypothesized that by doing so, autocrine or paracrine signalling molecules that promote embryo growth are retained in a high concentration surrounding the embryos and subsequently encourage the embryos to grow. The same phenomenon also occurs in relation to enzymes that embryos secrete to promote hatching from the zona pellucida around the blastocyst stage (Sawada, Yamazaki *et al.* 1990). The issue of embryo density becomes highly relevant in the consideration of microfluidic devices, as described further in the section on culture vessels. Unlike animal embryos, human embryos cannot be grown in groups to derive the benefits of group culture, particularly to the blastocyst stage. So volume reduction becomes the only viable approach to increase the embryo density per culture volume.

Apart from the physical volume of the culture media, other aspect of the culture environment such as gas composition, temperature, light, osmotic pressure, the culture vessel itself and the incubator are also important factors to be considered when optimizing the *in-vitro* culture environment for an embryo. This is because they all contribute to a complete system to provide a suitable environment for the embryo to grow. Because of this, the effect of each of these factors will be discussed below.

#### **2.1.4.4 The Gas Phase**

The two most commonly examined gas components relevant to embryo culture are oxygen and carbon dioxide. Carbon dioxide is essential for regulating the metabolism and pH of the culture medium by acting with bicarbonate and hydrogen ions in aqueous solutions, whereas oxygen is essential for the metabolic function of all cells. For oxygen, there are many studies showing that a low concentration enhances embryo development *in-vitro*, for example for mouse embryos the optimal oxygen concentration is 5 to 8% (Quinn and Harlow 1978; Umaoka, Noda *et al.* 1992), while for domestic animals such as sheep, goats and cows the optimal concentration is 7% (Thompson, Simpson *et al.* 1990; Batt, Gardner *et al.* 1991). Low oxygen concentration was also found in the reproductive tract of various other species (Mastroianni and Jones 1965; Fischer and Bavister 1993; Farrell and Foote 1995). In contrast, reduced embryo growth was reported under the normal atmospheric oxygen content of 21% (Whitten 1971; Balin,

Fisher *et al.* 1984; Pabon, Findley *et al.* 1989). It is believed that when the oxygen content is high, large numbers of toxic free oxygen radicals could be formed in the culture media (Noda, Matsumoto *et al.* 1991; Umaoka, Noda *et al.* 1992). As for carbon dioxide (CO<sub>2</sub>), there is increasing evidence to show that a CO<sub>2</sub> concentration elevated from 5% to 10% helps to enhance embryo growth (Carney and Bavister 1987; Farrell and Foote 1995). This also correlates well with the amount of CO<sub>2</sub> concentration found within the reproductive tract, which is close to this elevated value (Hallden, Li *et al.* 1992). One of the explanations for this is that the increased CO<sub>2</sub> content helps to decrease the pH level of the culture medium, and this helps to maintain favourable culture condition. Aside from this, it is also found that CO<sub>2</sub> has a stimulatory effect on the metabolism of the embryo and hence a higher CO<sub>2</sub> content in the culture media improves embryo growth (McLimans 1972; Carney and Bavister 1987).

#### **2.1.4.5 Temperature Regulation and Light Conditions**

Apart from the composition of the gaseous environment, it has been found that the temperature and lighting have an effect on embryo growth, with temperature in particular of fundamental importance to all culture systems in all species. Studies have found that the fluid temperature surrounding the embryo affects the morphology of the embryo such as organization of the cytoskeleton and intracellular transport of organelles (Schumacher and Fischer 1988). The media temperature is also critical in maintaining the suitable pH buffering in the culture medium, as is the case *in-vivo* where at a high temperature the solubility of CO<sub>2</sub> decreases and therefore causes the pH level of the culture media to increase (Rivera and Hansen 2001). Culture temperature is usually matched to the body temperature of the species, while it is slightly different in different species, the optimal value for the temperature is about 37 °C (Brinster 1969; Gardner and Lane 1999). Deviation from this temperature result in decreased cleavage rates and reduction in blastocyst development (Fischer, Schumacher *et al.* 1988; Pickering, Braude *et al.* 1990). Similar growth impairment was also found when the embryo was exposed to visible light for a certain period of time (Hirao and Yanagimachi 1978; Fischer, Schumacher *et al.* 1988). It is believed that this is due to the deterioration of the culture medium that occurs when it is exposed to short-wavelength light (MacMicheal 1986). There is also evidence that ultraviolet light, a component of standard candescent

light sources, can lead to genetic mutations in cells. In short, a low light illumination is preferred when cultivating embryos, under constant temperatures conditions.

#### **2.1.4.6 Osmotic Pressure of Culture Medium**

Previous studies discovered that embryos are very adaptable to a wide range of osmotic pressure from 250 to 300 mOsmol (Whitten 1971; McKiernan and Bavister 1990), although it must be noted that the development of embryos *in-vitro* is severely impeded when the osmotic pressure is higher than this range (Brinster 1965; Beckmann and Day 1993; Liu and Foote 1996). The major effect that the osmotic pressure of the culture medium has on the embryo, as with other cells, is the regulation of its volume: the embryo will change its volume to alleviate the perturbation in the preferable osmotic pressure (Baltz 2001). However, such a change in volume is a short term effect, as in the long run the adjustment of the intracellular content of the organic osmolytes respond to the change in external osmotic pressure and allow the embryo to regain its original volume (Baltz 2001). It is believed that such a capability of the embryo allows it to tolerate such changes to the external osmotic pressure. Although it is found that the osmotic pressure *in-vivo* in the oviduct fluid is in the high range (above 300 mOsmol) for various species (Olds and VanDemark 1957; Van Winkle, Haghghat *et al.* 1990; Elhassan, Tasca *et al.* 1999), it is believed that the combined action of the organic osmolytes, in the embryo and secreted by the reproductive tract, help to mediate a suitable osmotic pressure, and therefore it can survive in such a high osmotic pressure environment.

As for the pH of the culture media, it is found that a variety of species are insensitive to pH variation between 6 and 8 (Brinster 1965; Carney and Bavister 1987). Typical pH values of culture media are set to a fairly constant values of 7.3 – 7.4, even though the pH of the fluid within the reproductive tract is found to varies between 7.1 and 8.0, depending on the different phase of embryo development (Gardner and Lane 1999). Regulation of the pH of culture media is mainly controlled by the content of CO<sub>2</sub> diffused in it. In contrast, the pH of intracellular fluid within the cell (different from the pH of the culture media) has a large influence on the embryo health. It functions as a metabolic regulator which has a large influence on the development of the embryo. This was discussed in detail by Bavister in his review on this topic (Bavister 1995).

#### **2.1.4.7 Incubator Containment**

In most cell and embryo cultivations, incubators are commonly employed to control all the environmental factors mentioned above. The design of the incubator is hence important when it comes to regulating environmental factors for embryo growth such as the gaseous composition, humidity and temperature. In particular, the ability of the incubator to maintain the desired culture environment and to restore this environment after disturbances, such as when a human operator opens the incubator to retrieve the embryo for inspection, becomes the main focus for any incubator design (Gardner and Lane 1999). The importance of tight incubator control is highlighted by studies that report improved embryo development results if opening of the incubator is restricted or a modular incubator chamber that has a better capability to maintain the desired environmental factors is used (Gardner and Lane 1996). One example of this is the gaining popularity of the mini incubator (MINC), as an alternative to the conventional larger volume incubator. Study show that the MINC has considerably better environment recovery ability than conventional larger volume incubators, because the much smaller incubation volume permits the desired gas phase, temperature and humidity to be regulated much faster (Fujiwara, Takahashi *et al.* 2007). It is also found that the direct contact of the MINC heating plate with the culture dish provides a much faster and effective culture media temperature control compared with conventional the air convection incubator design (Cooke, Tyler *et al.* 2002). The development of alternative systems such as the Submarine Incubation System by Vajta (Vajita, Holm *et al.* 1997) continue to focus on improving the ability of the incubator to maintain environmental conditions such as constant temperature under normal operation.

#### **2.1.4.8 The Embryo Culture Vessel**

In comparison to the aspects of culture environment discussed above, there is even less research on the design of the culture vessels that provide a safe environment for embryo development. As detailed by Brinster in his review of mammalian embryo culture systems (Brinster 1969), the typical static culture vessel, as shown in Figure 2.2, consists of designs that provide a containment geometry for a fixed volume of culture medium. Most of them consist of vessels that hold culture media in a volume of 50  $\mu$ l to 10 ml, either in micro-drops that normally measure in volume of about 50 - 100  $\mu$ l, or in

a pool of culture media that fills the entire vessel. Depending on the culture techniques employed, the culture media are either covered with a layer of oil or regulated with a gas composition that supports embryo growth. Referring to Figure 2.2, most early embryo culture took place in the vessel configuration of type J – a test tube (Hammond 1949; Whitten 1956), or type K – a Carrel flask (Pincus 1941). In these vessels, the embryos were cultivated in a comparatively large culture medium volume in the range of micro-litres. With the finding that a smaller culture volume is favourable to embryo growth (as mentioned in Section 2.1.4.3), the micro-drop method and its variations, such as illustrated by Types A, B, D, G and H in Figure 2.2, became more popular (Sherbahn, Frasor *et al.* 1996). Particularly, Type A and F remain as the most frequently utilized culture vessels for recent embryo culture where they come in the form of petri-dishes or multi-well plates fabricated from plastic or glass. Note that most of these culture vessels are originally designed to culture a variety of other cell types such as suspended cells or cells that adhered to the surface, where they are comparatively 10 to 50 times smaller than the embryo and they are commonly cultured in a group (Glasgow, Zeringue *et al.* 2001) .

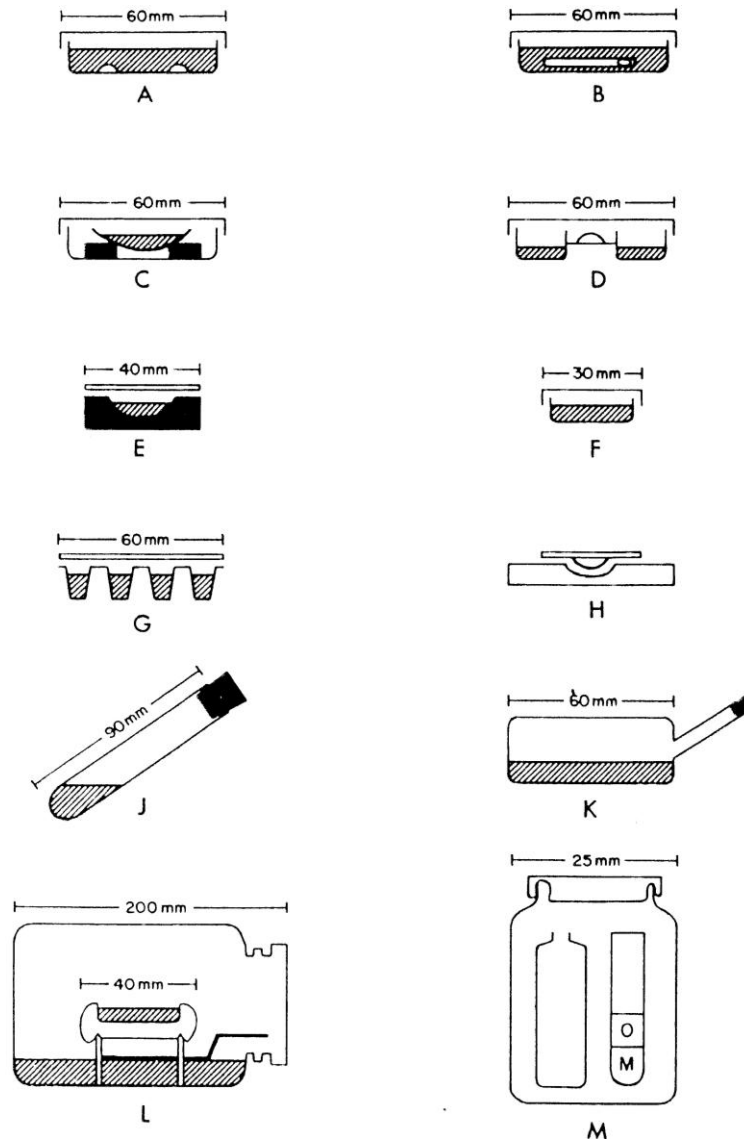


Figure 2.2: Typical static culture vessels employed to hold the embryos in place (Brinster 1969).

Practically all culture vessels used to culture embryos *in-vitro* today are static systems. That is, medium is contained under static physical conditions, in fixed volumes, without any fluid movement. In biological terms, this is different to the fluid environments that support embryos *in-vivo*, such as in the oviduct and uterus. The following section describes progress in modifications to the culture vessel in terms of volume, microenvironments and fluid movement.

## 2.2 Modification of Embryo Culture Vessels

While static culture vessels are popular due to their ease to set up, their potential performance drawbacks cannot be overlooked. Firstly, the metabolic activities carried out by embryos throughout their growth will alter the original composition of the culture media, causing the depletion of essential nutrients and the accumulation of metabolic waste (Gardner 1994; Bavister 1995). Such changes in the concentration of either the necessary or unwanted substances cannot be regulated in a static culture environment over extended culture periods. This alone results in the limited capacity of all static systems to support embryo growth. Secondly, as mentioned earlier, the embryo will change its physiology throughout its growth and hence the requirements for specific nutrient uptake will vary from the start to the end of the *in-vitro* culture. Although the use of sequential media under static culture conditions can address this need to a certain extent, this necessitates the embryo to adjust to a sudden change of environment, possibly resulting in physiological trauma, that can lead to increased mortality and developmental abnormalities (Gardner and Lane 1996). Moreover, embryos developing *in-vivo* experience a dynamic environment inside the reproductive tract that is very different from the static *in-vitro* culture environment (Hafez and Blandau 1969; Rousseau and Menezo 1993). Such a dynamic environment serves to maintain the continuous supply of nutrients and other essential growth factors and signaling molecules, while also diluting/removing metabolic waste (Bavister 1995).

### 2.2.1 Perfused Vessels

Perfusion systems represent methods of altering the medium environment within the culture vessel, whereby the containing volume is continuously replenished or recirculated from an external source. In order to address the drawback of static culture vessels in meeting the changing metabolic and signalling requirements of the developing embryo, dynamic perfusion culture systems<sup>2</sup> were created (Pincus and Werthessen 1938; Wilson, Zalesky *et al.* 1992; Goverde, Peeters *et al.* 1994; Lim, Reggio *et al.* 1997). Although the design for these systems vary, they generally have the components illustrated by the perfusion culture system employed by Lim (Lim, Reggio *et al.* 1997) as shown in Figure 2.3: a medium reservoir, a perfusion incubator containing the culture chamber that contains the embryo, a pump that drives the culture

---

<sup>2</sup> The notation “system” here refers to the combined setup of culture vessels and incubator.

media to flow through the system and a collector vessel (fraction collector) which retrieves expended media. Despite the extra effort, early studies comparing these perfusion culture systems with a static culture system found that they performed comparably. For example according to the comparative study by Pruitt, embryos produced from the conventional static culture system in a culture dish have a lower mean grade of morphological score of 1.15 (on a scale of 1-4 where 1 is the most desirable morphology) compared to the perfusion system which scored 2.20 (Pruitt, Forrest *et al.* 1991), while a similar comparison by Lim *et al.* found that only 31% of embryos developed to blastocyst stage under perfused conditions compared with 33% under static conditions, indicating no significant difference in developmental outcome (Lim, Reggio *et al.* 1996). It was suggested that the main reason for this is that the culture medium composition employed in their experiments was not ideal to support satisfactory embryo growth. For example, Pruitt commented that the possible poor outcomes of the perfusion system may have been due to the gelding serum employed in his experiment instead of the more popular fetal calf serum. It was believed that gelding serum does not contain the growth promoters for embryo growth, and that these components are present in fetal calf serum. Evidence for this was also suggested by a subsequent study by Lim *et al.*, who found that co-culture with bovine oviduct epithelial cells (which secrete embryotrophic factors that promote embryo development), and the addition of antioxidants, do improve embryo development to blastocyst stage (Lim, Reggio *et al.* 1997). Another possible factor was that the flow rate of the culture medium perfusion was set too high. In both comparative studies by Lim *et al.* they suspected that the culture medium flow rate of 30 – 38  $\mu\text{l}/\text{min}$  set in their experiments was detrimentally high compared with the flow rate of oviduct fluid *in-vivo* in the bovine species, which measures less than 10  $\mu\text{l}/\text{min}$  (Carlson, Black *et al.* 1970). In fact a flow rate that is very high ( $>60 \mu\text{l}/\text{min}$ ) was found to crack the zona pellucida and flatten the embryos. Apart from that, the chamber volume of the perfusion system (of Lim *et al.*) is in the range of 0.2 – 1.5 ml, very much larger than the micro-drops of culture medium employed (50 - 100  $\mu\text{l}$ ) in a static system or the micro-litres of oviduct fluid inside the reproductive tract (Hafez and Blandau 1969). This indicates that the benefits of a higher embryo per culture medium ratio are not available in these perfusion systems described so far.

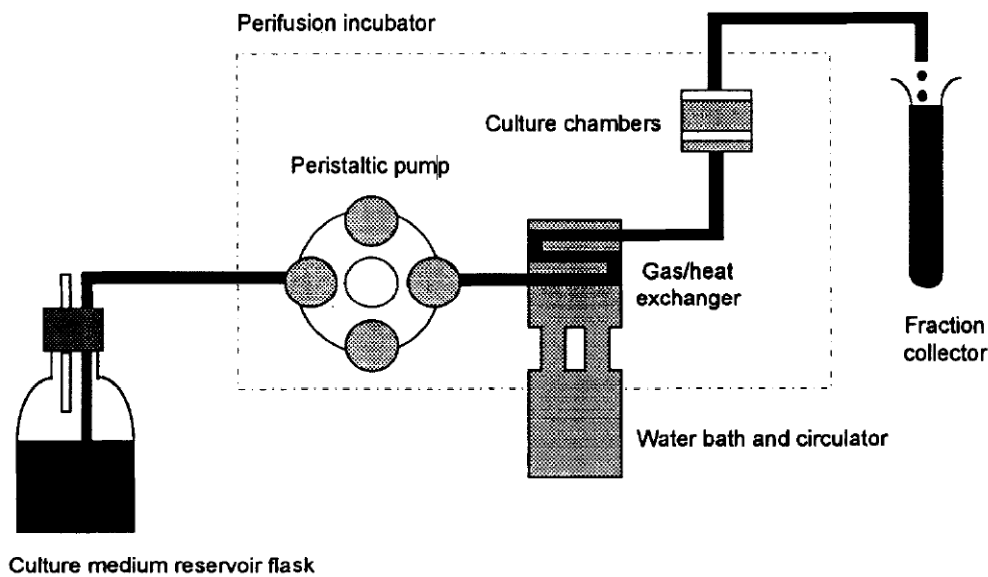


Figure 2.3: Schematic showing the typical components of a perfusion culture system (Lim, Reggio *et al.* 1996).

Nevertheless, these initial disappointing results do not detract from the potential practical benefits offered by perfusion culture systems, including adjustment of the content of the culture media without causing sudden disturbances to an embryo, and continuous harvesting of expended culture medium fractions for identification or quantification of embryotrophic and other important molecular factors produced by the embryo that may provide information about its growth.

### 2.2.2 Culture Vessels with Microcavities

In addition to medium perfusion, other studies have focused on improving the outcomes of embryo culture by optimizing the geometry and three-dimensional characteristics of the local area in the vicinity of embryos within the culture vessel. This has resulted from two main drivers: efforts to reduce the culture volume and to incorporate a suitable microenvironment. Both approaches have recently been integrated using microfluidics, which frequently employ the additional feature of medium perfusion or some kind of fluid movement.

The main idea is to mimic the *in-vivo* environment inside the reproductive tract, where the embryo grows naturally. A reason for this more optimal growth may be the

existence of complex cavity environments within the reproductive tissues that form a kind of “niche environment” inside the reproductive tract that creates a specially regulated environment to nurture the embryo. The idea of incorporating such a “niche environment” into the design of the culture vessels is inspired by other biological evidence from embryonic stem cells (Fuchs, Tumber *et al.* 2004; Li and Xie 2005). In the context of preimplantation embryos, the blastocyst itself represents an example of a niche microenvironment for the inner embryonic cells. While the structure and function of them differs from one type to another, in general the “niche environment” refers to a highly specialized hollow, fluid-filled micro-environment created by various types of cells, and all these different cells work together to perform a specific function. For example the “niche environment” for stem cells protects them from damage, regulates and maintains the normal function of the cells as well as providing extrinsic cues to signal how and when should the stem cells differentiate into other cell types (Fuchs, Tumber *et al.* 2004). By recreating an artificial environment that functions as a “niche environment”, it is hoped that a higher embryo cultivation success rate can be obtained, or at least improvements in the quality of embryos produced toward those of *in-vivo* standards.

The idea of reducing the volume of culture vessels originates from one of the discoveries in culture technique, which was that the proportion of embryos developing to the blastocyst stage is higher when ratio of embryo per culture medium volume is higher (Lane and Gardner 1992). In line with modification to the physical culture condition of embryo-to-volume ratio, it is believed that by reducing the culture volume surrounding the embryo, more autocrine/paracrine factors and metabolic by-products secreted by the embryos will be accumulated around it and a higher concentration of these factors will in turn promote embryo growth. More importantly, there is growing need to isolate and culture embryos individually in order to avoid aggregation of zona-free embryos (Wells and Powell 2000), as well as to counteract the situation where there is only one viable embryo available, or for identification purposes. Hence the benefit of having a higher ratio of embryo per culture media volume can only be achieved by reducing the culture volume.

There are a few notable examples which centre on this idea of reducing the culture volume. Among them is the Well-of-the-Well (WOW) system developed by Vajita (Vajita, Peura *et al.* 2000), and its variations such as the modified Well-of-the-Well system (Pereira, Dode *et al.* 2005) or microtube culture system (Roh, Choi *et al.* 2008). The idea here is to culture a single or a limited number of embryos inside a small cylindrical well with either a V-shape or a rounded bottom (Figure 2.4). Preparation of these micro-wells is performed by heating up a steel needle and then pressing it into the bottom of a 4-well dish, melting the bottom dish surface and forming the micro-wells with desired shapes. The cultivation itself is performed by placing the embryos in the micro-wells; these micro-wells are then filled with the appropriate culture medium, followed by an oil over-layer to prevent medium evaporation. There have been several favourable outcomes in using this culture system for bovine embryos, where a higher blastocyst development rate is reported and the quality of the blastocyst is higher when compared to the microdrop culture method (Vajita, Peura *et al.* 2000; Pereira, Dode *et al.* 2005; Roh, Choi *et al.* 2008). Another similar approach in reducing the culture volume and establishing a microenvironment is the Glass Oviduct (GO) culture system developed by Thouas (Thouas, Jones *et al.* 2003). In this system, the embryo is held vertically inside a micro-capillary tube containing a plug of culture medium. Using the GO system, a higher number of hatched blastocysts was obtained and the implantation rate was comparable to the conventional microdrop culture method, even when the embryo density is lower (Thouas, Jones *et al.* 2003). Compared to the WOW system, *in-vitro* culture using the GO system resulted in a higher blastocyst rate (Vajta, Lewis *et al.* 2001). Another advantage of the GO system over the WOW system is that they utilize commercially available culture components that do not require additional time and effort to prepare the micro-wells.

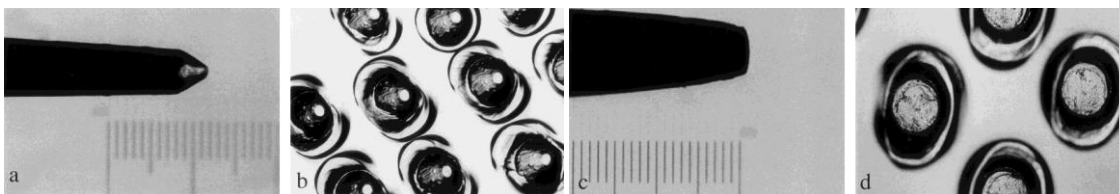


Figure 2.4: Cross-sectioned view (a, c) and top-down view (b, d) of the WOW culture systems, featuring the V-shaped bottom (a, b) and rounded bottom (c, d) (Vajita, Peura *et al.* 2000).

While reducing the volume of the culture vessel has brought many advantages, this approach still creates a culture environment dissimilar to the *in-vivo* condition, as it remains a variation on a static culture system, with inherent problems associated with fixed nutrient content and growth limitation, as discussed previously. Taka *et al.* found when using the WOW system, that embryo development to the blastocyst stage was actually suboptimal when smaller wells (500  $\mu\text{m}$  in diameter) were used, compared to the microdrop method (Taka, Iwayama *et al.* 2005). They reasoned that this is because, in their experiment with the smaller well of the WOW system, the embryo density is too high such that diffusion of toxic substances away from the embryo was limited. Overall, this study implies that over-reduction of the culture volume limits diffusion of harmful metabolic substances away from the embryo and the nutrients are depleted too fast such that it impairs embryo growth. Although it is possible to overcome this by replenishing the culture periodically with fresh medium, this again imposes the problem of environmental stressors on the embryo due to the change in pH, temperature and osmolarity when the embryo is being relocated to another medium. This problem, as well as others associated with culture in micro-volumes such as increased evaporation, difficulties in fluid handling, surface tension effects, rapid de-equilibration rates and more rapid build-up of metabolic waste products, may be overcome if some kind of fluid perfusion or dilution is introduced.

### **2.2.3 Perfused Microfluidic Vessels**

Microfluidics has emerged as a solution to the aforementioned problems, although it is still largely experimental in the application of embryo culture technology in ART. Research in this area has focused on introducing fluid perfusion from an external source into the design of culture vessels, while retaining the design feature of reduced culture volume. This concept also overlaps with that of bioreactors (from here onwards the term “bioreactor” refers to culture micro-vessels with medium perfusion). Earlier attempts at perfusion culture systems returned poor outcomes mainly because of the lack of suitability of equipment to handle small amounts of culture media, or to provide a very slow fluid perfusion rates that mimic the *in-vivo* culture condition in fluid-filled environments like the Fallopian tube (Thompson 2007). The introduction of design features and functionalities of microfluidic systems in a continuous flow bioreactor would address these drawbacks. Typically, microfluidic systems use micro-channels or

micro-chambers that can be fabricated using methods such as photolithography, laser ablation and injection moulding (Becker and Locascio 2002), to be similarly scaled to the size of a single embryo. Together with the fluid perfusion capability, microfluidic systems present a more suitable foundation to rationally design a bioreactor that can mimic the optimal *in-vivo* condition more closely. Due to the similar geometric features and scaling, the embryo is more likely to experience analogous fluid environments that exists inside the reproductive tract (Glasgow, Zeringue *et al.* 2001; Beebe, Wheeler *et al.* 2002; Thompson 2007). Also due to the small scale of any microfluidic system, the amount of culture medium utilized is very small compared to conventional perfusion culture systems and this will help to reduce the cost of performing embryo culture as some of the chemical components of the culture media such as growth factors are very costly (Glasgow, Zeringue *et al.* 2001).

Microfluidic systems have been investigated as alternative methods to perform other functions apart from embryo culture, such as embryo or gamete transfer and manipulation (Glasgow, Zeringue *et al.* 2001; Cho, Schuster *et al.* 2003; Suh, Phadke *et al.* 2003; Zeringue, Wheeler *et al.* 2004), *in-vitro* maturation and fertilization (Funahashi and Nagai 2000; Walters, Beebe *et al.* 2001; Suh, Zhu *et al.* 2006), as well as to combine them to form an integrated system which handles most aspects of the assisted reproduction – creating a lab-on-a-chip platform for assisted reproduction (Glasgow, Zeringue *et al.* 2001; Clark, Walters *et al.* 2003; Wheeler, Walters *et al.* 2007). Such microfluidic concepts may allow them to be integrated as embryo culture systems in an automated *in-vitro* embryo production platform, which may speed up overall embryo production, simplify some of the culture procedures and reduce the need for labour-intensive manual handling procedures. As evidence of this claim, various microfluidic culture systems have emerged demonstrating successful cultivation of different cell types using micro-channels (Horner, Miller *et al.* 1998; Park, Toner *et al.* 2006) and micro-chambers (Hung, Lee *et al.* 2005). In addition, the possibility of integrating some sub-processes such as microheaters, temperature sensors, micro-pumps and micro-valves has been demonstrated (Huang and Lee 2007). The high development potential of microfluidic systems is also reflected by the recent review on microfluidic cell culture systems by Meyvantsson and Beebe, which discusses the use of microfluidic platforms to design advanced cell culture systems retaining benefits such as high

scalability, high throughput and low culture media wastage (Meyvantsson and Beebe 2008). However, it must be noted that these microfluidic systems may be unsuitable for embryo culture because cells typically remain suspended in the flowing media while the embryo that is about 10 to 50 times larger appears to fill a considerable portion of a microfluidic channel, with other potential difficulties such as the need to track and reliably retrieve an individual embryo (Glasgow, Zeringue *et al.* 2001).

One of the notable microfluidic systems specifically designed to handle and culture mammalian embryos is the simplified micro-channel bioreactor system developed by Beebe and colleagues (Beebe, Trumbull *et al.* 1998; Glasgow, Zeringue *et al.* 2001; Beebe, Wheeler *et al.* 2002). Their microfluidic platforms include various micro-channel designs that demonstrate accurate placement and successful embryo survival within micro-channels, as well as embryo manipulations such as cumulus cell removal (Zeringue, Wheeler *et al.* 2004) and even zona pellucida removal (Zeringue, Wheeler *et al.* 2004). The basic outline of this micro-channel bioreactor is shown in Figure 2.5. Briefly, the design consists of an inlet funnel, which permits the loading or unloading of embryo and culture media, a constriction region, which holds the embryo in place while allowing culture media to perfuse past the embryo, and an outlet to facilitate the extraction of expended culture media. Both static culture (Walters, Clark *et al.* 2003; Raty, Walters *et al.* 2004) and dynamic culture with media perfusion (Beebe, Wheeler *et al.* 2002) have been performed using this bioreactor, using embryos from several species including the mouse and pig. Promising results were observed by these investigators for both static and dynamic culture on the micro-channel bioreactor, where a higher blastocyst rate was recorded in the micro-channel culture compared to the micro-drop culture.

As mentioned previously, the integration of the microfluidic platform into embryo culture is still not widespread and is largely at the experimental stage, since the understanding of the dominant physics governing microfluidic systems is not well established (Gravesen, Branebjerg *et al.* 1993; Atencia and Beebe 2005). Further research in this area is needed to understand how microfluidic flows such as high fluid viscosity, large surface to volume ratio, significance of surface tension influence the physiology of the growing embryo.

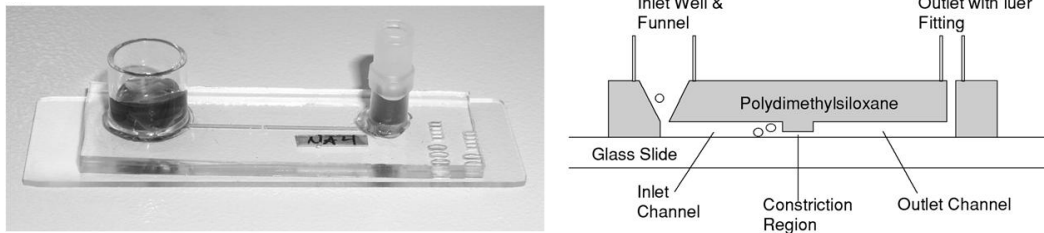


Figure 2.5: Photograph and conceptual sketch illustrating the microchannel culture system for the culture of mammalian embryos, developed by Beebe and his colleagues (Walters, Clark *et al.* 2004).

With the introduction of fluid perfusion, several operational issues need to be addressed. Firstly, present culture media are inappropriate to be utilized in microfluidic systems as commented by Wheeler in his review on microfluidic technologies for porcine embryos. This is because with the inclusion of fluid perfusion the mechanism of nutrient delivery to the embryo changes where, rather than depending on diffusion alone, the transport of nutrients or other substances may also be largely influenced by bulk flow movement in the microchannel (Wheeler, Clark *et al.* 2004). Apart from that, it is believed that the inappropriate perfusion rate of the culture medium causes unnecessary high shear stress to the embryo and may result in excessive depletion of autocrine/paracrine factors secreted by the embryos, thereby causing lower embryo viability. This was suggested by a study conducted by Hickman in examining static and dynamic embryo culture in a microfluidic culture system (Hickman, Beebe *et al.* 2002), which found that embryo development in a dynamic microfluidic bioreactor was significantly decreased compared with static microdrop or microfluidic bioreactors. More research is needed to determine suitable flow rates for culture medium perfusion to optimize such systems.

All in all, the approach of microfluidic bioreactors for cell culture is a growing area and further development is required before it becomes as routinely used as dishes for static cultures.

## 2.3 Fluid Flow in Microfluidic Systems

Extensive reviews are available, which discuss relevant theories, fabrication, testing, comparison and validation of microfluidic devices or systems, as well as their future potential (Gravesen, Branebjerg *et al.* 1993; Ho and Tai 1998; Gad-el-Hak 1999; Stone, Stroock *et al.* 2004; Atencia and Beebe 2005). The main focus of this section is to qualitatively review the notable attributes of the fluid flow in microfluidic systems relative to their macroscopic counterparts. This is done to understand how the physics of the flow in microfluidic platforms brings about benefits to bioreactor design.

By definition, microfluidics refers to devices or methods developed to manipulate fluid flow with length scales less than 1 mm (Stone, Stroock *et al.* 2004). The study of microscale phenomena has been going on since the 19<sup>th</sup> century, but in recent times that the pace of development for industry (Gravesen, Branebjerg *et al.* 1993; Gad-el-Hak 1999; Stone, Stroock *et al.* 2004; Atencia and Beebe 2005) and medicine (Wilding, Pfahler *et al.* 1994) has increased. This is mainly for two reasons. Firstly, the fabrication techniques that have enabled small-scale manufacturing have matured and they are becoming more accessible for laboratory usage. Most of these techniques stem from the development of integrated circuit fabrication techniques for integrated circuits (Ho and Tai 1998; Stone and Kim 2001). This opens up easier pathways to build and test microfluidic systems. Secondly, the demand has increased for microfluidic devices that tailor for a variety of applications in biology, medical and industrial fields, which require smaller scaled devices to optimize existing operations or to enable new techniques. Examples include studies on biological processes (Beebe, Trumbull *et al.* 1998; Glasgow, Zeringue *et al.* 2001; Wheeler, Walters *et al.* 2007) and the design of better sensors, which have higher detection ranges and faster frequency responses while reaching sizes that they do not interfere with the phenomena being measured (van Oudheusden 1992; Jiang, Tai *et al.* 1997; Ho and Tai 1998).

### 2.3.1 Highly Viscous Flow

As highlighted by Purcell in his famous paper discussing the environment experienced by micro-organisms (Purcell 1977), at such small scales, the dynamics of a fluid is very different from that at larger scales that we commonly experience. Due to the very small length scale of microfluidic systems, the Reynolds number ( $Re$ ) is typically the order of

unity or less. As this number describes the ratio of inertial to viscous forces, this directly implies that viscosity dominates inertia in influencing fluid behaviour. Thus one can expect predictable laminar flows, rather than turbulent flows common in industrial situations (Brody, Yager *et al.* 1996). This means that fluid flow control in a microfluidic system can be designed to be very precise and predictable, and for very small Reynolds numbers it is even possible to completely reverse the motion of the flow and return the fluid to its original state, a feat that is unachievable otherwise (Purcell 1977; Leal 1992; Brody, Yager *et al.* 1996). This capability opens up new possibilities to enhance existing flow control devices, such as allowing precise transport of small amounts of a liquid or solids to a target area (Bringer, Gerds *et al.* 2004), or provide a new means to fabricate very small structures such as the microfabrication of very fine fibers (Kenis, Ismagilov *et al.* 1999; Jeong, Kim *et al.* 2004). On the other hand, existing devices that rely on inertia no longer work and this is a reason why effective microfluidic devices have to be designed based on the controlling physics and not simply by miniaturizing existing macroscopic devices.

### 2.3.2 Diffusion Dominance

Related to the above discussion is that diffusion also becomes the dominant transport mechanism for the distribution of a solute in a fluid rather than advection. This is quantified by the dimensionless Peclet number,  $Pe$ , which describes the relative importance of diffusion and advection for species within the fluid. This is defined by  $Pe = UL/D_{solute}$ , where  $U$  is the average velocity of the flow,  $L$  is the characteristic length of the microfluidic system and  $D_{solute}$  is the diffusivity of the solute within the fluid. In a microfluidic system, both the length and velocity scales are typically small compared with typical macroscopic systems (Bird, Stewart *et al.* 2002). As for the Reynolds number when  $Pe$  is small ( $< 1$ ), the solute transport is more influenced by diffusion and this is relevant to nutrient delivery and metabolic waste management. This opens possibilities to manipulate the fluid flow. By utilizing this diffusion dominant property, new type of filters, which have high filtration efficiency and only require a small amount of sample have been devised (Brody and Yager 1997). Examples include the “H-filter”, which can extract particles or solutes in a stream of fluid (sample stream) by allowing it to be in contact with another stream of miscible fluid with different diffusivity (extraction stream). For the purpose of mixing fluids, this can be either

beneficial or detrimental depending on the purpose. In a scenario where minimal mixing of solutes is desired, such as having two different types of solutes or two solutes with different concentrations that travel side by side, this diffusion dominant effect is favoured as the slow but controlled mixing between these solutes forms a virtual barrier when the two different streams come into contact (Hibara, Nonaka *et al.* 2002; Zhao, Viernes *et al.* 2002). However, if rapid mixing between solutes is required, because diffusive transport is slow, it will require a longer time and/or an impractical long distance for complete mixing to occur (Stone, Stroock *et al.* 2004). In order to enhance mixing in a microfluidic system, it may be necessary to employ laminar chaos (Stone, Stroock *et al.* 2004). This can be achieved by applying passive mixing methods to generate a secondary flow depending on specially shaped structures such as obliquely oriented grooves (Stroock, Dertinger *et al.* 2002); or using active mixing methods that utilize localized forcing such as using piezoelectric fabricated surface to generate secondary fluid motion across a flow (Miyazaki, Kawai *et al.* 1991).

### **2.3.3 Large Surface Area to Volume Ratio**

The second key characteristic of any microfluidic system is that surface area to volume is large compared to that of macroscopic systems – this ratio maybe  $10^6$  larger (Gad-el-Hak 1999). Due to this difference in scale, several phenomena which are not significant in the macroscopic world stand out. For example, evaporation acts quickly on exposed liquid surfaces (Brody, Yager *et al.* 1996); homogenization of solutes or temperature gradients occur faster as the relatively larger surface area and smaller volume allow much faster equilibrium to be achieved (Atencia and Beebe 2005); and similarly the flow reaches an equilibrium profile faster as it enters a microchannel (Koo and Kleinstreuer 2003). Perhaps the most notable phenomenon is that the surface force has a much large influence on the fluid flow in the microscopic world (Ho and Tai 1998).

It is believed that this change to the force balance is the main reason for the deviation of properties such as friction factor, pressure gradient, temperature gradient or heat flux from the ones predicted by classical flow theories commonly appeared to macroscopic systems. This has been pointed out by a number of researchers (Pfhaler, Harley *et al.* 1990; Mala and Li 1999; Guo and Li 2003; Koo and Kleinstreuer 2003). With the increase of surface area per unit volume as the device length-scale decreases, the

various types of surface forces, such as the van der Waal, electrostatic and steric forces, which are negligibly small for macroscopic systems, can become very significant. This presents opportunities as well as difficulties. For one, it provides a new means of moving fluids in the microfluidic platforms other through pressure gradients. There are several notable examples:

- Capillary action can overcome gravity and pull liquid across an enclosed microstructure. This occurs when the adhesive intermolecular forces between the liquid and the adjacent surface of the structure are stronger than the cohesive intermolecular forces within the liquid (Rowlinson and Widom 2002). This provides an approach to drive fluid flow within microstructures only by adjusting the surface properties of the microstructure to achieve the desired flow characteristics and thus may eliminate the need for cumbersome external forcing (Atencia and Beebe 2005).
- The electro-osmosis force (EOF) can generate liquid flow by applying an electric field along a microstructure containing a liquid. This is possible due to electrokinetics – the interaction between electric currents on the surface of a microstructure and charged electrolytes within a fluid (Saville 1977; Stone, Stroock *et al.* 2004). The EOF generates a plug flow profile instead of the usual parabolic profile generated by pressure driven flow and this allows the transport of solutes without dispersion as they travels along channels or pipes (Long, Stone *et al.* 1999; Herr, Molho *et al.* 2000). This is useful for applications such as studying targeted drug delivery to a specific location or driving slow fluid movement in a microfluidic system.

For the case of immiscible fluids, the combination of strong surface tension and laminar flow provides a consistent way to produce and manipulate droplets with very precise control. This is demonstrated by the use of a “T-junction”. It is a T-shaped channel geometry which forces two streams of immiscible fluids to merge in such a way that one liquid forms droplets dispersed in the other (Tan, Fisher *et al.* 2004; Utada, Lorenceau *et al.* 2005). One notable application for this in is the operation of an inkjet printer nozzle in outputting minute but precise amounts of ink (Bassous, Taub *et al.* 1977). The surface tension of a liquid can be altered by adjusting the surface properties, such as hydrophobicity, and this can be used to create an interface to separate two

streams of immiscible fluids, analogous to a water/oil interface in the macroscopic world. Such interfaces are useful for efficient exchange of dissolved gas between two streams of fluid (Zhao, Viernes *et al.* 2002; Hibara, Iwayama *et al.* 2005).

Despite the potential benefits that stem from the relatively large ratio of surface area-to-volume, the potential difficulties also need to be borne in mind. Firstly, depending on the characteristics of the system surfaces, some solutes may exhibit a high tendency to stick to these surfaces. This problem is experienced with adhesion of proteins to a PDMS surface (Roach, Song *et al.* 2005). Such adhesion not only greatly depletes the free solute in the fluid but the adhesion also forms a permanent attachment (Atencia and Beebe 2005) to the surface and alters the original geometrical features (Dickinson and Matsumura 1994). Secondly, if gas bubbles are present in a liquid flow, the very small radius of curvature of the gas-liquid interface is linked to strong surface tension (Matsumoto and Colgate 1990), with the net effect of impeding the fluid flow in the microfluidic system. This necessitates using a large pressure difference to drive bubbly liquid (Pfhaler, Harley *et al.* 1990; Brody, Yager *et al.* 1996).

#### **2.3.4 Rarefaction Effects**

In addition to the main characteristics discussed above in Section 2.3.1 through 2.3.3, the gas flow in microfluidic systems exhibits another phenomenon which is not present in liquid flow: the rarefaction effect.

In the macroscopic world, the air flow is always regarded as incompressible so long as the local Mach number,  $Ma$ , the dimensionless ratio of the air speed to the speed of sound, is less than about 0.3 (White 2003). However, this is not the case with air flow in microfluidic systems. As pointed out by Gad-el-Hak (Gad-el-Hak 1999), the small dimension of the microfluidic system limits the number of gas molecules present. This may significantly alter the density of the gas where it is rarefied, subsequently increasing the compressibility of the gas flow, even if it is flowing at  $Ma < 0.3$  (van den Berg, Seldam *et al.* 1993; Arkilic, Schmidt *et al.* 1997). This rarefaction effect in turn will induce a non linear pressure distribution on the flow (as the gas is more compressible) and implies that a much higher pressure than the one predicted using

conventional flow theories is needed to drive the gas flow (Colin 2005; Barber and Emerson 2006).

Another interesting phenomenon appears in the microfluidic gas flow, also due to the rarefaction effect, is a change to the no-slip condition at solid walls. This assumption states that fluid molecules adjacent to a solid wall do not move but instead stick to the surface. This does not hold true and the effect of this “wall slip” become increasingly important. This phenomenon has been observed in many microchannel gas flow investigations, where the measured gas flow properties such as pressure drop, shear stress and mass flow rate are found to be different from the values calculated using continuum-based flow models with no-slip boundary conditions (Pong, Ho *et al.* 1994; Beskok, Karniadakis *et al.* 1996; Arkilic, Schmidt *et al.* 1997). It must be noted that this effect is not significant in liquid flows as the liquid molecules in comparison are much denser than gas molecules. For example, the mean free path of a typical liquid molecule such as water is 0.3 nm (Koo and Kleinstreuer 2003), while for a gas such as air the mean free path is 70 nm for standard conditions (Arkilic, Schmidt *et al.* 1997). The tightly packed liquid molecules do not allow the molecules adjacent to the wall to move by much, and hence the wall slip effect is negligible in liquid flow (Koo and Kleinstreuer 2003).

The reason for this “wall slip” is that as the gas become more rarefied, the mean free path between the molecules (the distance which measures how far the gas molecule would travel before colliding with another gas molecule) becomes larger and this allow the molecules adjacent to the solid surface to travel further and faster before colliding with the surface, therefore increasing the degree of wall slip (Kennard 1938; Bird 1976; Edwards 1977). The direct implication of the wall slip effect is that the viscous shear stress is reduced and correct prediction of gas flows using continuum-based flow theories require modifications to cater for this (Kennard 1938; Beskok, Karniadakis *et al.* 1996). The degree of wall slip and consequently the degree of validity of the continuum model can be represented by the dimensionless Knudsen number ( $Kn$ ), where it is defined as the ratio between the mean free path of the gas molecules and the characteristic length of the device or system in which the gas is moving through (Knudsen 1909).  $Kn > 10$  signifies a high degree of wall slip corresponding rarefied gas

so that the gas flow needs be modelled as a free molecule flow, while  $Kn < 0.01$  represent a low rarefaction and hence the wall slip is negligible, and the gas flow can be modelled assuming as a continuum. Between  $0.01 < Kn < 10$ , the gas flow can be further categorized into two regime: the slip-flow regime:  $0.01 < Kn < 0.1$  and the transition regime:  $0.1 < Kn < 10$  (Beskok, Karniadakis *et al.* 1996; Gad-el-Hak 1999). These different regimes determine the suitability of approximations based on either continuum or molecular-based theories for modelling the gas flow.

## 2.4 Proposed New Micro-Bioreactor Design

As shown by the review on embryo culture vessel modifications, previous attempts of reducing the culture volume and applying microfluidic concepts into the bioreactor design have been met with successful outcomes of obtaining better mammalian embryo growth, where an increasing number of embryos are grown to the blastocyst stage and the overall embryo quality is better. Given these promising outcomes, it is enticing to examine if combining both approaches could provide an even greater improvement. The initial idea for this new bioreactor design is shown in Figure 2.6. Termed the “cavity micro-bioreactor”, the device consists of a microchannel and an array of micro-cavities situated at the bottom surface of the channel. The microchannel facilitates the perfusion of culture media through the bioreactor, perhaps mimicking the dynamic *in-vivo* fluid flow environment inside the reproductive tract. The micro-cavities fulfil the role of the “niche environment” for the embryo by providing in a reduced effective culture volume and a sheltered micro-environment for embryo growth while at the same time permitting unobstructed exchange of nutrients, gases and other substrates via the cavity opening. With these two features, it is believed that the artificial *in-vitro* culture environment provided by this bioreactor design more closely imitates the overall *in-vivo* conditions. It must be noted that the inspiration for this design comes from Gardner in his proposed concept of a dynamic embryo culture system (Gardner 2008). This facilitates the change of composition of the culture media without moving the embryos. A similar concept has been devised by Park and his colleagues intended to grow bioartificial liver cells (Horner, Miller *et al.* 1998; Park, Berthiaume *et al.* 2005). That bioreactor has a microchannel for the perfusion of culture media and a grooved surface at the bottom of the microchannel, which acts as the platform to seed the hepatocytes cells. In using this bioreactor, they found that the liver cells experienced reduced shear stress, which is beneficial for them, while adequate oxygen was supplied to the liver cells that have a high oxygen uptake rate. The main dissimilarity between this and the proposed cavity micro-bioreactor is that the latter one has an open channel design as shown in Figure 2.6 while the microchannel bioreactor has an enclosed channel design. The open surface design allows easier placement and relocation of embryos; an oil-layer is distributed on top of the culture media to prevent evaporation of the culture media as in any microfluidic system significant evaporation of fluid will occur due the very small amount of working fluid.

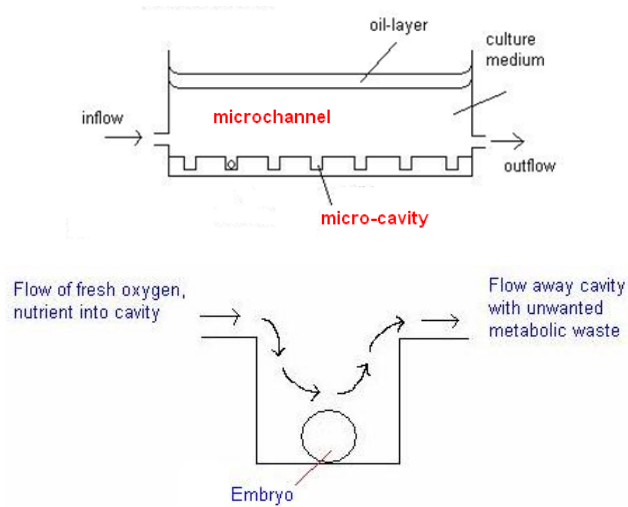


Figure 2.6: Conceptual sketches showing the two design features of the cavity micro-bioreactor: the microchannel that permits continuous perfusion of the culture medium, and the micro-cavity housing the embryo and protecting it from the oncoming flow while still allowing substrate exchange to and from the embryo.

#### 2.4.1 Evaluation of Micro-Bioreactor Design

With the bioreactor prototype established, the next step is to examine its feasibility. In general, this initial testing phase can be broken down into three iterative stages:

- Numerical parametric studies
- Experimental testing
- Performance evaluation and refinement

As shown in Figure 2.7, these three stages are interconnected and form an iterative procedure for testing the feasibility of this bioreactor. Starting with the parametric studies stage, numerical simulations are carried out to model the fluid environment and solute distribution inside the micro-bioreactor. These studies determine the influence of changing design parameters on the fluid flow and solute transport within the micro-bioreactor. They thus refine bioreactor geometry and operation settings to at least serve as an initial guide for the experimental program. For example, by using outcomes from culture medium inflow-rate studies together with the physiochemical information on the best oxygen content and shear stress to promote embryo growth, the culture medium inflow rate, which is one of the operational settings for the bioreactor, can be tuned.

Based on this set of initial design parameters, the experimental testing stage can begin by constructing a prototype of the bioreactor. At this stage other relevant experimental factors need to be decided on. These include microfluidic aspects of the bioreactor such as the mechanism to drive the medium perfusion, the nature of the oil layer and culture media interface, and other embryo culture aspects such as embryo loading and unloading, and incubation procedures to suite the micro-bioreactor.

Lastly, the bioreactor performance can be evaluated and compared with that of existing bioreactors and to expectations. This can provide further input to the iterative loop if the performance is not ideal, or it appears that the performance can be improved by undertaking further changes.

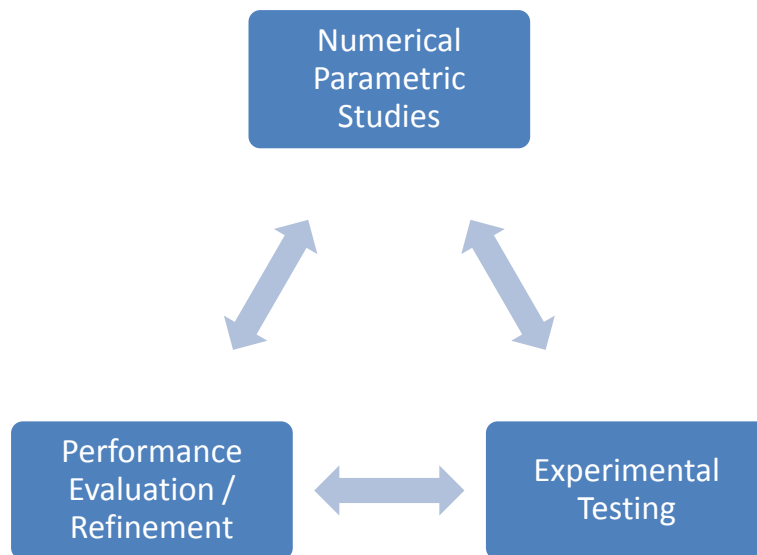


Figure 2.7: The three main phases of concept evaluation for realizing the micro-bioreactor concept.

### 2.4.2 Motivation for Parametric Studies

The numerical parametric studies, (i.e., stage 1 of the design loop), form the main body of research described in this thesis. The main objective is to provide an understanding of how controllable parameters (are likely to) affect embryo development within the cavity bioreactor, and to allow optimisation of, and improvements to, actual laboratory and clinical bioreactors. The other objective is to employ these parametric studies to further develop numerical modelling as a useful tool to aid micro-bioreactor development. Note that the specific parametric studies mentioned here refer to investigations into input

solute concentration, inflow rate and bioreactor geometry on factors affecting embryo growth such as shear stress, and local concentrations of dissolved gas, nutrient and waste products. The main reason to utilize numerical modelling to conduct these parametric studies, as opposed to actually constructing the bioreactor and conducting experiments, is that they provide a rapid and inexpensive way to explore a wide range of parameter space and provide data that can be difficult to measure in experiments. Changes to geometrical features can be easily and inexpensively implemented in numerical models compared to constructing physical prototypes. Of course there are definite limitations which constrain the capacity of numerical modelling, for example, at present it does not model biological aspects of the embryo or the physiochemical reactions that take place on the embryo surface.

The two specific objectives of this thesis are explained here. Initially, the parametric studies function as an approach to predict the optimal initial dimensions and operating parameters for the bioreactor prototype. This is achieved by devising several parameter space studies on the geometric features and the functional aspects of the micro-bioreactor. These parametric studies find out how changes to these factors influence the fluid condition within the bioreactor, and how would these changes affect the physiological factors that influence embryo growth such as solute concentration and shear stress. The parametric studies conducted in this project are as listed here below, where each sub study focuses on one aspect of the bioreactor design:

- *Cavity aspect-ratio, width and shapes*: The three studies here aim to find out the impact of changing the length, depth, width and shape of the cavity affects the fluid conditions around the embryo.
- *Culture media inflow rate and height*: These studies aim to investigate favourable settings for the perfusion of culture media in the bioreactor.
- *Embryo growth*: This study is devised to explore the situation where the embryo changes size and metabolic needs as it matures.
- *Multiple embryos or multiple cavities*: These studies investigate the scenarios of cultivating several embryos in a single cavity or having several cavities located in proximity where each cavity cultivates an embryo, in essence evaluating the possibilities of increasing the embryo production.

After this initial stage, experiments should be conducted on a physical bioreactor. At the commencement of this research program, a sequential experimental program was planned but at this stage is running a little behind schedule, so that the design loop sequence has not yet been completed. Of course, the experimental program was not a planned component of the research program reported here. In future work, after the experimental testing on embryo culture has been performed, the culture outcomes will be used to validate the predictions from these parametric studies. Quantitative discrepancies between the parametric studies and the experiments will be examined to find out any short-comings of the numerical model and refinements will be made to improve on it. Other factors not currently included in the model may also need to be added, such as production of factors controlling growth and development. Improvements to the numerical model may contribute much to speed up the refinement of bioreactor design as a robust and accurate tool that can emulate the environment experienced by the embryo precisely, and can easily handle parameter space studies and overcome restrictions hindering earlier models. Ultimately, it is hoped that this preliminary study will assist with the development of more complete numerical models that can accurately predict the physiochemical parameters experienced by an embryo, leading to much better optimisation and understanding of bioreactor design.

### **2.4.3 Overview of Numerical Modelling**

In general, there are three types of approach used to model microfluidic flow. These are analytical approximations, continuum fluid modelling and discrete fluid modelling (Nguyen and Wereley 2006).

#### **2.4.3.1 Analytical Model Approximations**

Analytical model approximation, as the name implies, is the attempt to use simple analytical models to approximate the fluid flow in a microfluidic system. These models are generally derived from macroscopic fluid mechanics, such as flow models which describe the flow-pressure characteristics for a number of microfluidic devices (Gravesen, Branebjerg *et al.* 1993). Successful utilization of this approach has been reported in the flow modelling of simple microfluidic devices such as valves (Tiren, Tenerz *et al.* 1989; Jensen and Gravesen 1993) and channels (Manz, Miyahara *et al.* 1990; Young, Gray *et al.* 1993; Koo and Kleinstreuer 2003), where the predicted flow

rates are in good agreement with the measured values. Brody *et al.* have also successfully utilized this approach to model the fluid flow in microchannels and demonstrated that the analytical model predictions compare favourably with experimental results (Brody, Yager *et al.* 1996). Flow modelling in a more complex system such as in a microfluidic chip with several types of sensors and actuators has also been undertaken with limited success by subdividing the system into several elements. These can be described individually with simple analytical models, and individual models of these elements are then interconnected using circuit simulation tools such as Bond graphs (van de Pol, Breedveld *et al.* 1990), SPICE (Swart and Nathan 1992; Rasmussen, Mavriplis *et al.* 2001) or others similar programs (Perera and Rao 1990; Zengerle and Richter 1994).

While this modelling approach requires the least computation and is relatively easier to carry out compared with the other two modelling approaches, there are several drawbacks which limit its use. For one, it can only handle a limited selection of flow quantities such as averaged flow velocities, flow rates or pressure drops. This limits the types of analysis that can be employed to analyse the flow or incorporate other types of modelling such as solute transport. Besides that, the accuracy of these models depends heavily on the correct assumptions to the type of flow (Gravesen, Branbjerg *et al.* 1993). In a more complex fluid flow situation, such as for the type of microfluidic device considered here, analytical modelling approximation is not ideal for quantitative predictions (Gravesen, Branbjerg *et al.* 1993). Augmentation of these simple models is required, such as including empirical relations consistent with the underlying approximations of the approach.

#### **2.4.3.2 Discrete Fluid Modelling**

Discrete fluid modelling, also termed *molecular-based flow modelling*, approximates the flow by viewing the fluid as a collection of discrete particles such as molecules (and perhaps atoms, ions and electrons). It then describes the condition of the fluid in terms of the positions, velocities and thermodynamic state of these particles. This approach becomes more important for cases in which the continuum fluid approximation breaks down, such as (rarefied) gas flows in MEMS devices or flows experienced by spacecraft as they cruise through a rarefied atmosphere in high earth orbit. The macroscopic

properties of the fluid such as density, velocity and pressure can be computed by suitable averaging procedures (Gad-el-Hak 1999). This is in direct contrast to continuum fluid modelling that approximates the fluid as a continuous and indefinitely indivisible unit. Discrete fluid modelling can be subdivided into two categories: the deterministic approach and the probabilistic approach (Kogan 1973; Allen and Tildesley 1987).

The deterministic approach, mainly represented by molecular dynamics (MD) simulations (Alder and Wainwright 1957; Alder and Wainwright 1958), is the most fundamental method, where the fluid condition is modelled in such a way that each of the particles in the fluid is assigned a random velocity according to the Boltzmann distribution. The interactions between particles are described through a two-body potential and the time evolution of each particle position is determined by integrating Newton's equation of motions (Cercignani 1988). As the MD simulation is derived based on the most basic sets of equations from classical or quantum mechanics, in principle they can be applied to model any types of flow without limitations (Haile 1993; Koplik and Banavar 1995). However, there is a practical limitation which prevents MD simulations from being the method of choice for fluid modelling: MD simulations require significant computational resources, as in MD simulations the computation of the trajectory of a single particle need to account for its interaction with other particles in the fluid volume under consideration, hence if  $N$  numbers of particles are present in the model, the amount of computations required is proportional to  $N^2$ . This implies that as the size of the computation volume and the total number of particles increase, the computational resources required will increase phenomenally, and this in turn poses a serious limitation on the system size that can be handled by MD simulations (Koplik and Banavar 1995; Gad-el-Hak 1999). As quoted by Gad-el-Hak, given the state-of-the-art of MD simulations in the late 1990s, the computation time for realistic MD simulations for a sizable fluid volume requires a computational time of thousands of years (Gad-el-Hak 1999).

The probabilistic approach, alternatively, focuses on computing the probability of finding a particle at a particular position and state within a defined volume of fluid. The probability distribution is then determined constrained by appropriate conservation

equations to obtain the mean number, momentum and energy of particles within the computing volume (Schaaf and Chambre 1961; Bird 1994). This method is mainly developed to address the modelling of gas flow in which the interaction between the particles is infrequent – rarefied flow, where the  $Kn$  of the flow is larger than 0.001 (Muntz 1989; Bird 1994). The notable example of this method is the direct simulation Monte Carlo method (DSMC), which is most suitable to handle modelling of rarefied gas (Bird 1978). To date, it has been successfully applied to many studies of rarefied gas where the continuum models break down (Cheng 1993; Bird 1994; Oran, Oh *et al.* 1998). It must be noted that while the probabilistic approach is relatively much less computationally demanding than the deterministic approach, the required computation time is still very large compared to continuum modelling of gas flows (Oran, Oh *et al.* 1998). All in all, while discrete fluid modelling is the most versatile model because it can theoretically model any type of fluid at any conditions, the computational cost is still prohibitive, especially for parameter studies in microfluidic devices.

#### **2.4.3.3 Continuum Fluid Modelling**

Continuum fluid modelling is the modelling approach which approximates the fluid as a continuous medium that uniformly fills up the entire volume that it occupies. The variation of the physical quantities such as energy and momentum are defined everywhere and variation of these values are continuous from point to point throughout the fluid. Under normal circumstances, the continuum assumption holds true if the distance between the molecules or the mean free path, is small compared with the characteristic length scale of the fluid volume – the mean free path is typically smaller than  $10^{-6}$  m for a gas and  $10^{-8}$  m for a liquid (Nguyen and Wereley 2006). With this assumption differential equations can be derived, which express conservation of mass, momentum and energy. These need to be supplemented by a constitutive relation expressing the relationship between stress and rate of strain, and potentially an equation of state (Landau and Lifshitz 1987; Sherman 1990; Gad-el-Hak 1999; White 2003). The most common equations employed to describe the motion of fluids are the Navier-Stokes equations which are essentially Newton's second law for fluid motion that assume a linear relationship between stress and strain rate. By applying the appropriate boundary and initial conditions, the differential equations can be solved either analytically or numerically depending on the complexity of the problem (Landau and

Lifshitz 1987; White 2003). The numerical approach in solving the differential equations using computer methods, termed *computational fluid dynamics* (CFD), is gaining more popularity in recent years due to the advancement in computational capacity of modern computers. More types of numerically complex problems can now be resolved with sufficient accuracy and acceptable computational times (Anderson 1995; Ferziger and Peric 1999).

There are many studies of microfluidic flows which successfully utilize continuum fluid modelling. Koo and Kleinstreuer have utilized it to study the liquid flow in microchannels, where it was found that the numerical results compared favourably with experimental observations (Koo and Kleinstreuer 2003). Zeng *et al.* used continuum fluid modelling (CFD) to conduct parametric studies in characterizing the solute concentration and shear stress experience by cells in a microchannel bioreactor (Zeng, Lee *et al.* 2006). The continuum fluid model was also utilized by Horner *et al.* to simulate the fluid flow and solute transport in a microchannel bioreactor for growing bio-artificial liver cells (Horner, Miller *et al.* 1998). These and numerous others similar studies (Olivier and Truskey 1993; Spiga and Morini 1994; du Toit 2002) indirectly establish the applicability of continuum fluid model to handle microfluidic flows. This is further backed up by several authors in reviewing the fluid mechanics of microfluidic devices (Gad-el-Hak 1999; Nguyen and Wereley 2006).

One attractive feature of applying continuum fluid modelling to handle microscopic fluid flow, apart from the established history of successful applications as mentioned above, lies in the versatility that it offers compared to the other two modelling approaches. In comparison to analytical modelling, continuum fluid modelling is able to handle more complex flow conditions which would be intractable. In comparison to discrete fluid modelling, continuum fluid modelling is computationally less demanding since it approximates the fluid as a continuous medium even at the discretisation level rather than as a huge numbers of atoms and molecules (Gad-el-Hak 1999). Apart from this, depending on the nature of the flow being modelled, the governing differential equations potentially may be further simplified to reduce the complexity in resolving the flow (Landau and Lifshitz 1987; White 2003).

Of course, a limitation of continuum fluid modelling is the large deviation of predictions when the model is employed outside the continuum assumptions. For example, Pfahler *et al.* found that liquid transport in microchannels deviates from the prediction of Navier-Stokes equations such that the measured friction factor is substantially higher when the  $Re$  is smaller than 0.01 (Pfahler, Harley *et al.* 1990). Similarly, Mala and Li found that the flow characteristics in a microtube depart significantly from those predicted by a continuum model when the diameter of the tube was decreased. This manifested in a higher measured friction factor and pressure drop, and it was found that the surface roughness of the tube wall had a significant influence on the flow. This implied that the surface forces become increasingly dominant as the size of the tube decreases (Mala and Li 1999). As mentioned previously, this continuum assumption breaks down when the characteristic length scale governing the fluid is small and comparable to the mean free path of the molecules or atoms (Nguyen and Wereley 2006). When this occurs, modifications to the continuum model such as enforcing slip boundary conditions to the fluid solid interface (Dussan 1976; Den 1990; Koplik and Banavar 1995) or replacement of the fluid viscosity with an apparent viscosity (Israelachvili 1986; Migun and Prokhorenko 1987) can be undertaken to retain the usability of the model.

#### **2.4.3.4 Selection of Numerical Method for Parametric Studies**

After reviewing the three modelling approaches, the continuum approach is considered the most appropriate to simulate the culture media (liquid) flow within a micro-bioreactor. To provide one final argument, as the proposed initial dimension of the micro-bioreactor is similar to the grooved micro-channel bioreactor for bio-artificial liver cells, which has demonstrated successful applicability of the continuum fluid modelling (Horner, Miller *et al.* 1998), it is logical to believe that a similar approach will be successful for modelling the micro-bioreactor described here.

## 2.5 Conclusions

The chapter began by reviewing the general aspects of embryo culture systems. The definition and a brief overview of the importance of *in-vitro* mammalian embryo culture were provided. Next the history of the development of embryo culture systems was given, and the development was categorized into three aspects: culture media formulation, culture techniques and culture environment. The major discoveries and actions taken to improve embryo culture relevant to each three aspects were reviewed in detail. Particular attention was paid to the modification of the culture vessels, or bioreactors employed for embryo culture, as in the past it received little attention compared with culture media formulation and culture techniques. From there, the concepts of microfluidics and the “niche environment” were introduced as possible approaches to seek further improvement in the embryo culture bioreactor design. A review of the attributes of microfluidic fluid flow has been conducted to understand its attractiveness in improving embryo and cell cultures. Based on the findings from these reviews, a new bioreactor design incorporating the two aforementioned approaches was devised. A prototype bioreactor was designed, and a method to test its feasibility and provide improvements was suggested. That involved the iterative procedure of (i) conducting parametric studies, (ii) constructing the prototype and culturing embryos in it, and then (iii) evaluating the performance of the bioreactor based on embryo culture outcomes and planning further refinement to improve on the bioreactor concept. This thesis is mainly concerned with the first stage of this development loop: to conduct numerical parametric studies to examine the changes in various parameters of the bioreactor, such as geometric features, fluid flow characteristics and chemical solute transport. This will provide an understanding of the underlying physics and will also provide a quantitative database on how controllable parameters affect embryo development within the cavity bioreactor. While stages two and three of the design loop are not part of this current study, it is hoped that this work will feed into the redesign of, or optimisation of and improvements to, actual laboratory and clinical bioreactors.

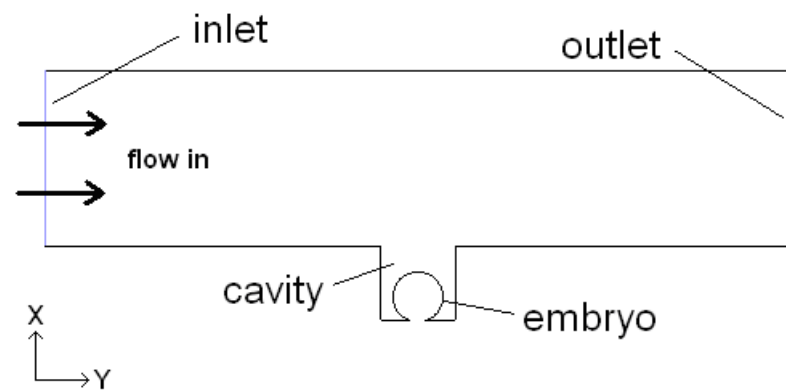
## 3.0 Methodology

---

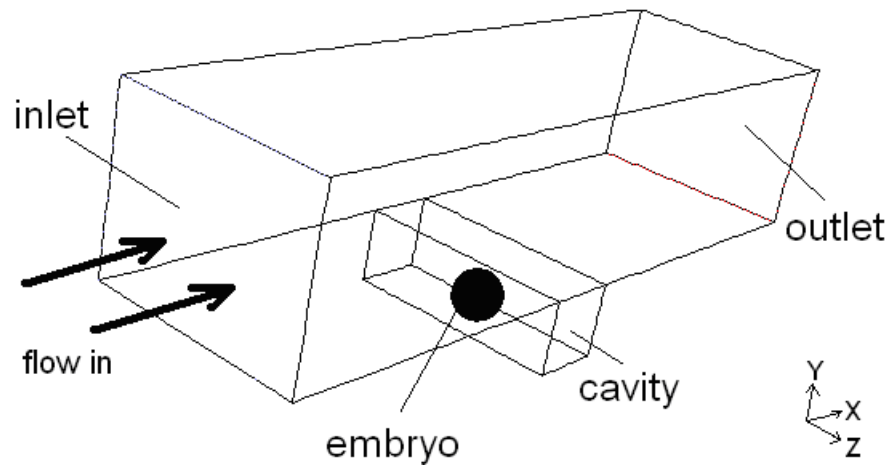
This chapter discusses the mathematical model and numerical methods employed to conduct the parametric studies. It begins with a description of the physical model, which explains the geometric and functional features of the micro-bioreactor and the parameters to be studied. This is followed by a description of the mathematical model and how it is implemented numerically to simulate the fluid flow. The factors concerned with setting up the numerical model are then discussed, such as discretisation of the fluid domain, the grid generation strategy, procedures for ensuring the flow is resolved and the selection of appropriate boundary conditions. Finally, some preliminary studies are used to validate the numerical model, including a grid resolution study and comparisons with relevant similar studies.

### 3.1 Physical Model

The two-dimensional (2D) and three-dimensional (3D) CFD models of the prototype bioreactors created for the parametric studies are shown in Figure 3.1. As can be seen they are consistent with the micro-bioreactor concept portrayed in Figure 2.6. In these models, the culture medium moves from the inlet to the outlet across the open channel. The embryo, represented by a circle in the 2D model and a sphere in the 3D model, is positioned at the middle of the square cross-sectioned cavity situated at the center of the channel. The cavity dimensions are only slightly bigger than the embryo to be consistent with the micro-niche environment. The free surface at the top of the open channel is modelled as a flat surface with the assumption that the fluid movement in the channel does not alter the shape of this free surface. This assumption requires that the Froude number (the ratio of kinetic to gravitational potential energy) is small, and that the system length scale is larger enough so that gravity dominates surface tension. This latter assumption may not fully hold; however, it appears to be a reasonable first approximation and it seems unlikely that allowing free-surface distortion would significantly change the flow behaviour. Solute exchanges are simulated to represent the main metabolic activities of the embryo such as oxygen and nutrient uptake, and metabolic waste production. These functions relate the capability of the bioreactor to the physiological needs of the embryo. The simulation of the process of solute exchange is accomplished by applying a sink term at the embryo surface to simulate the intake of solutes from the culture medium surrounding the embryo or applying a source term to simulate the production of solutes from the embryo.



(a) 2D CFD model



(b) 3D CFD model

Figure 3.1: Schematic of the (a) 2D and (b) 3D cavity micro-bioreactor CFD models in general: The circle or sphere represents the embryo located in the cavity situated along the perfusion channel.

There are eight parameters being studied in this thesis as mentioned in Section 2.4.2 in the literature review chapter. They can be categorized into four groups:

1. Cavity aspect ratio, width and shape
2. Culture medium flow rate and height
3. Embryo growth
4. Multiple cavities and embryos

The detailed description of the objective for each study is presented in their relevant result chapters, but in brief the parametric studies on the first group alter the length, width, depth and shape of the cavity and quantify how these factors affects the fluid flow and solute transport in the bioreactor; the second group examines the influence of

the perfusion rate and upstream channel height of the culture medium; the third group investigates the influence of embryo physiology on the performance of the bioreactor by changing the embryo size and solute exchange rate where the different values on these two factors reflect the measured changes to embryo physiology at different growth stages; while the fourth group looks at the prospect of increasing the number of embryos cultured in a micro-bioreactor by examining different scenarios of culturing several embryos in the same cavity or having several cavities to hold embryos in the same channel. Overall, studies including this diverse range of parameters should provide valuable insights into the design and performance of micro-bioreactors.

The solute concentrations in the vicinity of the embryo and the shear stress experienced by the embryo were chosen to characterise the embryo environment. These variables were monitored as the input parameters were varied, generally one at a time. Dimensionless representations of those variables were used, i.e.

$$\mathbf{C} = \frac{C}{C_{ref}}, \quad (3.1)$$

$$\boldsymbol{\tau} = \frac{\tau}{\tau_{ref}}, \quad (3.2)$$

where  $\mathbf{C}$ ,  $\boldsymbol{\tau}$  are the normalized solute concentration and shear stress on the embryo respectively, and  $C_{ref}$ ,  $\tau_{ref}$  represent the reference or default solute concentration and shear stress, the respective solute concentration and shear stress experienced by the embryo prior to the changes on the parameters. These two dependent parameters were chosen because previous studies have indicated that the mortality of the embryo is largely affected by the chemical composition of the culture fluid (Balin, Fisher *et al.* 1984; Batt, Gardner *et al.* 1991; Bavister 1995; Houghton, Thompson *et al.* 1996) and embryo shear stress (Xie, Wang *et al.* 2006; Rappolee 2007; Zhong, Xie *et al.* 2007).

In overview, the numerical simulations are set up as follows. The *embryo* is fixed at the middle of the cavity and the culture medium is allowed to perfuse into the bioreactor cavity as it flows along the channel. Two metabolic characteristics of the embryo are

simulated: oxygen uptake, which is one of the species required by growth and development, and lactate production, a waste product of the cells. Of course, other chemical factors are important for the health and well-being of embryos, such as growth factors and suppressors, however, this initial research program does not yet include these. The methodology can accommodate the addition of other chemical species as more empirical data becomes available to feed into the modelling. The metabolism of the mouse embryo is chosen to provide input parameters for the numerical simulations since there have been many studies conducted on mouse embryos, as can be seen from the literature review.

### 3.2 Mathematical Model

As indicated in the previous section, the numerical code employed to model the fluid condition in the micro-bioreactor has to be able to handle both fluid flow and solute transport. The numerical simulations conducted for the parametric studies were performed using the commercial CFD code *Fluent 6.2.16*. There are two main reasons that this software package was chosen for the studies. Firstly, this CFD software consists of a complete package for simulating and analysing fluid flow, including the following components:

- A pre-processor *GAMBIT 2.3.16* – used to generate the mesh. Also used to identify boundaries within the mesh system for the application of boundary conditions.
- An unstructured finite-volume solver that is responsible for resolving the governing equations that describe the physics of the fluid to obtain the desired flow variables.
- A built-in post-processing capability that enables visualizing the flow. It can generate contour plots, vector plots and particle trajectory plots, and can be used to extract point or integral flow properties.

Secondly, it includes the versatility to model other aspects of flow problems, such as solute transport within the fluid. This software provides the capabilities required for this project, and so has been chosen to use, rather than spending a considerable time developing a customized solver. Although the code may not be optimized to handle any particular flow, since for the current problem the flow is typically diffusion dominated, difficult to model flow features such as shear layers and boundary layers are avoided. Thus one can expect reasonably good convergence rates as the grid is refined. Moreover, if necessary, an optimized code for simulating the fluid flow and solute transport can be developed once this first stage of confirming the feasibility of this micro-bioreactor design has been accomplished.

Basically, *Fluent* utilizes the finite-volume based method to resolve the Navier-Stokes, species transport and the mass conservation equations, which govern the physics of the fluid and solute transport. (The latter is termed as *species* transport in *Fluent*). By applying the proper boundary conditions on the fluid domain, these equations can be

solved to obtain the fluid and solute fields such as the velocity, shear stress and solute concentration. The two primary assumptions when modelling the flow and solute conditions in the micro-bioreactor are:

- The fluid flow in the micro-bioreactor is incompressible. The requirement for this to be true is that the Mach number is small, which will certainly be true for the low flow rates that occur in perfused bioreactors.
- The fluid flow and solute transport are assumed to reach a steady-state. This is because the steady-state solver is used to obtain the flow solution and is consistent with the low Reynolds numbers involved. For the set of simulations in which the embryo changes size, it is assumed that the development timescale is much larger than the flow adjustment timescale so that a good approximation to the flow solution can be constructed as a set of quasi-steady flow solutions corresponding to the embryo size at different times.

Detailed derivations and discussions of these equations are contained in the following texts: White (White 2003) and Landau & Lifshitz (Landau and Lifshitz 1987) for the derivations of continuity and Navier-Stokes equations; Tosun (Tosun 2007) and Incropera & Dewitt (Incropera and Dewitt 2000) for derivations of the solute transport equation. These equations are briefly presented below.

The Navier-Stokes equations are essentially the momentum conservation equations for a Newtonian fluid. Taking the further assumptions that the viscous fluid flow is incompressible and time-invariant, the dimensionless mathematical expression for the vector form is

$$-\nabla \mathbf{p} + \nabla \cdot \left( \frac{1}{Re} \nabla \mathbf{u} \right) - \mathbf{u} \cdot \nabla \mathbf{u} = \mathbf{0} , \quad (3.3)$$

where  $\mathbf{u}$  denotes the normalized velocity vector,  $\mathbf{p}$  is the normalized kinetic pressure term (i.e., the pressure divided by the density) and  $Re$  is the Reynolds number characterizing the relative importance of convection to diffusion on the flow

$$Re = \frac{\rho u L}{\mu} , \quad (3.4)$$

where  $u$ ,  $\rho$  and  $\mu$  are the relevant velocity scale, the density and the viscosity of the fluid respectively, and  $L$  is a characteristic length scale of the flow system. As can be seen, the Navier-Stokes equations contain a pressure force term, a viscous stress term and the convective acceleration term from left to right, respectively. Note that the gravitational force term is omitted, since it can be combined with the pressure within the fluid. It is necessary for interface problems, however, as discussed before it is assumed that there is no surface distortion, or at least the effect of surface distortion on the predicted flow fields is minimal.

The continuity equation is the other equation that governs fluid flow. This prescribes the law of mass conservation on the flow. Again, assuming that the fluid is incompressible and the flow is invariant in time, the expression for the dimensionless form of the continuity equation is

$$\nabla \cdot \mathbf{u} = 0, \quad (3.5)$$

where the only term in the equation is the velocity divergence term since the density is assumed constant.

Lastly, the conservation equation of chemical species describes the distribution and transport of a non-reactive solute in a culture medium. Again under the conditions of flow incompressibility and time-invariance, the dimensionless form of this equation is

$$\mathbf{S} + \nabla \cdot \left( \frac{1}{Pe} \nabla \mathbf{C} \right) - \mathbf{u} \cdot \nabla \mathbf{C} = 0, \quad (3.6)$$

where  $S$  is the dimensionless solute source or sink term which either generates or withdraw solutes into the fluid domain and  $Pe$  is the Peclet number of the flow (Equation 3.7) – a dimensionless parameter, which relates the importance of mass convection relative to mass diffusion (Deen 1998)

$$Pe = \frac{UL}{D}, \quad (3.7)$$

As can be seen, the three terms in the solute transport equation are a source or sink term, a diffusion term and a convection term, respectively.

Overall, by solving Equation 3.3, 3.4 and 3.5, one can obtain the velocity, pressure and solute fields within the flow system and specifically around the embryo. The processes of resolving these numerically are described in the next section.

### 3.3 Numerical Model

The solution algorithm used by *Fluent* to resolve the governing equations is called the *segregated solver* (Fluent 2005). The governing equations, which are non-linear and coupled, are iteratively solved by sequentially updating the equations starting from an initial guess. Because of the non-linear nature of the equations, convergence is not guaranteed but relies on the use of under-relaxation parameters, effectively to nurse the iterative solution towards convergence. The standard approach employed by *Fluent* is known as the *SIMPLE* algorithm (Patankar and Spalding 1972), although there is a choice of other solvers available, which are mostly variations to this approach. The steps are:

1. The solution fields are initialized usually from extrapolating from the boundary values.
2. Any fluid properties are updated if necessary. For example, the viscosity may be temperature dependent (although not for this problem). Then the Navier-Stokes equations (Equation 3.3) are updated one equation at a time to give a set of updated velocity component fields based on the current pressure field estimate.
3. As the velocity fields obtained in Step 2 may not satisfy the continuity equation (Equation 3.5), a *Poisson* equation is derived from the continuity equation and momentum equations to correct the pressure, and obtain necessary adjustments to the pressure and velocity fields so that continuity is satisfied. The Poisson equation is solved iteratively as well. Generally only a few iterations are performed during this step because the Navier-Stokes equations will not yet be converged.
4. Depending on the problem, other flow scalars such as solutes, energy or turbulence are resolved using the previously updated values up to this step. For this case of the modelling of the micro-bioreactor, Equation 3.6 is resolved.
5. The solution fields at this step are checked for convergence, i.e., whether they satisfy the discretised equations sufficiently well. This is measured by a set of residuals for each equation. The convergence criteria are set by the user. If the convergence criteria are met, the iterative process is halted and the solutions are outputted, else the iteration continues by returning to step 2.

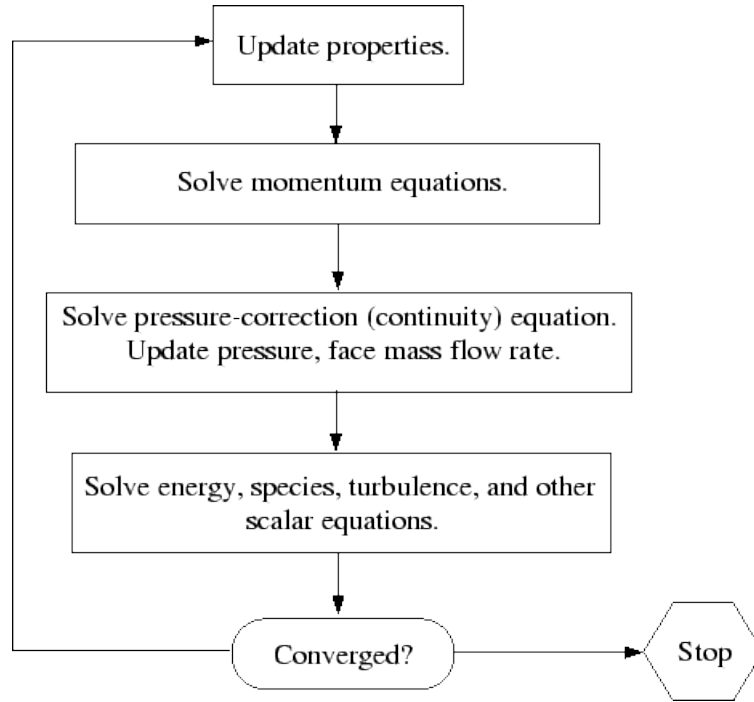


Figure 3.2: Flow chart showing the iterative solution algorithm of the segregated solver (Fluent 2005).

The strategy to obtain approximate solutions to the governing equations involves converting them into algebraic expressions using the finite-volume method and then resolving these algebraic equations based on the iterative procedures as mentioned above. This step is generally called *discretisation*. In the following subsections, the finite-volume method, the design and creation of the computational grid, boundary conditions and convergence criteria selected, are discussed in more detail.

### 3.3.1 Finite Volume Method and Spatial Discretisation

Equation 3.3 and 3.6 are clearly similar in form (since they are based on similar conservation principles). By replacing the velocity vector of Equation 3.3 and the solute concentration of Equation 3.6 with a general variable  $\Phi$ , representing the pressure and solute source terms as a generalized source term  $S_\phi$ , and replacing  $(1/Re)$  and  $(1/Pe)$  with a general diffusion coefficient  $\Gamma$ , both equations can be represented in the following form, giving a generalised transport equation for quantity  $\Phi$  (Versteeg and Malalasekera 2007)

$$S_\phi + \nabla \cdot (\Gamma \nabla \phi) - \nabla \cdot (\phi \mathbf{u}) = 0. \quad (3.8)$$

The finite-volume method is the technique utilized by *Fluent* to convert the partial differential transport equation above into an algebraic equation which can be solved iteratively as discussed above. As discussed in detail by Versteeg and Malalasekera (Versteeg and Malalasekera 2007), this is achieved by dividing the entire fluid volume into a collection of smaller fluid volumes, also termed as cells, elements or *finite volumes*, where the variables of interest such as velocity, density or solute concentration are (in this case) located at the centroid of these cells. The governing transport equation (Equation 3.8) is then integrated over each cell to obtain the discretized form, which express the conservation principle of the variables of interest within each cell

$$\int_V \mathbf{S}_\phi dV + \int_V \nabla \cdot (\Gamma \nabla \phi) dV - \int_V \nabla \cdot (\phi \mathbf{u}) dV = 0, \quad (3.9)$$

where  $V$  represent the volume of a cell. Using the divergence theorem, the second convection term and the third diffusion term of the Equation 3.9 is expressed as the integrals over the surface area  $A$  of the cell so to emphasize the balance of the surface flux of  $\phi$  in the discretized governing transport equation

$$\int_V \mathbf{S}_\phi dV + \int_A \mathbf{n} \cdot (\Gamma \nabla \phi) dA - \int_A \mathbf{n} \cdot (\phi \mathbf{u}) dA = 0. \quad (3.10)$$

Here  $\mathbf{n}$  refers to the vector normal to the surface element  $dA$ . To this stage it can be seen that the partial differential equation has been transformed into a suitable integral form of Equation 3.10, which can be discretized into an algebraic form while still preserving the conservation principle (Versteeg and Malalasekera 2007)

$$\left( \begin{array}{c} \text{Net rate of} \\ \text{creation or destruction} \\ \text{of } \phi \\ \text{inside the cell} \end{array} \right) + \left( \begin{array}{c} \text{Net rate of} \\ \text{increase of } \phi \\ \text{due to} \\ \text{diffusion across the} \\ \text{cell boundaries} \end{array} \right) - \left( \begin{array}{c} \text{Net rate of} \\ \text{decrease of } \phi \\ \text{due to} \\ \text{convection across the} \\ \text{cell boundaries} \end{array} \right) = 0.$$

The re-expression of Equation 3.10 into an algebraic form is discussed in detail by Versteeg and Malalasekera (Versteeg and Malalasekera 2007). Briefly, by integrating

Equation 3.10 over a cell, an algebraic form of the transport equation is formed where each integral term is approximated so that it is expressed in terms of values of  $\Phi$  of the current and neighbouring cells. The integral form is evaluated for each cell leading to a large set of coupled algebraic equations. This system can then be solved using the iterative process of Figure 3.2 to evaluate the solution fields ( $\Phi$ ) in the fluid domain.

When expanding the integral form Equation 3.10 into the relevant algebraic form, one would require evaluating the value of  $\Phi$  at the surface of each cell ( $\Phi_{face}$ ) and the respective convective fluxes across the surface boundaries. The second-order upwind differencing scheme is selected for this latter step. As explained by Versteeg, Malalasekera (Versteeg and Malalasekera 2007), and Anderson (Anderson 1995), the upwind differencing scheme takes into account of the flow direction when evaluating the value of  $\Phi_{face}$  at the surface boundaries by selectively choosing values of  $\Phi$  at the centroid of appropriate neighbouring cells. For example, if the flow is moving forward, the values of  $\Phi$  at the current cell and at the adjacent backward cell are used when calculating  $\Phi_{face}$ ; else if the flow is moving backward, the values of  $\Phi$  at the current cell and the adjacent forward cell are considered. The benefit with this is that it ensures that the solution of the discretized equation is stable, especially important in the case where there are sharp gradients or discontinuities within the flow such as with boundary layers. The method is consistent with the fact that convection transports variables with the flow so that upstream values should contribute to the solution rather than downstream values (Anderson 1995). As the name implies, second-order upwind differencing has second-order accuracy. This is achieved by employing a Taylor series expansion up to second order during the evaluation of  $\Phi_{face}$  (Barth and Jespersen 1989). It also helps to mitigate the unwanted artificial diffusion, which plagues first-order upwind differencing (Anderson 1995).

With regard to the Navier-Stokes equations, the pressure gradient term which forms the main momentum source term is not known a priori. As the flow is assumed to be incompressible, the density is hence constant and this means that the mass conservation equation is not in the form of a transport equation. The coupling of pressure and velocity constraints the evaluation of the flow field whereby if the incorrect pressure is evaluated, the related flow velocity field will not satisfy the continuity equation. In

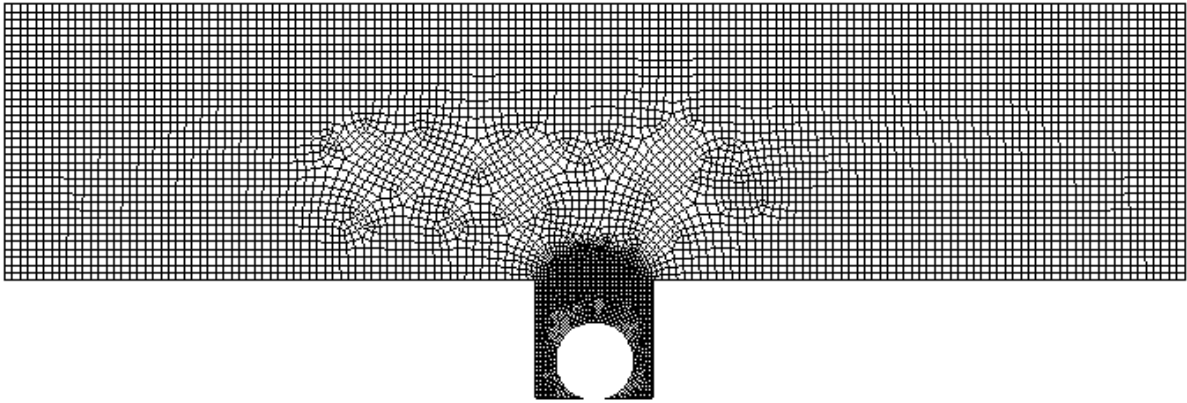
order to address this problem, the *semi-implicit method for pressure linked equations* (SIMPLE) algorithm is employed to calculate the correct value for the pressure. Developed by Patankar and Spalding (Patankar and Spalding 1972), the algorithm initially guesses and iteratively corrects the pressure. It begins with providing an initial guess of the pressure field  $p^*$  across all the cells, and then substitute it into the discretized Navier-Stokes equation to yield an initial approximation on the velocity field  $u^*$ . Next,  $u^*$  is substituted into the continuity equation to evaluate the required pressure correction field  $p'$  such that by correcting the initial  $p^*$  with  $p'$ , the corrected pressure field  $p$  together with the initially evaluated  $u^*$  would satisfy the continuity equation better. This iterative procedure is continued to progressively improve the pressure field until the required convergence criteria is met. The details of the derivation of the algorithm and its application to the discretized Navier-Stokes equation are provided by Versteeg, Patankar and Anderson (Patankar and Spalding 1972; Anderson 1995; Versteeg and Malalasekera 2007).

### **3.3.2 The Computational Grid**

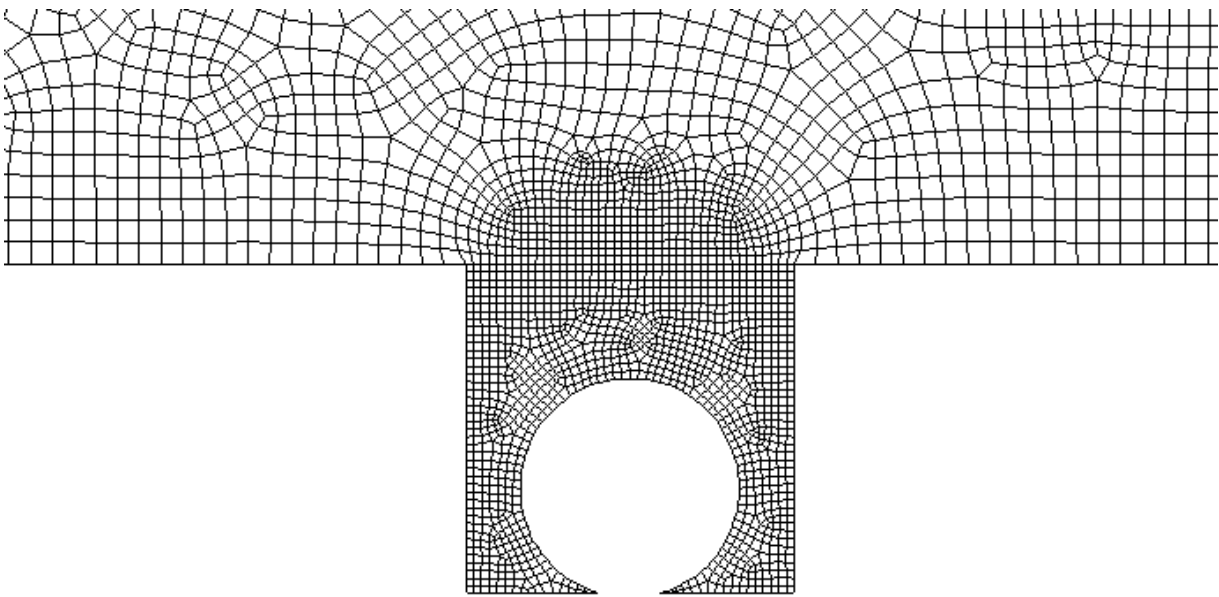
This section focuses on the creation of the 2D and 3D computational grids intended for the parametric studies. The “generic” grids are presented here, where this means the grids without modifications of any parameters. They were created using the pre-processor *Gambit 2.3.16* which offers various approaches to construct the geometry of the fluid domain and a large number of algorithms to sub-divide it, commonly termed “meshing”. Overall, all the computational grids were created using the unstructured grid approach (Anderson 1995; Versteeg and Malalasekera 2007). This provides the maximum geometric flexibility to mesh the fluid domain and offers the versatility of varying the mesh density as required. This translates to efficient use of computing resources as the higher mesh density only needs to be applied to the region of interest, typically near no-slip boundaries or where flow gradients are high. A lower mesh density can be applied elsewhere to conserve computational storage and minimize the overall computing time. More details on grid generation are discussed in the following texts: (Liseikin 1999; Chung 2002; Versteeg and Malalasekera 2007). The discussion here is on the strategy taken to optimize the mesh structure for computation efficiency, and the algorithm utilized to sub-divide the fluid domain.

The 2D generic grid is illustrated in Figure 3.3 while the 3D generic grid is illustrated in Figure 3.4. Notably, they consist of two regions: the cavity region with a higher mesh density and the channel region with a coarser mesh requirement (Figure 3.3a and 3.4a). Higher mesh density is used in the cavity primarily because it is expected that the flow varies more quickly in the neighbourhood of the embryo since the geometry variation is greatest there. Because both the Reynolds and Peclet numbers are small the problem is diffusion dominated for both the fluid and solute. This means that there won't be strong velocity solute gradients. Outside the cavity, it is expected that the flow and solute gradients will be even smoother because of the simple geometry. Hence the mesh density in the channel is chosen to be lower than within the cavity. Of course, a subsequent resolution study is conducted to check that the flow is fully resolved.

The *paving algorithm* is employed to generate the mesh for the 2D study. This automatically generates an unstructured mesh on the defined surface. Quadrilateral elements are chosen for construction (Gambit 2005). Quadrilateral elements are preferred over triangular elements (which are more versatile to model complex geometries) as they provide a better solution stability (Liseikin 1999). The different mesh densities are obtained by paving the two regions separately, with different basic element sizes. The meshing strategy applied here is simple: firstly, the edge of the fluid domain is meshed with the appropriate size depending whether it is around the cavity or channel. Next, the fluid domain in the cavity is meshed before attempting to mesh the channel. By applying this "edge pre-mesh" strategy, only the mesh close to the embryo (Figure 3.3b) and out to the cavity opening (Figure 3.3a) is unstructured, while the mesh distribution further out in the channel approaches a uniform distribution, similar to a structured mesh.



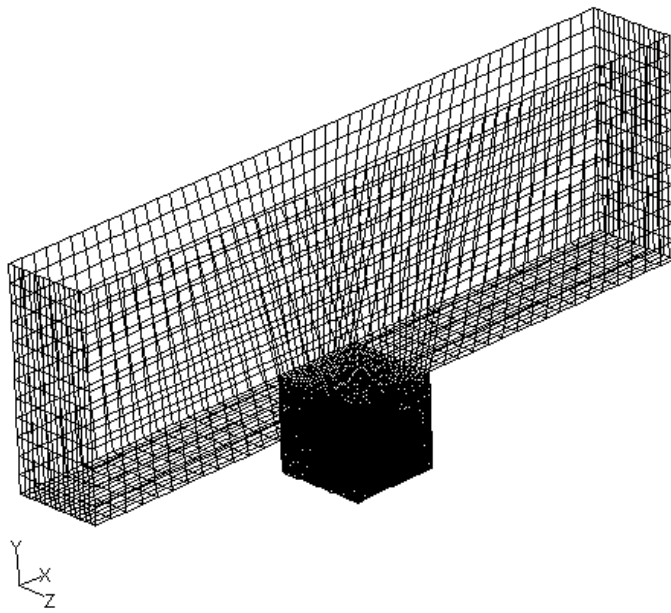
(a) Entire 2D generic grid



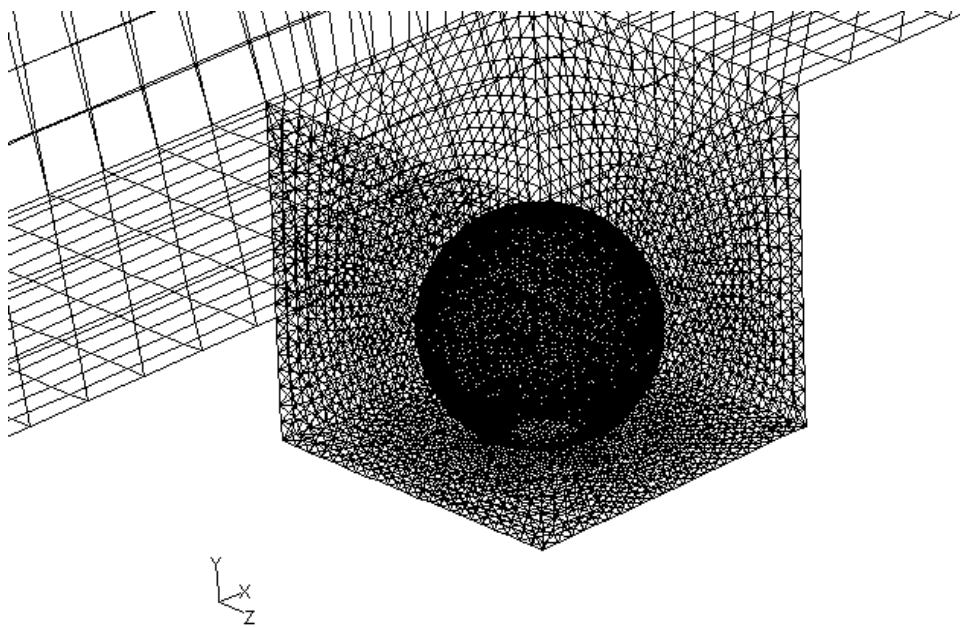
(b) Zoomed in view of the grid around the embryo

Figure 3.3: (a) The entire domain of the generic 2D computational grid showing the unstructured mesh and mesh compression applied around the fluid domain near the embryo in the cavity; (b) Zoomed in view showing the finer mesh within the cavity transitioning to a coarser mesh outside the cavity.

Alternatively, the 3D generic grid is created using two meshing schemes. The coarse mesh on the fluid domain in the channel is generated using the map meshing scheme that enforces a rectangular, structured grid with hexahedral elements as the base shape of the cells. As shown in Figure 3.4a, a fairly uniform and rectangular structured mesh is generated on the fluid domain in the channel by using this combination of the map scheme with the hexahedral elements (Gambit 2005). Such a simple mesh configuration offers the benefit of demanding lower computational resources and improved solution stability. As for the fluid domain in the cavity, the spherical embryo surface coupled with the flat surface of the cavity walls creates a complex geometry to be meshed as the interaction between the highly curved surface and the flat surface creates a situation where it is difficult to implement a structured grid. Therefore, the finer mesh of the fluid volume in the cavity is created using the geometrically versatile *TGrid* meshing scheme with the default tetrahedral/hybrid elements as the base shape for each cell (Gambit 2005). The TGrid meshing scheme creates a mesh primarily consisting of tetrahedral elements but it includes other elements such as hexahedral, wedge or pyramidal elements if it encounters a pre-meshed surface with quadrilateral elements. The strategy of “face pre-meshing” is applied here. It is the strategy of pre-meshing the surface before attempting to generate a volume mesh, similar to the “edge pre-meshing” used for the 2D mesh construction. Specifically, this is accomplished by firstly pre-meshing the surface of the channel with quadrilateral surface elements using the map meshing scheme and pre-meshing the surface of the cavity and embryo with triangular surface elements using paving scheme. Volume meshing is then accomplished using map and TGrid schemes. As can be seen from Figure 3.4a, such a strategy is able to provide a coarse, uniform and fairly structured volume mesh on the fluid domain in the channel, while a finer tetrahedral mesh results in the fluid volume within the cavity where a high density triangular surface mesh is used to discretize the surface of the spherical embryo (Figure 3.4b).



(a) Entire 3D generic grid



(b) Zoomed in view of the grid around the embryo showing only the surface meshes.

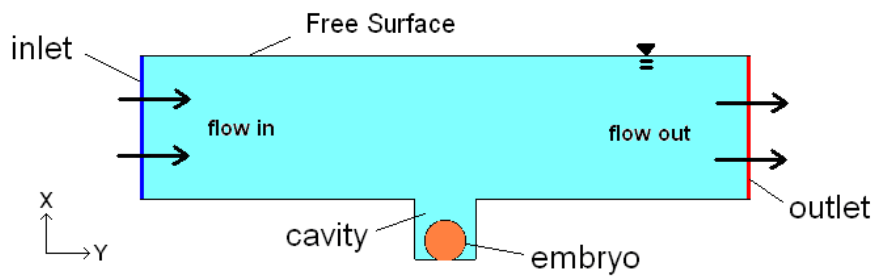
Figure 3.4: (a) Similar to the 2D grid, the entire domain of the unstructured generic 3D computational grid showing the mesh compression applied to provide a finer mesh around the fluid domain near the embryo in the cavity while maintaining a coarser mesh in the channel; (b) Zoomed in view of the grid showing the finer mesh at the fluid domain in the cavity around the embryo to capture more details of the flow and solute transport.

### 3.3.3 Boundary Conditions

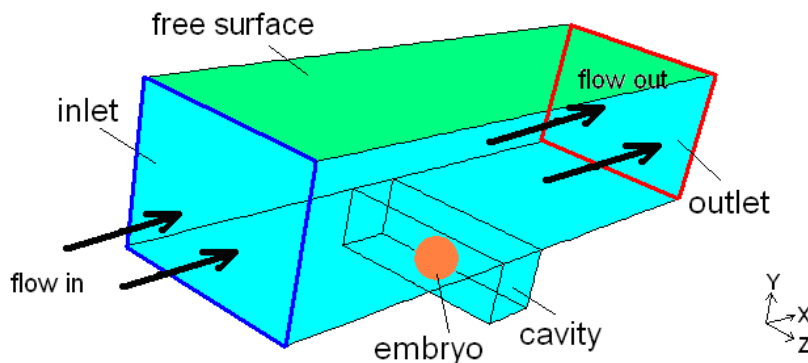
The specifications of the boundary conditions (BCs) for the 2D and 3D generic models are illustrated in Figure 3.5. They can be summarized as follows: at the entrance of the channel, a velocity inlet is implemented; at the solid bioreactor walls and embryo surface a no-slip condition is imposed; at the free surface of the fluid, a zero stress condition is applied; also at the embryo surface, solute source and sink conditions are set, expressing the solutes exchange from the embryo surface; and finally at the inlet the oxygen concentration is specified at a preset level. All these boundary conditions are defined under *Gambit* and the values for them can be readily modified using the graphical user interface of *Fluent*.

The velocity inlet BC is responsible for controlling the inflow rate of the culture medium. The inflow rate is defined by specifying the velocity and the direction of flow from the blue entrance surface (Figure 3.5). Due to the connection of the inlet surface with the free surface at the top and no-slip surface at the bottom the velocity profile across the depth of the channel bears a parabolic shape. The inflow of pre-defined oxygen content within the culture medium coming in from the channel entrance is simulated by defining a constant oxygen concentration at the entrance surface; specifically this is achieved by setting the desired mass fraction of oxygen at the entrance surface. At the other end of the channel, the outflow BC is set at the red surface (Figure 3.5). The outflow BC functions by extrapolating the information regarding the flow from within the fluid domain and updates the outflow velocity and pressure in a manner that is consistent with a fully-developed flow assumption.

The free surface of the culture medium at the top of the channel is modelled with a zero stress condition. The primary assumption of this BC is that there is negligible deformation of the surface. As discussed previously, this requires a low Froude number and neglect of surface tension effects. The surface of the embryo and the remaining surfaces of domain are set to no-slip walls. The shear stress on the walls and hence the shear stress imposed on the embryo depends solely on the velocity gradient, assuming that the fluid viscosity is constant throughout the fluid.



(a) Boundary conditions for the 2D generic model



(b) Boundary conditions for the 3D generic model

Figure 3.5: The sketch of both 2D (a) and 3D (b) models showing the position and type of the boundary conditions present.

The lactate source BC and oxygen sink BC that represent the solute exchange into and out of the embryo are defined by setting appropriate values for the source term in all source/sink volumes – the discretized small fluid volumes adjacent to the embryo surface as shown in Figure 3.6. For the lactate source, the desired values for the source is set by specifying the mass flux (in  $\text{kg}/\text{m}^3\text{s}$ ) of lactate species on all the source volumes, while for the oxygen sink, the desired values for the sink is specified by setting the negative mass flux of oxygen species at all the sink volumes. It must be noted that the solute exchange rates defined here are assumed to be independent of others variables, such as solute concentration and temperature. The main reason for this is that information on the variation of the solute exchange rate for embryos is not available. Studies on the metabolism of embryos show that a significant change to the metabolism rate only occurs after at least 1 day, for example a mouse embryo only changes its oxygen uptake rate after 18 – 24 hours, which corresponds well to the progression of the growth stages (Houghton, Thompson *et al.* 1996). Consequently, it is deduced that a constant solute exchange rate would function as a first-order

approximation to the solute exchange between embryos with their surrounding culture medium. While this is not an ideal approximation, it can be modified in future work as better models become available.

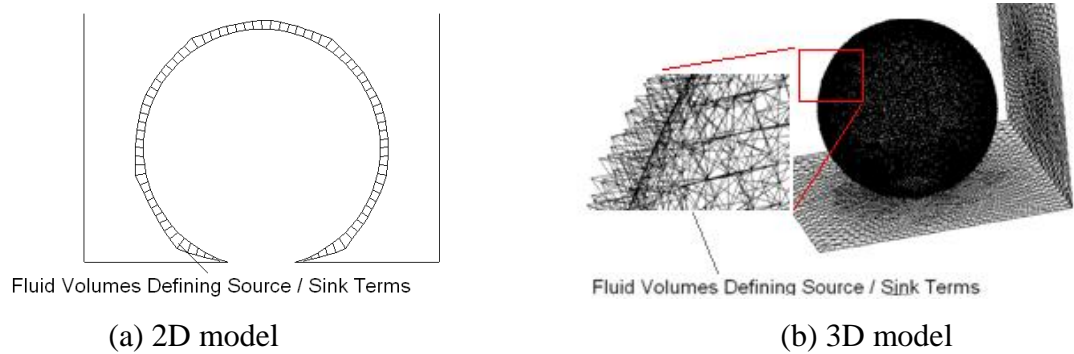


Figure 3.6: Zoomed in view showing the discretized fluid volumes adjacent to the surface of the embryo where the solute source or sink term are defined for both 2D and 3D models: (a) quadrilateral surface elements for the 2D model and (b) tetrahedral volume elements 3D model.

The default values used for the BCs and key dimensions of the bioreactor model are tabulated in Table 3.1. Here the default values refer to the BC settings that are enforced when they are not being altered for the purpose of a particular parametric study. The default length and depth of the cavity are set as 50% larger than the size of the embryo to reflect the small yet accommodating “niche environment”. The size of the embryo chosen is the average size of an embryo prior to the blastocyst stage (Thouas, G A, private communication). The default inflow rate of the culture medium is set at a value such that the flow Reynolds number in the micro-bioreactor is around 0.1, which is typical for a microfluidic system as shown in the review of microfluidic flows in the previous chapter. The default lactate production and oxygen uptake rate are set based on the average exchange rate of the respective solutes for a mouse embryo over the five growth stages (from the 1-cell stage to the blastocyst stage). The data is obtained from metabolic rate measurements for the mouse embryo by Houghton *et al.* (Houghton, Thompson *et al.* 1996). The preset oxygen concentration at the inlet reflects the 21% oxygen that is available in most culture media (Gor and Lucassen 1993; Bavister 1995; Gardner and Lane 1999).

Embryo diameter	100 $\mu\text{m}$
Cavity length x depth x width	150 x 150 x 300 $\mu\text{m}$
Culture medium inflow rate	0.001 m/s
Lactate production rate	$9.427 \times 10^{-13}$ mol/hr
Oxygen uptake rate	$2.145 \times 10^{-13}$ kg/hr
Preset oxygen concentration at inlet	$2.189 \times 10^{-4}$ mol/L

Table 3.1: Default values for the model dimensions and boundary conditions when they are not being altered by any of the parametric studies.

The properties of the culture medium utilized in the simulations are tabulated in Table 3.2. The density and viscosity of the fluid chosen are obtained from the measurement on available culture media and these values are typical for most culture media employed in existing culture practice (internal source: Thouas, G A). The diffusivity values of lactate and oxygen are acquired from measured data from Himmelblau (Himmelblau 1964), where the measured diffusivity of lactate and oxygen dissolved in salt water is used, since the culture medium is basically water with dissolved minerals essential for embryo growth (Biggers 1987; Bavister 1995). Note that due to the unavailable data on the diffusivity of lactate and oxygen *together* in the same fluid, the interaction between the diffusion of lactate and oxygen when they are present in the same fluid could not be modelled. Therefore, the simulations of lactate production and oxygen uptake are separated: when simulating the scenario of oxygen uptake, only the oxygen species are present in the simulated culture medium; when simulating the scenario of lactate production, oxygen species is not present in the simulated culture medium.

Density	1000 kg/m <sup>3</sup>
Viscosity	0.016 kg/ms
Lactate diffusivity	$1.45 \times 10^{-9}$ m <sup>2</sup> /s
Oxygen diffusivity	$3.2 \times 10^{-9}$ m <sup>2</sup> /s

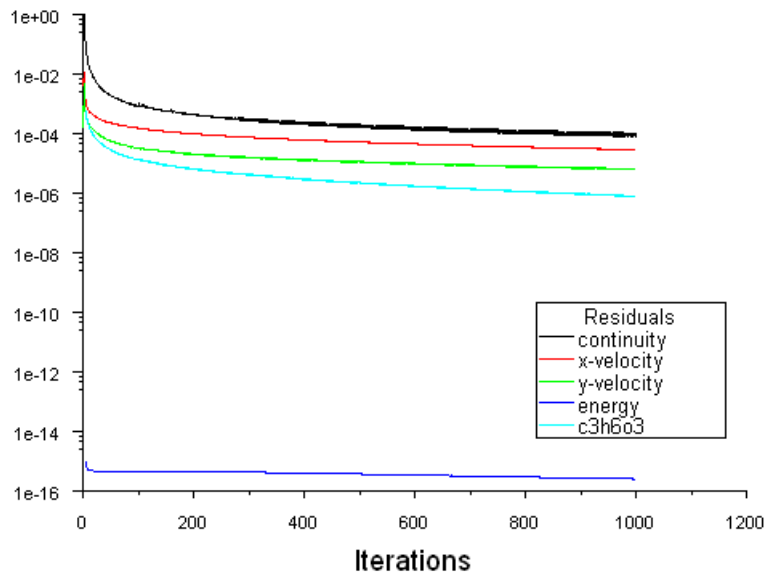
Table 3.2: Properties for the culture medium modelled in the simulations.

### 3.3.4 Convergence Criteria

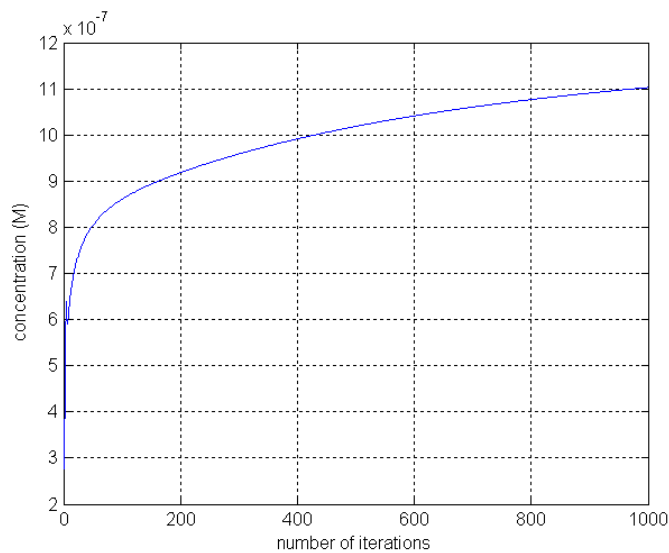
As mentioned previously, the iterative procedure used to obtain the flow solution is halted when the convergence criteria are met. The criteria which determine convergence are that the residual levels, i.e., the  $L_2$  norms of the error in satisfying the discretised equations, are all reduced to be below predefined thresholds, typically 0.001. In

addition, the averaged lactate and oxygen concentration, as well as the shear stress on the embryo surface, are monitored and convergence is assumed when the variation is less than 0.001% for at least 500 iterations.

On this point, as revealed in the simulations conducted, it is found that when deciding the solution has converged it is not sufficient that the equation residuals are below the convergence thresholds. The convergence of the variable of interest may still be comparatively large. This can be seen from the plots of the residual variations and the approach to convergence of the variable of interest (lactate concentration) in Figure 3.7. At the 1000<sup>th</sup> iteration the residuals have been reduced below the nominal convergence criteria (0.001), but it is not the case for the lactate concentration. Subsequently, it is necessary to observe the convergence behaviour on all variables of interest.



(a) Residual levels for mass, momentum and solute flux



(b) Lactate concentration

Figure 3.7: Plots showing the change in residual against the change in the resolved lactate concentration for the same number of iterations. As can be noted the residuals satisfy the convergence criteria by the 1000<sup>th</sup> iteration but this is not the case for lactate concentration.

### **3.4 Model Validations**

With the numerical model defined, the next task that needs to be performed before utilizing it to conduct studies is to validate its credibility. This validation process is divided into three tasks: grid resolution studies, validation of fluid flow modelling and justification of the solute transport modelling.

#### **3.4.1 Grid Resolution Studies**

Theoretically, as the grid cell size becomes smaller, the solution provided by the model should approach the analytical solution, termed the grid-independent solution. However, more cells imply a higher computational cost (computing time and storage) is required to model the flow. Subsequently, grid resolution studies are necessary to determine the optimum grid size for discretizing the fluid domain. Here, optimum means a grid size which allows the model to sufficiently resolve the flow, yet it does not require an unreasonable amount of computational resources.

The procedures for performing the grid resolution study are summarized below:

1. A reference grid is constructed. The resolution of this grid is characterized by the cell size on the embryo surface.
2. The grid resolution indicator is selected. Typically this indicator changes as the characteristic grid resolution is changed.
3. A few models are generated with a different grid sizes and simulations are conducted to determine how the change on the characteristic grid size affects the selected flow indicator. The grids are selected to keep the same relative grid point distribution between the different parts of the domain for the different grids, so that Richardson extrapolation is possible in the step below. The relationship between the grid size and the grid resolution indicator is plotted.
4. Using Richardson's extrapolation (Richardson 1910), the grid independent solution is obtained by extrapolating the solution to zero cell size.
5. With the grid independent solution obtained and the relationship showing the change of grid size with the indicator, the optimum grid size is decided considering the available computational resources and the acceptable accuracy for the numerical modelling.

The following two sub sections discuss the processes used to obtain the optimum grid size for both the 2D and 3D models, and the final selected grid sizes for each. The characteristic cell size here refers to the distance between the two nodes that form the discretized surface or volume, as illustrated in Figure 3.8 below.

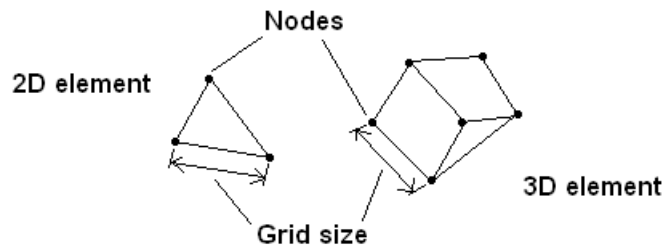


Figure 3.8: Sketches showing the difference between the 2D and 3D elements and the definition of characteristic cell size.

### 3.4.1.1 2D Grid Resolution Study

For the 2D model, the embryo surface cell size is selected as the characteristic cell size. This cell size is kept as constant as possible within the cavity, given the limitations of the paving meshing algorithm. Outside the cavity in the channel the base cell size is set to a value that is 3 times larger than inside the cavity. Averaged lactate concentration on embryo surface is chosen as the convergence indicator. For the resolution study, the cell size is decreased from 40  $\mu\text{m}$  to 0.5  $\mu\text{m}$ . The outcomes are shown in Table 3.3 and the relationship between the grid resolution and lactate concentration is plotted in Figure 3.9. It is observed that as the cell size is reduced, the lactate concentration approaches a constant value. By fitting a second-order polynomial to the data, the y-intercept is found to be  $5.18 \times 10^{-5}$  M. This is the extrapolated grid independent value.

As the resolution was increased, the time taken for the solution to reach convergence increased substantially. As seen from the table when the cell size is reduced below 1  $\mu\text{m}$  the required number of iterations increases dramatically: at grid size of 2.5  $\mu\text{m}$  the required number of iterations is 7000, while for a cell size of 1  $\mu\text{m}$  the required number of iterations is 38000. Increasing the resolution by 2.5 times increases the number of iterations 5-fold. Moreover, if the cell size is reduced to 0.5  $\mu\text{m}$ , the required number of iterations is 121000, which translates to an increase of 17-fold. In addition, the time per iteration increases as the square of the spatial resolution. Subsequently, to ensure that

the solution time remains reasonable while maintaining acceptable accuracy, a grid size which resolves solution to within 3% of the estimated “true” solution is selected as the grid size for subsequent simulations. This grid had a characteristic cell size of 3.5554  $\mu\text{m}$ .

Characteristic grid size	Total no. of elements in model	Embryo surface lactate concentration	No. of iterations till convergence
$\mu\text{m}$		M	
40.0	227	2.9999E-05	1000
20.0	799	4.2575E-05	1000
10.0	3168	4.6475E-05	1000
5.0	12578	4.9832E-05	4000
2.5	50310	5.0740E-05	7000
1.0	314653	5.1385E-05	38000
0.5	1258424	5.1719E-05	121000

Table 3.3: The outcomes of the grid resolution study for 2D generic model.

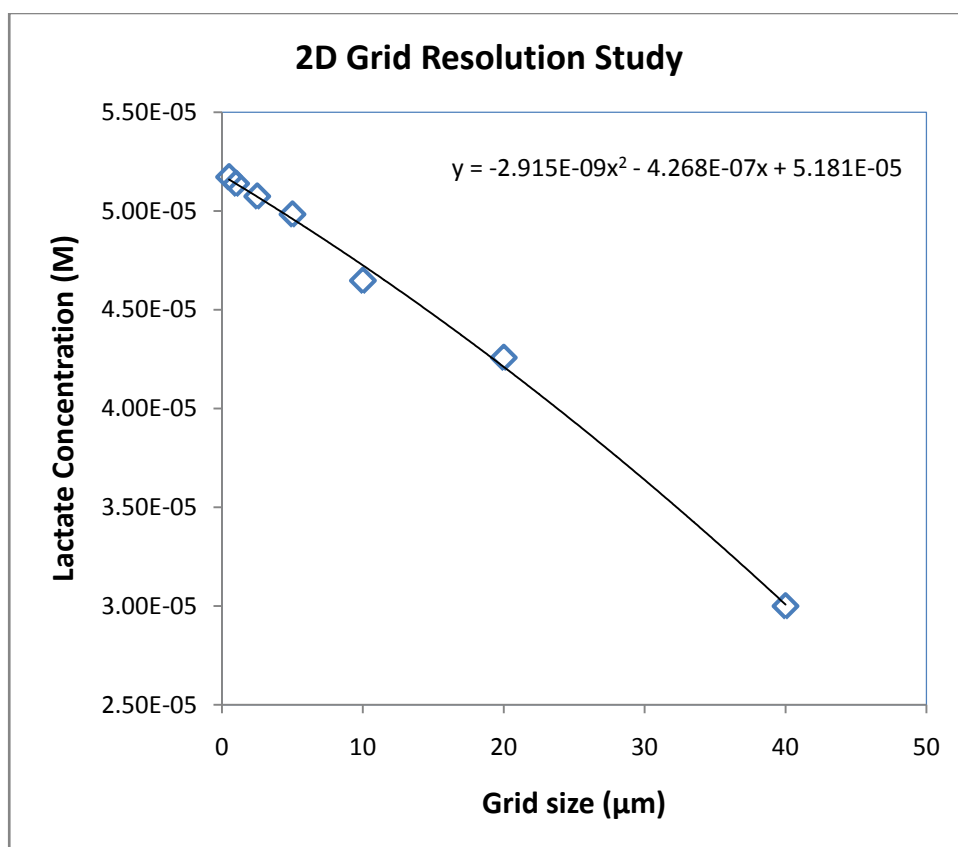
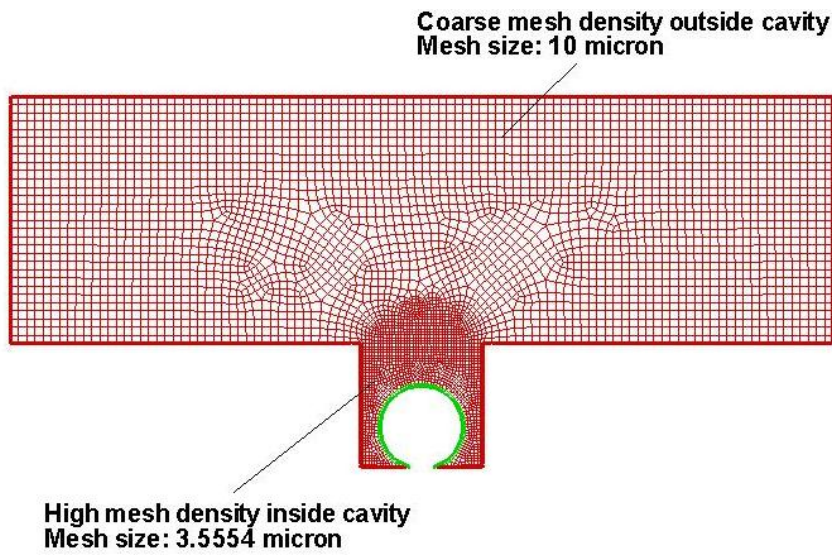


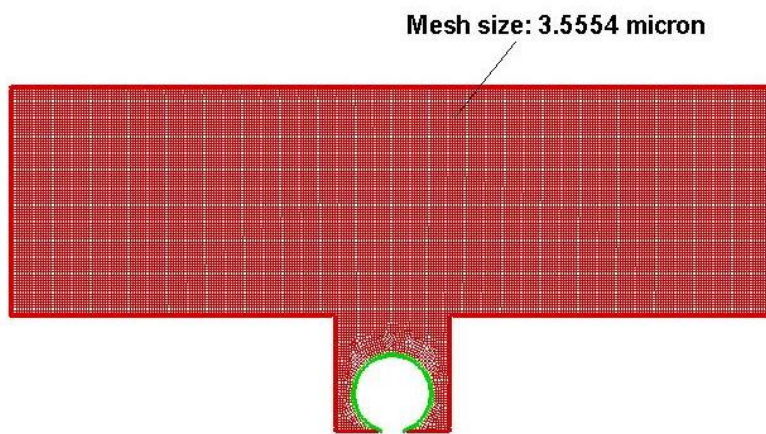
Figure 3.9: Change of lactate concentration on the embryo surface with respect to the characteristic grid size.

To improve the computational efficiency, the meshing of the entire domain is prepared such that the mesh density further away from the cavity is less dense than the mesh density inside the cavity. The reason for this is because further away from the cavity less mesh resolution is required to properly resolve the flow. To determine if such a mesh density distribution would compromise the accuracy of the solution, the solution on the optimized grid (Figure 3.10a) is compared with that on a uniform grid with the same fine grid resolution throughout the fluid domain (Figure 3.10b). The uniform mesh has a mesh size of 3.5554  $\mu\text{m}$  specified for the entire domain, while the optimized mesh has mesh size of 3.5554  $\mu\text{m}$  inside the cavity and a larger mesh size of 10  $\mu\text{m}$ , which is 3 times larger, outside the cavity along the channel. Simulations are then conducted and the calculated lactate concentrations of the embryo surface from both grids are compared.

From the simulations, the measured lactate concentration for the optimized grid is  $5.428 \times 10^{-5}$  M, while for the uniform grid it is  $5.438 \times 10^{-5}$  M. This translates to a discrepancy of 0.17 % between the two mesh configurations, which is very small. In addition, it can be seen on Figure 3.11, that there is no discernable difference in the lactate concentration distribution between the optimized grid and the uniform grid, even at the cavity opening (Figure 3.11b). Hence, it is deduced that the *optimized* mesh adequately resolves the flow over the entire domain. This mesh is used for the 2D models for the rest of the investigations.



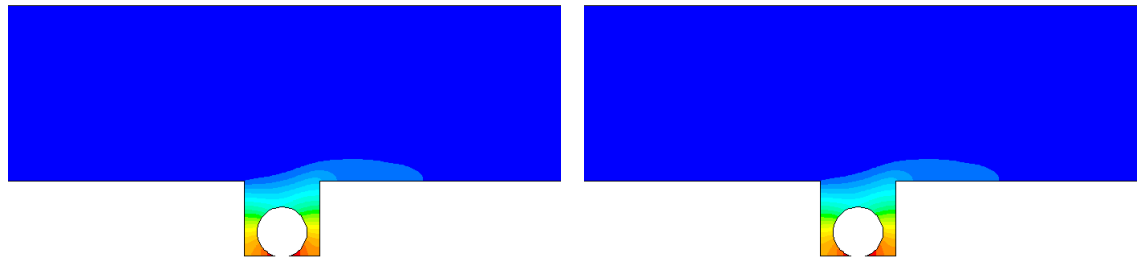
(a) Optimized grid



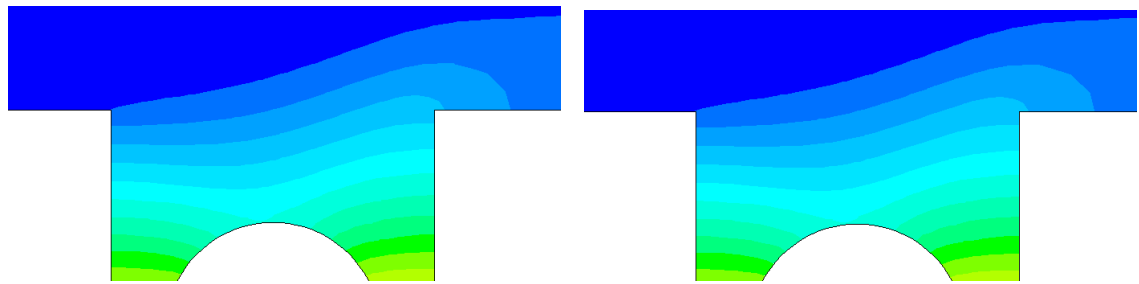
Uniform mesh density throughout entire mesh

(b) Uniform grid

Figure 3.10: The (a) optimized and (b) uniform grid for the 2D generic model.



(a) Contour of lactate concentration between the optimized grid (left) and uniform grid (right)



(b) Zoomed in view of the concentration contour near the cavity opening

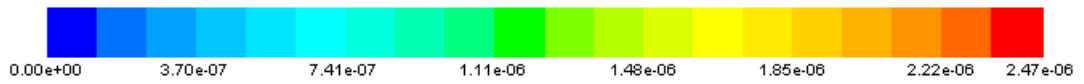


Figure 3.11: (a) Contour plots of lactate concentration (measured in M) in the flow for both the optimized grid (left) and uniform grid (right); (b) Zoomed in view on the cavity opening.

### 3.4.1.2 3D Grid Resolution Study

A similar grid resolution study was carried out for the 3D generic model. Again, the cell size at the embryo surface is selected as the characteristic size and this time the averaged oxygen concentration on the embryo surface is chosen as the resolution indicator. Similar to the optimized grid of the 2D generic model, mesh compression is applied to obtain a finer mesh over volume in the cavity. The grid resolution is 3 times larger than that of the discretized fluid volume in the channel. The characteristic cell size is varied from 2.5  $\mu\text{m}$  to 20  $\mu\text{m}$ , as tabulated in Table 3.4, and four simulations are conducted to evaluate how the oxygen concentration at the embryo surface changes with grid size. It must be noted that due to significant higher computational expense of the 3D simulations (for 3D simulations, solving 5 iterations requires 60 s, as opposed to 2D simulations solving 5 iterations requires 2 s), only four grid sizes were used for the study.

Grid size $\mu\text{m}$	Total no. of elements in the model	Embryo surface oxygen concentration M	No. of iterations till convergence
20	7843	2.1603E-04	174
10	56642	2.1591E-04	505
5	409369	2.1587E-04	1343
2.5	3200355	2.1585E-04	3844

Table: 3.4: The outcomes from the 3D grid resolution study.

The outcome of the resolution study is plotted in Figure 3.12. As can be seen, the oxygen concentration varies smoothly with grid size. By fitting a second order polynomial curve to the data, it is deduced that the grid-independent solution is  $2.158 \times 10^{-4}$  M. Also, as can be seen on Table 3.4, as the grid cell size decreased from 20  $\mu\text{m}$  to 2.5  $\mu\text{m}$ , the total number of elements of the entire model increases 400-fold from 7843 cells to 3.2 million cells, and correspondingly the number of iterations until convergence increases dramatically as well. Subsequently, after considering the available computational capacity and time constraints, the optimum grid size is selected to be 10  $\mu\text{m}$  where this will provide a solution that only deviates 0.035% from the grid independent solution. This is felt to be entirely satisfactory accuracy for the 3D parametric studies. Note, the large number of iterations required for convergence in the

fine grid cases, even though this is effectively a linear problem at these low Reynolds numbers.

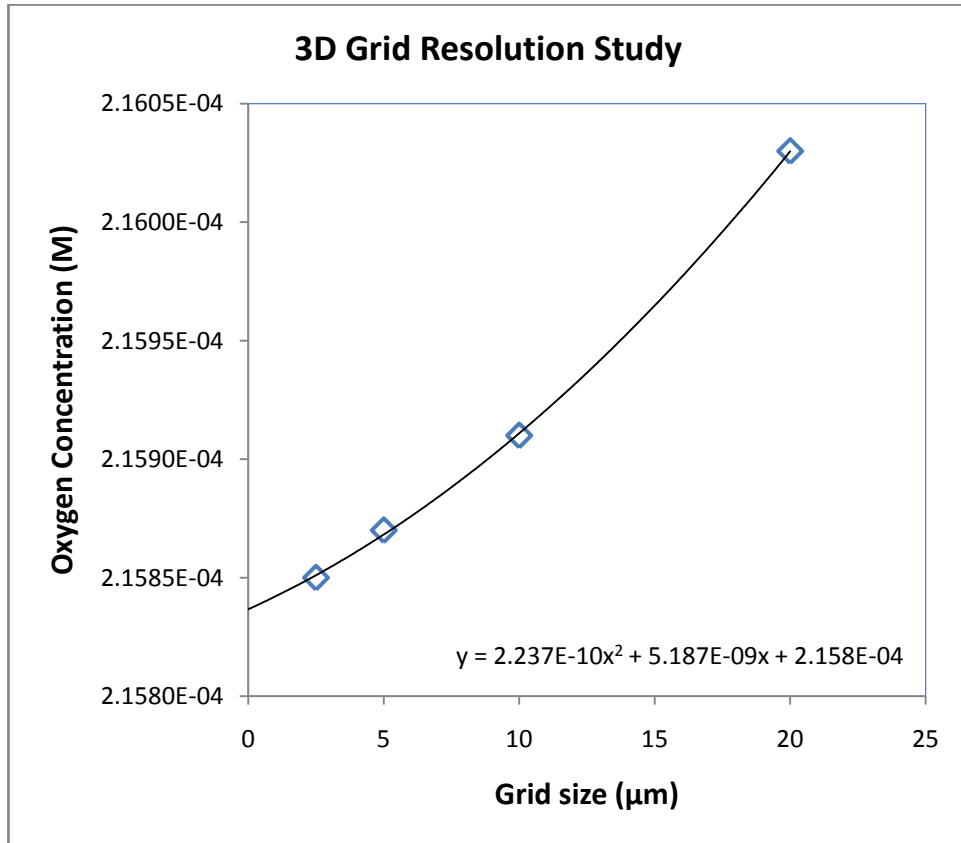


Figure 3.12: Change of oxygen concentration on the embryo surface with respect to the characteristic grid size.

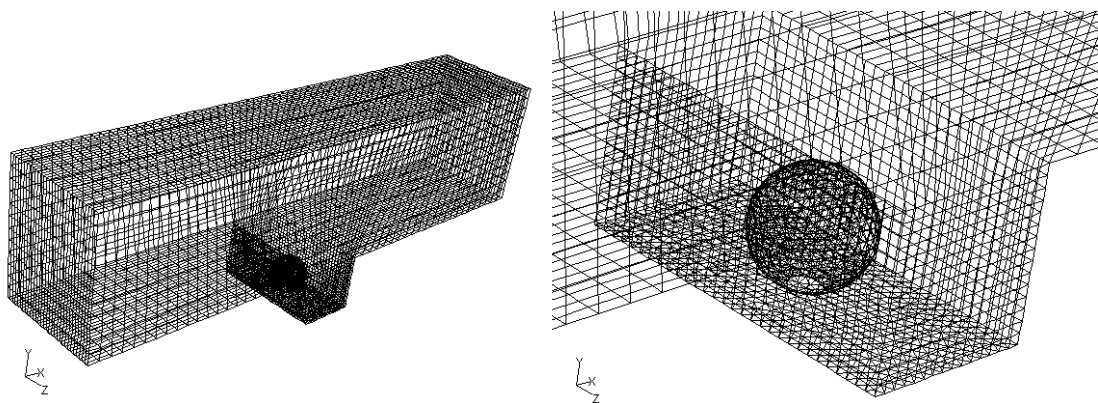


Figure 3.13: The overall (left) and zoomed in view (b) of the 3D generic grid. Only surface meshes are shown.

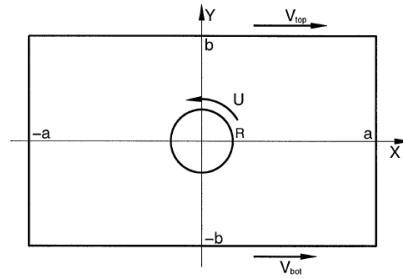
### **3.4.2 Validation of Fluid Flow Modelling**

With satisfactory grid sizes for both 2D and 3D models decided, the next task is to validate the predictive capability of the model against other work from the literature. In particular, this validation step provides confidence that the models have been implemented correctly within the framework provided by the software and that the software can make useful predictions for this problem.

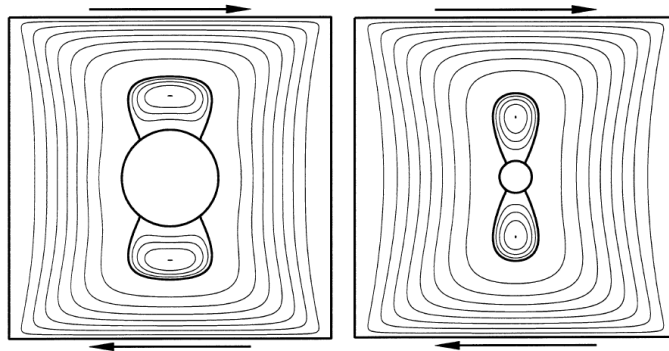
#### **3.4.2.1 Model Validation on 2D Model**

The numerical investigation by Galaktionov *et al.* on the Stokes flow in a rectangular cavity containing a cylinder (Galaktionov, Meleshko *et al.* 1999) was chosen as appropriate for validating the 2D model, since the flow problems are quite similar. By reproducing their work, the capability of the 2D model in predicting the flow structure and due to the presence of a cylinder inside the cavity can be assessed.

The details of the numerical setup are given in Galaktionov *et al.* (Galaktionov, Meleshko *et al.* 1999). In brief, the study aimed to predict the 2D creeping flow of an incompressible viscous fluid in a lid-driven cavity with a cylinder inside (Figure 3.14a). The top and bottom plate of the cavity are driven to induce flow inside the cavity and a cylinder is situated at the middle of this cavity. Various parameters, such as the dimensions of the cavity and cylinder, cylinder rotation rate and cavity surface translation rate were varied, and the flow structure changes in response to varying these parameters were qualitatively analysed in the form of streamfunction plots.



(a) Problem definition



(b) Square cavity with static cylinder

Figure 3.14: The problem definition for the cavity flow study by Galaktionov *et al.*; (b) Two particular case studies selected for the validation study (Galaktionov, Meleshko *et al.* 1999).

Two particular cases were selected to simulate using a similar local grid structure of the 2D model developed for the micro-bioreactor. The two cases are: dual lid-driven square cavity flow with two different cylinder sizes, one with normalized radius of  $R_0 = 0.3$ , the other with  $R_0 = 0.1$ . The two lids are driven at the same rate but in the opposite direction as shown in Figure 3.14b. The dimensions of the cavity, lid translation velocity, fluid density and viscosity are set, such that it results a flow with  $Re = 0.01$ , corresponding to the typical condition experienced in a Stokes flow. These exact conditions for the flows as portrayed in Figure 3.14b are reproduced using the 2D numerical model for the micro-bioreactor.

The resolved streamfunctions for both cases are plotted and compared with the outcomes by Galaktionov, as shown in Figure 3.15. As can be seen from the plots, majority of the streamlines predicted by the 2D model matched well with the outcomes from Galaktionov. For both cases with large and small cylinders, all the main flow features such as the outer large streamlines and the two smaller streamlines near the

cylinder were successfully predicted by the 2D model (Figure 3.15a and 3.15b). The size of these streamfunction profiles predicted by the 2D model matched well with the prediction by Galaktionov. Subsequently, it can be said that the 2D model for the micro-bioreactor is validated where it is convinced that the model can simulate the anticipated flow field that will be encountered in the cavity.

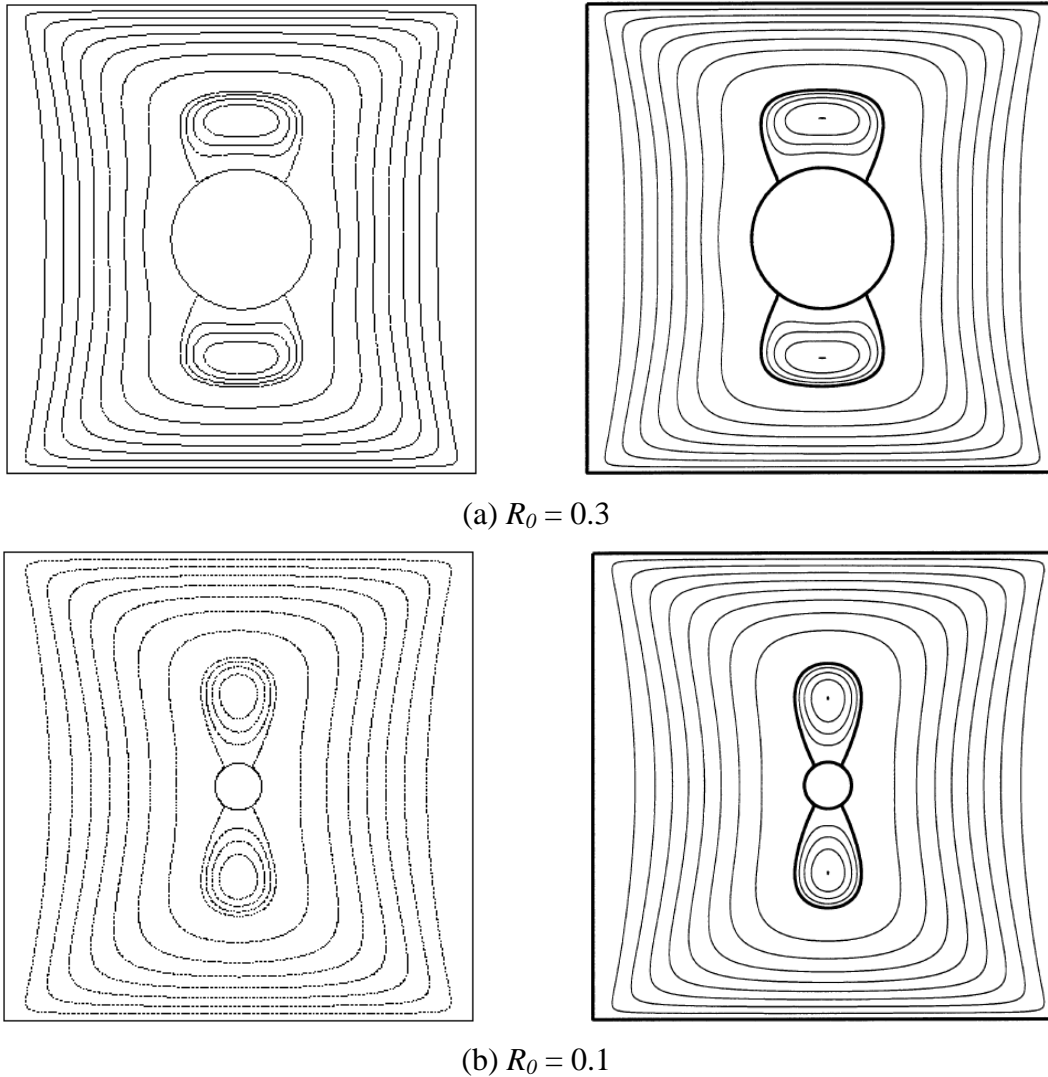


Figure 3.15: Streamfunction plots for both cases of (a)  $R_0 = 0.3$  and (b)  $R_0 = 0.1$  predicted by the 2D model (left) compared with the respective streamfunction plots from Galaktionov (right).

### 3.4.2.2 Model Validation on 3D Model

Another validation study was also undertaken using a 3D test case: the numerical study of Chiang *et al.* in modelling the flow in a 3D lid-driven cavity (Chiang, Sheu *et al.* 1998). It must be noted that, originally, it was intended to find a case study with a cavity geometry with a body inside, because of the similarity to the current problem. However, a suitable test case could not be found and the cavity flow problem seemed reasonably appropriate.

In brief, the numerical study carried out by Chiang *et al.* plans to investigate the effect of increasing the flow  $Re$  has on the flow in a cavity, where they aimed to find out the critical  $Re$  that cause instabilities to start occurs and the evolution of the flow recirculation in the cavity as  $Re$  is varied. In their study they employed a finite volume based incompressible flow model to numerically simulate the flow inside a lid-driven cavity, and have conducted both steady and unsteady simulations to model the flow from  $Re = 10$  to  $Re = 3200$ . In regards to the validation study, only the two cases of steady-state low  $Re$  lid-driven cavity flow is selected for simulation using the 3D model. The validation of the 3D model starts with constructing the flow model as indicated in Chiang's paper (Figure 3.16). A rectangular box with span to width ratio of 3:1 and depth to width ratio of 1:1 is constructed to represent the lid-driven cavity. The 3D cavity measured 3m by 1m by 1m. Non-uniform grid spacing of 34 x 91 x 34 resolution (higher grid density at cavity corner) was employed, following the exact meshing specification from the paper. For the purpose of validating the 3D model, two steady simulations were conducted at the two low Reynolds number condition of  $Re = 10$  and 100. The top wall is set to translate while the rest of the walls are defined as the stationary, no-slip walls.

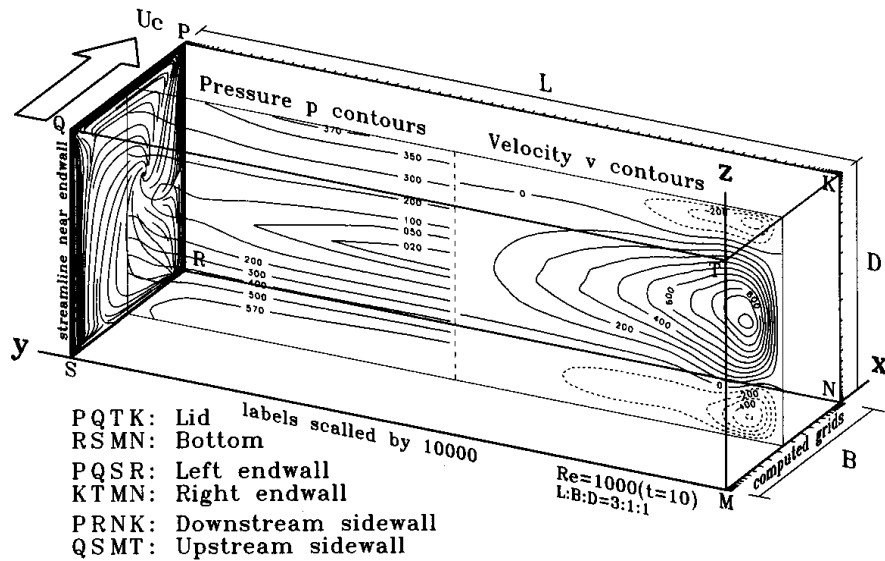
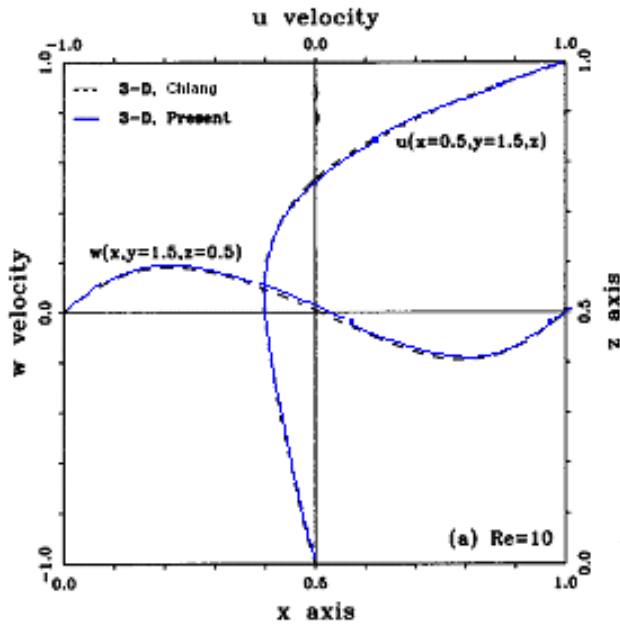
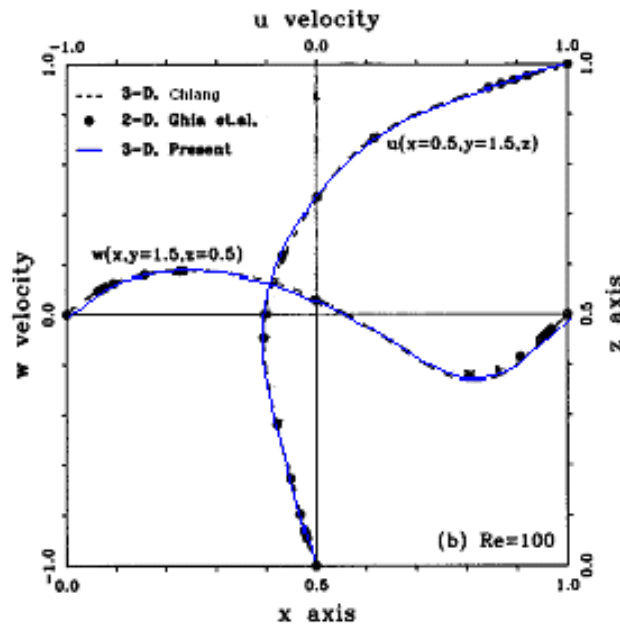


Figure 3.16: Illustration of the 3D lid-driven cavity investigated, together with a cross section view at the middle of the cavity showing the pressure and velocity contour and streamline plots at the right wall (Chiang, Sheu *et al.* 1998).

The flow predicted by the 3D model is compared with the outcomes from Chiang’s paper by looking at the velocity profiles at the mid cavity horizontal ( $x = 0.5$ ) and vertical ( $z = 0.5$ ) plane as well as the streamlines at the cross section face at  $y = 2.5$ . As can be seen on Figure 3.17, velocity profiles along the center line ( $x = 0.5, z = 0.5$ ) from the simulation coincide well with Chiang’s results as can be seen by the blue line that adheres well to the dotted data points for both  $Re = 10$  and  $Re = 100$ . Also can be seen on Figure 3.18 the streamlines predicted by the 3D model matches well with the outcomes from Chiang *et al.* where  $Re = 10$ , the core of the flow circulation is found to be located near the moving lid while for  $Re = 100$ , this core is found to be siding to the right side; both locations of the core predicted matches well with Chiang’s results. It must be noted that due to the 3D presentation approach undertaken by *Fluent* it is found that the streamlines across the span of the cavity (through the page) are overlapped onto the 2D projection plane, therefore it is not surprising that there are some “peculiar” streaks occur across the cavity (Figure 3.18b, bottom). Nevertheless, overall it can be said that good comparisons of results were found between present simulations and Chiang’s numerical works. All in all, it can be deduced that the 3D model for the micro-bioreactor is validated where it is convinced that the model can simulate the anticipated flow field that will be encountered in the cavity.

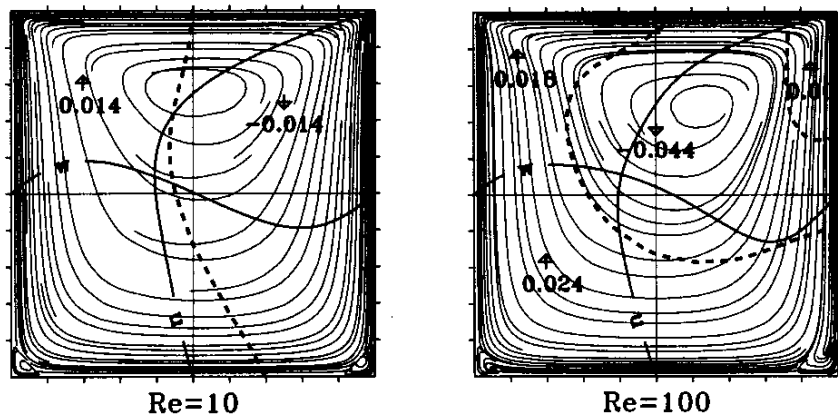


(a)  $Re = 10$

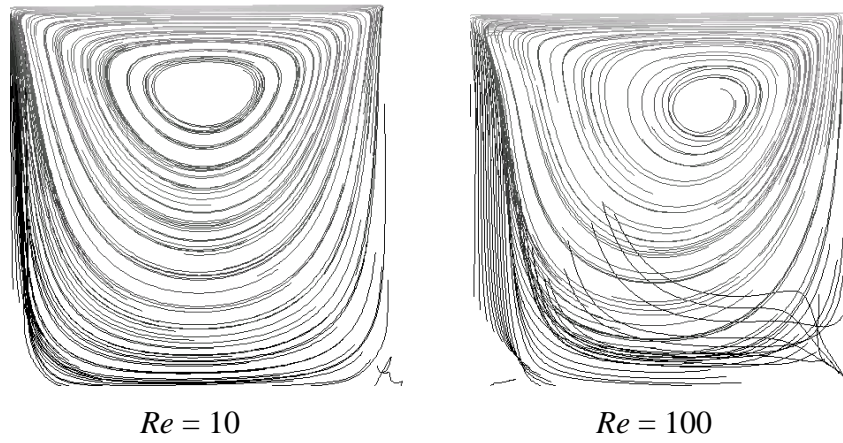


(b)  $Re = 100$

Figure 3.17: Comparison between Chiang et al, Ghia et al and present simulations for  $x$ -velocity and  $z$ -velocity along the lines of  $x = 0.5$  and  $z = 0.5$  in the middle of the cavity (Chiang, Sheu *et al.* 1998). The blue line represent the results evaluated by the 3D model, the dotted lines is the results from Chiang *et al.*



(a) Outcomes from Chiang *et al.* (Chiang, Sheu *et al.* 1998)



(b) Results predicted using 3D model

Figure 3.18: Comparison of streamline at cross section plane at  $y = 2.5$  between Chiang *et al* and present simulation: (a) Results from Chiang *et al* simulations; (b) Results predicted using 3D model.

### 3.4.3 Validation of Solute Transport Modelling

Similar to the validation of fluid flow modelling, the justification of solute transport modelling is carried out to ascertain the capability of the numerical model in simulating solute transport accurately. In particular, the validation study aims to find out how well the micro-bioreactor numerical model simulates the distribution and the exchange of solutes in the micro-bioreactor. Basically, the validation process is about reproducing the similar study by previous researcher in examining solute transport in fluid flow, comparing the outcomes with the published results and assessing the capability of the model from there. It must be noted that due to the shortage of studies on solute transport modelling in 3D, the validation study conducted here only focus on the 2D model and it is assumed the solute transport capability of the 3D model will mainly be similar to the 2D model. The validity of the solute transport modelling of the 3D model is to be examined once there is available experimental or other numerical data to perform the validation study.

The numerical study conducted by Horner *et al.* in examining the oxygen and lactate transport in a grooved perfusion flat-bed bioreactor (Horner, Miller *et al.* 1998) is chosen for this validation study. The main reason that for this selection is that the geometry and functional aspects of the bioreactor studied by Horner *et al.* is very similar to the structure of the micro-bioreactor: it consists of a channel which allow fluid perfusion to occur and cavity is located at the bottom surface of the channel which house the subject to be grown. In their study, Horner *et al.* examined how the change on culture condition would and operating parameters of the bioreactor influences the solute transport into and out of the hematopoietic cells. Specifically, they modelled the oxygen uptake and lactate production (as a form of metabolic waste production) of the hematopoietic cells using a finite-element solver (*FIDAP*) on the grooved perfusion bioreactor and non-grooved bioreactor, which is essentially a microchannel with a flat surface. The hematopoietic cells are seeded at the bottom surface of the non-grooved bioreactor and seeded in the groove of the grooved bioreactor, as shown in Figure 3.19. For the purpose of the validating the solute transport modelling, it would be ideal to reproduce some part of their study using the numerical model of the micro-bioreactor and compared the modelling outcomes with Horner's work, so to assess how well it handle the simulations on oxygen uptake and lactate production.

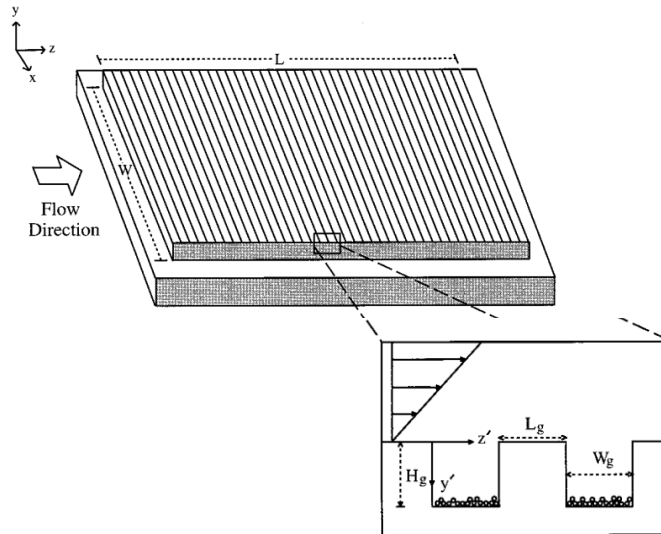


Figure 3.19: Illustration of the grooved perfusion flat-bed bioreactor examine by Horner *et al.* (Horner, Miller *et al.* 1998).

A few simulations were conducted to reproduce the similar results published by Horner *et al.* They include:

- Oxygen transport in grooved and non-grooved bioreactor under different uptake rates with 20% inlet oxygen content at culture medium flow rate of 2.5 mL/min
- Lactate transport in grooved and non-grooved bioreactor under different production rates at culture medium flow rate of 2.5 mL/min

The details on the simulation setups and dimensions of the grooved and non-grooved bioreactor are summarized in Table 3.5 where they follows the relevant details from Horner's paper (Horner, Miller *et al.* 1998). Note that the rate of solute transport, the oxygen uptake and lactate production in Horner's simulations are assumed to be independent of others variables such as solute concentration and temperature, which is the same to the solute transport modelling of the micro-bioreactor.

<b>Model</b>	
Dimension	2D
Viscous	Laminar
Species model	Non-volumetric reaction
	Inlet diffusion enabled
	Energy diffusion enabled
Discretisation	2 <sup>nd</sup> order for all
<b>Fluid Properties</b>	
Species	Medium (H <sub>2</sub> O-liquid), oxygen (liquid) or lactate
Density evaluation	Volume-weighted mixing law
Viscosity evaluation	Constant
Mass-diffusivity evaluation	Constant dilute approximation
<b>Boundary Conditions</b>	
Inlet	Velocity inlet
Outlet	Outflow
Top wall, groove, bottom wall	Stationary wall
Species uptake or production	Fluid source (+ value) or sink (- value)

Table 3.5: Summary on the *Fluent* setup on model, fluid properties and boundary conditions for the solute transport modelling validation study.

As can be seen from Figure 3.20 and Figure 3.21 respectively which plot the oxygen concentration and lactate concentration trend change along the length of the grooved and non-groove bioreactor (the oxygen and lactate concentration here refers to the concentration on the seeded cell on the bioreactor surface), the trend changes for predicted by the numerical model coincide well with the results by Horner *et al.* The discrepancies between them, in comparing the concentration values at 6 cm, are at most 0.25% (for the grooved bioreactor at oxygen uptake rate of 2.0  $\mu\text{mol/hr}$ ) for oxygen transport and at most 0.40% (for the grooved bioreactor at lactate production rate of 6.0  $\mu\text{mol / hr}$ ) for lactate transport. Such a small discrepancies between the outcomes predicted by current model with Horner's results instils a large confidence on the current model to model the solute transport in the micro-bioreactor accurately.

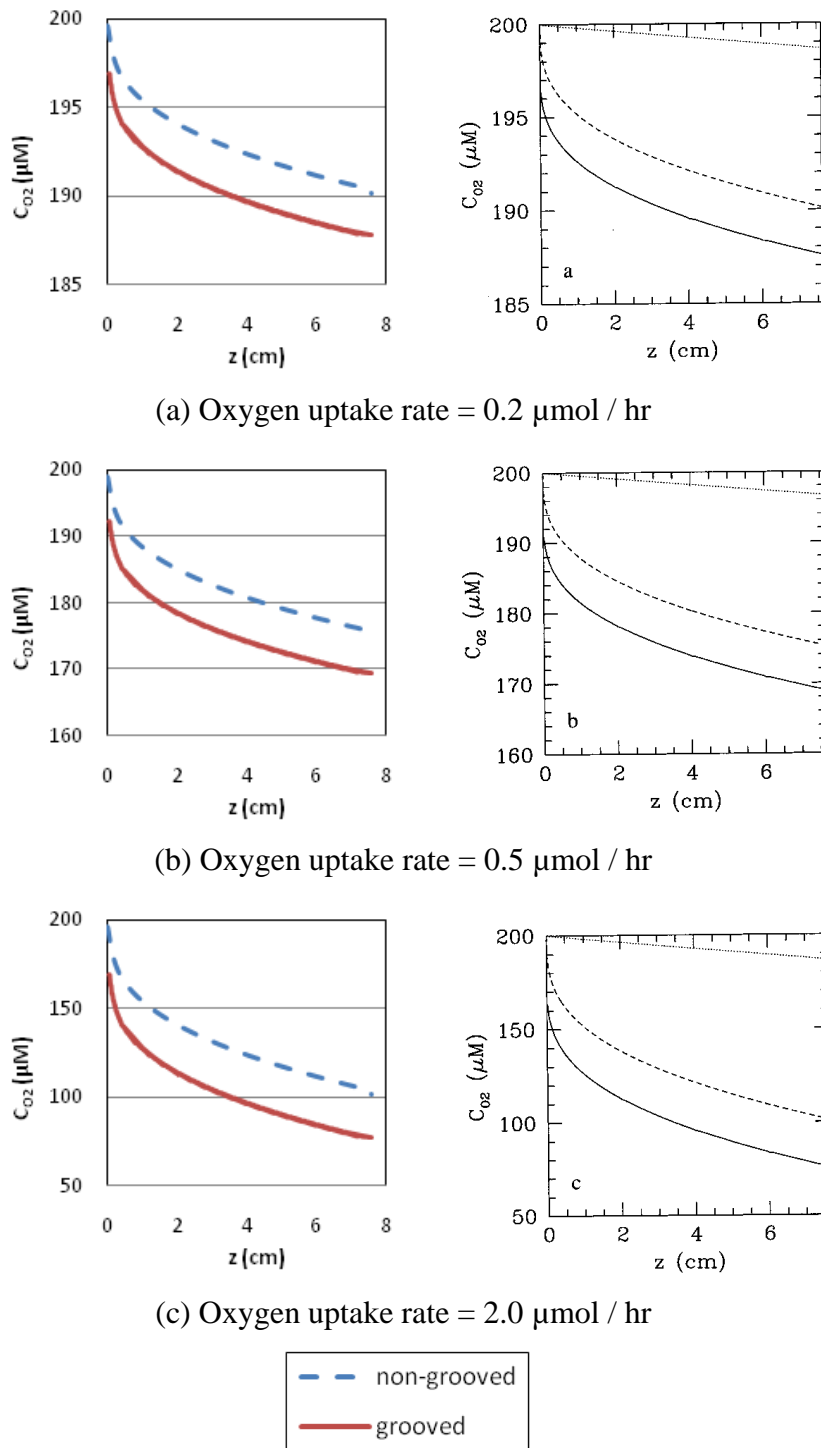
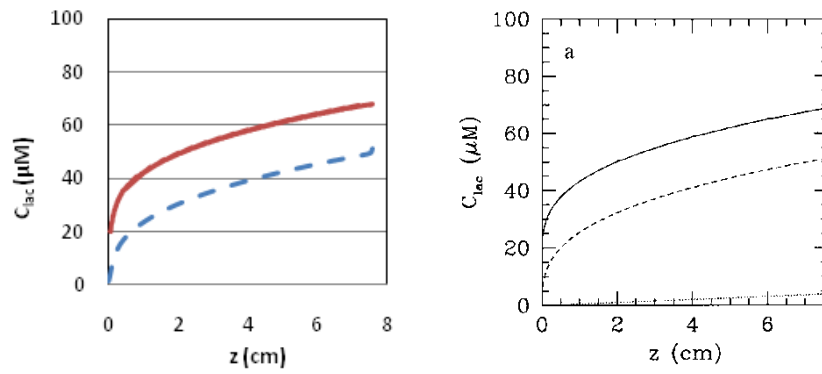
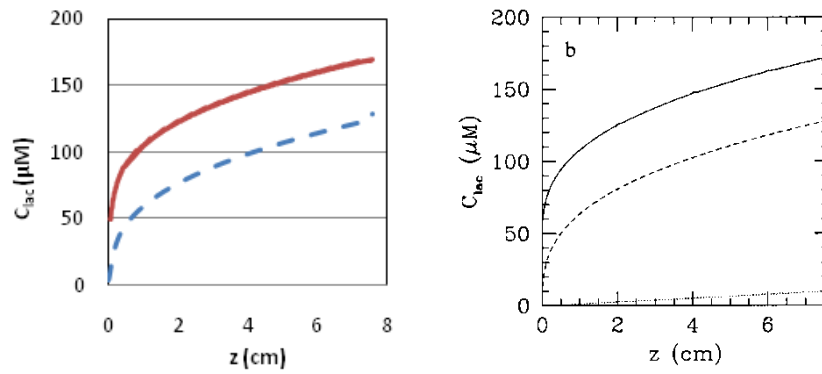


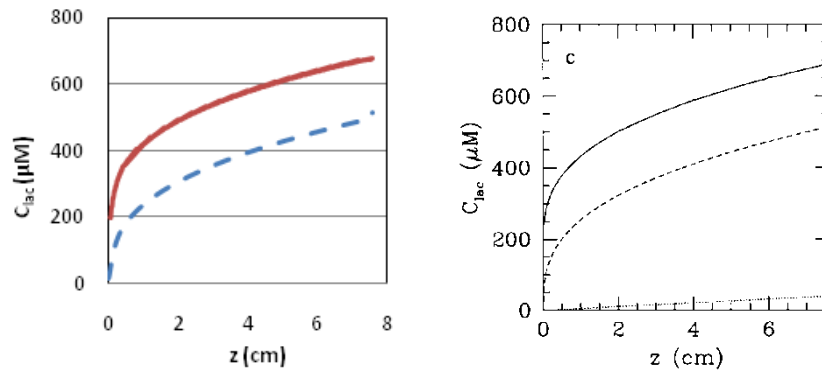
Figure 3.20: Oxygen concentration (with 20% inlet oxygen) comparison between grooved (solid line) and non-grooved (dashed line) at different uptake rates ranging from (a) small uptake rate of  $0.2 \mu\text{mol/hr}$  to (c) large uptake rate of  $2 \mu\text{mol/hr}$ ; (left) outcomes predicted by current model; (right) Horner's results.



(a) Lactate production rate =  $0.6 \mu\text{mol} / \text{hr}$



(b) Lactate production rate =  $1.5 \mu\text{mol} / \text{hr}$



(c) Lactate production rate =  $6.0 \mu\text{mol} / \text{hr}$

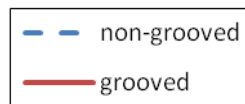
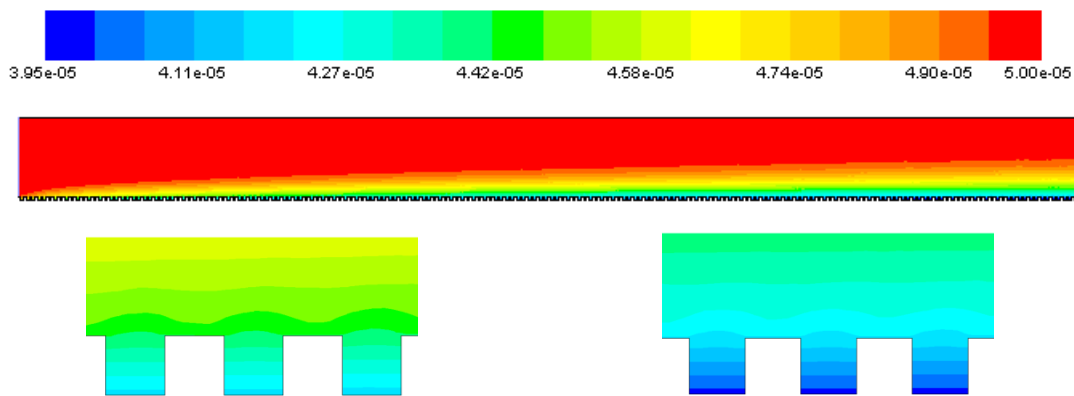


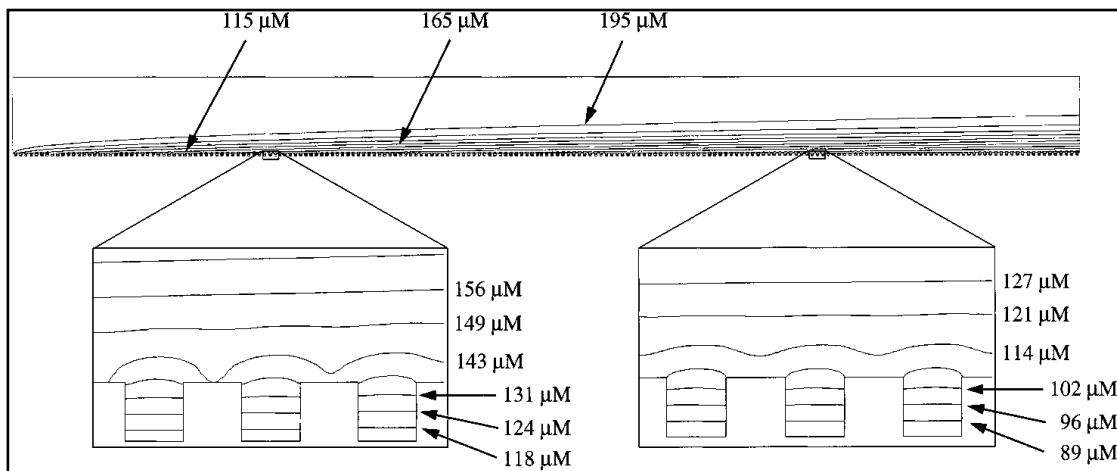
Figure 3.21: Lactate concentration comparison between grooved (solid line) and non-grooved (dashed line) at different uptake rates ranging from (a) small production rate of  $0.6 \mu\text{mol/hr}$  to (c) large production rate of  $6 \mu\text{mol/hr}$ ; (left) outcomes predicted by current model; (right) Horner's results.

The comparison of the contour plots of oxygen and lactate as shown in Figure 3.22 and Figure 3.23 respectively also revealed the same finding where the oxygen and lactate

distribution for the entire grooved bioreactor evaluated using current model are similar to the respective concentration contour plots by Horner *et al.* The solute distributions in the within the grooves, as depicted in the inserts, also revealed the same finding. Therefore, with such good agreement between them, it can be said that the solute transport modelling of the numerical model to simulate the micro-bioreactor has been validated.

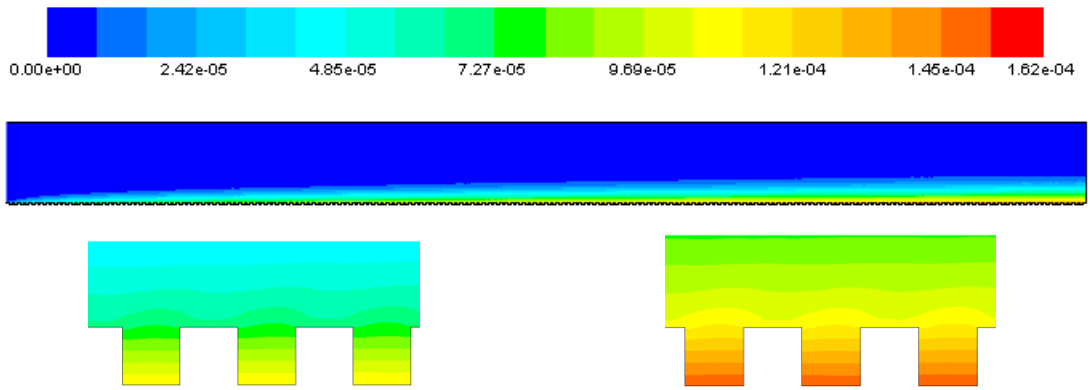


(a) Oxygen concentration contour predicted by current model

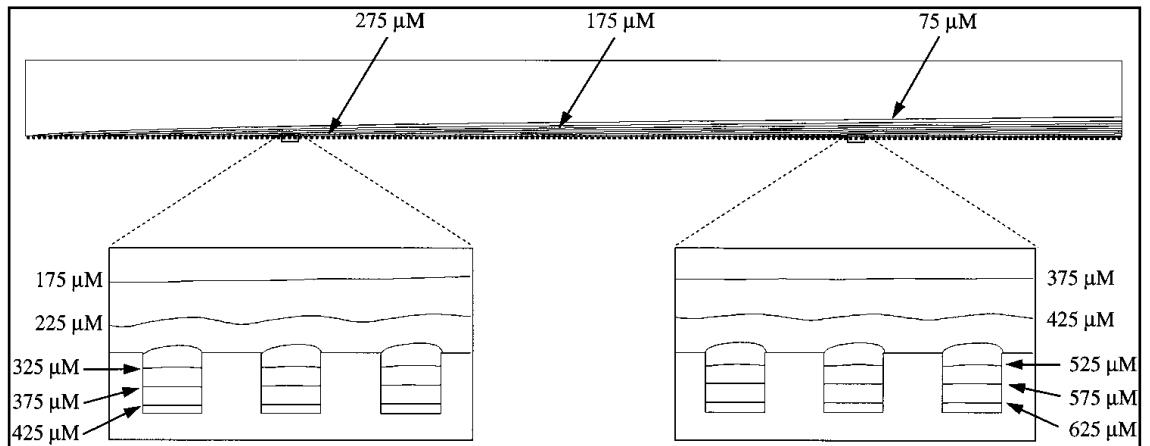


(b) Oxygen concentration contour by Horner *et al.*

Figure 3.22: Contour plot comparison for oxygen concentration (measured in M) with culture medium flowing at a rate of 2.5 mL/min and overall oxygen uptake rate of 2  $\mu\text{mol/hr}$ ; (a) predicted by current model; (b) Horner's results



(a) Lactate concentration contour predicted by current model



(b) Lactate concentration contour by Horner *et al.*

Figure 3.23: Contour plot comparison for lactate concentration (measured in M) with culture medium flowing at a rate of 2.5 mL/min and overall lactate production rate of 6  $\mu\text{mol/hr}$ ; (a) predicted by current model; (b) Horner's results.

### **3.5 Conclusion**

As to conclude, the mathematical and numerical models devised to numerically study the feasibility of the micro-bioreactor have been discussed in details, covering the physical aspects of the micro-bioreactor that concern its operation, the mathematical formulation of the governing equations which are employed to numerically model fluid flow and solute transport and the numerical aspects that deals with conducting finite-volume CFD simulations. Validation of the numerical model has been carried to justify the capability of the model in simulating fluid flow and solute transport. All in all, preparation of the numerical model has been completed and it is ready to be utilized on the parameter studies.

# 4.0 Two-Dimensional Parametric Studies

---

The aim of this chapter is to provide a broad parameter study based on a two-dimensional numerical model of the niche micro-bioreactor. A two-dimensional model is used because it is considerably less expensive, both in terms of setting up the model and in the computational resources (computer time and memory) required. However, two-dimensional modelling should still provide considerable understanding of the effect of the control parameters on performance, restrict the focus of the three-dimensional studies in the next chapter, and allow expertise in modelling and analysis to be developed.

The chapter is structured as a set of sub-studies each focussing on the influence of a different parameter. These sub-studies involve: (1) the cavity aspect ratio; (2) changes due to embryo growth; (3) the inflow rate; (4) the height of culture medium; and (5) interactions between multiple cavities.

#### 4.1 Default Setup of the Two-Dimensional Micro-Bioreactor

The boundary conditions and dimensions of the default micro-bioreactor model are specified in Table 4.1. These values represent the default setup for the bioreactor and embryo before any parameters are altered for the subsequent sub-studies. The simulated lactate, oxygen concentration and shear stress averaged across the embryo surface are tabulated in Table 4.2. Termed as the *default values*, they are also used to normalize the corresponding results provided by the parametric studies. The objective of doing this is to reflect the relative changes of lactate concentration, oxygen concentration and shear stress after parameters are varied. To be specific, all the results on lactate and oxygen concentration, and shear stress, presented in this chapter are normalized by dividing by the default or reference values for each.

Embryo diameter	100 $\mu\text{m}$
Cavity length x depth	150 x 150 $\mu\text{m}$
Channel length x depth	10150 x 350 $\mu\text{m}$
Culture medium inflow rate	0.001 m/s
Lactate production rate	$9.427 \times 10^{-13}$ mol/hr
Oxygen uptake rate	$2.145 \times 10^{-13}$ kg/hr
Preset oxygen concentration at inlet	$2.189 \times 10^{-4}$ mol/L

Table 4.1: Default values for the model dimensions and boundary conditions.

Default lactate concentration	$1.63 \times 10^{-6}$ M
Default oxygen concentration	$2.12 \times 10^{-4}$ M
Default shear stress	$2.70 \times 10^{-4}$ Pa

Table 4.2: Default values of lactate, oxygen concentration and shear stress averaged across the embryo surface. These were found from a simulation using the default values.

## 4.2 Cavity Aspect Ratio Parametric Study

This parameter study focuses on examining and understanding how changes in cavity aspect ratio (AR) affects the flow properties and solute transport inside the cavity. The cavity AR is defined as the ratio of the length to depth of the cavity. Thus, it is a dimensionless number characterizing the cavity shape. Several previous studies of the flow structure in cavities (Shen and Floryan 1985; Galaktionov, Meleshko *et al.* 1999) found that changing the size of the cavity affects the fluid flow topology inside the cavity; it is believed that the flow topology affects the solute concentration in the cavity and shear stress distributions on the embryo surface. The solute concentration distribution within the cavity is a good indicator of how well the bioreactor supplies nutrients and oxygen to the embryo, removes metabolic waste produced by growing embryos or retains the embryotrophic factors essential to cell growth. The level of shear stress induced by the fluid flow affects embryo growth; indeed excessive shear can cause premature embryo death.

In this section, the flow geometry, boundary conditions and solute properties specific to this parameter study are first presented. The main outputs are lactate and oxygen concentration distributions as well as surface shear stress changes with AR. These are reported and analysed. Some implications to bioreactor design and utilization are discussed.

### 4.2.1 Problem Setup

As described above, for this study the design parameter that is being altered is the cavity AR, defined as the ratio of length ( $L$ ) to depth ( $D$ ) of the cavity (Figure 4.1). Five model geometries have been created for this study, as shown in Figure 4.2, covering a representative range of AR (Table 4.3). The AR varies between 0.25 and 4.0, based on the following approach: the length of the cavity was increased to increase the AR from 1.0 to 4.0 (Figure 4.2a to 4.2c); alternatively, the depth of the cavity was increased to decrease the AR from 1.0 to 0.25 (Figure 4.2c to 4.2e). Such configurations covered the range of cavity shape from a shallow cavity with wide opening to a deep cavity with small opening. This AR range was found to be large enough to cover the majority of the possible solute transport and shear stress change behaviour. The depth of the cavity was set to a constant at 50  $\mu\text{m}$  higher than the diameter of the embryo to ensure it was fully

enclosed within the synthetic niche environment of the cavity. Similarly, the length of the cavity was set to be larger than the diameter of the embryo by 50  $\mu\text{m}$ , such that the embryo is always contained within a small environment enclosed by the cavity side walls, as the depth of the cavity is increased.

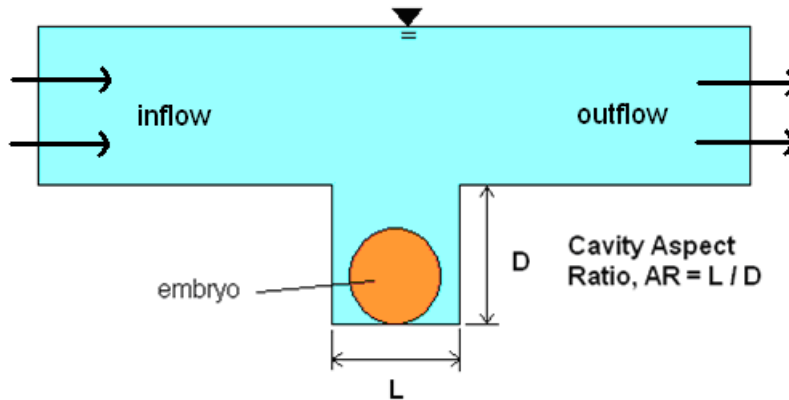


Figure 4.1: Sketch of the bioreactor model showing the length and depth that define the AR.

Aspect ratio, AR	Length, $L$	Depth, $D$
	$\mu\text{m}$	$\mu\text{m}$
4.0	600	150
2.0	300	150
1.0	150	150
0.5	150	300
0.25	150	600

Table 4.3: Tabulated values showing the aspect ratios considered for the AR parametric study.

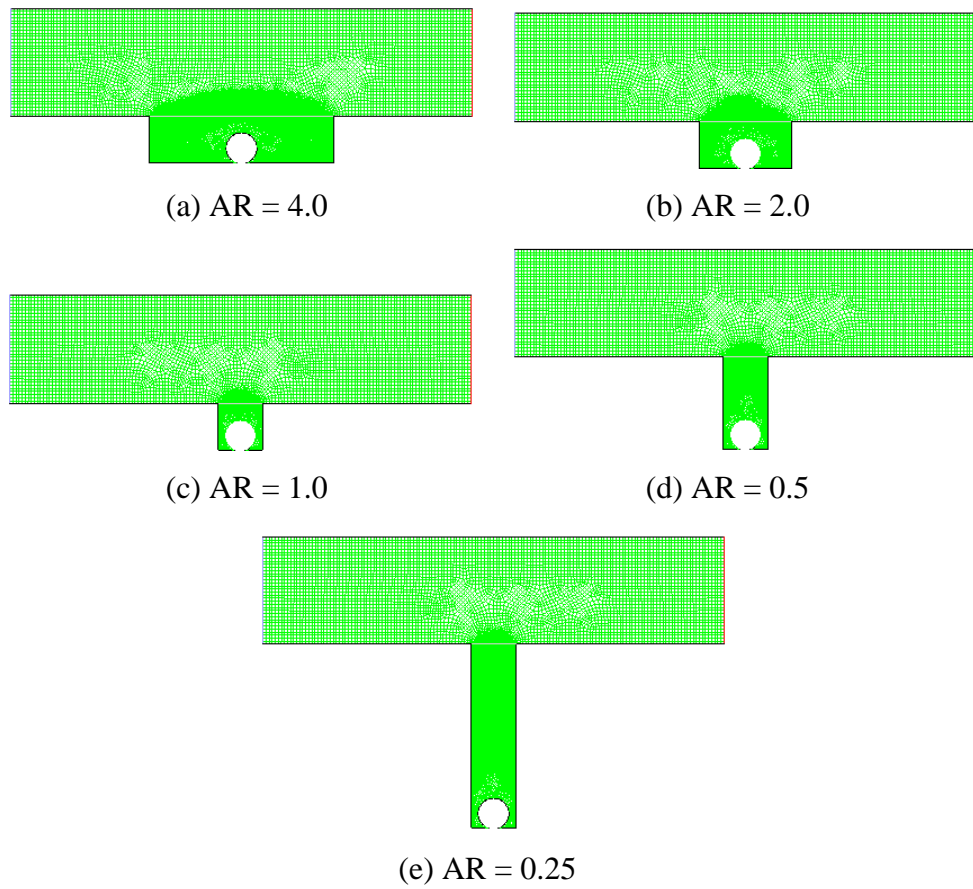


Figure 4.2: The five meshed numerical models for the cavity AR parametric study, with cavity AR varied from 4.0 (a) to 0.25 (e).

### 4.2.2 Flow Structures in the Cavity

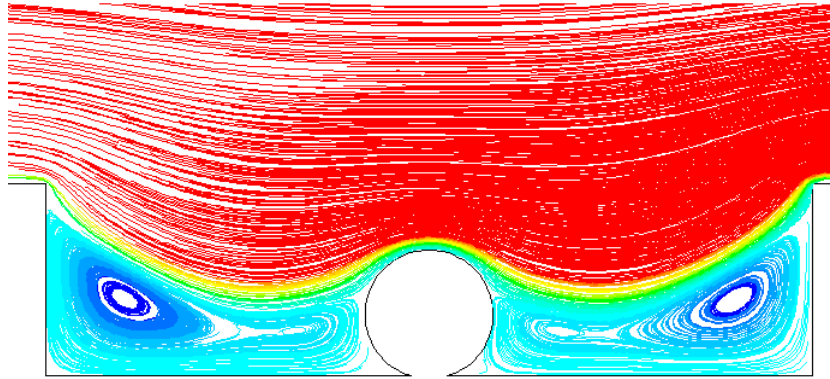
The flow streamlines in the neighbourhood of the cavity are presented to provide insight into, and understanding of, how the flow changes the solute transport and shear stress distribution as the cavity AR is altered. Flow topology changes are observed as AR changes.

For AR of 4.0 (Figure 4.3a), the large cavity opening allows some of the bulk flow in the main channel to penetrate into the cavity to contact the embryo body. Two weaker but large flow recirculations are induced beside the embryo, but notably the cores of these recirculations are quite far from the embryo. When AR is decreased to 2.0 (Figure 4.3b), the relative opening of the cavity is reduced. In turn, this reduces the bulk flow penetration into the cavity. Again, two relatively weak flow recirculations are formed beside the embryo but their cores are closer to the embryo body.

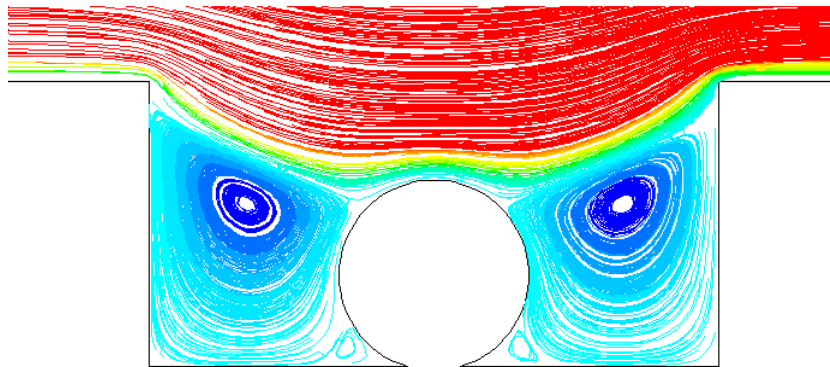
As the AR decreased to 1.0, the cavity shape becomes square and the flow topology starts to change (Figure 4.3c). The two flow recirculations beside the embryo body reduce in size and move closer to the upper side of the body. Two smaller recirculations are also formed below the main recirculations, beside the embryo. At the bottom of the cavity the flow appears to be virtually stagnant as no flow recirculations are observed.

As AR is decreased further, the depth of the cavity is increased. The two main flow recirculations merge into a large recirculation on top of the embryo body. As shown in Figure 4.3d, for the case of AR of 0.5, only one large recirculation is detected on top of the body. Two smaller recirculations with weaker strengths appear beside it, while the flow around the bottom of the cavity appears to be stagnant. When AR is decreased further to 0.25, two large recirculations form above the embryo body, where the one closer to the cavity opening is significantly stronger (Figure 4.3e). The embryo body is bathed in a stagnant flow at the bottom of the cavity.

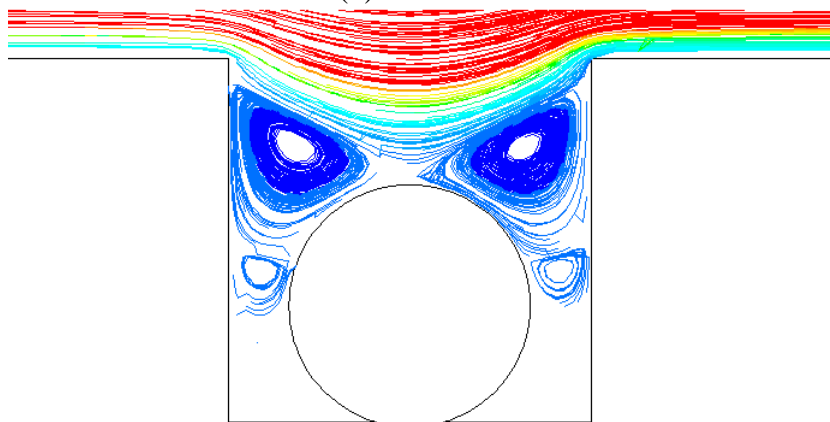
Note that the basic findings described above are supported by the numerical work of Shen and Floryan (Shen and Floryan 1985), who examined the evolution of flow structures in an open cavity where the aspect ratio is altered between 0.25 and 4.0.



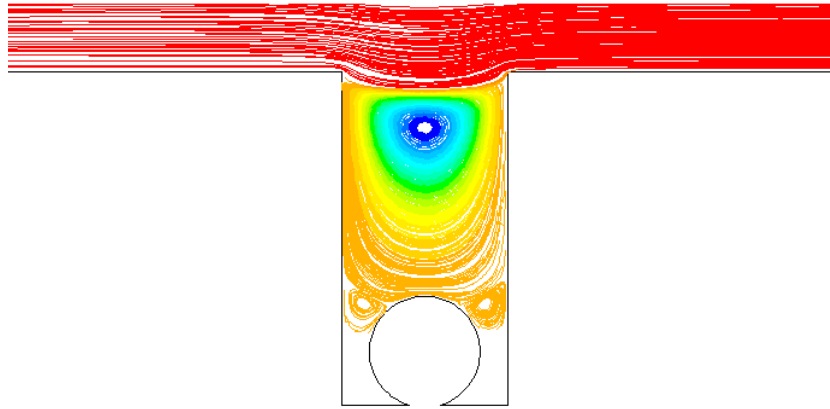
(a) AR = 4.0



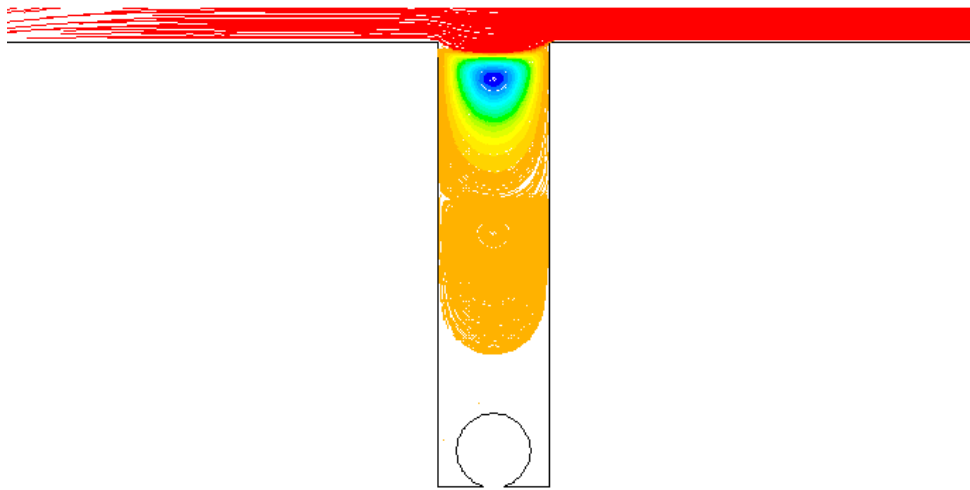
(b) AR = 2.0



(c) AR = 1.0



(d) AR = 0.5



(e) AR = 0.25



Figure 4.3: Streamfunction plots of flow in the cavities indicating the structure and the strength of the flow recirculations (measured in kg/s).

### 4.2.3 Solute Concentration Changes with AR

Changes of lactate and oxygen concentration due to AR variation are presented in Figure 4.4. The reported values of averaged lactate and oxygen concentration across the embryo surface have been normalized with their respective reference values (Table 4.2). These two plots show that as AR is increased from 0.25 to 1.0, the solute concentration initially changes quickly. Lactate concentration drops rapidly (around a 400% decrease), while oxygen concentration rises sharply (around 10% increase). When AR is increased further from 1.0 to 4.0, the drop of lactate concentration level and rise of oxygen concentration level begins to level off. It seems reasonable that the solute concentration would asymptote further as AR is increased beyond 4.0.

Aspect ratio, AR	Lactate concentration	Normalized lactate concentration	Oxygen concentration	Normalized oxygen concentration
	M		M	
4	5.36E-07	0.329	2.16E-04	1.018
2	7.50E-07	0.460	2.15E-04	1.014
1	1.63E-06	1.000	2.12E-04	1.000
0.5	3.44E-06	2.112	2.06E-04	0.972
0.25	7.05E-06	4.327	1.95E-04	0.918

Table 4.4: Tabulated values showing the change of lactate and oxygen concentration averaged across the embryo surface when AR is altered. The concentration values are normalized with the default solute concentration given in Table 4.2.

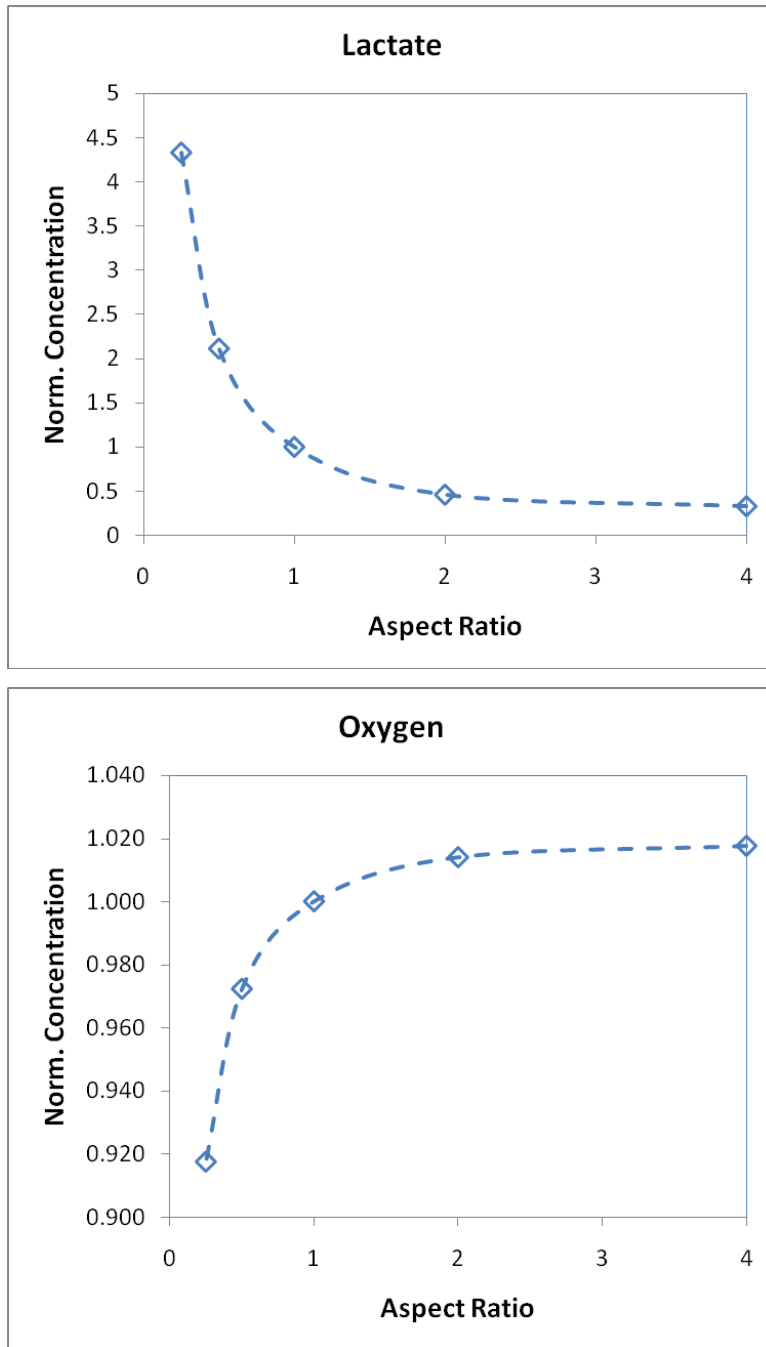


Figure 4.4: The normalized concentration of lactate and oxygen averaged across the embryo surface with respect to AR.

The initial rapid changes in the solute concentrations are consistent with the rapid changes to the flow topology in the cavity (Figure 4.3) as aspect ratio is varied. For a cavity with  $AR < 1$ , the cavity opening is much smaller (relative to cavity depth). This has the immediate effect of significantly reducing flow penetration directly into the cavity, and because of the low Reynolds number, the induced flow recirculations reduce in strength rapidly with depth. At such low Reynolds numbers, solute transport is clearly controlled by diffusion.

When the cavity  $AR$  is larger than one, the relatively wide cavity opening allows a sizeable bulk flow from the main channel to enter the cavity, which in turn produces strong flow recirculations within it. In particular, the bulk flow across the top of the cavity directly affects fluid flow below the level of the top of the embryo, so that it is bathed in fresh rather than recirculating fluid. As the speed of the main flow is fixed for this parameter study, the immediate flow and fluid environment of the embryo becomes primarily controlled by the main flow over the top of the cavity. This causes the solute concentration variation in the cavity to level off as  $AR$  is increased to larger values.

Also from Figure 4.4 and Table 4.4, it is observed that the variation in oxygen concentration is much less than the variation in lactate concentration. Further comments on this are given in the next chapter in section 5.5.

#### **4.2.4 Solute Distribution around the Embryo**

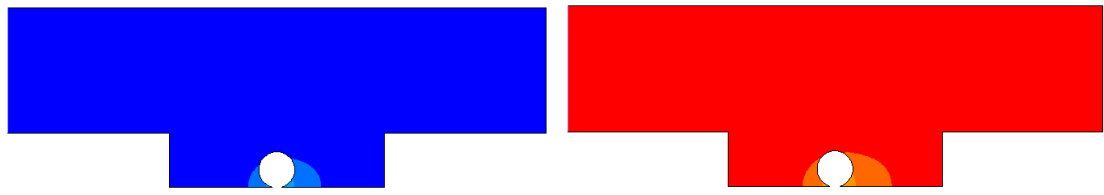
The solute distribution around the embryo is examined to better understand the solute concentration level variation as  $AR$  is altered. Firstly, the solute distribution of the entire modelling domain is inspected, as shown in Figure 4.5 below. The distribution trend of both lactate and oxygen remains similar regardless of the different  $AR$ .

When  $AR$  is larger than one, the wide cavity opening promotes solute transport across the cavity. This is evidenced in the streamline plots (Figure 4.3a, 4.3b), where the bulk flow from the main channel penetrates into the cavity and induces two large flow circulations to enhance the solute transport. This causes the solute concentration level in the cavity to be almost identical to that in the main perfusion channel. Regions of high lactate concentration and low oxygen concentration are found near the embryo (Figure

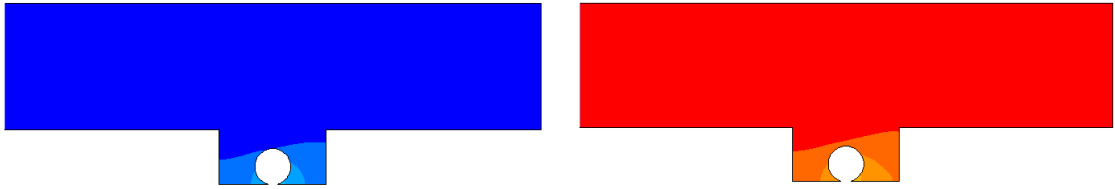
4.5a, 4.5b). As the cavity AR is increased, this region grows to fill the cavity bottom; higher lactate concentration and lower oxygen concentration are observed around the embryo.

As the cavity shape became square ( $AR = 1.0$ ), the narrow opening restricts the bulk flow entering the cavity; the two large flow circulations are compressed and weakened, as shown in the streamline plot in Figure 4.3c. This hinders the solute transport in the cavity, causing the lactate produced by the embryo to start to accumulate in the cavity and this raises the concentration level in the cavity. At the same time, less oxygen is supplied into the cavity and to the embryo, enlarging the oxygen deficit region to fill the entire cavity (Figure 4.5c). The lactate concentration level in the cavity in this case is overall much higher, while the oxygen concentration level is overall much lower than for a shallow, wide cavity with AR larger than 1.0.

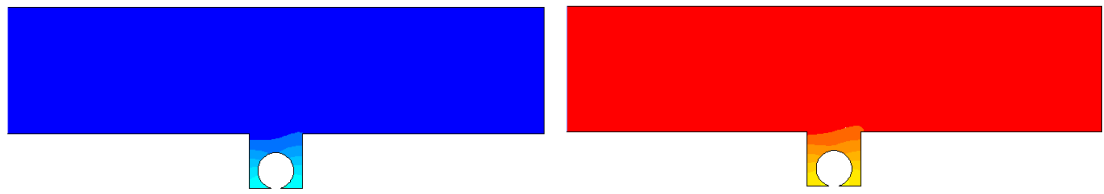
As AR is decreased to 0.50, the two flow recirculations above the embryo merge into a large yet weaker recirculation (Figure 4.3d). Now the bulk flow from the main channel cannot reach the embryo; the fluid movement adjacent to the embryo is mainly the weaker flow recirculation. This further impedes the solute transport in the cavity (Figure 4.5d), which causes even more lactate produced by the embryo to remain around it. For the same reason, oxygen transport into the cavity slows down and further lowers the concentration level in the cavity. As the depth of the cavity continues to increase, more flow recirculations are formed in the cavity. Since the strength of the flow recirculation deeper into the cavity is low (Figure 4.3e), solute transport into the cavity, and especially around the embryo, is very slow. Consequently, the lactate produced by the embryo remains due to the stagnant condition and a similarly, the surrounding fluid is also depleted of oxygen (Figure 4.5e).



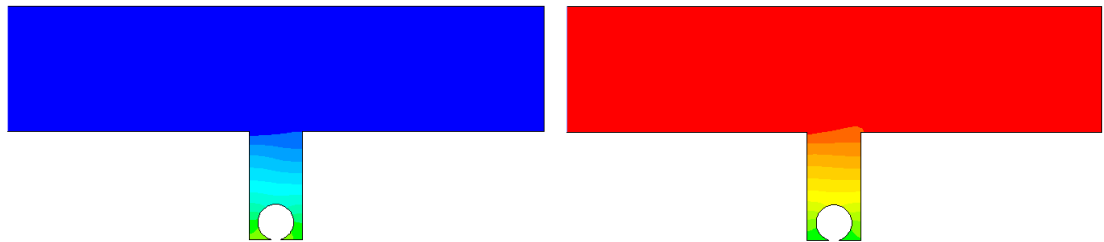
(a) AR = 4.0



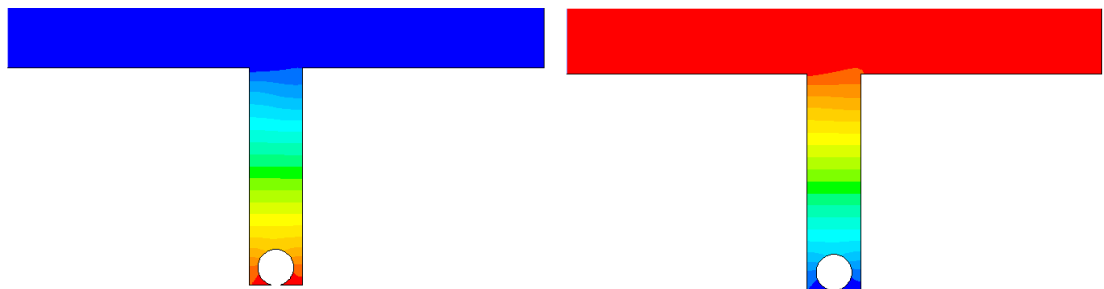
(b) AR = 2.0



(c) AR = 1.0



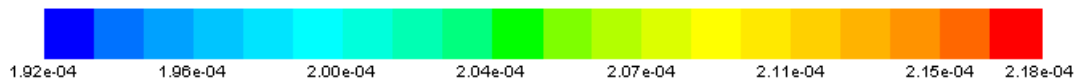
(d) AR = 0.5



(e) AR = 0.25



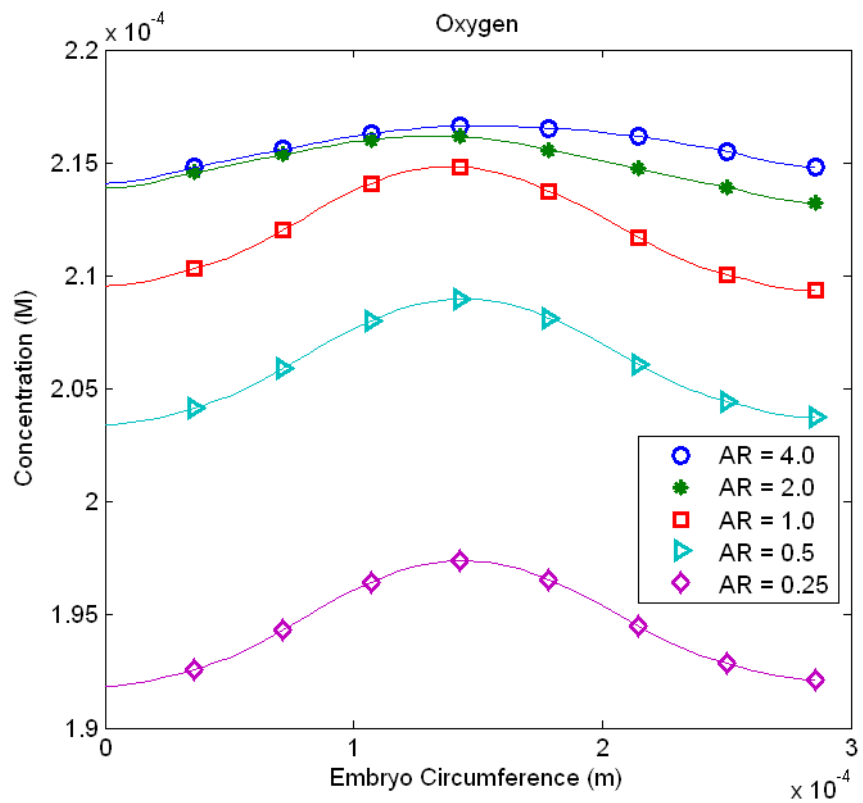
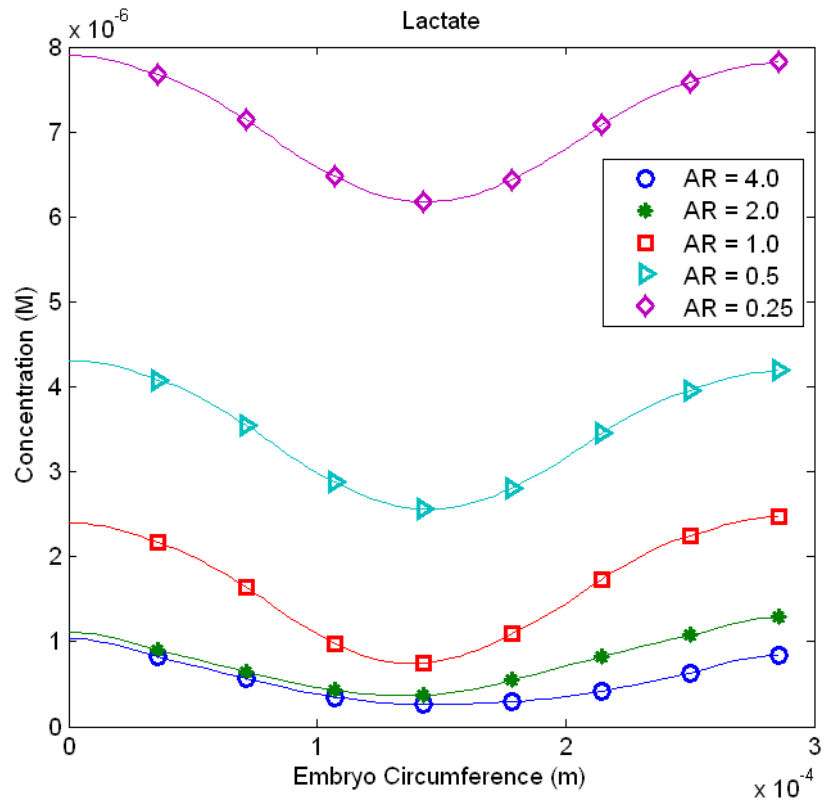
(Lactate concentration measured in M)



(Oxygen concentration measured in M)

Figure 4.5: Lactate (left) and oxygen (right) distribution. Here the contour level range for lactate and oxygen respectively is set to be the same for all the different AR to highlight the overall magnitude change as aspect ratio is altered.

From Figure 4.6 one can notice that regardless of the different AR, the solute concentration distribution profiles on the embryo remains similar. For lactate, the highest concentration appears at the bottom of the embryo. The concentration level then drops progressively to the lowest value at the top of the embryo. For oxygen, the exact opposite situation is observed. The lowest concentration is found at the bottom of the embryo. This concentration level then increases gradually to the highest value at the top of the embryo. These profiles can be explained by looking at the streamline plots in Figure 4.3. Regardless of different AR, the top of the embryo appears in contact with the bulk flow (Figure 4.3a, 4.3b) or the main flow recirculations (Figure 4.3c, 4.3d, 4.3e). These flow features help to accelerate the solute transport around the top region of the embryo, causing lactate to be removed and oxygen to be supplied there. In contrast, at the bottom the flow is stagnant, which causes the solute transport to be very slow.



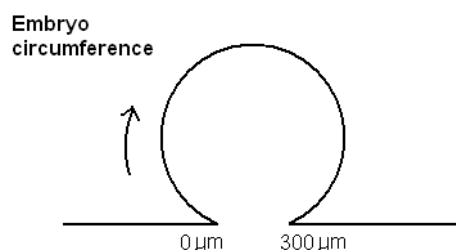


Figure 4.6: Lactate (top) and oxygen (bottom) concentration distribution on the embryo surface for different AR. The circumference here measures from the left bottom point to the right bottom point on the embryo. This notation is used for all the following plots.

#### 4.2.5 Implications for Solute Transport

Summarizing the outcomes from the lactate and oxygen modelling, some conclusions can be drawn. Firstly, it is found that solute transport is impaired by deep cavities while it is very much affected by perfusion outside the cavity in the case of shallow cavities. This observation is useful when tuning the bioreactor design, for example to remove undesirable solutes produced by the embryo, a shallow cavity ( $AR > 1$ ) could be employed. Conversely, for the case where one needs to retain embryotrophic factors produced by the embryo (which promotes embryo growth), a deeper cavity should be employed. A practical bioreactor design involves balancing these effects. Apart from these qualitative conclusions, the profiles give quantitative information about the variation of solute concentration around the embryo for a particular flow rate. The effect of the flow rate will be given in a later study in this chapter.

For this particular flow rate, the concentration changes as AR increases beyond 4 are minimal, indicating that cavity aspect ratios larger than 4 have a decreasing effect. Also of interest, the relative solute concentration variation around the embryo does not alter much as AR changes. However, solute concentration does vary considerably and this may have implications for optimal embryo growth, although this is beyond the scope of the current parametric study.

#### 4.2.6 Embryo Surface Shear Stress Changes with AR

In general, the shear stress on the embryo surface increases rapidly with AR (Figure 4.7). The stress level here refers to the averaged shear stress across the circumference of the modelled embryo surface. From Table 4.5 we can see that the stress level increases by

$10^5$  when AR is raised from 0.25 to 1.0, corresponding to the depth of the cavity decreasing. The stress level variation rate then slows and there is only a 10-fold increase as AR increases from 1.0 to 4.0. The stress level appears to asymptote as the AR is increased further beyond 4.0, corresponding to the embryo surface becoming increasingly exposed to the free stream.

Aspect ratio, AR	Shear stress Pa	Normalized shear stress
4	5.03E-03	1.86E+01
2	2.00E-03	7.41E+00
1	2.70E-04	1.00E+00
0.5	1.91E-05	7.08E-02
0.25	4.45E-09	1.65E-05

Table 4.5: Tabulated values of the averaged shear stress across embryo surface for different AR. The shear stress is normalized with the default shear stress given in Table 4.2.

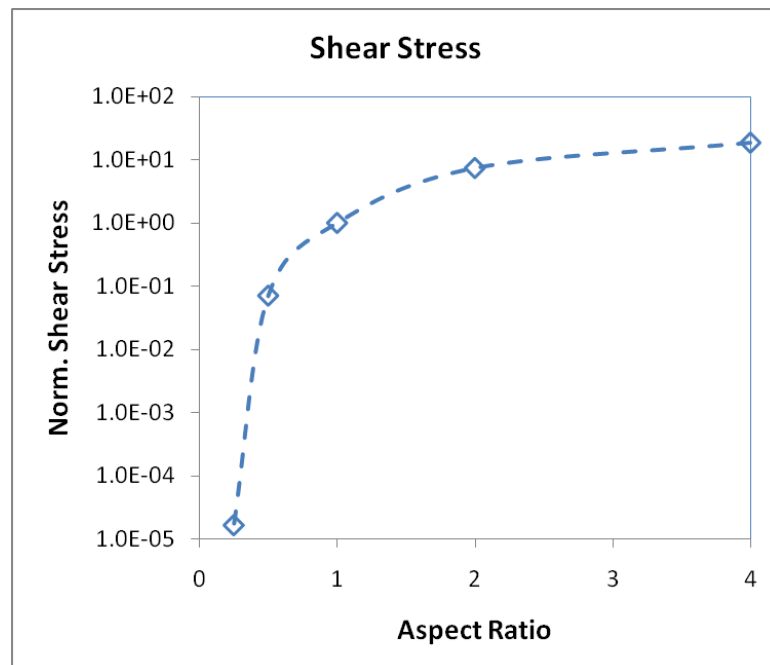


Figure 4.7: Averaged shear stress across the embryo surface as AR is varied from 0.25 to 4.00.

The reason for the observed variation again can be directly related to flow topology changes when the AR is altered. As the cavity is deepened, a greater number of flow recirculation regions occur within the cavity. As shown on Figure 4.3d and 4.3e, the deeper the cavity, the weaker the strength of the recirculation. The shear stress is proportional to the normal velocity gradient, which can be at least approximately related to the strength of the flow circulation, since the velocity falls to zero at the surface. Thus, an embryo in a deeper cavity will experience a much lower shear stress as the recirculating flow adjacent to it is much weaker. On the other hand for shallower cavities the channel flow directly interacts with the top of the embryo. This suggests that the shear stress should level off as more of the embryo directly experiences the channel flow, as the aspect ratio gets larger.

#### **4.2.7 Local Shear Stress Distribution on Embryo Surface**

A more detailed investigation of the stress distribution on the embryo surface was conducted to map the local features of the shear stress induced on the embryo surface. Firstly, the stress level for different AR is compared (Figure 4.8). From the figure, it is clear that the stress level on the embryo in a wide, shallow cavity is much higher than that in the square or deeper cavities, as shown by the single peaked stress level at the top of the cavity. Due to the large magnitude difference in stress between AR of 4.0 and 0.25, plots of all the stress distributions together on the same axes could not be presented usefully. Hence the stress distributions are examined individually (Figure 4.9).

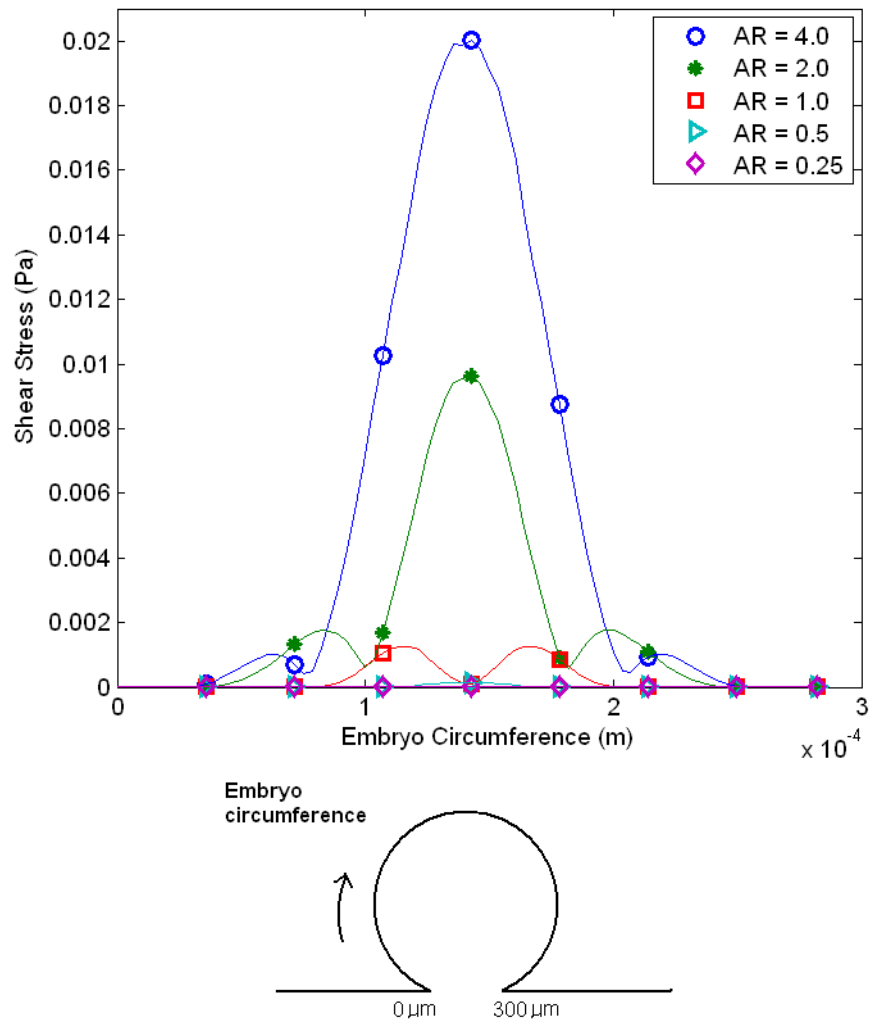
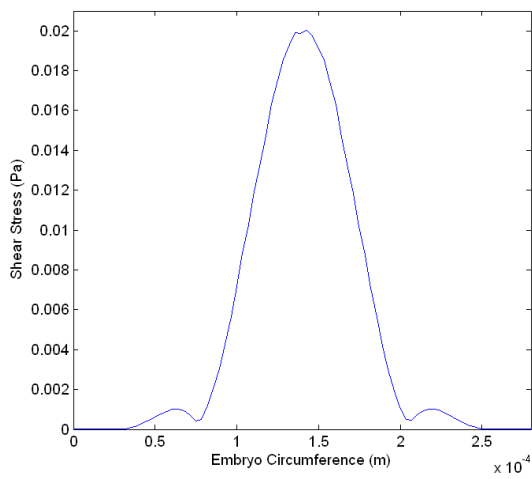
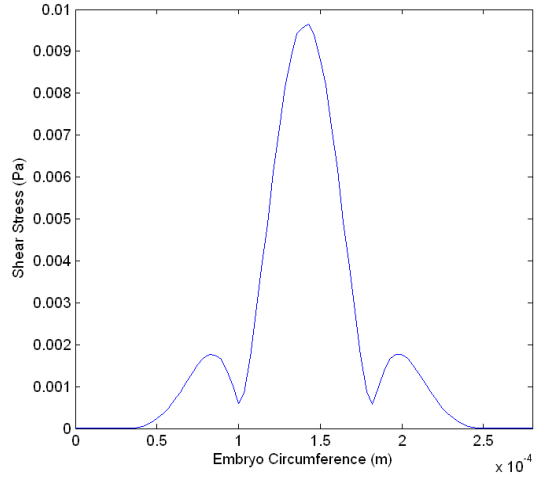


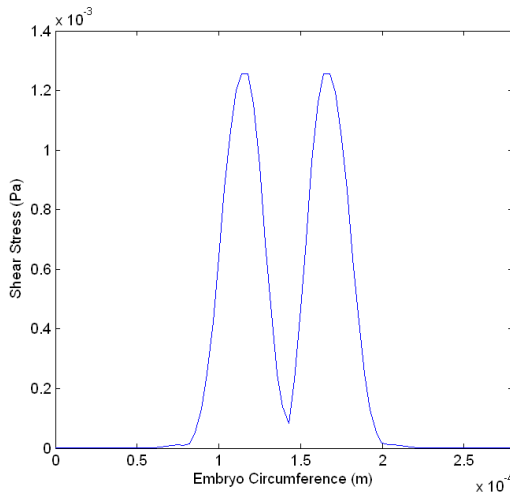
Figure 4.8: Comparison of embryo surface shear stress distribution along the embryo circumference for different AR.



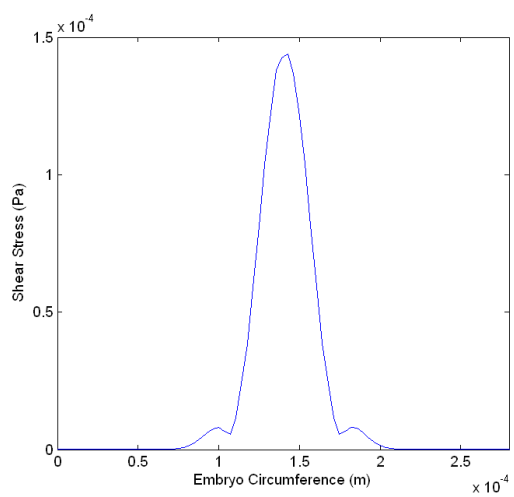
(a) AR = 4.00



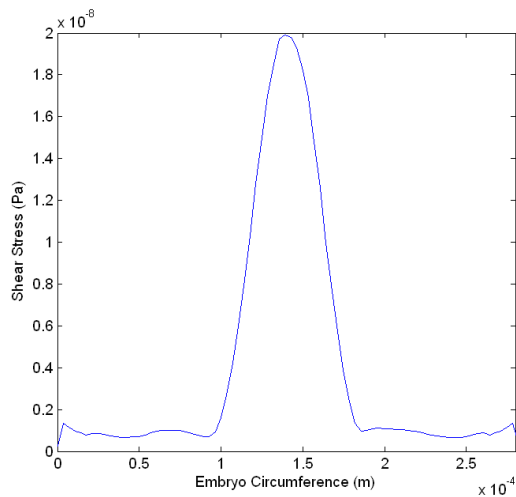
(b) AR = 2.00



(c) AR = 1.00



(d) AR = 0.50



(e) AR = 0.25

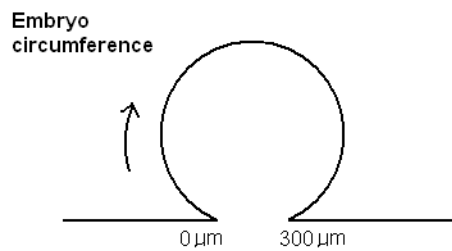


Figure 4.9: Shear stress distributions along the embryo circumference for five different AR.

First of all, the stress distribution on an embryo in a wide shallow cavity is examined. For the case of  $AR = 4.0$ , the maximum peak stress is 90% larger than the two local maxima next to it. The occurrence of these peak stresses correspond well to the position of flow recirculations and bulk flow touching the embryo (Figure 4.3a). The maximum peak stress occurs at the top of the embryo, which coincides with the location where the strong bulk channel flow shears across the surface of the embryo. The two smaller peak stresses occur at the locations at which the two big side recirculations brush the embryo surface. As the strengths of these flow recirculations are weaker than the bulk flow, lower peak stresses are induced there.

For the case of  $AR = 2.0$ , a similar stress distribution profile can be seen (Figure 4.9b). The only difference between it and the stress profile for  $AR = 4.0$ , is that the two lower peak stresses are relatively higher (the maximum peak stress is 81% higher than the two peaks beside it). The location of these peak stresses again can be explained by the occurrence of the bulk flow and flow recirculations within the cavity (Figure 4.3b).

In a square cavity, two peak stresses occur around the top region of the embryo (Figure 4.9c), which agree well with the location of the two flow recirculations appearing near the cavity opening (Figure 4.3c). The stress at the lower region of the embryo is close to zero, which is expected, as the fluid there is relatively stagnant.

For a deep cavity with  $AR = 0.5$  and  $0.25$ , the stress distribution has the following profile: a single peak stress at the top of the embryo, with the stress level dropping down and levelling out around the lower section of the embryo (Figure 4.9d, 4.9e). The only difference between them is that the stress level for embryo in the deeper cavity with  $AR$  of  $0.25$  is about  $10^4$  lower than the other (peak stress of  $2 \times 10^{-8}$  Pa against  $1.4 \times 10^{-4}$  Pa). This peak stress is coherent with the formation of a big but weak flow recirculation on top of the embryo, as shown in the corresponding streamline plots in Figure 4.3d and 4.3e. The size of the difference in peak stress between these two cases is interesting, presumably caused by the failure of the bulk channel flow to penetrate into the cavity barely at all for the deeper cavity.

#### **4.2.8 Implications for Shear Stress Changes**

The maximum level of shear stress is found for the cavity with the largest aspect ratio, and presumably this will increase slightly as the aspect ratio is further increased. This indicates that one can significantly reduce the shear stress exerted on the embryo by reducing the cavity AR. Reducing the AR to less than one can decrease the magnitude of the shear stress greatly, while increasing the AR to more than four offers only small changes to the shear stress. These observations may be useful when considering the design of a micro-bioreactor to control stress levels to desirable levels for embryo growth.

The shear stress distribution on the embryo surface varies depending on the position where the flow circulations and bulk flow interact with (or *touch*) the embryo. This means that it is possible to pinpoint the location of localized maximum shear by looking at the flow structures inside the cavity, and this may prove useful if it is not possible to measure the shear stress on the embryo surface.

#### **4.2.9 Conclusion and Summary**

In this section, the effects of cavity aspect ratio on the solute transport and shear stress distribution were studied for set values of the other control parameters. The streamlines in the cavity were examined; these highlight the flow structure changes as the AR is varied. It is found that broadly there are two regimes with different flow topologies as the AR was varied: AR larger than one and smaller than one.

When AR is larger than one, the large cavity opening allowed stronger bulk flow penetration into the cavity. This also creates two large flow recirculations on both sides of the embryo. These features enhance the solute transport but induce a large shear stress on the embryo. Both solute concentrations of lactate and oxygen, as well as the surface shear stress, asymptote as AR becomes larger, showing that as the cavity opening becomes larger the fluid environment becomes more and more influenced by the unchanged bulk flow.

When AR is smaller than one, the small cavity opening hinders flow penetration into the cavity. A set of weaker flow recirculations is produced in the cavity. These flow structures reduce solute transport and the shear stress on the embryo surface.

The solute concentration distributions remain similar in shape as AR is altered. Local maxima of oxygen concentration and local minima of lactate concentration are found at top of the embryo. Conversely, the shear stress distribution does vary in shape as AR is altered. Local maxima of the shear stress occur at the location at which the flow recirculations or bulk flow are in contact with the embryo.

### 4.3 Culture Medium Inflow Rate Parametric Study

The inflow rate of the culture medium is the main parameter governing fluid perfusion for the bioreactor. It is of vital importance to investigate the impact of altering this parameter since solute transport and shear stress are clearly strong functions of it. Not surprisingly, previous studies on a grooved perfusion flat-bed bioreactor (Horner, Miller *et al.* 1998) and a microchannel bioreactor (Zeng, Lee *et al.* 2006), which are similar in concept to the micro-bioreactor here, report notable changes in solute concentration in the cavity when the inflow rate of culture medium is modified.

In this section, the modelling and simulation setup specific to this study is explained prior to the analysis and discussion of results. The *Peclet* number is introduced as the governing parameter controlling solute transport. Particle trajectories are used to aid in explaining the flow behaviour within the cavity. The solute transport and flow-induced shear stress are then analysed, and implications of these results are discussed before the section is concluded.

#### 4.3.1 Problem Setup

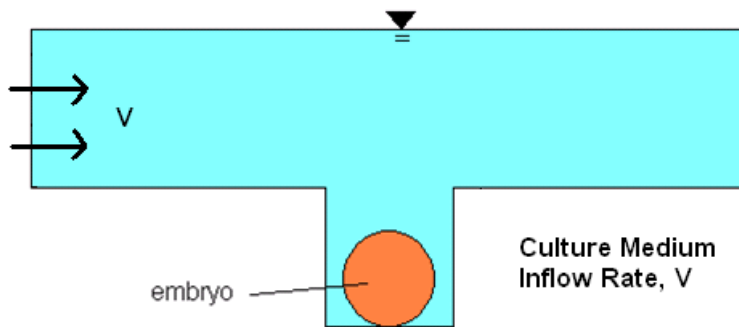


Figure 4.10: A sketch of the bioreactor model indicating the parameter of interest in this study: the inflow rate,  $V$ , of the culture medium.

In this study, the parameter investigated is the inflow rate,  $V$ , of the culture medium. The inflow rate here specifically refers to the inflow velocity of the culture medium across the inlet surface (Figure 4.10). The initially uniform fluid velocity entering at the inlet forms a semi-developed boundary layer before passing across the cavity, as shown in Figure 4.11. The transition to a full-developed flow is a function of the Reynolds number – the case shown is for the highest Reynolds number studied, taking the longest

for the entry flow to become fully developed. Recall, the top surface is a free surface and the bottom surface is a no-slip wall.

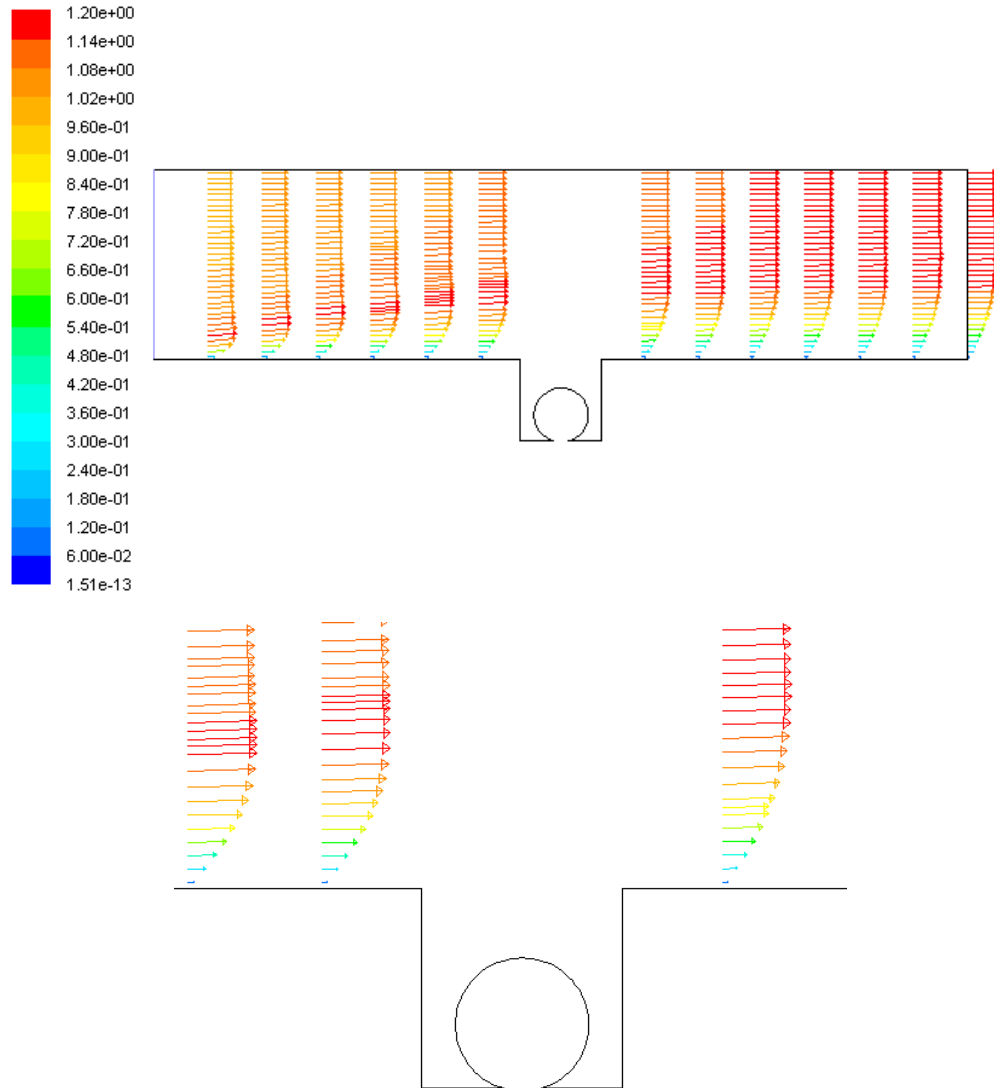


Figure 4.11: Typical plots of velocity vectors (measured in m/s) showing the evolution of the velocity from a plug flow at the entrance (top). The velocity profile immediately before encountering the cavity approaches the equilibrium half-parabolic shape (bottom).

The range of  $V$  (from 1 m/s to  $1 \times 10^{-9}$  m/s) investigated is tabulated in Table 4.6 below. It is found that it provides adequate scope to cover the majority of the solute transport and fluid condition changes due to the inflow rate variation, as indicated by the flow Peclet number ( $Pe$ ) and Reynolds number ( $Re$ ) ranges given in the table. The definition and role of  $Pe$  is explained in the next section. For the subsequent presentation of the

solute concentrations, the  $Pe$  values for lactate and oxygen are employed to characterise the predictions, while the  $Re$  is chosen to non-dimensionalise the results for the shear stress. Note that there is a fixed relationship between both non-dimensional parameters, since for biological applications the temperature is fixed at body temperature, so that the diffusivities of momentum and each of the solutes are effectively constant.

Inflow rate, $V$	$Pe$ (lactate)	$Pe$ (oxygen)	$Re$
m/s			
1.00E+00	1.03E+05	4.69E+04	9.38E+01
1.00E-01	1.03E+04	4.69E+03	9.38E+00
1.00E-02	1.03E+03	4.69E+02	9.38E-01
1.00E-03	1.03E+02	4.69E+01	9.38E-02
1.00E-04	1.03E+01	4.69E+00	9.38E-03
1.00E-05	1.03E+00	4.69E-01	9.38E-04
1.00E-06	1.03E-01	4.69E-02	9.38E-05
1.00E-07	1.03E-02	4.69E-03	9.38E-06
1.00E-09	1.03E-04	4.69E-05	9.38E-08

Table 4.6: Specific values of the inflow rate chosen for this study along with their associated flow Reynolds and Peclet number.

#### 4.3.2 Peclet Number: Relevance in Solute Transport

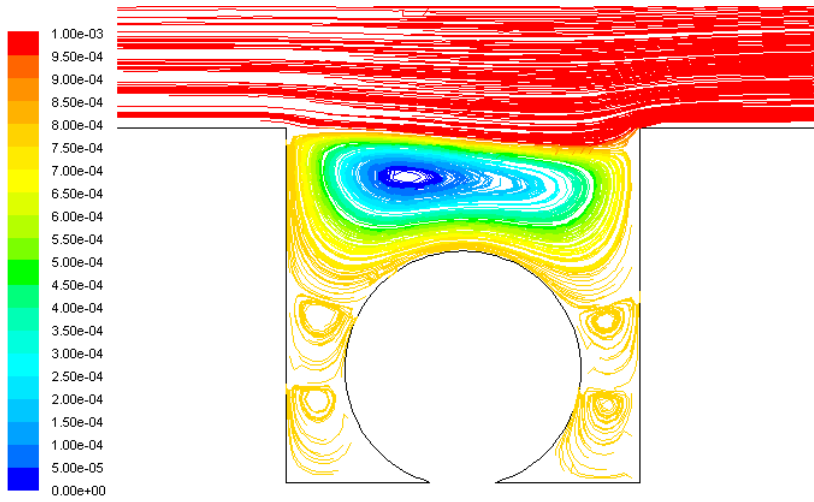
To describe the solute transport behaviour,  $Pe$  is introduced to relate the solute concentration variation as the inflow rate changes. For mass transfer in a laminar flow, such as application of the micro-bioreactor,  $Pe$  is typically employed to indicate the importance of mass convection relative to mass diffusion (Deen 1998). The definition of  $Pe$  is given in Equation 3.7 (Section 3.2). Basically, for a given cavity geometry and preset culture medium,  $Pe$  becomes the governing parameter for the solute distribution. For the case here, in which the length scale and diffusivities are effectively set, the Peclet number is directly related to the inflow speed; however, it is useful to characterise the problem using this non-dimensional parameter because it directly indicates the relative importance of advection to diffusion.

Another important dimensionless parameter relevant to this problem is the Schmidt number,  $Sc$ , the ratio of momentum to solute diffusivity (Deen 1998). For this problem, since the temperature is effectively fixed,  $Sc$  is constant for each solute species:  $Sc_{\text{oxygen}}$

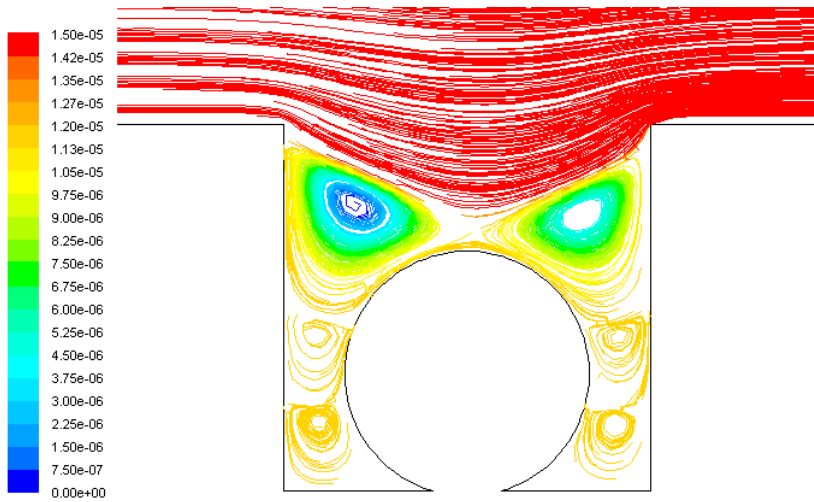
$\approx 500$  and  $Sc_{\text{lactate}} \approx 1100$ . This also means that diffusion is less important for solute transport than for momentum transport. The implications will be discussed later.

### **4.3.3 Particle Trajectories in the Cavity**

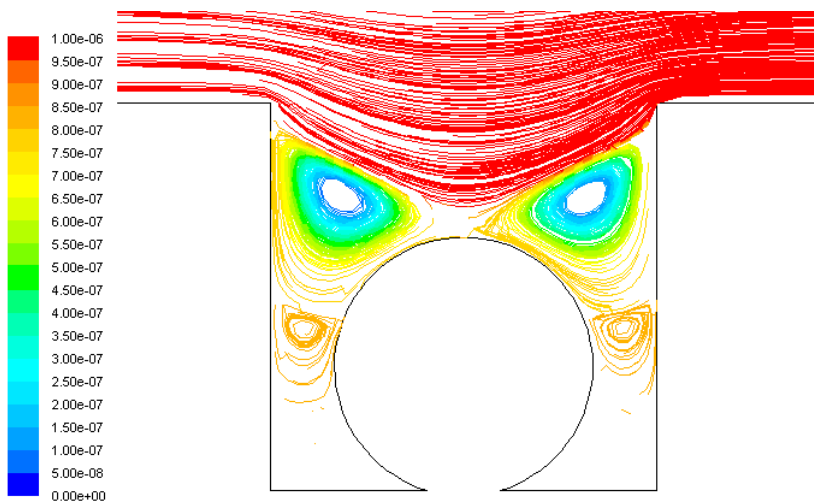
There are a few notable changes to the flow structures in the cavity as  $V$  is altered, especially when  $V$  is relatively large. When  $V$  is 1 m/s, ( $Re = 93.8$ ), convection is relatively important, and a large and strong flow recirculation is detected above the embryo. In addition, four smaller and weaker flow recirculations are formed beside the embryo (Figure 4.12a). As  $V$  is reduced to 0.1 m/s, convection is less dominant, and the previously large flow recirculation splits as the flow penetrates into the cavity. The four induced flow recirculations found previously still persist (Figure 4.12b). For  $V$  below approximately 0.01 m/s ( $Re \approx 1$ ) (see Figures 4.12c-e) there is little further change to the flow pattern. The flow becomes dominated by diffusion and the velocity field can be predicted by scaling from one Reynolds number to another.



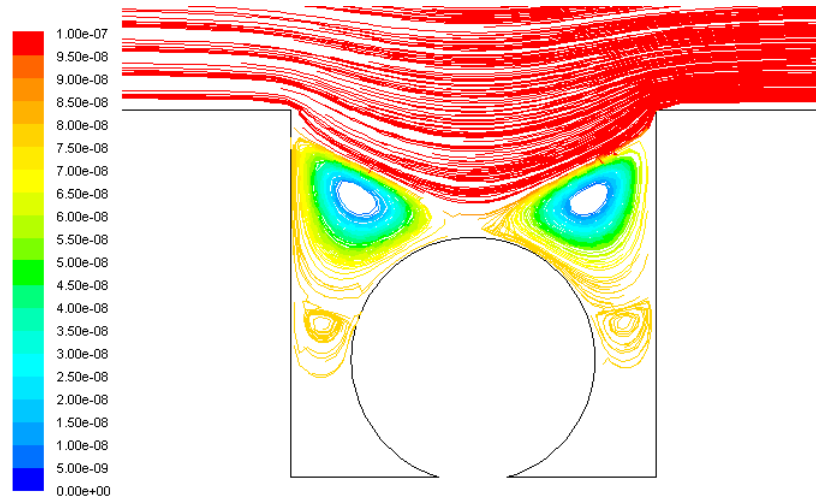
(a)  $V = 1 \text{ m/s}$



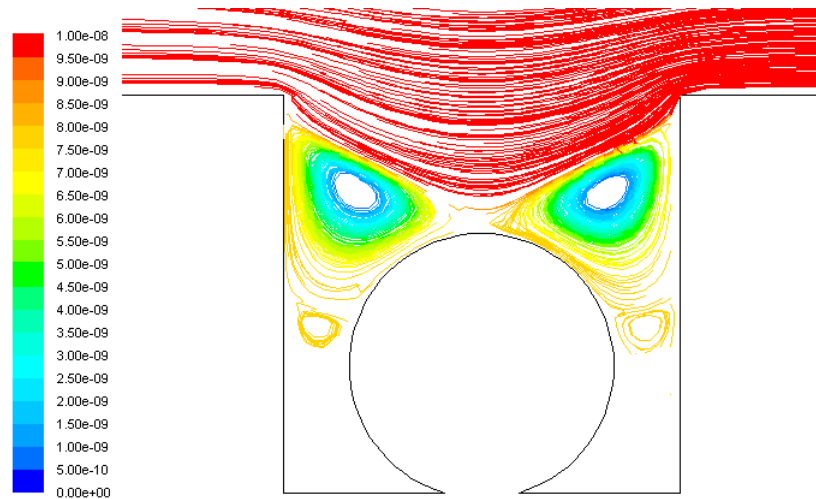
(b)  $V = 1 \times 10^{-1} \text{ m/s}$



(c)  $V = 1 \times 10^{-2} \text{ m/s}$



(d)  $V = 1 \times 10^{-3}$  m/s



(e)  $V = 1 \times 10^{-4}$  m/s

Figure 4.12: Streamline plots showing the flow structures in the cavity for different inflow rates. The flow recirculation strength is measured in kg/s.

As indicated above, the diffusion coefficients of the solutes are significantly lower than the diffusion coefficient for momentum (the kinematic viscosity); hence the solute distributions should show stronger variation over this Reynolds number range.

#### 4.3.4 Changes in Solute Transport

The change in solute concentration on the embryo surface is plotted against  $Pe$  in Figure 4.13. It is found that the normalized solute concentration asymptotes to a constant value of 3.53 for lactate and 1.01 for oxygen as  $Pe$  becomes smaller. When  $Pe$  becomes larger, lactate concentration decreases while oxygen concentration increases consistently. The

critical  $Pe$  values which mark these behavioural changes are 0.01 for lactate and 0.6 for oxygen.

These trends are consistent with the fact that fluid flow around the embryo changes from diffusion dominated when  $Pe$  is smaller than the critical value to advection dominated when  $Pe$  is larger than the critical value. In the diffusion dominant regime, the solute transport is mainly driven by the concentration gradient. In this case, the diffusivity of the solute governs its transport. As the diffusivities of lactate and oxygen are constants, this causes the solute concentration near the embryo to approach a fixed distribution corresponding to the quiescent case. On the other hand, when advection is dominant, solutes are transported by the movement of the fluid within the cavity. As the speed of fluid flow is increased, the faster bulk flow movement enhances solute transport and this causes more lactate to be advected away from, and more oxygen to be supplied to, the embryo. This is the cause for the lactate concentration decrease and oxygen concentration increase as  $Pe$  becomes larger.

By comparing the plots of  $Pe$  against solute concentration of lactate and oxygen, it is found that the critical  $Pe$  for lactate is lower than the critical  $Pe$  for oxygen. This is shown in Figure 4.13, where the lactate concentration starts to stabilize at  $Pe = 0.01$ , whereas oxygen concentration begins to stabilize at  $Pe = 0.6$ . This is presumably due to two factors: the difference in Schmidt numbers between two solutes; and the difference in the boundary conditions for two solutes, i.e., the fact that only oxygen is supplied from the inlet flow in addition to the different source/sink rates for the two solutes.

Another difference between the results for lactate and oxygen concentration is that oxygen concentration exhibits much less variation than lactate concentration. This is clearly linked to the non-zero oxygen concentration of the inflowing fluid. This is discussed further in Section 5.5.

$Pe$ (lactate)	Lactate concentration	Normalized lactate concentration	$Pe$ (oxygen)	Oxygen concentration	Normalized oxygen concentration
	M			M	
1.034E+05	5.756E-07	0.353	4.688E+04	2.157E-04	1.017
1.034E+04	8.835E-07	0.542	4.688E+03	2.144E-04	1.011
1.034E+03	1.309E-06	0.803	4.688E+02	2.132E-04	1.006
1.034E+02	1.630E-06	1.000	4.688E+01	2.120E-04	1.000
1.034E+01	2.144E-06	1.315	4.688E+00	2.102E-04	0.991
1.034E+00	2.950E-06	1.809	4.688E-01	2.087E-04	0.984
1.034E-01	5.054E-06	3.100	4.688E-02	2.087E-04	0.984
1.034E-02	5.786E-06	3.549	4.688E-03	2.087E-04	0.984
1.034E-04	5.882E-06	3.608	4.688E-05	2.087E-04	0.984

Table 4.7: Tabulated values showing the change of solute concentration averaged over the embryo surface as  $Pe$  changes. The solute concentrations are normalized with the corresponding default concentrations from Table 4.2.

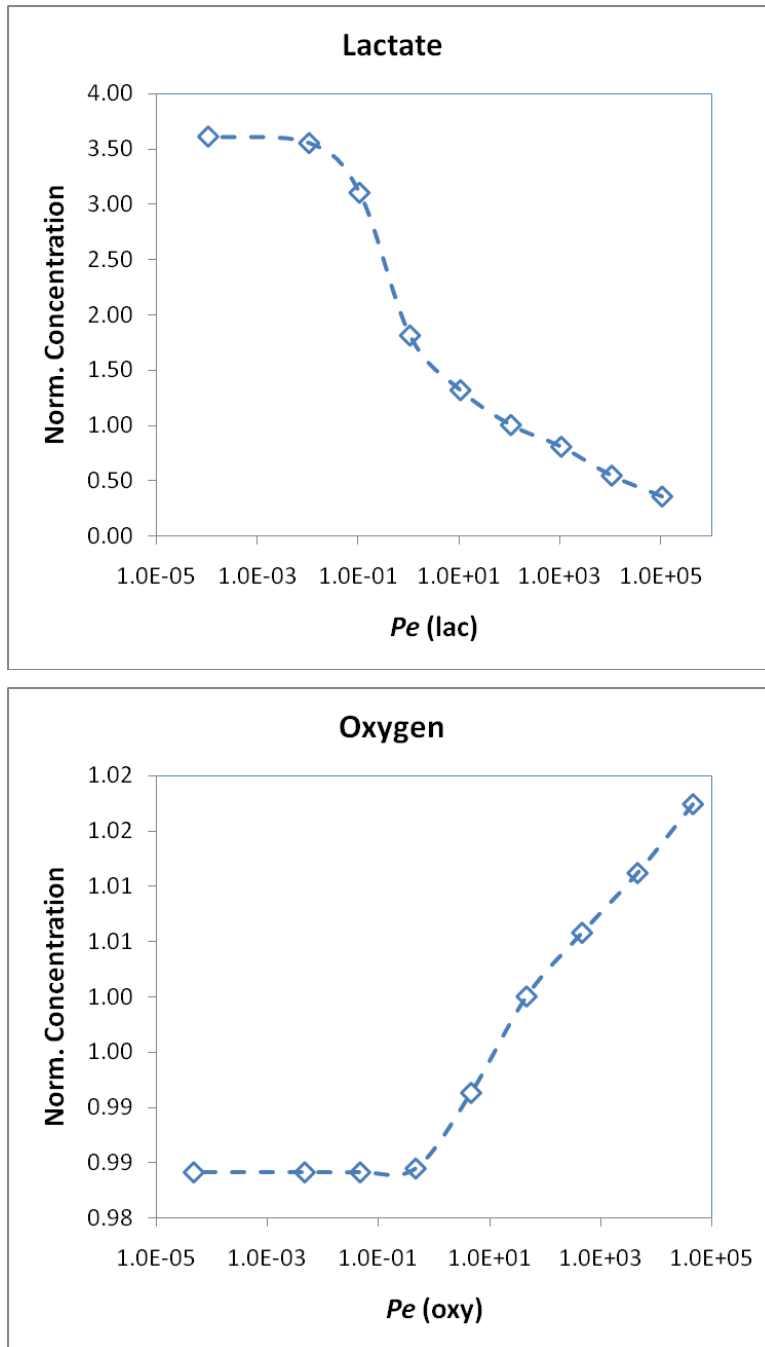


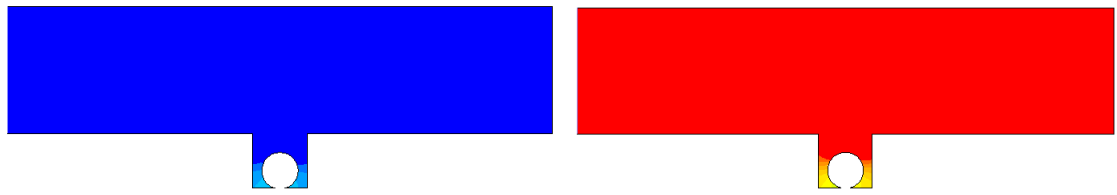
Figure 4.13: Changes of the solute concentration averaged over the embryo surface as  $Pe$  varies.

Examination on the solute concentration distribution in the modelling domain (Figure 4.14), especially at the region around the embryo, indicates that lowering the Reynolds number imposes a larger change to the solute distribution outside the cavity compared to the solute distribution inside the cavity.

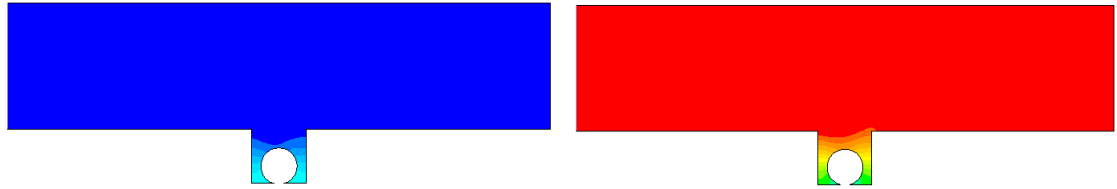
Solute distributions in the cavity in general have a fairly uniform gradient from the bottom to the top of the cavity. As highlighted in Figure 4.15, lactate and oxygen concentration distributions each have a similar shape for different Peclet numbers owing to the confinement of the cavity. For lactate, a high concentration level is found at the bottom of the embryo, where most of the lactate produced by the embryo is accumulated there as the solute transport at this location is impeded by minimal fluid movement; even for the highest Reynolds number cases considered (see Figure 4.12). This concentration level drops gradually as we transverse along the embryo circumference to the top of the embryo, where the lowest concentration level is observed. This corresponds well with the fact that the fluid movement is relatively stronger above the embryo helping to remove the lactate produced. Even without substantial advection, diffusion will be more efficient at the top in reducing lactate concentration there. On the other hand, for oxygen, a low concentration level is observed at the bottom of the embryo. Again, this is expected as the slow fluid movement at the bottom of the cavity hinders oxygen transport to this location so that transport is mostly through diffusion, even in the highest Reynolds number cases. The concentration level then rises gradually to a maximum value at the top of the embryo, once again consistent with the fact that the faster fluid movement here provides more oxygen.

For the highest Reynolds number cases studied, the concentration distribution of lactate and oxygen outside the cavity are similar. However, as  $Re$  is reduced, the solute distributions begin to differ as the effect of diffusion begins to surpass the effect of advection: for oxygen, a radial, uniform concentration gradient emanating from the embryo starts to form; for lactate, a concentration gradient occurs across the channel with the upstream of the cavity having a lower concentration level and the downstream of the cavity having a higher concentration level. Since oxygen has a higher diffusivity than lactate, oxygen experiences a stronger diffusion effect than lactate at the same

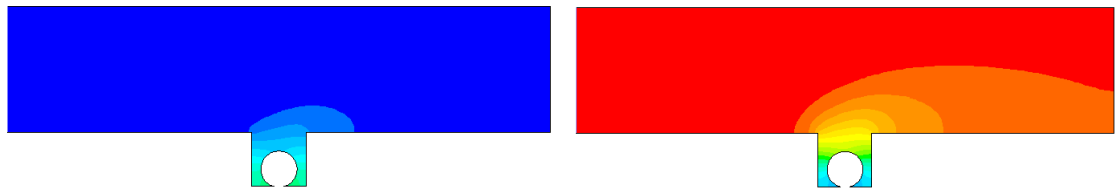
Reynolds number. A comparison of the solute concentration distribution on the entire modelling domain as  $Re$  decreases, in Figure 4.14, verifies this claim. As  $V$  drops from 1 m/s to  $1 \times 10^{-2}$  m/s, corresponding to  $Re$  changing from approximately 100 to 1, little difference is observed in the solute distribution (Figure 4.14a, 4.14b). As  $V$  falls to  $1 \times 10^{-4}$  m/s ( $Re \approx 0.01$ ,  $Pe_{\text{lactate}} \approx 10$ ,  $Pe_{\text{oxygen}} \approx 5$ ), the concentration gradient for oxygen is found to be much larger and extends out further than that for lactate (Figure 4.14c). This means that the bulk flow movement has a lesser effect on oxygen transport compared to lactate transport. As  $V$  is further decreased to  $1 \times 10^{-5}$  m/s, the concentration gradient profile for oxygen starts to stabilize and forms semi-circular shaped contours (Figure 4.14d to 4.14f, right). Comparatively, lactate requires a relatively slower  $V$  of  $1 \times 10^{-6}$  m/s to reach a similarly stabilized state with a transverse concentration gradient profile along the channel (Figure 4.14e and 4.14f, left).



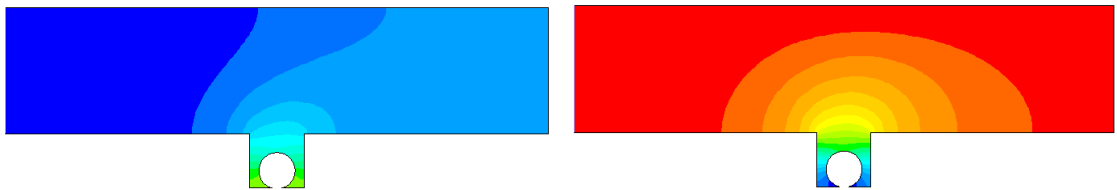
(a)  $V = 1 \text{ m/s}$



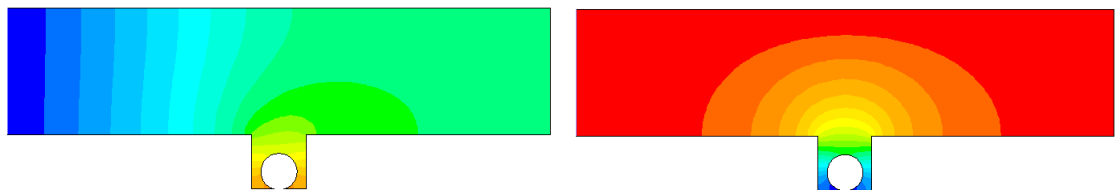
(b)  $V = 1 \times 10^{-2} \text{ m/s}$



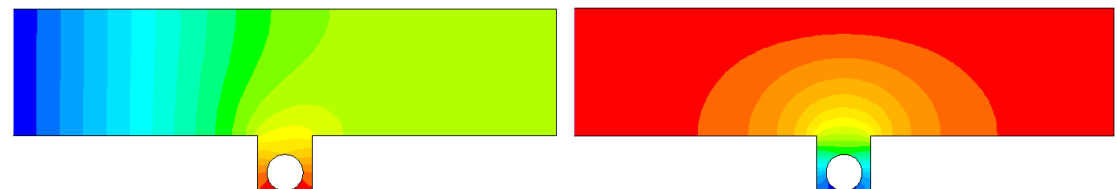
(c)  $V = 1 \times 10^{-4} \text{ m/s}$



(d)  $V = 1 \times 10^{-5} \text{ m/s}$



(e)  $V = 1 \times 10^{-6} \text{ m/s}$



(f)  $V = 1 \times 10^{-9} \text{ m/s}$



(Lactate concentration, measured in M)



(Oxygen concentration, measured in M)

Figure 4.14: Lactate (left) and oxygen (right) distribution. Here the contour level range for lactate and oxygen is set to be the same respectively to highlight the overall magnitude change as  $V(Re)$  is altered.

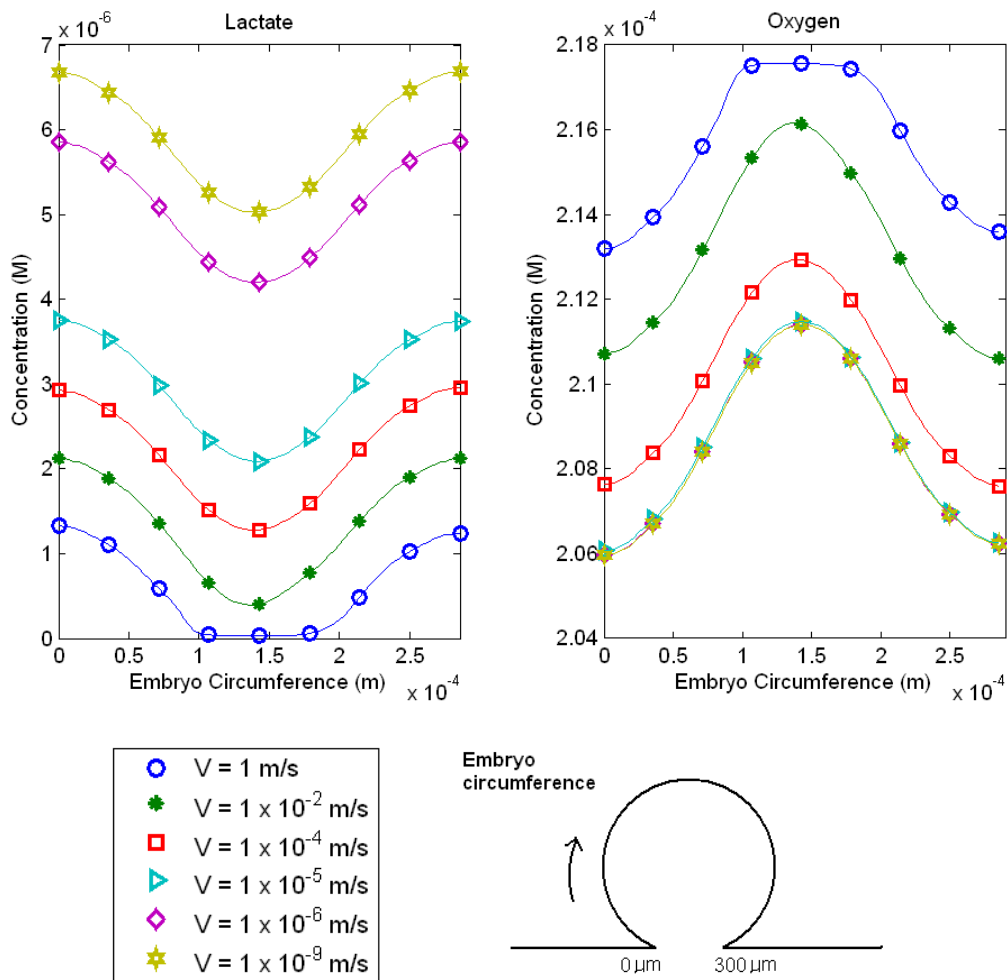


Figure 4.15: Comparison of lactate (top) and oxygen (bottom) concentration distribution on the embryo surface for different inflow rates

### 4.3.5 Implication for Solute Transport

Assuming that the diffusivities of the fluid and solutes are independent of species concentration and temperature (which is appropriate for this simulation of mouse embryo growth at 37°C), not surprisingly, species transport changes with respect to

inflow velocity can be categorized into two types: diffusion dominant for low  $V$  and advection dominant for high  $V$ .

There are three governing, but connected, parameters: the Reynolds number and the two solute Peclet numbers. Importantly, the Schmidt numbers of the two solutes are different, and they both differ significantly from unity. Hence while the flow undergoes transition from advection to diffusion dominated around  $Re \approx 1$ , the transition for oxygen and lactate occur at much lower Reynolds numbers, when the corresponding Peclet numbers reach approximately unity. This occurs for oxygen first before lactate. In this regime the oxygen and lactate concentrations in the neighbourhood of the embryo approach the no-flow case. These numerical experiments will provide some quantitative guidance on the appropriate operating domain once some more information on the optimal embryo environment becomes available from experimental programs.

Clearly the solute distributions at the embryo surface are non-homogeneous; especially noticeable is the distinct gradient between the bottom and the top of the embryo. Even the commonly used static flow embryo culture systems where the embryo sits on the bottom of a flask are likely to have concentration gradients between the bottom and top (due to the bottom surface limiting radial diffusion). While it has not been established whether such concentration profiles would be detrimental to embryo growth, this study ascertains that altering the inflow velocity within the range considered here does not affect the shape of the solute distributions within the cavity substantially although it does affect the levels, given constant absorption/excretion rates imposed in these simulations. Clearly, this latter assumption is somewhat of a crude idealisation and more work is required to construct a model allowing the local solute environment to influence solute uptake and waste generation.

#### **4.3.6 Changes in Embryo Shear Stress**

As indicated by Table 4.8 and Figure 4.16, embryo surface shear stress increases by  $10^9$  as the Reynolds number increases from  $Re = 1 \times 10^{-7}$  to  $Re = 100$ . This is expected, since as  $V$  increases, the flow past the cavity speeds up which also speeds up the flow circulations in the cavity, inducing a proportionately higher shear stress across the embryo surface.

Inflow velocity, $V$	$Re$	Shear stress	Normalized stress level
m/s		Pa	
1.000E+00	9.375E+01	1.624E+00	5.979E+02
1.000E-01	9.375E+00	3.427E-02	1.262E+01
1.000E-02	9.375E-01	2.716E-03	1.000E+00
1.000E-03	9.375E-02	2.703E-04	9.953E-02
1.000E-04	9.375E-03	2.703E-05	9.952E-03
1.000E-05	9.375E-04	2.703E-06	9.954E-04
1.000E-06	9.375E-05	2.709E-07	9.975E-05
1.000E-07	9.375E-06	2.784E-08	1.025E-05
1.000E-09	9.375E-08	1.484E-09	5.466E-07

Table 4.8: The shear stress (averaged across embryo surface) as  $V$  ( $Re$ ) varies is tabulated here. The shear stress is normalized by the default shear stress indicated in Table 4.2.

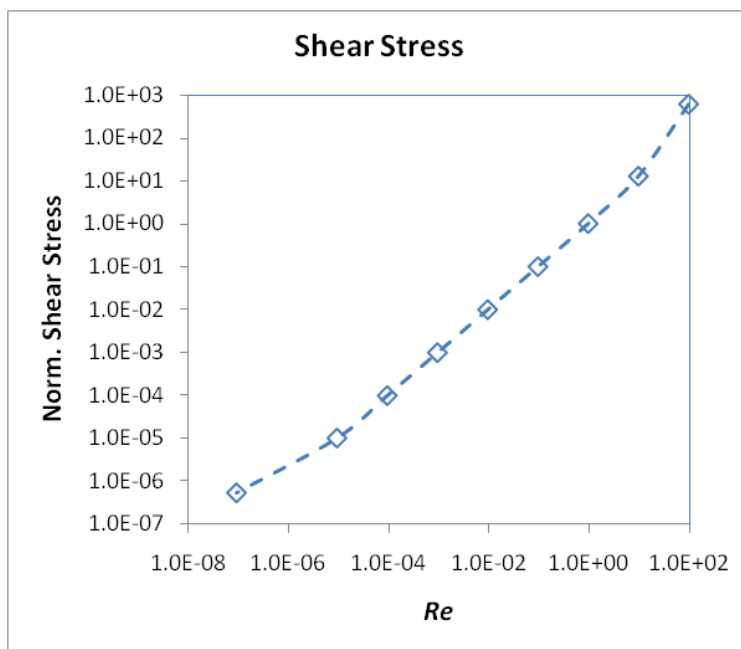
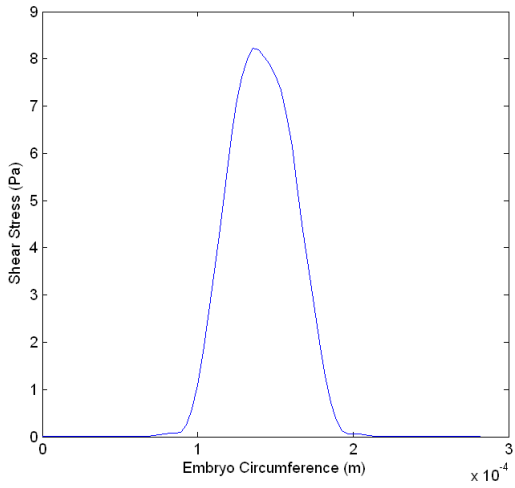


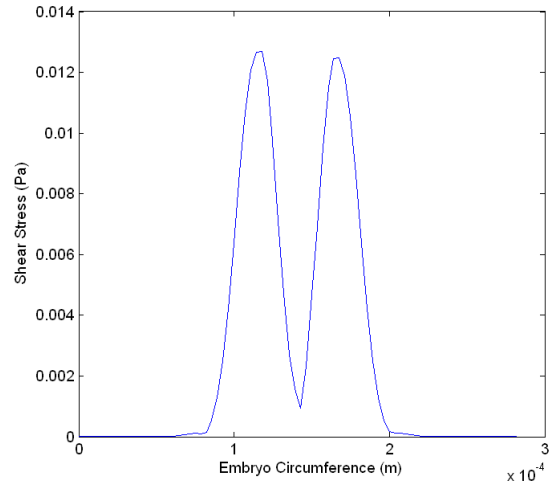
Figure 4.16: Normalized average shear stress across the embryo surface as  $V$  (indicated by  $Re$ ) is varied between 1 m/s and  $1 \times 10^{-9}$  m/s ( $Re$  variation from 93.8 to  $9.38 \times 10^{-8}$ ).

The distribution of shear stress along the embryo circumference is plotted in Figure 4.17. Similar to what was found in previous parametric studies, the distribution of the shear stress has a close connection with the flow structures within the cavity. Particularly, the locations of the peak stresses correspond well with the locations at which the flow recirculations interact with the embryo surface. When  $V$  is at 1 m/s ( $Re \approx 100$ ), a large

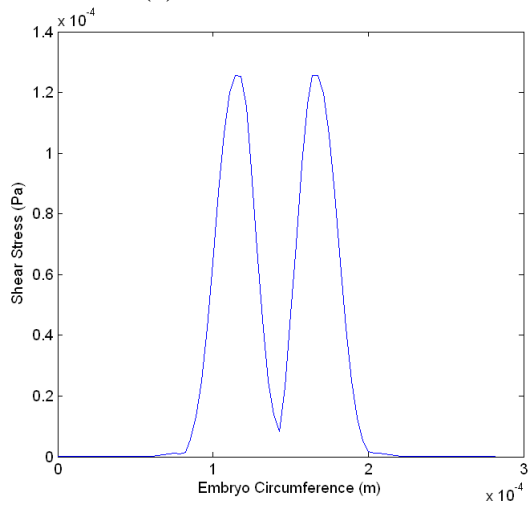
flow recirculation sits above the embryo and four smaller eddy recirculations appear beside it (Figure 4.12a). As the strength of the large flow recirculation is much higher than the induced eddy recirculations, this causes the peak shear stress to occur at the top of the embryo, (Figure 4.17a). As  $V$  drops, the main recirculation of the previous state breaks into two smaller recirculations (Figure 4.12b), and consequently this leads to the single shear stress maximum to split into two peaks. The other recirculations are too weak to induce any significant stress levels on the embryo (Figure 4.17b). As  $V$  is decreased further, moving into the diffusion dominated regime, the peaks become symmetrical and there is little further change to the shape of the overall stress distribution (Figure 4.12c to 4.12e). In this regime the shear stress at any point is directly proportional to the inflow velocity (or the Reynolds number).



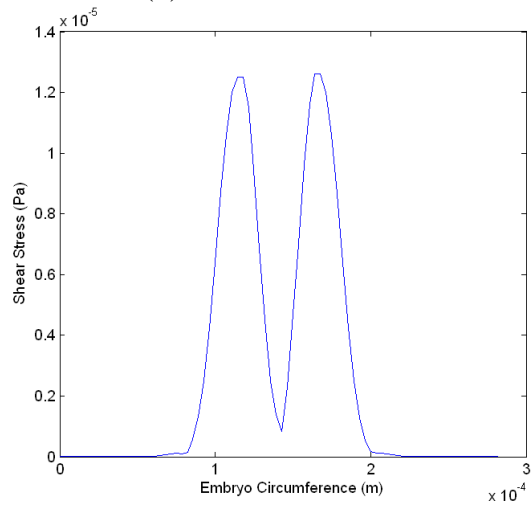
(a)  $V = 1 \text{ m/s}$



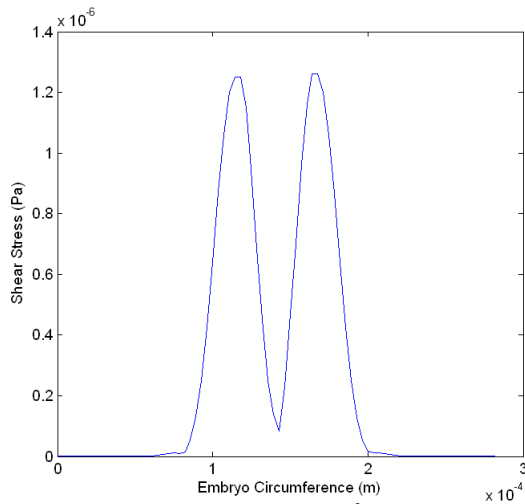
(b)  $V = 1 \times 10^{-2} \text{ m/s}$



(c)  $V = 1 \times 10^{-4} \text{ m/s}$



(d)  $V = 1 \times 10^{-5} \text{ m/s}$



(e)  $V = 1 \times 10^{-6} \text{ m/s}$

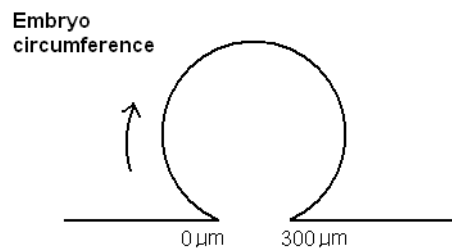


Figure 4.17: Shear stress distribution along the embryo surface for the variation of  $V$  from  $1 \text{ m/s}$  to  $1 \times 10^{-9} \text{ m/s}$ .

#### **4.3.7 Implications for Shear Stress Changes and Summary**

In general and unsurprisingly, decreasing the inflow rate significantly lowers the shear stress on embryo surface. As evidenced from Figure 4.16, a logarithmic decrease of  $Re$  induces a logarithmic decrease in the shear stress level. For Reynolds numbers of unity or below the relationship is effectively linear, since the flow pattern within the cavity remains (virtually) the same.

The shear stress distribution is determined by the main flow structures within the cavity. This finding is also observed in other parametric studies. This suggests that one can at least qualitatively predict the stress distribution on the embryo by observing the flow structure around the embryo. This may be useful in the application of growing embryos or any other cell types given visualisation is easier to implement experimentally than measuring the shear stress.

Combining the results presented in this subsection with those from the aspect ratio study show the strong dependence of shear on the rapidly spatially varying flow environment of this type of bioreactor. For practical bioreactors these results indicate that good control over the embryo shear stress can be accomplished through a combination of inflow rate and cavity aspect ratio changes.

## 4.4 Culture Medium Height Parametric Study

This section details an investigation into the effect of the height of the culture medium on the operation of the micro-bioreactor. The setup is illustrated in Figure 4.18 below. The *height* is the distance measured from the free surface of the culture medium to the bottom surface of the channel.

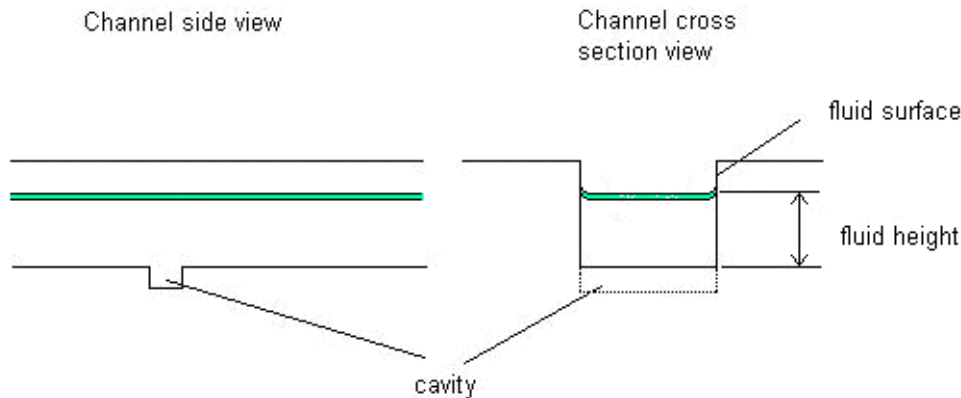


Figure 4.18: Sketch showing the height of the culture medium in the channel.

Due to the open channel design of the bioreactor, the height of this culture medium could depend on the inflow rate at the channel inlet given that the geometry of the channel is fixed. Alternatively a downstream weir could be used to control the height independently of the flow rate. The height will have some impact on the solute transport and shear stress on the embryo, especially in the low Reynolds number regime, where the initially uniform inflow velocity will relax to the equilibrium velocity profile well before reaching the cavity.

In this section, the setup of the models and simulations for this study is described. As previously, an analysis of the results of solute transport in the form of lactate production and oxygen uptake by the embryo is given. This is followed by an examination of the effect on the shear stress distribution. The section concludes by discussing the implications for bioreactor performance.

### 4.4.1 Problem Setup

In order to evaluate the effect of inflow fluid height, six geometric models are constructed to simulate the flow in the bioreactor for the steady-state case. The difference between these models is in the culture medium height ( $D_f$ ), as illustrated in

Figure 4.19 below. Other geometric features of the model such as cavity depth, length and embryo size, as well as the boundary conditions of the simulations, such as culture medium inflow rate, solute transport exchange rate and material properties, are fixed for all the simulations.

The culture medium heights selected for this study are tabulated in Table 4.9. It is found that this range of fluid height is sufficient to provide a good qualitative parametric study. In presenting the findings, the heights ( $D_f$ ) are normalized by the cavity depth,  $D$ , to form non-dimensional culture medium heights, i.e.,  $D_f^*=D_f/D$ . Here,  $D$  is fixed at 150  $\mu\text{m}$ .

Medium height, $D_f$ $\mu\text{m}$	Normalized Medium height, $D_f^*$
75	0.5
150	1.0
225	1.5
350	2.3
450	3.0
750	5.0

Table 4.9: Values of the modelled culture medium height selected for this study.

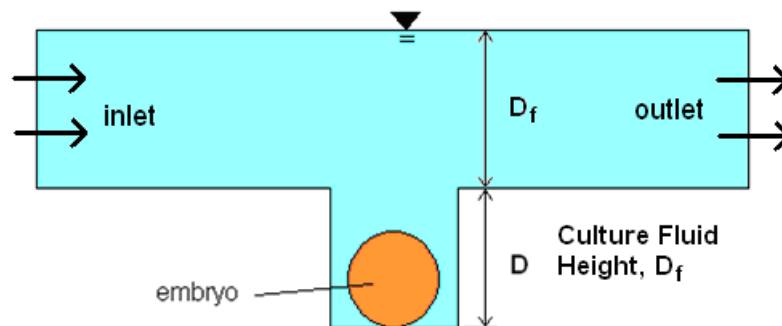


Figure 4.19: Sketch of the 2D model showing the two heights: the height of the culture medium  $D_f$  and cavity depth  $D$ .

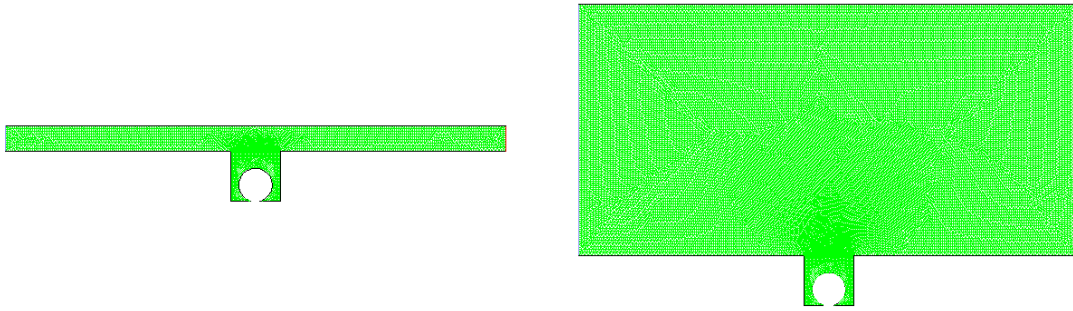


Figure 4.20: Two meshed models for fluid height parametric study: a shallow fluid height of  $D_f^* = 0.5$  (left) and a deep fluid height of  $D_f^* = 5.0$  (right).

#### 4.4.2 Solute Concentration Changes with Culture Medium Height

It is observed that the solute concentration on the embryo changes consistently (Figure 4.21), with lactate concentration increasing and oxygen concentration decreasing as  $D_f^*$  is increased. The variation is only slightly non-linear. Note that this default case corresponds to  $Re \approx 0.1$ ,  $Pe_{\text{lactate}} \approx 100$ ,  $Pe_{\text{oxygen}} \approx 50$ . When  $D_f$  is 50% of the depth of the cavity, the lactate concentration is 17% below the default lactate concentration and the oxygen concentration is 0.4% above the default oxygen concentration. However, when  $D_f$  is increased to 500% of the cavity depth, there is a 9% increase in lactate and a 0.24% decrease in oxygen concentration from the default values. Also, the magnitude change of oxygen is found to be considerably less than lactate. The reason for this is explained in Section 5.5.

Normalized medium height, $D_f^*$	Lactate concentration	Oxygen concentration	Normalized lactate concentration	Normalized oxygen concentration
	M	M		
0.5	1.36E-06	2.130E-04	0.833	1.004
1.0	1.47E-06	2.126E-04	0.904	1.003
1.5	1.55E-06	2.123E-04	0.949	1.001
2.3	1.63E-06	2.120E-04	1.000	1.000
3.0	1.68E-06	2.119E-04	1.030	0.999
5.0	1.77E-06	2.115E-04	1.090	0.998

Table 4.10: Tabulated values showing the averaged solute concentrations evaluated from the simulations for different fluid heights. The normalized fluid height is obtained by dividing the fluid height by the cavity depth. The solute concentrations are normalized with the respective default lactate and oxygen concentration from Table 4.2.

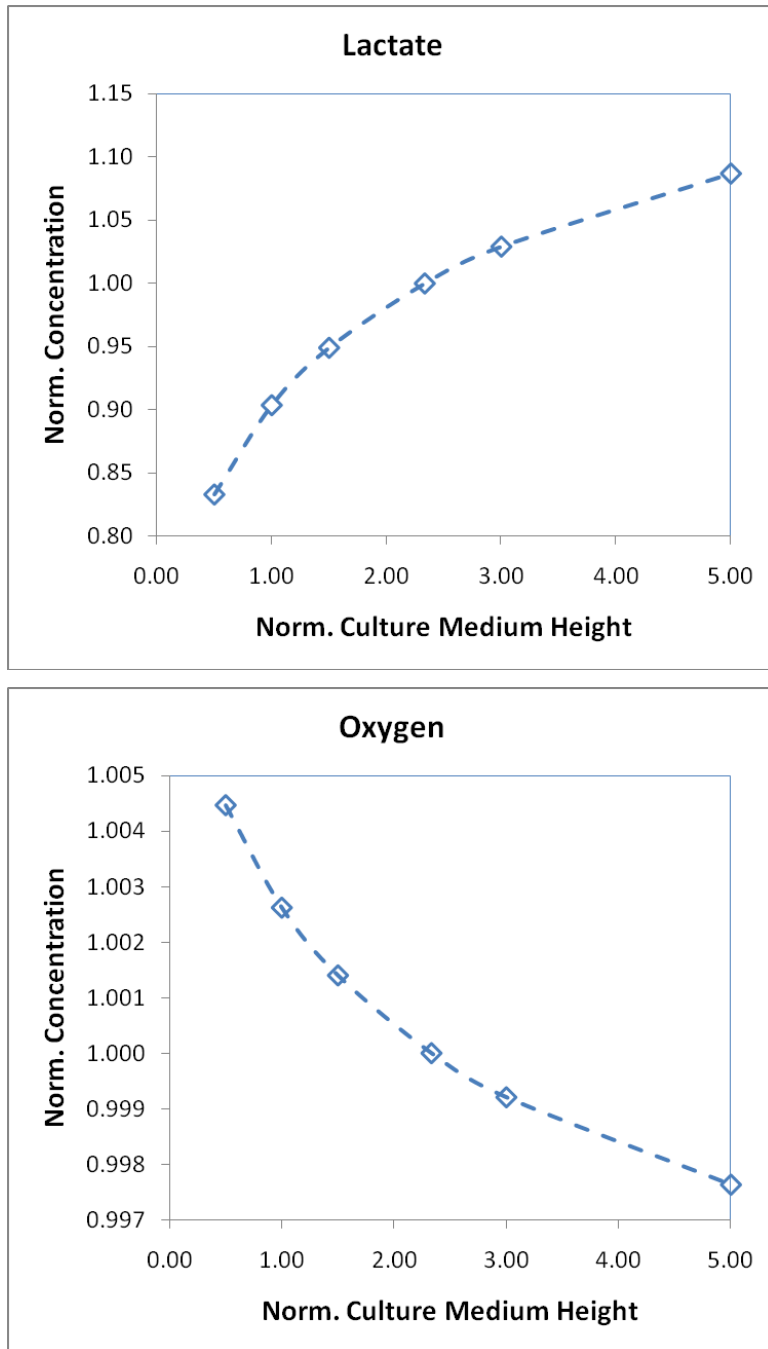


Figure 4.21: Lactate (top) and oxygen (bottom) concentration changes with  $D_f^*$ .

From the observations above, solute transport is reduced when the depth of the culture medium flowing through the channel is larger. This effectively means that less lactate is being removed from the cavity, causing the lactate concentration in the cavity to rise. Concurrently, less oxygen is being transported into the cavity, causing the oxygen concentration to drop.

An inspection of the local flow environment at the cavity opening indicates that as  $D_f^*$  increases, the horizontal fluid velocity flowing across the opening decreases as shown in Figure 4.22. This is because as the fluid becomes shallow, the free surface of the channel is closer to the bottom of the channel, directly increasing the velocity gradient extending from the bottom surface of the channel to the top free surface, as shown in Figure 4.23. When the fluid is shallow, the faster fluid movement at the cavity opening induces a stronger flow recirculation in the cavity, enhancing solute transport, causing more lactate to be removed from, and more oxygen to be supplied to, the cavity. The opposite occurs when the fluid is deeper.

A further understanding of this behaviour can be achieved by considering the velocity profile immediately upstream of the cavity. For the low Reynolds number considered here the velocity should effectively reach its equilibrium half-parabolic profile prior to passing across the top of the cavity. This means that the normal velocity gradient at the surface will be proportional to the channel depth. Thus, it should be the velocity gradient – rather than the inflow velocity – that approximately determines the strength of the recirculation within the cavity. Effectively increasing the channel height should give a similar result to decreasing the Reynolds number. For the base case considered here, the Peclet numbers are still considerably greater than unity; hence solute transport is dominated by advection, while the flow is diffusion dominated. Thus, from the latter, decreasing the depth should result in an approximately proportional increase in cavity circulation, which is borne out from the results in Table 4.11, and hence a corresponding increase in solute transport through advection.

Normalized medium height, $D_f^*$	Averaged velocity across opening	Horizontal velocity component	Vertical velocity component
	m/s	m/s	m/s
0.5	3.40E-04	3.12E-04	9.83E-09
1.0	1.94E-04	1.81E-04	2.41E-08
1.5	1.31E-04	1.23E-04	-1.27E-09
2.3	8.44E-05	7.97E-05	-4.09E-09
3.0	6.47E-05	6.11E-05	8.93E-09
5.0	4.02E-05	3.82E-05	1.70E-08

Table 4.11: The change in  $D_f^*$  brought about a change in the averaged velocity across the cavity opening, together with their respective horizontal and vertical velocity component.

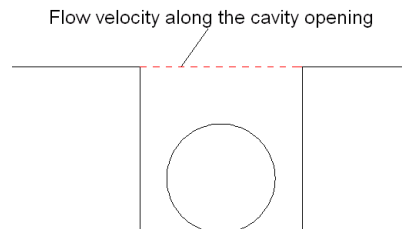
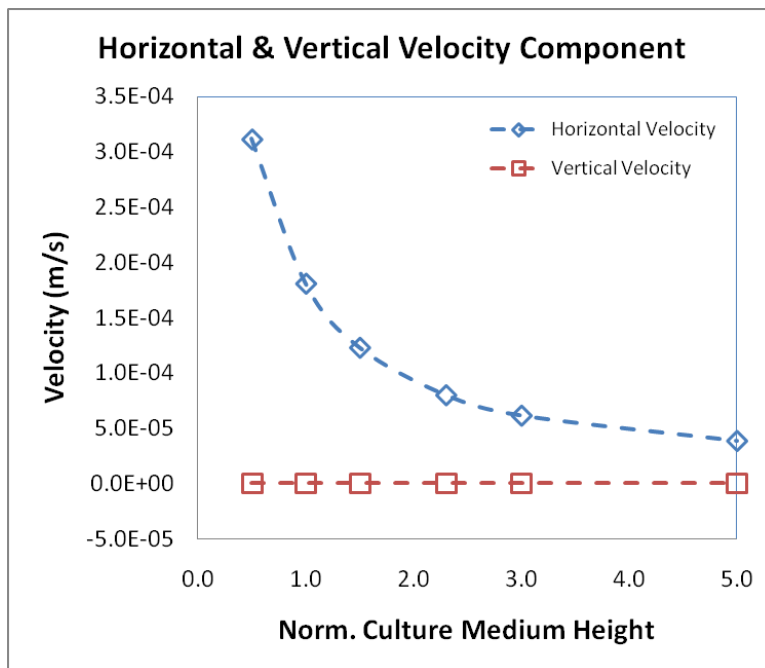
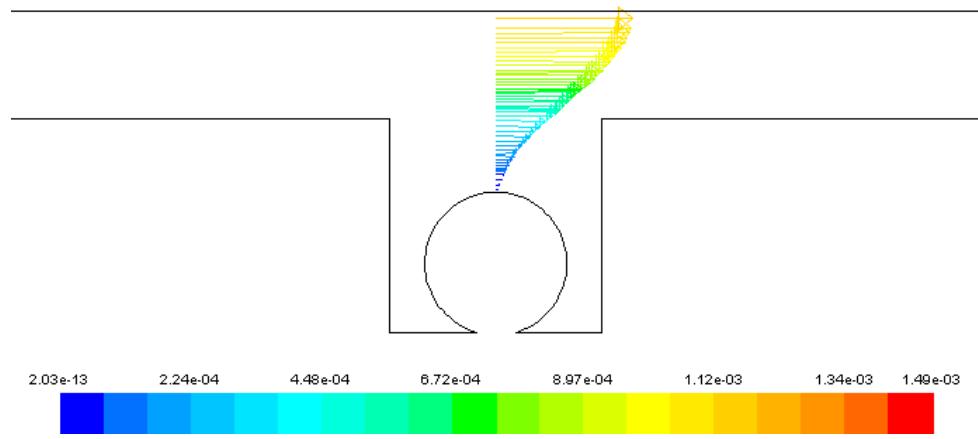
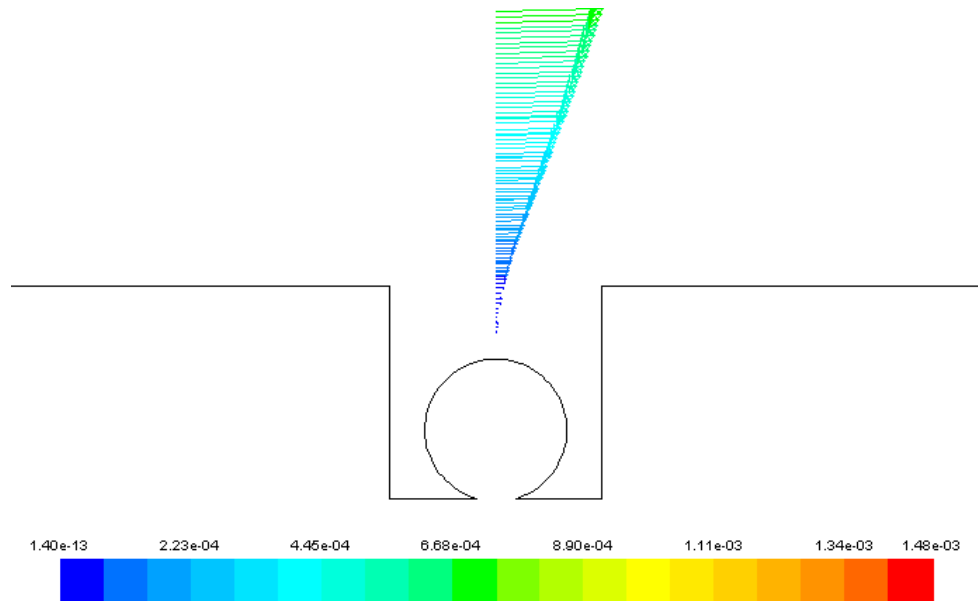


Figure 4.22: Averaged horizontal and vertical velocity components of the averaged velocity across the cavity opening for five different fluid heights.



(a)  $D_f^* = 0.5$



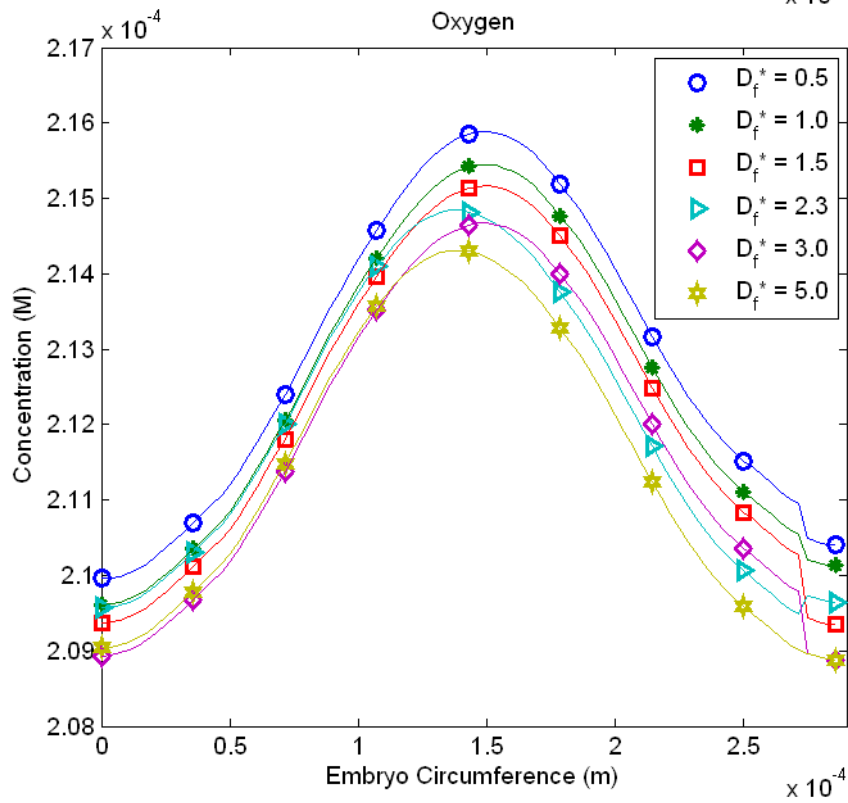
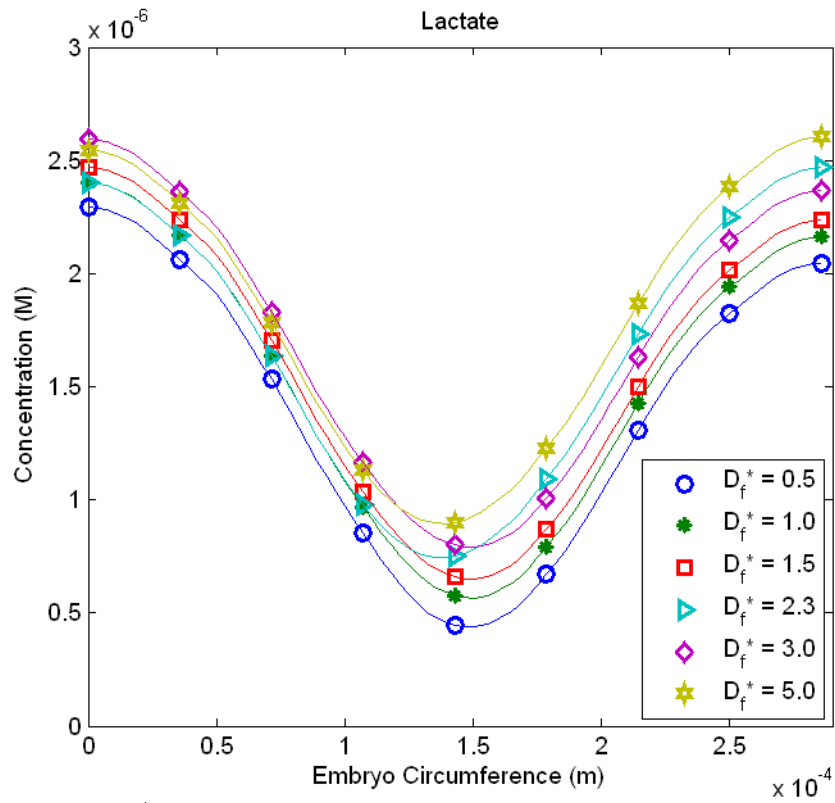
(b)  $D_f^* = 5.0$

Figure 4.23: Velocity (measured in m/s) vector plots demonstrating how the vertical velocity gradient changes as  $D_f^*$  changes. Note the velocity gradient at the height level of the cavity opening: (a) a lower  $D_f^*$  induces faster fluid movement; while (b) a higher  $D_f^*$  causes a slower flow movement.

### 4.4.3 Solute Distribution around the Embryo

In general, the distribution profiles of solute around the embryo remain similar regardless of the  $D_f^*$  changes. This can be seen from the solute concentration plots of lactate and oxygen in Figure 4.24. Similar to the previous studies, for lactate, the profile starts off with a high concentration level at the lower part of the embryo. This concentration level then drops to the lowest value at the top of the embryo. The exact opposite situation occurs for oxygen concentration. The most apparent difference as  $D_f^*$  is varied is in the overall magnitude of the concentration level. This finding reinforces the hypothesis of small solute concentration changes due to  $D_f^*$  changes mentioned previously in Section 4.4.2.

In more detail, low oxygen concentration occurs in the lower region of the cavity as this region clearly receives less oxygen (Figure 4.25, right). Towards the cavity opening the solute concentration is relatively much higher. The curvy iso-concentration lines at the cavity opening indicate that the concentration distribution is much affected by the flow penetration from the main channel. Similar observations are found for lactate concentration distribution (Figure 4.25, left) with the distribution reversed.



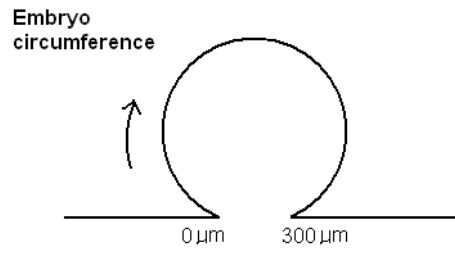
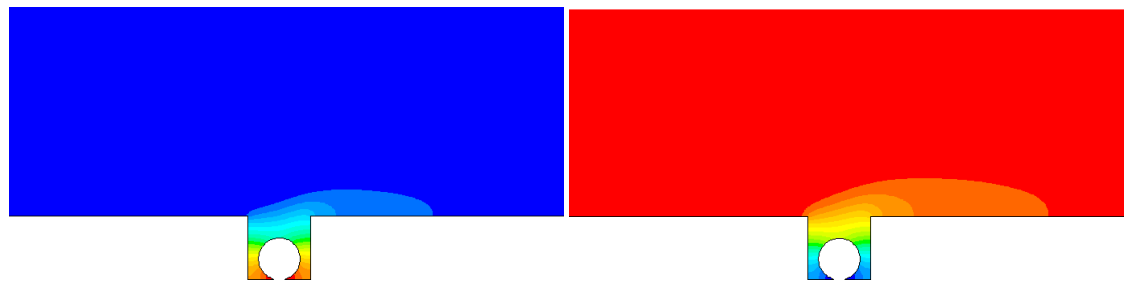
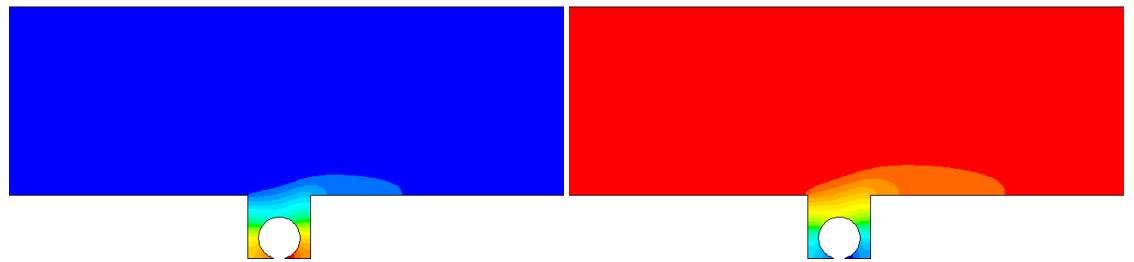


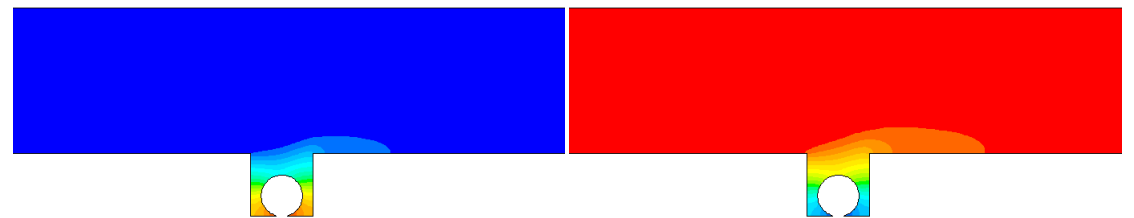
Figure 4.24: Lactate (top) and oxygen (bottom) concentration distribution on the embryo surface for different  $D_f^*$ .



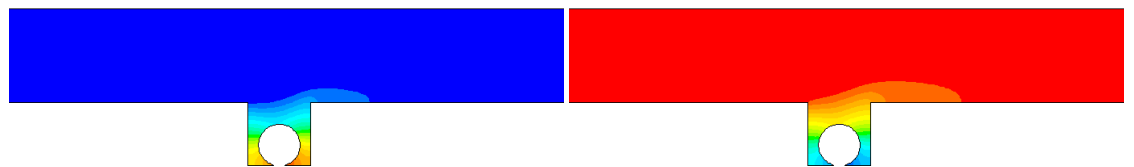
(a)  $D_f^* = 5.0$



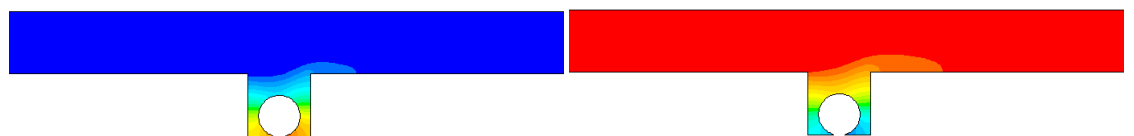
(b)  $D_f^* = 3.0$



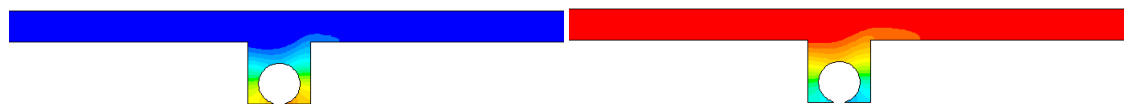
(c)  $D_f^* = 2.3$



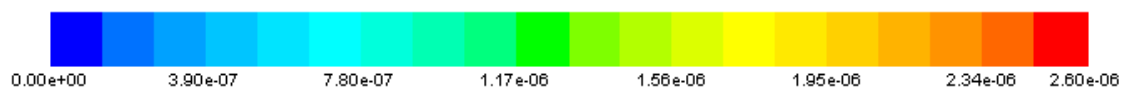
(d)  $D_f^* = 1.5$



(e)  $D_f^* = 1.0$



(f)  $D_f^* = 0.5$



(Lactate concentration, measured in M)

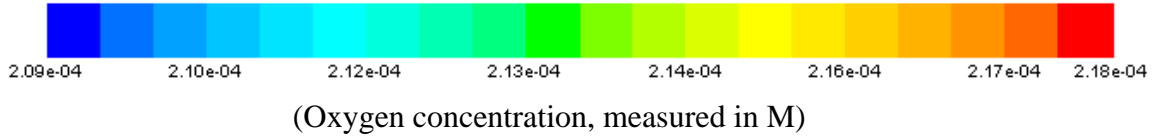


Figure 4.25: Lactate (left) and oxygen (right) concentration distribution for different  $D_f^*$ .

#### 4.4.4 Implication for Solute Transport

A drastic change of the solute concentration is detected when the fluid height is increased up to the depth of the cavity ( $D_f^* = 1.0$ ). This change then becomes less drastic as  $D_f^*$  is increased further. This shows that solute transport is more sensitive when the height of the culture medium flowing in the channel is shallow. This is not surprising since  $D_f^*$  is effectively a measure of the velocity gradient length scale to the cavity width. If this is reduced to below unity, there should be a more significant readjustment as the fluid passes over the cavity. This is clearly observed from the particle tracer plots, where the  $D_f^* = 0.5$  case is clearly different from the others. Fluid penetration into the cavity is much greater.

Broadly, for the parameters studied here, the solute concentration distribution profiles on embryo surface and the concentration contours in the cavity are similar regardless of the different  $D_f^*$ . This suggests that a change in fluid height does not have much impact on the solute distribution around the embryo in the cavity. However, recall that the base parameters used for this series of simulations correspond to  $Re \approx 0.1$ ,  $Pe_{\text{lactate}} \approx 100$ ,  $Pe_{\text{oxygen}} \approx 50$ . Since changing the depth is expected to have a similar effect to changing the Reynolds number, at least for the larger depths, the depth variation explored here still means that the flow is diffusion dominated and the solute transport is advection dominated for all cases.

#### 4.4.5 Shear Stress Changes with Culture Medium Height

Table 4.12 and Figure 4.26 uncover that the averaged shear stress across the embryo surface decreases sharply from 450% to 150% of the default shear stress, when  $D_f^*$  is elevated from 0.5 to 1.5. After that, the stress level stabilized to a steady drop down to 64.5% of the default shear stress, as the fluid height continued to increase from 1.5 to 5.0. This trend is considerably different from the trend change of solute concentration, where there is a near linear dependence (Figure 4.21).

Norm medium height, $D_f^*$	Shear stress	Normalized shear stress
	Pa	
0.5	1.21E-03	4.49
1.0	5.24E-04	1.94
1.5	3.62E-04	1.34
2.3	2.70E-04	1.00
3.0	2.39E-04	0.88
5.0	1.74E-04	0.65

Table 4.12: Tabulated values of the calculated averaged shear stress across the embryo surface for different  $D_f^*$ . The shear stress is normalized by the default shear stress as shown in Table 4.2.

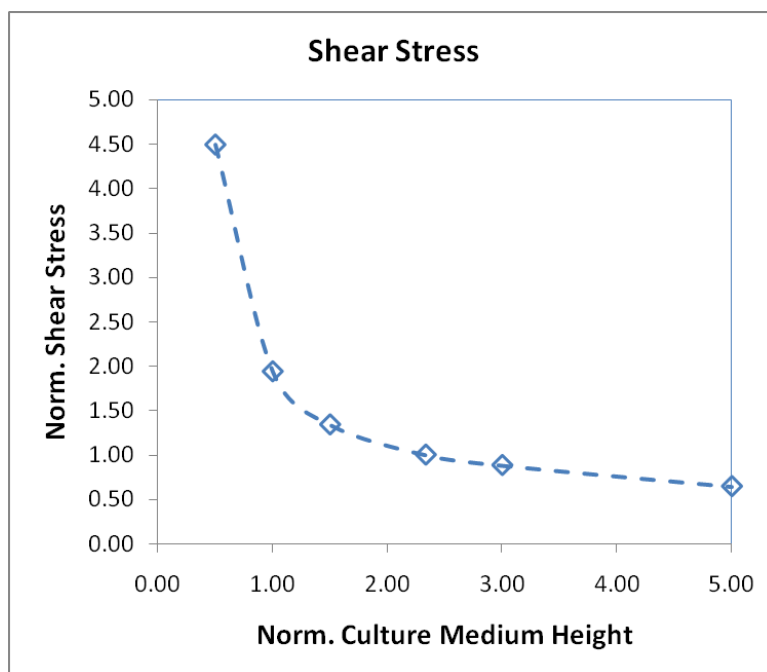


Figure 4.26: Changes of the normalized averaged shear stress distribution across the embryo surface as  $D_f^*$  varies.

The cause can be related to the variation of the local velocity field as  $D_f^*$  is varied. As shown in Figure 4.22, the horizontal velocity decreases sharply then gradually levels off as  $D_f^*$  changes from a shallow to a deep height. This will slow the flow recirculations in the cavity, which shear the embryo surface. As the surface shear stress is proportional to the normal velocity gradient at the embryo surface, this means that the shear stress will be high where the recirculation flow is tangential to the surface.

The overall magnitude of the shear stress on the embryo is closely related to the fluid condition near the cavity opening. A shallow culture medium flow in the channel leads to more culture medium entering the cavity, raising the flow velocity near the top of the embryo, and in turn speeding up the induced flow recirculations. A deep culture medium flow leads to lower penetration into the cavity, resulting in a much lower direct stress at the top of the embryo.

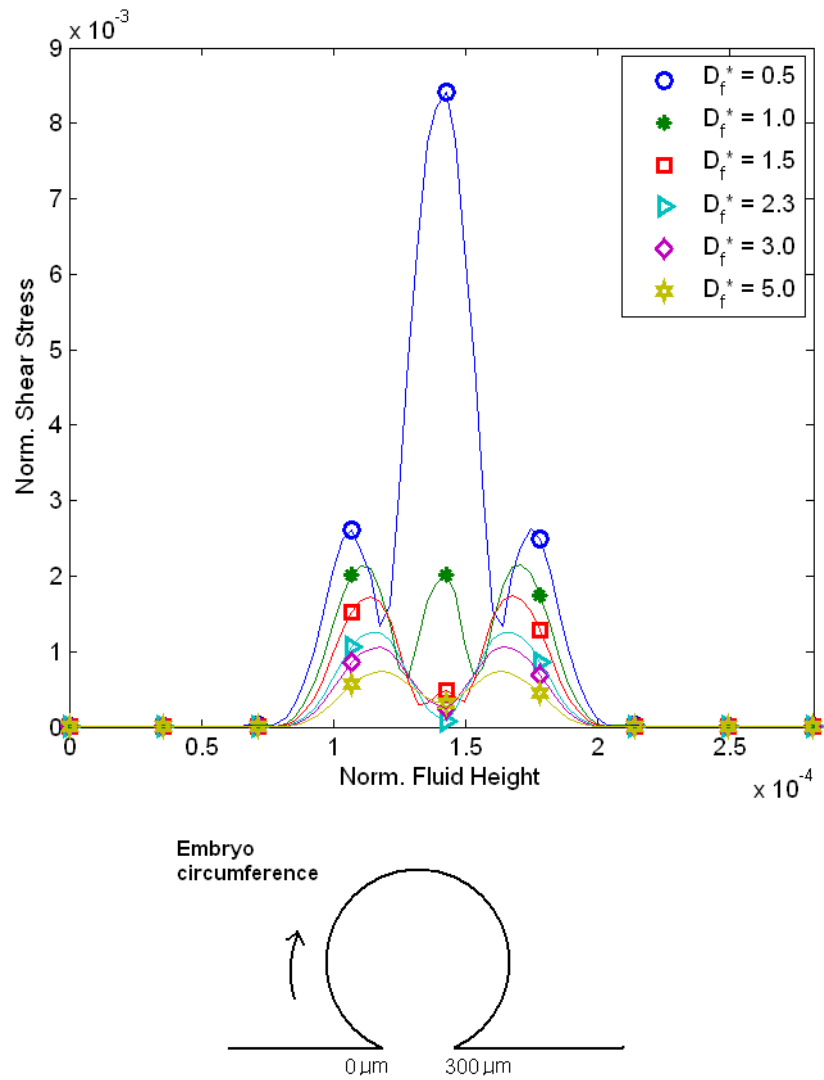
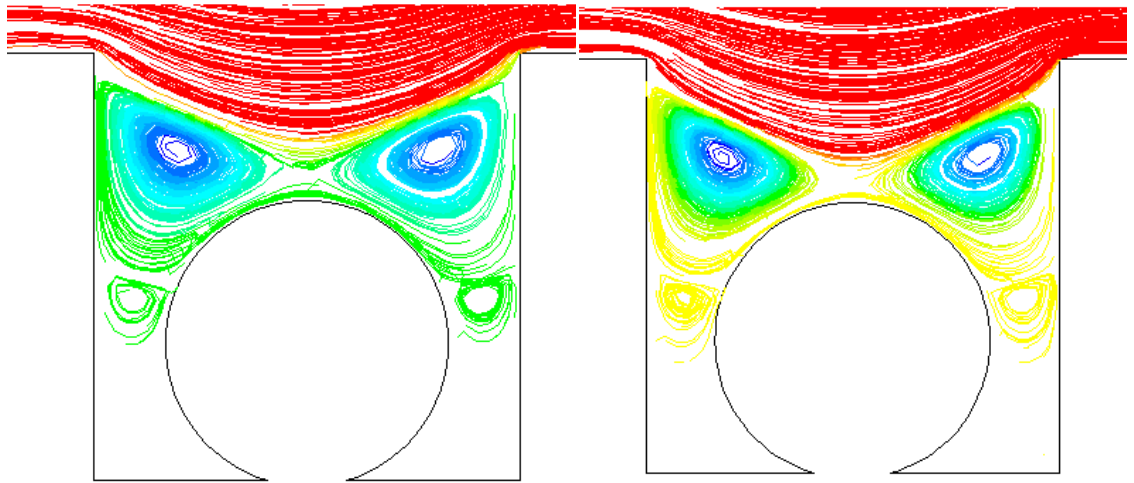


Figure 4.27: Comparison of embryo surface shear stress distribution along the embryo circumference for different  $D_f^*$ .

The shear stress distribution on the embryo surface differs with different  $D_f^*$ . On the whole, multiple peaks of stress occur around the top section of the embryo surface. Starting with  $D_f^* = 0.5$ , three peaks are detected, with the middle peak that corresponded to the top point on the embryo, having a significantly higher peak stress. If  $D_f^*$  is increased to 1.0, the magnitude of these peaks drop, the most significant change being the level of the middle peak is reduced significantly from previous value. If  $D_f^*$  is further increased to 2.3, the middle peak is then much lower than the two surrounding peaks. Further increases lead to a further reduction in the magnitude of the side peaks as would be expected.

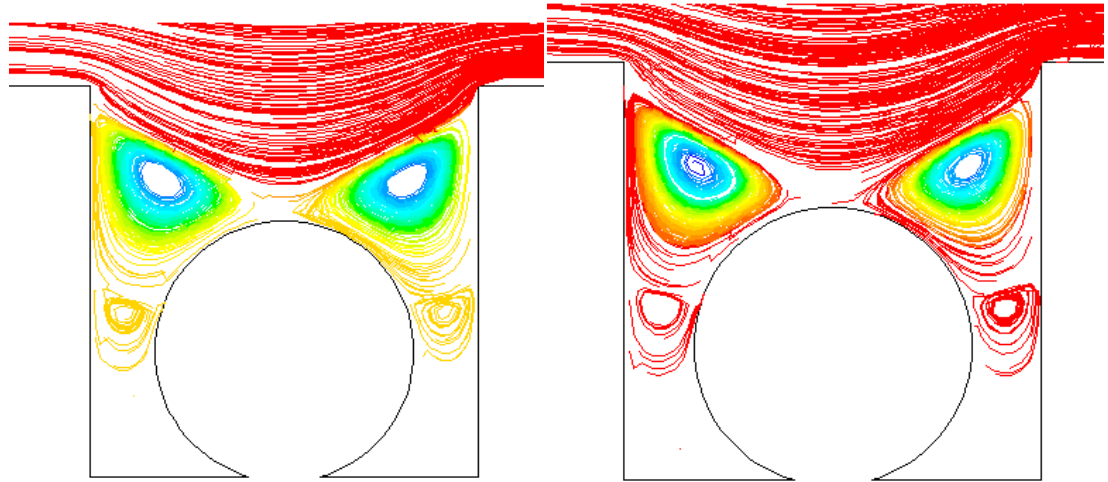
Similar to previous studies, the changes can be understood by relating them to the interaction between fluid flow structures in the cavity with the embryo surface, as presented in particle trajectory plots of Figure 4.28. For the case of shallow fluid heights ( $D_f^* = 0.5$ , Figure 4.28f), fluid flow from penetration into the cavity directly reaches the top part of the embryo as implied above; this causes a high peak stress to occur there. The two flow recirculations at the sides of the embryo cause two smaller stress peaks to be induced there.

The main differences from this case are as follows. As  $D_f^*$  is increased the penetration reduces so that the channel fluid does not reach the top of the embryo. For larger height ratios the side recirculations link up to form a separatrix above the top of the embryo; this results in the stress peak at the top of the embryo disappearing. The side recirculations maintain a similar shape over the range of  $D_f^*$  studied, with the main difference that their centres migrate towards the top of the embryo for increasing  $D_f^*$  as their strength reduce (see Figures 4.28a-e).



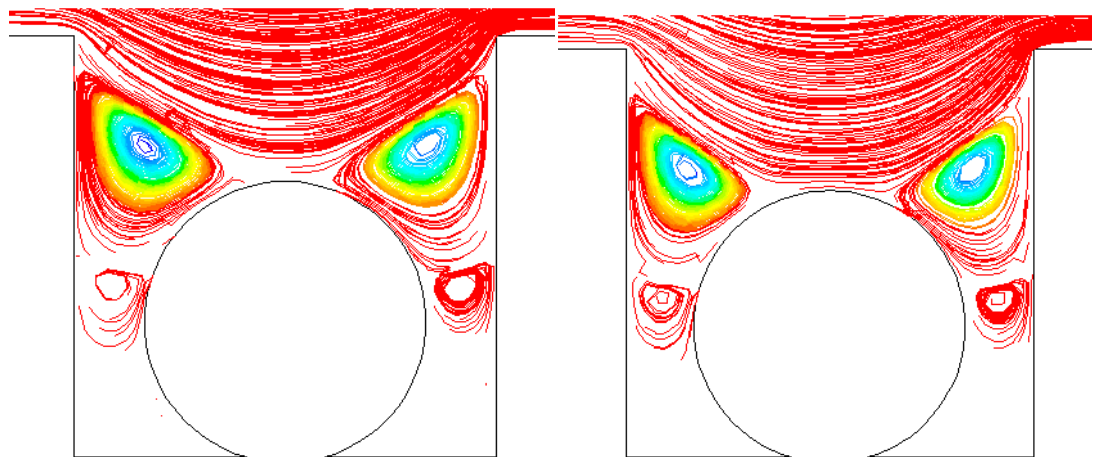
(a)  $D_f^* = 5.0$

(b)  $D_f^* = 3.0$



(c)  $D_f^* = 2.3$

(d)  $D_f^* = 1.5$



(e)  $D_f^* = 1.0$

(f)  $D_f^* = 0.5$



Figure 4.28: Particle trajectory plots demonstrating how the flow recirculations around the embryo change as  $D_f^*$  changes. The colours indicate the value of the streamfunction measured in kg/s.

#### 4.4.6 Implication for Shear Stress Changes

To summarize, increasing the height of the culture medium alleviates the embryo shear stress. The drastic fall in shear stress occurs when  $D_f$  is increased up to the depth the cavity. Fluid heights larger than the depth of the cavity will continue to decrease the shear stress, but the effect reduces once the channel fluid does not penetrate enough to directly interact with the top surface of the embryo. Consequently, it may be advisable to maintain a level of culture medium larger than the depth of the cavity ( $D_f^* > 1.0$ ) to ensure the embryo does not experience large local stresses that might be detrimental to its growth and viability.

Shear stress distribution is clearly far from uniform and varies as  $D_f^*$  is altered. The most significant effect is the very large peak stress that occurs at the top of the embryo when the height of the culture medium is smallest ( $D_f^* = 0.5$ ). For  $D_f^* > 1.0$  the peaks reduce in magnitude and there is less variation around the circumference.

Clearly, these results are dependent on Reynolds number. Broadly, the previous studies show shear stress varies almost directly with Reynolds number. Fluid media depth changes can be considered to be effective Reynolds number changes – since the velocity scale at the top of the cavity can be related to the velocity gradient of the channel fluid multiplied by an appropriate length scale, such as the cavity width. For small  $D_f^*$ , there is considerable direct penetration of the channel flow into the cavity potentially leading to very high and undesirable stress at the top of the embryo. This needs to be taken into account in optimising bioreactor design.

#### 4.4.7 Conclusion and Summary

For this study, six models were created, each with a different  $D_f^*$ , to examine the solute transport and shear experienced by an embryo. Attention is focussed on the fluid environment around the cavity opening, where the flow velocity at the opening and particle trajectories within the cavity were observed. This is because the fluid

environment there is the dominating factor in controlling the solute transport and shear stress.

It is established that a small  $D_f^*$  brings about faster solute transport but higher shear stress, with the opposite true for large  $D_f^*$ . The solute concentrations change at a near constant rate with  $D_f^*$ , while the shear stress at first drops drastically, when  $D_f$  is less than the depth of the cavity ( $D_f^* < 1.0$ ), and then the rate of change reduces when the fluid height is more than the depth of the cavity.

The surface solute concentration distribution on the embryo is virtually identical as  $D_f^*$  varies, with the lowest lactate concentration level and highest oxygen concentration level recorded at the top of the embryo. The shear stress distribution does differ with different  $D_f^*$ , with the profiles highly dependent on flow penetration from the channel into the cavity.

To conclude, it seems reasonable to require the height of the culture medium flowing in the channel to be at least deeper than the depth of the cavity, to reduce the direct shear from the channel flow.

## 4.5 Embryo Growth Parametric Study

During *in-vitro* cultivation, there are five stages which are commonly used to describe the growth of an embryo (Gor and Lucassen 1993). In essence, the growth phases of interest here include the period from after fertilization to before formation of the foetus.

These stages are:

1. 1-cell stage
2. 2-cell stage
3. 4-cell stage
4. morula stage
5. blastocyst stage

When cultivating from the 1-cell to the blastocyst stage, the embryo size is reported to enlarge about 50% from its initial size and varies its solute uptake and production rates. Chung (Chung 1973) completed an investigation on mouse embryo size changes as the embryo develops from a fertilized ovum to a foetus. In his paper, he observed that the embryo varies from 85  $\mu\text{m}$  to 110  $\mu\text{m}$  in diameter. Houghton *et al.* (Houghton, Thompson *et al.* 1996) reported different oxygen uptake and lactate production rates for these five distinct stages. From these findings, it is established that embryo growth is associated with changes of both embryo size, and substrate uptake and production. These features provide a quantitative characterisation of embryo development.

It is important to take into account the changes during embryo development, since these may mean adjustments should be made to controllable conditions of the bioreactor for optimal embryo viability. This is the focus of this section.

### 4.5.1 Problem Setup

For this study, the growth stages of a typical mouse embryo are used. Each of the five growth stages lasts for approximately one day. The combined data on embryo size changes from internal sources (Thouas, GA, private communication), and oxygen uptake and lactate production rate changes from Houghton *et al.* (Houghton, Thompson *et al.* 1996), are used to adjust solute source and sink rates for the current simulations. These data are tabulated in Table 4.13. They are provided for the five different growth stages, from the 1-cell stage to the blastocyst stage. The simulations are set up as

steady-state problems corresponding to each of these five stages. This assumes that the different stages can be treated as quasi-steady problems. For example, for the 1-cell stage, the embryo size is set to 70  $\mu\text{m}$ , oxygen uptake rate is set to  $2.0163 \times 10^{-13}$  kg/hr and lactate production rate is set to  $7.54 \times 10^{-13}$  mol/hr. To achieve this, five geometric models were created to simulate them (Figure 4.29) where each model differs from others in embryo size, lactate production and oxygen uptake rates. Other geometric features of the model such as cavity depth, length and the boundary conditions of the simulations, such as culture fluid inflow rate and material properties were fixed for all simulations.

Embryo growth stage	Day	Embryo diameter, $D_{\text{embryo}}$	Oxygen uptake rate, $-S_{\text{oxy}}$	Lactate production rate, $S_{\text{lac}}$
		$\mu\text{m}$	kg/hr	mol/hr
1-cell	1	70.00	2.016E-13	7.540E-13
2-cell	2	86.00	2.231E-13	1.290E-12
4-cell	3	91.00	2.188E-13	7.840E-13
Morula	4	78.00	2.016E-13	2.596E-12
Blastocyst	5	107.00	5.892E-13	1.180E-11

Table 4.13: Summary on the embryo size and solutes exchange rate of a mouse embryo collected from several sources (see text for details).

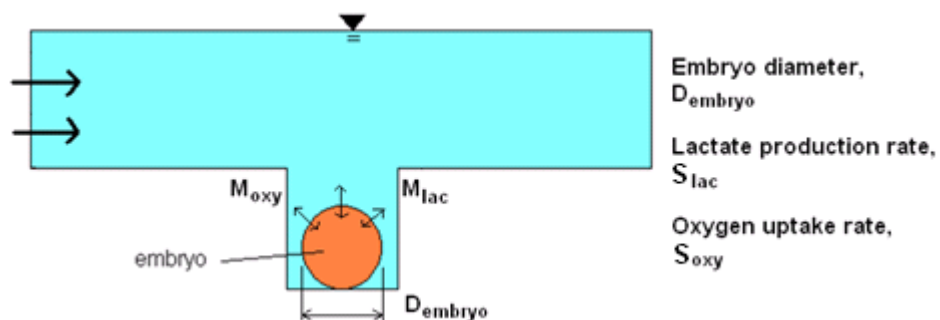


Figure 4.29: Sketch of 2D model showing the two factors characterizing embryo growth: embryo size indicated by the embryo diameter and solutes exchange rate indicated by lactate production rate and oxygen uptake rate.

#### 4.5.2 Embryo Growth at Different Stages

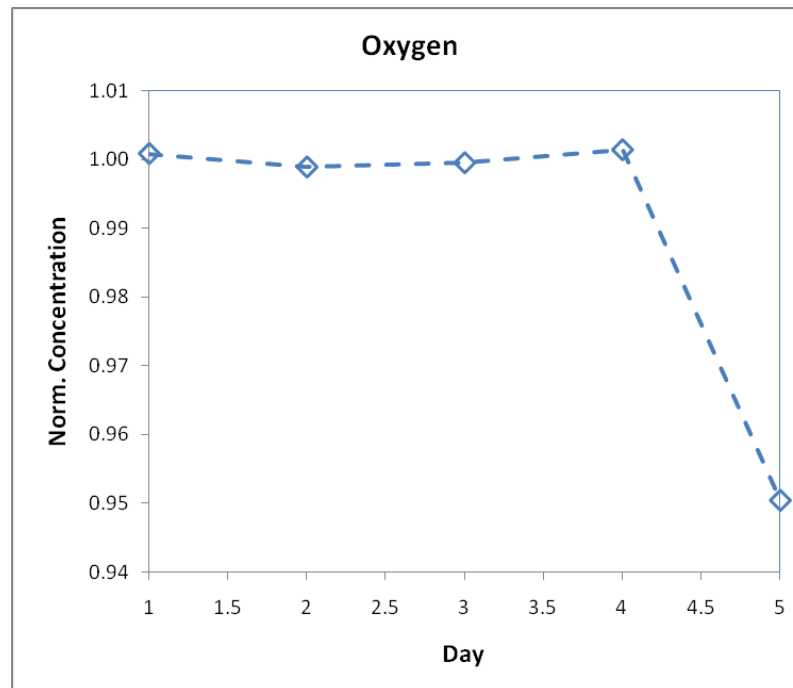
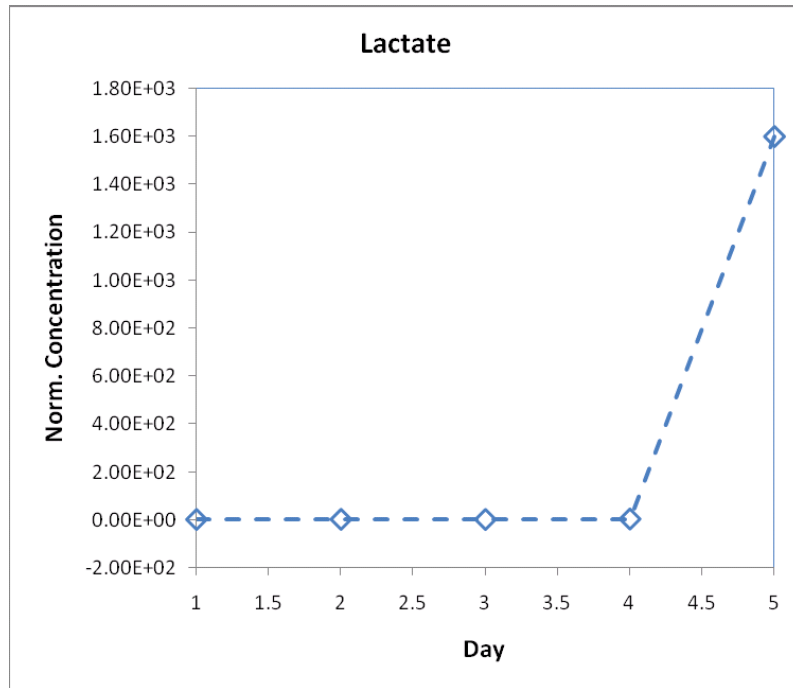
Utilizing the embryo growth data tabulated in Table 4.13, ten sets of simulations were conducted (five on simulating lactate production and five on simulating oxygen uptake)

to simulate lactate and oxygen exchange in the bioreactor for all five individual growth stages. The changes to the overall lactate and oxygen concentrations, and the shear stress on embryo for these five growth stages were then examined.

Embryo growth stage	Day	Oxygen concentration	Normalized oxygen concentration	Lactate concentration	Normalized lactate concentration	Shear stress	Normalized shear stress
		M		M		Pa	
1-cell	1	2.122E-04	1.001	1.35E-06	0.83	5.72E-04	2.12
2-cell	2	2.118E-04	0.999	2.24E-06	1.37	4.72E-04	1.75
4-cell	3	2.119E-04	1.000	1.35E-06	0.83	4.15E-04	1.53
Morula	4	2.123E-04	1.001	4.54E-06	2.79	5.36E-04	1.98
Blastocyst	5	2.015E-04	0.951	2.60E-03	1600	2.97E-04	1.10

Table 4.14: The overall concentration of lactate and oxygen as well as shear stress formed on the embryo (averaged across the embryo surface) recorded for all five stages of growth. The normalized quantities were obtained by dividing each value with its respective default value for lactate and oxygen concentration, and shear stress from Table 4.2.

As shown in Table 4.14 and Figure 4.30, the solute concentration changes for different stages of embryo growth (indicated by the different days in the Figure 4.30) reveal only small changes to the concentrations from the 1-cell stage to the morula stage. Then from the morula stage to the blastocyst stage, a large change in concentration is detected, where the lactate concentration increases 1600% from the default lactate concentration, while oxygen concentration drops 5% from the default oxygen concentration. Variation to the shear stress is very different from the solute concentration changes, where the stress level does not exhibit any notable increase or decrease as the embryo matures into the blastocyst stage. Note that the reason that the total variation in lactate concentration is different from that of the oxygen concentration is explained in Section 5.5.



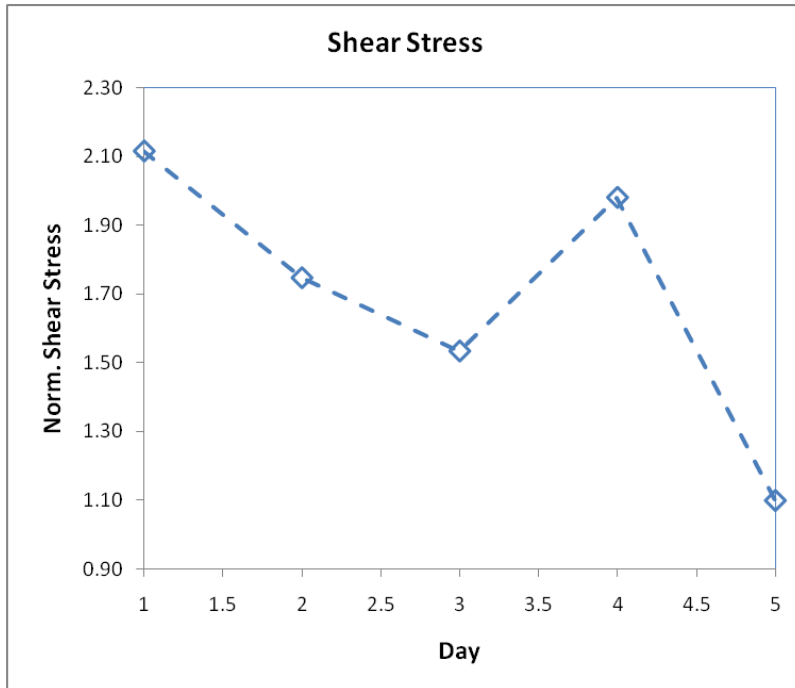


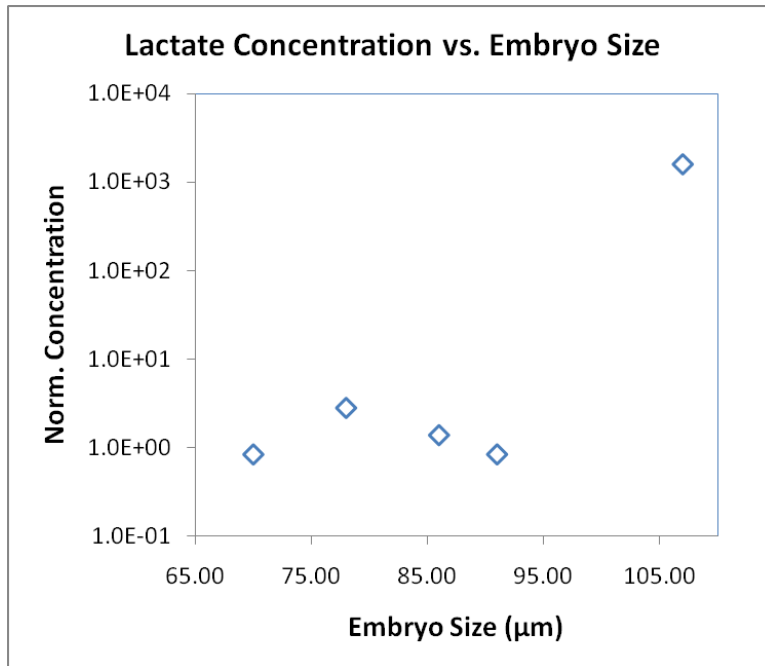
Figure 4.30: Plots showing the overall lactate, oxygen concentration and the shear stress on the embryo (averaged across the embryo surface) for all five days of embryo growth.

### 4.5.3 Establishment of Governing Factors

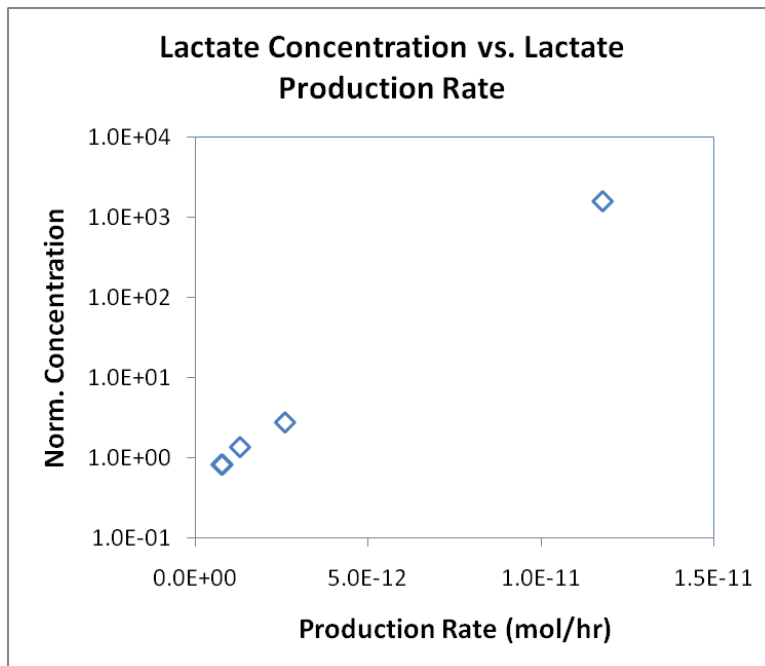
In this set of simulations, three factors (embryo size, oxygen uptake and lactate production) vary between the different runs. Clearly, the shear stress is only affected by embryo size, since it changes the flow within the bioreactor and the flow is independent of solute transport. In addition, the oxygen level at the embryo surface will not be affected by the lactate production rate, and similarly the lactate level will not be influenced by the oxygen uptake rate, although both will be affected to some degree by the embryo size. On the other hand, oxygen uptake should be related to lactate production, i.e., waste production should be related to food intake, and embryo growth must also be related to oxygen uptake. Unfortunately, exploring these latter relationships is beyond the scope of the current research. While there will be a direct correlation between the solute levels and the uptake/production rate, the correlation with embryo size over the 5 stages of growth is less clear, although it could be studied independently. One aim of the study in this section is to examine these correlations using a statistical analysis.

Firstly, for the solute levels, establishing the influence of solute production/uptake and embryo size are initially assessed by plotting the solute levels against those variables. It

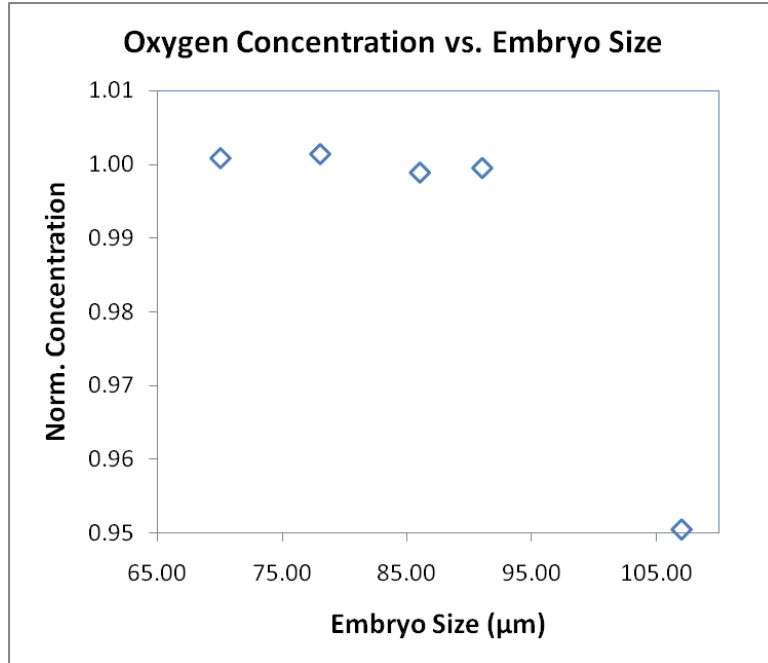
is observed from Figure 4.31 that the lactate/oxygen level has a better correlation with the production/uptake rate (see Figures 4.31b and 4.31d). The correlation with embryo size is less strong (Figure 4.31a and 4.31c). Although the results are not statistical in nature and the influence of each parameter could be determined by independent simulations, for the purpose of the present study a non-parametric correlation method, the Spearman rank correlation, is used to determine the correlation ratio between the input and output variables. This determines how well an *arbitrary* monotonic function can describe the relationship between two variables. Such a method was utilized by Gauthier to detect trends on chemical concentration changes (Gauthier 2001). The key feature of this correlation approach is that it is nominally suitable to handle few data points, such as in the case here.



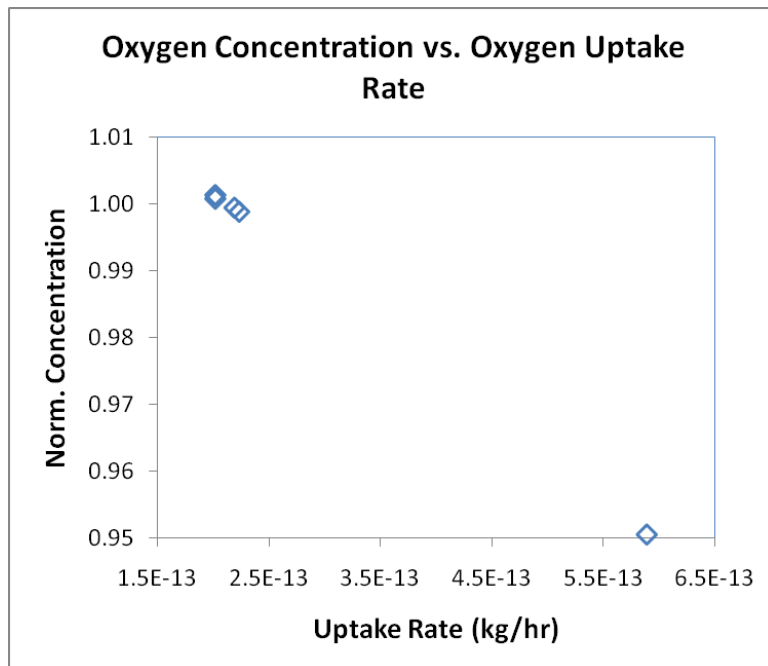
(a) Lactate concentration vs. embryo size



(b) Lactate concentration vs. production rate



(c) Oxygen concentration vs. embryo size



(d) Oxygen concentration vs. uptake rate

Figure 4.31: Scatter plots showing the relationships between the embryo size (a, c) and the solute exchange rate (b, d) with the lactate and oxygen concentration on the embryo.

The data for the plots were obtained from Table 4.13 and 4.14.

Using this method, firstly the correlation ratios were calculated using the lactate and oxygen concentration, and shear stress data recorded in Table 4.14 and they are tabulated in Table 4.15 below. Next, comparisons of the correlation ratio of embryo size against solute concentration and solute exchange rate against solute concentration are made to reveal which parameter (embryo size or solute exchange rate) associates better with the variation of the solute concentration. A +1 or -1 correlation ratio means perfect positive or negative correlation between the two parameters while zero correlation ratio indicates no correlation between the two parameters. In short, this means that a larger correlation value suggests a better correlation between the two parameters. The correlations are verified to be significant at 95% probability by comparing the calculated ratio to the corresponding critical values for Spearman's rank correlation coefficient (Gauthier 2001). The calculated correlation ratios proved to be significant as they were found to larger than the corresponding critical value for 95% probability.

Relationship	Correlation ratio
Embryo size - oxygen concentration	-0.8
Oxygen uptake rate - oxygen concentration	-0.9
Embryo size - lactate concentration	0.6
Lactate production rate - lactate concentration	1.0

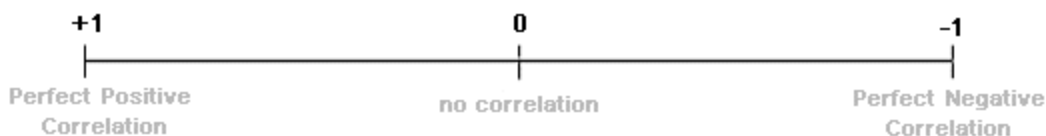
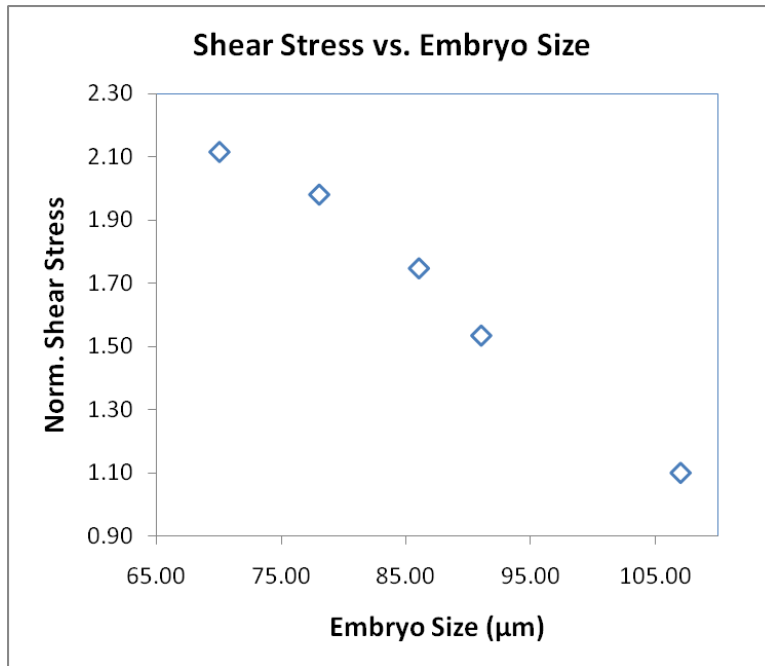


Table 4.15: Comparison of the calculated correlation ratios for embryo size and solutes exchange rates with respect to the overall solute concentrations recorded on the embryo.

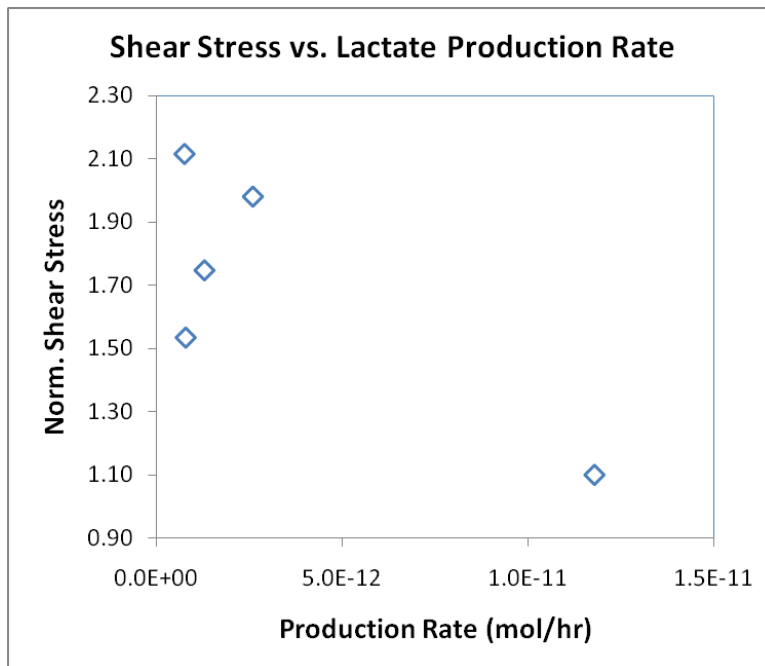
As revealed in Table 4.15, as expected, the solute exchange rates (lactate production and oxygen uptake rate) correlate better with concentration changes than embryo size. For oxygen, the correlation ratio for embryo size (-0.8) is lower than the correlation ratio for oxygen uptake rates (-0.9), implying that oxygen uptake rates are more closely related to the change of oxygen concentration in the cavity. For lactate, the correlation ratio for the lactate production rate (1.0) is also higher than the correlation ratio for embryo size (0.6). All the correlation results corresponded well with the findings from the scatter

plots in Figure 4.31. Therefore, this suggests (not surprisingly) that the solute exchange rate has a larger influence on the solute concentration on the embryo and subsequent analyses on solute concentration distributions focus on this.

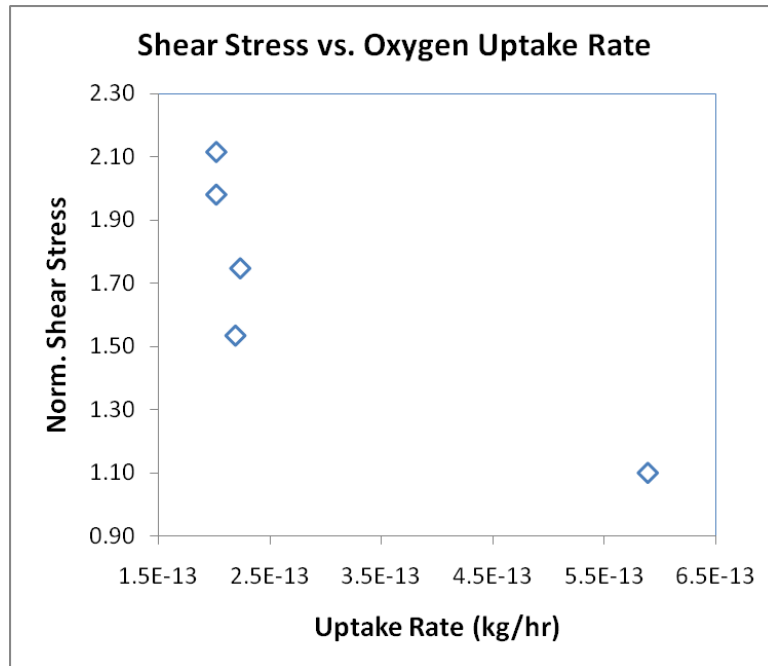
The same method was used to determine the controlling factors for shear stress. In particular, the following three factors were examined: embryo size, oxygen uptake rate and lactate production rate. This is done as a test of the approach since the governing equations indicate that the flow field, and hence the shear stress, does not depend on solute transport. Scatter plots of these three factors against the shear stress are presented in Figure 4.32 below. As can be observed, embryo size (Figure 4.32a) exhibits a clear monotonic relationship compared with lactate production and oxygen uptake (Figure 4.32b and 4.32c respectively).



(a) Shear stress vs. embryo size



(b) Shear stress vs. lactate production rate



(c) Shear stress vs. oxygen uptake rate

Figure 4.32: Scatter plots showing the relation of (a) embryo size, (b) lactate production rate and (c) oxygen uptake rate with the overall shear stress on the embryo. The data for the plots were obtained from Table 4.13 and 4.14.

The correlation ratios for the case of shear stress were calculated again based on the data of the overall shear stress on the embryo tabulated in Table 4.14. The observed clear correlation from the scatter plot of shear stress against embryo size is well supported by the calculated Spearman’s rank correlation coefficient of -0.9 (Table 4.16). Unfortunately, the correlation coefficients for the other two variables (-0.8 for oxygen uptake rate and -0.6 for lactate production rate) are also relatively large despite the independence of the variables. This probably indicates that there is insufficient data to use for statistical analysis, despite the general acceptance of the test for small data sets. In any case further analysis on embryo shear stress will be focused on the quantitative relationship with changing embryo size.

Relationship	Correlation ratio
Embryo size – embryo shear stress	-0.9
Oxygen uptake rate – embryo shear stress	-0.8
Lactate production rate – embryo shear stress	-0.6

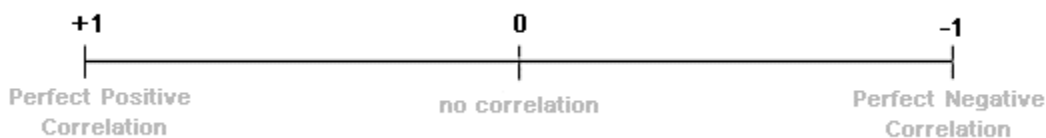


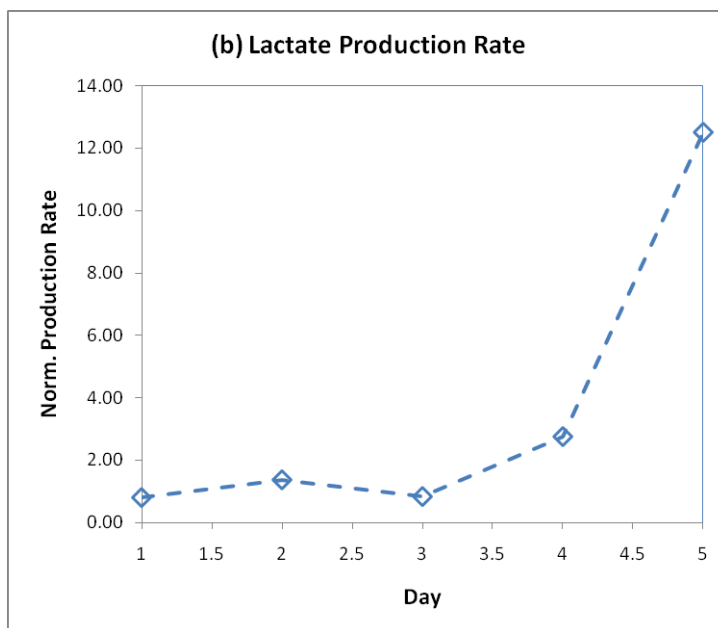
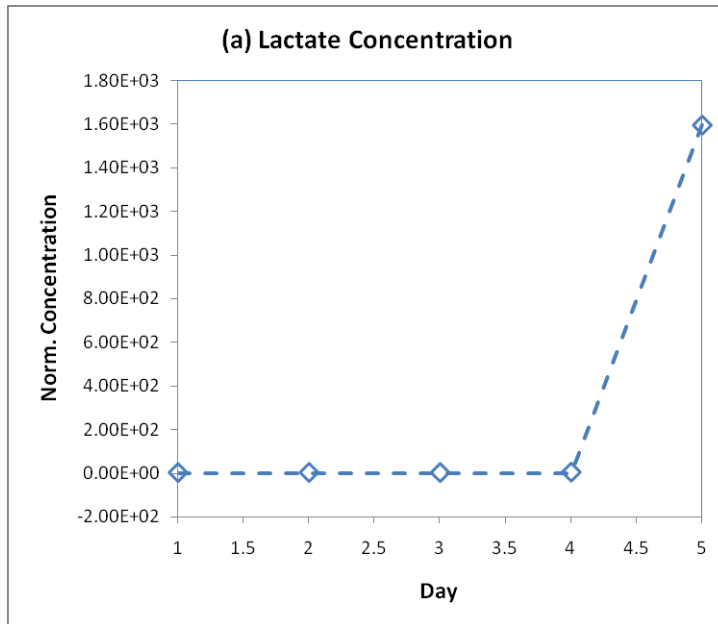
Table 4.16: Comparison of the calculated correlation ratios of embryo size and solutes exchange rates with respect to the shear stress formed on the embryo.

#### 4.5.4 Variation of Solutes Concentration

As shown in Figure 4.33, and as expected, the variation in lactate concentration demonstrates a positive correlation with the lactate production rate. From day 1 to day 3, lactate production rate did not vary much and the lactate concentration on the embryo was found to be comparatively constant for the first 3 days. On day 4 and day 5, a sharp rise of lactate production rate occurs. Correspondingly, the similar sharp increase of lactate concentration by 1600% from the default concentration is observed. Likewise, the change in oxygen concentration has a negative correlation with the change in oxygen uptake rate. From day 1 to day 3 oxygen uptake does not change much and this is reflected by the moderately consistent oxygen concentration for these 3 days. On day 4 and 5, the oxygen uptake increases significantly and this corresponds well with the

significant oxygen concentration level decrease down to 5% from the default oxygen concentration level.

The reasons for these changes are clear. When the lactate produced from the embryo surface increases with no change to the flow conditions, more of this lactate must remain in the cavity for longer. Similarly, as the amount of oxygen consumed by the embryo increases, this will lower the oxygen concentration level within the cavity.



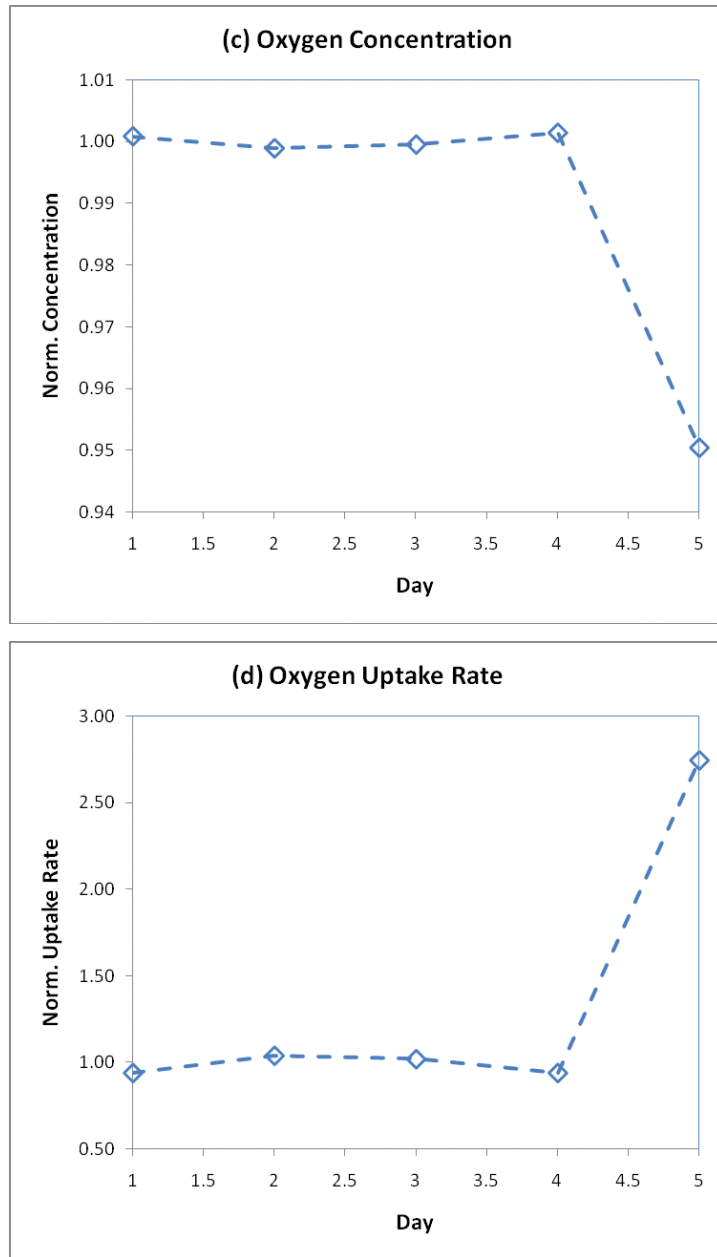


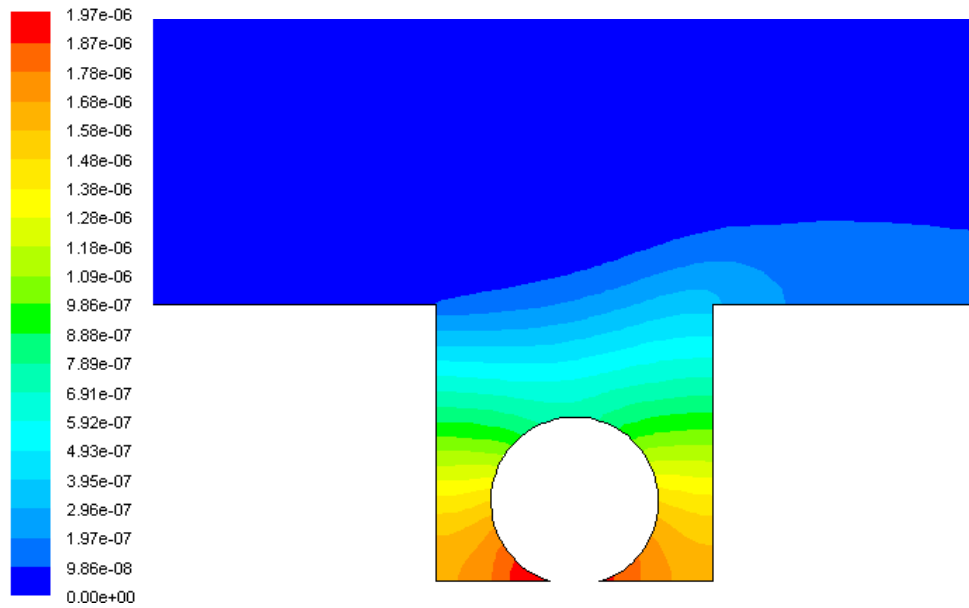
Figure 4.33: For all five days of the embryo growth, the solutes concentrations (a, c) are compared with the solutes exchange rates (b, d) to show how they are related to each other. The data for the plots are provided in Tables 4.13 and 4.14.

#### **4.5.5 Solutes Distribution around the Embryo**

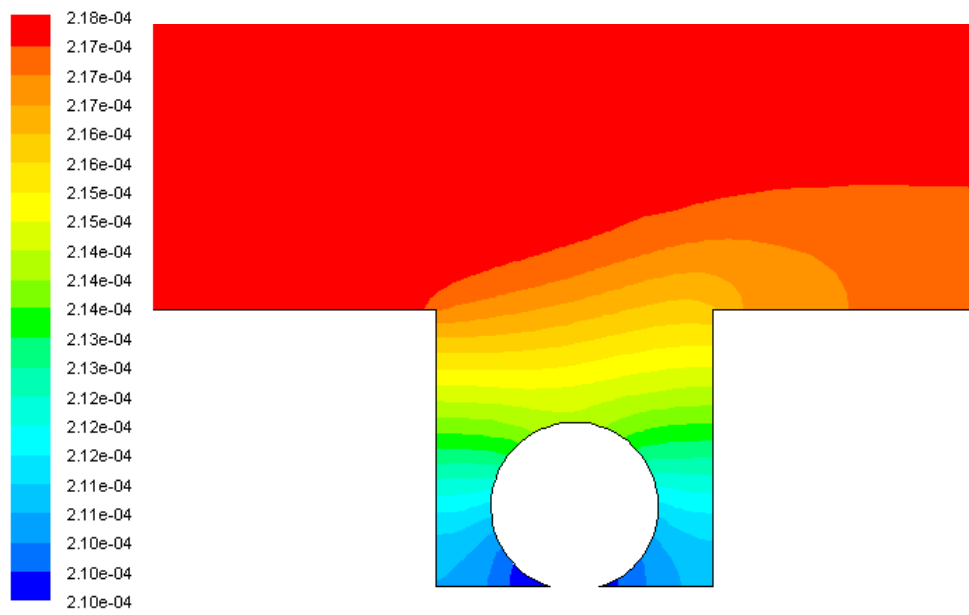
Typical distributions of lactate and oxygen in the cavity are illustrated in Figure 4.34. (These are repeated from Figure 4.25, but are shown here for convenience). Recall, the large solute variation between the bottom and the top of the cavity. This is due to the very slow flow towards the bottom of the cavity causing lactate accumulation and oxygen depletion.

Due to the unchanged flow and boundary conditions, other than the increase of lactate production and oxygen uptake, the lactate and oxygen distribution pattern around the embryo does not vary much when maturing from the 1-cell stage to the blastocyst stage. As shown in Figure 4.35 only the overall magnitudes change, with the circumferential profiles remaining similar.

A discussion of the circumferential solute variations has been given in sections 4.3.4 and 4.4.3, and hence will not be repeated here. However, the profiles are provided in Figure 4.34 for completeness.

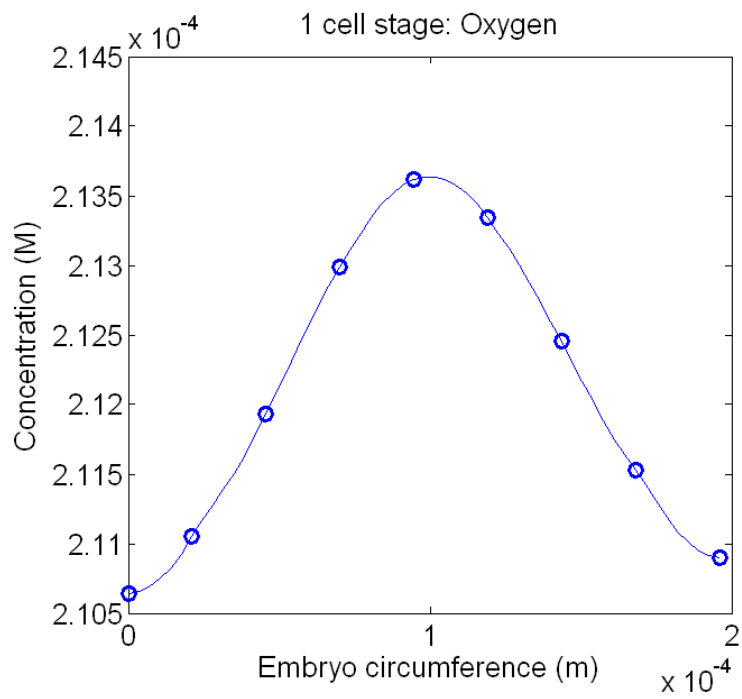
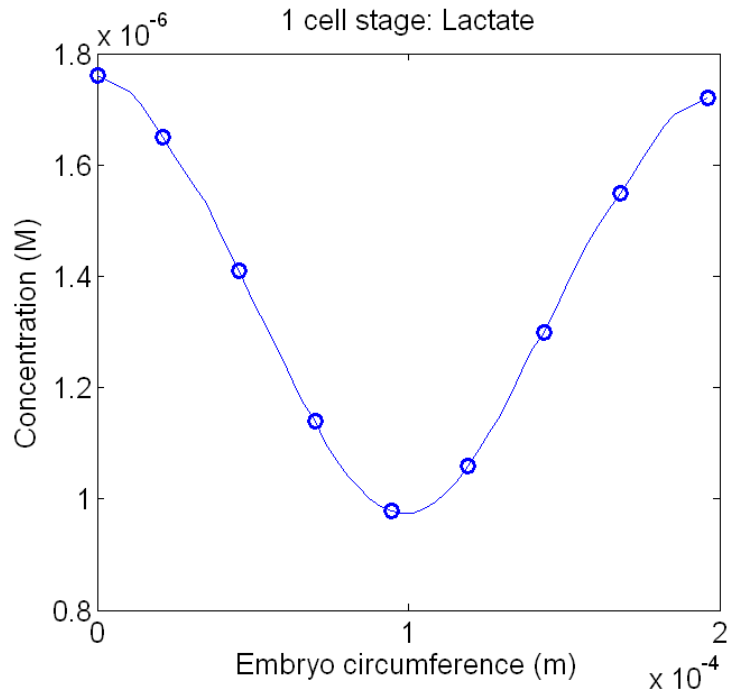


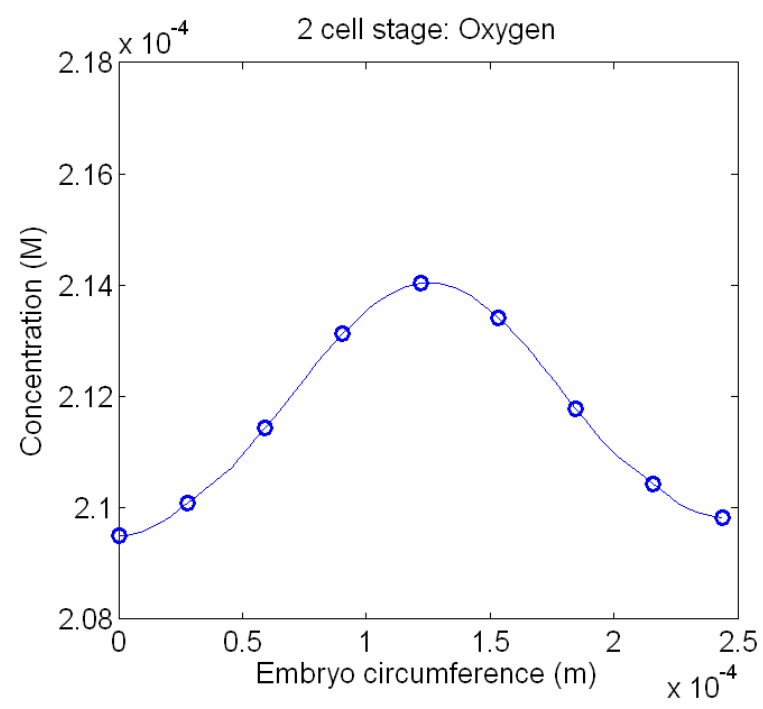
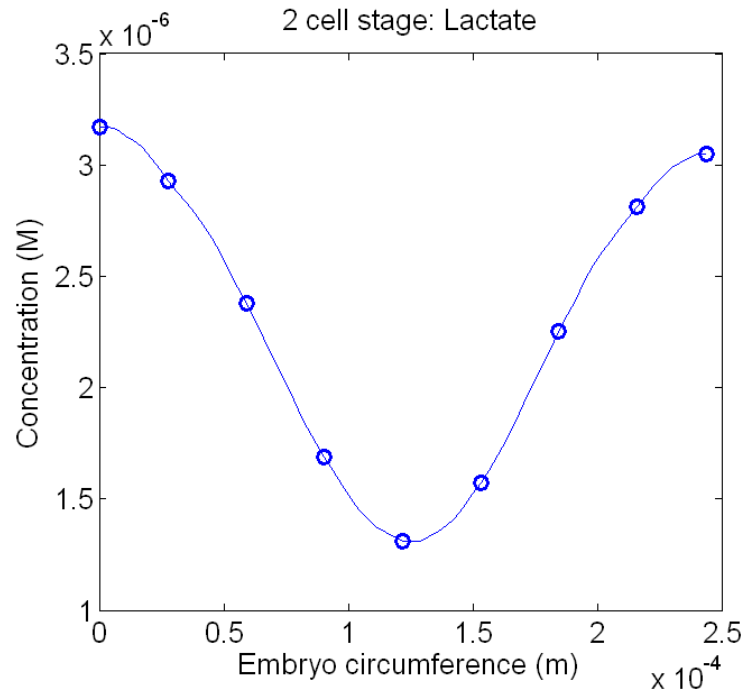
(a) Lactate distribution

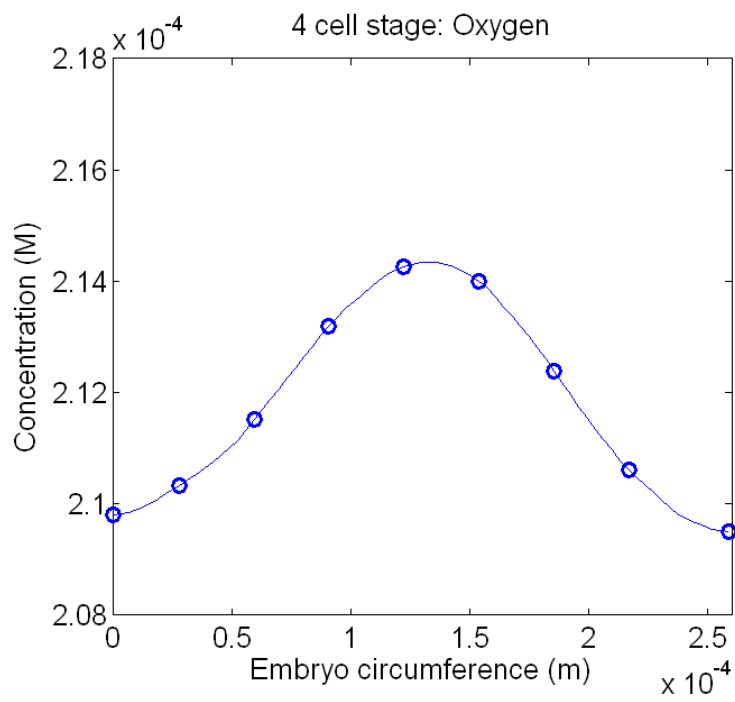
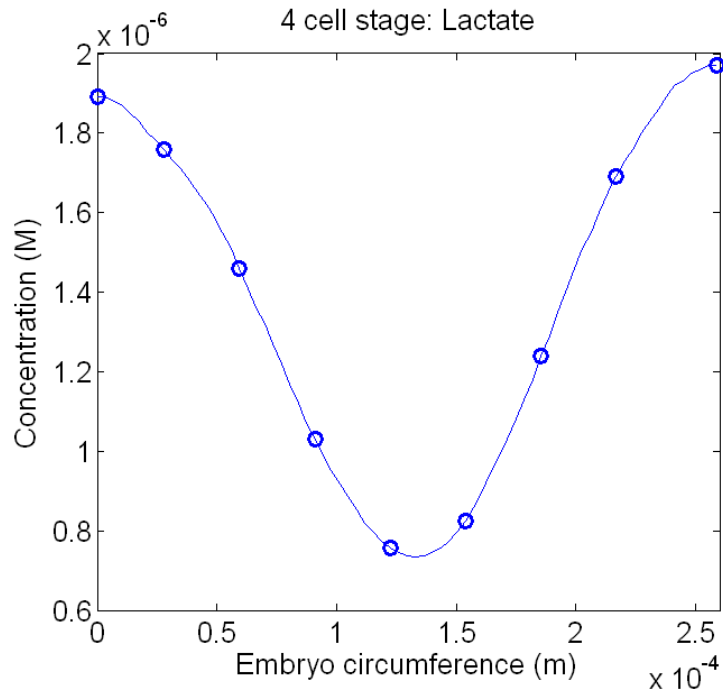


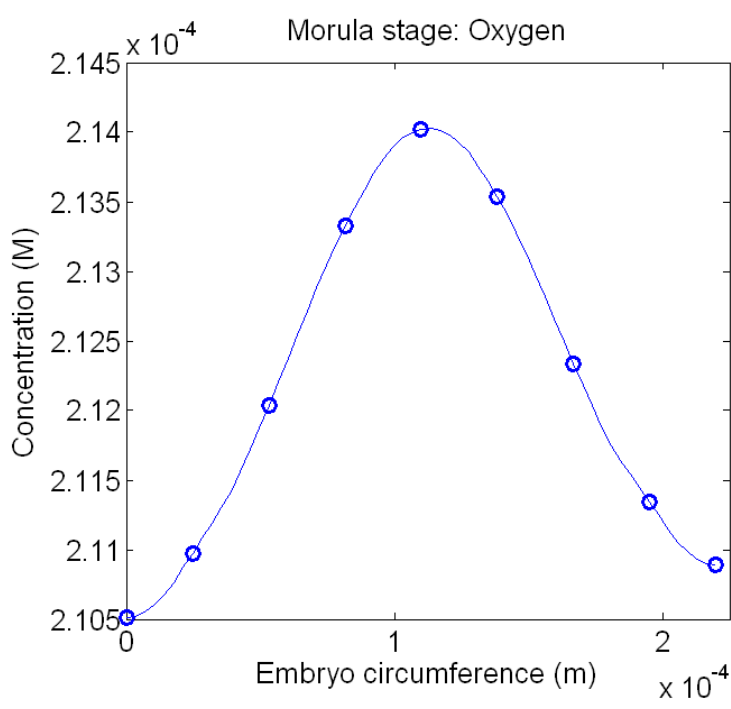
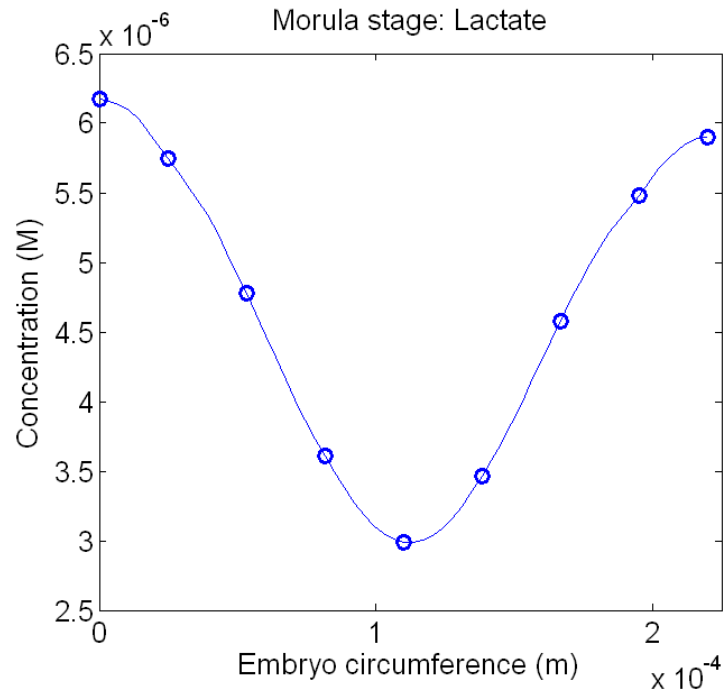
(b) Oxygen distribution

Figure 4.34: Contour plots of (a) lactate and (b) oxygen concentration (measured in M) around the embryo at the 4-cell stage. Solute distributions at other growth stages have a similar distribution.









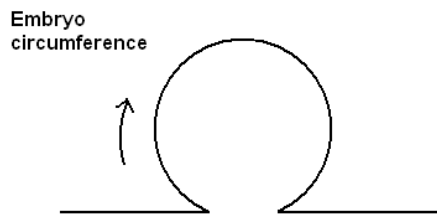
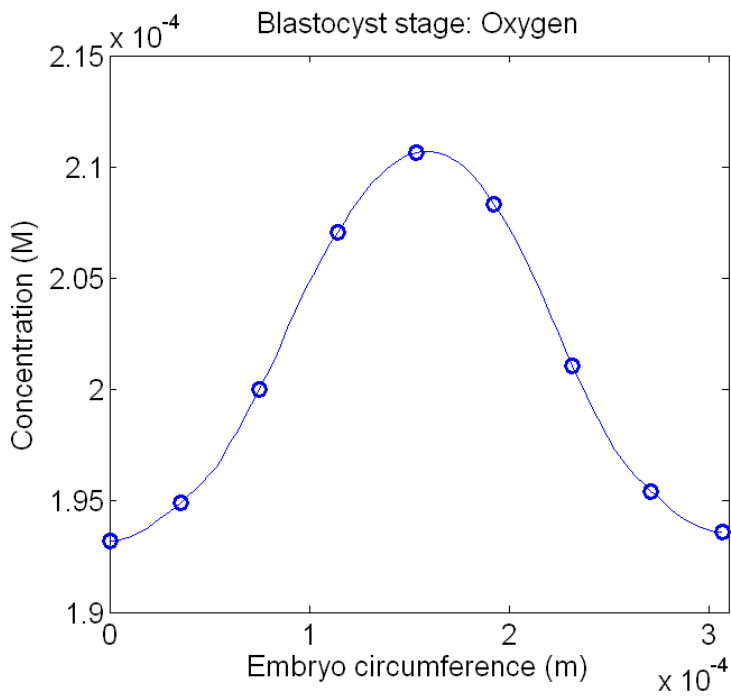
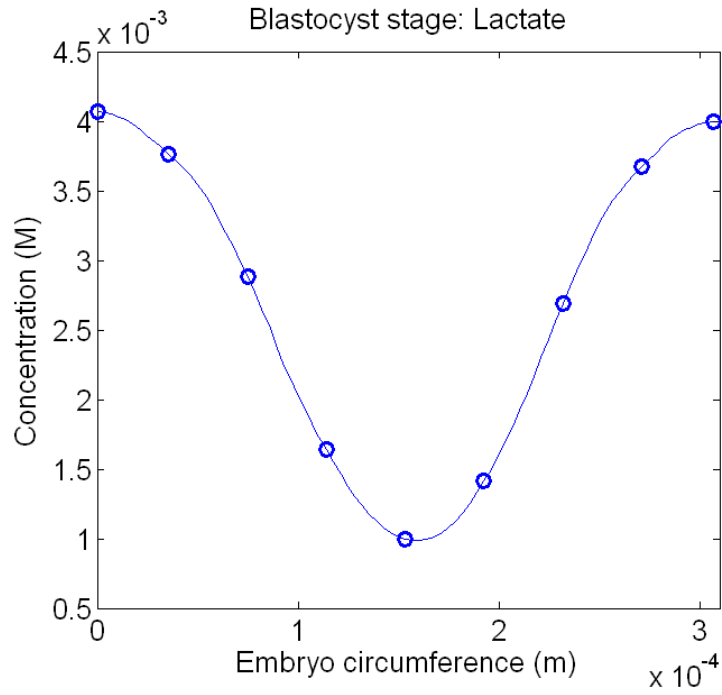


Figure 4.35: Distributions of lactate (left) and oxygen (right) on the embryo surface for all five days of the embryo growth.

#### **4.5.6 Implication for Solute Transport**

As demonstrated from the observations above, while they do not affect the solute distribution patterns significantly, the changes in the solute exchange rates of the embryo throughout the growth period can potentially have a substantial impact on the design of the bioreactor, or at least on selecting the controllable operating conditions. This is due to the substantial variations in the magnitude of the uptake/excretion rates of the embryo, particularly when the embryo reaches the final blastocyst stage. For that final stage, the oxygen uptake rate increases 3-fold and the lactate production rate increases 16-fold from the initial 1-cell stage values. Oxygen delivered to the embryo may not be adequate if the oxygen supply is maintained at the same level as that during the 1-cell stage. Similarly, if the culture fluid perfusion rate in the channel remained unchanged, the lactate produced by the embryo during the blastocyst stage may oversaturate the cavity and cause harmful side effects to the embryo.

With these findings, one can optimize the operation of the bioreactor to ensure the performance of the bioreactor does not degrade and provide the best time-dependent environment for the embryo cultivation. For example, one can continuously monitor and adjust the preset oxygen concentration level such that it provides adequate oxygen supply to the embryo throughout all the growth stages. Similarly, the flow rate of the culture medium can be increased to speed up the removal of excess lactate around the embryo during the blastocyst stage.

#### **4.5.7 Variation of Shear Stress**

The plots of embryo surface shear stress and embryo size from day 1 to day 5 in Figure 4.36 once again demonstrate the inverse relationship between embryo size and the surface shear stress. From day 1 to day 3, the increase in embryo diameter causes a 60% decrease in shear stress. From day 3 to day 4, the 40% increase in shear stress corresponds well to a decrease in the embryo diameter. The shear stress then reduces to the lowest value from day 4 to day 5 as the embryo grows to its largest size.

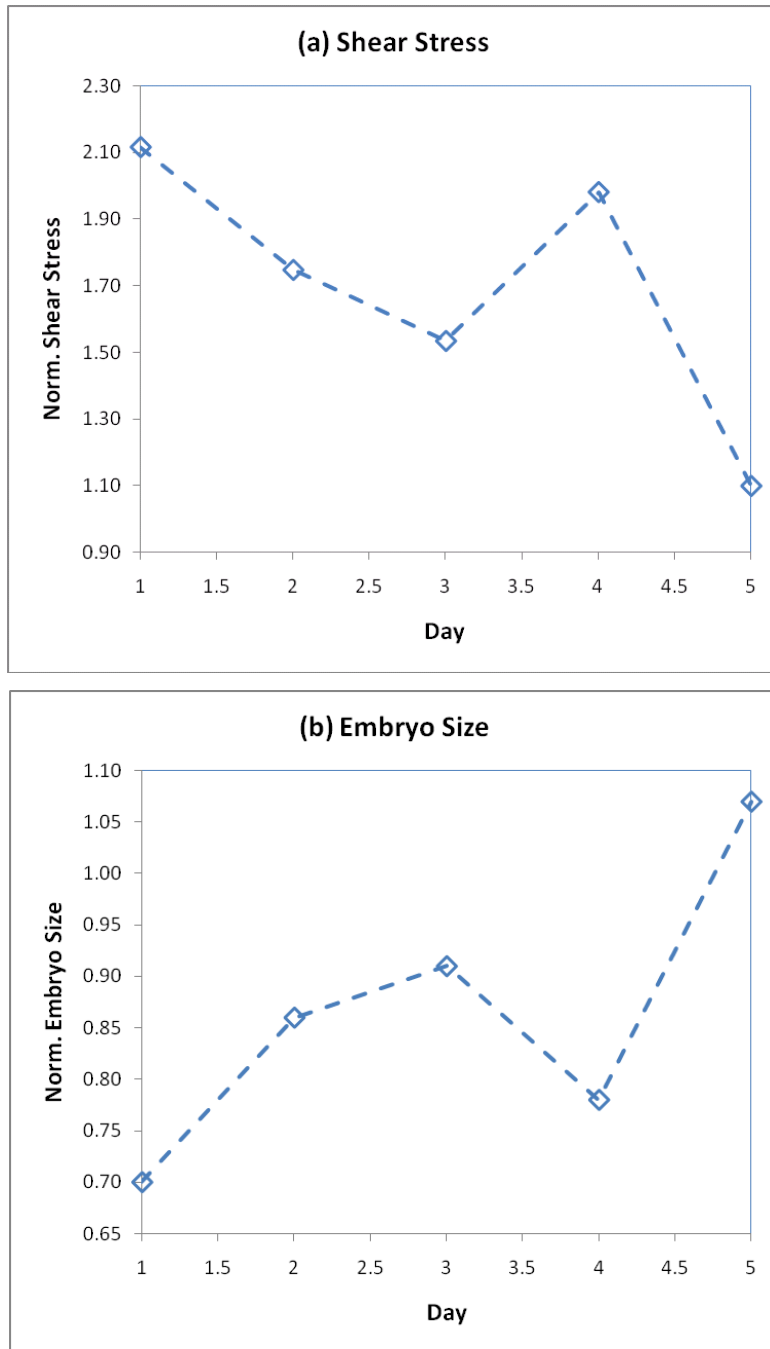


Figure 4.36: For all five days of the embryo growth, the shear stress (a) was compared with embryo size (b) to show how they are related to each other. Again, the data for the plots is from Tables 4.13 and 4.14.

Such observation of surface shear stress behaviour can be explained by the fact that as the embryo size changes, the flow topology in the cavity varies considerably. As shown in Figure 4.37 below, when the embryo is small (Figure 4.37a, 4.37d), a single flow recirculation is detected above the embryo; as the embryo enlarges (Figure 4.37b, 4.37c, 4.37e), this flow recirculation splits into two weaker flow recirculations. The stronger single flow recirculation induces a larger local shear stress than the weaker smaller flow recirculations at the top of the embryo.

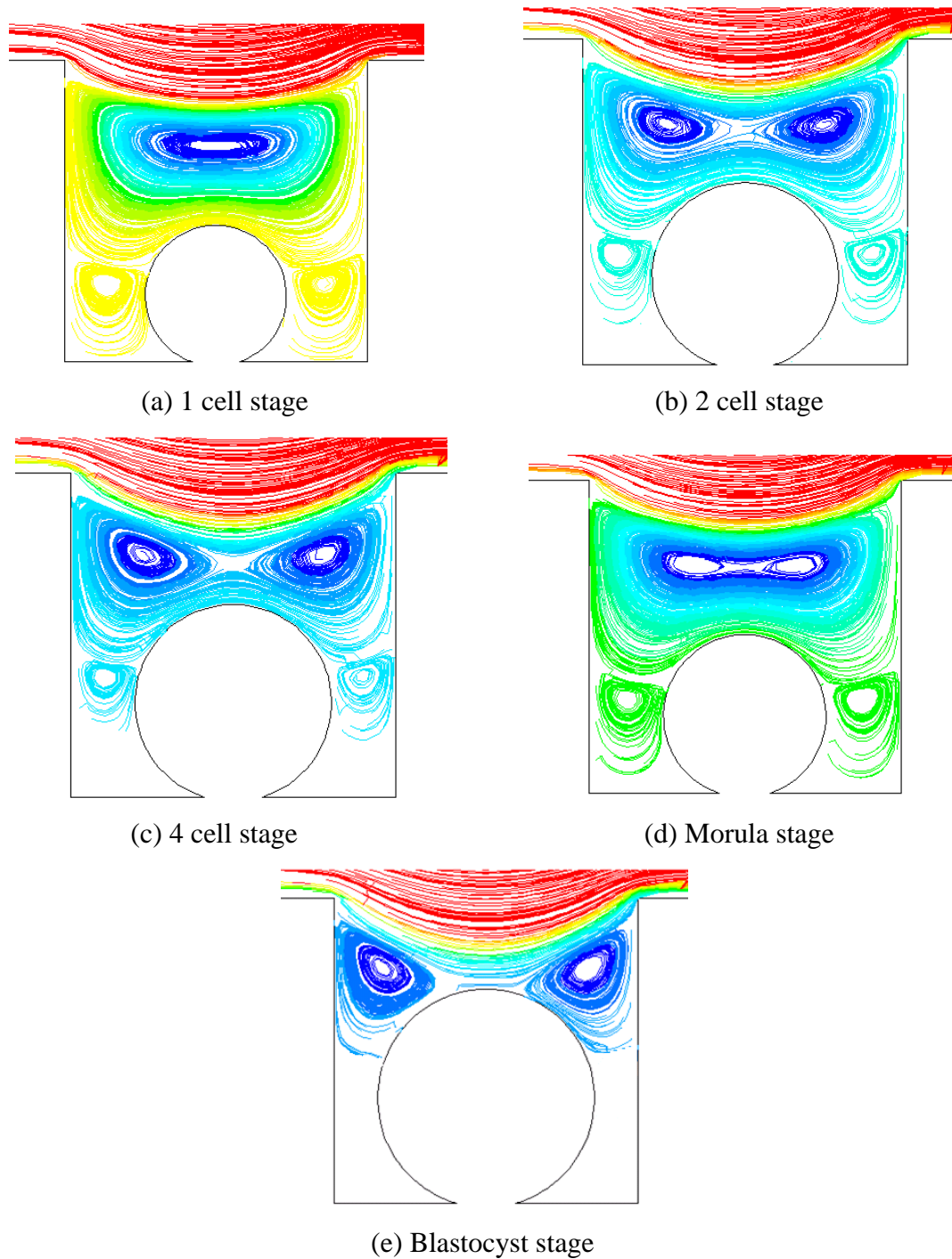
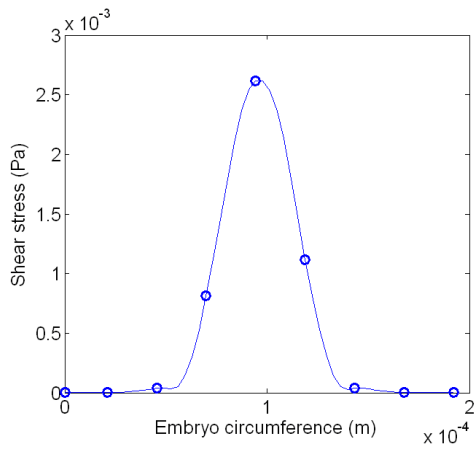


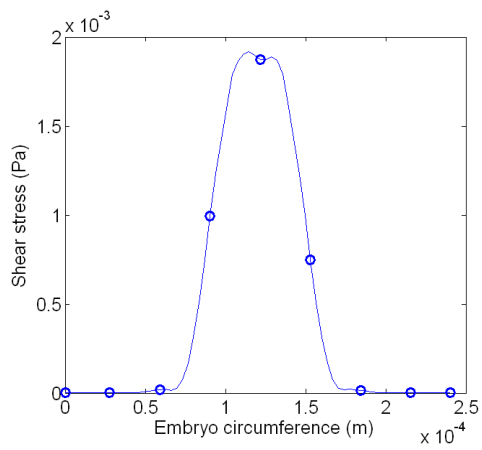
Figure 4.37: Streamfunction plots showing strength the flow circulation (measured in kg/s) within the cavity for all 5 growth stages.

#### **4.5.8 Shear Stress Distribution on the Embryo**

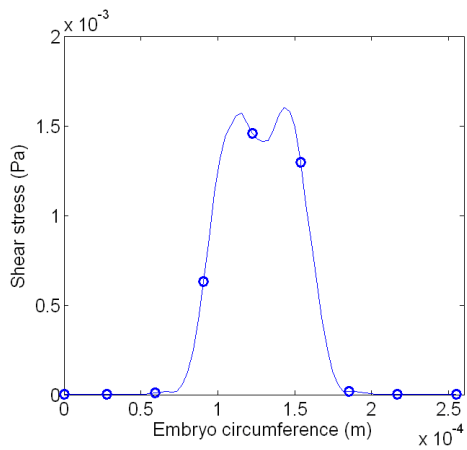
For all five growth stages, the shear stress distribution on the embryo surface in general has the following variation (Figure 4.38): starting with a very low stress level at the bottom, the shear stress increases to higher values at the top of the embryo. The variation between them can be observed at the peak stress region at the top of the embryo. For the 1-cell and morula stages, a single peak is detected (Figure 4.38a, 4.38d); for 2-cell and 4-cell stages when the embryo is larger (Figure 4.38b, 4.38c), twin peaks are detected and for blastocyst stage, which has the largest size, triple peaks are detected (Figure 4.38e). As found previously, the number of peaks found mirror the flow recirculations in the cavity (Figure 4.37). For instance, at the 1-cell stage, a single flow recirculation corresponds to the occurrence of a single peak; at the 4-cell stage, 2 flow recirculations are detected and these cause the twin peaks found at the top of the embryo. At the blastocyst stage, it can be observed from Figure 4.37e, the top of the embryo is in contact with 2 flow recirculations and the bulk flow from the channel. Therefore, three peaks are found for this stage.



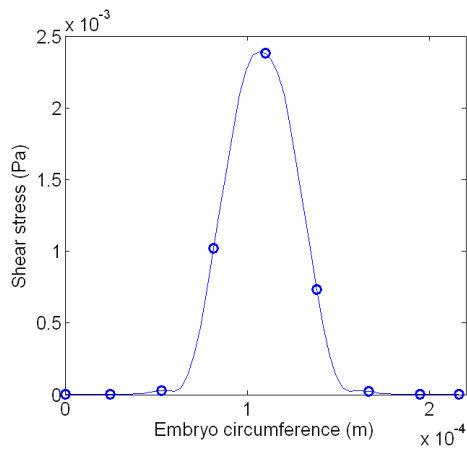
(a) 1 cell stage



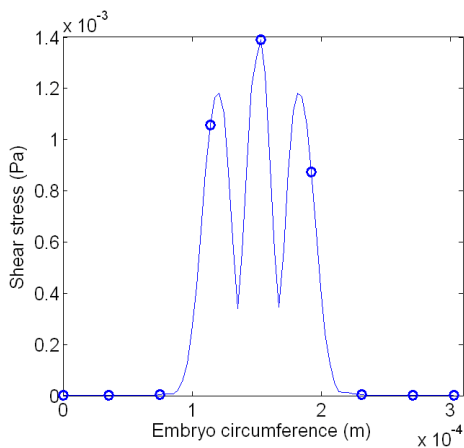
(b) 2 cell stage



(c) 4 cell stage



(d) Morula stage



(e) Blastocyst stage

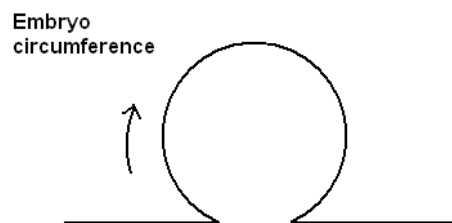


Figure 4.38: Distributions of shear stress on the embryo surface for all five days of the embryo growth.

#### **4.5.9 Implications for Shear Stress Changes**

Gathering these results, it can be summarized that changing the embryo size alters the flow structure within the cavity and thus varies the overall shear stress on the embryo surface. This stress is higher when the embryo is smaller because the channel flow sets up a strong recirculation immediately above the embryo, and perhaps surprisingly, the stress decreases as the embryo becomes larger (as the embryo top gets closer to the faster flowing channel fluid). *For the flow rate considered for this study*, the peak stress occurred for the 1-cell stage, when the embryo has its smallest size. For that reason, to ensure that the induced shear stress throughout embryo growth is not too large to harm the embryo, one can adjust the safe stress level to be no higher than the acceptable stress level established during the 1-cell stage. For other flow rates (or Reynolds numbers) guidance on the shear stress generated at the embryo is available from the previous parametric study on the flow rate.

#### **4.5.10 Conclusions and Summary**

This parameter study aimed to determine how embryo growth affects lactate and oxygen concentrations within the cavity, and embryo shear stress by treating each growth stage as quasi-steady, so that the environment for each stage could be examined separately.

As the embryo matures from the initial 1-cell stage up to the final blastocyst stage, the solute exchange rates and the size of the embryo change significantly. Due to these changes, factors such as oxygen saturation of the inlet flow and inflow rate may need to be varied over the incubation time to provide good growth conditions. For example, during the initial growth stages, the culture fluid inflow rate might be set to a lower value to reduce the maximum shear stress experienced by the embryo. As the lactate production rate and oxygen uptake rate at these initial stages is not high, a low culture medium perfusion rate may suffice to ensure an adequate amount of oxygen is advected to the embryo as well as to remove the excess lactate. During the later growth stage, especially during the blastocyst stage, a higher perfusion rate may be needed to ensure more oxygen is supplied to the embryo and the large amount of lactate is advected out of the cavity, as during these later growth stages both the oxygen uptake rate and lactate production rate are significantly higher. The shear stress experienced by the embryo at

this stage is lower than for the 1-cell stage and this can offset the high shear stress induced by the high perfusion rate.

## 4.6 Multiple Cavities Parametric Study

To increase the rate of embryo cultivation, one possible strategy is to have several cavities in close vicinity and grow embryos individually inside each cavity. This configuration offers the benefit of creating a “niche environment” around each embryo, while increasing the number of embryos being grown in a single bioreactor unit. Investigating the effect of the fluid flow and solute transport in a bioreactor with such a configuration is the primary objective of this parameter study.

Note that this sort of configuration also has other potential implications not explicitly considered here. For example, it is clear that various factors secreted by cells can act to enhance or suppress or modify future growth. If the growing cells are placed in close proximity, it is possible that such chemical signalling could play a strong role in cell development. The chemical signalling will be looked at indirectly through solute transport (especially lactate flow) between cells.

Due to the time constraints, investigations of multiple cavity configurations focus on the following two aspects:

- Cavity spacing
- Interaction between different numbers of cavities

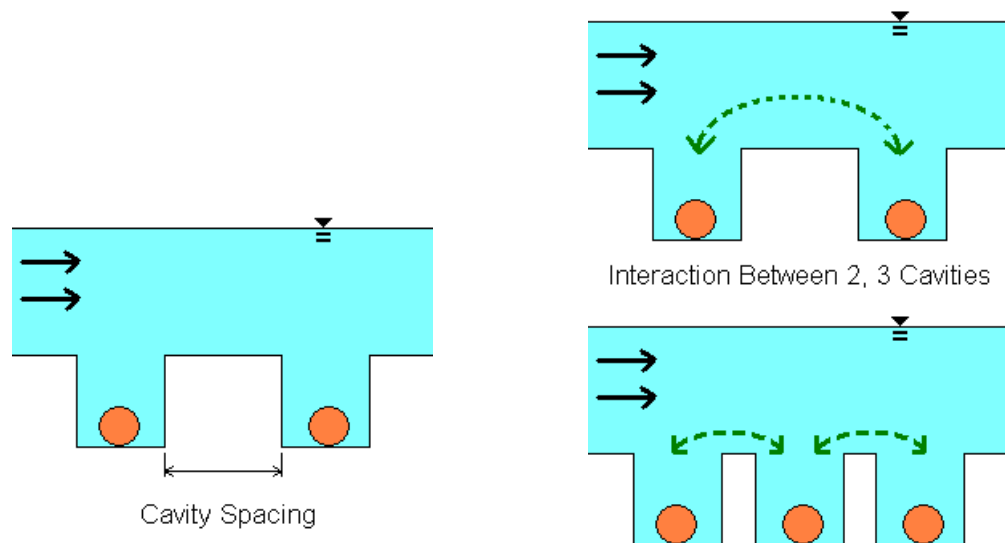


Figure 4.39: Sketches showing the two aspects examined in the multiple cavities parametric study.

As illustrated in Figure 4.39, within the limits of two-dimensional simulations, a configuration with multiple cavities is achieved by arranging one cavity with another in tandem. Given this framework, it is interesting to study the effect of varying the spacing between the cavities, as the proximity of neighbouring cavities is expected to cause some interference in the solute transport and shear stress formation on the embryo in each cavity. It is expected that as the distance increases, such interference/communication will decrease and this sub-study on cavity spacing aims to quantify this.

An extended sub-study concentrates on determining how increasing the number of cavities in the bioreactor influences the flow and solute exchange for each embryo. Specifically, the aim is to find out the degree of interference of each cavity with the others, and to quantify it, where the interference here refers to the changes to solute transport and shear stress from the single cavity case.

Initially, this section starts with a description of the problem setup specific for both parametric sub-studies. It then focuses on the sub-study of cavity spacing followed by another sub-study of the interaction between two and three cavities. As before, in each of the sub-studies, the analysis of solute transport and shear stress formation on the embryo forms the basis of these investigations. The implication of the outcomes from these sub-studies is then discussed before the section is concluded.

#### **4.6.1 Problem Setup**

The first sub-study on cavity spacing ( $L_s$ ) is conducted by constructing a number of geometric models with two cavities: each model differs from another in terms of the spacing between the two cavities, as shown in Figure 4.40. The spacing  $L_s$  covers a comprehensive range from 10  $\mu\text{m}$  to 4000  $\mu\text{m}$ , encompassing significant to very limited interaction. Steady-state simulations are conducted using these models, with other features such as embryo size, depth, length of the cavity and channel, as well as culture fluid inflow rate, solute transport exchange rate and material properties fixed.

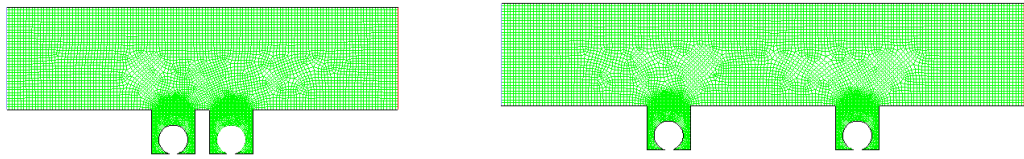


Figure 4.40: Two of the meshed geometric models featured in the cavity spacing sub-study, showing the difference in  $L_s$ : 50  $\mu\text{m}$  (left) and 500  $\mu\text{m}$  (right)

The second sub-study on the interaction between multiple cavities focuses on the differences in the interaction between two cavities and between three cavities. Using the geometric models as shown in Figure 4.41, steady-state simulations are conducted to compute the solute concentration in the bioreactor and the shear stress distribution on the embryo. Here, the spacing between cavities is set to  $L_s = 200 \mu\text{m}$ . The decision for choosing this spacing was made based on the first sub-study on cavity spacing described above. It was found that starting from this spacing the flow interference between cavities starts to diminish. As the objective here is to study the interaction between cavities, it is vital to ensure that the cavities are not too far apart such that interference between them becomes insignificant.

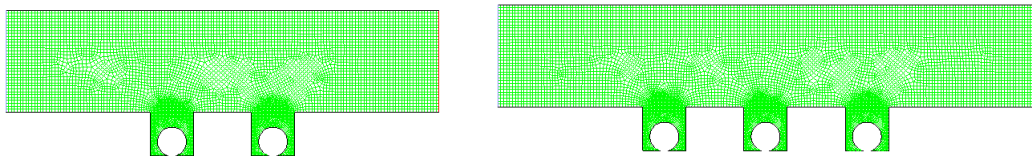
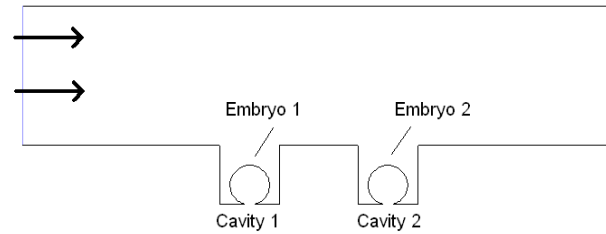


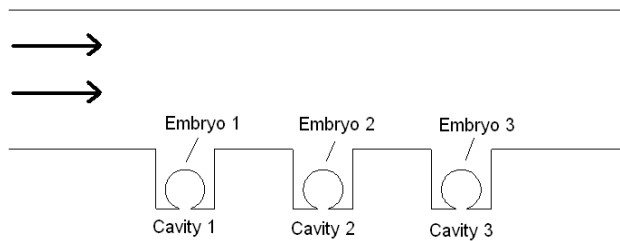
Figure 4.41: Two meshed geometric models employed in the sub-study of interaction between multiple cavities: two cavities (left) and three cavities (right). Each cavity is 200  $\mu\text{m}$  apart. Recall the cavity width is 150  $\mu\text{m}$ .

For both sub-studies, the culture fluid flows left to right. Each of the embryos in their separate cavity is modelled to release lactate and absorb oxygen at the same rate individually. In order to identify the location of the cavity and embryo for several cases in this study, cavities and embryos are identified by the notation in Figure 4.42, for the front, middle or rear cavity along with the respective embryo.

The findings are presented in terms of normalized cavity spacing  $L_s^*$ , where  $L_s^*$  is obtained by dividing  $L_s$  by the length of the cavity,  $L$ , i.e.,  $L_s^* = L_s/L$ .



(a) Two cavities



(b) Three cavities

Figure 4.42: Notation used to identify the cavity location. (a) For the case of two cavities, Cavity 1 refers to the front cavity while Cavity 2 refers to the rear cavity. (b) For the case of three cavities, Cavity 1 refers to the front cavity, Cavity 2 refers to the middle cavity and Cavity 3 refers to the rear cavity. Similar notations are used in identifying individual embryos.

#### 4.6.2 Cavity Spacing: Flow Structure Variation

In order to get a handle on the change in solute transport and the shear stress as  $L_s^*$  is varied, initially the variation of flow structure is examined. It is found that the presence of the rear cavity affects the fluid flow into and out of the front cavity. This is due to the low Reynolds number ( $Re \approx 0.1$ ), so that diffusion is important allowing a significant upstream effect. The size of the effect can be gauged by the vertical velocity contour plots given in Figure 4.43. For the two largest cavity spacings ( $L_s^* = 6.67, 26.67$ ), the velocity contours for each cavity appear similar and reasonably symmetric about the vertical centreline. For the smallest spacing,  $L_s^* = 0.33$ , there is clearly a strong effect – both with the reduction in symmetry and between the upstream and downstream cavities. For the intermediate case,  $L_s^* = 1.33$  there is still clearly an effect, but it is not strong.

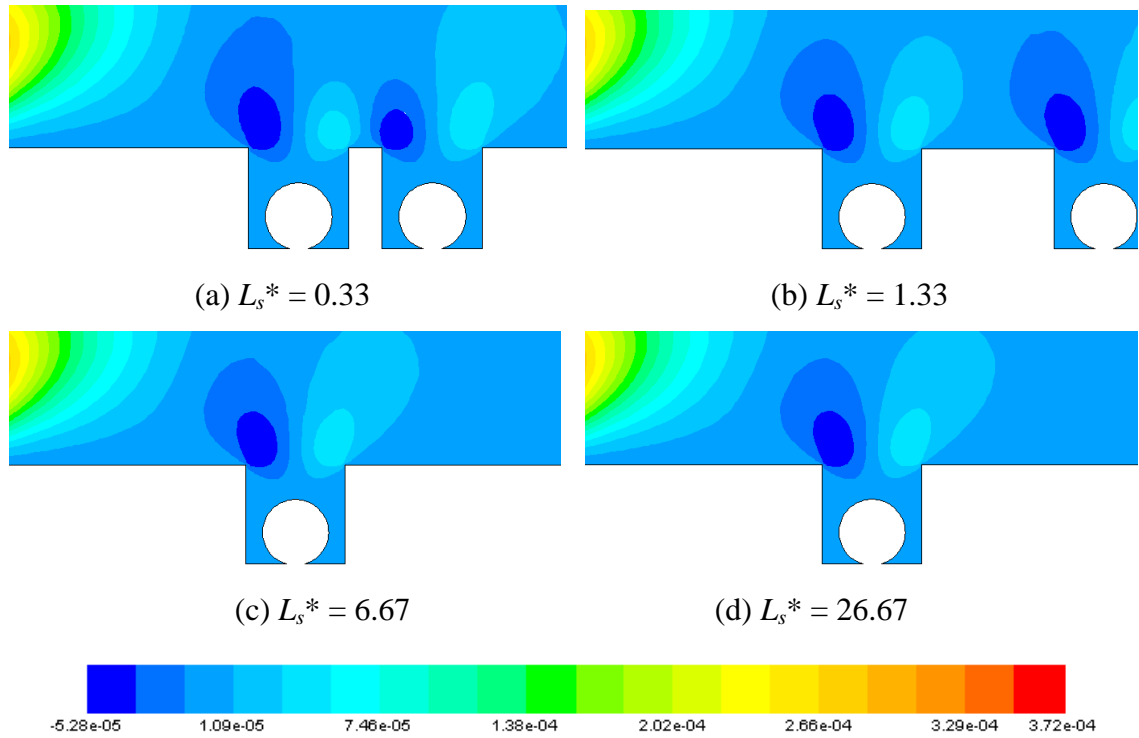


Figure 4.43: Contour plots showing the vertical velocity component (measured in m/s) in the front cavity as  $L_s^*$  is increased from a small value to large value.

Further investigations reveal that non-negligible interference occurs when the cavity spacing is smaller than 1.67 times of the cavity length. Evidence is provided in Table 4.17 and Figure 4.44, where the velocity at sample points decreases sharply and then stabilizes as  $L_s^*$  is increased from 0.07 to 1.67. Note that the velocity at Point 1 stabilizes at  $L_s^*$  of 1.33, while the velocity at Point 2 stabilizes at  $L_s^*$  of 1.67. Beyond  $L_s^* = 1.67$ , the interference between the cavities, in terms of affecting the flow in each cavity, is very small.

		Point velocity		Normalized point velocity	
Cavity spacing, $L_s$	Normalized cavity spacing, $L_s^*$	Point 1	Point 2	Point 1	Point 2
$\mu\text{m}$		m/s	m/s		
10	0.07	3.897E-09	-4.280E-09	3.897E-06	-4.280E-06
20	0.13	3.881E-09	-4.163E-09	3.881E-06	-4.163E-06
30	0.20	3.867E-09	-4.084E-09	3.867E-06	-4.084E-06
40	0.27	3.854E-09	-4.027E-09	3.854E-06	-4.027E-06
50	0.33	3.844E-09	-3.986E-09	3.844E-06	-3.986E-06
100	0.67	3.819E-09	-3.897E-09	3.819E-06	-3.897E-06
150	1.00	3.809E-09	-3.864E-09	3.809E-06	-3.864E-06
200	1.33	3.800E-09	-3.847E-09	3.800E-06	-3.847E-06
250	1.67	3.799E-09	-3.842E-09	3.799E-06	-3.842E-06
300	2.00	3.798E-09	-3.839E-09	3.798E-06	-3.839E-06
350	2.33	3.797E-09	-3.837E-09	3.797E-06	-3.837E-06
400	2.67	3.798E-09	-3.839E-09	3.798E-06	-3.839E-06
450	3.00	3.797E-09	-3.836E-09	3.797E-06	-3.836E-06
500	3.33	3.797E-09	-3.837E-09	3.797E-06	-3.837E-06
600	4.00	3.799E-09	-3.838E-09	3.799E-06	-3.838E-06
700	4.67	3.797E-09	-3.838E-09	3.797E-06	-3.838E-06
800	5.33	3.798E-09	-3.838E-09	3.798E-06	-3.838E-06
1000	6.67	3.798E-09	-3.836E-09	3.798E-06	-3.836E-06
2000	13.33	3.796E-09	-3.841E-09	3.796E-06	-3.841E-06
3000	20.00	3.796E-09	-3.837E-09	3.796E-06	-3.837E-06
4000	26.67	3.798E-09	-3.836E-09	3.798E-06	-3.836E-06

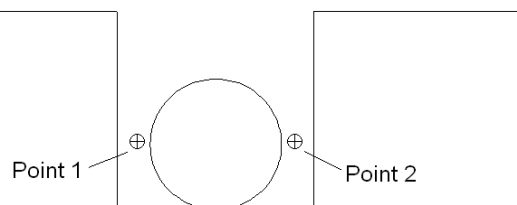


Table 4.17: The vertical velocity components at point 1 and 2 around the embryo demonstrating the evolution as  $L_s$  increases. The normalized velocity components are obtained by dividing them with the inflow velocity (0.001 m/s).

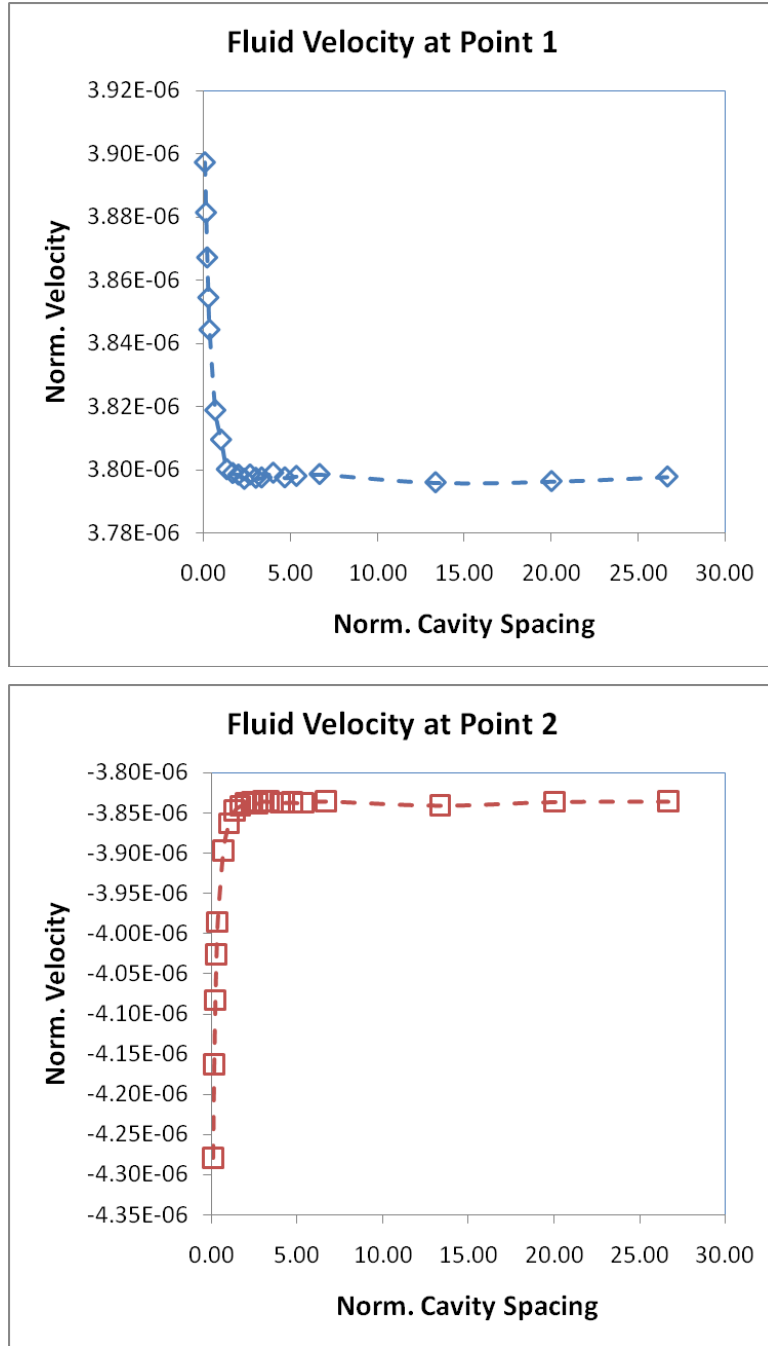


Figure 4.44: Plots of vertical velocity components at points 1 and 2 revealing that as  $L_s^*$  becomes larger the velocity components rapidly stabilize.

### 4.6.3 Cavity Spacing: Change of Solute Concentration

For the purpose of quantifying the effect of changing  $L_s^*$  on altering the solute transport around the embryo, the solute concentration of lactate and oxygen on the embryo surface (Table 4.17 and Figure 4.42) is examined.

Firstly, solute transport for the front cavity (Cavity 1) is examined. The solute concentration on the embryo in this cavity does not change much as  $L_s^*$  is increased from 0.067 to 26.67. There is a minor change in the solute concentration when the two cavities are very close ( $L_s^* = 0.067 \sim 1.67$ ). This is shown by the rise in normalized lactate concentration from 0.995 to 0.999 and slight fall in normalized oxygen concentration level from 1.0001 to 1.0000. These trends seem to be explained by the accelerated fluid flow across the cavities due to the presence of the rear cavity in close vicinity. As  $L_s^*$  increases, the solute concentration quickly approaches the level for an isolated cavity.

In contrast, for the rear cavity (Cavity 2), the normalized lactate concentration recorded on the embryo decreases sharply from 1.116 to 1.011 while the normalized oxygen concentration increases rapidly from 0.9963 to 0.9996 when  $L_s^*$  is increased up to 6.67; these variations start to stabilise as  $L_s^*$  increased above 6.67. Aside from that, it must be noted that regardless of the change, lactate concentration on the embryo in the rear cavity is always higher than that in the front cavity. In a similar sense for oxygen, the concentration level recorded in the rear cavity is always lower than that for the front cavity.

From these observations, it is evident that solute transport in the front cavity has a larger impact on the rear cavity. When  $L_s^*$  is small, a reasonable fraction of the lactate produced from the embryo in the front cavity passes through the rear cavity, causing the overall lactate concentration in the rear cavity to rise. Likewise for oxygen, some of the oxygen flowing into the front cavity from the inlet is absorbed by the embryo, decreasing the availability for the rear embryo. As  $L_s^*$  is increased, the growing distance between the two cavities allows more lactate produced by the embryo in the front cavity to be advected and diffused to the main flow in the channel rather than being transported into the rear cavity. This directly lowers the lactate concentration in

the rear cavity. Similarly, the larger distance between the cavities allows more oxygen from the channel flow to be passed into the rear cavity to the embryo, raising the oxygen concentration level there. When the two cavities are very far apart, the solute distributions in the rear cavity approach the isolated cavity case, indicating that interference becoming increasing less significant.

Norm. cavity spacing, $L_s^*$	Lactate concentration		Norm. lactate concentration		Oxygen concentration		Normalized oxygen concentration	
	Cavity 1	Cavity 2	Cavity 1	Cavity 2	Cavity 1	Cavity 2	Cavity 1	Cavity 2
	M	M			M	M		
0.067	1.6222E-06	1.8198E-06	0.9951	1.1163	2.1205E-04	2.1124E-04	1.0001	0.9963
0.133	1.6232E-06	1.8109E-06	0.9957	1.1108	2.1205E-04	2.1128E-04	1.0001	0.9965
0.2	1.6236E-06	1.8035E-06	0.9959	1.1062	2.1205E-04	2.1131E-04	1.0001	0.9966
0.267	1.6243E-06	1.7970E-06	0.9964	1.1023	2.1205E-04	2.1133E-04	1.0001	0.9967
0.333	1.6258E-06	1.7902E-06	0.9972	1.0981	2.1204E-04	2.1136E-04	1.0001	0.9969
0.667	1.6270E-06	1.7642E-06	0.9980	1.0822	2.1204E-04	2.1146E-04	1.0001	0.9974
1	1.6279E-06	1.7477E-06	0.9985	1.0720	2.1204E-04	2.1153E-04	1.0000	0.9977
1.333	1.6281E-06	1.7361E-06	0.9987	1.0649	2.1204E-04	2.1158E-04	1.0000	0.9979
1.667	1.6283E-06	1.7263E-06	0.9988	1.0589	2.1203E-04	2.1162E-04	1.0000	0.9981
2	1.6283E-06	1.7189E-06	0.9988	1.0543	2.1203E-04	2.1165E-04	1.0000	0.9982
2.333	1.6282E-06	1.7128E-06	0.9988	1.0506	2.1203E-04	2.1168E-04	1.0000	0.9984
2.667	1.6282E-06	1.7073E-06	0.9987	1.0473	2.1203E-04	2.1170E-04	1.0000	0.9985
3	1.6282E-06	1.7027E-06	0.9987	1.0445	2.1203E-04	2.1172E-04	1.0000	0.9985
3.333	1.6282E-06	1.6988E-06	0.9987	1.0421	2.1203E-04	2.1173E-04	1.0000	0.9986
4	1.6279E-06	1.6924E-06	0.9986	1.0381	2.1204E-04	2.1176E-04	1.0000	0.9988
4.667	1.6280E-06	1.6874E-06	0.9986	1.0350	2.1204E-04	2.1178E-04	1.0000	0.9989
5.333	1.6281E-06	1.6831E-06	0.9987	1.0324	2.1204E-04	2.1180E-04	1.0000	0.9989
6.667	1.6282E-06	1.6766E-06	0.9987	1.0284	2.1203E-04	2.1183E-04	1.0000	0.9991
13.333	1.6279E-06	1.6601E-06	0.9986	1.0183	2.1204E-04	2.1190E-04	1.0000	0.9994
20	1.6281E-06	1.6529E-06	0.9987	1.0139	2.1203E-04	2.1193E-04	1.0000	0.9995
26.667	1.6282E-06	1.6489E-06	0.9987	1.0114	2.1203E-04	2.1194E-04	1.0000	0.9996

Table 4.18: Tabulated values of lactate and oxygen obtained from the simulations. The concentration was normalized by the default solute concentrations from Table 4.2.

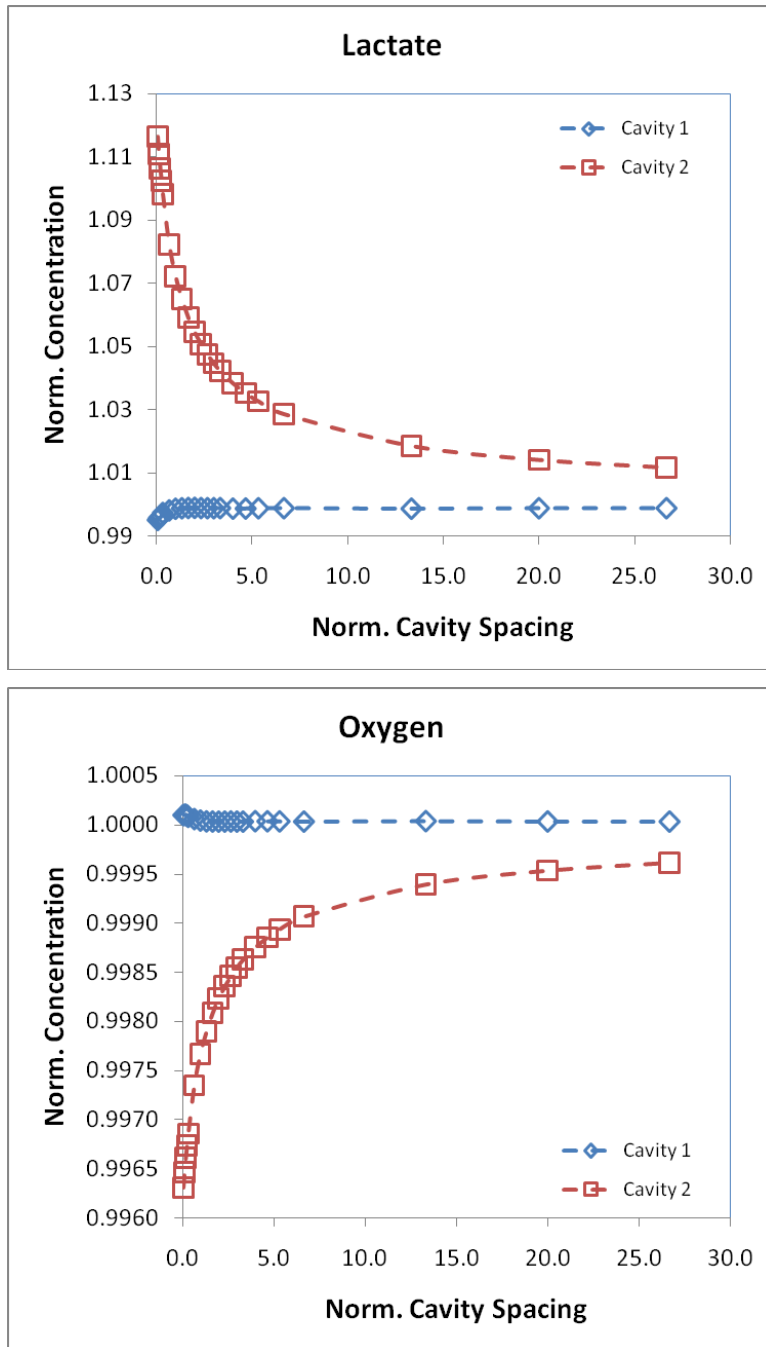
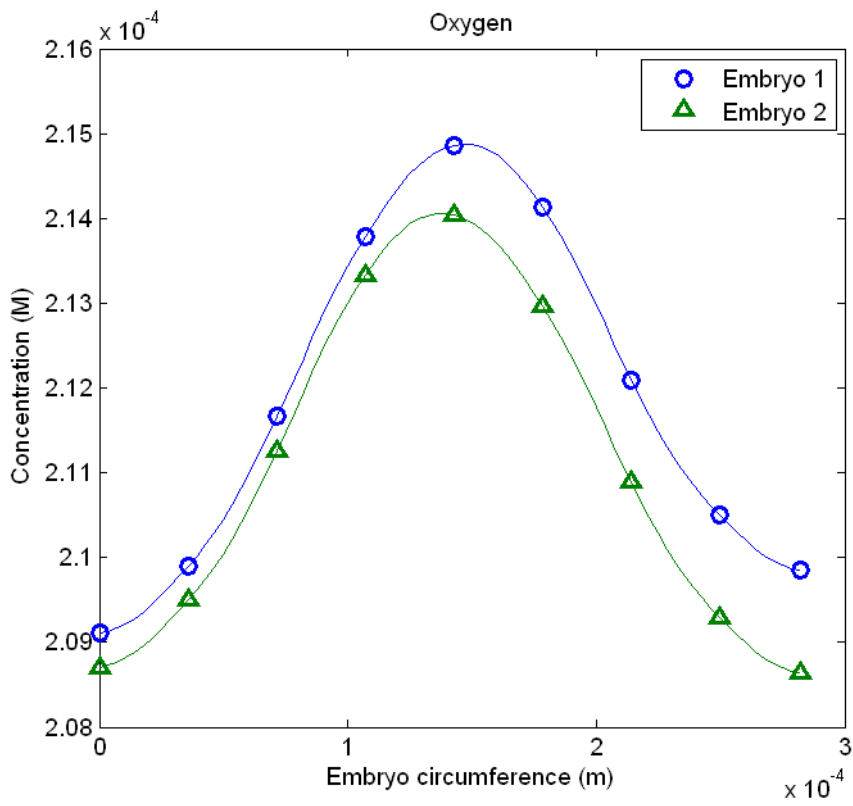
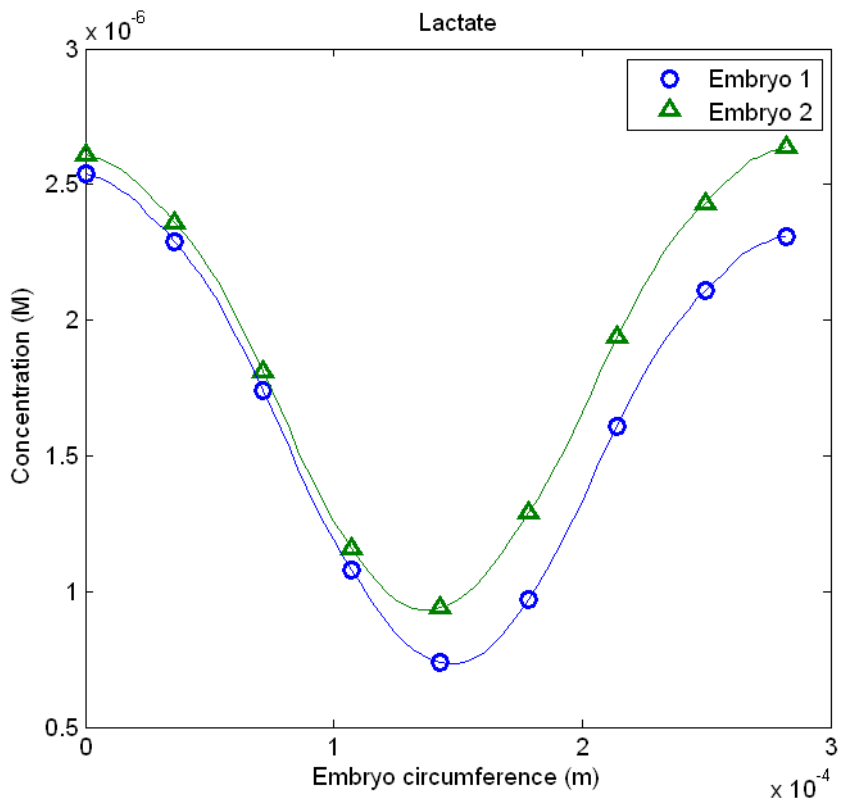


Figure 4.45: Plots showing the variation of the lactate and oxygen concentration (averaged across the embryo surface) due to the changes in  $L_s^*$ .

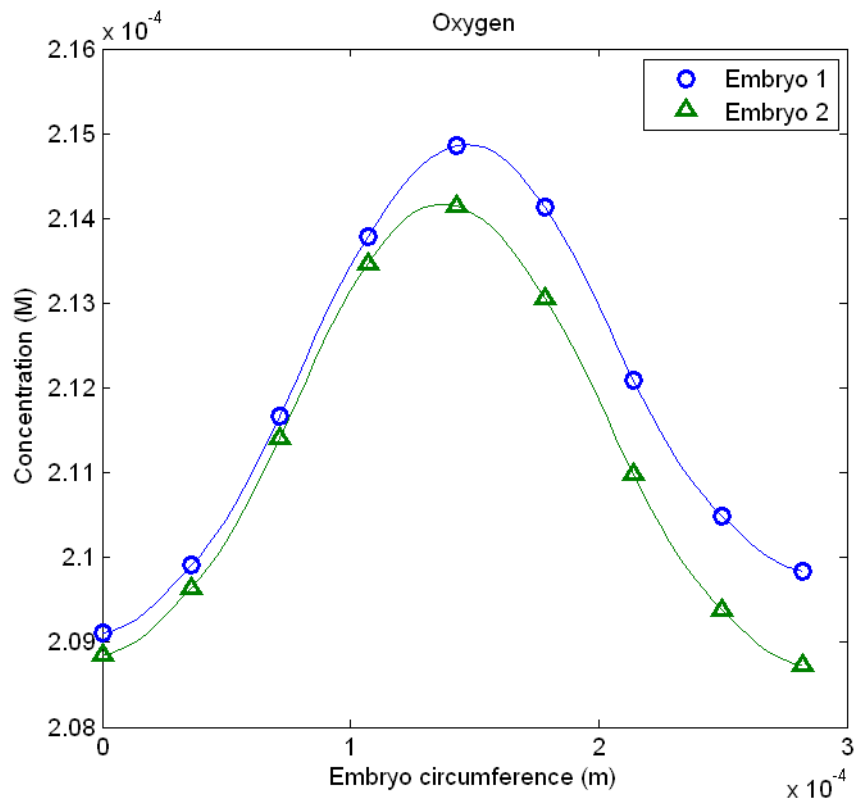
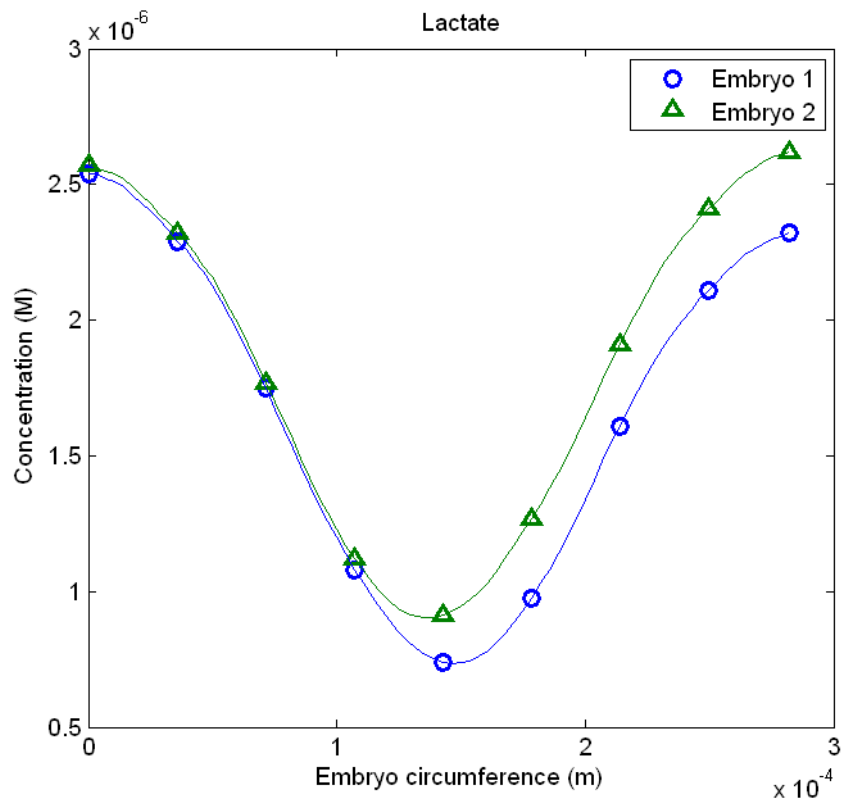
#### 4.6.4 Cavity Spacing: Solute Distribution around the Embryo

By examining the circumferential solute concentration profiles of Figure 4.46, it can be deduced that the distributions do not vary significantly in their general shape. Regardless of the cavity spacing, lactate concentration generally exhibits a downward bell-shaped profile (Figure 4.46, left) and oxygen shows an upward bell-shape profile (Figure 4.46, right). Again, this is due to the low flow velocities at the base of the cavity and much higher velocities towards the top.

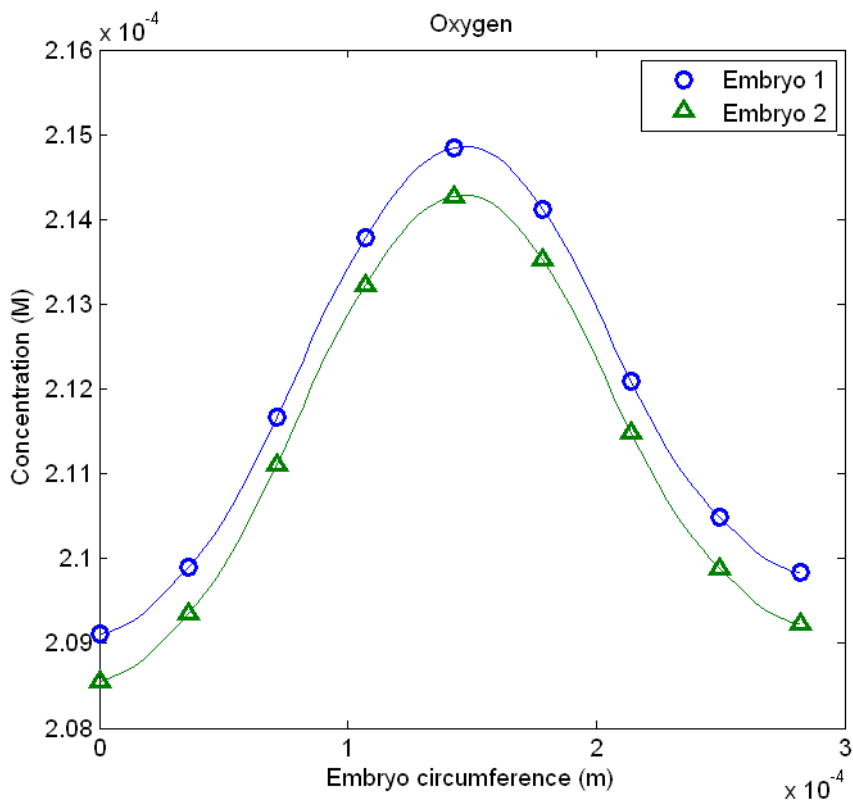
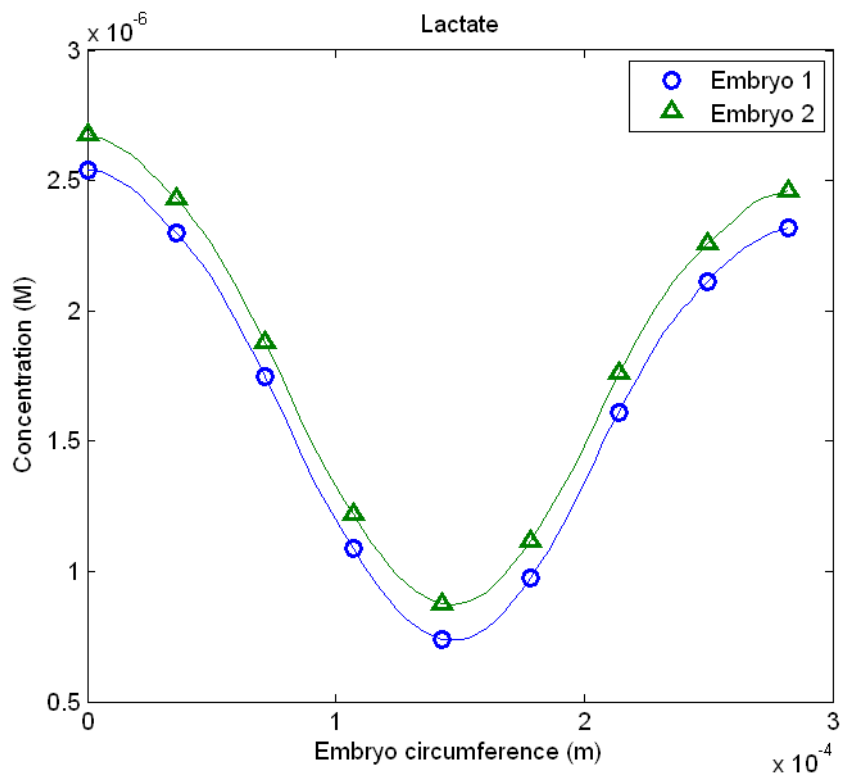
Focusing into comparing the solute concentration profiles between the front embryo (Embryo 1) and rear embryo (Embryo 2), one can notice the relatively subtle difference in the magnitude of the solute concentration when  $L_s^*$  is small ( $0.067 \sim 0.667$ ), as revealed by the gap between the concentration profiles of Embryo 1 and Embryo 2, shown in Figures 4.46a, 4.46b and 4.46c. This difference diminishes as  $L_s^*$  is increased to 26.67, as can be seen in Figure 4.46d to 4.46f, where the gap shrinks until both concentration profiles overlap.



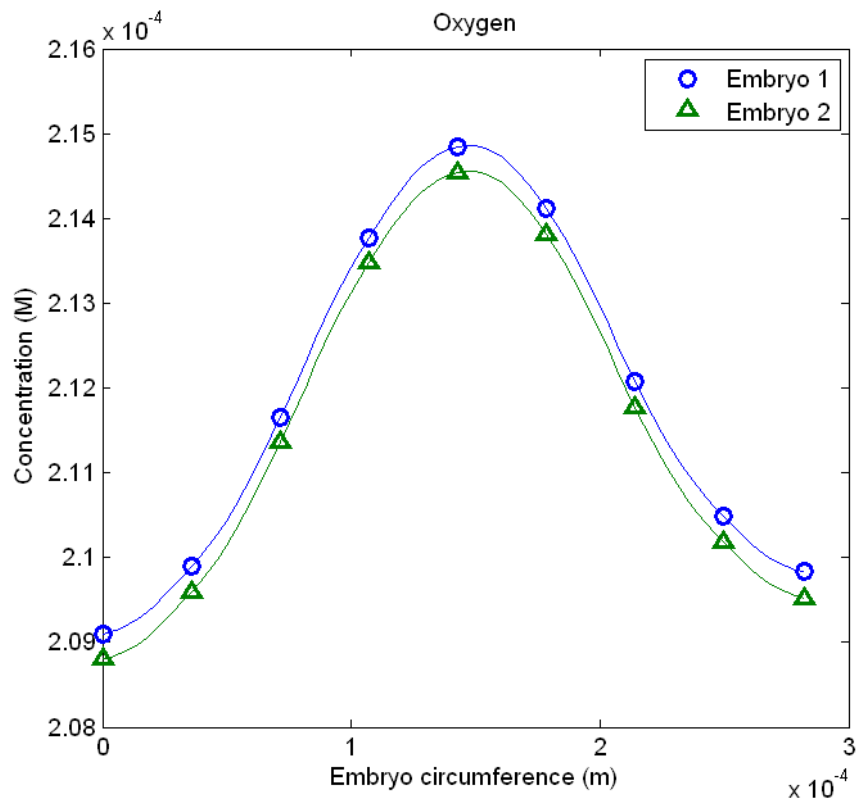
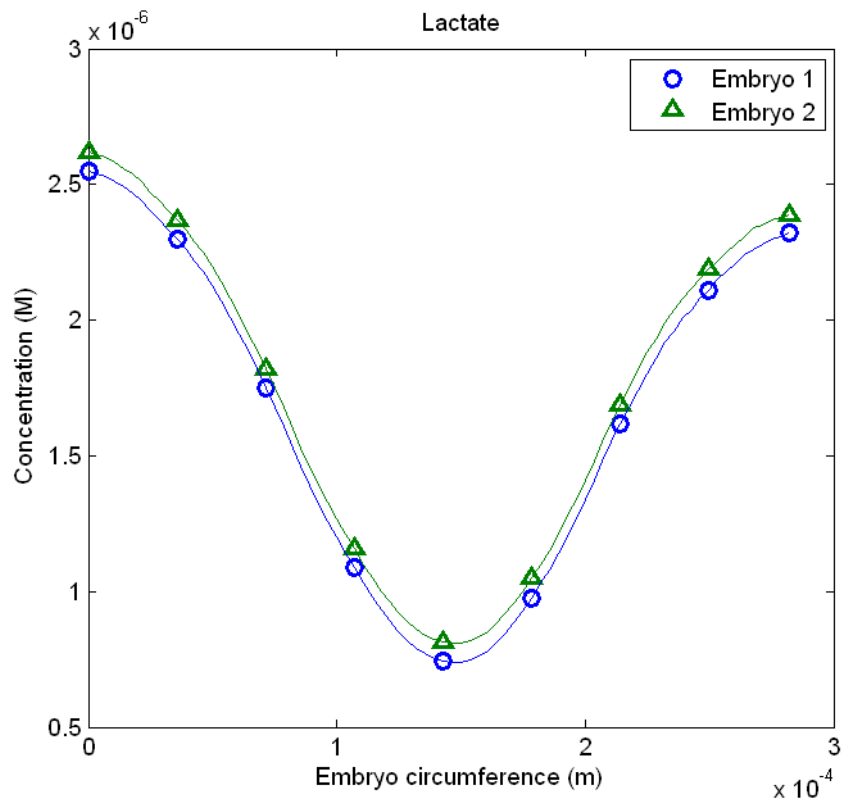
(a)  $L_s^* = 0.067$



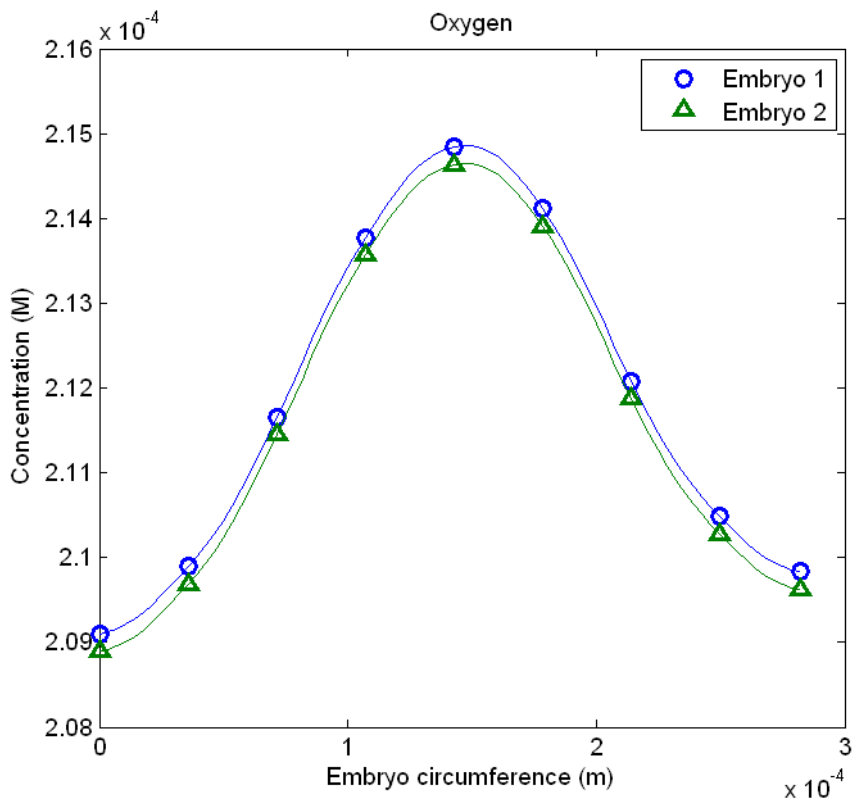
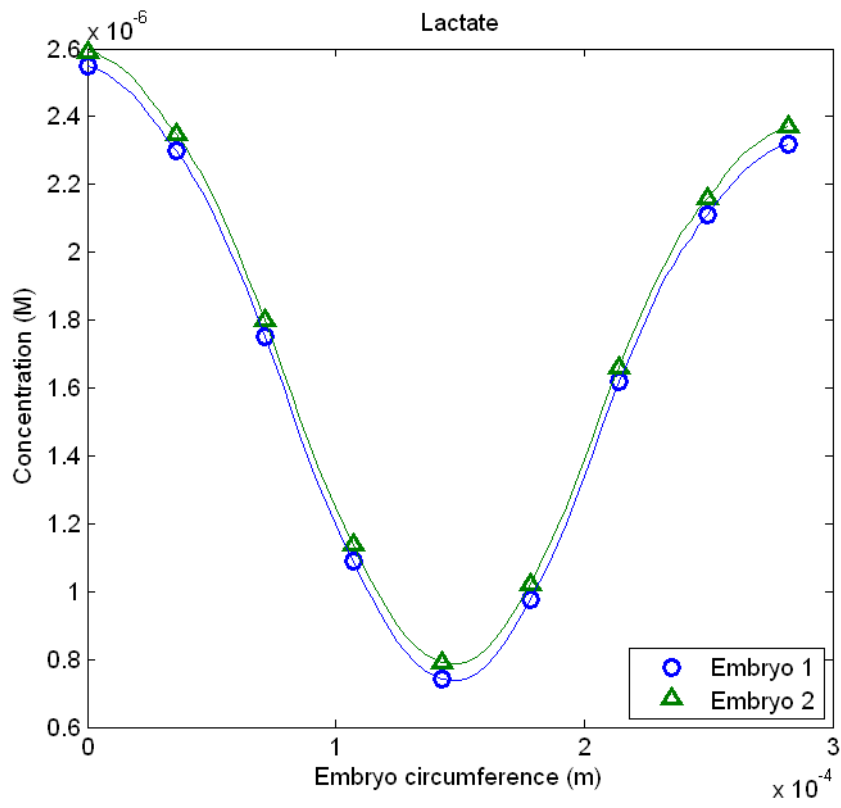
(b)  $L_s^* = 0.333$



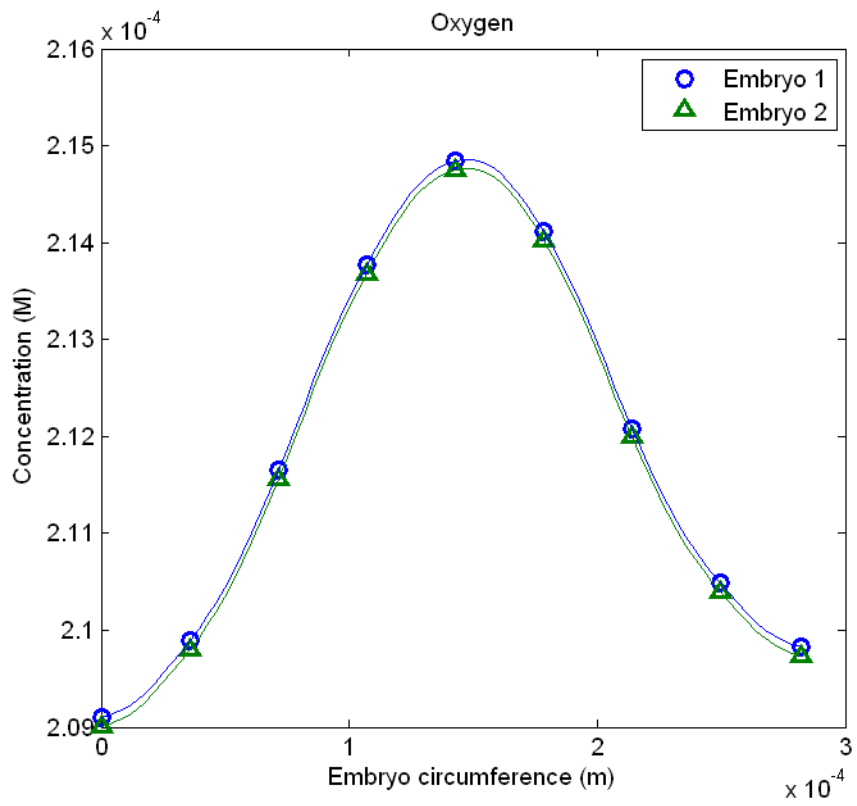
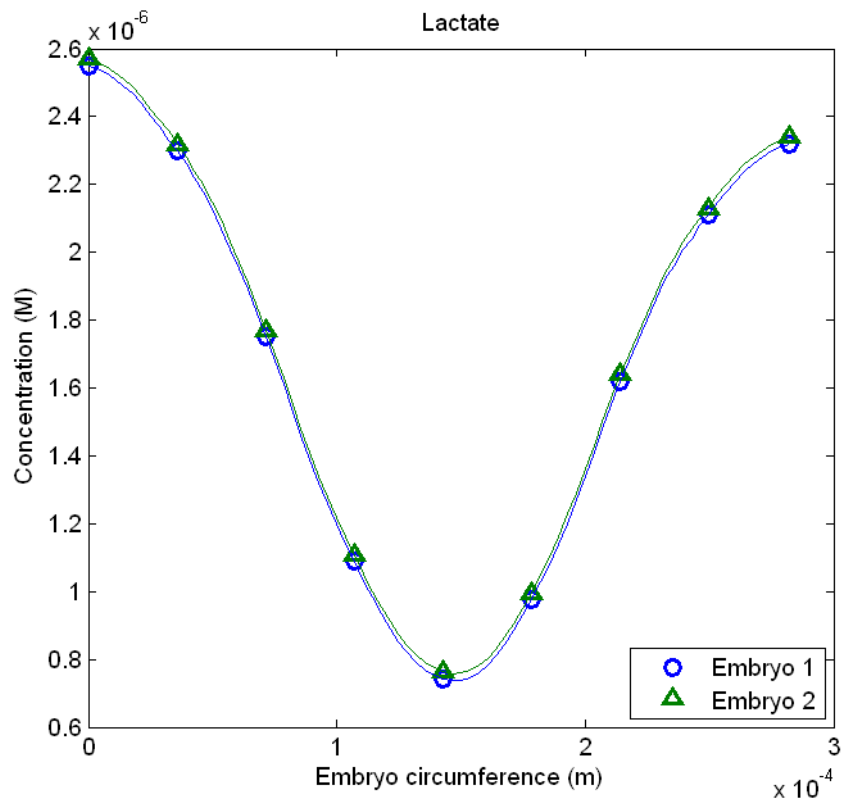
(c)  $L_s^* = 0.667$



(d)  $L_s^* = 3.333$



(e)  $L_s^* = 6.667$



(f)  $L_s^* = 26.667$

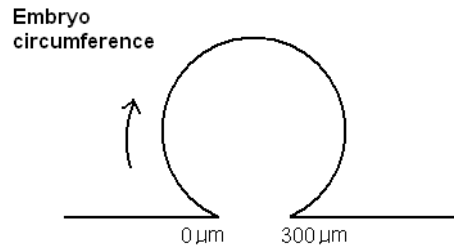


Figure 4.46: Evolution of the concentration distribution profiles of lactate (left) and oxygen (right) along the surface of the front embryo (Embryo 1), and rear embryo (Embryo 2), as  $L_s^*$  is increased from 0.067 to 26.667. Refer to Figure 4.42a for details on the notation of front and rear embryo.

#### 4.6.5 Multiple Cavity Interaction: Changes of Solute Concentration

Figure 4.47 summarises the oxygen and lactate levels in each of the cavities for the isolated and multiple cavity cases with the cavity separation equal to  $L_s^* = 1.33$ . This figure highlights two main features: the effective constancy of the solute levels within each cavity with the same sequence number, whether it belongs to a single or multiple cavity bioreactors; and the variation between cavities in the same bioreactor. For the case examined here lactate is about 11% higher in the third cavity of a three cavity bioreactor, while oxygen is only 0.35% lower.

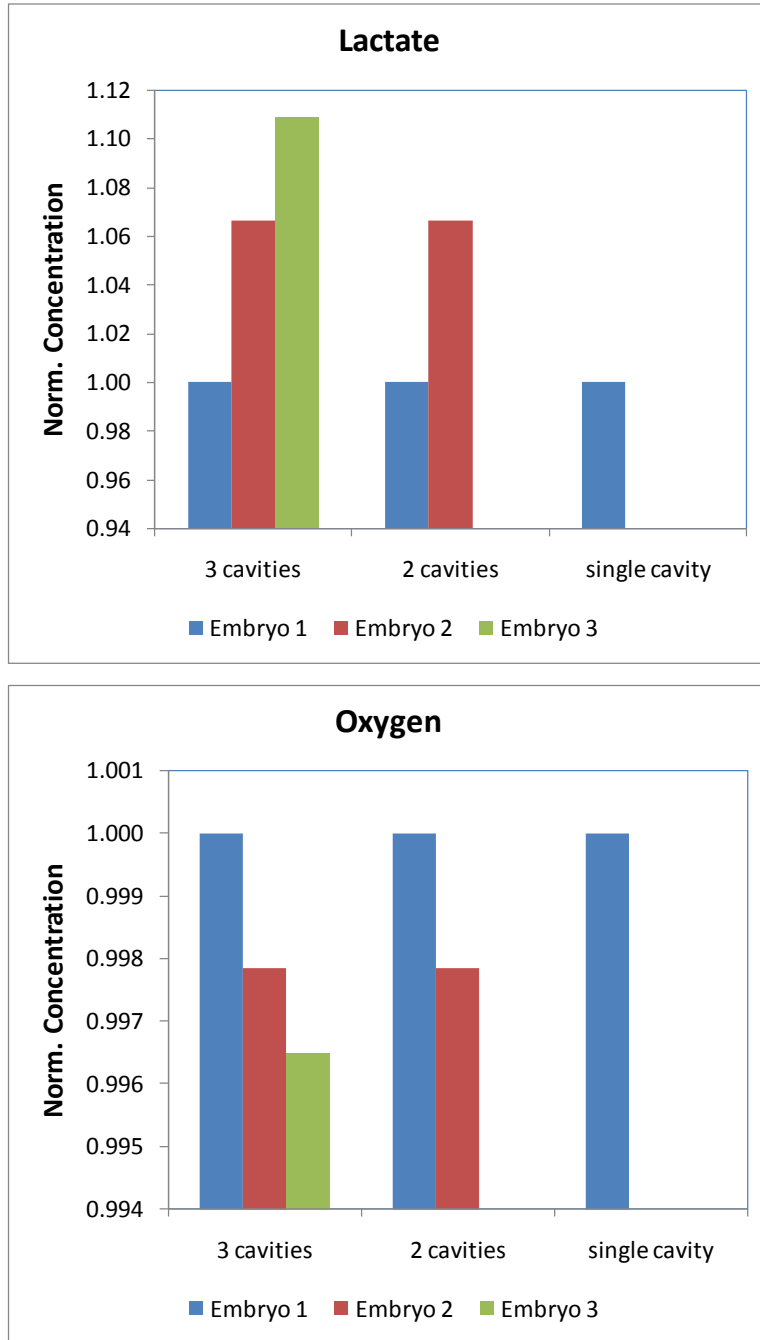
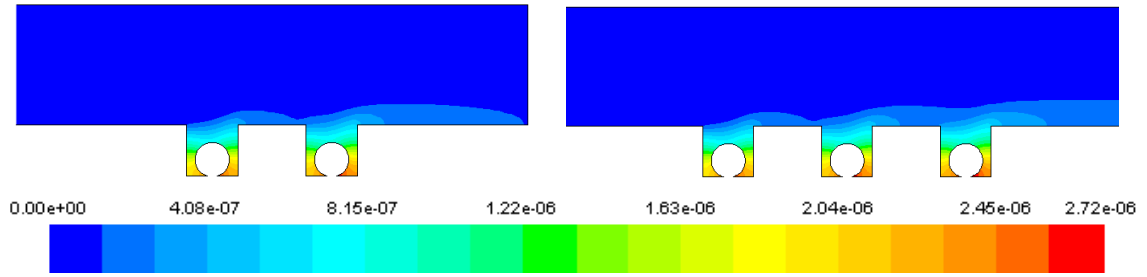
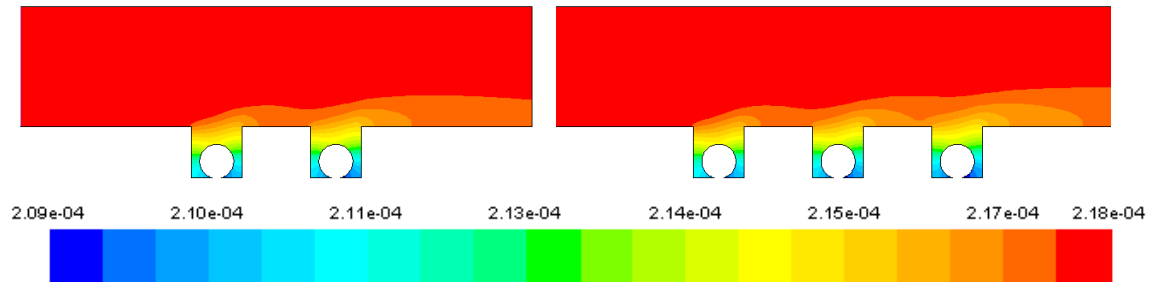


Figure 4.47: Normalized values of lactate and oxygen concentration averaged on the embryo surface for three cases of single, two and three cavities. The normalization is obtained by dividing the solute concentration level with the default lactate and oxygen concentration level. For the case of two cavities, Cavity 1 and 2 denotes front and rear cavity respectively; for the case of three cavities, Cavity 1, 2 and 3 denotes front, middle and rear cavity respectively.



(a) Lactate

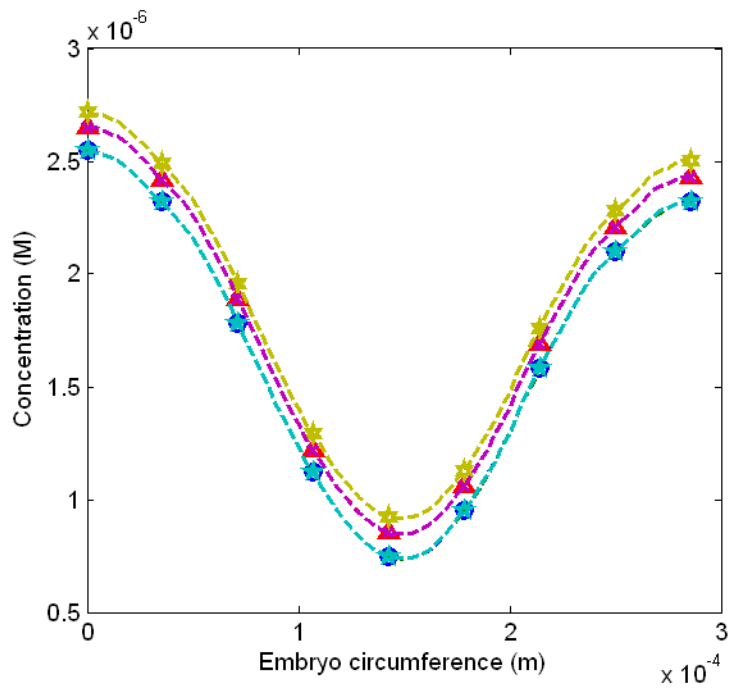


(b) Oxygen

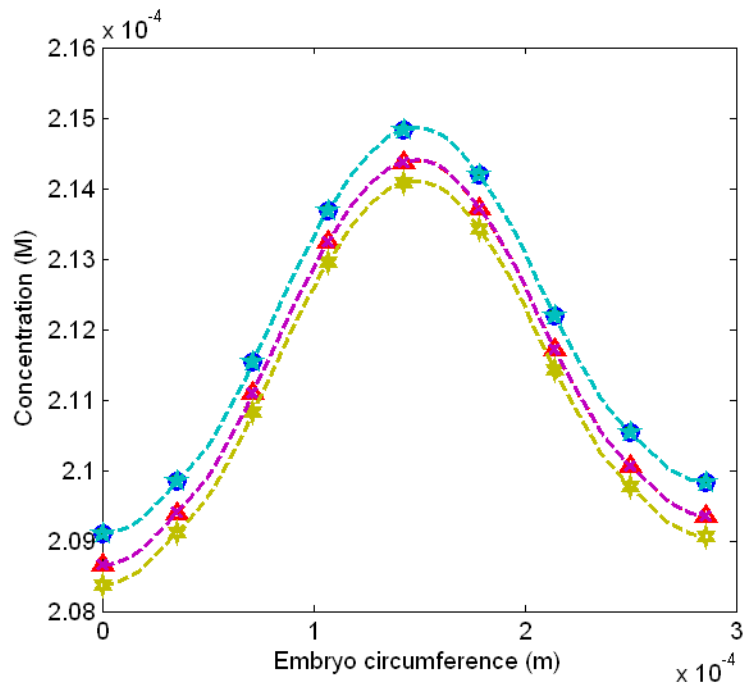
Figure 4.48: Contour plots of lactate (a) and oxygen (b) concentration (measured in M) in the bioreactor, highlighting how the front cavity affects the solute transport in the rear cavity.

#### 4.6.6 Multiple Cavity Interaction: Solute Distribution around the Embryo

It is also observed from Figure 4.48, and consistent with the findings presented in section 4.6.4, the distribution of solutes in and around different cavities remains similar regardless of how many cavities are situated in proximity. This is also shown by the solute concentration plots around the embryo represented by Figure 4.49, where the shape of the distribution profile is the same for each embryo. As for the two cavity case, the only dissimilarity between these distribution profiles is their overall magnitude, where the overall lactate concentration on embryo 1 is slightly lower than embryo 2, and the overall lactate concentration on embryo 2 is slightly lower than embryo 3 (Figure 4.49a). The lactate concentration on both embryo 1 in the case of two cavities and three cavities is essentially the same, where this is reflected in Figure 4.47. These trends are also observed on oxygen concentration in the opposite sense (Figure 4.49b).



(a) Lactate



Oxygen

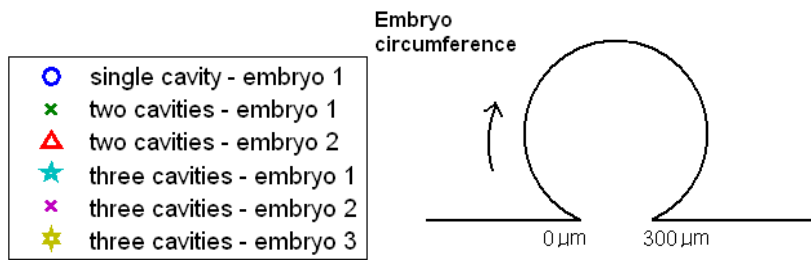


Figure 4.49: Plots of (a) lactate and (b) oxygen concentration distributions profiles for all the embryos in different cavities, emphasizing the similarity of the distribution profiles regardless of the number of cavities in proximity.

#### 4.6.7 Implication for Solute Transport

From the sub-study on cavity spacing, it can be concluded that when there are two cavities located in proximity, interference on the solute transport occurs between them and this interference becomes more important as the spacing,  $L_s$ , between the cavities shrinks. It is also found that the interference is insignificant when  $L_s$  is larger than 6.67 times of the cavity length. Note that this is considerably larger than the distance at which the flow within each cavity is no longer affected ( $L_s = 1.67$ ). This is presumably due to the lower diffusivities of lactate and oxygen relative to momentum, so that advection is more important for solute transport. The circumferential distributions of each solute around the embryo appear to be unaffected in shape by changes in  $L_s$ . Using these findings as a guide, one can regulate the solute transport in the bioreactor to tailor it for different requirements arising in embryo cultivation. For example, if it is necessary to retain the growth factors, the cavities should be placed nearer; if the aim is to prevent metabolic waste build up due to scaling up embryo cultivation, the spacing between cavities should be enlarged.

The sub-study on multiple cavity interaction revealed that having more cavities does not have much influence on the solute concentration within each. However, the distance between cavities can determine the amount of solute present around an embryo to some extent. One cavity is only able to extend its influence to an adjacent cavity if the spacing between them is small. In effect this means that one does not need to be concerned too much about the side effect of placing more cavities in proximity when trying scale up embryo production as doing so has little effect on solute transport in each individual cavity.

#### 4.6.8 Cavity Spacing: Changes to Shear Stress

As can be seen from Figure 4.50, the normalized shear stresses on both the embryos in the front and rear cavities increase rapidly by 14% when  $L_s^*$  is reduced from 1.667 to 0.067. This is anticipated due to the fact that when the two cavities are close to each other, the flow interference between the two cavities enhances the fluid movement in the cavities, directly increasing the shear stress. As the two cavities are moved further apart, this interference effect lessens and hence the shear stress drops. When  $L_s^*$  is larger than 3.333, the shear stress approaches the asymptotic level. These findings are consistent with those found when examining solute transport.

Also, it should be noted that there is an almost constant small stress level difference between the front cavity (Cavity 1) and rear cavity (Cavity 2). It is found that this occurs because the inlet flow disturbs the vertical velocity component at the front cavity while the rear cavity is not affected. As illustrated in Figure 4.43, for the cases of large  $L_s^*$ , the velocity gradient created at the inlet suppresses the vertical velocity gradient located at the upstream side of the front cavity, causing it to be smaller than the vertical velocity gradient located at the upstream side of the rear cavity. The difference in these velocity gradients translates to slight difference in the overall rate of fluid movement in the cavity, where this causes the constant shear stress gap to appear.

Normalized cavity spacing, $L_s^*$	Shear stress		Normalized shear stress	
	Cavity 1	Cavity 2	Cavity 1	Cavity 2
	Pa	Pa		
0.067	3.0824E-04	3.0578E-04	1.1405	1.1314
0.133	3.0017E-04	2.9665E-04	1.1106	1.0976
0.200	2.9179E-04	2.9116E-04	1.0796	1.0773
0.267	2.8686E-04	2.8708E-04	1.0614	1.0622
0.333	2.8740E-04	2.8406E-04	1.0634	1.0510
0.667	2.7888E-04	2.7668E-04	1.0318	1.0237
1.000	2.7694E-04	2.7313E-04	1.0247	1.0106
1.333	2.7482E-04	2.7223E-04	1.0168	1.0072
1.667	2.7462E-04	2.7080E-04	1.0161	1.0019
2.000	2.7455E-04	2.7126E-04	1.0158	1.0036
2.333	2.7373E-04	2.7166E-04	1.0128	1.0051
2.667	2.7395E-04	2.7080E-04	1.0136	1.0019
3.000	2.7341E-04	2.7038E-04	1.0116	1.0004
3.333	2.7360E-04	2.7058E-04	1.0123	1.0011
4.000	2.7302E-04	2.7069E-04	1.0102	1.0016
4.667	2.7281E-04	2.7058E-04	1.0094	1.0011
5.333	2.7352E-04	2.7083E-04	1.0120	1.0021
6.667	2.7342E-04	2.7042E-04	1.0116	1.0005
13.333	2.7292E-04	2.7109E-04	1.0098	1.0030
20.000	2.7331E-04	2.7065E-04	1.0112	1.0014
26.667	2.7338E-04	2.7090E-04	1.0115	1.0023

Table 4.19: Tabulated values of shear stress averaged across the embryo surface. The normalized versions of them were obtained by dividing the shear stress with the default shear stress as indicated in Table 4.2.

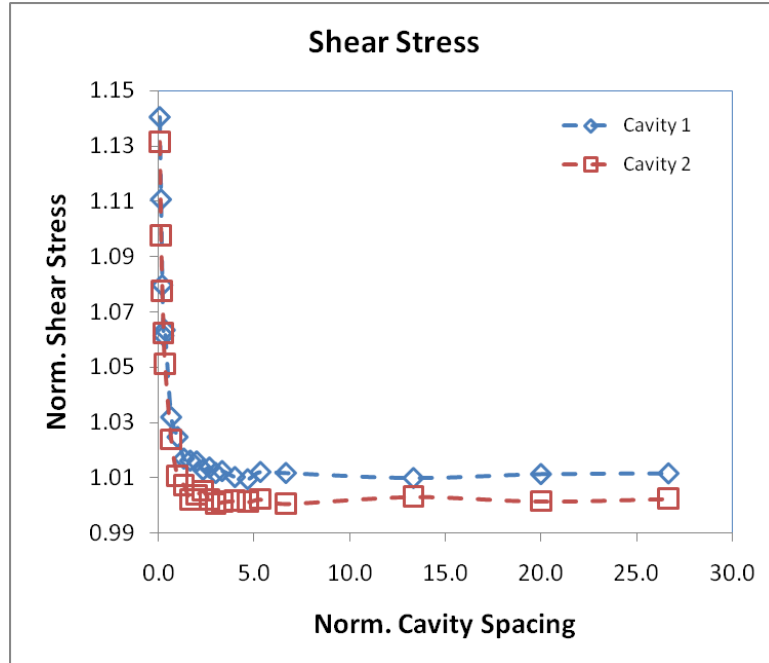


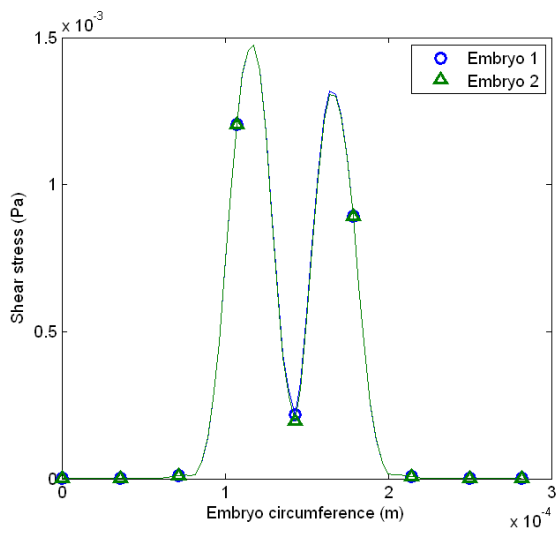
Figure 4.50: Plot showing the variation of the normalized shear stress (averaged across the embryo surface) due to the changes in  $L_s^*$ .

#### 4.6.9 Cavity Spacing: Shear Stress Distribution on the Embryo

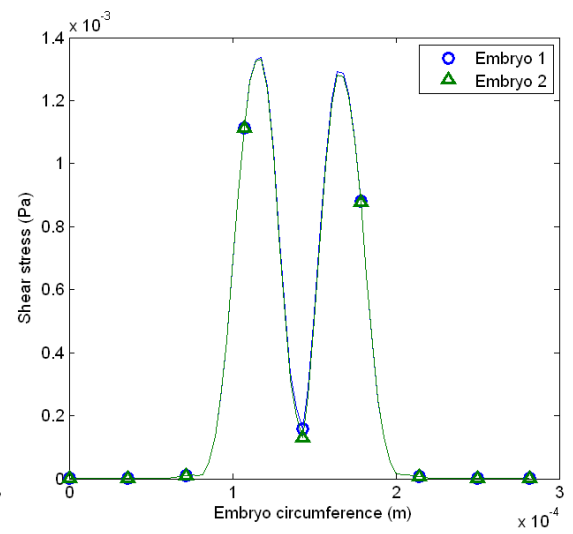
The shear stress distributions on both embryos are similar regardless of how far the two cavities are situated apart, as illustrated in Figure 4.51. This is further reinforced by the findings from the flow structures around the embryo (Figure 4.52), where they are similar irrespective of how far apart the two cavities are situated. Once again, the reason is that the flow interaction between cavities does not affect the flow structures within each cavity by very much. Evidence is provided in Figure 4.52, where the flow circulation in both cavities is similar. The variation in cavity spacing only causes a minor change in the flow structure, where the two circulations above the embryo are shifted further away from each other.

The stress distribution profiles imposed on the embryo is related to the flow structures. Twin peak of shear stress appear around the upper part of the embryo. These are caused by the two flow circulations around the upper part of the cavity, which speed up the fluid movement there directly creating a higher local shear stress at the upper part of the embryo. At the top of the embryo, a stagnation point between the two flow recirculations occurs and this results in a sharp drop in shear stress at this location. The fluid movement at the bottom of the embryo is significantly slower than that over the

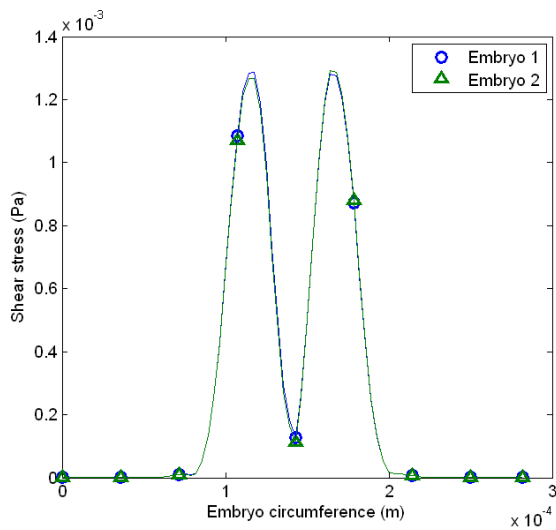
upper region of the cavity, since the fluid there is stagnant. This is why the shear stress at the bottom of the embryo is negligibly low.



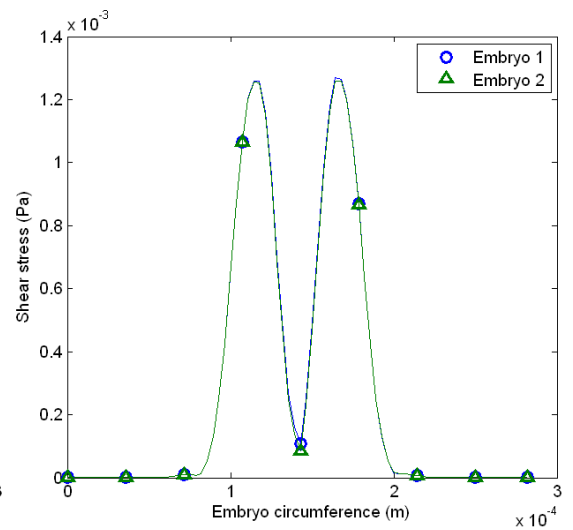
(a)  $L_s^* = 0.067$



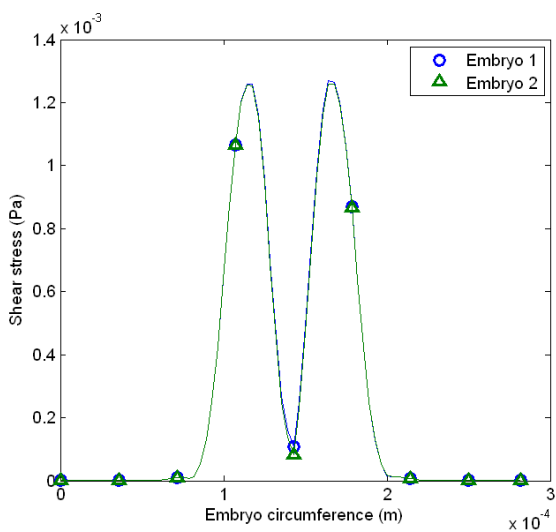
(b)  $L_s^* = 0.333$



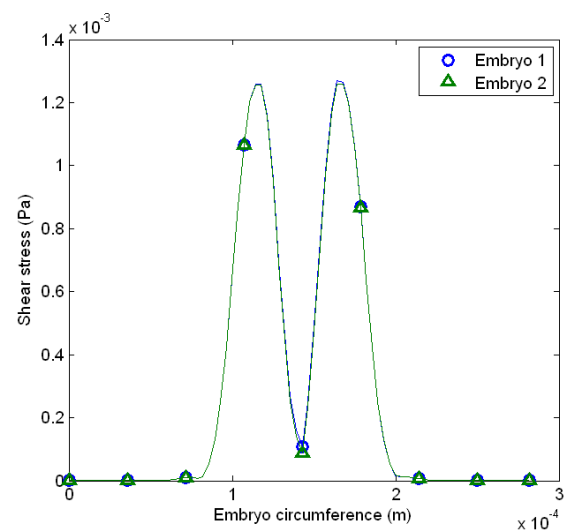
(c)  $L_s^* = 0.667$



(d)  $L_s^* = 3.333$



(e)  $L_s = 6.667$



(f)  $L_s = 26.667$

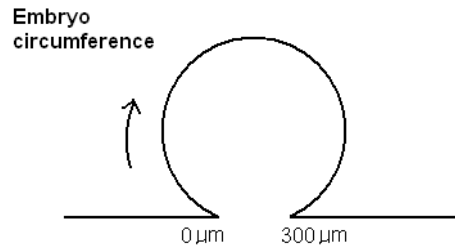


Figure 4.51: Shear stress distributions on the two embryos located in different cavities spaced apart from  $L_s^* = 0.067$  to  $L_s^* = 26.667$ .

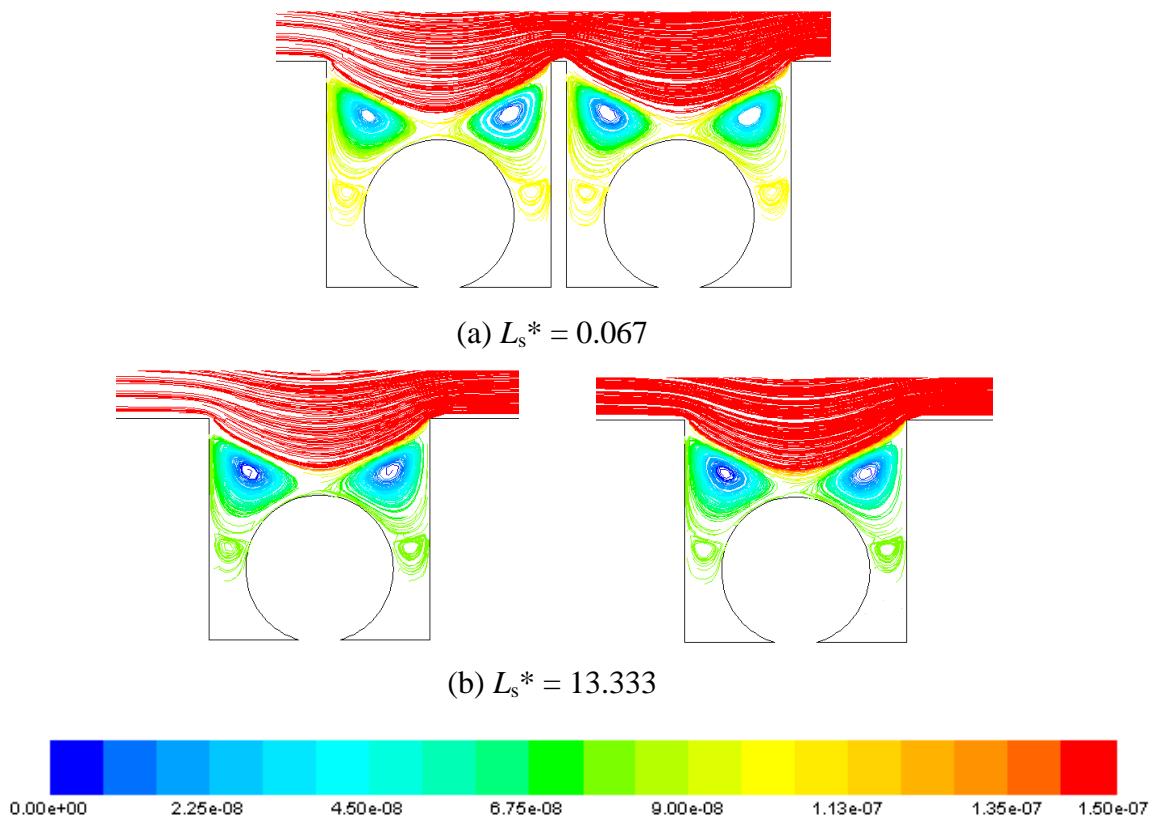


Figure 4.52: Streamline plots indicating the flow structures in the cavities for the case of (a)  $L_s^* = 0.067$ , which represents situation where the cavities are in close proximity, and (b)  $L_s^* = 13.333$ , which represents the situation where they are far apart. The strength of the flow recirculation is measured in kg/s.

#### 4.6.10 Multiple Cavity Interaction: Change of Shear Stress

The overall shear stress imposed on the embryos is slightly higher when several of the cavities are located closely. Looking at the shear stresses comparison in Figure 4.53, one can observe that the highest shear stress is caused when there are more cavities in close proximity. This is expected because when multiple cavities are in proximity they

speed up the fluid movement. This is evidenced from the smaller vertical velocity contours that appeared in between the cavities (Figure 4.54), where this smaller velocity contour highlighted the rapid velocity acceleration or deceleration when the fluid flow enters and exits the cavity. As shear stress is directly related to adjacent fluid movement, enhanced fluid movement will increase the induced shear stress. The occurrence of these smaller vertical velocities is caused by minor flow interference between the cavities. Note that the overall shear stress variation between sequential embryos for the spacing chosen here is only about  $\pm 1\%$ .

As we compare the shear stresses on the different embryos in a bioreactor with multiple cavities, the stresses decrease progressively from upstream to downstream. This is understandable as some of the flow momentum is lost after the fluid passes each cavity. Because of this, the fluid flow passing over the next adjacent cavity becomes locally slower and hence the shear stress induced on the embryo in that cavity is slightly lower.

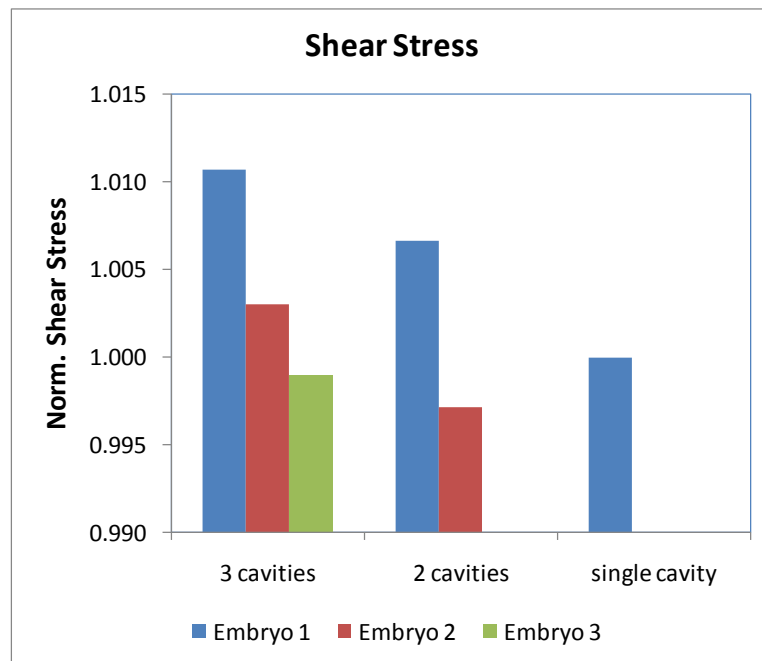


Figure 4.53: The normalized surface shear stress for three cases of single, two and three cavities in the bioreactor is presented. The normalization process involved dividing the stress level with the default shear stress indicated in Table 4.2. Embryo 1 denotes the embryo located in Cavity 1, Embryo 2 denotes the embryo located in Cavity 2 and so on. Cavity 1 is place in front of Cavity 2 and Cavity 3.

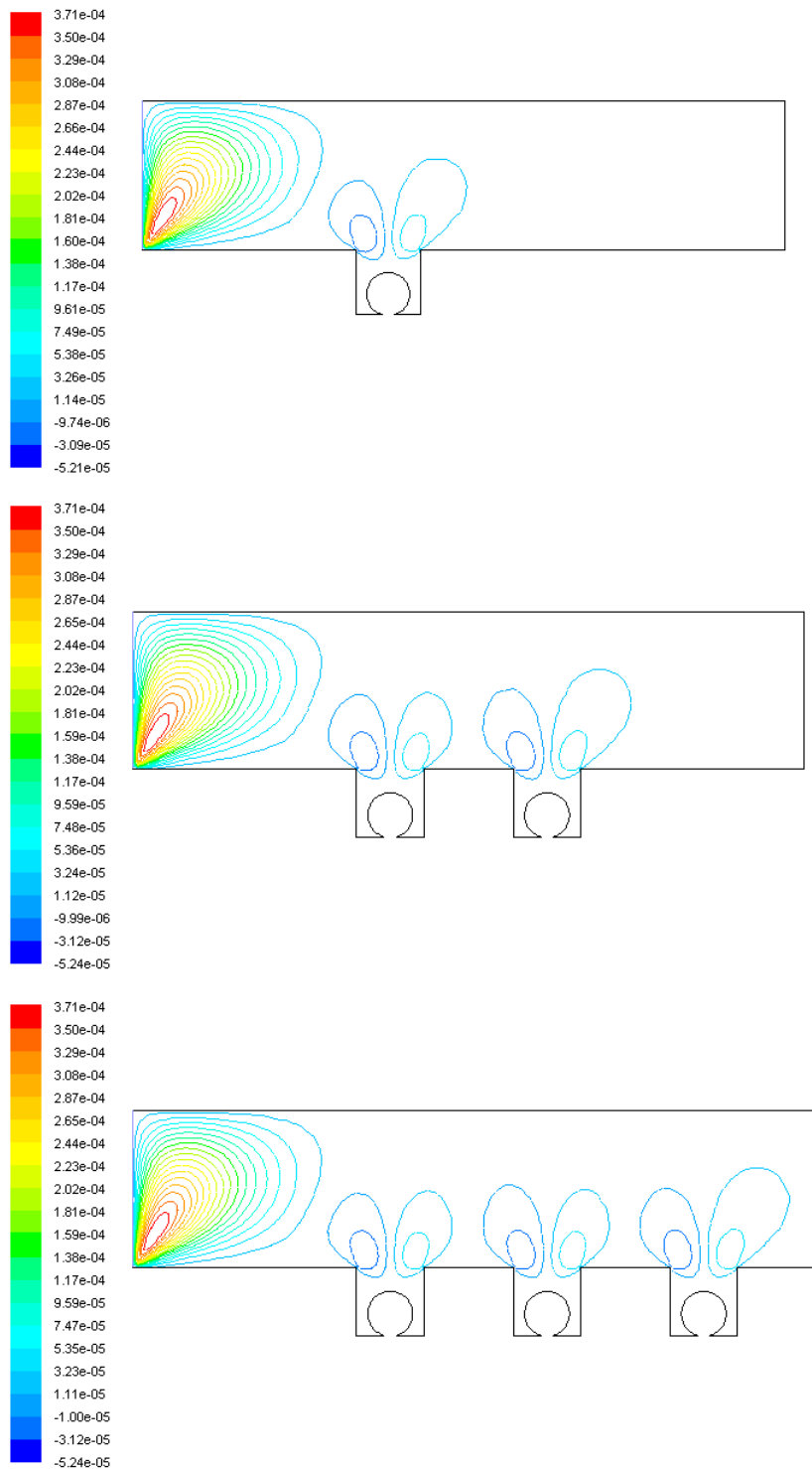


Figure 4.54: Vertical velocity (measured in m/s) contours for single and multiple cavities. Notice that the contour at the upstream edge of the cavity for the case of single cavity is smaller than the downstream ones for multiple cavities.

#### 4.6.11 Multiple Cavity Interaction: Shear Stress Distribution on the Embryo

As can be seen in Figure 4.55, the embryo surface shear stress distribution on all embryos is effectively the same regardless of which cavity they are situated in and irrespective of how many cavities are located in proximity. This is consistent with the previous stress distribution analysis for the cavity spacing study.

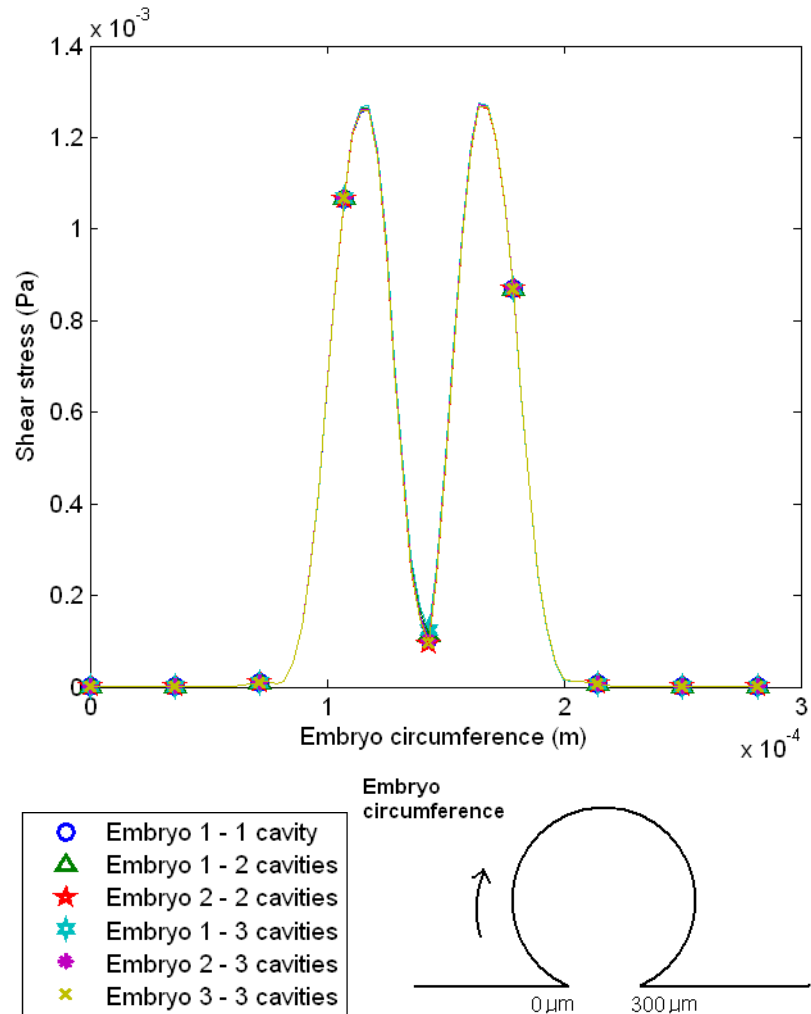


Figure 4.55: Shear stress distribution on the surface of all embryos in the case of single, two and three cavities.

#### 4.6.12 Implication for Shear Stress Changes

From this sub-study on multiple cavity bioreactors, it is found that the overall shear stress for both embryos increase by the order of 10% when the cavities are very close. This is due to the fast fluid movement produced due to the flow interference caused by the cavities. As this interference only has a limited range effect for the Reynolds

number chosen for this study, its influence on the fluid movement dies away rapidly as the two cavities are moved further away. As detailed in the study, this critical spacing is typically about 1.667 times the cavity length, which is comparatively small. In any case, the overall change to the stress from the single cavity case is relatively minor, and will be much more affected by changing the inflow rate. Hence, it is possible to scale up the productivity of the bioreactor by adding more cavities without compromising the viability of the embryos.

#### **4.6.13 Conclusions and Summary**

As an attempt to examine one of the strategies to scale up embryo production, this study on multiple cavities configuration was broken down into two sub-studies: cavity spacing and cavity interaction. For the sub-study on cavity spacing, several CFD models of a bioreactor with two cavities with different spacings were constructed, while for the sub-study on cavity interaction, three CFD models each with single, two and three cavities were built. Steady-state flow simulations were conducted on all of them to simulate the bioreactor operation, focusing on emulating the solute exchange and fluid movement in the bioreactor. The outcomes on the solutes concentration and shear stress were then examined to gauge the influence on the performance of the bioreactor due to changing the cavity spacing and having a different number of cavities in proximity.

The key findings of these sub-studies appears to be that for the reference case geometry and flow rate used, both solute concentration levels and shear stress are not strongly affected by using multiple cavities even in when they are in close proximity. Variations from the base case of a single cavity were determined to be up to 10% for stress and lactate levels, and less than one percent for oxygen. This seems to indicate that the use of multiple cavity bioreactors is a good way to increase production rates.

#### **4.7 Final Comments**

Of course, the studies presented in this chapter have focused on a *two-dimensional bioreactor*. As described previously, this approach was taken to allow a reasonably thorough examination of parameter space, to at least provide a basis for the considerably more expensive three-dimensional studies presented in the next chapter. Despite their two-dimensionality, these studies are still somewhat restricted in their coverage of parameter space, since they are mainly based on varying parameters one at a time from a *default case*. However, it is still believed that they provide a good deal of guidance for bioreactor construction and optimisation once more

# 5.0 Three-Dimensional Parametric Studies

---

While the two-dimensional modelling provides some guidance for designing a niche micro-bioreactor, to obtain better quantitative predictions, it is necessary to undertake full three-dimensional modelling. These models are both more time-consuming to construct, in terms of building the meshes, and also to run, in terms of computer time and memory requirements. Nevertheless, it is important to undertake some three-dimensional modelling, which may provide a comparison for the two-dimensional models and perhaps also even provide enough information to approximately rescale two-dimensional predictions to apply to three-dimensional bioreactors. This chapter details the findings from three three-dimensional (3D) parametric studies undertaken on varying the cavity width, shape and the inclusion of multiple embryos in a cavity.

## 5.1 Default Scenario on Three-Dimensional Micro-Bioreactor

The boundary conditions and dimensions of the default or reference micro-bioreactor model are specified in Table 5.1. As with the two-dimensional studies, these settings provide reference values allowing comparisons to be made as each parameters is varied. As before, in this chapter, the results for lactate and oxygen concentration, and shear stress, are presented in normalized form.

Embryo diameter	100 $\mu\text{m}$
Cavity length x depth x width	150 x 150 x 300 $\mu\text{m}$
Channel length x depth x width	10150 x 350 x 300 $\mu\text{m}$
Culture medium inflow rate	0.001 m/s
Lactate production rate	$9.427 \times 10^{-13}$ mol/hr
Oxygen uptake rate	$2.145 \times 10^{-13}$ kg/hr
Preset oxygen concentration at inlet	$2.189 \times 10^{-4}$ mol/L

Table 5.1: Default values for the model dimensions and boundary conditions.

Default lactate concentration	$5.19 \times 10^{-7}$ M
Default oxygen concentration	$2.16 \times 10^{-4}$ M
Default shear stress	$1.30 \times 10^{-3}$ Pa

Table 5.2: Default values of the lactate and oxygen concentrations and shear stress averaged across the embryo surface.

## 5.2 Cavity Width Parametric Study

Using three-dimensional CFD modelling, this study assesses the influence of the width of the cavity on solute transport and shear stress. As shown in Figure 5.1, the width of the cavity,  $B$ , is defined as the distance between the two side walls. Note that this distance represents the width of the entire bioreactor (width of both the channel and the cavity). The reason for this is that changing the cavity width will alter the transverse flow structure in the cavity, as reported by Shankar in his review of the fluid flow in a lid-driven cavity (Shankar and Deshpande 2000). With three-dimensional (3D) simulations, this effect can be investigated numerically as opposed to the limiting two-dimensional (2D) simulations that assume the cavity and embryo has infinite width.

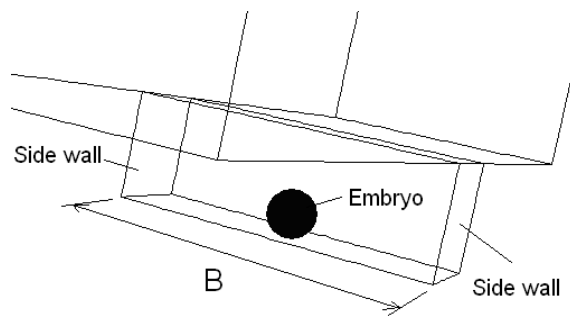


Figure 5.1: Schematic of the idealized cavity micro-bioreactor numerical model showing the first parameter to be studied: cavity width,  $B$ .

In addition, a brief secondary study is conducted to compare the two-dimensional (2D) and three-dimensional (3D) modelling. This is undertaken to gain a better understanding of the limitation of 2D models in predicting the performance of the bioreactor. While 3D modelling is able to emulate the flow closer to the actual condition compared to 2D modelling, the latter is still important in the sense that it offers a much less resource-intensive model with which to work. Also, one can obtain the results faster than for a 3D model, whilst at the same time acknowledging the limitation of a 2D model.

This section starts with the description of the setup used. An analysis is then presented with attention drawn to the changes in solute transport and shear stress formation as the width is varied, followed by a discussion of the implication of the study. Next the comparison of the 2D and 3D modelling is presented and discussed.

### 5.2.1 Problem Setup

For this study, as shown in Figure 5.2, ten geometric models were constructed, each with a width increment of 150  $\mu\text{m}$  (Table 5.3). Steady-state simulations were conducted to simulate the fluid and solute movement in the bioreactor where the culture fluid was simulated to enter the bioreactor at the inlet at one side, allowed to perfuse through the channel passing over the cavity, and finally to exit the bioreactor at the outlet on the other side. The width of the cavity,  $B$ , was varied between 150  $\mu\text{m}$  and 1500  $\mu\text{m}$ . The dimensionless representation of  $B$  is  $B^*$ , which reflects the variation of the cavity width relative to the embryo size of 100  $\mu\text{m}$  (fixed for this study). Other features of the model were maintained at the default values.

Width, $B$	Normalized width, $B^*$	Width, $B$	Normalized width, $B^*$
$\mu\text{m}$		$\mu\text{m}$	
150	1.5	900	9.0
300	3.0	1050	10.5
450	4.5	1200	12.0
600	6.0	1350	13.5
750	7.5	1500	15.0

Table 5.3: Tabulated values of the cavity width  $B$  chosen for the study. The normalized cavity width  $B^*$  is obtained by dividing the cavity width by the diameter of the embryo (100  $\mu\text{m}$ ).

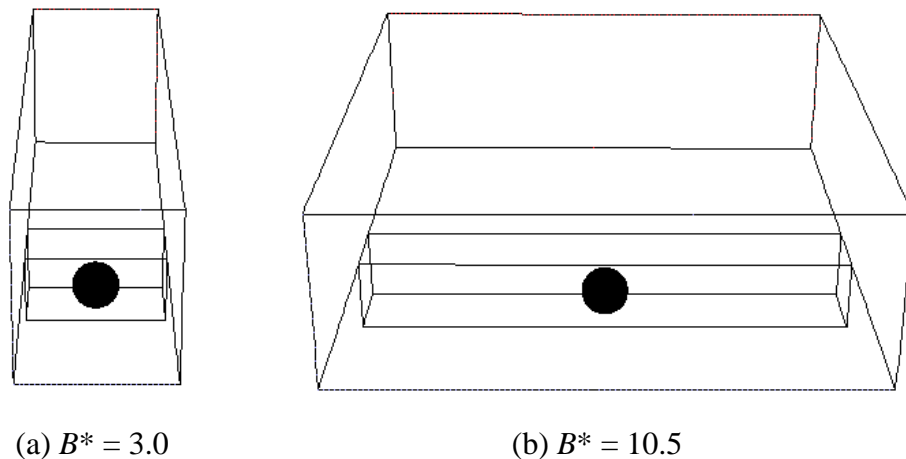


Figure 5.2: Two geometric models, each with  $B^*$  of (a) 3.0 and (b) 10.5 utilized in the cavity width investigation are shown here to indicate the key difference between each of the ten models intended for the cavity width study.

The models for the 2D and 3D comparison are given in Figure 5.3. Basically, there are three models: a 2D model as depicted in Figure 5.3a; a 3D cylindrical embryo model as shown in Figure 5.3b; and a 3D spherical embryo model as illustrated in Figure 5.3c and which represents the actual bioreactor in 3D. The 3D cylindrical embryo model is basically a 2D model extended in the spanwise direction. It served the purpose of relating the 2D model (Figure 5.3a) with the 3D model comprising a spherical embryo (Figure 5.3c); as mentioned before, a 2D model is assumed to have an infinite width. Therefore the circle, which represents the embryo in the 2D model, when projected in 3D, has a cylindrical rather than spherical shape.

Apart from the difference mentioned above, all the models share similar features such as the same cross section, dimension of the channel, embryo diameter and height of the culture fluid. The width of the 3D model was selected to be 750  $\mu\text{m}$ , decided on the basis of the finding from the prior cavity width investigation that at this width, the flow interference caused by side walls becomes less significant. This is important because the 2D model assumes an infinite width, which means that there is no side wall interference.

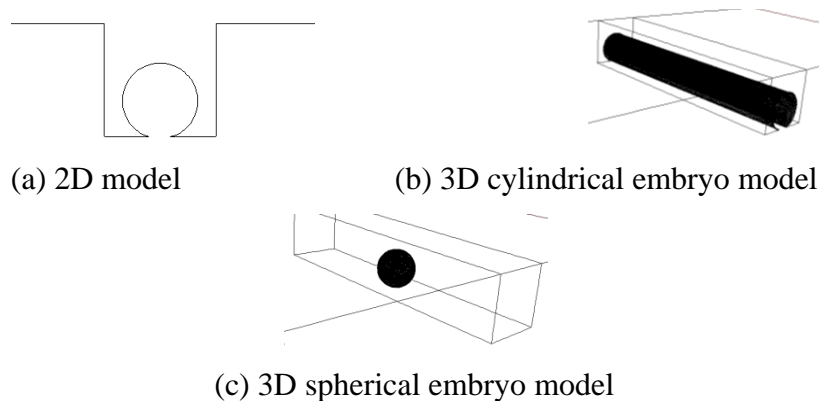


Figure 5.3: Comparison study between different types of model: (a) 2D model; (b) 3D model with cylindrical embryo; (c) 3D model.

### 5.2.2 Solute Concentration Changes

The solute transport variation as the cavity width changes was first examined, where the concentration here refers to the averaged solute concentration across the embryo surface. As shown in Table 5.4 and Figure 5.4, a sharp drop in lactate concentration by 55% and a rapid rise in oxygen concentration by 0.54% are recorded when  $B^*$  is increased from 1.5 to 6.0. The rate of change then reduces and becomes insignificant as  $B^*$  continues to

increase. This suggests that when the two side walls of the cavity are close together, the smaller cavity opening restrains the solute movement into and out of the cavity. This diminishes the solute transport, as more lactate was found to accumulate and less oxygen was supplied into the cavity. Also, the magnitude of the variation of oxygen concentration is found to be much lower than variation of lactate concentration; explanation is provided in Section 5.5.

Normalized cavity width, $B^*$	Lactate concentration	Oxygen concentration	Normalized lactate concentration	Normalized oxygen concentration
	M	M		
1.5	7.496E-07	2.1498E-04	1.444	0.9957
3.0	5.192E-07	2.1591E-04	1.000	1.0000
4.5	4.764E-07	2.1610E-04	0.918	1.0009
6.0	4.674E-07	2.1615E-04	0.900	1.0011
7.5	4.671E-07	2.1615E-04	0.900	1.0011
9.0	4.685E-07	2.1615E-04	0.902	1.0011
10.5	4.651E-07	2.1616E-04	0.896	1.0012
12.0	4.685E-07	2.1615E-04	0.902	1.0011
13.5	4.697E-07	2.1615E-04	0.905	1.0011
15.0	4.714E-07	2.1614E-04	0.908	1.0011

Table 5.4: Tabulated values of the simulated averaged solute concentration on the embryo surface, with the normalized lactate and oxygen concentration calculated by dividing them by their respective default concentration highlighted in Table 5.2.

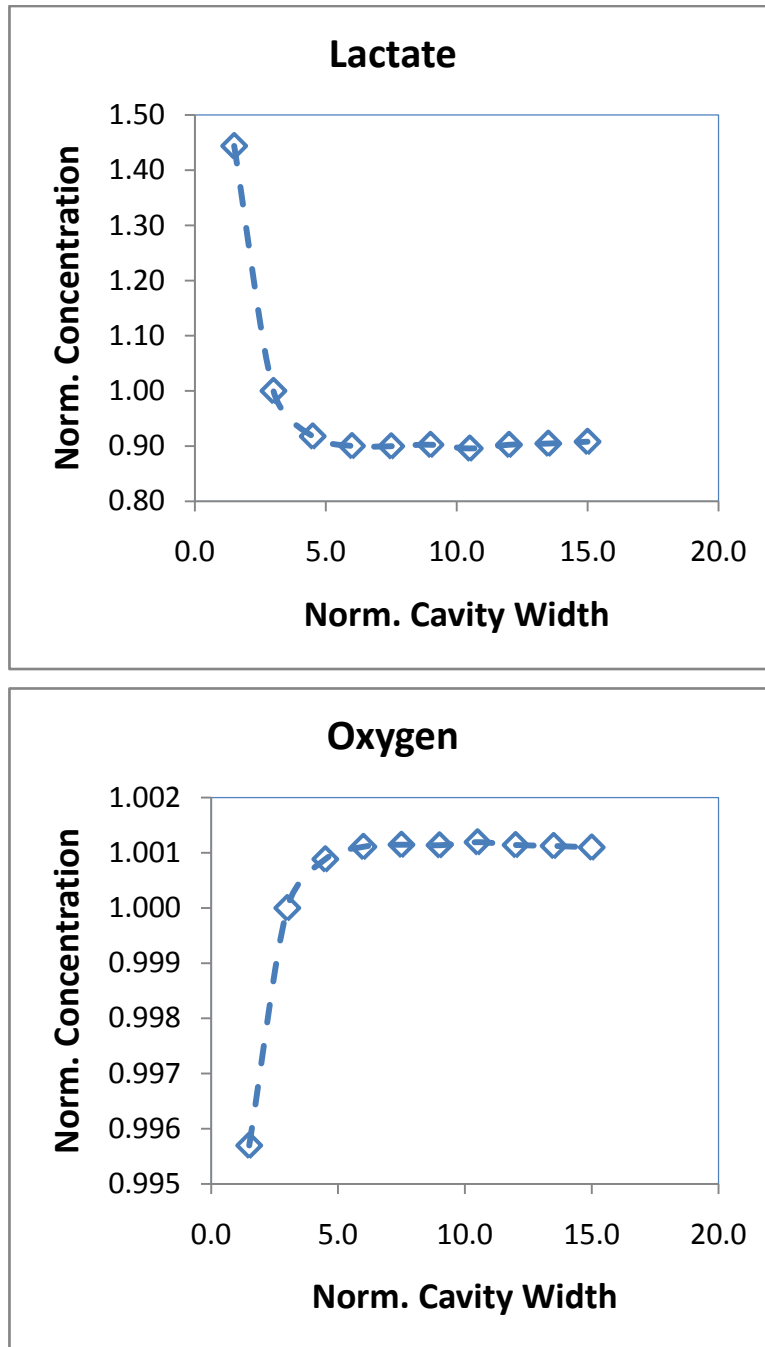


Figure 5.4: Changes of the lactate (top) and oxygen (bottom) concentration averaged across the embryo surface for lactate as  $B^*$  increases.

The effect of the smaller cavity opening in restraining the solute transport is clearly shown in Figures 5.5 and 5.6. With a narrow cavity, the small cavity opening restricts lactate from being expelled from the cavity, and with the two side walls situated closely, lactate is more prone to accumulate around the embryo. This raises the overall lactate concentration (Figure 5.5a). Likewise, the small opening also limits the amount of oxygen being transported into the cavity and thus lowers the overall oxygen concentration (Figure 5.6a). Conversely, with a wide cavity, the larger  $B^*$  promotes solute transport around the embryo as the larger volume allows more lactate to diffuse away from the embryo, and the larger cavity opening also permits more lactate to be transported out of the cavity (Figure 5.5b). Similarly, more oxygen is able to be transported to the embryo when the cavity opening is large. As a result, this raised the overall oxygen concentration level on the embryo (Figure 5.6b). Of course, these effects are expected but it is important to establish their magnitude.

As  $B^*$  increases, the cavity opening and the cavity volume eventually are sufficiently large that they do not affect the solute transport to and from the embryo. This can be seen in Figures 5.5b and 5.6b by the large contour plot area of the low lactate concentration and high oxygen concentration further away from the embryo, towards both ends of the cavity. It is found that at steady-state, the solute concentrations in these two regions are saturated with the same solute concentration as found in the channel. Consequently, even if the cavity opening continues to enlarge, the concentration gradient around the embryo would not differ by much, leading to the asymptoting of the solute concentrations as  $B$  increases.

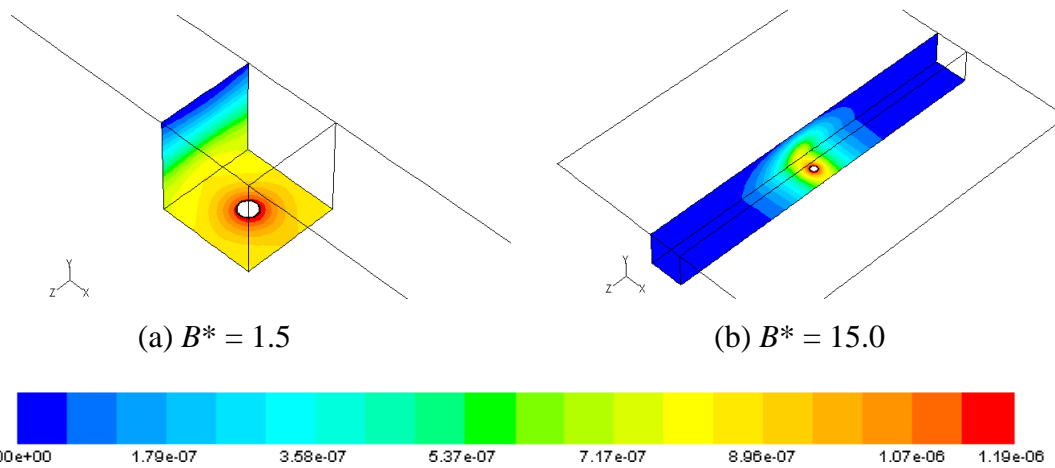


Figure 5.5: Contour plots of lactate concentration (measured in M) on the bottom and rear cavity walls for (a) a narrow cavity of  $B^* = 1.5$  and (b) a wide cavity of  $B^* = 15.0$ , showing the stark difference in distribution of lactate produced.

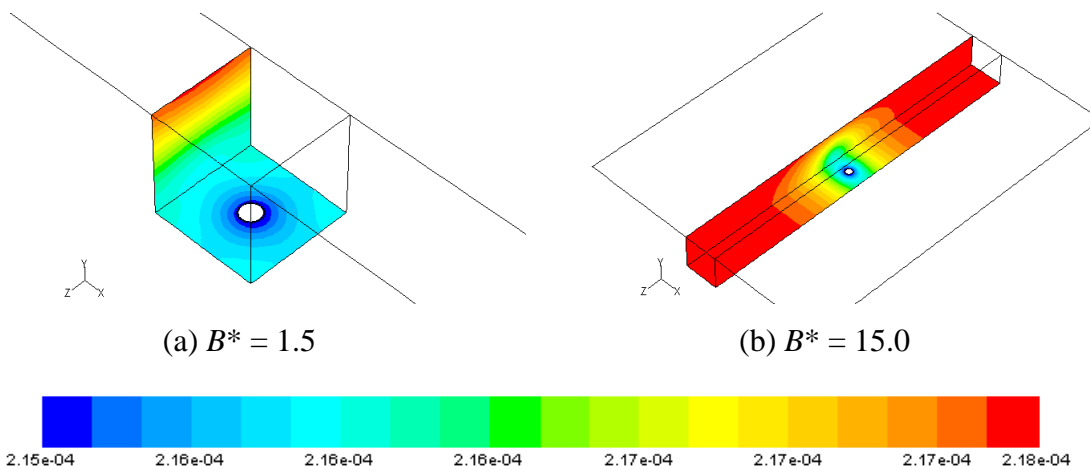
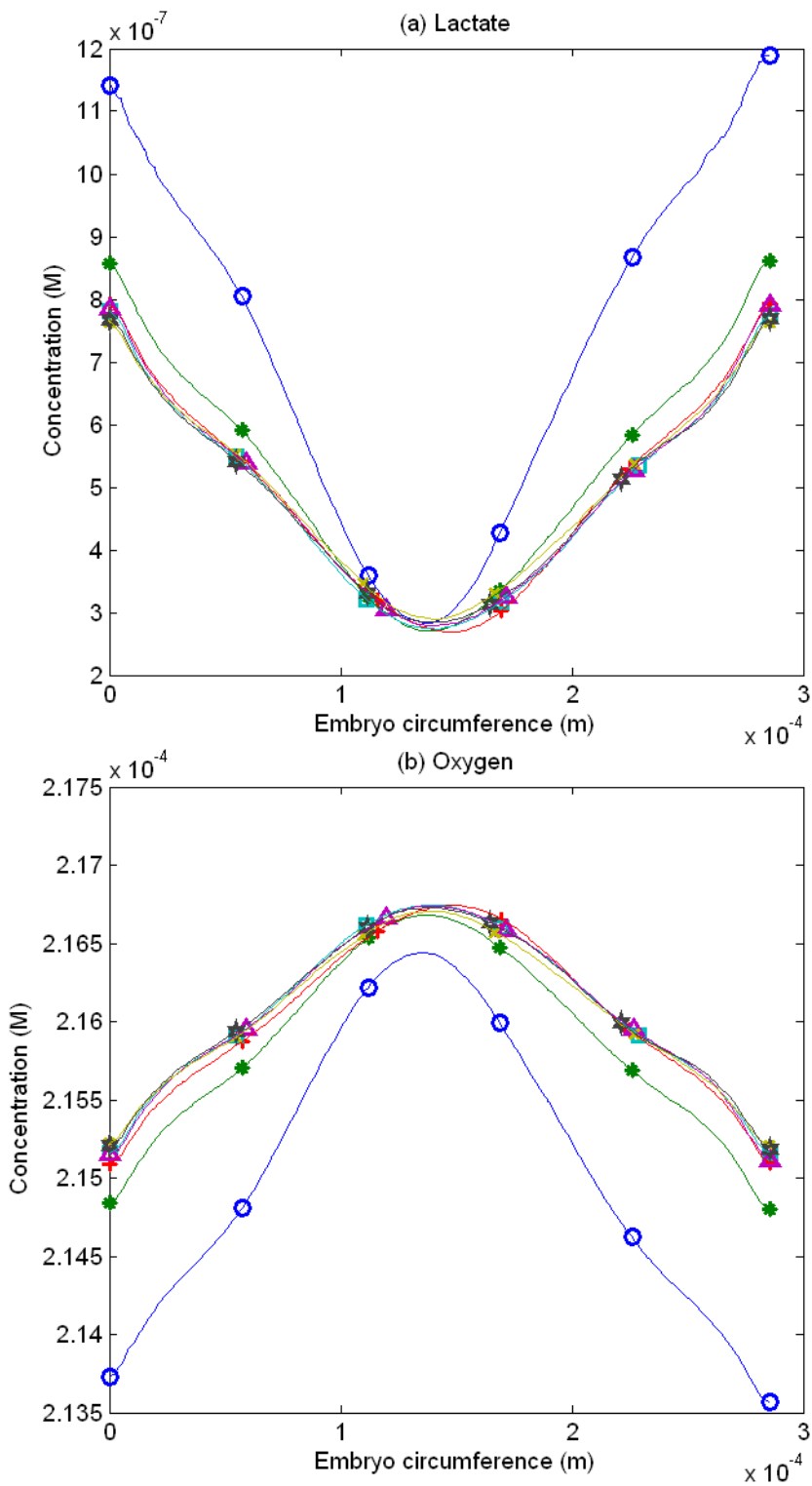


Figure 5.6: Contour plots of oxygen concentration (measured in M) on the bottom and rear cavity walls for (a) a narrow cavity of  $B^* = 1.5$  and (b) a wide cavity of  $B^* = 15.0$ , showing the contrast in the distribution of oxygen around the embryo.

### 5.2.3 Solute Distribution on the Embryo

As shown in Figure 5.7 and 5.8, the distribution of the solutes does not change much as  $B^*$  varies. The distributions are similar to those observed for the two-dimensional models, with a considerable concentration gradient between the top and the bottom of the cavity. Lactate levels are highest at the base of the embryo and oxygen levels are the highest at the top for the reasons discussed in the previous chapter.

The notable difference of the solute distribution profile as  $B^*$  varies is the rate of change of the solute concentration level: the rate of change is steep when  $B^*$  is smaller than 1.5, corresponding to strong confinement; as  $B^*$  increases further than that, the rate of change quickly becomes moderate. Figures 5.7 and 5.8 provide circumferential lactate and oxygen concentration plots for the *lengthwise* (along the flow, XY-direction) and *spanwise* (perpendicular to the flow, YZ-direction) directions. For a small width ( $B^* = 1.5$ ), at the bottom of the embryo, the highest lactate concentration and the lowest oxygen concentration were detected. As  $B^*$  is increased, the overall lactate concentration decreases and the overall oxygen concentration increases, and they converge when  $B^*$  is larger than 3.0. Again, this is expected because from a previous finding that solute transport is impeded when the cavity width is narrow.



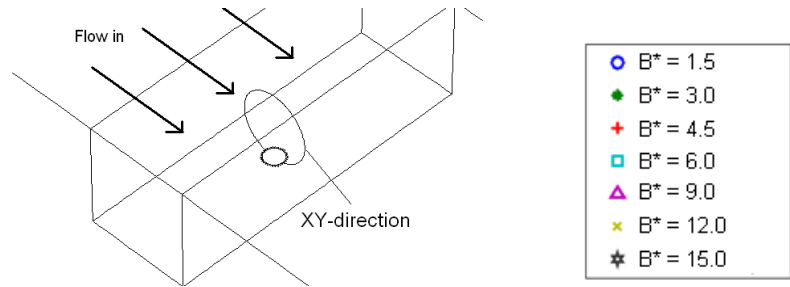
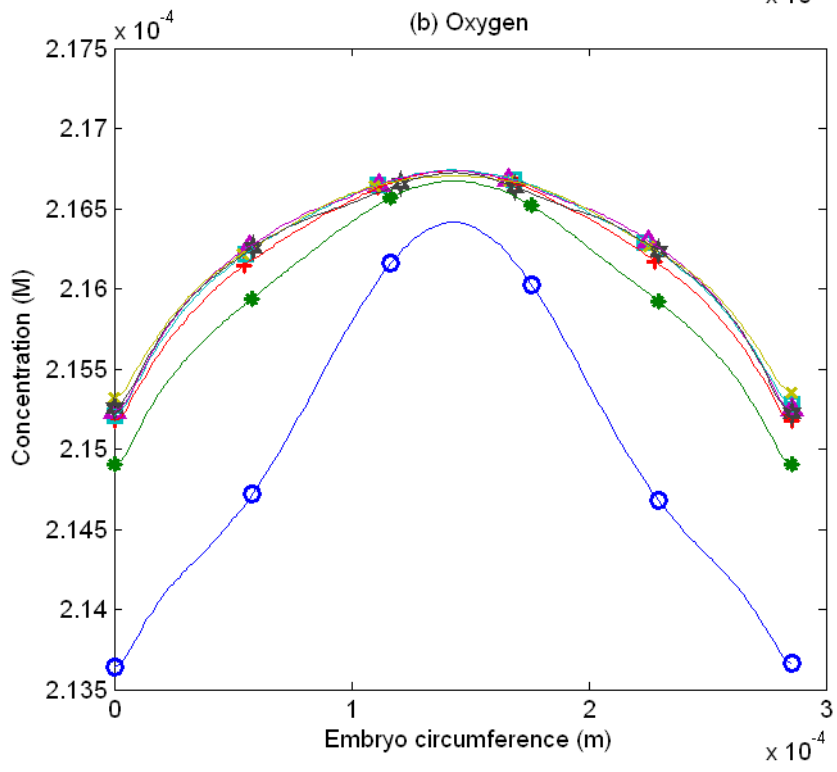
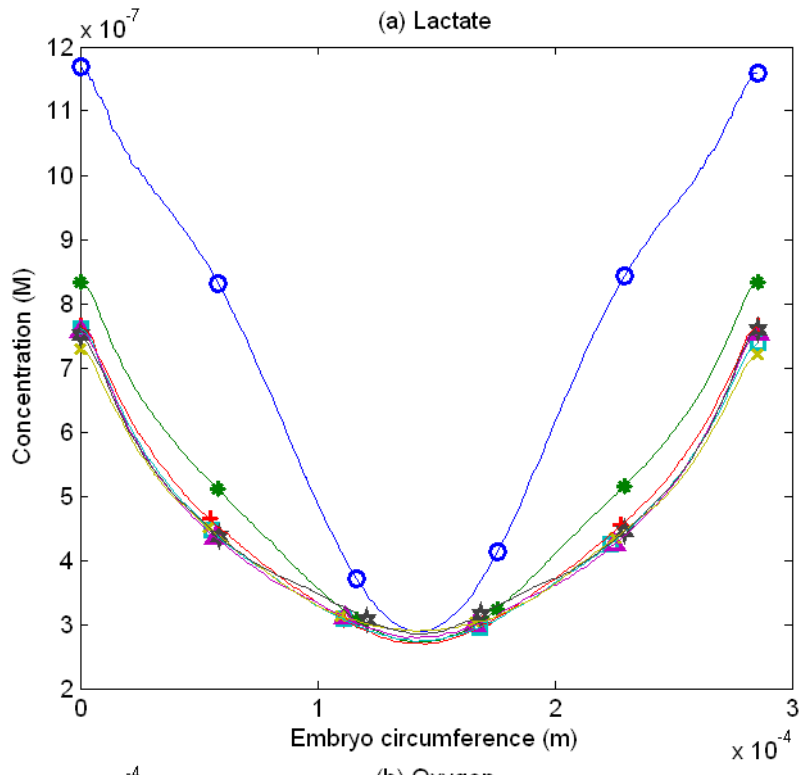


Figure 5.7: (a) Lactate and (b) oxygen distribution on the embryo surface at the XY-direction (as indicated in the insert).



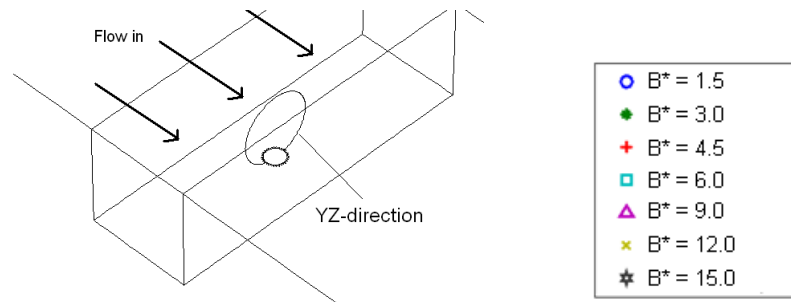
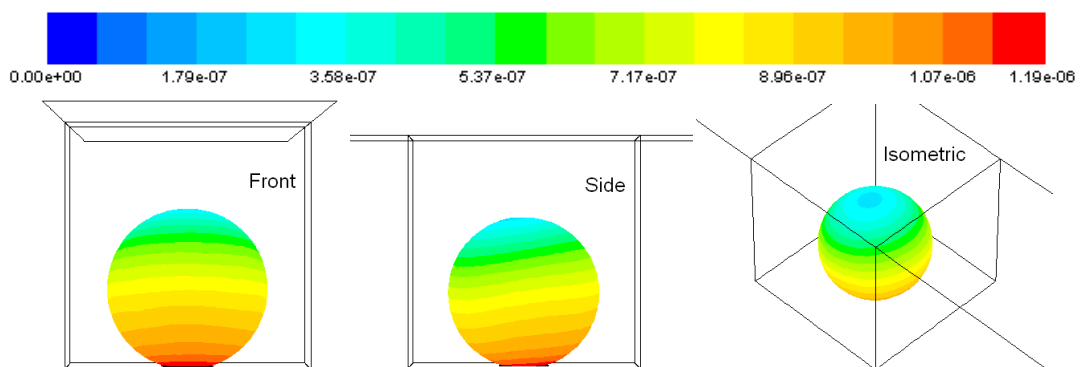
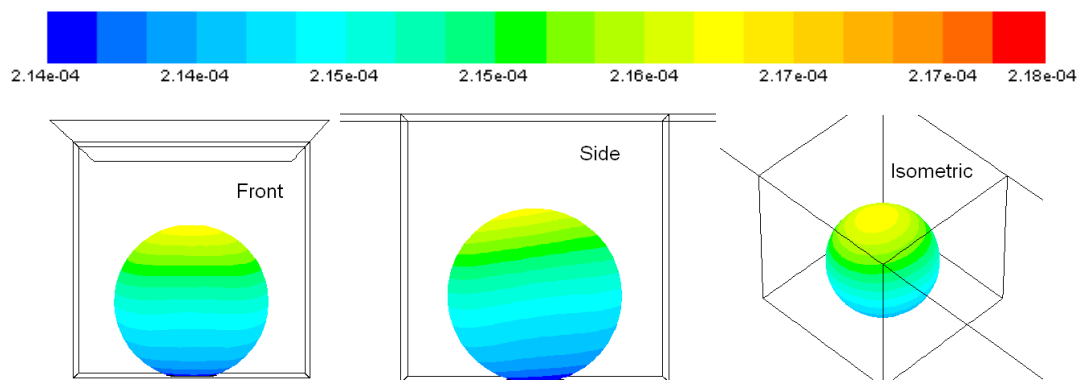


Figure 5.8: (a) Lactate and (b) oxygen distribution on the embryo surface at the YZ-direction (as indicated in the insert).

As shown in Figure 5.9, when width is the same as the length of the cavity, the solute concentration contours are fairly level across the embryo surface. This can be explained by combination of a cubical cavity and low Reynolds number used for this case leading to a reasonable symmetric flow about the XY and YZ centre planes.



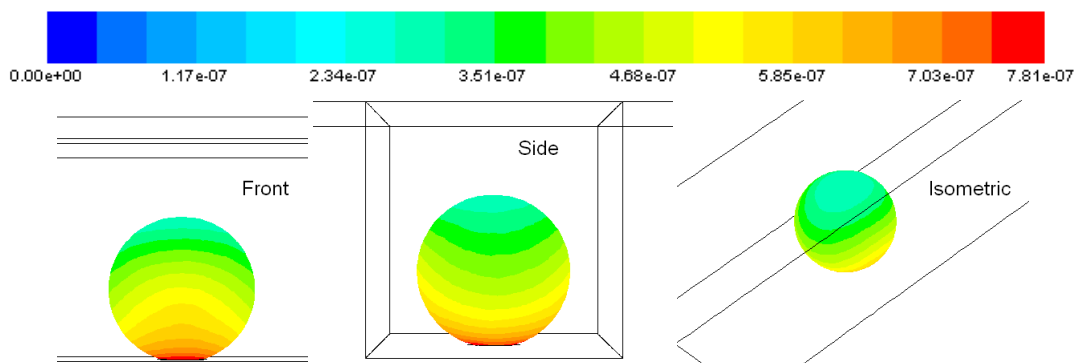
(a) Lactate: fluid flow from left to right when viewed at the side view.



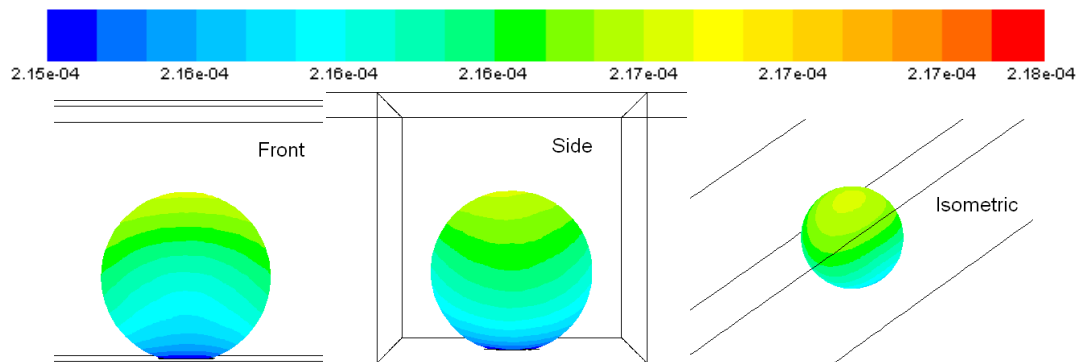
(b) Oxygen: fluid flow from left to right when viewed at the side view.

Figure 5.9: Contour plots of the (a) lactate and (b) oxygen concentration (measured in M) on the embryo surface when the cavity has a narrow width of  $150\ \mu\text{m}$ , where the front, side and isometric view of the embryo are shown.

When  $B$  is larger than  $150\ \mu\text{m}$  (Figure 5.10), the cavity symmetry is broken and the solute contours in each direction on the embryo are more curved. In particular, it can be deduced that when the cavity wall is close to the embryo, solute movement at the bottom of the embryo is obstructed, causing the lactate to build up and oxygen depletion to occur. If the cavity side walls are further away, this blockage is relieved; explaining the formation of the wavy contours on the surface in Figure 5.10.



(a) Lactate: fluid flow from left to right - side view.



(b) Oxygen: fluid flow from left to right - side view.

Figure 5.10: Contour plots of the (a) lactate and (b) oxygen concentration (measured in  $M$ ) on the embryo surface when the cavity has a wider width of  $600\ \mu\text{m}$ , where the front, side and isometric views of the embryo are shown.

#### 5.2.4 Implication for Solute Transport

Gathering all the outcomes from the observations on the solute transport, two implications can be made on varying the cavity width. First, it is found that reduced solute transport results when the cavity is narrow, particularly when  $B^*$  is smaller than 1.5. As  $B^*$  is increased, the solute transport improves until  $B^*$  is around six times the

diameter of the embryo ( $B^* = 6.0$ ), beyond which little improvement occurs. It must be noted that the value of this critical width is dependent on the embryo size and Peclet numbers; determination of this width for other sizes may require further simulations.

Second, it is found that the distance between the embryo surface and the cavity side walls directly affects the solute distribution on the embryo. Particularly, a small distance tends to create a blockage of the solute transport, while this blockage quickly disappears as the distance grows larger. With this, one can adjust the solute distribution pattern on the embryo by adjusting  $B^*$ , depending on the different requirements for the cultivation of different embryo types.

### **5.2.5 Shear Stress Changes**

The variation of the shear stress averaged across the embryo surface is examined first. As shown in Table 5.5 and Figure 5.11, the average shear stress is the highest when  $B^*$  is the smallest, at 1.5. As  $B^*$  increases to 4.5, a sharp drop in the shear stress by 56% is recorded. As  $B^*$  increases further, the shear stress variation stabilized to a consistent linear drop. This trend is similar to that for the solute concentration changes, suggesting a similar mechanism: more closely located cavity side walls induce a large interference to the shear stress on the embryo; this interference diminishes as  $B^*$  increases.

Contrary to the change in solute concentration, the shear stress continues to decrease at a consistent rate of 2.3% per unit  $B$ . It is believed that this occurs because the varying distance between the embryo surface and the cavity side walls continues to alter the fluid flow in the cavity as  $B^*$  continues to change. It is speculated that only when  $B^*$  is increased much larger that this change will eventually diminish. This is because the fluid flow in the bioreactor is in the range of very low Reynolds number; the viscous communication between the embryo surface and the side walls acts over a large distance.

Normalized cavity width, $B^*$	Shear stress Pa	Normalized shear stress
1.5	2.032E-03	1.562
3.0	1.301E-03	1.000
4.5	1.183E-03	0.909
6.0	1.155E-03	0.888
7.5	1.118E-03	0.859
9.0	1.093E-03	0.840
10.5	1.059E-03	0.814
12.0	1.033E-03	0.794
13.5	1.004E-03	0.772
15.0	9.746E-04	0.749

Table 5.5: Tabulated values indicating how the variation on  $B^*$  alters the overall shear stress averaged across the embryo surface. The normalized version of this shear stress is calculated by dividing them by the default shear stress as shown in Table 5.2.

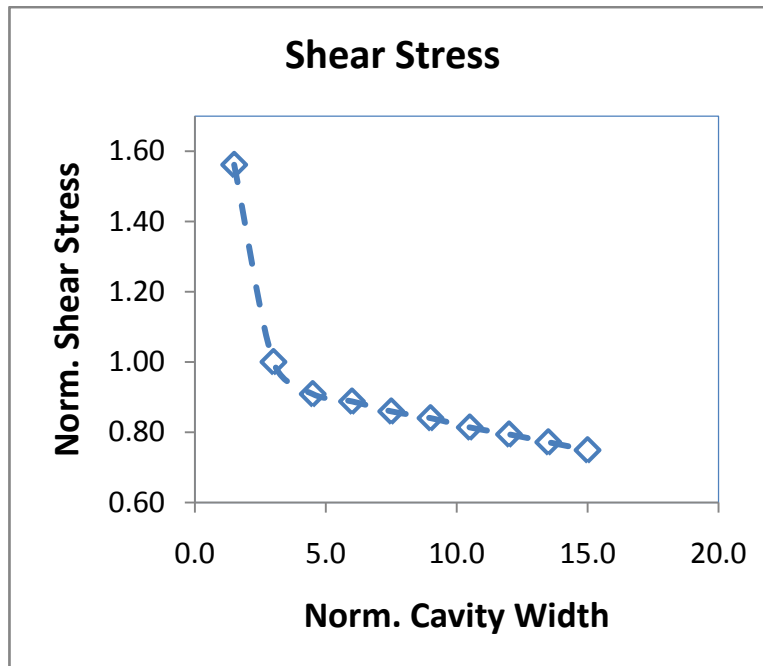


Figure 5.11: Plot showing the variation of the surface shear stress averaged across the embryo surface with respect to the increasing normalized cavity width,  $B^*$ .

The velocity contours of the secondary flow perpendicular to the main flow are examined in order to find out the actual cause of such viscous interference. As shown in Figure 5.12, the velocity contour at the middle plane of the cavity, which intersects the

embryo, was examined to identify the cause of such shear stress behaviour. As revealed in these plots, due to the low Reynolds number flow condition in the bioreactor ( $Re \sim 0.1$ ), the viscous effect is dominant in the flow, causing a large velocity gradient to occur from the side walls of the channel. As the top surface of the channel is modelled as a free surface, the high velocity region (marked by the red contour region in Figure 5.7) is attached to the top surface.

As  $B^*$  is varied, the shape of the velocity contours in the cavity changes. A small  $B^*$  causes an interference of the viscous boundary layers to occur between the two side walls. As can be seen in Figure 5.12a (right), the *compressed* velocity contours extend well into the cavity, accelerating the fluid flow there. This means that for a narrower cavity, the fluid movement above the embryo is relatively faster, causing a higher shear stress on the embryo. Alternatively, as  $B^*$  increases, the compression of the velocity contours is relaxed showing the fluid is not accelerated as much, as can be seen in Figure 5.12b (right) and 5.12c (right). Here, the higher speed velocity contours only extend a little into the cavity compared with the previous case for a narrow cavity. Therefore, the fluid movement around the embryo is comparatively much slower, explaining why the shear stress induced is lower when  $B^*$  is smaller. It must be noted that this interference is only significant when  $B^*$  is less than 4.0, where the starkest increase of stress occurs, as shown in Figure 5.6.

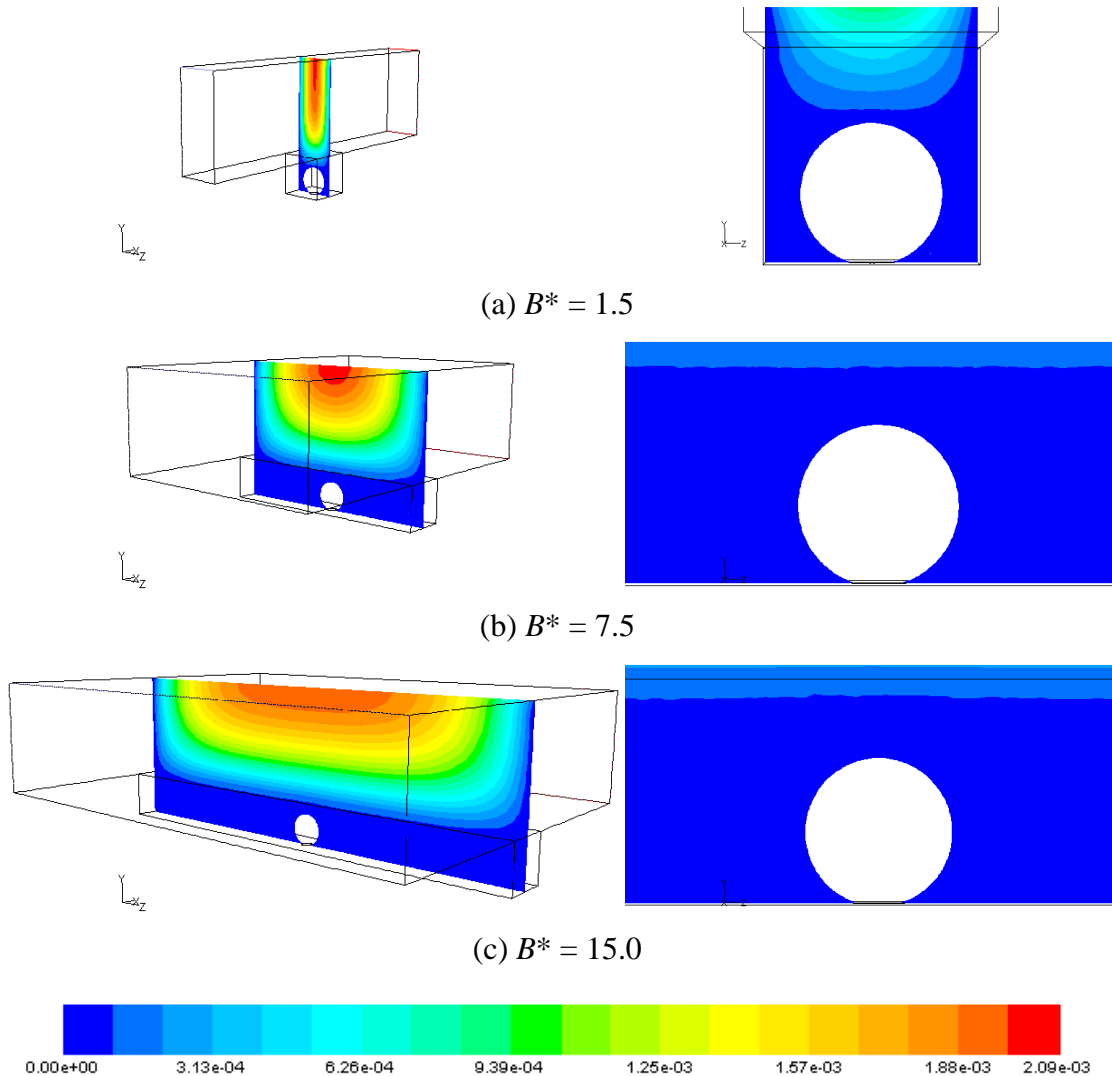
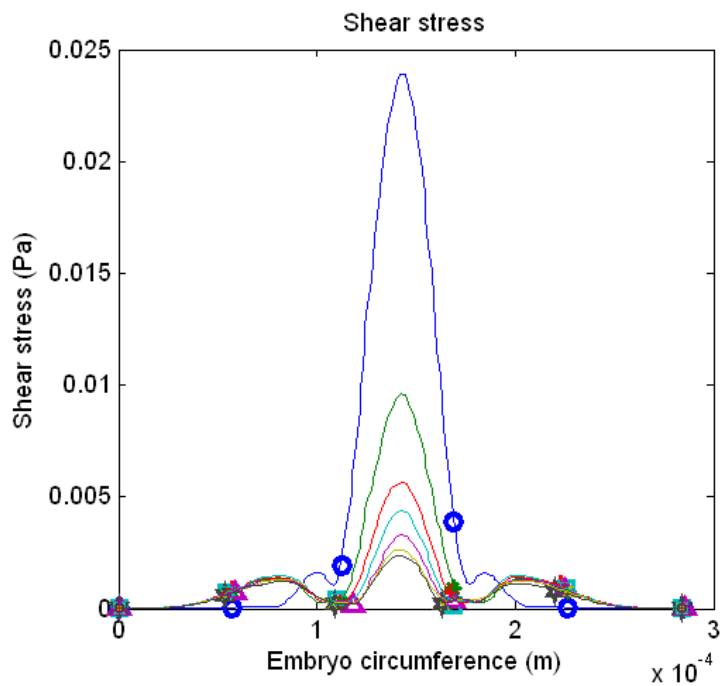


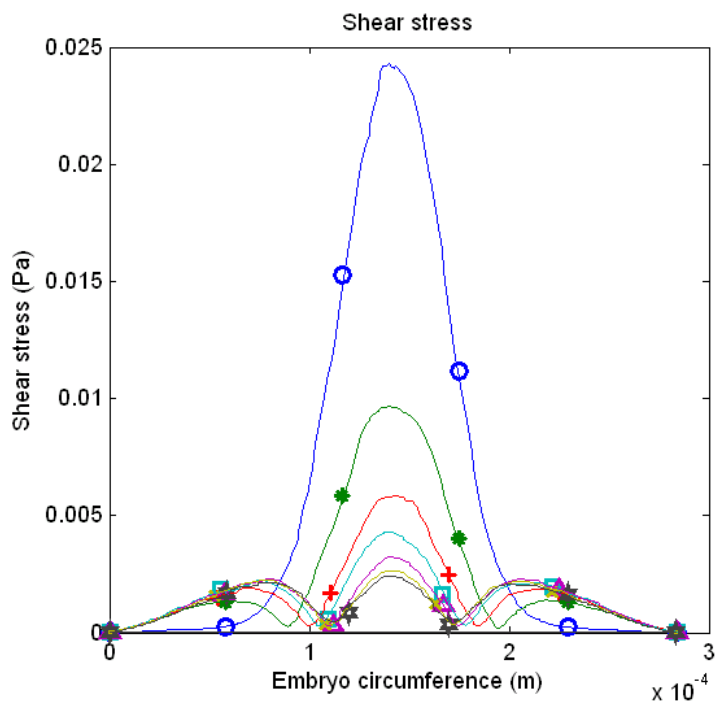
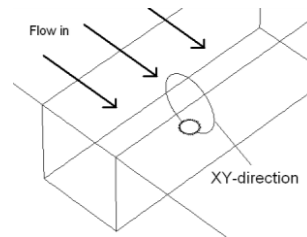
Figure 5.12: Velocity magnitude (measured in m/s) contour plots at the middle of the bioreactor for three different cavity widths on the left: (a)  $B^* = 1.5$ , (b)  $B^* = 7.5$ , (c)  $B^* = 15.0$ , together with the close up view on the right, detailing the velocity contours near the embryo. Here, the influence of the side walls in causing the velocity changes at the middle cross section of the bioreactor is highlighted.

### 5.2.6 Shear Stress Distribution on the Embryo

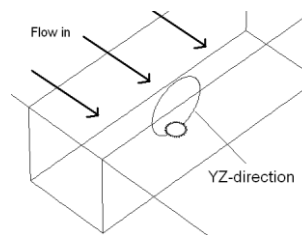
To examine this in a little more detail, the circumferential shear stress profiles on the embryo in the XY and YZ centre planes are examined. In general, as shown in Figure 5.13a, the shear stress profile in the flow direction has three peaks in the stress located near the top of the embryo, as found for the two-dimensional investigations. The highest peak stress occurs right at the top of the embryo (this is referred as the middle peak stress for subsequent discussion). When  $B^*$  is smaller than 1.5, the three peak stresses are grouped closely around the top of the embryo and the highest middle peak stress is recorded. This middle peak stress decreases drastically as  $B^*$  is increased up to 3.0. The two adjacent peak stresses, while not changing much in magnitude, move further around from the top point. When  $B^*$  exceeds 3.0, the middle peak stress continues to decrease in magnitude, while the two adjacent peaks remain almost the same. The shear stress profiles perpendicular to the flow (Figure 5.13b) exhibits a similar trend change. The main difference is that when  $B^*$  is small, there is only a single peak stress found in the YZ-direction compared to the three peak stresses detected in the XY-direction.



(a) XY-direction



(b) YZ-direction



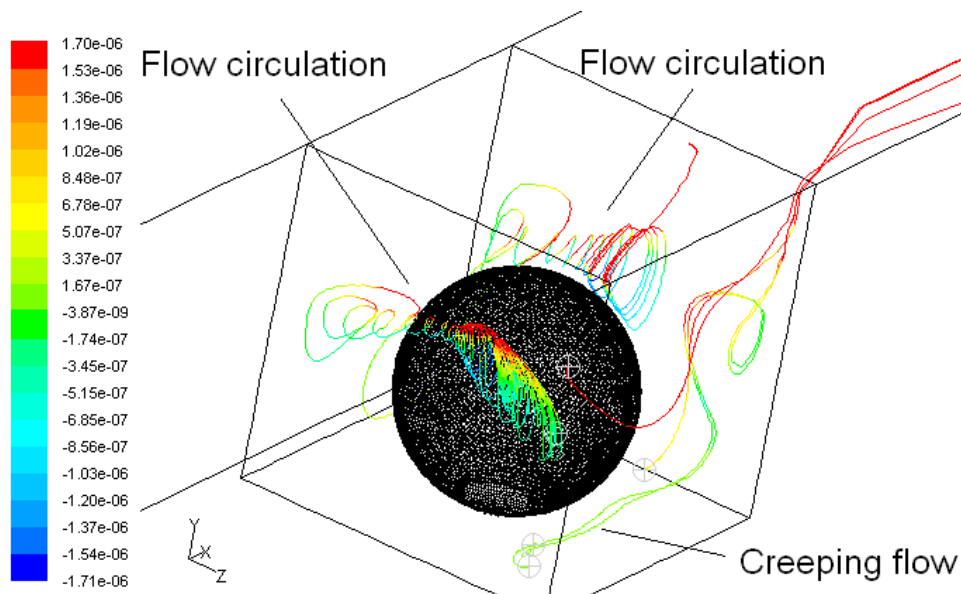
- $B^* = 1.5$
- ◆  $B^* = 3.0$
- ✦  $B^* = 4.5$
- $B^* = 6.0$
- △  $B^* = 9.0$
- ×  $B^* = 12.0$
- ★  $B^* = 15.0$

Figure 5.13: Shear stress distribution on the embryo surface in the (a) XY-direction and the (b) YZ-direction as indicated in the inserts.

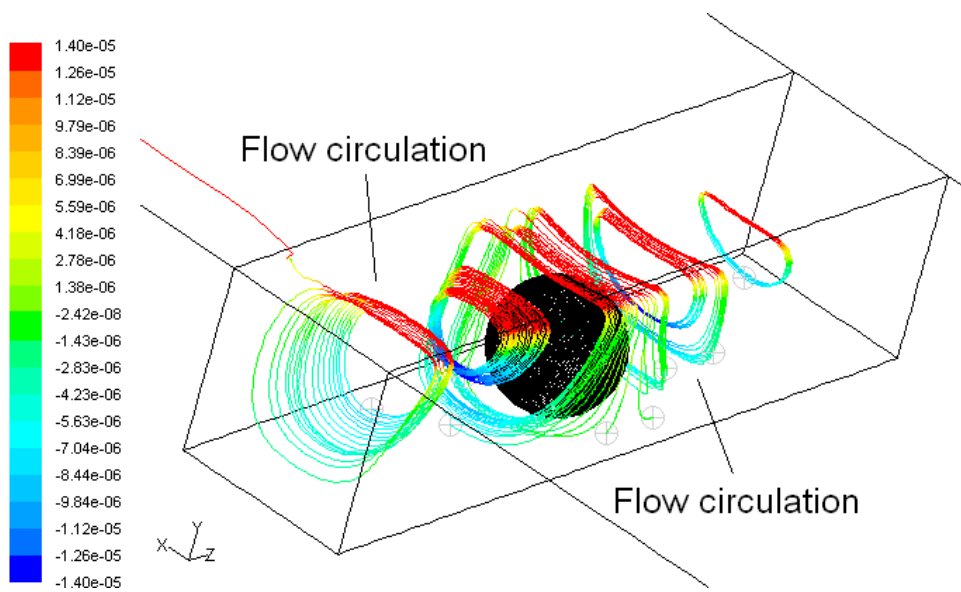
The occurrence of such stress distribution profiles on the embryo and how they change can be understood by looking at the fluid movement in the cavity. This is accomplished by looking at the particle trajectories in Figure 5.14. Here, the particles are released at several locations near the embryo in order to examine the trajectories of the particles travelling in the cavity around the embryo.

For the case of a narrow cavity with  $B^* = 1.5$ , it is found that recirculating flow mainly occurs around the upper region of the embryo, close to the cavity opening. This is shown in Figure 5.14a, where flow recirculation is detected around the upper part of the cavity. At the lower part of the embryo near the bottom of the cavity, the flow is very slow. The reason that such flow structures appear in a narrow cavity is that due to the proximity of the two side walls, the flow is dominated by viscosity. The strong fluid movement in the channel causes high shear; this tapers off quickly away from this region where the flow is much slower.

For the case of a wide cavity, such as shown here in Figure 5.14b for  $B^* = 6.0$ , flow recirculation, over the entire span, appears in the direction of the main flow (XY-direction). As can be seen in Figure 5.14b, the flow recirculation in most parts of the cavity takes a similar form. The embryo at middle in the cavity does not disturb this flow circulation pattern very much, as can be seen in the particle trajectory plots; in the middle of the cavity, the trajectories continue to circulate and wrap around the embryo. This can be explained by the fact that as the cavity width increases, the viscous interaction between the two side walls is less. This leads to a difference between the multiple embryo surface peak stresses in a wide cavity, which is less than when the cavity is narrow. The fluid movement is again found to be fastest near the cavity opening due to the proximity to the channel flow. This explains why the peak stresses always appear around the top region of the embryo.



(a)  $B^* = 1.5$



(b)  $B^* = 6.0$

Figure 5.14: Trajectory plots of particles released at several locations around the embryo shown here to illustrate the change of fluid movement in the cavity for (a)  $B^* = 1.5$  and (b)  $B^* = 6.0$ . The colours on the particle paths indicate the magnitude of the flow velocity (measured in m/s).

The typical shear stress distribution on the embryo is illustrated by the embryo surface shear stress contour plots shown in Figure 5.15. Here, only two distributions are displayed as, from previous findings on the examination of the shear stress distribution changes, they provide the representative examples. One arises when the cavity is narrow ( $B^* \leq 1.5$ ), the other when the cavity is wide ( $B^* > 1.5$ ). These plots provide a more complete picture of the variation over the entire embryo surface. In a narrow cavity, significant shear stress is detected only on top of the embryo as revealed in Figure 5.15a, with the highest stress located right at the tip of the embryo. The shear stress is negligibly small elsewhere on the embryo. In a wide cavity such as the one shown in Figure 5.15b, the peak stresses, while occupying a much wider area on the embryo, differ by little. As expected, these shear stress distributions correlate well with the flow structures in the cavity, which were described previously.

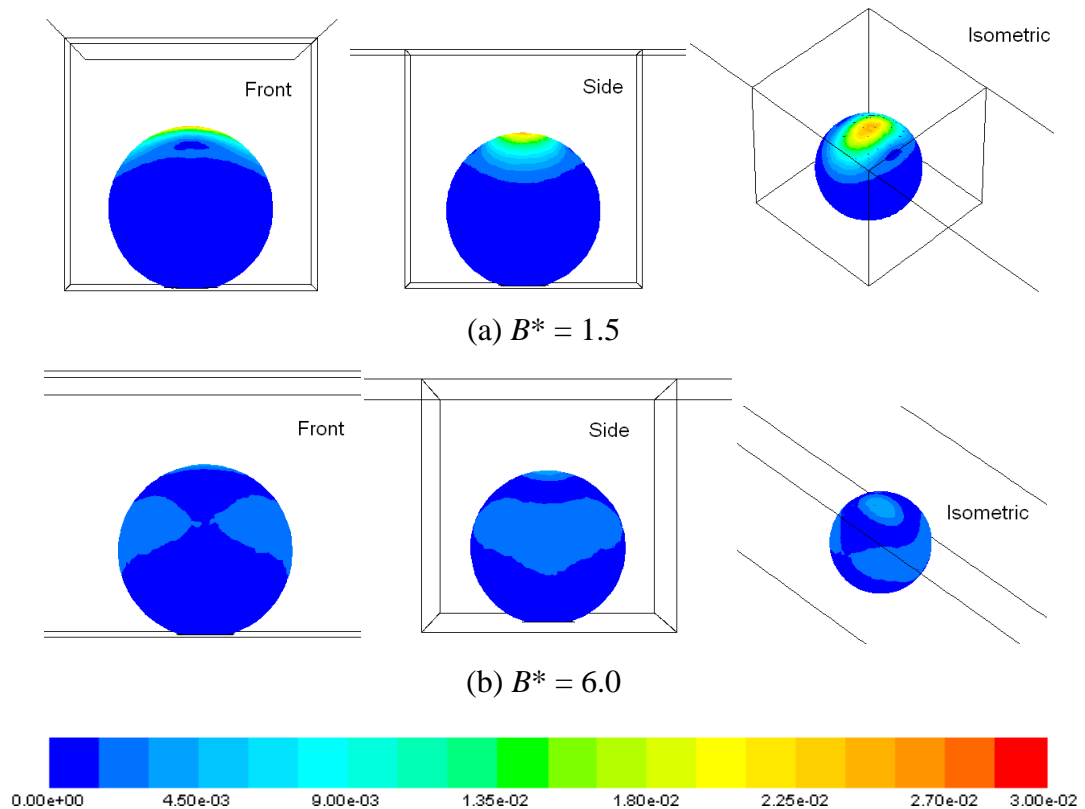


Figure 5.15: Contour plots of the shear stress (measured in Pa) on the embryo surface when the cavity has (a) a narrow width of  $B^* = 1.5$  and (b) a wider width of  $B^* = 6.0$ , where the front, side and isometric views of the embryo are shown. The fluid flow is from left to right in the side view.

### **5.2.7 Implication for Shear Stress Changes**

A few implications can be made from the observations on the shear stress formation and distribution on the embryo. First, in regards to the overall shear stress changes with different  $B^*$ , it can be concluded that a significant change in the level of shear stress is recorded when  $B^*$  is smaller than the critical width. This critical width is defined as the width at which the drastic change in shear stress starts to reduce, representing the point at which the viscous effect interference due to both side walls becomes insignificant. This critical width is important, as it allows one to alter the shear stress on the embryo to some extent by adjusting  $B^*$  within this critical width range.

From this study, it is also found that the viscous interference between the side walls and the embryo surface has an influence on a very wide region due to the condition of very low Reynolds number flow. Setting the width of the cavity so as to render such interference insignificant may not be viable, as the width of the cavity has to be set very large. Consequently, this issue has to be taken into consideration when optimizing the shear stress condition experienced by the embryo in deciding the suitable  $B^*$ .

Finally, when examining the shear stress distribution on the embryo, it is discovered that the top region of the embryo consistently experiences a higher shear stress compared with other parts of the embryo. When the cavity width is smaller than the aforementioned critical width, the top of the embryo experiences an excessively high shear stress – 10 times higher than for wide cavities. If it is required to design the bioreactor to have such narrow cavity, it may be necessary to devise some measures to either reduce this excessive stress or try to redistribute the stress more evenly. Presumably this can be accomplished by increasing the depth to move the embryo away from the direct influence of the fast-flowing fluid of the channel.

### **5.2.8 Comparison of 2D Model against 3D Model**

In this comparison study, the amount of lactate/oxygen exchanged across the embryo and the shear stress experienced by it for a 2D model are compared with the results for two 3D models with similar cross section: the 3D model with a cylindrical embryo and the 3D model with a spherical embryo.

As can be seen from Table 5.6, the discrepancies between the 2D model and both 3D models are noteworthy. The 3D cylindrical embryo model records a lactate concentration 81% lower than the 2D model, and an oxygen concentration of 63% lower than the 2D model. For the 3D spherical embryo model, the recorded lactate concentration is 57% lower while the oxygen concentration is 46% lower than the 2D model. The discrepancies for the shear stress have a trend different to that of the solute concentration. The shear stress calculated by the cylindrical embryo model is 81% higher than the 2D model while the spherical embryo model records a stress value 312% higher than the 2D model. In general, the 2D model predicts a higher solute concentration and a lower shear stress than the 3D models, suggesting that fluid movement calculated by the 3D models is more vigorous.

Looking at the solutes and shear stress distributions on the embryo along the flow (XY-direction), as indicated in Figure 5.16, it is found that apart from the magnitude dissimilarity, the solute distribution profiles for both 2D and 3D models are similar. In contrast, the shear stress distribution profiles for the 2D and 3D models are different. As can be seen in the stress distribution plots in Figure 5.16, the 3D models predict three peak stresses while the 2D model predicts only two peak stresses.

	Lactate concentration	% difference with 2D model
	M	
2D model	1.084E-06	-
3D model (cylinder)	2.070E-07	80.90
3D model (sphere)	4.667E-07	56.94

(a) Lactate

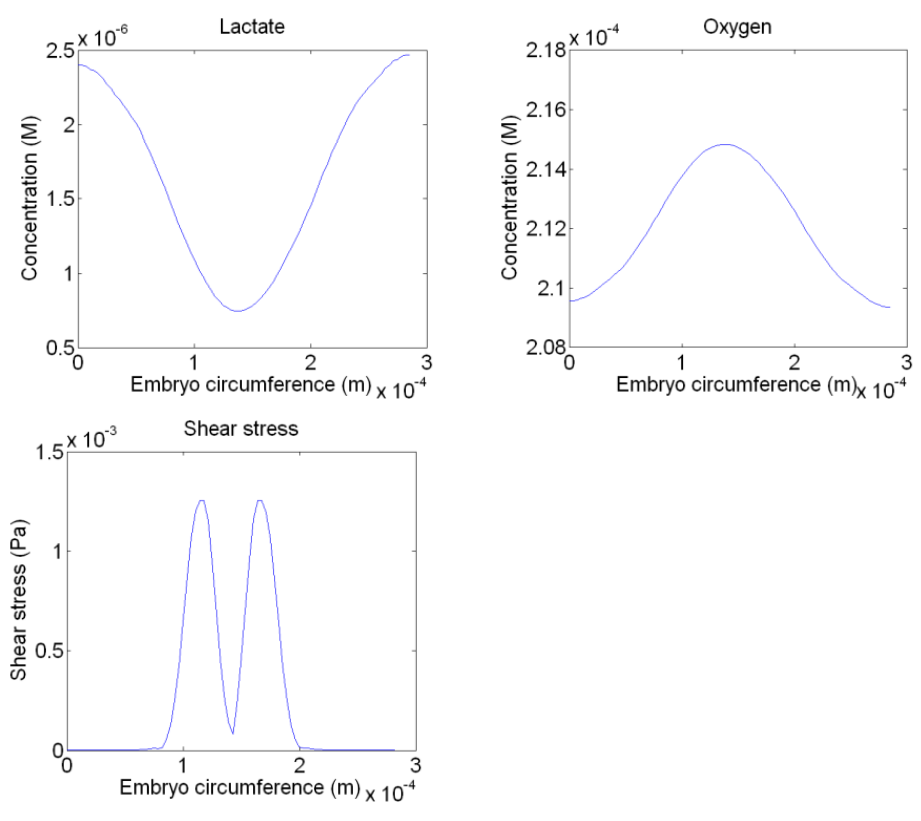
	Oxygen concentration	% difference with 2D model
	M	
2D model	5.119E-06	-
3D model (cylinder)	1.886E-06	63.16
3D model (sphere)	2.744E-06	46.39

(b) Oxygen

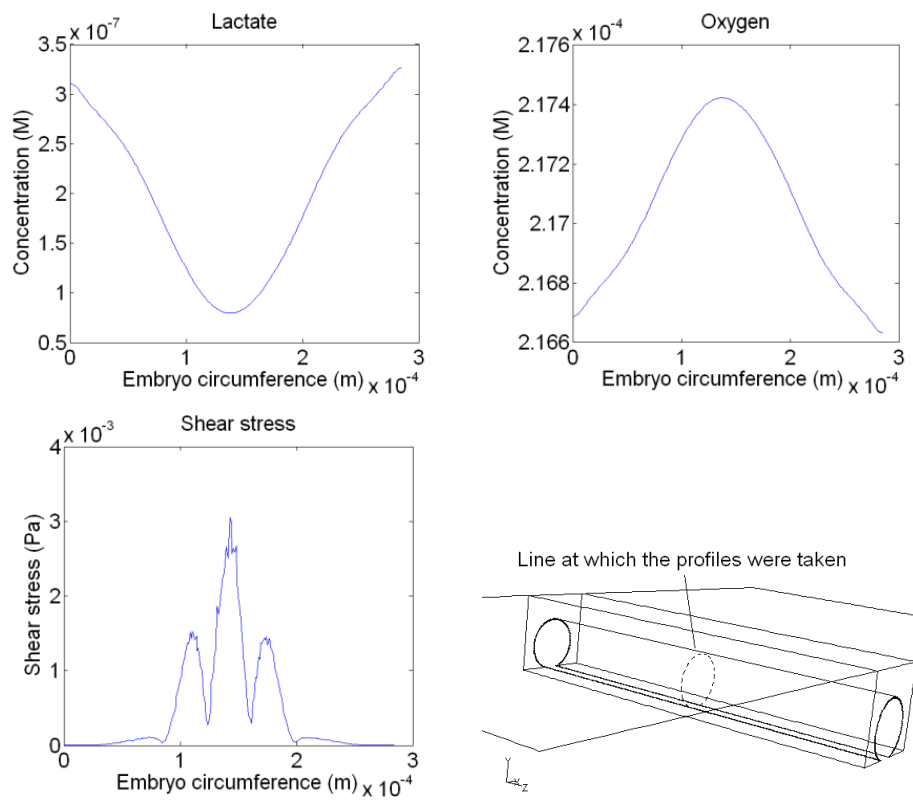
	Shear stress	% difference with 2D model
	Pa	
2D model	2.703E-04	-
3D model (cylinder)	4.883E-04	80.68
3D model (sphere)	1.112E-03	311.60

(c) Shear stress

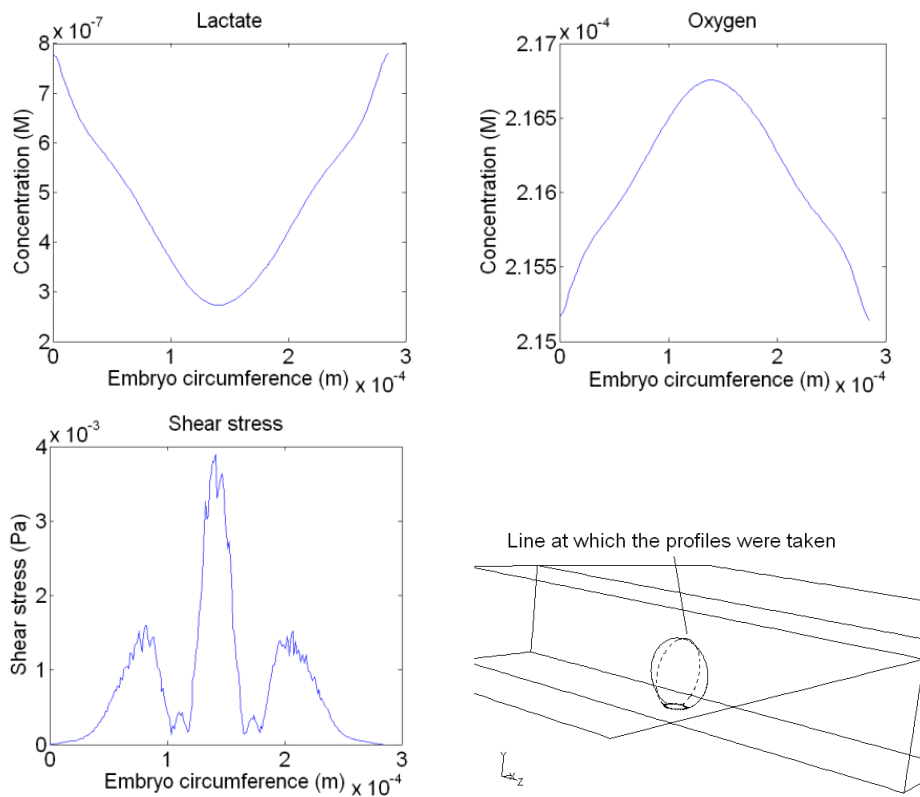
Table 5.6: Comparison of (a) lactate, (b) oxygen concentration and (c) shear stress summed over the embryo surface for all three models, with the percentage value showing the discrepancies between the 2D and the 3D models.



(a) 2D model



(b) 3D cylindrical model

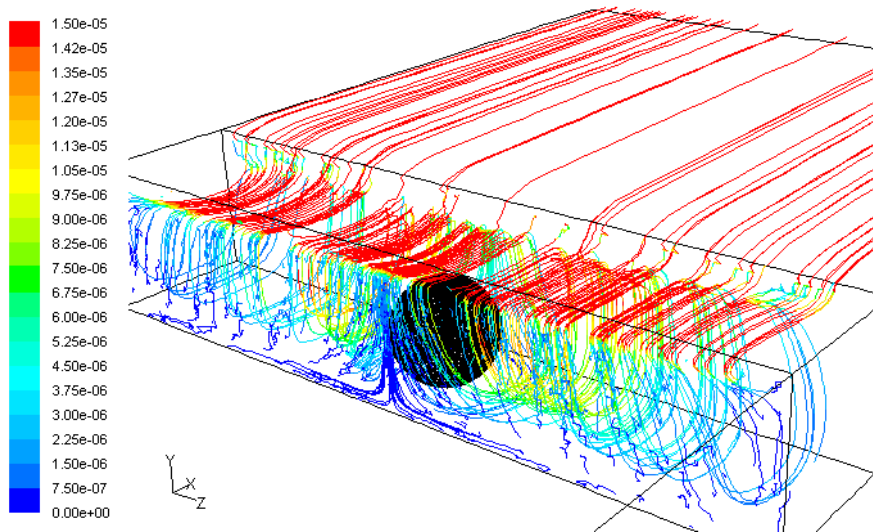


(c) 3D spherical model

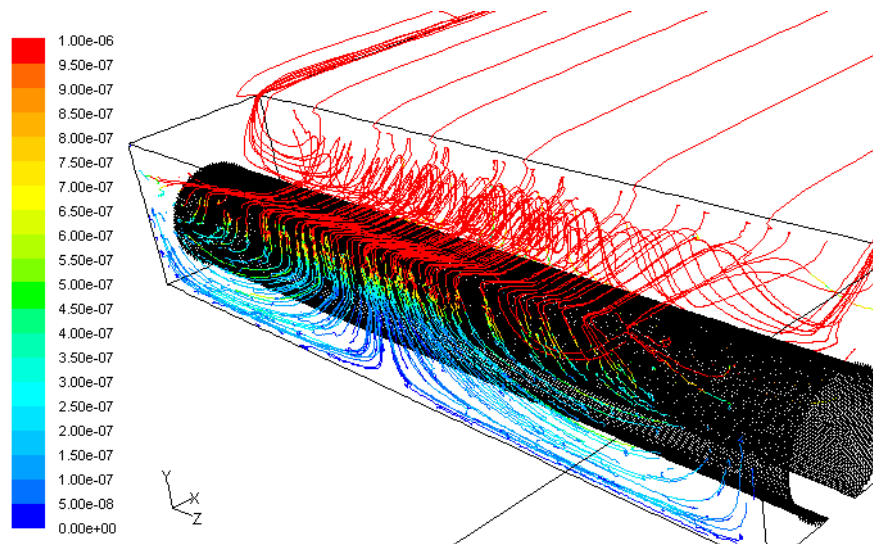
Figure 5.16: Comparison of the distribution of lactate, oxygen concentration and shear stress on the embryo for (a) the 2D model, (b) the 3D cylindrical embryo model and (c) the 3D spherical model. Note that for the 3D models, the distribution profiles obtained refer to the distribution at the middle of the embryo measured along the width, as indicated by the *dotted* line in the inserts.

The outcomes from the 2D model and 3D spherical embryo model were analysed first. All the findings from the overall solutes concentrations and shear stress, as well as their respective distributions on the embryo, clearly show the main difference between the 2D and the 3D model: that is, the presence of fluid movement along the width of the cavity. In a 2D model, the fluid movement in this direction is by definition zero, yet this is not the case for a 3D model, as demonstrated by Figure 5.17a. Here, it is found that large flow circulations occurred across the entire width of the cavity, and transverse fluid movement was detected pushing fluid towards the embryo in the middle. One explanation for this is that the 3D models utilized here only have a finite width of 750  $\mu\text{m}$ , which does not provide a true infinite width condition as imposed by the 2D model. The velocity is zero at the side walls of the cavity and the channel. Because of the low Reynolds number, this influences the velocity far away from these walls causing a flow that is far from two-dimensional.

The change in shear stress is more sensitive to the changes in fluid movement (either in the direction along the flow or perpendicular to the flow) compared to solute transport as shown by the numerous previous studies in the thesis. The movement of solutes is governed more by the diffusivity of the solute itself. This is why a 3D spherical model predicts an overall shear stress 3 times higher than does the 2D model, which is far in excess of the difference in the solute concentration.



(a) 3D cylindrical embryo model



(b) 3D spherical embryo model

Figure 5.17: Particle trajectory plots indicating the flow patterns for (a) the 3D cylindrical embryo model and (b) the 3D spherical embryo model. The 3D cylindrical embryo model was intended to mimic the 2D model with infinite width. The colour contour plots indicate the velocity magnitude (measured in m/s) of the flow in the cavity, where it is capped at  $1 \times 10^{-6}$  m/s to highlight the relatively small change in velocity in the cavity compared with the flow in the channel, which is much faster.

In regard to the 3D cylindrical embryo, one interesting finding here is that this model records a large difference in solute concentrations from the 2D model, since it is supposed that the 3D cylindrical embryo model reflects the 2D model projected in 3D. This discrepancy can be explained by the fact that there is considerable fluid movement along the width simulated by the 3D model, as revealed in Figure 5.17b. Here, the particle trajectory plot clearly shows the two fluid circulations in the spanwise direction meeting up at the middle width of the cavity. Consequently, this completely nullifies the intended purpose to represent the 2D model in 3D. Similar to the case of the 3D spherical embryo model, the width of the cavity is not large enough to render the viscous interference due to the side walls to be insignificant and a true infinite width condition is not achieved.

In summary, while it is found that the solute transport and the fluid flow predicted by the 3D spherical embryo model is starkly different from the 2D model, it must be stressed that a 2D model is still able to predict the form of the solute distribution around the embryo and provide at least order of magnitude estimates of solute and stress levels. The results show that the effects of the side walls are substantial. At low Reynolds numbers, viscosity causes considerable altering of the streamwise velocity across the width of the channel, and there are very substantial induced three-dimensional flows within the cavity. While this is not surprising considering that similar studies by Shankar (Shankar and Deshpande 2000) highlighted the significant of spanwise flow in a 3D lid-driven cavity model, more studies are needed to explore this, so that a better understanding of the 2D and 3D models can be achieved.

### **5.2.9 Conclusion and Summary**

This study focused on exploring the width of the cavity as the design parameter for the bioreactor. Using a three-dimensional model, the width of the cavity along with the bioreactor was expanded from 150  $\mu\text{m}$  to 1500  $\mu\text{m}$  and the solute transport and fluid flow variation due to the width change were quantified by examining the solute concentration and shear stress condition around the embryo. A secondary study on examining the difference between a 2D model and a 3D model was undertaken to explore the credibility of a 2D model in describing the flow in the bioreactor. This is

achieved by constructing 3D models that have the same cross section as the 2D model and assigned them with a width that is supposed to be free of end wall effects.

Gathering all the outcomes from the main cavity width research, it was found that poor solute transport and high shear stress are induced on the embryo when the cavity width is small; when the cavity width is reduced to smaller than a critical width, drastic changes in solute concentration and shear stress were detected. Using this information, one can adjust the width of the bioreactor to achieve a desired solute transport performance or to control the shear stress formed on the embryo. Such implementation is most efficient when the width adjustment is carried out within the critical width. Also from the study, it was found that the drop in solute transport performance and the high shear stress induced when the cavity is narrow is caused by the large viscous interference originating from the side walls (due to the very low Reynolds number condition), which in turn affects the solute transport and fluid movement around the embryo. It is anticipated that such interference is unavoidable unless the width the cavity is very large and one needs to take into consideration this issue when designing and optimizing the bioreactor.

The secondary study comparing the 2D and 3D models revealed that there are distinct differences in the predictions of the two models, due to the interference of the viscous effects from both of the side cavity walls. Despite this, both types of model may have their place: for example, a 2D model is relatively faster to set up and obtain preliminary results, (which may be subsequently scaled to an equivalent 3D model), while a 3D model has a direct representation of the actual bioreactor.

To conclude, the three-dimensional study on cavity width demonstrated the importance of utilizing three-dimensional CFD simulations in designing and optimizing the bioreactor, indirectly justifying the need to conduct more 3D studies.

### **5.3 Cavity Shape Parametric Study**

There are several techniques available to fabricate a micro-bioreactor. They generally include micromachining of silicon and glass, soft lithography, imprinting or embossing, injection moulding and laser ablation (Ho and Tai 1998; Stone and Kim 2001). These fabrication techniques are able to form complex three-dimensional structures with a multitude of shapes (Fiorini and Chiu 2005), and sized in the range of 15 to 30  $\mu\text{m}$  (Becker and Locascio 2002).

Focusing on the cavity in the micro-bioreactor, a number of choices of the cavity shape can be made. From the previous two-dimensional (2D) parametric study on the aspect ratio and the three-dimensional (3D) study on the cavity width, it is found that altering the dimension of the cavity changes the flow structure in it, which has a direct impact on the solute transport and shear stress formation on the embryo. Based on these findings, a 3D parametric study on different cavity shapes was conducted to find the advantages and disadvantages that different cavity shapes have on the fluid environment around the embryo. This information can be utilized to decide the most suitable cavity shape to breed embryos.

This section starts with a description of the shapes selected for the investigation and outlines the specific model and simulation setup for the parametric study. Solute transport and fluid flow around the embryo are inspected. The solute concentration and shear stress on the embryo are measured and analysed in order to understand how the fluid flow and solute transport around the embryo react to the different cavity shapes. Based on these findings, the benefits and shortcomings of each cavity shape are compared and discussed before the study is concluded.

#### **5.3.1 Problem Setup**

Four cavity shapes were selected for this study after considering the time and computational resources constraints. As shown in Figure 5.18 below, they are:

- Square cavity: the common square cross-sectioned cavity employed for all the other 2D and 3D studies.
- Round-grooved cavity: similar to the square cavity except for the rounded cavity floor compared with the flat surface in the square cavity

- Sharp-grooved cavity: rectangular V-shaped cavity with deep sharp groove.
- Hole cavity: cavity with a circular side wall and flat bottom surface; the cavity opening is smaller than the other three shapes.

These four shapes were chosen based on the possible fabrication techniques and the viable base material to fabricate the bioreactor. It must be noted that other aspects of the manufacturing process such as equipment availability, overall fabrication costs, speed and capability are not taken into consideration as they are not within the scope of this preliminary study.

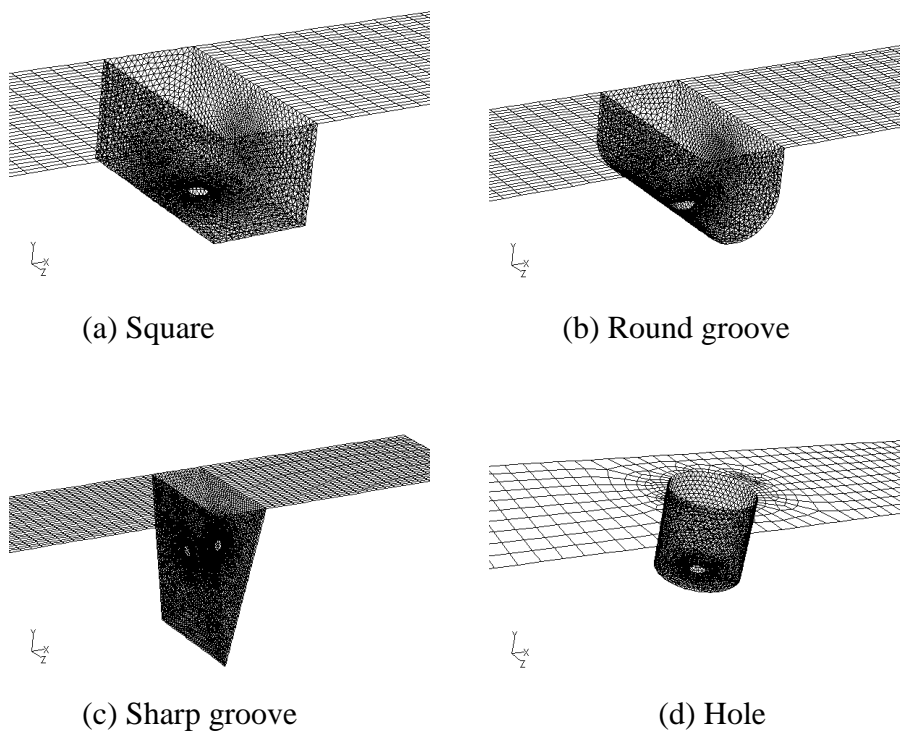


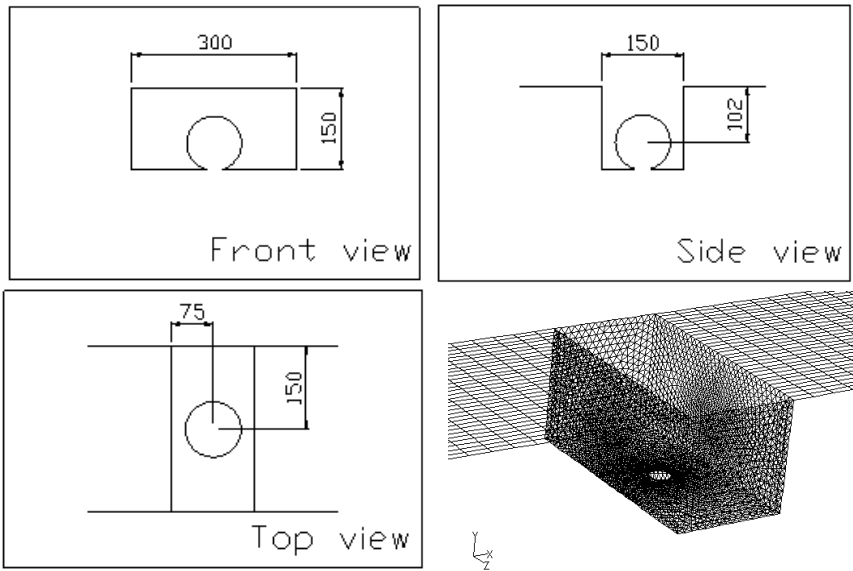
Figure 5.18: Meshed models of the four shapes chosen for this cavity shape study.

Geometric details specific for each cavity shape are presented in Figure 5.19, where the drawings of front, side and top view, as well as the meshed models in isometric view are shown. As highlighted, the common features that relate these four shapes are:

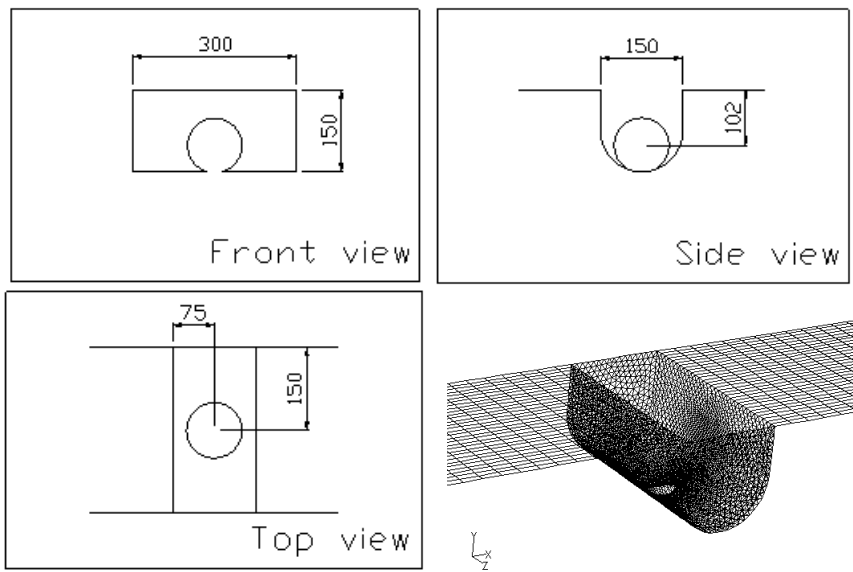
- The depth of the embryo from the cavity opening is the same.
- The location of cavity measured from the inlet is the same.
- The embryo is located in the middle on the bottom wall of the cavity.

By ensuring these features on all four cavities to be the same, the factors that might alter the fluid condition and solute transport other than the shape of the cavity were eliminated. This assures that the fluid and solute condition changes found in the study are solely caused by the shape variation.

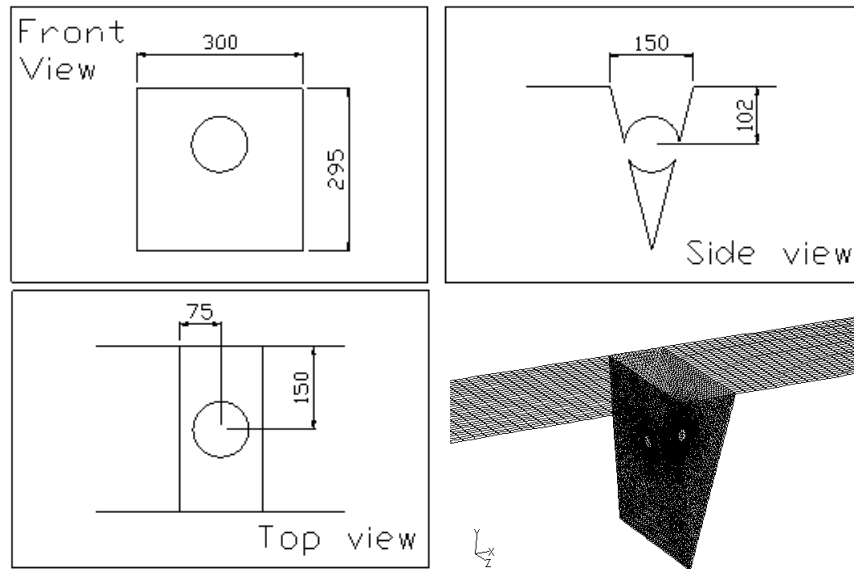
For all the simulations conducted in this study, several parameters of the CFD solver and the model were kept constant. The solute exchange rate of lactate and oxygen and the material properties of the culture fluid were fixed. The culture medium was set to perfuse through the bioreactor in the channel from the inlet to the outlet at the rate of 0.001 m/s. This made the fluid flow in the bioreactor viscous dominated ( $Re \approx 0.1$ ). The top surface of the channel was modelled as a free-surface wall to emulate the interface between oil layer and culture medium.



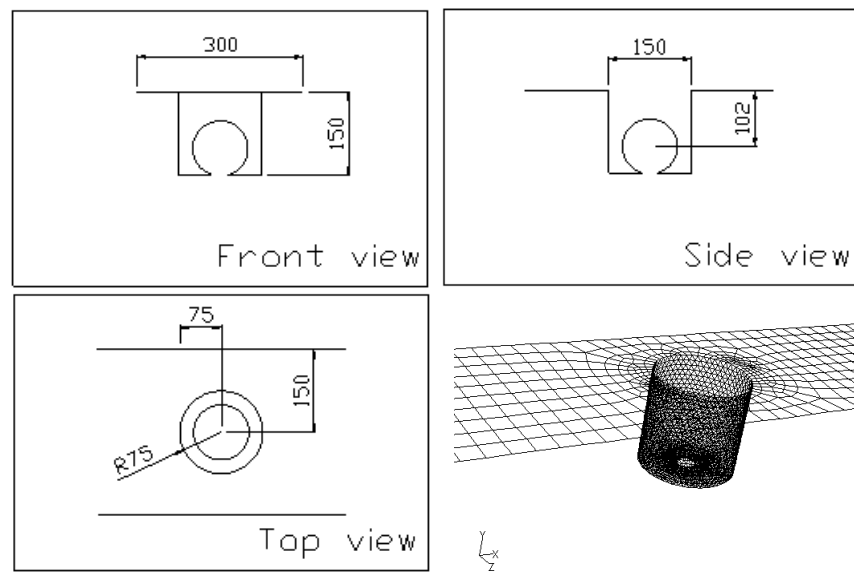
(a) Square



(b) Round-groove



(c) Sharp-groove



(d) Hole

Figure 5.19: Drawings illustrating the front, side and top view as well as the meshed model in isometric view are shown for all four shapes chosen for the study.

### 5.3.2 Comparison of Overall Solute Concentration

Initially, the overall lactate and oxygen concentrations on the embryo surface are examined. The amount of lactate and oxygen recorded on the embryo located in these cavities provides an indication of the capability of each cavity shape in transporting solutes. As shown in Figure 5.20, the lactate and oxygen content in the square, round and sharp groove-shaped cavities are marginally similar. Among them, the square-shaped cavity comparatively has the most active solute transport, where the lowest normalized lactate concentration of 0.9988 and highest normalized oxygen concentration 1.0000 were recorded on the embryo located in this cavity shape. This implies that the square-shaped cavity offers the best solute transport since more lactate is removed from the cavity and more oxygen is being transported into it. The solute transport capability of the round groove-shaped cavity is lower than the square cavity followed by the sharp groove-shaped cavity. In contrast, the hole-shaped cavity held the highest lactate level (215% higher than the default lactate concentration) and lowest oxygen level (0.96% lower than the default oxygen concentration); this indicates that the hole-shaped cavity offers the poorest solute transport.

Cavity shape	Lactate concentration	Oxygen concentration	Normalized lactate concentration	Normalized oxygen concentration
	M	M		
Square	5.186E-07	2.159E-04	0.999	1.0000
Round groove	5.571E-07	2.158E-04	1.073	0.9994
Sharp groove	6.034E-07	2.156E-04	1.162	0.9986
Hole	1.117E-06	2.138E-04	2.151	0.9904

Table 5.7: Tabulated values of the overall lactate and oxygen concentration averaged across the embryo surface for all four cavity shapes. The normalized versions were obtained by dividing the respective solute concentration with the default values indicated in Table 5.2.

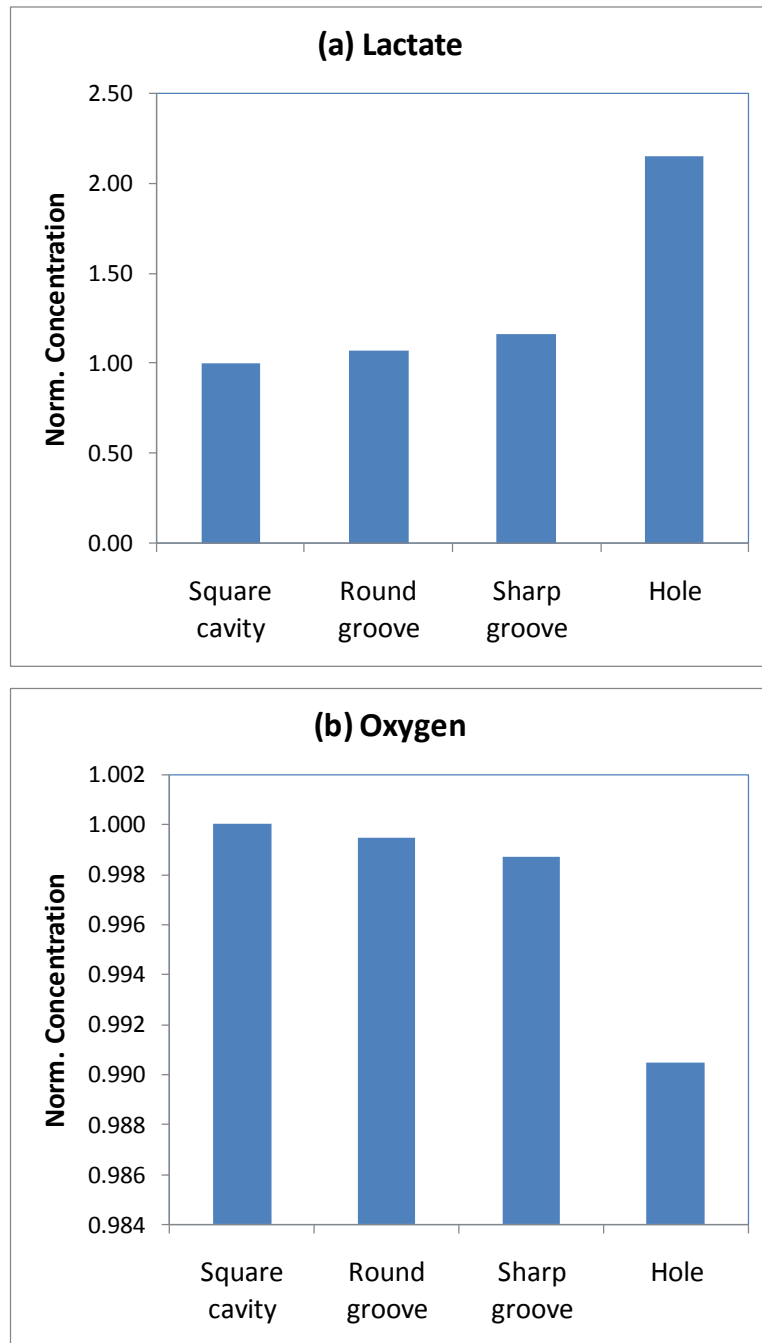


Figure 5.20: Comparison of the normalized (a) lactate and (b) oxygen concentration on the embryo surface for all four different cavity shapes.

To understand the reason for such variation of the solute transport as the cavity shape is altered, the lactate and oxygen distributions in the cavity are analysed. The contour levels of the lactate and oxygen located at the two middle planes are examined. One of the middle planes is located in the direction along the flow (XY-direction); the other one is located in the direction perpendicular to the flow (YZ-direction).

As shown in the lactate and oxygen contour plots in Figure 5.21 and 5.22 respectively, it is found that the overall lactate concentration is generally lower, while the overall oxygen concentration is generally higher in a square, round groove and sharp groove-shaped cavity than in a hole-shaped cavity. This is due to the larger cavity opening of the former three cavity shapes compared with the hole-shaped cavity, which allows more lactate to be advected from the cavity and similarly more oxygen to be transported into the cavity. Since the sizes of the cavity opening for square, round groove and sharp groove-shaped cavity are the same, it is not surprising that these three cavities recorded a similar overall solute concentration on the embryo. Apart from that, the smaller cavity volume of the hole-shaped cavity restricts solute movement around the embryo, which contributes to the lactate accumulation and oxygen deficiency in the cavity, as illustrated by the green to yellow contour levels in Figure 5.21d and the blue to green contour levels in Figure 5.22d, which cover the majority of the embryo surface. On the other hand, the larger cavity volume of the square, round groove and sharp groove-shaped cavities allows the lactate produced to dissipate further away from the embryo, lowering the lactate concentration on the embryo (as shown by the light blue contour level spreading out from the embryo in Figures 5.21a to 5.21c). At the same time, more oxygen at both sides of the cavity is able to reach the embryo in the middle of the cavity, causing the overall oxygen concentration to be higher (as shown by the yellow contour level spreading out from the embryo in Figure 5.22a to 5.22c).

In the comparison of the three cavity shapes that yield similar solute concentration, one can observe that the rounded bottom surface of the round groove-shaped cavity offers less cavity space at the bottom of the embryo compared with the square-shaped cavity that has a flat bottom surface. This further restrains the solute movement there and, as a result, more lactate builds up (Figure 5.21b) and higher oxygen deficiency occurs (Figure 5.22b), in a round groove-shaped cavity compared with a square-shaped cavity.

As for the sharp groove-shaped cavity, the V-shaped bottom severely impedes the solute transport below the embryo as shown by the higher lactate concentration level in Figure 5.21c and the lower oxygen concentration in Figure 5.22c at the region immediately below the embryo. This is because the V-shaped structure together with the embryo form a blockage that traps the solute at the bottom of the embryo. Also, it is generally known that in a V-shaped cavity as such, the flow circulation deeper into the cavity is increasingly slower (Moffatt 1964). Consequently, the overall lactate concentration is comparatively much higher while overall oxygen concentration is comparatively much lower in a sharp groove-shaped cavity compared with the other two cavities.

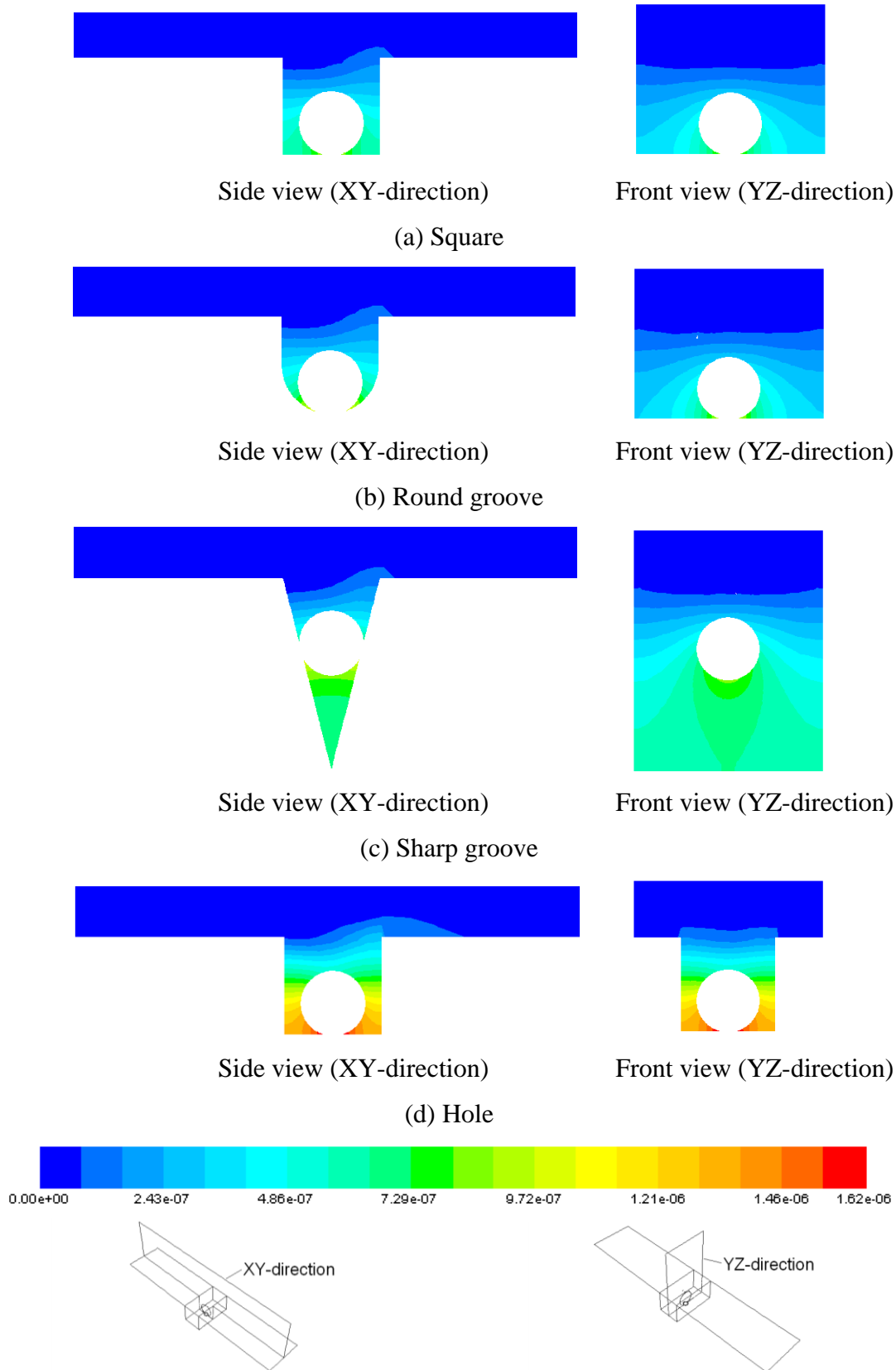


Figure 5.21: Contour plots of lactate concentration (measured in M) in all four cavities in the direction along the flow (XY-direction) on the left and perpendicular to the flow (YZ-direction) on the right.

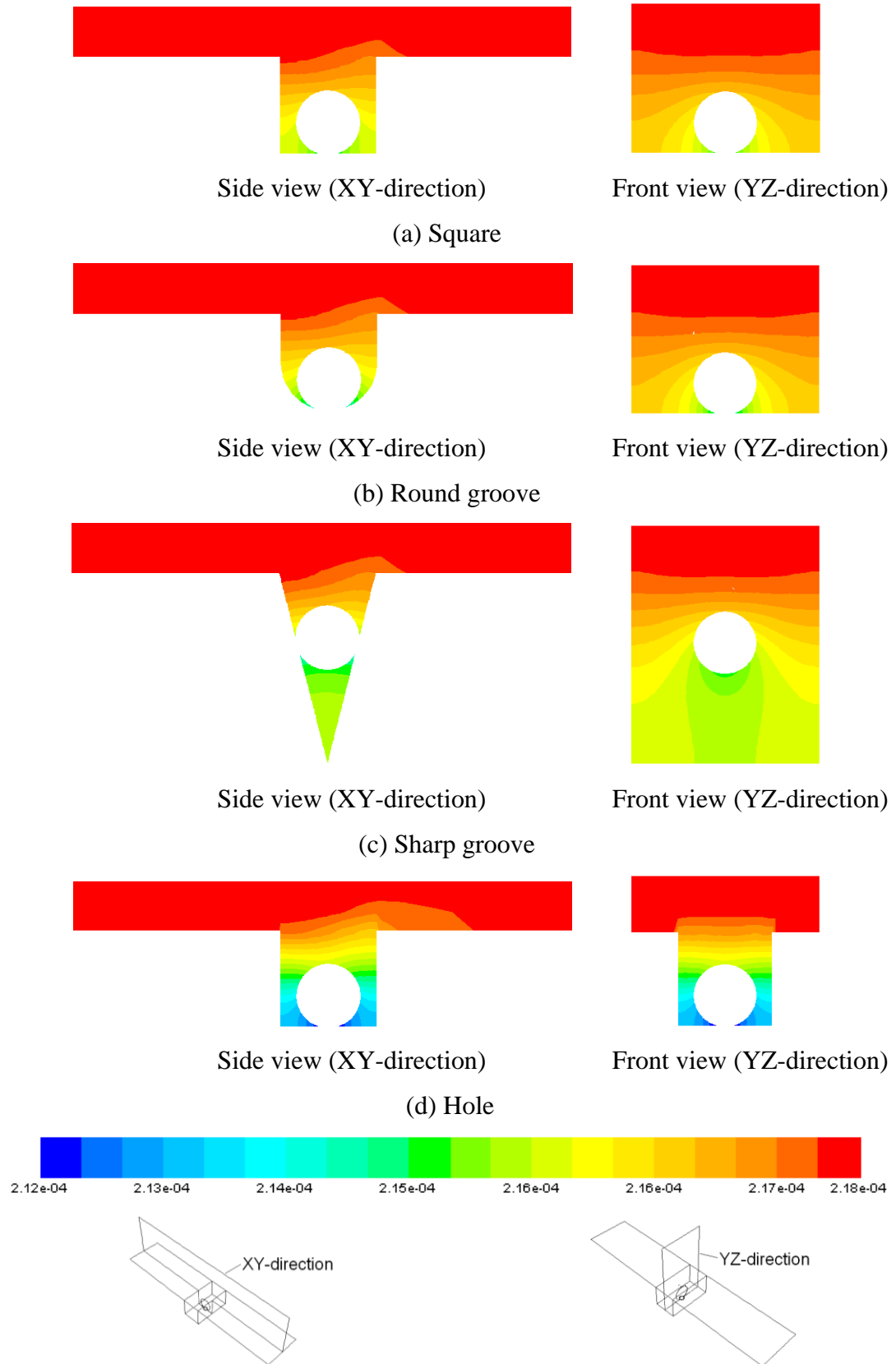


Figure 5.22: Contour plots of oxygen concentration (measured in  $M$ ) in all four cavities in the direction along the flow (XY-direction) on the left and perpendicular to the flow (YZ-direction) on the right.

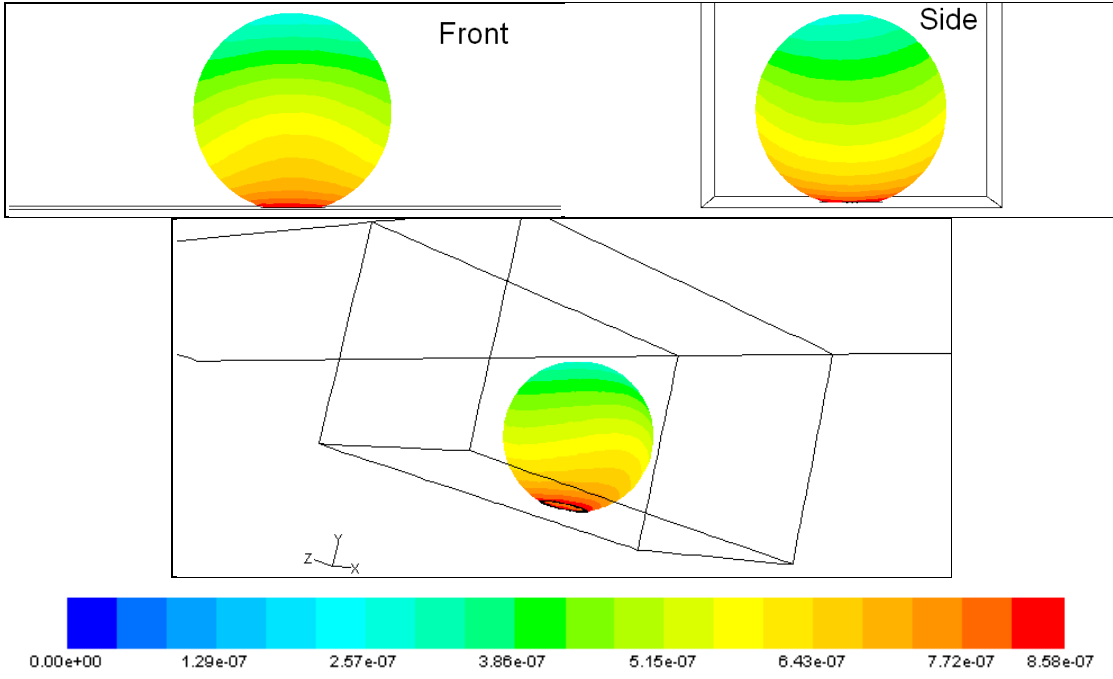
### 5.3.3 Comparison of Solute Distribution

In observing the solute distributions on the embryo, it is found that in general the solute concentration varies gradually from the bottom to the top of the embryo at an established gradient: lactate concentration changes from the highest level at the bottom of the cavity to the lowest level at the top of the embryo (Figure 5.23), while oxygen changes from the lowest level at the bottom of the cavity to the highest level at the top of the embryo (Figure 5.24). Such trends of the solute distributions result from solute transport at the top of the embryo being the most active, as it is closer to the cavity opening where the solutes are transported into and out of the cavity by the faster fluid flow in the channel.

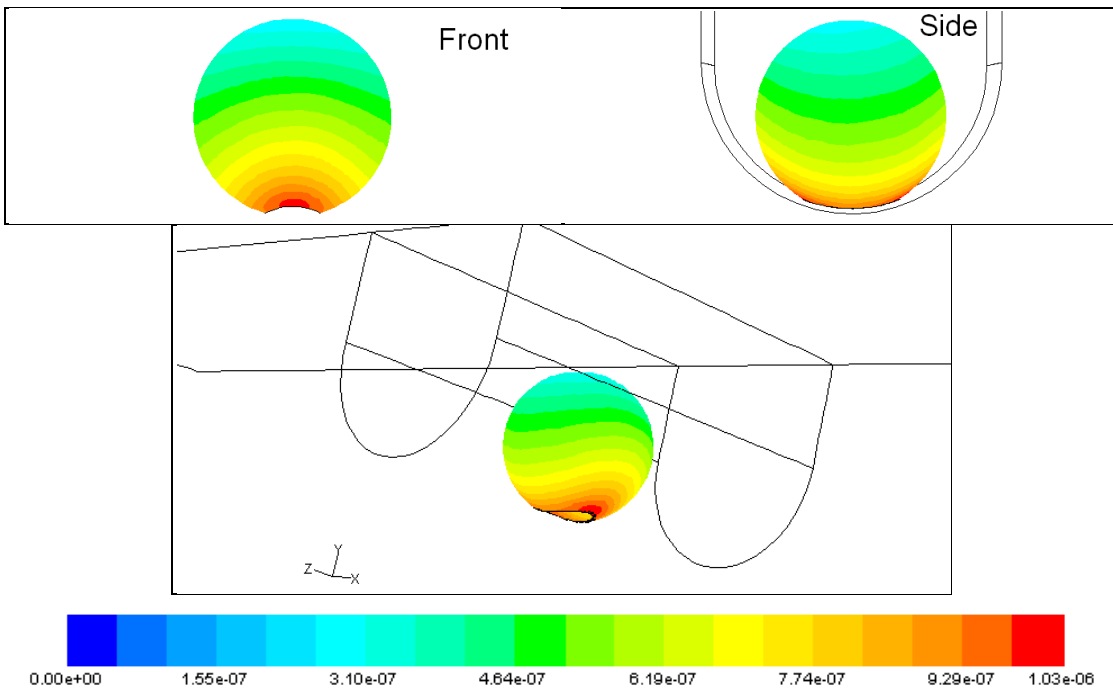
The main dissimilarity between the solute distributions for these four cavity shapes is the shape of the profile on the surface. In particular, the square, round groove and sharp groove-shaped cavities all have curvy contours (Figure 5.23a to 5.23c, 5.24a to 5.24c) while the hole-shaped cavity has a straight and level contour (Figure 5.23d, 5.24d) on the embryo surface. It is speculated that this occurs because with a hole-shaped cavity, the distance of the embryo surface to the cavity circular side wall is the same in all directions. On the contrary, for the square, round groove and sharp groove-shaped cavities, the distance orthogonally from each of these side walls to the embryo surface is different. This leads to a trend of the solute distribution on the embryos in the square, round groove and sharp groove-shaped cavities (Figure 5.23a to 5.23c, 5.24a to 5.24c respectively), That is, if the side wall is closer to the embryo surface, the concentration contours exhibit an upward curvature, while if the side wall is further away from the embryo surface, a downward curvature results.

The occurrence of these concentration contour curvatures is explained here. The upward curvature of the concentration contour reflects that when the side wall is close to the embryo, solute transport is impeded due to the restricted space. This causes more lactate to accumulate here as well as a lower amount of oxygen to be transported there. Alternatively, if the side wall is placed further from the embryo, the situation is reversed; where the solute transport is no longer impeded as much, and the solute movement toward and away from the embryo is more active. Lactate produced by the embryo

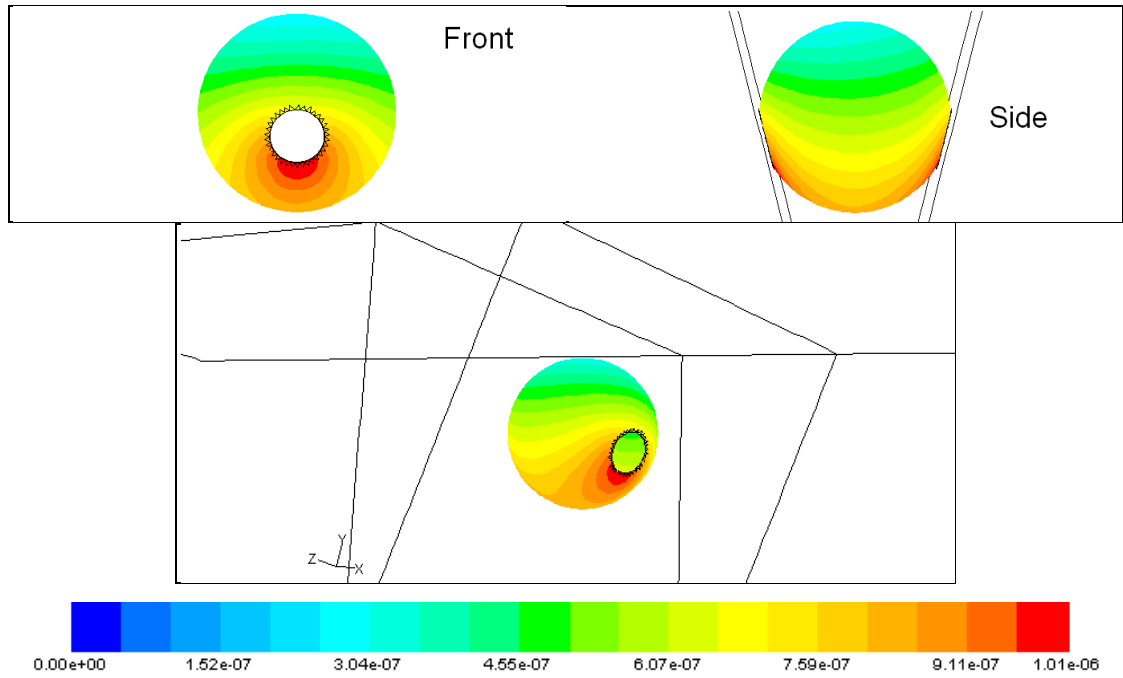
tends to diffuse away from the embryo, as can be seen by the low lactate concentration contour level (yellow contour level); this tends to be restricted at the bottom of the embryo (Figure 5.23a to 5.23c, 5.24a to 5.24c, side views). Similarly, more oxygen from other regions of the cavity and from the channel is transported to the embryo, as can be seen by the high oxygen concentration contour (shown by the green contour level), which tends to occupy more than half of the embryo surface. This can be seen in the side views of the concentration contour plots.



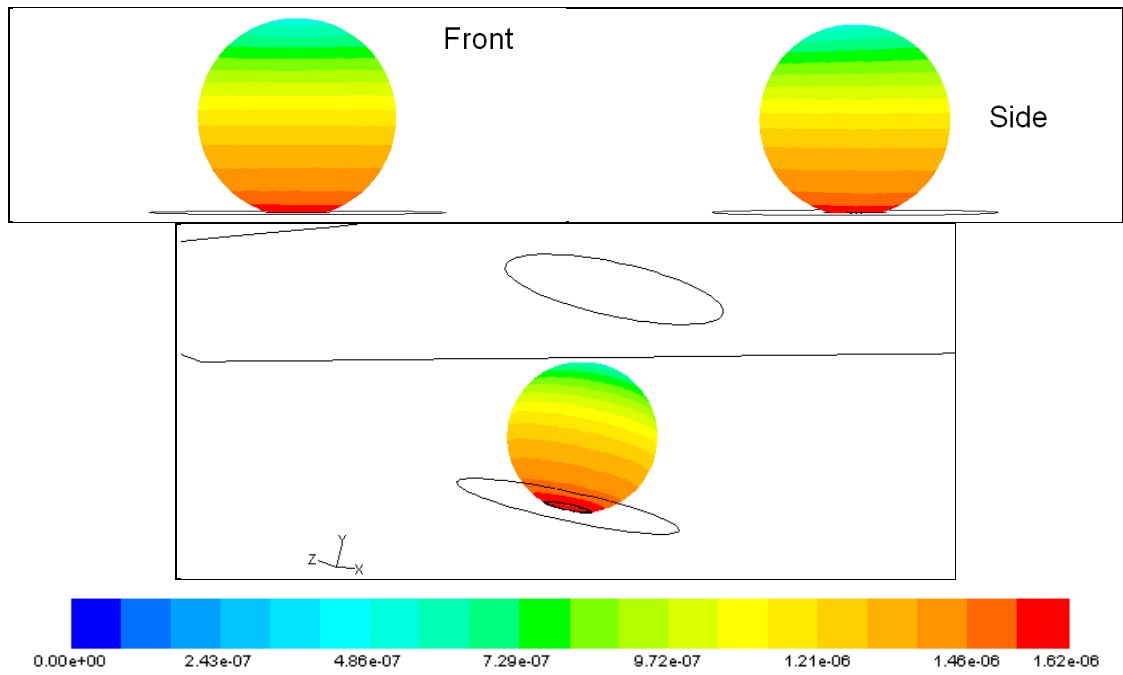
(a) Square



(b) Round groove

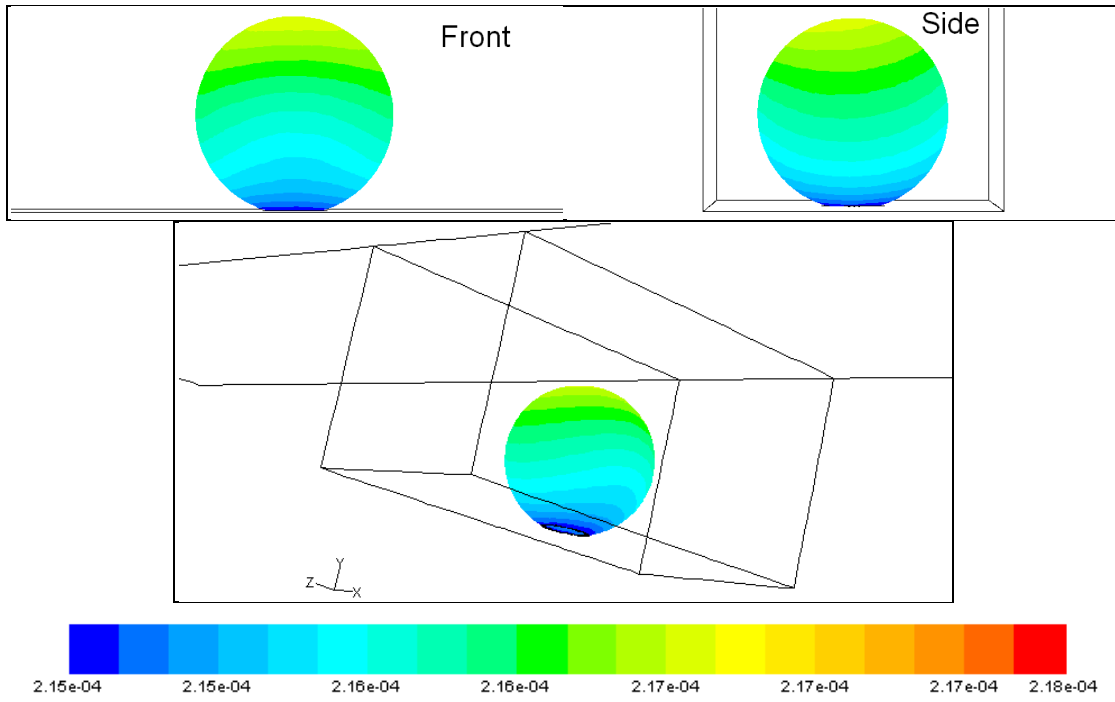


(c) Sharp groove

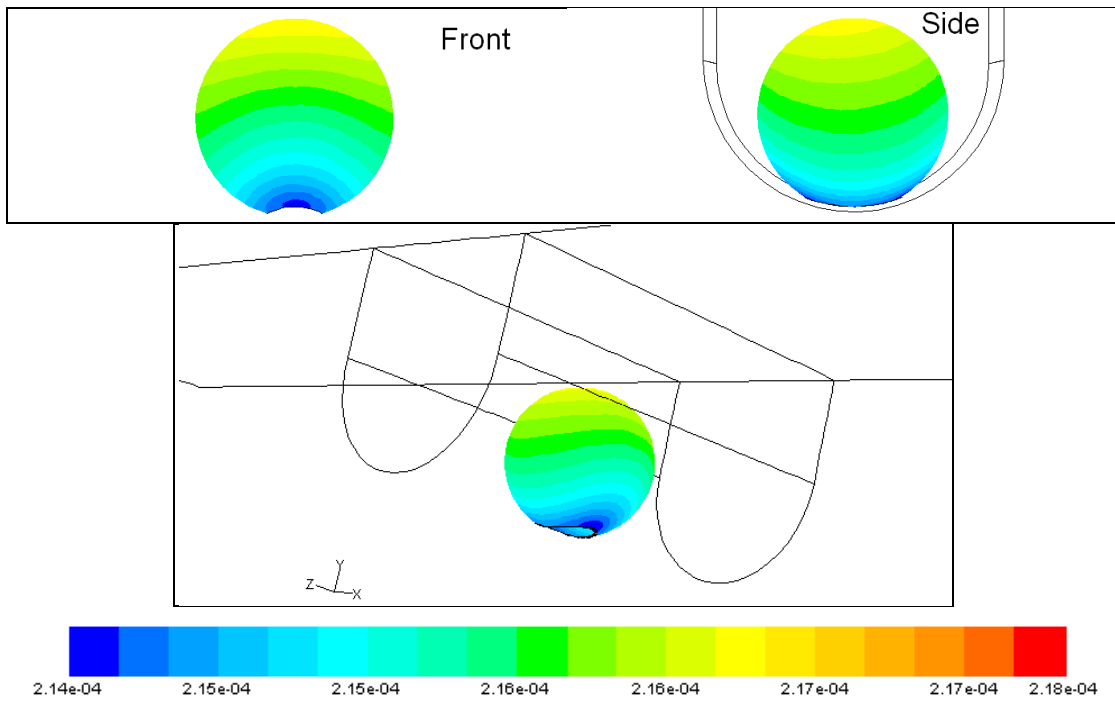


(d) Hole

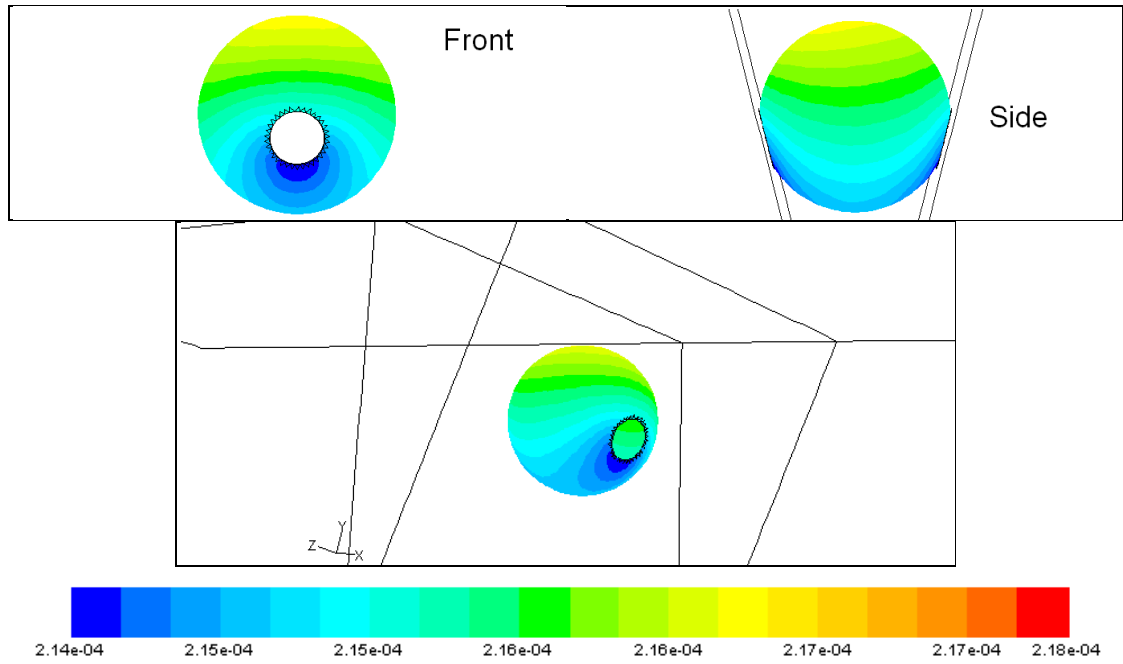
Figure 5.23: Contour plots of lactate concentration (measured in M) on the embryo surface for all four types of cavity shapes where the front, side and isometric view are shown



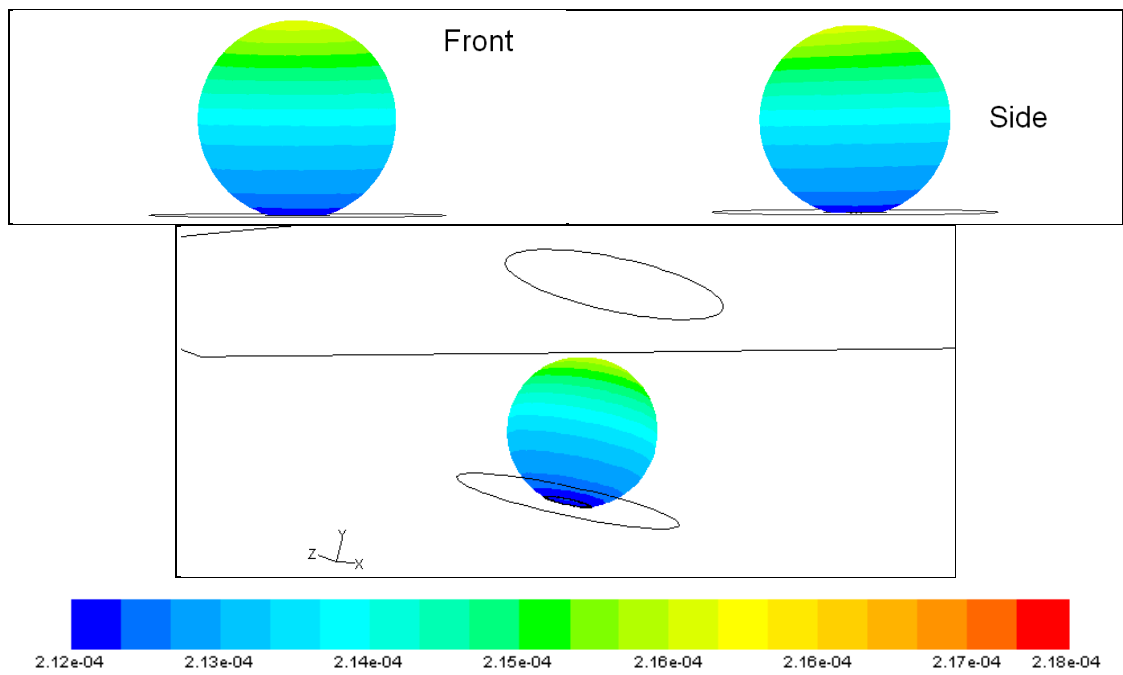
(a) Square



(b) Round groove



(c) Sharp groove



(d) Hole

Figure 5.24: Contour plots of oxygen concentration (measured in  $M$ ) on the embryo surface for all four types of cavity shapes. The front, side and isometric views are shown.

### 5.3.4 Comparison of Overall Shear Stress

In this section, the difference in the overall shear stress experienced by the embryo due to different cavity shapes is presented. As summarized in Figure 5.25, the square and round groove-shaped cavities induce a similarly high shear stress (around 98% of the default shear stress) on the embryo. This is followed by the sharp groove-shaped cavity for which is found a lower stress level of 70% of the default shear stress. The hole-shaped cavity provides the least stress on the embryo, where the stress level recorded is only 39% of the default shear stress. The overall discrepancy between the highest and the lowest shear stress is a significant 61%. It would be beneficial therefore to find out the cause for such a variation to gain a better understanding of why changing cavity shape affects the shear stress induced. To achieve this, the fluid movement in the cavity is examined by studying the velocity contour plots of the flow in the cavity, as depicted in Figure 5.26.

Cavity shape	Shear stress	Normalized shear stress
	Pa	
Square	1.296E-03	0.9962
Round groove	1.260E-03	0.9685
Sharp groove	9.078E-04	0.6975
Hole	5.042E-04	0.3875

Table 5.8: Tabulated values of the overall shear stress averaged across the embryo surface. The normalized shear stress is calculated by dividing the respective stress values with the default shear stress shown in Table 5.2.

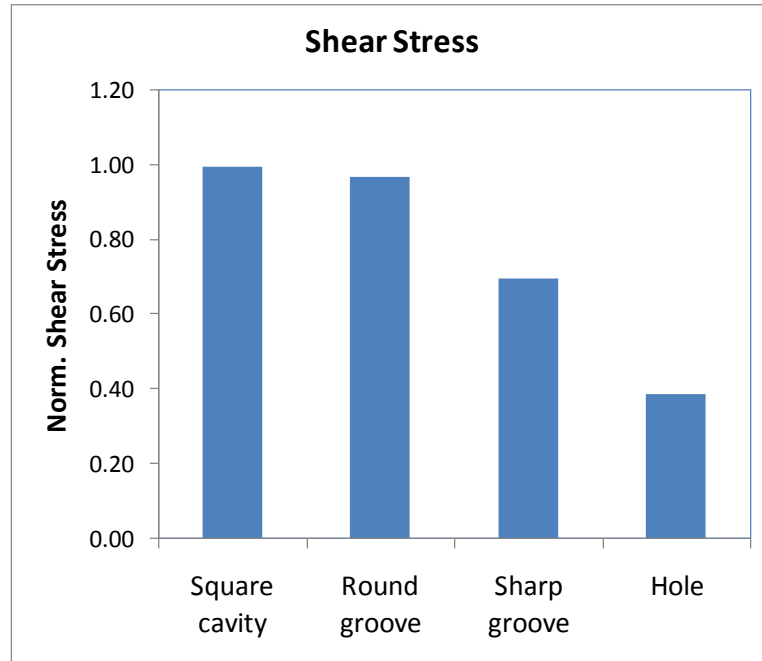


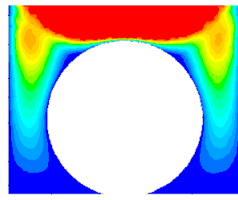
Figure 5.25: Comparison of the shear stress on the embryo surface for all four cavity shapes.

In comparing the velocity contours for all four shapes (Figure 5.26), it can be seen that majority of the fluid flow around the embryo in a square or round groove-shaped cavities is relatively fast. This is shown by the close vicinity of the yellow velocity contour, indicating the moderate flow circulation in the cavity, and the red velocity contour, indicating the fast channel flow. These faster fluid movements stimulate a relatively high shear stress on the embryo. In addition, it is not surprising that these two cavity shapes produce a similar velocity contour around the embryo because they are geometrically similar in terms of cavity opening and cavity volume. As a result, the fluid movement within them is similar. While the shape of the cavity bottom is different for both cavities, this did not affect the fluid movement by much, as shown by the velocity contours in the XY-direction in Figure 5.26a and 5.26b.

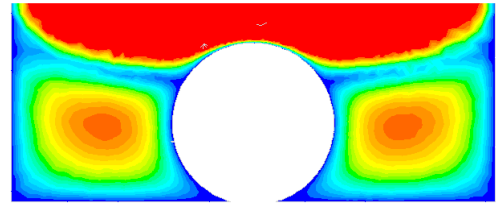
While the sharp groove-shaped cavity has an opening of size similar to the previous two cavity shapes, the transverse flow circulation in it is small (as illustrated by the XY-direction velocity contour in Figure 5.26c), implying that the shear stress due to the flow circulation is small. In addition, the V-shaped cavity bottom promotes the formation of *Moffatt* vortices, which represent a sequence of eddy recirculations decreasing in size and strength rapidly (Moffatt 1964). This implies that the fluid movement below the

embryo is much weaker than that above the embryo. Together, these factors result in a shear stress induced on this embryo that is lower than the ones in a square or round groove-shaped cavity.

Finally, as seen in Figure 5.26d, slow flow recirculations are detected around the embryo in a hole-shaped cavity, as shown by the light blue velocity contour surrounding the embryo. Also, the contact area with the channel flow on this embryo is smaller than the other three cases. This is because a hole-shaped cavity has a much smaller cavity opening that impedes much of the fluid flow from the channel from going into and out of the cavity. Apart from that, there is the least amount of space in the cavity available for flow circulation in a hole-shaped cavity. Subsequently, all these factors lead to the lowest stress occurring on the embryo in a hole-shaped cavity.

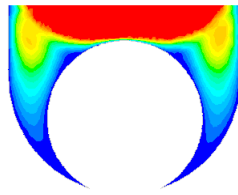


XY-direction

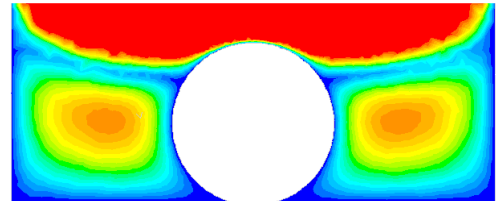


YZ-direction

(a) Square

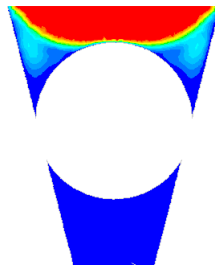


XY-direction

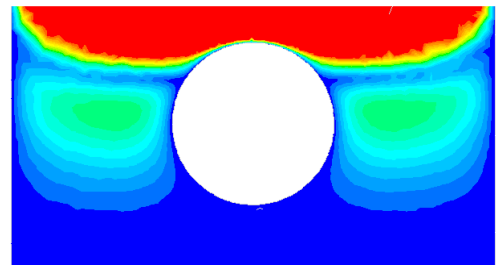


YZ-direction

(b) Round groove

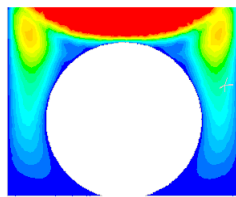


XY-direction

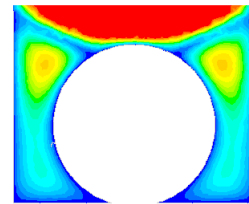


YZ-direction

(c) Sharp groove

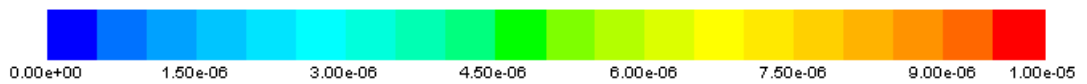


XY-direction



YZ-direction

(d) Hole



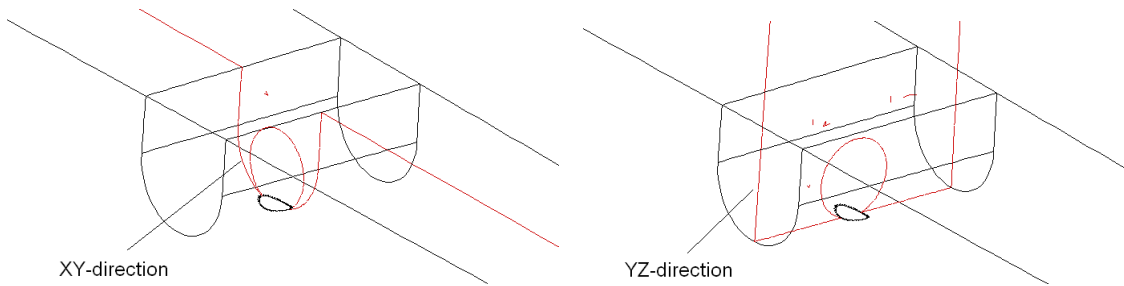


Figure 5.26: Velocity magnitude (measured in m/s) contour plots in the two planes in the middle of the cavity along the flow (XY-direction) and perpendicular to the flow (YZ-direction) in the cavity for all four cavity shapes, highlighting the magnitude and direction of the fluid movement around the embryo. The range of the velocity magnitude displayed is restricted up to  $1 \times 10^{-5}$  m/s in order to emphasize the very slow fluid movement in the cavity compared with the fluid flow in the channel.

### 5.3.5 Comparison of Shear Stress Distribution

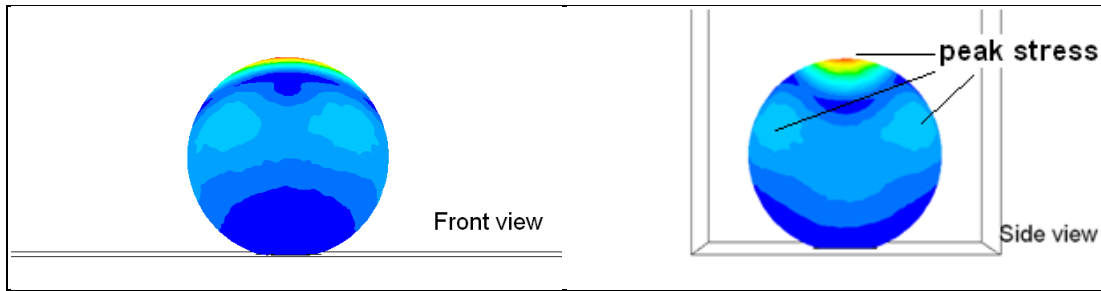
The shear stress distribution on the embryo in all four different cavity shapes, represented by the stress contour plots in Figure 5.27, is related to the fluid movement in the cavity as shown by the particle trajectory plots in Figure 5.28. The change of the shear stress induced on the embryo due to the variation of cavity shape was analysed by looking at the stress distribution at three locations on the embryo surface: the top region, the upper region and the lower region of the embryo.

First, it can be observed that the highest peak stress was formed at the top of the embryo, regardless of the cavity shape. This is shown by the yellow stress contour on the top of the embryo in a square, round groove and sharp groove-shaped cavities (illustrated in Figures 5.27a, 5.27b and 5.27c, respectively). In a hole-shaped cavity, a similar peak stress was also detected at the top of the embryo (Figure 5.27d), although the magnitude of this peak stress is not as high as in the previous three cases. The occurrence of this peak stress can be explained by the fact that the fast fluid movement in the channel extends into the cavity and reaches the top of the embryo; this fast fluid flow in turn induces a relatively high shear stress in this region. This explanation is evidenced by the particle trajectory plots in Figures 5.28a, 5.28b and 5.28c, where the streaks of red particle trajectories, representing fast fluid flow were found to appear on top of the embryo located in a square, round groove and sharp groove-shaped cavity. Due to the smaller cavity opening, there is a lower amount of fast fluid flow from the channel

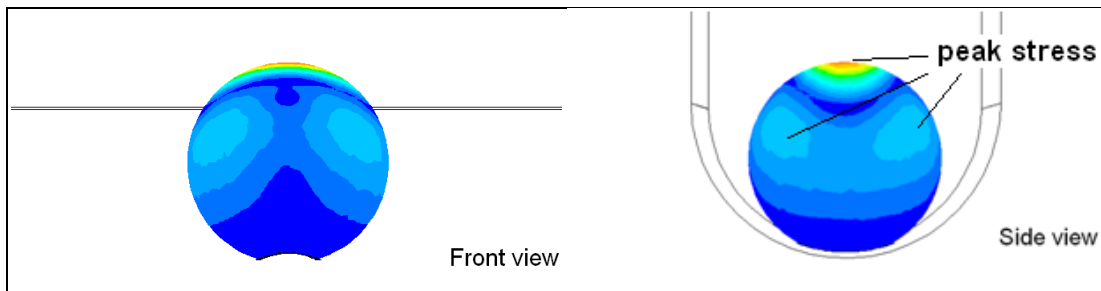
reaching the embryo in a hole-shaped cavity, as can be seen by the shorter red particle path in Figure 5.28d. This explains the relatively smaller peak stress at the top of the embryo in a hole-shaped cavity.

In the upper region of the cavity in a square, round groove and sharp groove-shaped cavity, four peak stresses, whose magnitudes are smaller than the peak stress at the top of the embryo, were detected. This is indicated by the light blue shear stress contour patches shown by the side view plots in Figures 5.27a, 5.27b and 5.27c. The occurrence of these peak stresses is due to the formation of the large flow recirculations on each side of the embryo. As indicated in Figures 5.28a, 5.28b and 5.28c, respectively, for a square, round groove and sharp groove-shaped cavity, these two large flow circulations, which are as large as the embryo, expand from the embryo surface to the side walls at the edge of the cavity. These flow recirculations align well with the upper region of the embryo and explain the formation of the two peak stresses on each side of the embryo. In a hole-shaped cavity, the two flow circulations besides the embryo were restricted by the smaller cavity volume. The cores of the flow recirculations are not aligned at the centre of the embryo but slightly above it (Figure 5.28d). As a result, the upper region of this embryo only experiences a peak stress on each side; these peaks are located closer to the top region of the embryo.

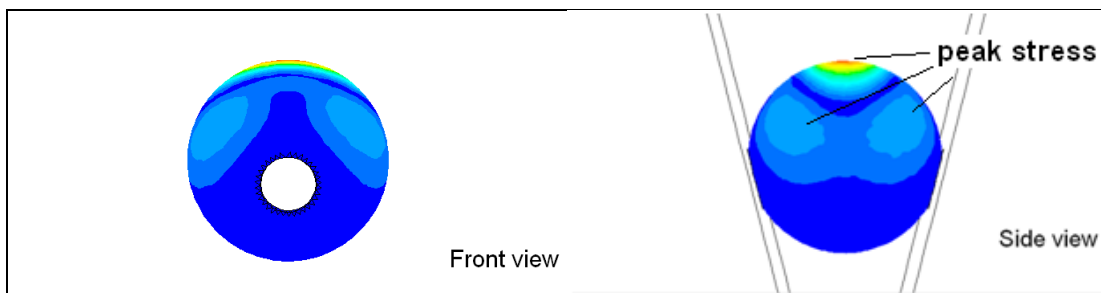
Lastly, for all the different cavity shapes, a slow rate of flow circulation was detected, as shown by the blue particle trajectories that appear at the bottom of the cavity in Figure 5.28. This is expected, as at the bottom of the cavity the fluid movement is generally much slower than the fluid flow near the upper region of the embryo or in the channel. Thus, the stress level there is comparatively lower than elsewhere, as demonstrated by the emergence of blue stress contour patches in Figure 5.27. Also, it must be noted that in a sharp groove-shaped cavity, the fluid movement deeper in the V-shaped bottom is generally very slow. Therefore, the fluid movement there does not have much impact on the shear stress induced on the embryo.



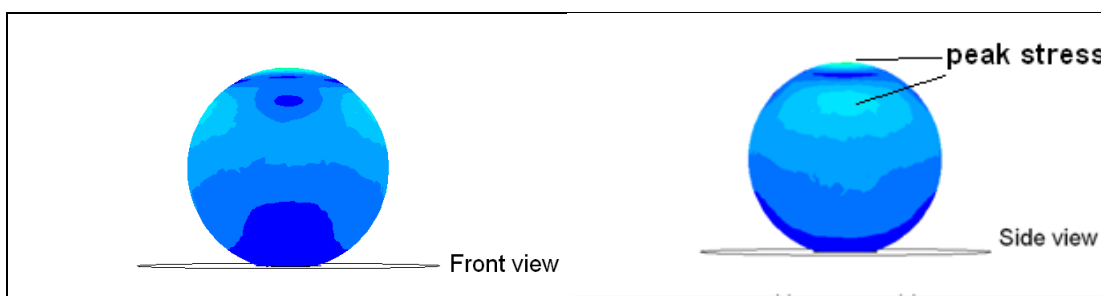
(a) Square



(b) Round groove



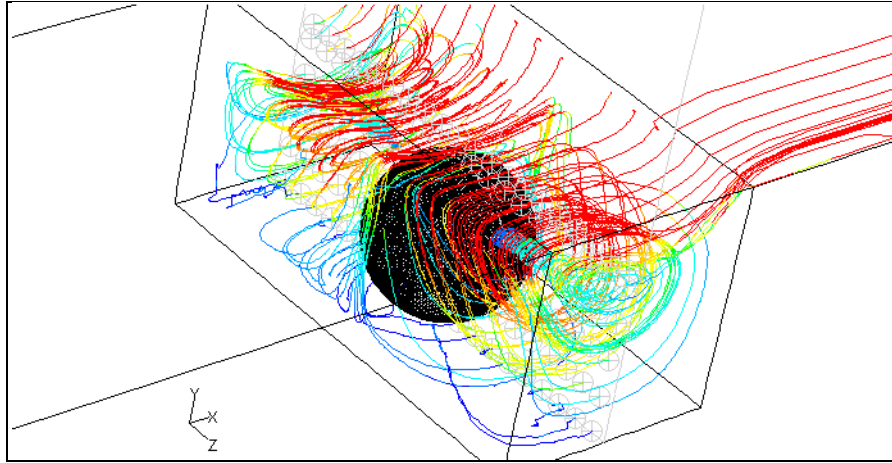
(c) Sharp groove



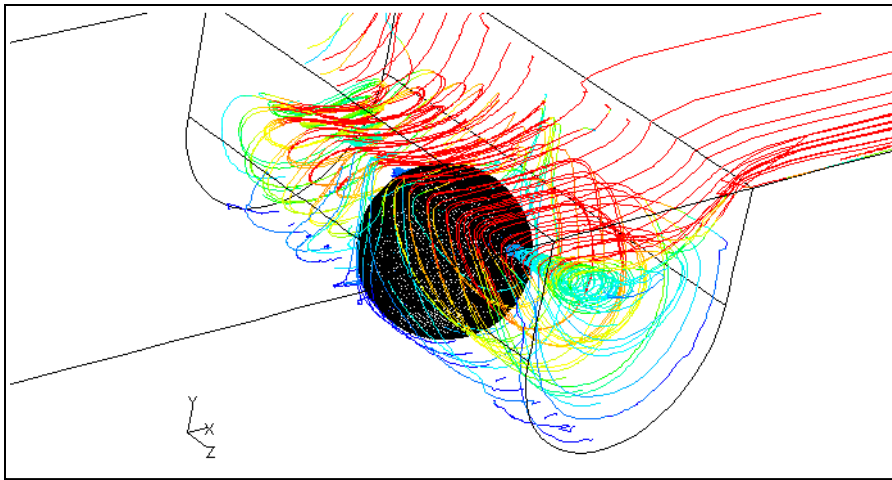
(d) Hole



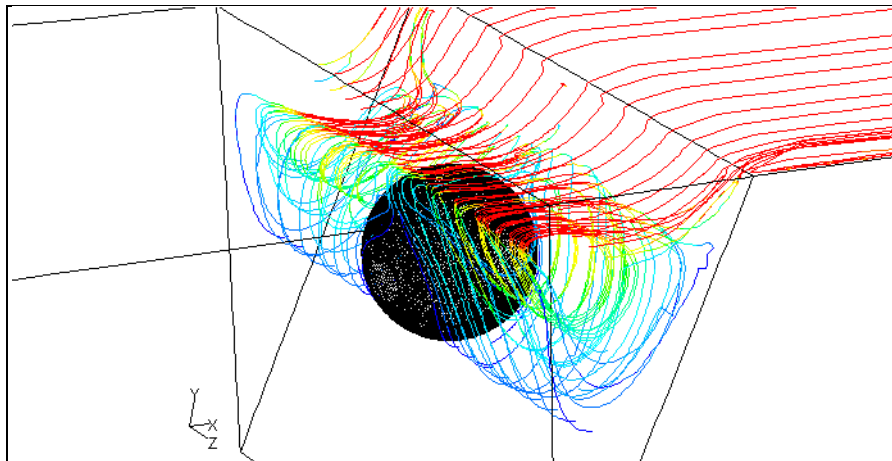
Figure 5.27: Contour plots showing the shear stress (measured in Pa) on the embryo induced by all four cavity shapes.



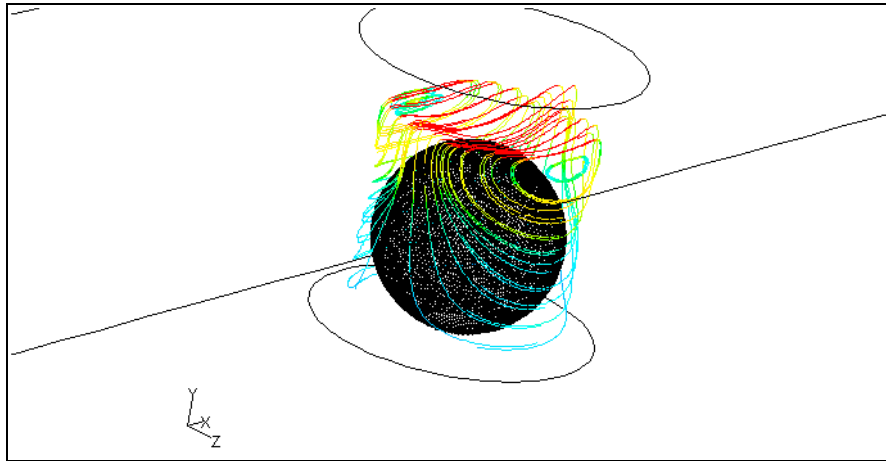
(a) Square



(b) Round groove



(c) Sharp groove



(d) Hole

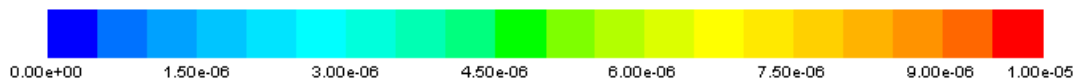


Figure 5.28: Particle trajectories plots highlighting the fluid movement around the embryo. The colour on the trajectories indicates the rate of the fluid movement (measured in m/s).

### 5.3.6 Implication for Solute Transport and Shear Stress Changes

Overall from this study, it can be summarized that a cavity with large opening and a large volume promotes solute transport and induces a faster fluid movement in the cavity. Consider the solute transport and shear stress as a whole. Since the square or round groove-shaped cavities have relatively large cavity openings and volumes, they similarly provide a favourable solute transport capability to the embryo but could induce a detrimentally high shear stress on it. The flat bottom surface of the square-shaped cavity and the rounded bottom surface of the round groove-shaped cavity cause little difference in the solute concentration around, and the shear stress imposed on, the embryo. This implies that both shapes have a similar impact on the solute transport and shear stress formation. On the other hand, a hole-shaped cavity induces the lowest shear stress on the embryo. However, it provides a poor solute transport capability compared with the other cavity shapes, as this cavity shape has a relatively small cavity opening and restricted cavity volume for fluid movement to occur.

The sharp groove-shaped cavity however has a solute transport capability similar to that of the square and round groove-shaped cavities, yet it induces a relatively lower shear stress on the embryo. The reasons that this cavity shape is able to provide such

conditions are that this shape creates a large cavity opening that favours solute transport, while the deep V-shaped bottom greatly reduces the shear stress formed on the embryo. From these findings, it is deduced that the sharp groove cavity shape offers the best cavity shape (of those tested) to breed embryos. *Note that this conclusion is made based on the assumptions that the embryo cultivation is optimal when the bioreactor provides a fast solute transport and incurs a low shear stress on the embryo.*

The solute distribution on the embryo is predominantly governed by the distance of the side walls to the embryo surface rather than the shape of the cavity surface, as demonstrated by the negligible solute concentration difference between a square, round groove or sharp groove-shaped cavity. As the side wall is located closer to the embryo surface, the solute transport at the region between the embryo and the side wall deteriorates; a solute-movement blockage is formed preventing solutes from moving into and out of this region. Therefore, it is established that this distance is a key factor to consider when designing a bioreactor if one needs to alter the solute distribution on the embryo. Conversely, the shear stress distribution depends on the overall fluid movement in the cavity. This is shown by the cases of square and round groove-shaped cavities; these have a similar stress distribution because the flow circulation in these two cavities is similar.

### **5.3.7 Conclusion and Summary**

This study explored the effects that different cavity shapes have in influencing the operation of the bioreactor. Four cavity shapes - square, round groove, sharp groove and hole - were chosen for the study. 3D simulations were conducted to simulate the steady-state operation of the bioreactor, and the key factors of solute concentration and embryo surface shear stress that affect the embryo growth were measured. The differences between these factors were examined and analysed to understand how they affect the bioreactor operation. Implications of these findings were discussed.

Of the four cavity shapes compared, square and round groove-shaped cavities offer a similarly high solute transport rate and form a similarly high shear stress on the embryo. In contrast, a hole-shaped cavity produces about a low solute transport rate yet the stress it caused to the embryo is also low. The sharp groove-shaped cavity offers a high solute transport rate similar to the square and round groove-shaped cavities, yet it imposes a

substantially lower shear stress on the embryo. The solutes and shear stress distribution on the embryo surface were found to be respectively governed by the proximity of the side walls to the embryo and the profile of fluid movement within the cavity.

To conclude, this study achieved its objective in determining the effect that different cavity shapes have in altering embryo growth and subsequently the operation of the bioreactor. It emphasized the importance of choosing the right cavity shape in designing a bioreactor that provides optimal embryo growth and uncovered some key factors that should be focused on when deciding on a proper cavity shape.

## 5.4 Multiple Embryos Parametric Study

Similar to Section 4.6, this parametric study explores another strategy to scale up the embryo cultivation: that is, culturing several embryos in the same cavity. This approach requires only a little modification to the bioreactor by elongating the width of bioreactor to fit more embryos; it does not compromise the usability of the bioreactor. However, it is anticipated that if there more embryos in the cavity, factors that influence the operation of the bioreactor will be altered. For example, the overall rate of solute production or uptake will increase and the fluid condition in the cavity will be different from the case where there is only one embryo in the cavity. Therefore, this study is conducted to explore the condition when there is more than one embryo in the cavity, and to address the question of how do different numbers of embryos contribute to changing the flow condition, solute transport and shear stress.

As with the other parametric studies, this section first outlines the specific problem setup for this study: the details of the placement of the embryo in the cavity and the maximum number of embryos employed in the study. Results of the overall solute transport and shear stress formation on the embryo are analysed and the causes for these changes are discussed. Distribution of the solutes concentration and shear stress on the embryo are also inspected. Implications of these results and integration of them into refining the bioreactor design for production scale-up are explored to conclude the study.

### 5.4.1 Problem Setup

For all the simulations conducted in this study, the solute exchange rate of lactate and oxygen for each of the embryos is the same and the material properties of the culture fluid are kept constant. Culture fluid was simulated to perfuse through the bioreactor in the channel from the inlet to the outlet at the rate of 0.001 m/s ( $Re \approx 0.1$ ). Again, the top surface of the channel was modelled as a zero stress wall.

The aforementioned strategy of increasing the number of embryos within a cavity was accomplished by locating several embryos side-by-side, within the allowable width of the cavity, as illustrated in Figure 5.29. Numerical modelling of this scenario is made possible by the use of three-dimensional CFD models. It must be noted that while there are several choices of arranging the embryos to fit in the cavity, the configuration as

shown in Figure 5.29 is chosen for the following reason: the cross section of the cavity is at most 50% larger than the diameter of the embryo to ensure that the concept of a “niche environment” is enforced. Therefore, it is only viable that more embryos can be added in the cavity by placing them along the width.

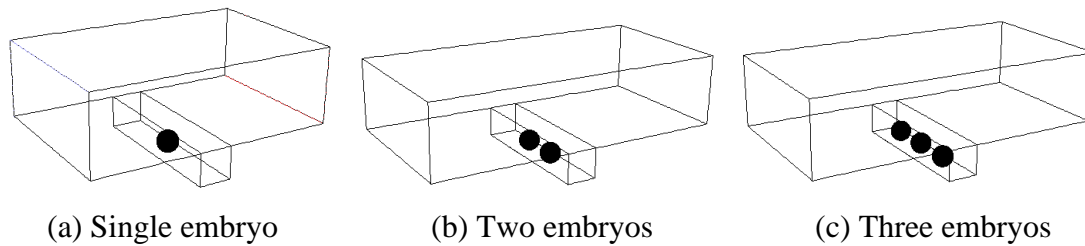
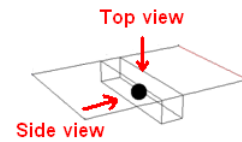
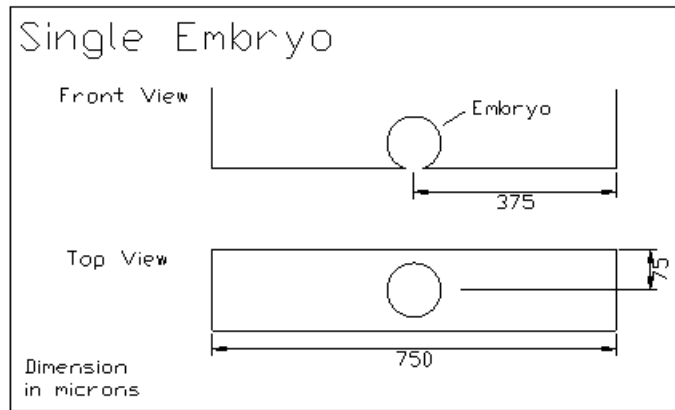
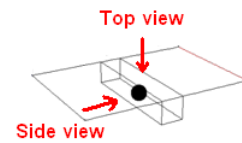
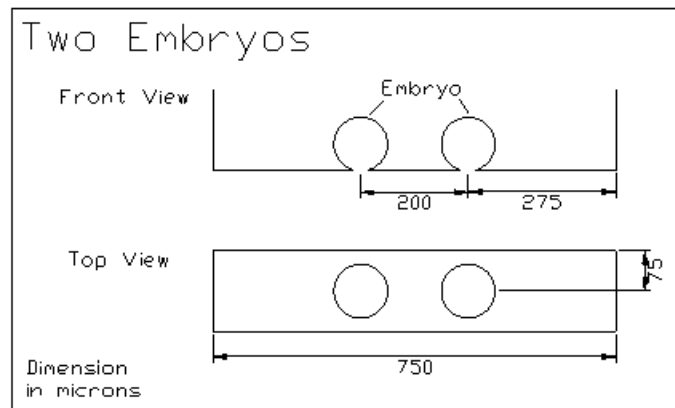


Figure 5.29: Sketches showing the three CFD models employed in the study. They respectively contain one, two and three embryos.

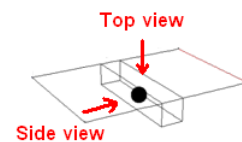
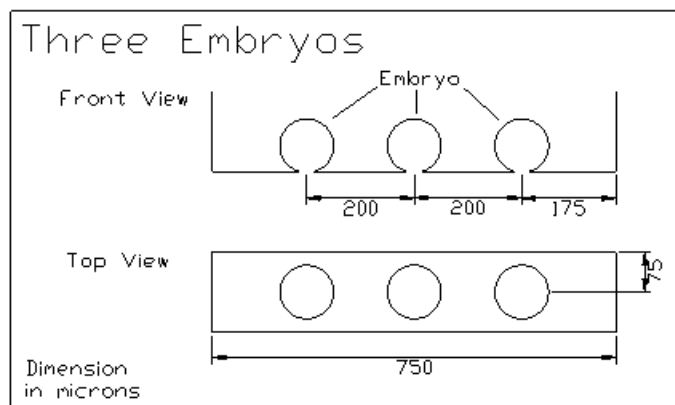
Due to the time and resources constraints, only the cases of single, two and three embryos are considered in this study. The standard size of the embryo is  $100\ \mu\text{m}$  in diameter, where this size was employed throughout this entire thesis, apart from the embryo growth parametric study. The placement of the embryos is given in Figure 5.30. For the case of multiple embryos, each embryo is situated  $200\ \mu\text{m}$  (measured from the centre of one embryo to another) apart. It is assumed that this distance offers enough room between the embryos for solute exchange to occur, for example, oxygen provision or waste product dissipation. Apart from this, it was also assumed that the embryos located in the cavity are stationary in the presence of fluid movement in the bioreactor. These assumptions are to be tested as one of the future work for this project.



(a) Cavity A: Single embryo



(b) Cavity B: Two embryos



(c) Cavity C: Three embryos

Figure 5.30: Schematics of the front and top view of the cavity and the embryos for all three cases of single, two and three embryos. The focus here is on the position of the embryos in the cavity.

For the discussion in the rest of this section, the naming for these three cavities that contain one, two or three embryos is expressed as follows:

- Cavity A: cavity with a single embryo
- Cavity B: cavity with two embryos
- Cavity C: cavity with three embryos

Note that while only half the cavity width needs to be modelled in each case due to symmetry, the entire system was modelled here. In fact, because of the way the meshing was done, it would be more time consuming to set up the symmetric models.

#### **5.4.2 Comparison of Overall Solutes Concentration**

The changes to the overall solute concentration of lactate and oxygen on the embryo surface are first examined. As the number of embryos in the cavity increases, the overall lactate concentration is higher while the overall oxygen concentration is lower. This is shown in Figure 5.31, where in Cavity B, the lactate concentration on both the embryos is 23% higher than the single embryo in the Cavity A. Similarly, all three embryos in Cavity C experience a higher lactate concentration compared with the two embryos in Cavity B, with the outermost two embryos and the middle embryo, respectively, experiencing a lactate concentration of 33% and 45% higher than the single embryo. The opposite is true for oxygen, where the single embryo in Cavity A records the highest oxygen concentration. This is followed by the two embryos in Cavity B, which experience an oxygen concentration 0.19% lower than the embryo in Cavity A. The three embryos in Cavity C all record a lower oxygen concentration than those in Cavities A and B, with the outermost two embryos and the middle embryo, respectively, experiencing an oxygen concentration of 0.28% and 0.37% lower than the single embryo. It is also observed that the change in the oxygen concentration is much smaller than the change in the lactate concentration; the explanation for this is given in Section 5.5.

Embryo configuration	Embryo position	Lactate concentration	Normalized lactate concentration	Oxygen concentration	Normalized oxygen concentration
		M		M	
1 embryo	-	4.6713E-07	1.00	2.1615E-04	1.0000
2 embryos	left embryo	5.7363E-07	1.23	2.1575E-04	0.9981
	right embryo	5.7369E-07	1.23	2.1575E-04	0.9981
3 embryos	left embryo	6.2159E-07	1.33	2.1555E-04	0.9972
	middle embryo	6.7812E-07	1.45	2.1535E-04	0.9963
	right embryo	6.2188E-07	1.33	2.1555E-04	0.9972



Table 5.9: Tabulated values of the overall lactate and oxygen concentration averaged across the embryo surface for all embryos in the three cases studied. The normalized lactate and oxygen concentration are obtained by dividing them by the solute concentration recorded from the single embryo case.

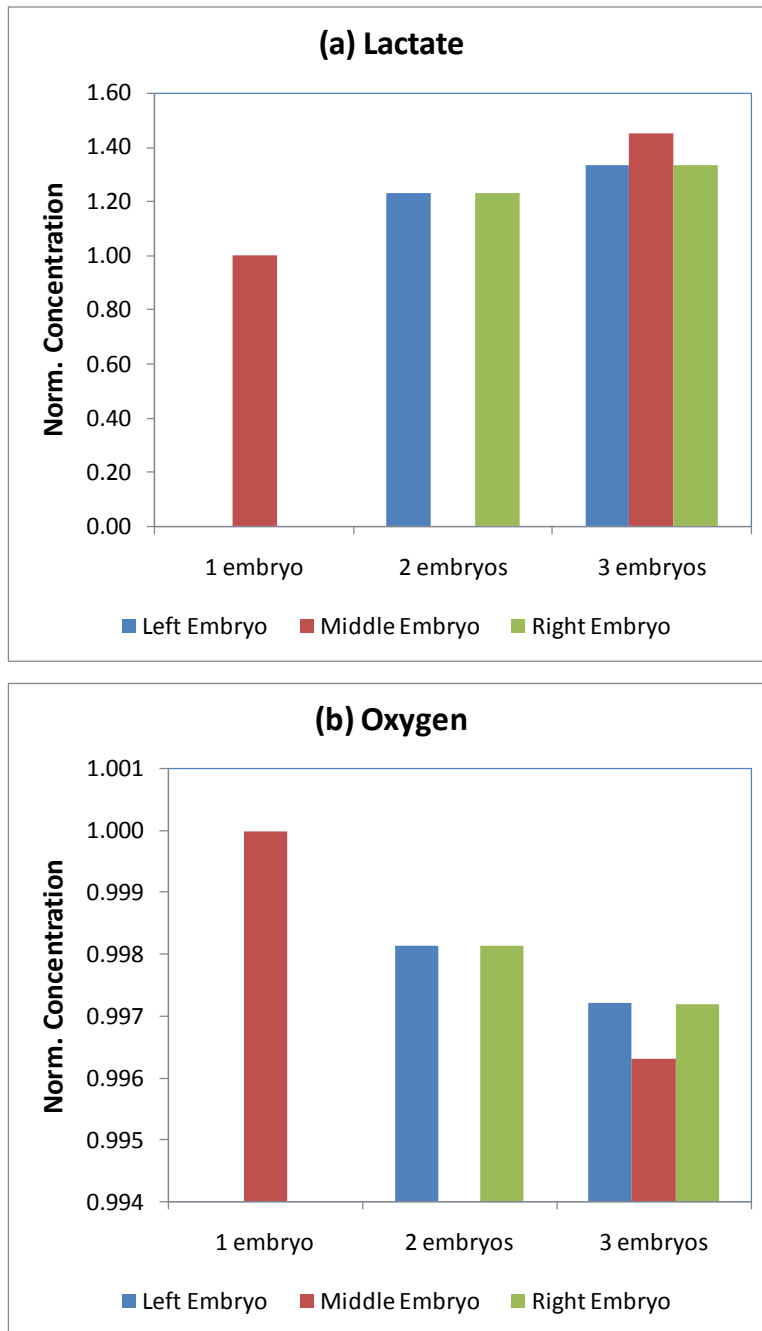


Figure 5.31: Comparisons of the overall (a) lactate and (b) oxygen concentration averaged across the embryo surface for the cases of single, two and three embryos. Refer to the inserts in Table 5.9 for the indication of the specific embryos in each case.

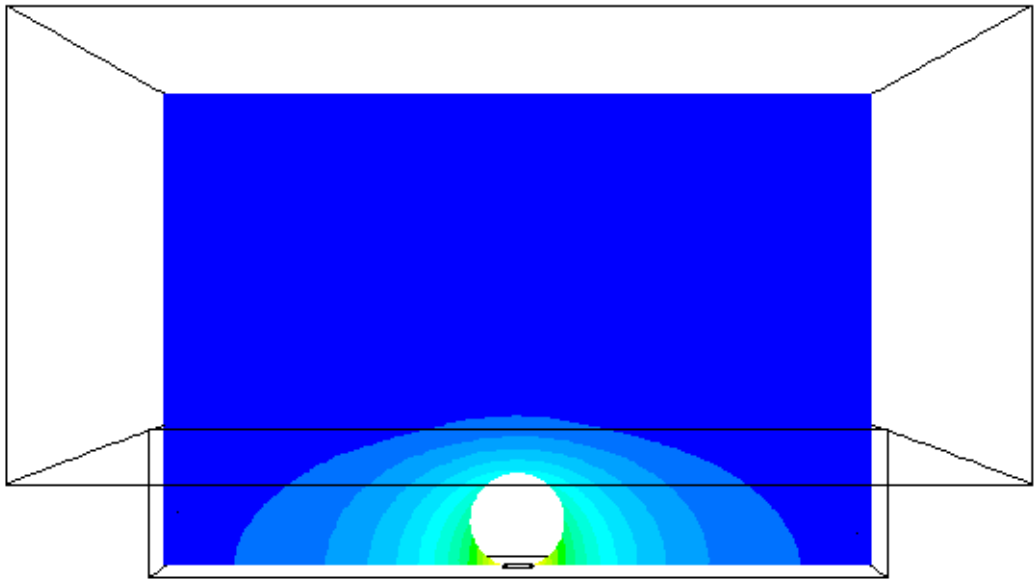
The reason for such a change in solute transport can be uncovered by looking at the distribution of lactate and oxygen around the embryo. For lactate, as the number of embryos in the cavity increases, the amount of lactate filling up the cavity increases, as shown in Figure 5.32 by the higher concentration of lactate around the embryos in Cavity B and C compared with Cavity A. This is expected because each of the embryos is releasing lactate at the same rate and the proximity between the embryos does not allow the lactate produced to have enough room to be diffused away. Aside from that, since each of the embryos is consuming oxygen at the same rate, the cavity with more embryos will exhibit a stronger oxygen deficit. The proximity of the embryos prevented much fresh oxygen from being supplied to the region between the embryos. This is clearly shown in Figure 5.33 by the oxygen concentration contours for Cavity B and Cavity C. A large region of low oxygen concentration is detected around the embryos, compared with the concentration contours in Cavity A, where this region of low oxygen concentration is lower.

In the upper region of the cavity, the faster fluid movement in the channel promotes solute transfer into and out of the cavity through the cavity opening. This is why the fluid region above the embryo demonstrates much lower lactate concentration and much higher oxygen concentration. Alternatively, the fluid region at the bottom of the cavity is relatively stagnant as it is far away from the faster fluid flow in the channel. As a result, solute transport around the bottom of the embryos is relatively dormant, as shown by the lactate accumulation and oxygen deficiency in the contour plots.

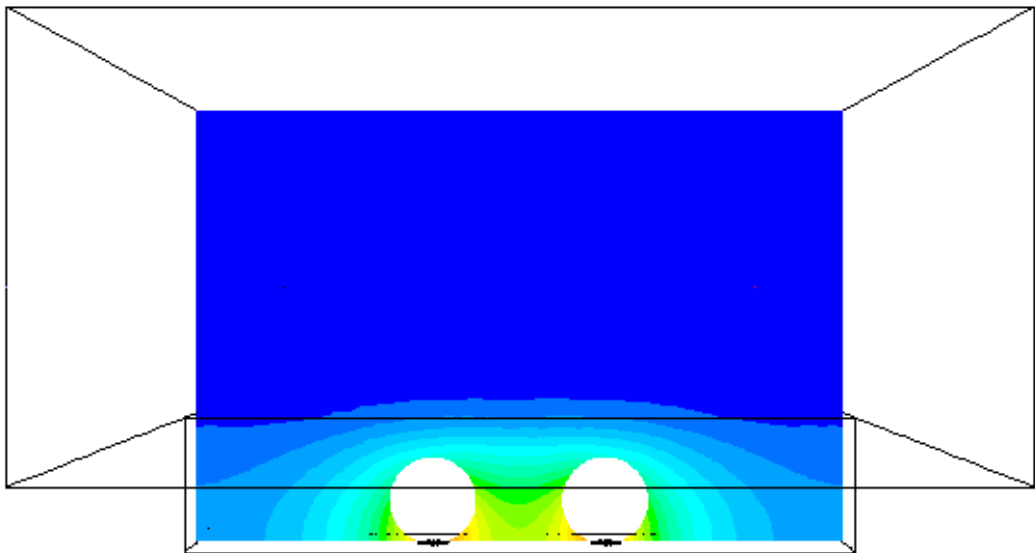
With two embryos in the cavity, one can observe that both embryos in Cavity B record the same amount of lactate and oxygen on the surface (Figure 5.31). The distributions of both lactate (Figure 5.32b) and oxygen (Figure 5.33b) in the cavity also exhibit this symmetry as expected.

With three embryos in the cavity, it is found that the middle embryo experiences a higher lactate concentration and the lower oxygen concentration than the left and right embryos. Again due to symmetry, the same solute concentration is recorded for the left and right embryos adjacent to the cavity side walls. See Figure 5.32c for lactate and Figure 5.33c for oxygen. By similar reasoning, the middle embryo experiences the

highest lactate concentration due to the accumulation of lactate produced by the adjacent left and right embryos. At the same time, it suffers a higher oxygen deficiency as a result of the adjacent left and right embryos also consuming oxygen at the same rate, which in turn depletes oxygen availability around the middle embryo.



(a) Cavity A: single embryo



(b) Cavity B: two embryos

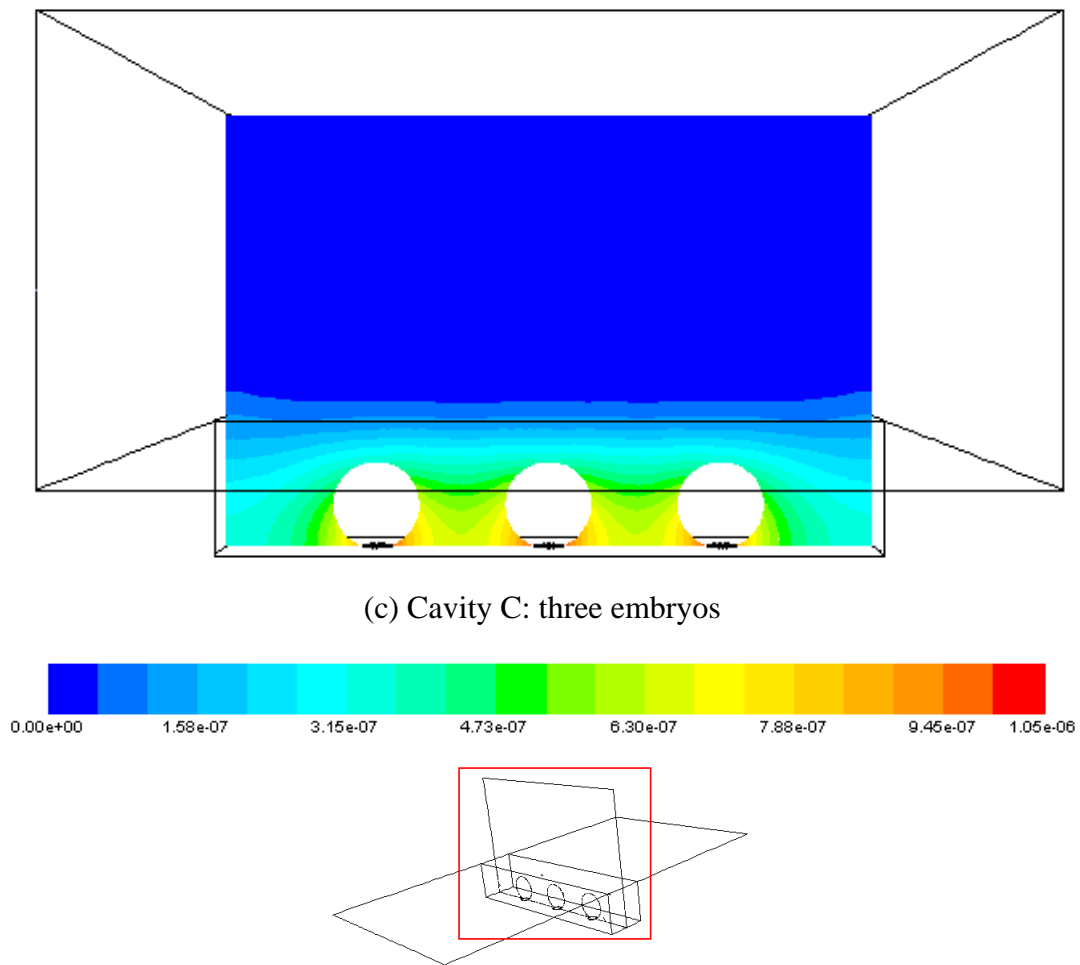
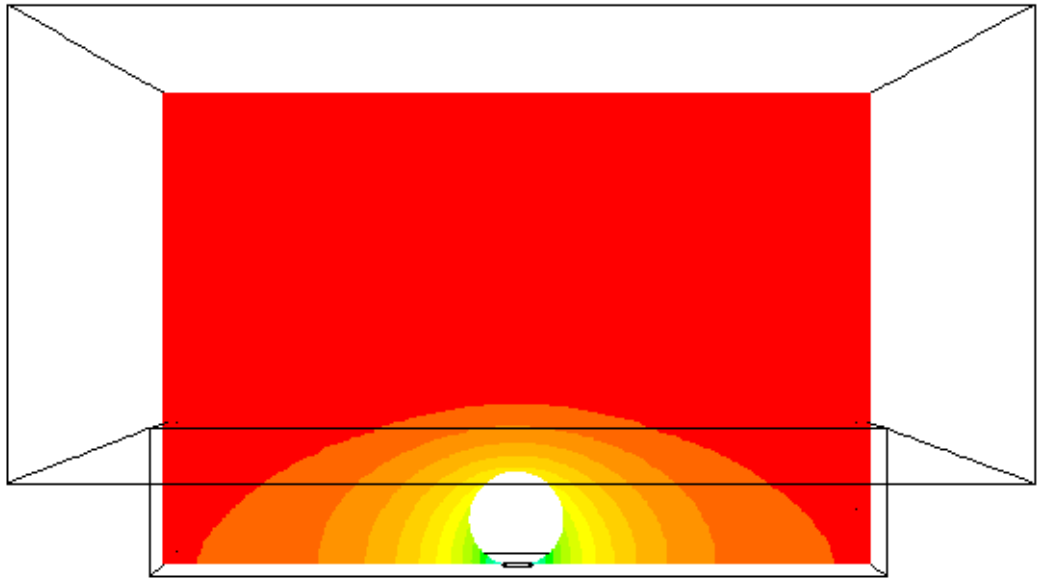
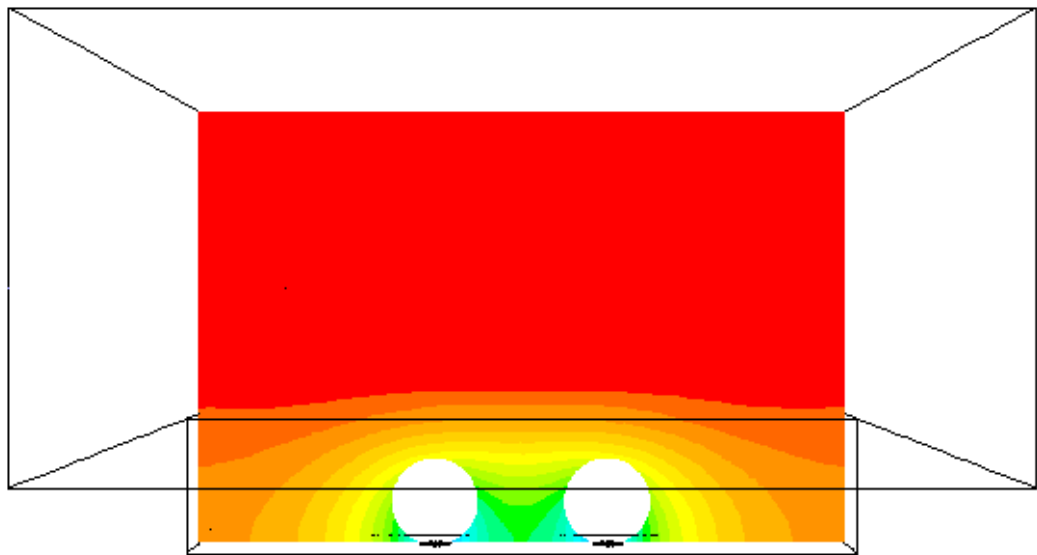


Figure 5.32: Contour plots of lactate distribution (measured in M) around the embryo, where this is represented by the contour slice at the middle plane located perpendicular to the streamwise flow as shown in the insert.



(a) Cavity A: single embryo



(b) Cavity B: two embryos

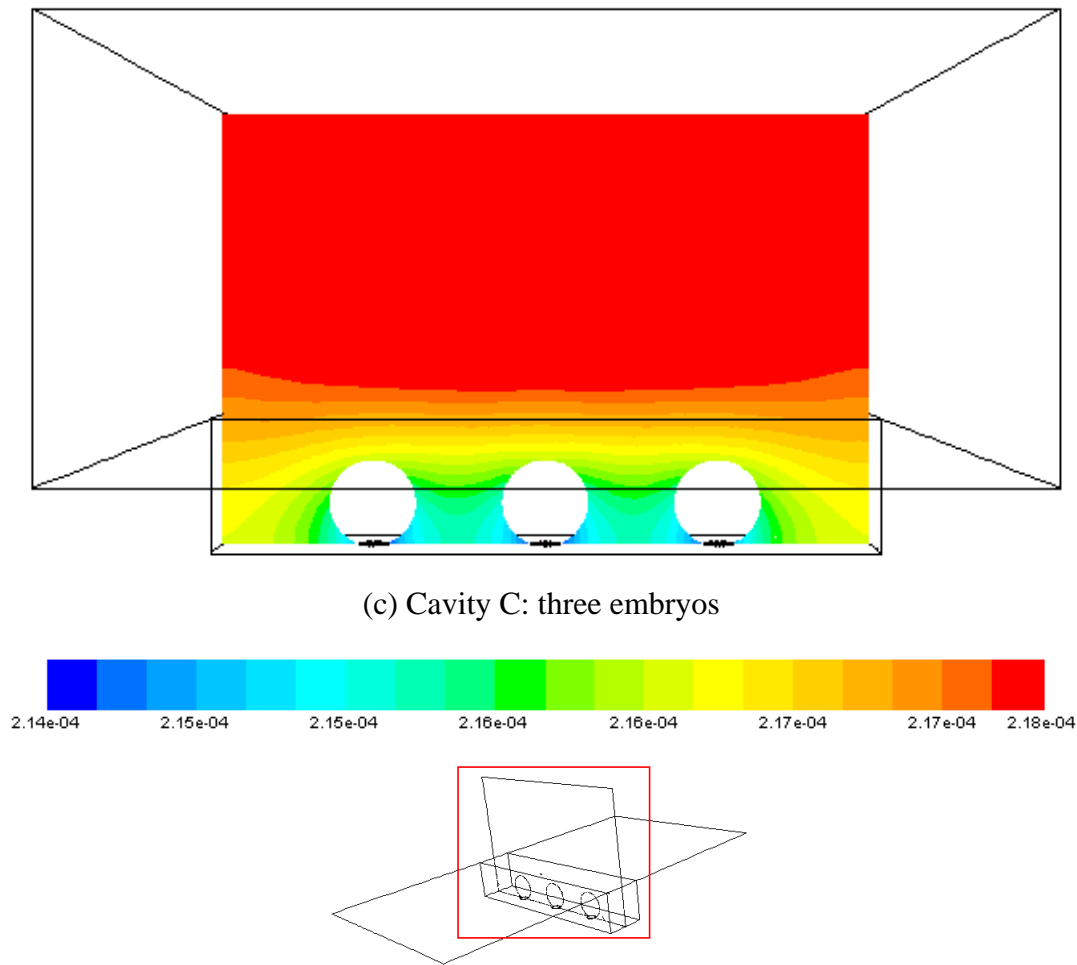


Figure 5.33: Contour plots of oxygen distribution (measured in  $M$ ) around the embryo for the plane shown in the inset.

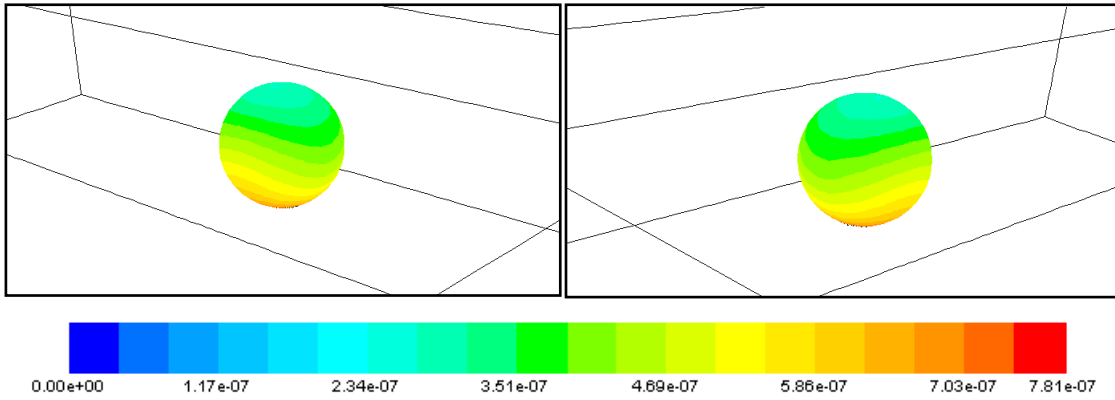
### 5.4.3 Solutes Distributions on the Embryos

As demonstrated by the contour plots of lactate and oxygen concentration at the embryo, in Figure 5.34 and 5.35 respectively, the solute concentrations on all the embryos in general vary smoothly from the bottom to the top of the embryo. The overall pattern is similar to the previous single embryo studies, with a large gradient from top to bottom for the reasons given previously.

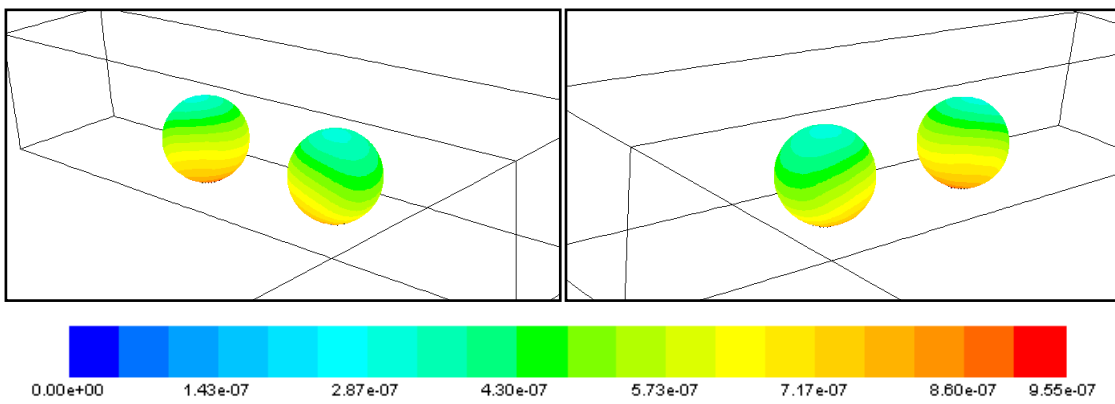
The difference in the solute distributions between each embryo is the profile of the contour levels, in particular the curvy nature of the contour levels. From the previous study on the cavity shape (Section 5.3), it was established that the shape of these profiles is primarily affected by the distance of the embryo surface to the adjacent side walls: if the embryo surface is closer to the side wall, the contour level changes faster

from low to high concentration, or vice versa. The reason for this is that the smaller distance leads to a poor solute transport to occur within the confined region. With this, one can gain a better understanding on the detailed differences in the contour level profiles.

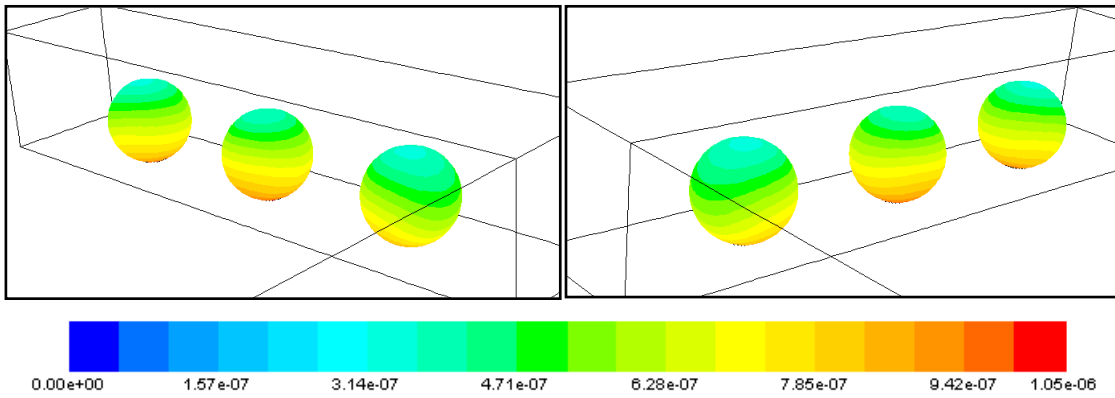
Starting with the single embryo in Cavity A, it is observed that the contour levels facing the side walls, which are much further from the embryo surface, change much more slowly from highest to lowest (or vice versa) than the ones facing the front and rear cavity walls, which are much closer to the embryo (Figures 5.34a and 5.35a). With two embryos in Cavity B, similar findings can be observed; in addition, the contour levels on the sides of the embryos facing each other change rapidly (Figures 5.34b and 5.35b). The reason for this is that that solute transport in between the embryos is more restrictive due to the proximity of these embryos; the lactate produced by them tends to accumulate faster and oxygen depletion also occurs faster. The same observation is found for the three embryos in Cavity C, especially for the middle embryo, which experiences the fastest change in solute concentration from the bottom to the top of the embryo (Figures 5.34c and 5.35c). This is because the middle embryo is sandwiched between the left and right embryos, and the solute transport between these embryos is very much restricted.



(a) Cavity A: single embryo

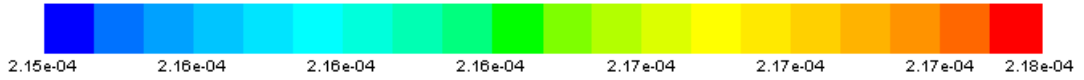
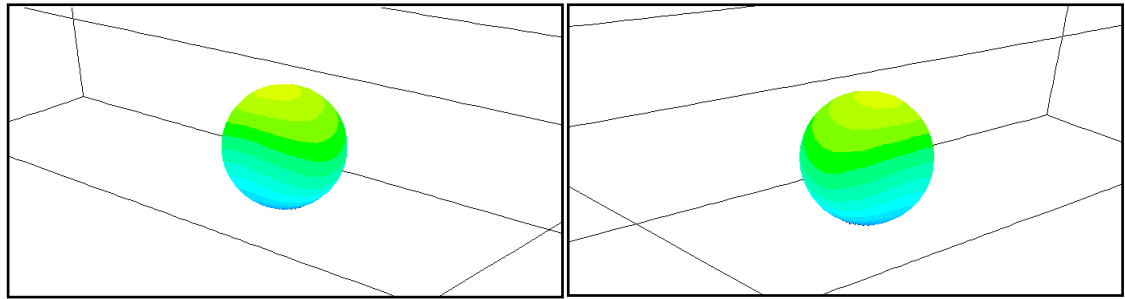


(b) Cavity B: two embryos

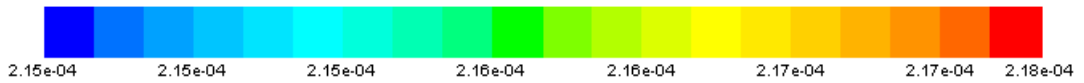
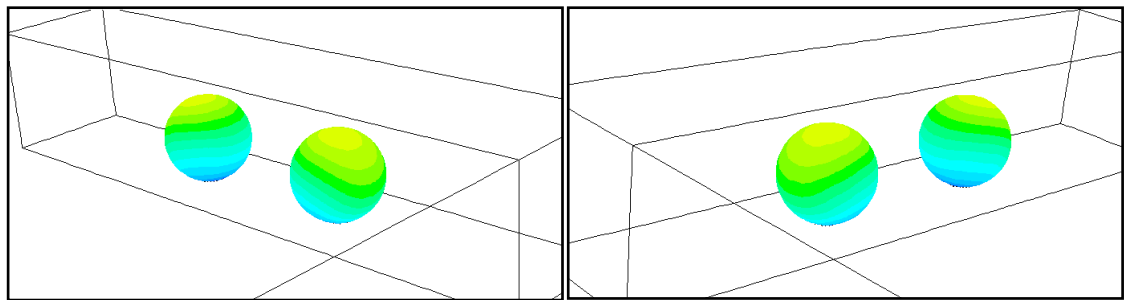


(c) Cavity C: three embryos

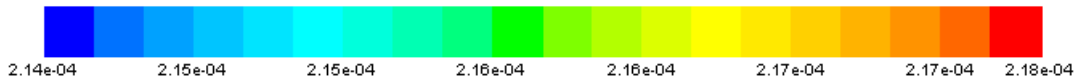
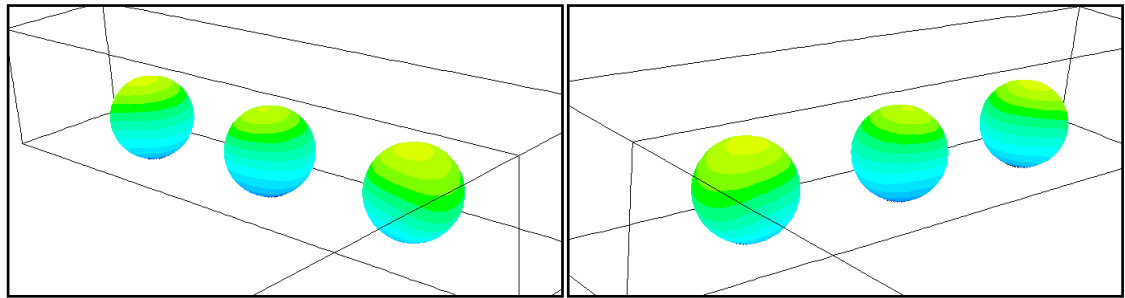
Figure 5.34: The left and right diagonal views of the lactate concentration (measured in M) contour plots on the embryos in Cavity A, B and C, showing the lactate distributions on the embryo surface.



(a) Cavity A: single embryo



(b) Cavity B: two embryos



(c) Cavity C: three embryos

Figure 5.35: The left and right diagonal views of the oxygen concentration (measured in M) contour plots on the embryos in Cavity A, B and C, showing the oxygen distributions on the embryo surface.

#### 5.4.4 Comparison of Overall Shear Stress

In this section, the overall shear stress experienced by the embryos is examined. As can be seen from Figure 5.36, the single embryo in Cavity A experiences the highest shear stress. The two embryos in Cavity B experience a shear stress that is 4.8% lower than the single embryo. As for the three embryos in Cavity C, it is found that the outmost two embryos adjacent to the side walls experience a stress that is about 20% lower than that experienced by the single embryo in Cavity A. However, the middle embryo on the contrary records a high shear stress similar to the single embryo in Cavity A. On the whole, the discrepancies in the overall shear stress between the embryos are not large, with the maximum recorded discrepancy of 20% between the highest and lowest stress.

Embryo configuration	Embryo position	Shear stress	Normalized shear stress
		Pa	
1 embryo	-	1.12E-03	1.00
2 embryos	left embryo	1.06E-03	0.95
	right embryo	1.07E-03	0.95
3 embryos	left embryo	8.93E-04	0.80
	middle embryo	1.12E-03	1.00
	right embryo	8.93E-04	0.80

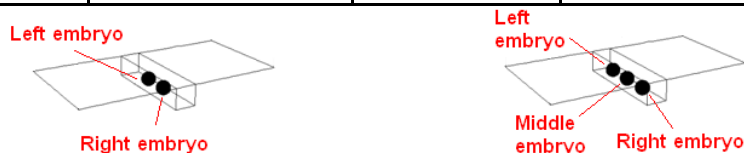


Table 5.10: Tabulated values of the overall shear stress averaged across the embryo surface for all the embryos in the three cases of single and multiple embryos. The normalized shear stress is obtained by dividing the stress level by the shear stress recorded from the single embryo case.

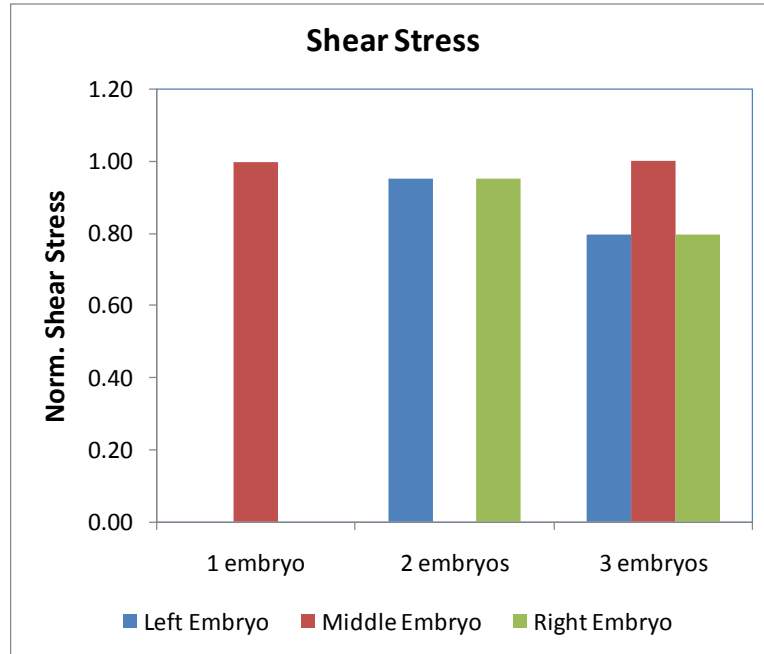


Figure 5.36: Comparisons of the overall shear stress on the embryo surface for the cases of single, two and three embryos. Refer to the inserts in Table 5.10 for the indication of the specific embryos in each case.

The reason for these differences is explored by examining particle trajectory plots around the embryo and the velocity contours in the middle of the cavity (Figure 5.37).

First, the overall fluid movement in the cavity is examined. As can be seen in the trajectory plots, the fluid movement in the cavity consists of major spanwise flow circulations that occur across the entire cavity. The rate of the fluid movement is the fastest near the cavity opening, where the fluid movement is accelerated by the fast channel flow. As the fluid is being circulated to the bottom of the cavity, the fluid movement slows down considerably. This is expected for a typical cavity flow circulation. The placement of embryos in the cavity breaks down the continuity of this flow circulation along the width. As can be seen in the trajectory plots, the slanted flow circulation that wraps around the embryo does not change the shape of the flow circulations, regardless of the number of embryos present in the cavity.

The major change that is detected with the presence of these embryos is that they speed up the fluid movement near them. This can be seen in the velocity contour plots (Figure

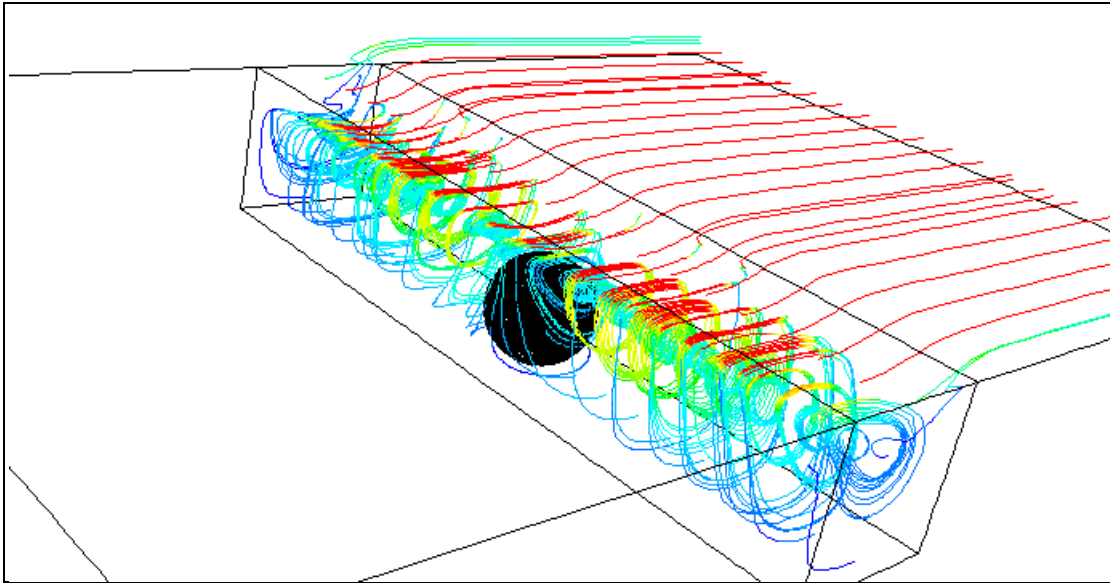
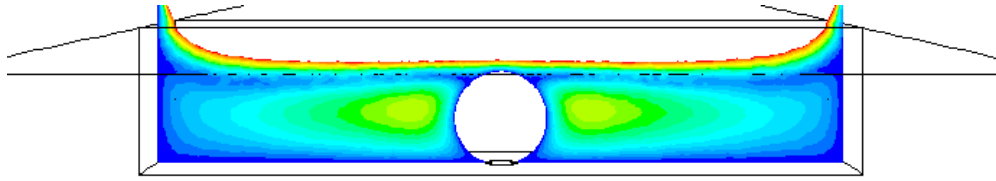
5.37a, 5.37b and 5.37c, top), where the green and yellow velocity contours indicate faster fluid movement. From here, two observations can be made. First, it is found that the magnitude of the flow circulation is proportional to the distance between the embryo surface and the cavity side wall; if this distance is larger, the strength of the flow circulation increases. This finding coincides with the similar finding in the cavity shape study (Section 5.3). Second, the fluid movement in between the embryos is notably faster than the fluid movement at other locations in the cavity. It is suggested that this is caused by the spherical surface of the embryo, which directs the flow circulation that wraps around the embryos, allowing a relatively faster rate of flow.

The two findings above can be used to explain the condition of the shear stress formed on the embryos in the three cases of a single, two and three embryos. Starting with Cavity A (Figure 5.37a), as there is only one embryo located at the middle of the cavity, the distance between the embryo surface to the cavity side wall is the largest amongst the three cases. This implies that the fluid movement besides the embryo is the fastest, which explains why it records the highest shear stress.

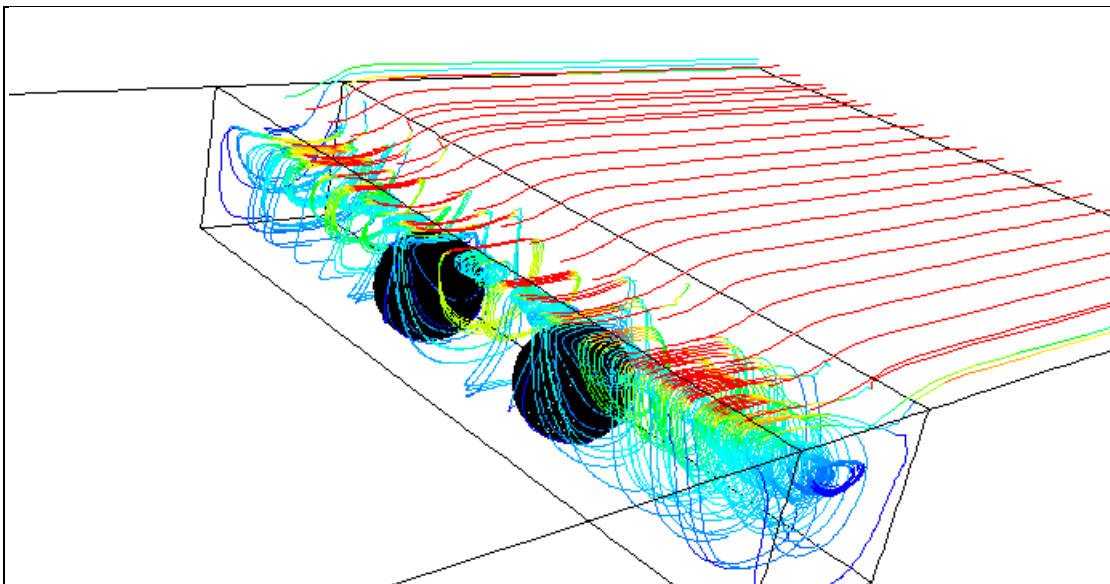
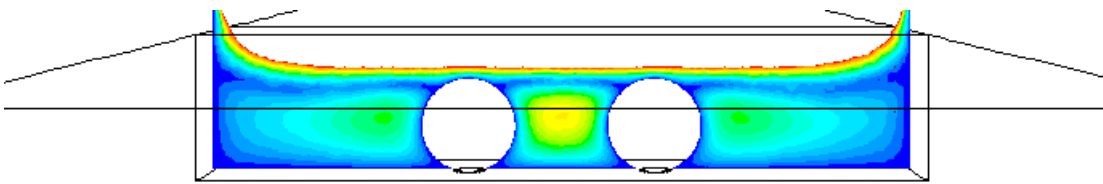
In Cavity B (Figure 5.37b), the location of the two embryos results in the distance between the embryo surface to the side wall being smaller, hence the rate of flow circulation in between the side wall and the embryo is slower and shear stress induced on this side of the embryo is smaller. However, the flow circulation in between the two embryos is much faster, as shown by the yellow velocity contour. Hence, the rate of fluid movement on this side of the embryo is larger. When considering the entire embryo surface, the overall shear stress is therefore only marginally smaller than the single embryo in Cavity A. Also, as noted above, these two embryos experience the same shear stress because they were located symmetrically in the cavity.

In Cavity C, the outmost left and right embryos are located closest to the side walls, hence the fluid movement there is the slowest and the shear stress induced on the embryo surface facing the side wall is the smallest. On the other side, where the left and right embryos face the middle embryo, the spherical surface of these embryos streamline the fluid movement in between them to be relatively faster, and the shear stress induced on these sides on the left and right embryo is larger. All in all, the overall

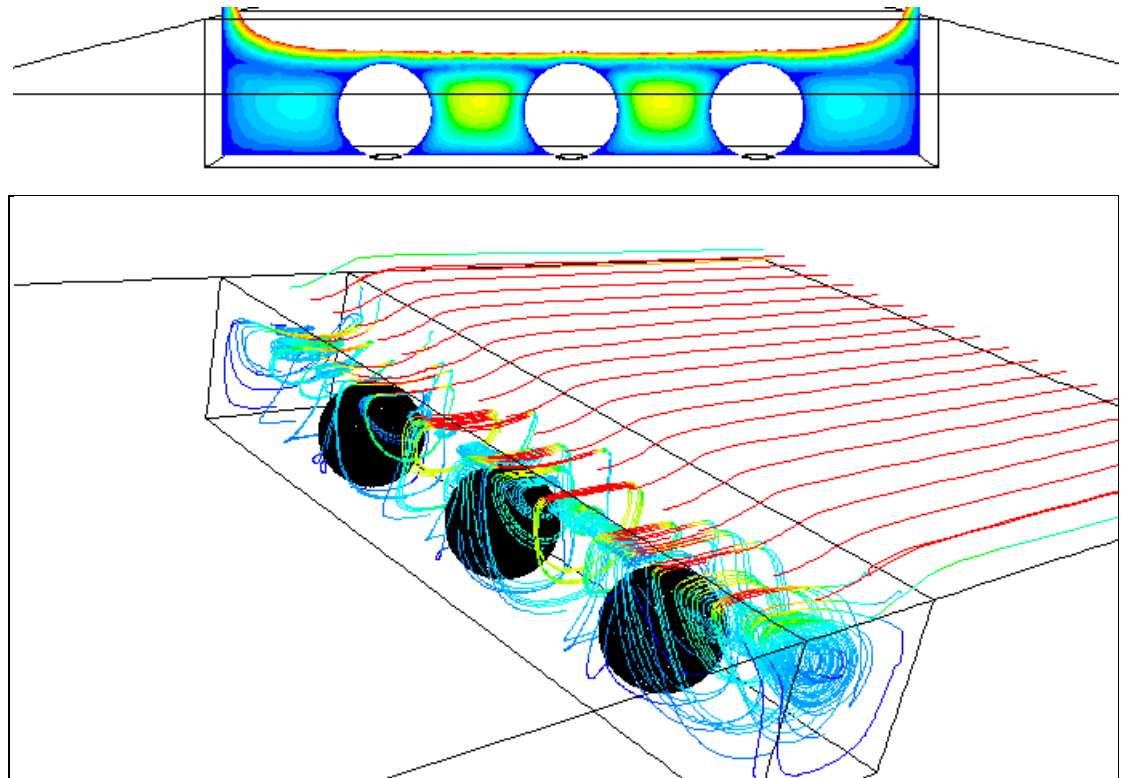
shear stress experienced by them is again much smaller than the other two cases. As for the middle embryo, since both sides of it are facing the spherical surfaces of the left and right embryos, fluid movement around the middle embryo is faster and therefore, it is not surprising that it records a similarly high shear stress to the single embryo in Cavity A.



(a) Cavity A: single embryo



(b) Cavity B: two embryos



(c) Cavity C: three embryos

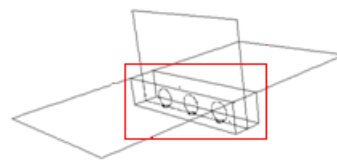
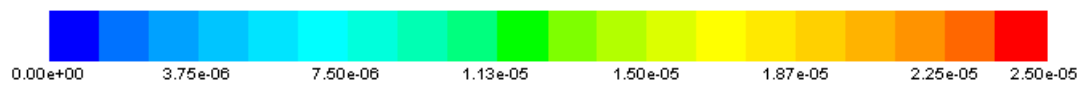


Figure 5.37: Contour plots (top) show the velocity magnitude of the fluid movement around the embryos for all three cases, while particle trajectories plots (bottom) indicate the fluid movement around the embryos; both aim to give a clear representation of the fluid flow in the cavity. The contour slice is positioned at the middle of the cavity as shown in the inset. The colour contour indicates magnitude of fluid velocity in m/s.

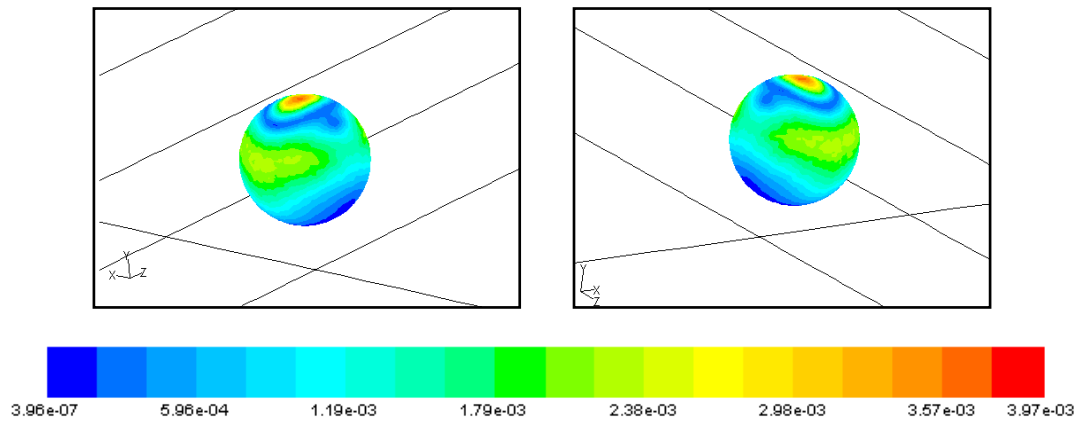
### 5.4.5 Shear Stress Distribution on Embryos

The shear stress distributions on the embryo are illustrated in Figure 5.38 on both the left and right diagonal views to give a better perspective of the stress distribution surrounding the entire embryo. In general, the stress distribution can be categorized into three regions on the embryo: the top region, the upper region and the lower region. As mentioned previously, such distribution is closely related to the condition of the fluid movement in the cavity shown in Figure 5.37.

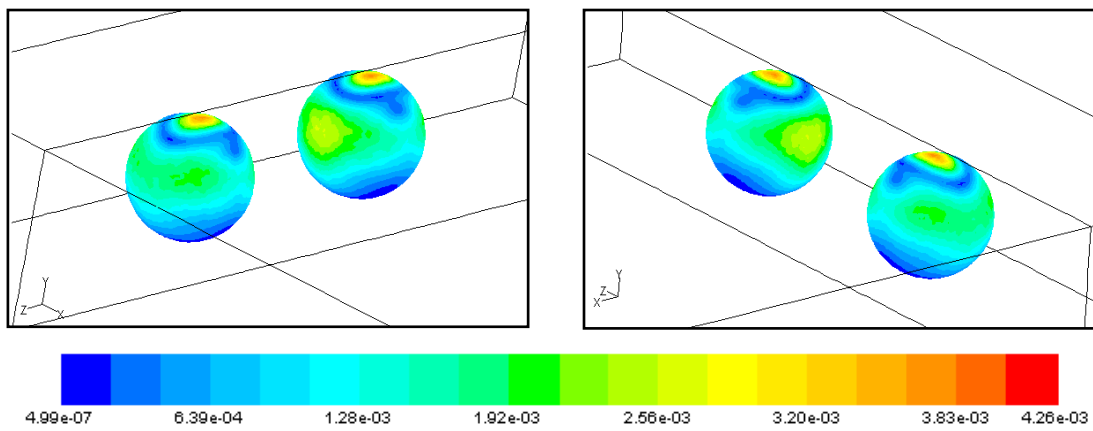
The top sections of all embryos experience the highest peak stress, indicated by the red stress contour area shown in Figure 5.38. Once again, this is easily understandable since the fluid flow in the channel, which is much faster than the cavity flow circulation, enters the cavity through the opening (shown by the red trajectories in Figure 5.37) and is in contact with the top surface of the embryo. This fast fluid flow then induces a relatively very high shear stress on the embryo. This observation is also found for all the previous studies, suggesting that the high peak stress is always located at the top of the embryo. On the contrary, over the lower section of the embryo, the shear stress is lower as shown by the light and dark blue stress contour zones in Figure 5.38. This corresponds well with the very slow fluid movement at the bottom of the cavity, which is clearly highlighted by the blue and dark blue particle trajectories in at the bottom of the cavity shown in Figure 5.37.

Over the upper section of each embryo, two smaller peak stresses (when compared with the highest peak stress at the top) are detected residing on both sides on the embryo surface facing the cavity side walls. These are highlighted by the green and yellow contour zones on the embryo surfaces shown in Figure 5.38. The location of these peak stresses and the magnitude of the stress depend on the fluid movement around the embryo. Specifically, as can be seen in the particle trajectory plots in Figure 5.37, the core of the flow circulation is found to align with the upper region of the embryo. As the fluid circulation near the core is fast, as shown by the light green and yellow particle paths, it causes a high peak stress over the upper section of the embryos. In addition, the difference in magnitude of the peak stresses corresponds well to velocity contours shown in Figure 5.37. For example, in Cavity C, the peak stress on the outermost embryos on the side facing the cavity side wall is much lower than the peak stress on

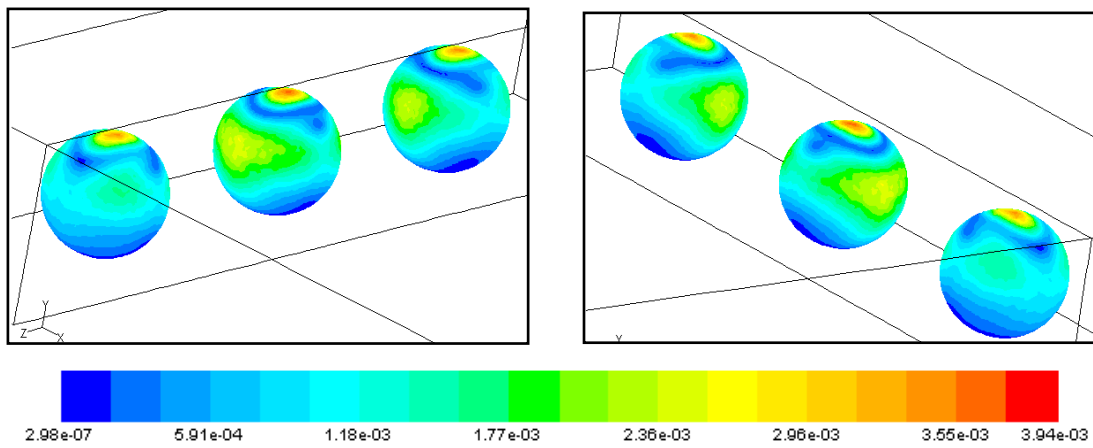
the other side of the embryo; this corresponds well with the slower flow circulation in the region between the embryo and the side wall. In the region between the embryos, the flow circulation is faster and, as a result, the peak stress induced at this side of the embryo is higher.



(a) Cavity A: single embryo



(b) Cavity B: two embryos



(c) Cavity C: three embryos

Figure 5.38: Contour plots indicating the surface shear stress (measured in Pa) on the embryos, with the left and right figures each showing the left diagonal and right diagonal views, respectively.

#### **5.4.6 Implications for Solute Transport and Shear Stress Changes**

A few implications can be made from this study with multiple embryos in a cavity. In regard to the solute transport, it is discovered that increasing the number of embryos cultured in the cavity moderately deteriorates the solute transport around them. This is expected since more embryos in the same cavity will raise the overall nutrient consumption and waste production of the bioreactor, which subsequently decreases the efficiency of the bioreactor. The distance between one embryo to the other embryos or to the side walls is related to the deterioration of the solute transport: if this distance is shortened, the solute transport in the corresponding fluid volume near the embryo is weakened. As a by-product of this finding, the distribution of solutes on the embryo surface is also greatly influenced by this distance. The solute concentration on the embryo surface facing the cavity walls or another embryo is higher if this distance is smaller. All these findings imply that while it is unavoidable that solute transport within the cavity will deteriorate if more embryos are being cultured together, there is a limited control on the solute concentration in the cavity by the means of adjusting such a distance.

With the addition of more embryos into the cavity, the overall shear stress experienced by each of the embryo does not differ by much, with the maximum recorded differences of 20%. The overall shear stress experienced by the embryos and the stress distribution on them are primarily influenced by the fluid movement around them. The fluid movement in the cavity predominantly consists of a series of large flow circulations filling up the entire cavity. The flow circulation in the region between the embryo and the cavity side walls is generally slower than the flow circulation that occurs in between two embryos. This is well reflected by the dissimilarity in the overall shear stress for each embryo and different peak stresses occurring in the upper region of the cavity for the different embryos. It can be deduced that if there is more than one embryo cultured in the cavity, the embryos located in the middle of the cavity will experience a higher stress while the embryos located near the edge of the cavity will have a lower stress.

While it is certain that increasing the number of embryos is a seemingly easy way to scale up the embryo production, one must take into consideration the shortcomings of

this strategy: that is, an efficiency drop in the solute transport and a different shear stress across the embryos.

#### **5.4.7 Conclusion and Summary**

This section detailed the investigation of another strategy to scale up the embryo production: instead of setting up multiple cavities in the bioreactor (as explored in Section 4.6), more embryos are being cultivated in a single cavity. Three-dimensional CFD simulations were employed in this investigation. Due to the constraints of time and computational resources, the maximum of embryos cultured in a cavity was limited to three. Three cases were set up for the investigation where each case consisted of one, two and three embryos, respectively, in the cavity. Steady-state simulations were carried out to model the fluid flow and solute transport within the bioreactor for all three cases. The solute concentration around, and shear stress on, the embryos were examined to characterize and quantify the change of these two factors that affect embryo growth, in order to understand the effect of culturing more embryos in the a single cavity.

The study found that the addition of more embryos into the cavity deteriorates the solute transport efficiency of the bioreactor by a small margin. As more embryos are added to the cavity, the increased proximity of one embryo to another raises the consumption or production of solutes within the cavity. This in turn causes a blockage effect on the solute transport, such that the solute is impeded from being transported into and out of the cavity. Also, depending on the distance between one embryo to another or to the side walls, the solute distribution on the embryo surface changes such that the gradient of the solute concentration differs. As for the shear stress induced on the embryo, while the difference between them is not significant, the addition of more embryos causes the shear stress experienced by each of them to be unequal. This is because the appearance of these embryos breaks down the spanwise major flow circulation across the cavity, causing the fluid movement at different locations to have different rates of flow circulation. With multiple embryos in the cavity, the embryos residing near the edge of the cavity experience smaller stress than the embryos located around the middle of the cavity. The distribution of shear stress on the embryo depends on the rate of fluid around the embryos: faster fluid movement around the embryo induces a local peak stress at the corresponding spot on the embryo.

To conclude, this study provided us a brief insight in the scenario of adding more embryos in a single cavity. It is certainly viable to employ such a strategy to increase embryo production as long as the numbers of embryos added do not overcrowd the cavity so that the operational efficiency of the bioreactor is not compromised. It is recommended that more parametric studies should be undertaken to explore this scale-up strategy in more detail, such as changing the distance between embryos, since this approach demonstrates great potential to increase embryo production.

## 5.5 Explanation on the Small Variation of Oxygen Concentration

From all the parametric studies conducted, it is found that the variation of oxygen concentration averaged across the embryo surface is considerably less than the variation of lactate concentration. This is shown in Table 5.11, where the maximum changes in averaged surface concentration for lactate and oxygen calculated from all the parametric studies are listed. The maximum change for a particular parametric study is evaluated by subtracting the largest solute concentration with the smallest one and the difference is presented in the form of percentage difference. In general, the variation in lactate concentration is about 9.5 to 84 times higher than the variation in oxygen concentration.

Parametric Studies	Maximum Change in Lactate Concentration	Maximum Change in Oxygen Concentration
	%	%
Cavity Aspect Ratio	92.40	9.72
Cavity Width	37.96	0.55
Cavity Shape	53.57	0.96
Culture Medium Inflow Rate	90.21	3.25
Culture Medium Height	23.16	0.68
Embryo Growth	99.95	5.03
Multiple Cavities	9.79	0.35
Multiple Cavities (Cavity Spacing)	10.86	0.38
Multiple Embryos	31.11	0.37

Table 5.11: Maximum changes in the lactate and oxygen concentration averaged across the embryo surface evaluated from all the parametric studies.

The reason for this is that the preset oxygen concentration at the inlet tends to dominate the oxygen depletion at the embryo, while for lactate, there is no background level. By disregarding the inlet oxygen concentration, the net amount of oxygen consumed by the embryo can be calculated. It is found that this amount of oxygen consumed is similar to the amount of lactate produced from the embryo. This is evidenced in Table 5.12, which shows that the maximum variation of the oxygen consumed is relatively similar to the maximum variation of the lactate produced.

Parametric Studies	Maximum Variation in Lactate Production	Maximum Variation in Oxygen Consumption
	%	%
Cavity Aspect Ratio	92.40	91.34
Cavity Width	37.96	30.18
Cavity Shape	53.57	40.76
Culture Medium Inflow Rate	90.21	77.66
Culture Medium Height	23.16	23.32
Embryo Growth	99.95	66.60
Multiple Cavities	9.79	11.53
Multiple Cavities (Cavity Spacing)	10.86	12.39
Multiple Embryos	31.11	22.52

Table 5.12: Maximum variation in the net amount of lactate and oxygen exchanged across the embryo surface evaluated from all the parametric studies.

Generally, the finding here implies that the difference in magnitude for the trend change of lactate and oxygen concentration is caused by the approach undertaken to present the result on the solute concentration. It does not alter the fact that the amounts of lactate and oxygen exchanged into and out of the embryo are comparatively similar. This is expected since the lactate production rate and oxygen uptake rate specified in the simulations are also comparatively similar as shown in Table 3.1.

## 6.0 Conclusions

---

This chapter reviews the parametric studies undertaken and attempts to relate the results to the objectives of this thesis. In particular, the significance of these studies to influence the design of micro-bioreactors is highlighted and possible utilisations of the results from the parametric studies are discussed. In order to simplify the complex analysis of fluid flow with the solute transport, several assumptions were made. The impact of these assumptions is examined, in order to identify the limitations of the existing CFD modelling.

## 6.1 Relevance of the Parametric Studies

The parametric studies undertaken cover four design aspects of the micro-bioreactor: cavity dimensions, perfusion of culture medium, embryo growth and multiplication of embryo production. This has been done to compare the parameters that relate to the same design aspect and also gain a better understanding of their capacity to influence the operation of the micro-bioreactor. Each study uses lactate production, oxygen uptake and shear stress formation as indicators of bioreactor performance. Essentially, they provide a measure for assessing many scenarios encountered in the operation of a micro-bioreactor used to cultivate embryos.

### 6.1.1 Cavity Dimensions

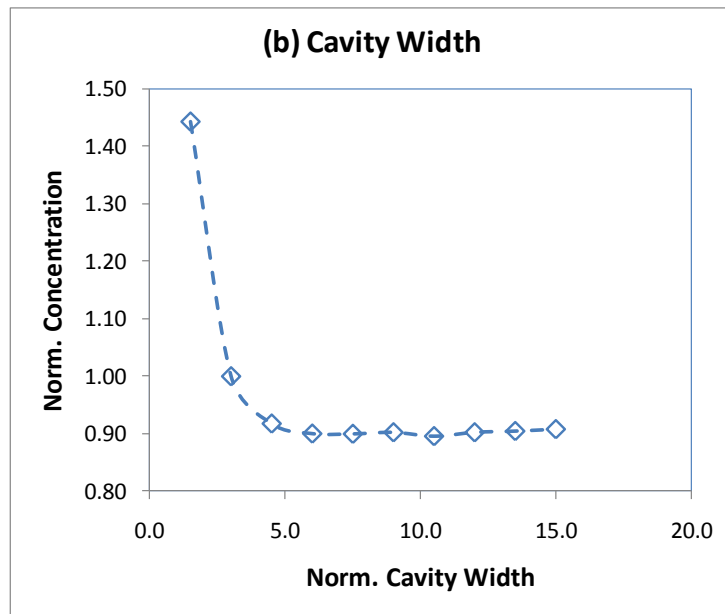
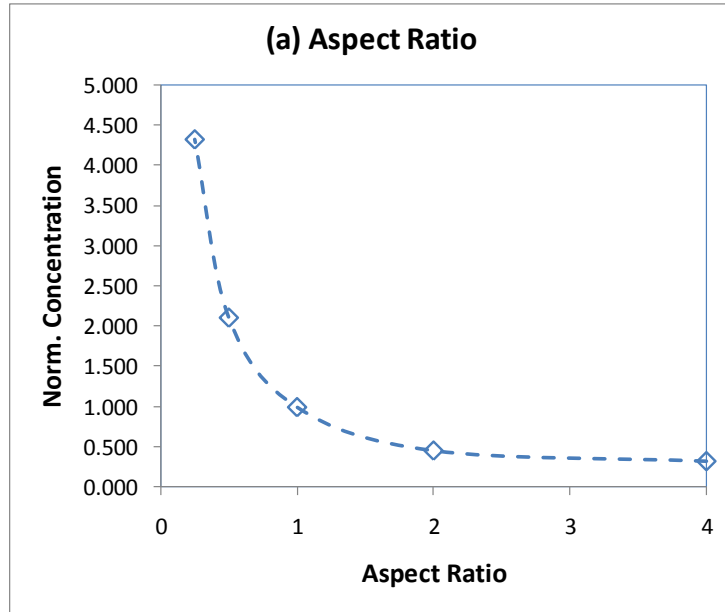
The cavity aspect ratio (AR), width and shape parametric studies examine the effects of modifications to the cavity dimensions. In particular, the three parameters which characterise the shape and size of the cavity are compared, in order to quantify their effect in moderating the solute environment of the embryo and the induced shear stress on the embryo surface.

In regard to solute production, the effect of changing the cavity AR has a greater impact on influencing the lactate concentration around the embryo, than does altering the cavity width and shape. This is highlighted by the 450% increase in lactate concentration when the AR is decreased to 0.25, as shown in Figure 6.1a. This result can be contrasted to the 45% increase in lactate concentration when the normalized cavity width is decreased to a length 50% larger than the embryo, as shown in Figure 6.1b. A maximum of 215% increase in lactate concentration is recorded by changing the cavity shape to a hole shape (Figure 6.1c). Results on oxygen concentration also show similar trends when the cavity AR, width and shape are altered. This is demonstrated by a 10% decrease in oxygen when the AR is decreased to 0.25, as shown in Figure 6.2a. A 4.3% decrease was recorded when the cavity width was half of the diameter of the embryo, as shown in Figure 6.2b. A maximum of 0.95% decrease was recorded when the cavity shape is a hole, as shown in Figure 6.2c. As the cavity AR and width are further increased, changes to the solute concentrations diminish and the concentration level asymptote to a constant. The direct implication of these results is that modifying the cavity AR is an effective measure to control the solute transport around the embryo. This method

should be considered when trying to augment the solute concentration around the embryo.

The changes to the solute concentrations caused by changes in the cavity AR, width and shape suggest that varying the depth of the cavity has the greatest impact on altering the solute concentration around the embryo. The largest change in solute concentration occurs when the depth of the cavity is altered such that the AR is decreased to less than one ( $AR < 1$  implies the cavity depth is larger than length). It is predicted that as the cavity depth increases, the embryo is located at a greater distance from the cavity opening, which promotes the accumulation of solutes and prevents more solutes reaching the embryo from the channel. Evidence for this is provided by the cavity shape parametric study, where for the case of sharp groove-shaped cavity, little change in solute concentrations is detected, even though the depth of the cavity is larger than for all other cases. This is a result of the embryo being positioned at the same height as in other cavities. From this finding, it is identified that the depth of the cavity, or the distance of the embryo from the cavity opening, should be a high priority design choice, as this parameter has a large influence on solute transport.

In addition, there exist critical values in varying cavity AR and width. If these parameters are increased beyond these critical values, negligible change to the solute concentrations around the embryo will occur. This is clearly illustrated by the settling trend of lactate and oxygen concentrations as cavity AR is increased beyond an aspect ratio of 2 (Figure 6.1a and 6.2a) and the cavity width is increased beyond a length 6 times that of the embryo size (Figure 6.1b and 6.2b). These critical values of cavity AR and width can be utilized to assist in regulating the amount of solute around the embryo, such that the AR and width are below these critical values in order that changes in these parameters may be used to control solute transport.



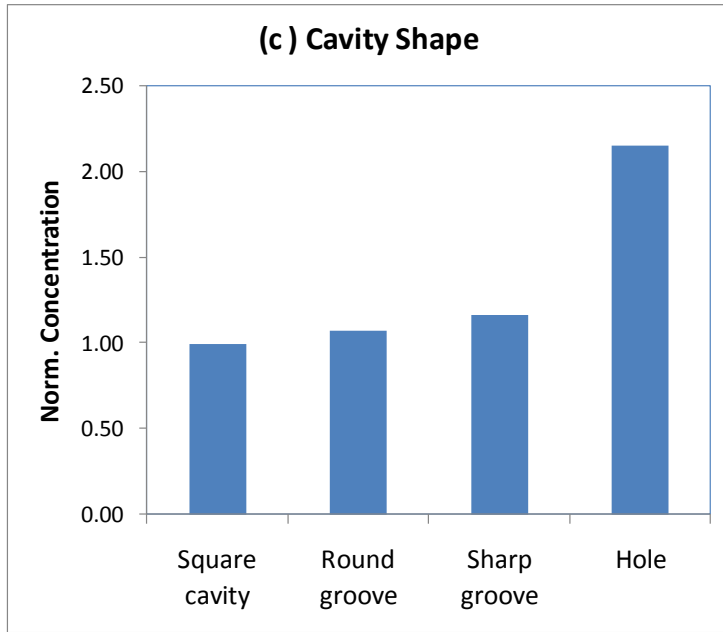
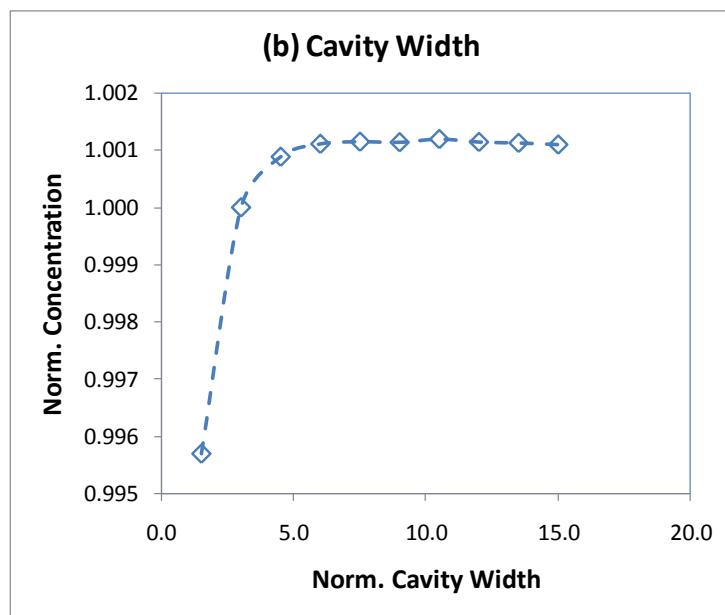
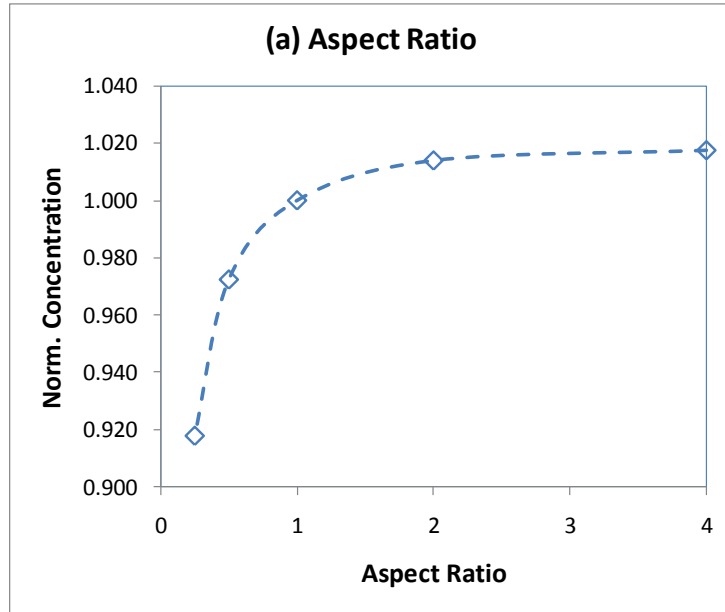


Figure 6.1: Effects of changing cavity aspect ratio, width and shapes on the lactate concentration on the embryo surface.



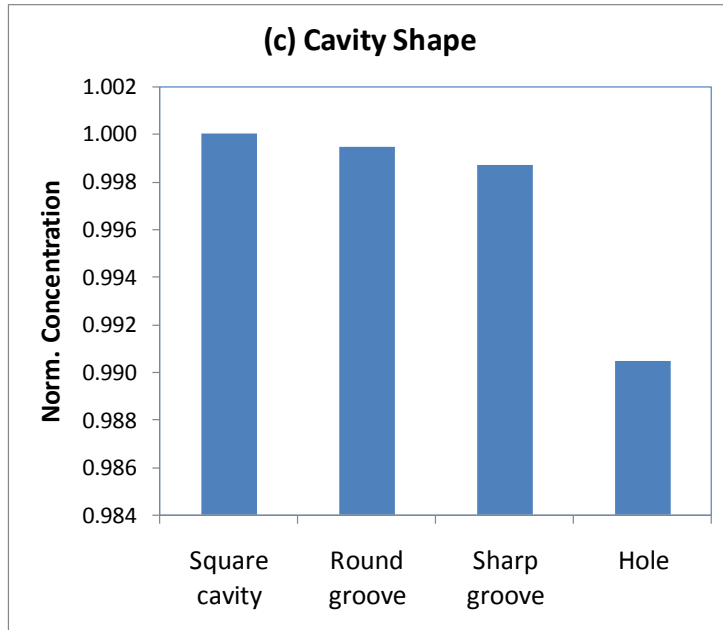


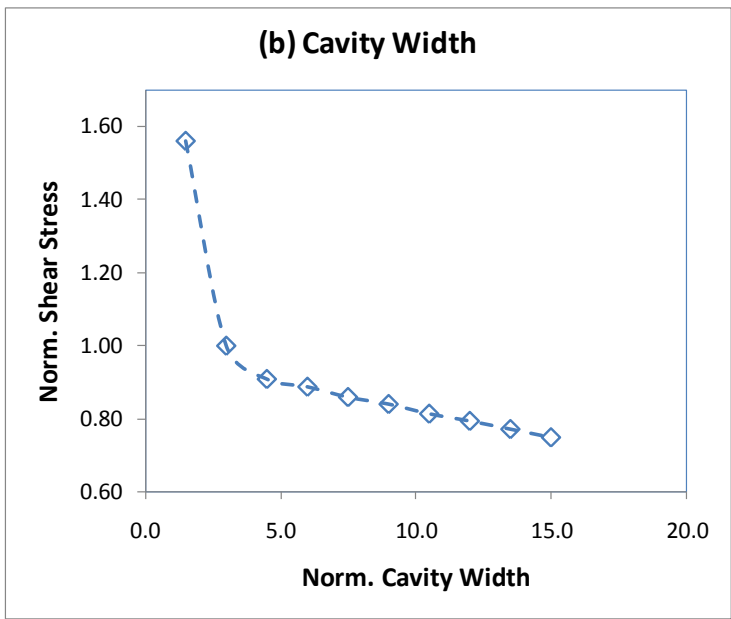
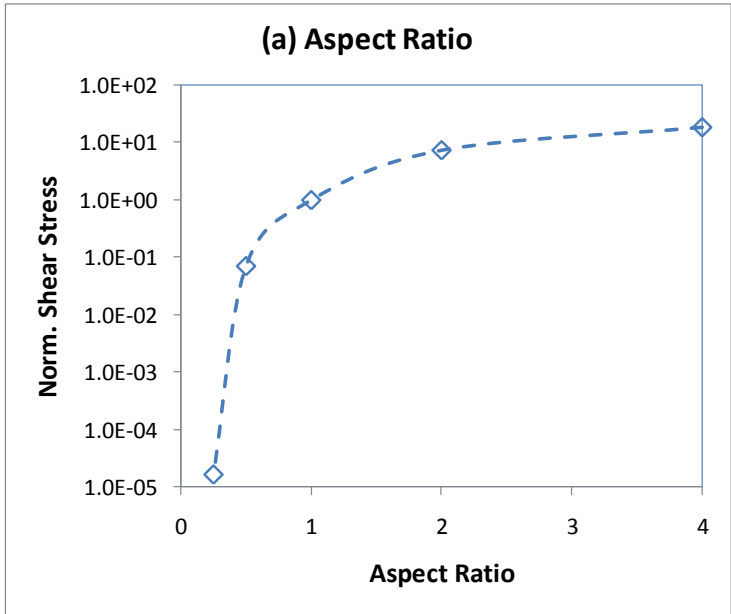
Figure 6.2: Effects of changing cavity aspect ratio, width and shape on the oxygen concentration on the embryo surface.

Shear stress as a function of cavity AR, width and shape are plotted in Figures 6.3a, 6.3b and 6.3c respectively. Analogous to the study of solute transport, the change in cavity AR produces the largest change in shear stress when compared to the other two parameters of width and shape. This is clearly shown by the logarithmic increase in the normalized shear stress from  $1 \times 10^{-5}$  to  $1 \times 10^{-1}$  when AR is varied logarithmically, as shown in Figure 6.3a. When cavity width is increased, a change of only 1.62 to 0.78 is observed, as shown in Figure 6.3b. When the cavity shape is changed from a square to a hole, a minimum normalized stress of 0.4 is recorded, as shown in Figure 6.3c. Again, these results suggest that modifications of the cavity AR are most useful in adjusting the stress level experienced by an embryo, as opposed to cavity width and shape.

In depth examination of the shear stress changes reveals that drastic stress level variation occurs when the cavity is deep and/or narrow. This is evidenced in Figure 6.3, where the most drastic shear stress changes occur when variation of cavity AR occurs below 0.5, and the cavity width decreases below 3 times the size of the embryo. In addition, the lowest shear stress occurred when a hole-shaped cavity was used. The reason for this is that a small cavity reduces flow circulations to occur around the embryo. This reduction results in lower shear stress, as the shear stress induced on the embryo surface is directly proportional to the rate of fluid movement around it. The

implication of this is that to reduce the shear stress induced on the embryo, a design with a small cavity to house the embryo should be used. While it was found that a larger cavity width contributes to a decrease in the shear stress, it is noted that the overall change in shear stress due to the cavity width variation is far smaller than the dramatic stress reduction when the cavity AR is decreased.

Another notable observation on varying the cavity AR and width is that the change in shear stress diminishes when AR is greater than 2 (Figure 6.3a) and normalized cavity width is greater than 3 (Figure 6.3b). These critical values for both cavity AR and cavity width mark the limits at which a change in these values will vary the stress level on the embryo. Larger values do not result in a significant change in the shear stress. These results should be considered when designing a cavity in order to minimize the shear stress.



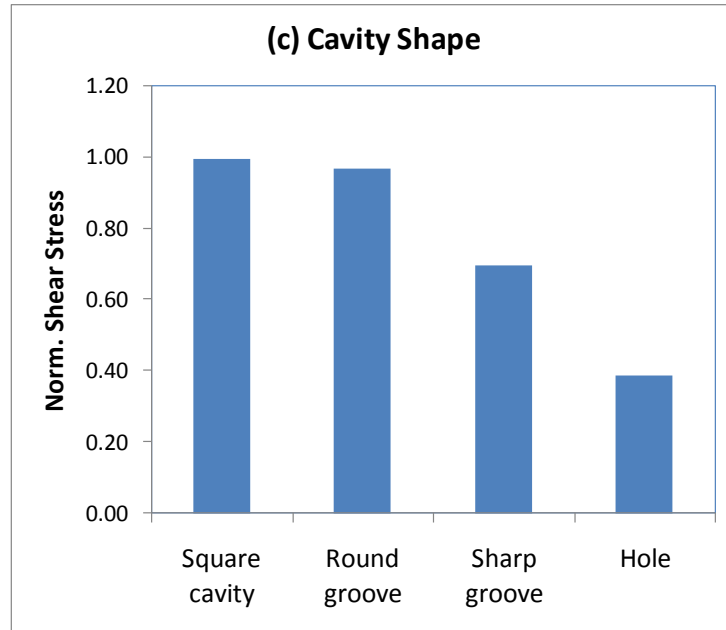


Figure 6.3: Effects of changing cavity aspect ratio, width and shapes on the embryo surface shear stress.

To conclude, modifying the AR of the cavity incurs the largest change in solute transport and shear stress on the embryo, in contrast to modifying the cavity width or shape. Therefore, cavity designs should focus on the AR parameter when designing the cavity of the micro-bioreactor. It is recommended that designers focus on the AR parameter when implementing micro-bioreactor cavities.

### 6.1.2 Perfusion of Culture Medium

The two parametric studies that focused on the perfusion of culture medium involved varying the inflow rate,  $V$  and adjusting the (normalized) height of the culture medium,  $D_f^*$ . The impact on fluid flow and solute transport due to these changes are now given.

As shown in Figure 6.4 for lactate and Figure 6.5 for oxygen, variation in the concentration of these two solutes is larger when  $V$  is varied, when compared to changing  $D_f^*$ . This is clearly shown by the 350% decrease of lactate concentration (Figure 6.4a) and 3.25% increase in oxygen concentration (Figure 6.5a), as  $V$  increases. When  $D_f^*$  is increased, only a 26% increase in lactate concentration (Figure 6.4b) and a 0.7% decrease in oxygen concentration is observed, as shown in Figure 6.5b. With this observation,  $V$  should be designated as the primary means to adjust the solute concentration around the embryo surface, rather than altering  $D_f^*$ . Furthermore, the

influence of changing  $V$  is comparable to that of varying the cavity AR. However, there is greater flexibility in adjusting the flow rate of the culture medium to alter the solute concentration around the embryo. The flow rate of the culture medium can be varied after the embryo cultivation period has begun, which is not the case for cavity AR.

In regard to the variation of  $V$ , the changes of solute concentrations stabilise when  $V$  is very slow, such that the corresponding  $Pe$  is very small, as shown in figure 6.4a and 6.5a. The value of  $V$  at which the changes of the solute concentrations stabilise to a constant value, the critical  $V$ , is different depending on the different types of solute, with each having a different diffusivity. When  $V$  is increased to a value greater than the critical value, the solute concentrations exhibit a linear trend change. The implication of this observation is that the critical  $V$  can be defined as the minimum inflow rate at which there is still some influence on the solute concentration around the embryo.

Concerning the change of  $D_f^*$ , the depth of the channel fluid, it can be seen that the trend changes of the solute concentration follows a parabolic profile, such that the rate of change of the solute concentration decreases as  $D_f^*$  increases. Notably, the change of solute concentration is marginally steeper when  $D_f^*$  is small, as shown in Figure 6.4b and figure 6.5b. When  $D_f^*$  is increased from 0.5 to 1.0, an 8.5% increase in lactate and 0.18% decrease in oxygen is detected. When  $D_f^*$  is increased to over 3.0, a 5.6% increase in lactate and 0.15% decrease in oxygen is observed. This means that a deep culture medium is less sensitive to changing the solute concentration in response to a change in  $D_f^*$ , such as increasing or decreasing  $V$ . The implication of this in regard to the operation of the micro-bioreactor is that it may be preferable to have a large  $D_f^*$  for the culture medium flowing in to the channel.

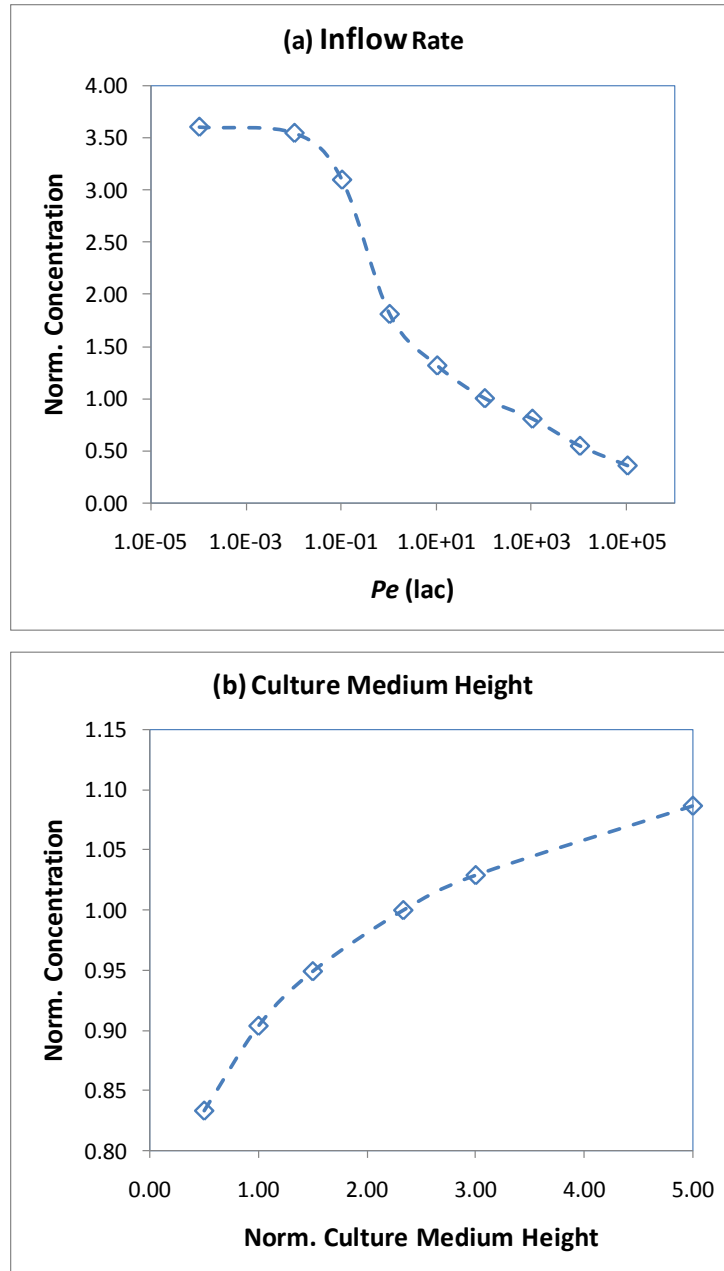


Figure 6.4: Changes to the lactate concentration on the embryo surface when (a) the inflow rate and (b) height of the culture medium flowing in the channel are varied.

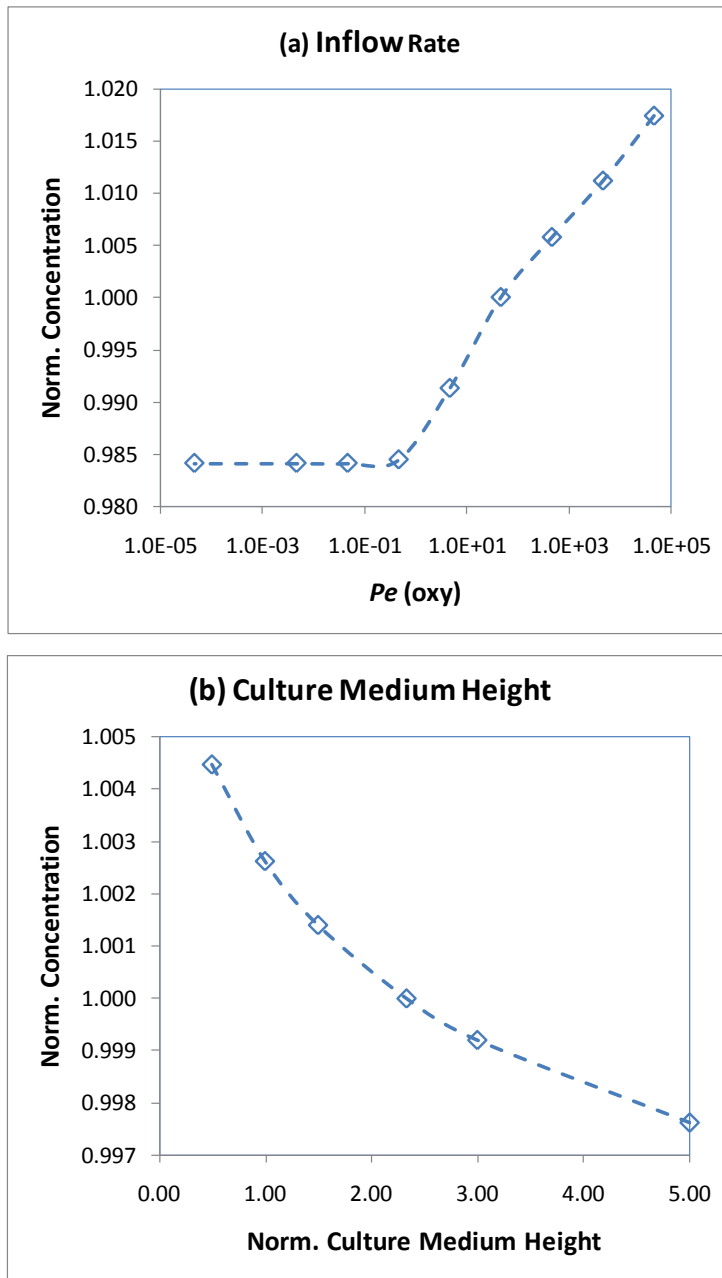


Figure 6.5: Changes to the oxygen concentration at the embryo surface when (a) the inflow rate and (b) height of the culture medium flowing in the channel are varied.

By comparison, varying  $V$  is even more effective at controlling the shear stress on the embryo, as opposed to manipulating the solute concentrations around the embryo. This is clearly shown by the logarithmic decrease in shear stress as  $V$  is reduced logarithmically (Figure 6.6a). In contrast, changing  $D_f^*$  to augment the stress level is less effective as changing  $V$ . This can be seen in Figure 6.6b, where only a 4-fold decrease in shear stress is detected when increasing  $D_f^*$  from 0.5 to 5.0. These observations imply that controlling the perfusion of the culture medium is a preferable means to reduce the shear stress experienced by the embryo. While it is also noted that changing the cavity AR also brought about a substantial change in the stress level (Figure 6.3a), the stress variation diminishes as cavity AR is increased to a value larger than 2. This observation once again supports that varying  $V$  is the best approach to control the shear stress experienced by the embryo.

When examining changes in  $D_f^*$  alone (Figure 6.6b), it is found that when the cavity height is shallow, a steeper change in shear stress results. For example, shear stress drops 57% as  $D_f^*$  increases from 0.5 to 1.0. This steep change is observed when the change in  $D_f^*$  is below 1.0, less than the height of the cavity. When the change in  $D_f^*$  is higher than 1.0, the rate of change in shear stress results in a shallow descent, with an average drop of 25% in shear stress observed when  $D_f^*$  is increased beyond 1.0. Similar measurements are observed for solute transport, where a shallow height of culture medium flowing into the channel leads to a more sensitive change to the solute concentration. In the results given in Figure 6.6b, a shallow height causes an even more responsive variation to the shear stress. Therefore, similar to the case with solute transport, it is suggested that a shallow flow of culture medium in the channel should be avoided in order to prevent a large fluctuation in shear stress occurring due to the unintended changes in  $D_f^*$ .

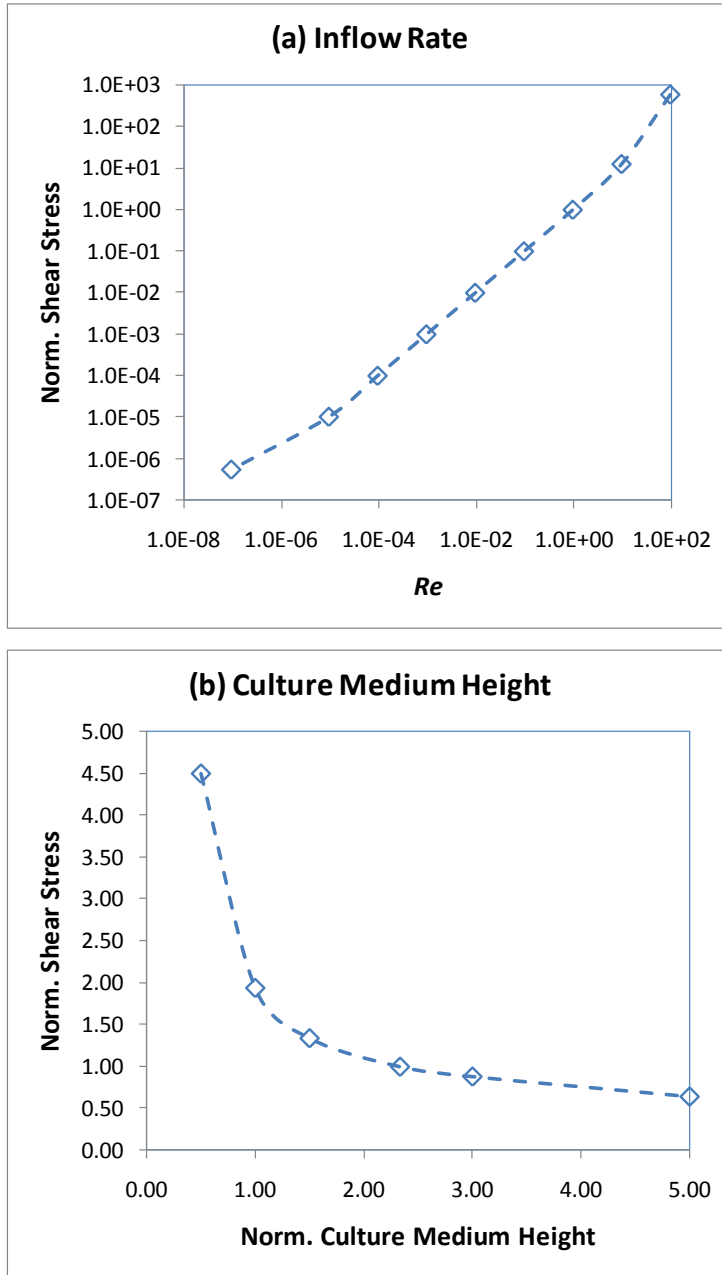


Figure 6.6: Changes to the shear stress on the embryo surface when (a) the inflow rate and (b) height of the culture medium flowing in the channel, are varied.

Overall, the two parametric studies on the perfusion of culture medium have identified that modifying the inflow rate is the preferable option to adjust the shear stress and solute concentration around the embryo. The flow of culture medium in the channel should also be as deep as possible.

### **6.1.3 Embryo Growth**

This parametric study investigated the effect on solute concentration and shear stress from varying solute exchange rate and embryo size. The variation on the solute exchange rate and embryo size represent the effect of embryo growth from the 1-cell stage to the blastocyst stage. The outcomes from this study are plotted in Figure 6.7 to 6.9. In brief, the change in solute production rate is directly proportional to the change in the solute concentration on the embryo, while the change in solute uptake rate is inversely proportional to the solute concentration on the embryo. The embryo size is inversely proportional to the change in the shear stress experienced by the embryo.

The influence on the solute concentration around the embryo due to the change in solute exchange rate is very large. This is evidenced by the 1600% increase in lactate concentration as shown in Figure 6.7b. A 5% decrease in oxygen concentration is also observed as shown in Figure 6.8b. This is the highest increase observed in all studies conducted in this thesis. As a result, continuous regulation of the proper amount of solutes in the culture medium is required to ensure that an optimal environment occurs around the embryo. This is important as previous studies found that embryo growth is greatly compromised if the amount of the required solutes in the culture medium is incorrect. Possible regulation measures may include augmenting the perfusion rate of the culture medium or externally altering the amount of the relevant solute in the culture medium before passing it into the micro-bioreactor. As part of this study, the data on the solute concentration changes recorded during the embryo growth may be utilized to configure the composition of the culture medium such that the embryo is continually bathed in the optimal culture medium.

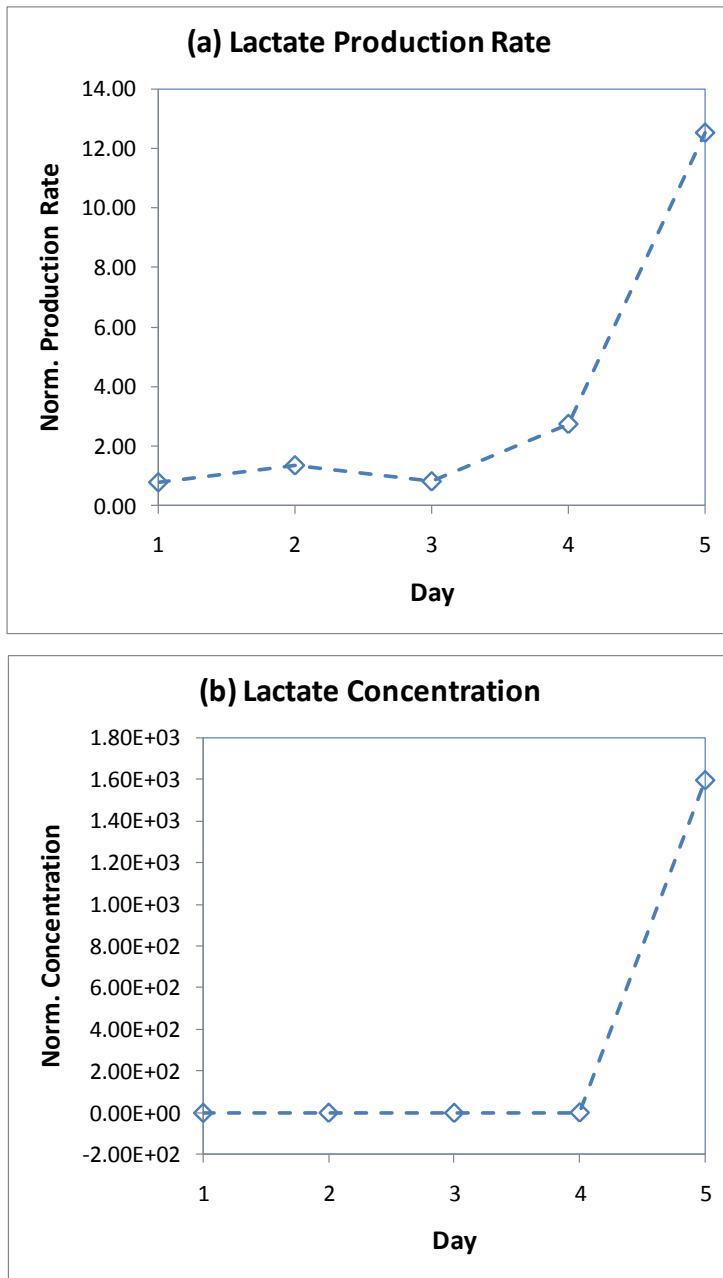


Figure 6.7: (a) the change in lactate production rate due to the embryo growth from day 1 to day 5 is compared with (b) the corresponding change in lactate concentration on the embryo surface.

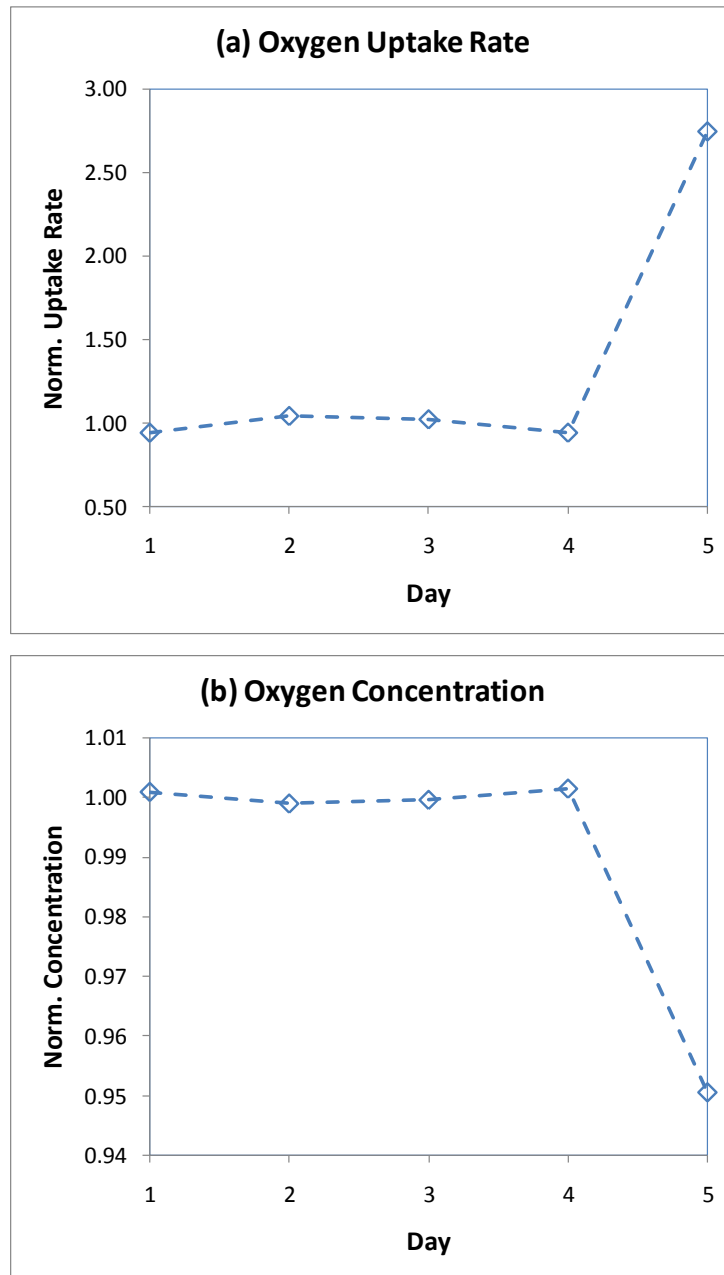


Figure 6.8: (a) the change in oxygen uptake rate due to the embryo growth from day 1 to day 5 is compared with (b) the corresponding change in oxygen concentration on the embryo surface.

As for the variation in shear stress, it is noted that the magnitude of the change is not large, as shown in Figure 6.9b, where a maximum 2-fold increase in shear stress is detected when the embryo is the smallest. This is in contrast to the variation in the inflow rate which incurs a 10-fold logarithmic decrease in shear stress. Also, the change in shear stress is not as sensitive as the change in solute concentration when influencing the embryo growth. As long as the shear stress experienced by the embryo does not exceed a maximum threshold (which differs depending on the types of the embryo), the embryo will continue to grow without any serious consequences (refer to Section 3.1). Consequently, only a slight change in the inflow rate might be necessary to offset a harmful shear stress increase that may arise from the size change of the embryo due to the growth.

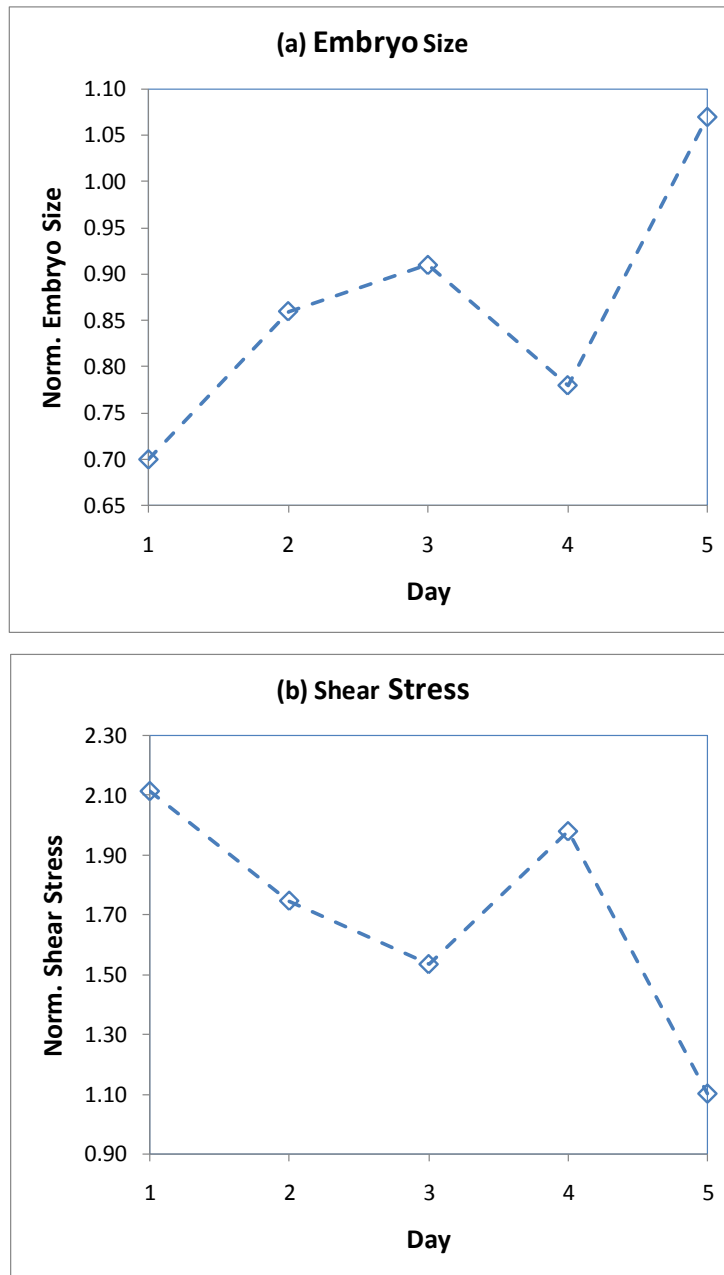


Figure 6.9: (a) the change in embryo size due to the embryo growth from day 1 to day 5 is compared with (b) the corresponding change in shear stress on the embryo surface.

#### **6.1.4 Scaling up Embryo Production**

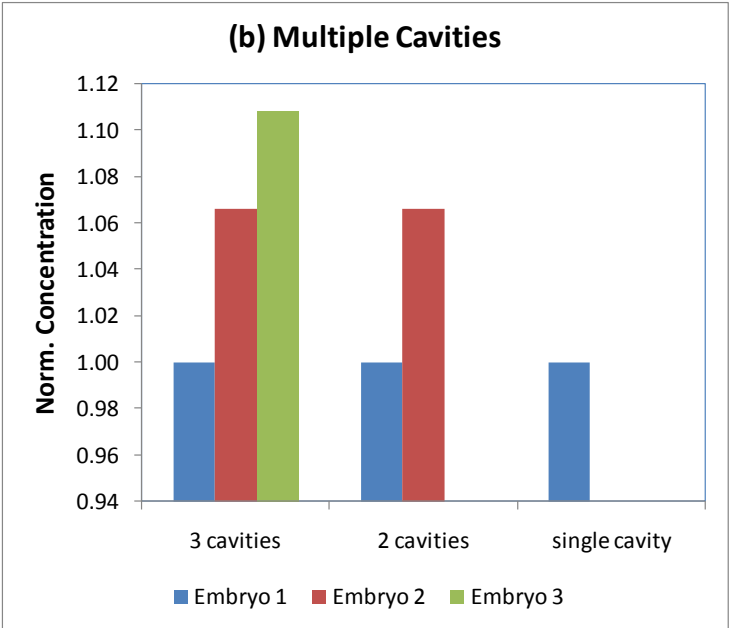
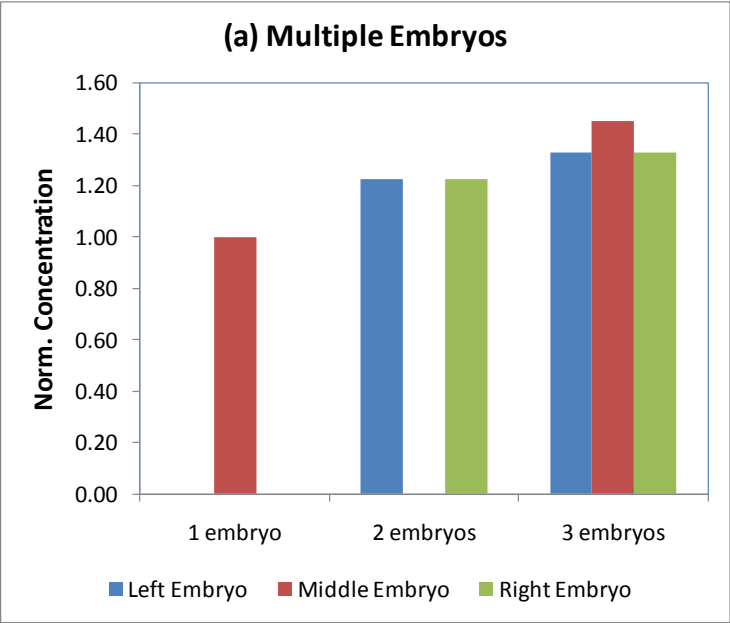
These parametric studies examined scaling up embryo production through setting up several experiments where several embryos are allocated to a cavity (multiple embryos study) and setting up several cavities in a micro-bioreactor (multiple cavities study). The results were then evaluated by examining the change in solute concentration and shear stress due to the addition of additional embryos or cavities. The multiple cavities study also examined variation in the spacing between cavities. Ultimately, the goal here is to study the perturbation to the solute transport and shear stress that may arise when increasing embryo production.

In general, these two approaches cause the unwanted side effect of uneven solute concentration across different embryos and poses a challenge in maintaining the same culture conditions for all embryos. In comparing these two approaches, increasing the number of embryos cultured in the same cavity induces a slightly larger change in the solute concentration than increasing the number of cavities present in the bioreactor. This is evidenced in Figure 6.10a, 6.10b, 6.11a and 6.11b, where increasing the number of embryos from one to three causes a maximum increase of 42% in lactate concentration and a 0.37% decrease in oxygen concentration of one of the embryos. Adding two more cavities to the bioreactor induced a maximum increase of 11% in lactate concentration and a 0.35% decrease in oxygen concentration on the embryo in one of the cavities. According to these findings, it can be deduced that the approach of adding more cavities has a slightly larger change in solute transport than packing more embryos in a cavity.

When the rate of change of the solute concentration is measured as more embryos or cavities are added into the micro-bioreactor, it is found that the rate of change of the solute concentration is fairly consistent when using both approaches to scale up embryo production. As shown in Figure 6.10a and 6.11a, increasing the number of embryos from one to two causes a 21% increase in lactate concentration and a 0.19% decrease in oxygen concentration, while a third embryo also causes an additional maximum increase of 21% in lactate concentration and a maximum 0.18% decrease in oxygen concentration. The increase in lactate and decrease in oxygen found when increasing the number of cavities is also similarly consistent, as shown in Figure 6.10b and 6.11b.

Increasing the number of cavities from one to two brought about a 6.2% increase in lactate concentration and a 0.2% decrease in oxygen concentration. Adding an additional cavity caused a further maximum of 5.9% increase in lactate concentration and a maximum 0.18% decrease in oxygen concentration. This finding here implies that adding more embryos or cavities would similarly cause a linear change in solute concentration. This further adds to the difficulty in keeping the same solute concentration across all embryos when scaling up embryo production.

When increasing the number of cavities, the spacing between cavities influences the change in the amount of solutes in the cavity/cavities downstream of the front cavity adjacent to the inlet. As this spacing becomes smaller, the solute concentration on the embryo in the rear cavity downstream is higher than the one found in the front cavity. This change in solute concentration on the rear embryo has a parabolic profile, where the change reduces to a constant concentration when the cavity spacing is about 10 times larger than the cavity length. Consequently, it is recommended that the spacing between the two cavities should be at least 10 times larger than the cavity length to ensure that the difference in solute concentration is kept as small as possible, in order to equalize the solute concentration on all embryos.



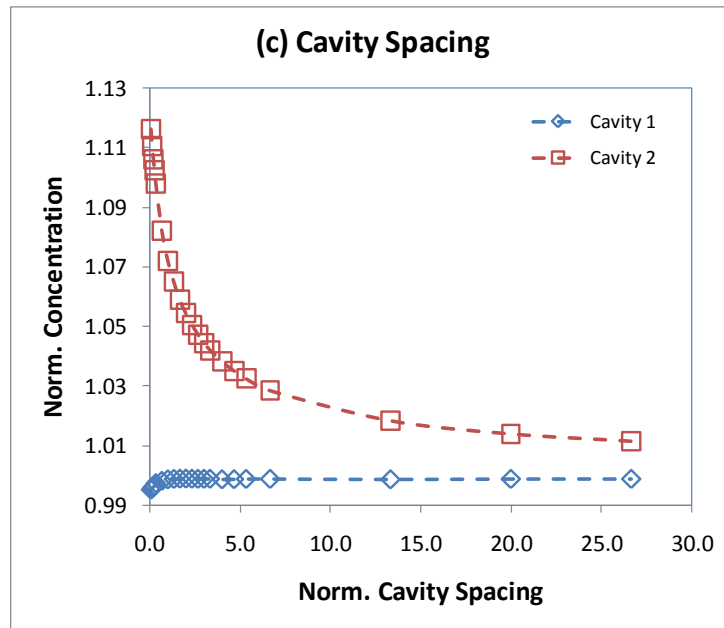
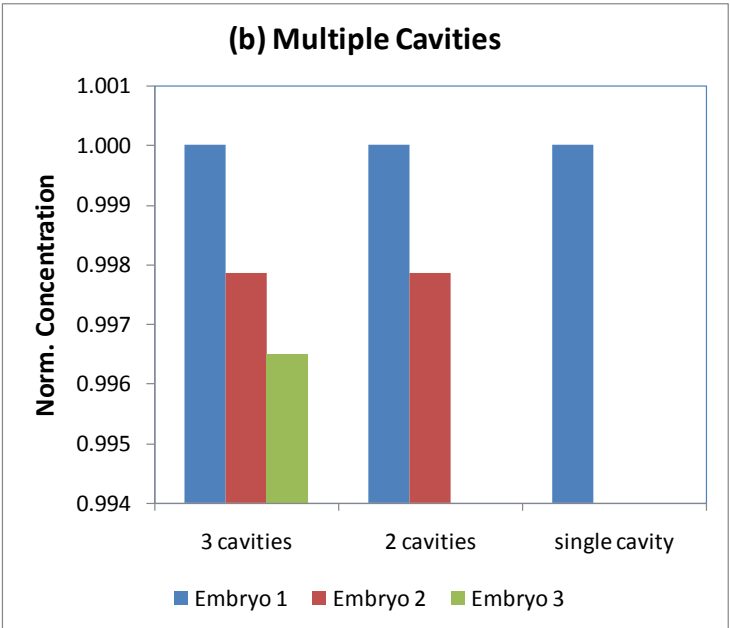
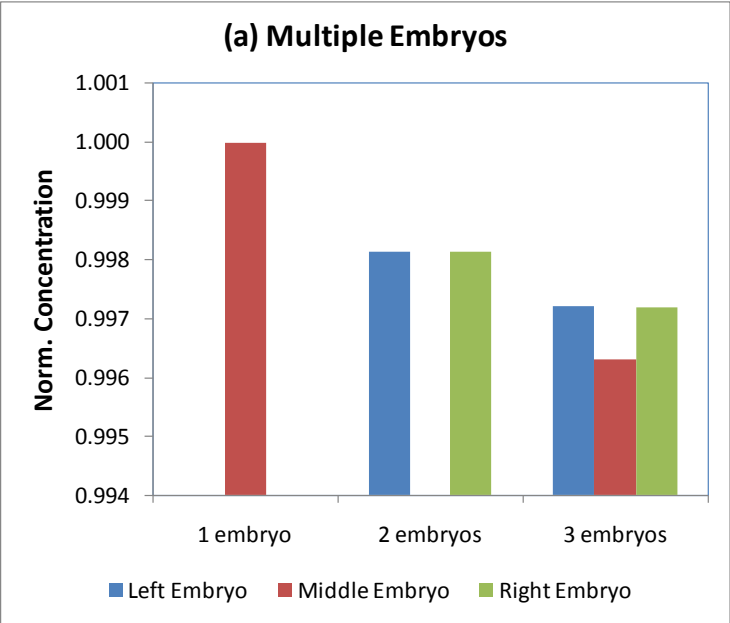


Figure 6.10: Comparisons of the lactate concentration on the embryo surface evaluated from the parametric studies of having multiple embryos or multiple cavities.



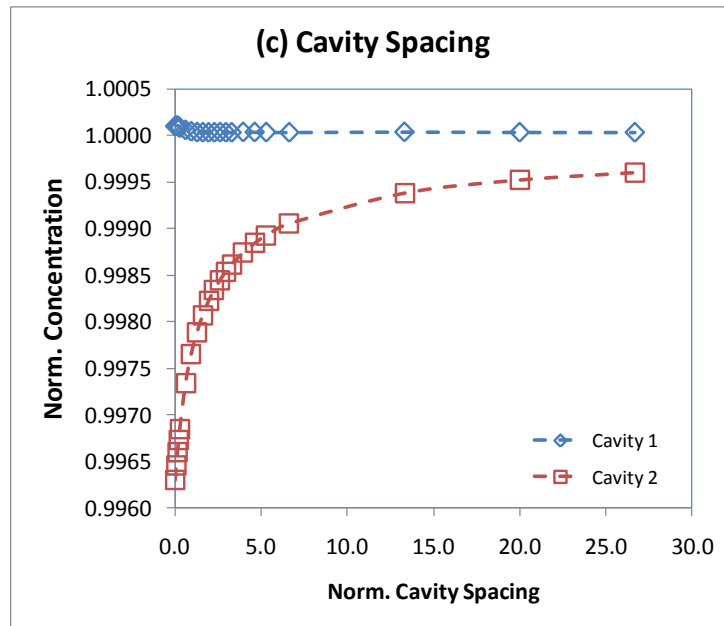
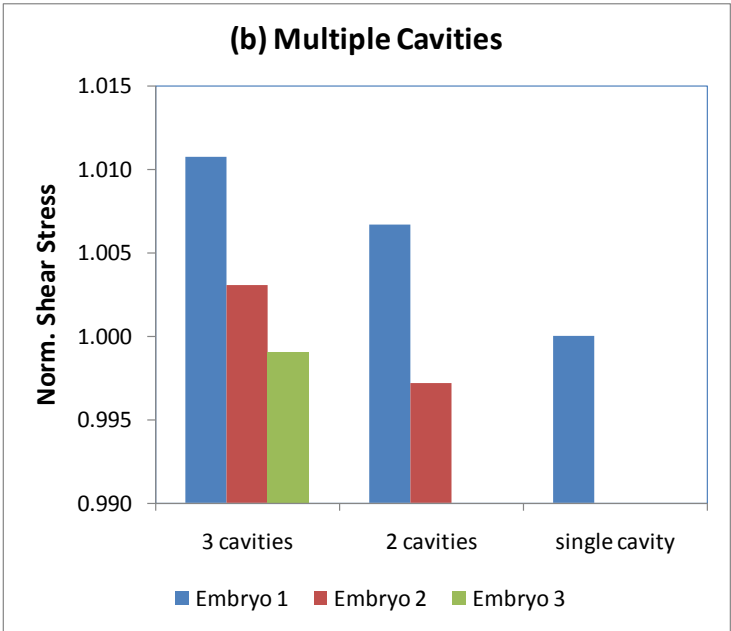
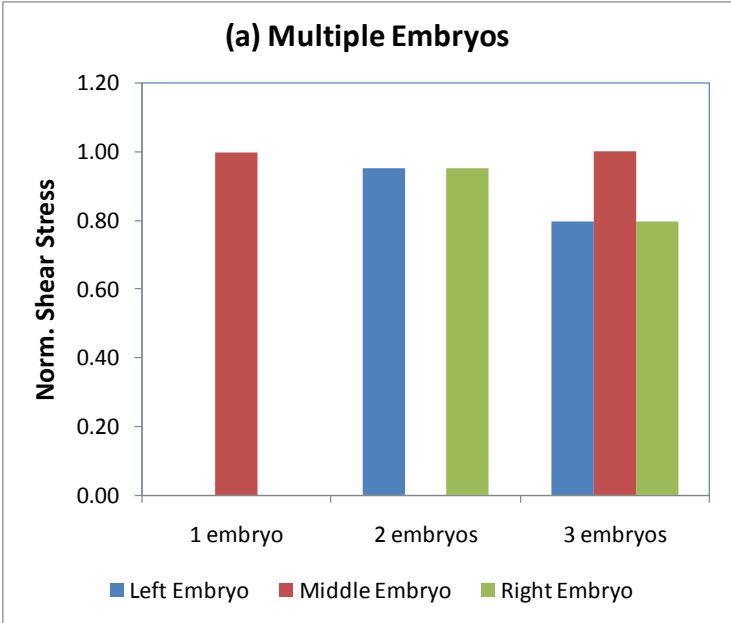


Figure 6.11: Comparisons of the oxygen concentration on the embryo surface evaluated from the parametric studies of multiple embryos or multiple cavities.

Analogous to the situation with solute transport, placing more embryos in the cavity or adding more cavities to the micro-bioreactor causes different embryos to experience different levels of shear stress. The shear stress variation due to increasing the number of embryos in the cavity is larger than the shear stress variation due to increasing the number of cavities in the micro-bioreactor. This is shown in Figure 6.12a and 6.12b, where a maximum 20% decrease in shear stress appears in the case of multiple embryos, while an overall change of 1.4% in shear stress (1.1% increase, 0.3% decrease) appears in the case of multiple cavities. Subsequently, in regard to the shear stress, the approach of adding more cavities to the micro-bioreactor is preferred when scaling up embryo production, as this approach causes less difference in shear stress across the embryos. This coincides with the findings for solute concentration, where adding more cavities also causes less difference in the solute concentration amongst the embryos.

The spacing between the cavities also has an influence on the shear stress experienced by the embryos in the cavity, where if this spacing is reduced to very small value, a large shear stress is incurred on all the embryos due to the flow interference caused by the cavities, as shown in Figure 6.12c. However, unlike the findings for solute concentration, such an influence on shear stress is only prominent when the cavities are

located very close, and this effect weakens quickly as the spacing increased. In particular, the shear stress experienced by all the embryos increases sharply when the spacing is less than the length of a single cavity, as highlighted in Figure 6.12c. Due to this, it is suggested that the spacing between the cavities should be longer than the length of the cavity, in order to avoid this build-up of shear stress.



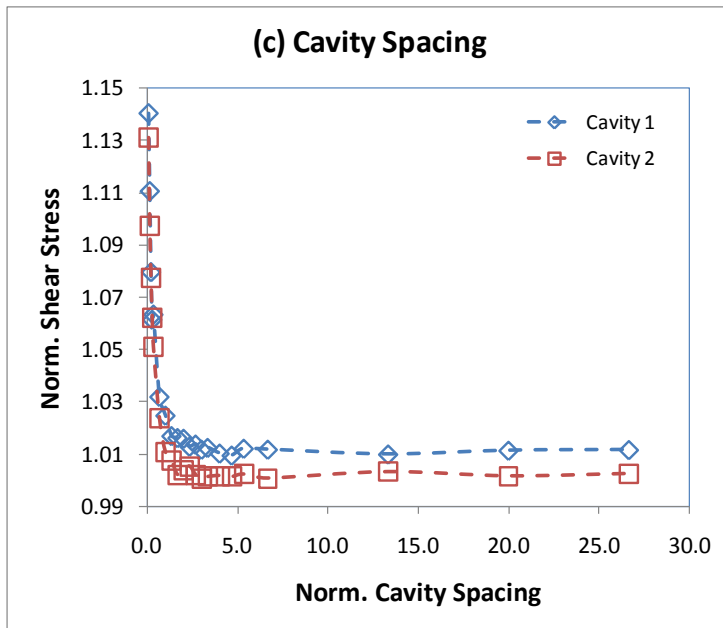


Figure 6.12: Comparisons of the shear stress on embryo surface evaluated from the parametric studies of multiple embryos or multiple cavities.

In summary, it is concluded that scaling up embryo production by placing more embryos in the same cavity, or adding more cavities to the micro-bioreactor, caused an uneven distribution of solute concentration and shear stress on each embryo. The addition of more embryos or cavities results in an escalation in the uneven distribution. As discussed, adding more cavities to the micro-bioreactor is the preferred approach, as this incurs less of the aforementioned side effect. While keeping the spacing between the cavities may help to alleviate this complication, better methods to homogenize the solute concentration on each embryo need to be developed to employ either of these scaling-up approaches.

## **6.2 Limitation of Numerical Model**

With the current numerical model, there are several assumptions made in terms of modelling on the fluid flow and solute transport. This is to simplify the model so that it could be handled using currently available numerical codes. The assumptions here may be translated as a limitation of the model, where the simplifications made could have restricted the potential of the model to simulate the fluid environment in the micro-bioreactor, to emulate the physiology and metabolism of the embryo, as well as to describe the interaction of different chemical solutes in the culture medium. This section discusses these limitations and suggests some possible measures to remedy them. These measures constitute recommendations for future project work.

### **6.2.1 Inadequacy of Model Capability, Validation and Optimisation**

The simulations conducted for all the parametric studies reported in this thesis model the fluid flow and solute transport under the steady-state condition. The assumption of steady-state condition here implies that the modelled fluid flow and solute transport occurring within the culture medium in the micro-bioreactor are time-independent. In other words, the condition of the fluid flow and solute transport is constant for an indefinite time. This assumption is made based on the reasoning that the culture medium perfusion and the time-scale for embryo growth are very much slower than the advection and diffusion flow time-scales. In summary, the flow and solute transport around the embryo is viewed as quasi-steady in terms of the embryo growth, and in particular, oxygen absorption and lactate production. This does not mean that these factors need to remain constant, just that if they change, then a new steady model is required.

While this assumption is used to reduce the computational time requirements, experimental studies may show that the constant uptake/production rates for solutes are not appropriate, for example, they may change considerably during growth, such as during cell division. In such a situation it may make more sense to employ a time-dependent numerical model despite the relatively larger cost.

As shown previously in the Methodology chapter, the numerical model has only been validated using other similar numerical studies, but not with actual experimental flow

systems close to the type of flow situation modelled here. The main problem here is that there may be important components of a real experimental bioreactor that are not included in this numerical model but which are of considerable importance to the growth and viability of embryos. This situation will be resolved as more experimental studies are undertaken and more experimental data are collected. Another problem with the numerical modelling is that it can suffer from various errors such as round-off, truncation, discretisation, domain-restriction and resolution errors. Of these, resolution studies were reported on in the Methodology section, showing that the simulation accuracy should be satisfactory. The discretisation or truncation errors reduce as the flow is better resolved, as the mesh is refined. Round-off errors also should not be an issue using the double precision version of the code with limited mesh sizes, given previous experience with *Fluent*. The computational domain size can have an effect. This is tied up with the application of incorrect or asymptotic conditions at domain boundaries, with the assumption that the flow and solute transport near the region of interest – the cavity – is appropriately modelled. This is discussed further below in the paragraph on boundary conditions.

An additional significant work to be undertaken in a future study is the optimisation of the numerical model to handle a fluid flow simulation with solute transport. As discussed previously in the Methodology section, the numerical model employed here is the generic CFD code *Fluent*, which has wide versatility to handle many types of flow modelling. The downside of this versatility is that the code is not optimized for any particular flow. In particular, for the problem here, the code takes an extraordinarily large number of iterations to converge for the fine grid cases, despite the relative linearity of the flow equations at low Reynolds numbers. There are various methods to speed up convergence – such as direct solvers using Newton-Raphson iteration (especially for the two-dimensional flows) or through the use of a multigrid solver. Furthermore the software may not be able to handle several modelling aspects concurrently, such as simulating the fluid flow with solute transport of several types of chemical species *together*. Subsequently, optimisation to the numerical code to tailor it for the application of simulating fluid flow and solute transport in a micro-bioreactor is recommended.

## 6.2.2 Assumptions on Culture Medium

There are several assumptions applied to the culture medium. The limitations of these assumptions in regards to the solute transport modelling are discussed in this section.

Firstly, and perhaps most importantly, the solute exchange rates of lactate production and oxygen uptake chosen for the parametric studies are assumed to have a zero-order reaction rate. This means that the solute exchange rate is independent of other solute conditions such as solute concentration, diffusivity and temperature. This assumption is contradictory to some experimental studies in the literature that state that the solute exchange of live cells (not the embryo) follows first-order Michealis-Menten kinetics – the solute exchange rate depends on the respective concentration of the surrounding solutes (Cohen 1973; Balis, Behnia *et al.* 1999; Patzer II 2004). Here in this thesis, the zeroth-order assumption has been made as there is not much information available regarding solute exchange for an embryo. While there are many studies conducted to measure the solute exchange on embryos such as oxygen consumption or nutrient uptake measurements, few studies examine the relation of solute exchange with surrounding physiological or chemical factors, such as the dependence of solute exchange rate on embryo metabolism or the concentration of chemical species in the culture medium surrounding the embryo. Consequently, a series of experimental parametric studies is needed to study the nature of solute exchange and to determine mathematical models that best describe the pattern of solute exchange for an embryo.. This is a major shortcoming of the current numerical model which, for instance, assumes a constant oxygen uptake rate independent of the available oxygen in the immediate environment. An appropriate model of the process is perhaps the number one addition to the current numerical model to improve its capabilities.

Secondly, the diffusion coefficients of the lactate and oxygen in the culture medium are assumed to be the standard diffusion coefficients of lactate and dissolved oxygen in saline water (Himmelblau 1964). These coefficients are generally dependent on temperature and density. For the case here, the temperature needs to be set to a constant incubator temperature, and it seems unlikely that it would be wise to vary this temperature very much. The assumption of constant density of the culture medium throughout the cultivation period (the fluid incompressibility assumption) holds true

since the cultivation of the embryo must occur in the standard atmospheric conditions and low Mach number, where no fluid compressibility will occur.

For the current set of simulations reported here, solute transport is undertaken in such a way that solute production is simulated separately from solute consumption. This means that two separate simulations are required, one to simulate the lactate production, another to simulate oxygen uptake. The main reason for setting up the simulation as such is that there is not enough information available yet to specify the combined diffusivity of all the solutes in the same culture medium. There are two negative outcomes of this. Firstly, more computational resources and time are required as every simulation needs to be conducted twice to separately model the solute production and the solute uptake. This translates to inefficient modelling of the solute transport. Note however that the flow solution is independent and is calculated first. Secondly, the actual embryo performs all solute exchange simultaneously. In order to remedy these effects, experimental studies to quantify the solutes diffusivities need to be carried out to gain a better understanding of the interaction between different solutes in the same culture medium. This can be achieved by setting up experiments to study the combined diffusivity of certain solutes in the same culture medium.

### **6.2.3 Assumptions on Boundary Conditions of the Model**

There are also several assumptions made on the boundary conditions (BC) that defined the modelled fluid domain in the micro-bioreactor. They include the culture medium-oil interface at the open surface of the channel and the BC that defined the embryo surface.

The interface between the culture medium and oil layer is modelled using a zero stress wall BC. As discussed previously, the function of the oil layer is to prevent the evaporation of the minute amount of culture medium in the microchannel. The application of this type of BC depends on the assumptions that the movement of the culture medium adjacent to the stationary oil layer would not be affected by the more viscous and less dense oil. It also assumes that the interface between the oil layer and the culture medium is stable over an indefinite time and does not deform under any circumstances. It is possible that these assumptions may not be true under certain conditions, for example at a very high inflow rate, but also since spatial dimensions are

small, surface tension may have a non-negligible effect. The validity of these assumptions therefore needs to be determined in order to ensure the validity of the numerical model. Again, experiments could be used to validate the assumption.

The embryo surface modelled in the simulations is assumed to be rigid and is fixed to the bottom surface of the cavity. The first assumption about the rigid embryo surface may not pose as large a drawback to the fluid flow and solute transport modelling. Real flow experiments, conducted by Beebe and his colleagues on embryo culture in a micro-channel bioreactor, found that the embryo does not deform in shape, even when the perfusion rate of the culture medium is several times higher than the *in-vivo* dynamic fluid culture condition (Beebe, Trumbull *et al.* 1998; Beebe, Wheeler *et al.* 2002). Nevertheless, it may be useful to create a numerical model with an embryo surface that can deform under large magnitudes of stress. Such a model could simulate the fluid flow around the embryo more accurately, since the deformation on the embryo surface may effectively alter the fluid flow around it. For example, the spherical embryo deformed into an elliptical shaped embryo. Ultimately, a deformable embryo surface is able to resemble the real embryo more closely.

The second assumption about the fixing of the embryo to a fixed point on the bottom surface may need to be examined further, as it is logical to expect that the embryo will roll along the bottom surface of the cavity, due to the perfusion of the culture medium at the channel on top of the cavity. Therefore, it is recommended to devise a dynamic BC that includes the description of embryo movement within the cavity, so as to obtain a more accurate description of the fluid flow condition in the cavity and around the embryo.

Finally, the inflow is taken to be uniform at the upstream boundary. For low Reynolds numbers, the flow reaches equilibrium prior to passing across the cavity. However, for the highest Reynolds number case studied, this did not quite occur. Since the most interest is at low Reynolds numbers, this is presumably not a problem.

### **6.3 Concluding Remarks**

This chapter has drawn conclusions by categorising parametric studies into four aspects that characterize the bioreactor design, comparing each of the parametric studies and discussing their relevance to the design and operation of the micro-bioreactor. Furthermore, suggestions have been given on how to best use the findings from the parametric studies to improve bioreactor design. Some of the major limitations of the numerical model employed to conduct the parametric studies have also been discussed, including limitations of the numerical model in predicting the fluid flow and solute transport that occur in the micro-bioreactor. Finally, the identified limitations act as a starting point to devise improvements to the numerical model.

## 7.0 Future Work

---

As stated in Section 2.4.1, numerical parameter studies can provide useful input to the development of a micro bioreactor. Ideally this study would be part of a larger joint numerical and experimental program, with the numerical simulations providing input into the experimental program and vice-versa. Unfortunately, the experimental component of the program was delayed, so the results reported in this thesis are still somewhat theoretical in nature. From the point of view of extending the numerical program, some other useful studies are listed below:

- Develop a more streamlined cavity design and conduct parametric studies to examine it. This is to find out the effectiveness of the streamlined cavity in providing better control on the transport of solutes into and out of the cavity, and to perhaps lead to a more uniform solute concentration (and shear stress) around the embryo.
- Examine the possibility of having porous cavity surfaces to actively augment and increase the uniformity of the solute concentration around the embryo. Such capability is desirable as it allows better control on the amount of solute present around the embryo (uncompromised growth requires the embryo to be bathed in a culture medium providing the proper solute environment).
- Implement a dynamic wall boundary condition to define the surface of the embryo. Such a wall boundary condition would allow the modelled embryo to react to its surrounding flow conditions, such as deforming its shape or allowing it to roll along the bottom of the cavity. In doing so, the fluid environment experienced by the embryo would be more closely emulated.
- Investigate different designs of the microchannel. This is to determine an optimal channel design to transport solutes to the embryo. The comparison between an open channel and closed channel is also suggested to determine which channel type is better in transporting the solutes from the inlet.
- Devise more ideas to scale-up embryo production and then numerically examine their effects in influencing the fluid flow and solute transport in the micro-

bioreactor. The numerical approach is preferable here since new ideas can be setup easily and economically using a numerical model. In contrast, it is relatively more time consuming and expensive to manufacture a series of micro-bioreactor prototypes with different designs.

- Implement a higher-order model for representing solute absorption/production incorporating the influence of the solute environment on uptake/production rates. Such models exist in the literature, although they have been developed for different types of cells. This would be a considerable improvement to the current model since it would provide a means of directly assessing how the solute environment affects embryo viability. Experiments are needed to provide input into such a model.

Apart from that, the numerical model utilized in the parametric studies requires further improvements. As discussed in Section 6.2, the improvements could focus on addressing some of the limitations of the existing numerical model (with some features more important than others):

- Construct prototypes of the micro-bioreactor and conduct flow experiments to validate some of the findings from the numerical studies. This allows the improvement and optimisation on the numerical model to be made, which in turn should provide improvements to further prototypes. This is very important.
- Develop a time-varying numerical model to handle more parametric studies such as investigating the effect of continuously changing the oxygen uptake rate. This will open up the possibility of simulating continuous embryo growth. This is important, but it would be useful to update of the solute uptake/production model (described above) first.
- Remodel the free surface of the open channel flow with dynamic surface boundary conditions such as the volume-of-fluid (VOF) boundary condition. Such boundary conditions can model the free surface more realistically as it takes into account the possible deformation of the fluid surface. This could be delayed until the experiments reveal whether surface tension causes significant surface distortion.
- Modify the numerical model such that it can simulate the uptake and production of different solutes *simultaneously*. This feature is desirable since it reduces the

number of simulations required to emulate all the solutes separately. This is useful for the reason of efficiency.

# Bibliography

---

- Alder, B. J. and Wainwright T. E. (1957). "Studies in molecular dynamics." Journal of Chemical Physics **27**: 1208 - 1209.
- Alder, B. J. and Wainwright T. E. (1958). Molecular dynamics by electronic computers. Transport Processes in Statistical Mechanics. I. Prigogine. New York, Interscience: 97 - 131.
- Allen, M. and Tildesley D. J. (1987). Computer Simulation of Liquids. Oxford, Clarendon Press.
- Anderson, J. D. (1995). Computational Fluid Dynamics: the Basics with Applications. New York, McGraw-Hill.
- Arkilic, E. B., Schmidt M. A., et al. (1997). "Gaseous slip flow in long microchannels." Journal of Microelectromechanical Systems **6**(2): 167 - 178.
- Atencia, J. and Beebe D. J. (2005). "Controlled microfluidic interfaces." Nature **437**: 648 - 655.
- Balin, A. K., Fisher A. J., et al. (1984). "Oxygen modulates growth of human cells at physiologic partial pressures." Journal of Experimental Medicine **160**(1): 152 - 166.
- Balis, U. J., Behnia K., et al. (1999). "Oxygen consumption characteristics of porcine hepatocytes." Metabolic Engineering **1**(1): 49 - 62.
- Baltz, J. M. (2001). "Osmoregulation and cell volume regulation in the preimplantation embryo." Current Topics in Developmental Biology **52**: 55 - 105.
- Barber, R. W. and Emerson D. R. (2006). "Challenges in modelling gas-phase flow in microchannels: from slip to transition." Heat Transfer Engineering **27**(4): 3 - 12.
- Barth, T. J. and Jespersen D. (1989). The design and application of upwind schemes on unstructured meshes. AIAA 27th Aerospace Sciences Meeting, Reno, Nevada, Technical Report AIAA-89-0366.
- Bassous, E., Taub H. H., et al. (1977). "Ink jet printing nozzle arrays etched in silicon." Applied Physics Letters **31**: 135 - 137.
- Batt, P. A., Gardner D. K., et al. (1991). "Oxygen concentration and protein source affect the development of preimplantation goat embryos *in vitro*." Reproduction, Fertility, and Development **3**(5): 601 - 607.
- Bavister, B. D. (1987). Studies on the developmental blocks in cultured hamster embryos. The Mammalian Preimplantation Embryo: Regulation of Growth and Differentiation *In Vitro*. B. D. Bavister. New York, Plenum Press: 219 - 249.
- Bavister, B. D. (1995). "Culture of preimplantation embryos: facts and artifacts." Human Reproduction Updates **1**(2): 91 -148.
- Becker, H. and Locascio L. E. (2002). "Polymer microfluidic devices." Talanta **56**(2): 267 - 287.
- Beckmann, L. S. and Day B. N. (1993). "Effects of media NaCl concentration and osmolarity on the culture of early-stage porcine embryos and the viability of embryos cultured in a selected superior medium." Theriogenology **39**: 611 - 622.
- Beebe, D., Wheeler M., et al. (2002). "Microfluidic technology for assisted reproduction." Theriogenology **57**: 125-135.

- Beebe, D. J., Trumbull J. D., et al. (1998). Microfluidics and bioanalysis systems: issues and examples. 20th Annual International Conference of the IEEE Engineering in Medicine and Biology Society.
- Beskok, A., Karniadakis G. E., et al. (1996). "Rarefaction and compressibility effects in gas microflows." Journal of Fluids Engineering **118**(3): 448 - 456.
- Biggers, J. D. (1987). Pioneering mammalian embryo culture. The Mammalian Preimplantation Embryo: Regulation of Growth and Differentiation In Vitro. B. D. Bavister. New York, Plenum press: 1-22.
- Biggers, J. D., Gwatkin R. B. L., et al. (1962). "Development of mouse embryos in organ cultures of fallopian tubes on a chemically defined medium." Nature **194**: 747 - 749.
- Biggers, J. D., McGinnis L. K., et al. (2004). "Enhanced effect of glycyl-L-glutamine on mouse preimplantation embryos *in vitro*." Reproduction Biomed Online **9**(1): 59 - 69.
- Biggers, J. D., McGinnis L. K., et al. (2005). "One-step versus two-step culture of mouse preimplantation embryos: is there a difference?" Human Reproduction **20**(12): 3376 - 3384.
- Biggers, J. D. and Stern S. (1973). "Metabolism of the preimplantation mammalian embryo." Advances in Reproductive Physiology **6**: 1 - 59.
- Biggers, J. D., Whittingham D. G., et al. (1967). Pattern of energy metabolism in the mouse oocyte and zygote. Proceedings of the National Academy of Sciences of the United States of America.
- Bird, G. A. (1976). Molecular Gas Dynamics. Oxford, Clarendon Press.
- Bird, G. A. (1978). "Monte Carlo simulation of gas flows." Annual Review of Fluid Mechanics **10**: 11 - 31.
- Bird, G. A. (1994). Molecular Gas Dynamics and the Direct Simulation of Gas Flows. Oxford, Clarendon Press.
- Bird, R. B., Stewart W. E., et al. (2002). Transport Phenomena, John Wiley & Sons Inc.
- Bongso, A. and Gardner D. K. (1999). Embryo development. Handbook of In Vitro Fertilization. A. O. Trounson and D. K. Gardner. New York, CRC Press: 167 - 179.
- Bongso, A., Sakkas D., et al. (1999). Coculture of embryos with somatic helper cells. Handbook of In Vitro Fertilization. A. O. Trounson and D. K. Gardner. New York, CRC Press: 181 - 203.
- Bringer, M. R., Gerds C. J., et al. (2004). "Microfluidic systems for chemical kinetics that rely on chaotic mixing in droplets." Philosophical Transactions. Series A, Mathematical, Physical, and Engineering Sciences **362**(1818): 1087 - 1104.
- Brinster, R. L. (1965). "Studies on the development of mouse embryos *in vitro* I: the effect of osmolarity and hydrogen ion concentration." Journal of Experimental Zoology **158**: 49 - 58.
- Brinster, R. L. (1965). "Studies on the development of mouse embryos *in vitro* II: The effect of energy source." Journal of Experimental Zoology **158**: 59 - 68.
- Brinster, R. L. (1965). "Studies on the development of mouse embryos *in vitro*. I. The effect of osmolarity and hydrogen ion concentration." Journal of Experimental Zoology **158**: 49 - 57.
- Brinster, R. L. (1969). Mammalian embryo culture. The Mammalian Oviduct: Comparative Biology and Methodology. E. S. E. Hafez and R. J. Blandau. Chicago, University of Chicago Press: 419 - 444.
- Brody, J. P. and Yager P. (1997). "Diffusion-based extraction in a microfabricated device." Sensors and Actuators **58**(1): 13 - 18.

- Brody, J. P., Yager P., et al. (1996). "Biotechnology at low Reynolds numbers." Biophysical Journal **71**: 3430 - 3441.
- Buster, J. E., Bustillo M., et al. (1985). "Biologic and morphologic development of donated human ova recovered by nonsurgical uterine lavage." Americal Journal of Obstetric and Gynecology **153**(2): 211 - 217.
- Carlson, D., Black D. L., et al. (1970). "Oviduct secretion in the cow." Journal of Reproduction and Fertility **22**: 549 - 552.
- Carney, E. W. and Bavister B. D. (1987). "Regulation of hamster embryo development *in vitro* by carbon dioxide." Biology of Reproduction **36**(5): 1155 - 1163.
- Cercignani, C. (1988). The Boltzmann Equation and Its Applications. Berlin, Springer-Verlag.
- Cheng, H. K. (1993). "Perspectives on hypersonic viscous flow research." Annual Review of Fluid Mechanics **25**: 455 - 484.
- Chiang, T. P., Sheu W. H., et al. (1998). "Effect of Reynolds number on the eddy structure in a lid-driven cavity." International Journal for Numerical Methods in Fluids **26**: 557-579.
- Cho, B. S., Schuster T. G., et al. (2003). "Passively driven integrated microfluidic system for separation of motile sperm." Analytical Chemistry **75**(7): 1671 - 1675.
- Chung, S. O. (1973). "Volume changes during the preimplantation stages of mouse egg development." Yonsei Medical Journal **14**: 63-90.
- Chung, T. J. (2002). Computational Fluid Dynamics. Cambridge, Cambridge University Press.
- Clark, S. G., Walters E. M., et al. (2003). "A novel integrated *in vitro* maturation and *in vitro* fertilization system for swine." Theriogenology **59**: 441.
- Cohen, S. R. (1973). "The rate equation and activation energies for the uptake of  $\alpha$ -aminoisobutyric acid by mouse brain slices." Journal of Physiology **228**(1): 105 - 113.
- Colin, S. (2005). "Rarefaction and compressibility effects on steady and transient gas flows in microchannels." Microfluid Nanofluid **1**(3): 268 - 279.
- Cooke, S., Tyler J. P. P., et al. (2002). "Objective assessments of temperature maintenance using *in vitro* culture techniques." Journal of Assisted Reproduction and Genetics **19**(8): 368 - 375.
- Dawson, K. (1990). Introduction: An outline of scientific aspects of human embryo research. Embryo Experimentation. P. Singer, H. Kuhse, S. Buckle, K. Dawson and P. Kasimba. New York, Cambridge University Press: 3 - 13.
- Deen, W. M. (1998). Analysis of Transport Phenomena. New York, Oxford University Press.
- Den, L. M. (1990). "Issues in viscoelastic fluid mechanics." Annual Review of Fluid Mechanics **22**: 13 - 34.
- Dickinson, E. and Matsumura Y. (1994). "Proteins at liquid interfaces: role of the molten globule state." Colloids and Surfaces B: Biointerfaces **3**: 1 - 17.
- du Toit, C. G. (2002). "Calculation of friction factors and Nusselt numbers for laminar flow in rectangular ducts using finite elements." Numerical Heat Transfer, Part B **41**: 397 - 407.
- Dussan, E. B. (1976). "The moving contact line: the slip boundary condition." Journal of FLuid Mechanics **77**: 665 - 684.
- Eckert, J., Pugh P. A., et al. (1998). "Exogenous protein affects developmental competence and metabolic activity of bovine pre-implantation embryos *in vitro*." Reproduction, Fertility, and Development **10**(4): 327 - 332.

- Edwards, R. (1977). Low density flows through tubes and nozzles. Rarefied Gas Dynamics. J. Potter. New York, American Institute of Aeronautics and Astronautics.
- Elhassan, Y. M., Tasca R. J., et al. (1999). "Levels of amino acids in bovine oviductal and uterine fluids in comparison to levels available in a culture medium supplemented with commercial stocks." Theriogenology **51**: 237.
- Farrell, P. B. and Foote R. H. (1995). "Beneficial effects of culturing rabbit zygotes to blastocysts in 5% oxygen and 10% carbon dioxide." Journal of Reproduction and Fertility **103**(1): 127 - 130.
- Ferziger, J. H. and Peric M. (1999). Computational Methods for Fluid Dynamics. New York, Springer.
- Fiorini, G. S. and Chiu D. T. (2005). "Disposable microfluidic devices: fabrication, function and application." BioTechniques **38**(3): 429 - 446.
- Fischer, B. and Bavister B. D. (1993). "Oxygen tension in the oviduct and uterus of rhesus monkeys, hamsters and rabbits." Journal of Reproduction and Fertility **99**(2): 673 - 679.
- Fischer, B., Schumacher A., et al. (1988). "Potential risk of light and room temperature exposure to preimplantation embryos." Fertility and Sterility **50**(6): 938 - 944.
- Fluent (2005). Fluent 6.2 User's Guide, Fluent Inc.
- Fong, C. and Bongso A. (1998). "Comparison of human blastulation rates and total cell number in sequential culture media with and without co-culture." Human Reproduction **14**(3): 774 - 781.
- Fuchs, E., Tumber T., et al. (2004). "Socializing with the neighbors: stem cells and their niche." Cell **116**: 769-778.
- Fujiwara, M., Takahashi K., et al. (2007). "Effect of micro-environment maintenance on embryo culture after *in vitro* fertilization: comparison of top-load mini incubator and conventional front-load incubator." Journal of Assisted Reproduction and Genetics **24**: 5 - 9.
- Funahashi, H. and Nagai T. (2000). "Sperm selection by a climbing-over-a-wall IVF method reduces the incidence of polyspermic penetration of porcine oocytes." Journal of Reproduction and Development **46**(5): 319 - 324.
- Gad-el-Hak, M. (1999). "The fluid mechanics of microdevices - the Freeman scholar lecture." Journal of Fluid Engineering **121**: 5 - 33.
- Galaktionov, O. S., Meleshko V. V., et al. (1999). "Stokes flow in a rectangular cavity with cylinder." Fluid Dynamics Research **24**: 81-102.
- Gambit (2005). Gambit 2.3 Documentation, Fluent Inc.
- Gardner, D. K. (1994). "Mammalian embryo culture in the absence of serum or somatic cell support." Cell Biology International **18**(12): 1163 - 1179.
- Gardner, D. K. (1998). "Changes in requirements and utilization of nutrients during mammalian preimplantation embryo development and their significance in embryo culture." Theriogenology **49**: 83 - 102.
- Gardner, D. K. (2008). "Dissection of culture media for embryos: the most important and less important components and characteristics." Reproduction, Fertility, and Development **20**(1): 9 - 18.
- Gardner, D. K. and Lane M. (1993). "Amino acids and ammonium regulate mouse embryo development in culture." Biology of Reproduction **48**(2): 377 - 385.
- Gardner, D. K. and Lane M. (1996). "Alleviation of the '2-cell block' and development to the blastocyst of CF1 mouse embryos: role of amino acids, EDTA and physical parameters." Human Reproduction **11**(12): 2703 - 2712.

- Gardner, D. K. and Lane M. (1997). "Culture and selection of viable blastocysts: a feasible proposition for human IVF?" Human Reproduction Update **3**(4): 367 - 382.
- Gardner, D. K. and Lane M. (1999). Embryo culture systems. Handbook of In Vitro Fertilization. A. O. Trounson and D. K. Gardner. New York, CRC Press: 206 - 264.
- Gardner, D. K. and Sakkas D. (1993). "Mouse embryo cleavage, metabolism and viability: role of medium composition." Human Reproduction **8**(2): 288 - 295.
- Gauthier, T. D. (2001). "Detecting trends using Spearman's rank correlation coefficient." Environmental Forensics **2**: 359-362.
- Glasgow, I. K., Zeringue H. C., et al. (2001). "Handling individual mammalian embryos using microfluidics." IEEE Transactions on Biomedical Engineering **48**(5): 570-577.
- Gor, D. and Lucassen E. (1993). In Vitro Cultivation of Animal Cells, Butterworth-Heinemann.
- Goverde, H. J., Peeters R. H., et al. (1994). "The development of a superfusion system for studying intracellular and secretory processes in embryos." In Vitro Cellular and Developmental Biology **30A**(12): 819 - 821.
- Gravesen, P., Branbjerg J., et al. (1993). "Microfluidics - a review." Journal of Micromechanics and Microengineering **3**(4): 168 - 182.
- Guo, Z. and Li Z. (2003). "Size effect on microscale single-phase flow and heat transfer." International Journal of Heat and Mass Transfer **46**(1): 149 - 159.
- Hafez, E. S. E. and Blandau R. J. (1969). The Mammalian Oviduct: Comparative Biology and Methodology. London, University of Chicago Press.
- Haile, J. M. (1993). Molecular Dynamics Simulations: Elementary Methods. New York, Wiley.
- Hallden, K., Li J., et al. (1992). "Increasing carbon dioxide from five percent to ten percent improves rabbit blastocyst development from cultured zygotes." Molecular Reproduction and Development **33**(3): 276 - 280.
- Hammond, J. (1949). "Recovery and culture of tubal mouse ova." Nature **163**: 28 - 29.
- Handyside, A. H. (1998). "Clinical evaluation of preimplantation genetic diagnosis." Prenatal Diagnosis **18**(13): 1345 - 1348.
- Harlow, G. M. and Quinn P. (1982). "Development of preimplantation mouse embryos *in vitro* and *in vivo*." Australian Journal of Biological Sciences **35**: 187-193.
- Heape, W. (1891). "Preliminary note on the transplantation and growth of mammalian ova within a uterine foster-mother." Proceeding of the Royal Society of London **48**: 457 - 458.
- Herr, A. E., Molho J. I., et al. (2000). "Electroosmotic capillary flow with nonuniform zeta potential." Analytical Chemistry **72**(5): 1053 - 1057.
- Heyman, Y., Menezo Y., et al. (1987). "*In vitro* cleavage of bovine and ovine early embryos: improved development using coculture with trophoblastic vesicles." Theriogenology **27**(1): 59 - 68.
- Hibara, A., Iwayama S., et al. (2005). "Surface modification method of microchannels for gas-liquid two-phase flow in microchips." Analytical Chemistry **77**(3): 943 - 947.
- Hibara, A., Nonaka M., et al. (2002). "Stabilization of liquid interface and control of two-phase confluence and separation in glass microchips by utilizing octadecylsilane modification of microchannels." Analytical Chemistry **74**(7): 1724 - 1728.

- Hickman, D. L., Beebe D. J., et al. (2002). "Comparison of static and dynamic medium environments for culturing of pre-implantation mouse embryos." Comparative Medicine **52**: 122 - 126.
- Himmelblau, D. M. (1964). "Diffusion of dissolved gases in liquids." Chemical Reviews **64**: 527 - 550.
- Hirao, Y. and Yanagimachi R. (1978). "Detrimental effect of visible light on meiosis of mammalian eggs *in vitro*." Journal of Experimental Zoology **206**(3): 365 - 369.
- Ho, C. and Tai Y. (1998). "Micro-electro-mechanical-systems (MEMS) and fluid flows." Annual review of Fluid Mechanics **30**: 579 - 612.
- Horner, M., Miller W. M., et al. (1998). "Transport in a grooved perfusion flat-bed bioreactor for cell therapy applications." Biotechnology Progress **14**: 689-698.
- Houghton, F. D., Thompson J. G., et al. (1996). "Oxygen consumption and energy metabolism of the early mouse embryo." Molecular Reproduction and Development **44**: 476 - 485.
- Huang, C. and Lee G. (2007). "A microfluidic system for automatic cell culture." Journal of Micromechanics and Microengineering **17**(7): 1266 - 1274.
- Huisman, G. J., Alberda A. T., et al. (1994). "A comparison of *in vitro* fertilization results after embryo transfer after 2, 3, and 4 days of embryo culture." Fertility and Sterility **61**(970 - 971).
- Hung, P. J., Lee P. J., et al. (2005). "A novel high aspect ratio microfluidic design to provide a stable and uniform microenvironment for cell growth in a high throughput mammalian cell culture array." Lab on a Chip **5**: 44 - 48.
- Incropera, F. P. and Dewitt D. B. (2000). Fundamental of Heat and Mass Transfer. New York, Wiley.
- Israelachvili, J. N. (1986). "Measurement of the viscosity of liquids in very thin films." Journal of Colloid and Interface Science **110**: 263 - 271.
- Jensen, O. S. and Gravesen P. (1993). "Flow characteristic of a micromachined diaphragm valve designed for liquid flows above 1 ml/min." journal of Micromechanics and Microengineering **3**(4): 236 - 238.
- Jeong, W., Kim J., et al. (2004). "Hydrodynamic microfabrication via "on the fly" photopolymerization of microscale fibers and tubes." Lab on a Chip **4**(6): 576 - 580.
- Jiang, F., Tai Y., et al. (1997). A flexible MEMS technology and its first application to shear stress sensor skin. Micro Electro Mechanical Systems, 1997, Nagoya, IEEE.
- John, D. P. and Kiessling A. A. (1988). "Improved pronuclear mouse embryo development over an extended pH range in Ham's F10 medium without protein." Fertility and Sterility **49**: 150 - 155.
- Jones, G. M., Trounson A. O., et al. (1998). "Evolution of a culture protocol for successful blastocyst development and pregnancy." Human Reproduction **13**(1): 169 - 177.
- Kane, M. T. (1987). In vitro growth of preimplantation rabbit embryos. The Mammalian Preimplantation Embryo: Regulation of Growth and Differentiation In Vitro. B. D. Bavister. New York, Plenum Press: 193 - 217.
- Kenis, P. J. A., Ismagilov R. F., et al. (1999). "Microfabrication inside capillaries using multiphase laminar flow patterning." Science **285**(5424): 83 - 85.
- Kennard, E. H. (1938). Kinetic Theory of Gases. New York, McGraw-Hill.
- Knudsen, M. (1909). "Die gesetze der molecular stromung und die inneren reibungstromung der gase durch rohren." Annalen der Physik (Leipzig) **28**: 75 - 130.

- Kogan, M. N. (1973). "Molecular gas dynamics." Annual review of Fluid Mechanics **5**: 383 - 404.
- Koo, J. and Kleinstreuer C. (2003). "Liquid flow in microchannels: experimental observations and computational analyses of microfluidics effects." Journal of Micromechanics and Microengineering **13**: 568 - 579.
- Koplik, J. and Banavar J. R. (1995). "Continuum deductions from molecular hydrodynamics." Annual Review of Fluid Mechanics **27**: 257 - 292.
- Lai, Y. M., Stein D. E., et al. (1992). "Evaluation of vero cell co-culture system for mouse embryos in various media." Human Reproduction **7**(2): 276 - 280.
- Landau, L. D. and Lifshitz E. M. (1987). Fluid Mechanics. Oxford, Pergamon Press.
- Lane, M. and Gardner D. K. (1992). "Effect of incubation volume and embryo density on the development and viability of mouse embryos *in vitro*." Human Reproduction **7**(4): 558-562.
- Leal, L. G. (1992). Laminar Flow and Convective Transport Processes. Boston, Butterworth-Heinemann.
- Li, L. and Xie Y. (2005). "Stem cell niche: structure and function." Annual Review of Cell and Developmental Biology **21**: 605 - 631.
- Lim, J. M., Reggio B. C., et al. (1996). "A continuous flow, perfusion culture system for 8- to 16-cell bovine embryos derived from *in vitro* culture." Theriogenology **46**: 1441-1450.
- Lim, J. M., Reggio B. C., et al. (1997). "Perifusion culture system for bovine embryos: improvement of embryo development by use of bovine oviduct epithelial cells, an antioxidant and polyvinyl alcohol." Reproduction, Fertility, and Development **9**(4): 411 - 418.
- Liseikin, V. D. (1999). Grid Generation Methods. New York, Springer.
- Liu, Z. and Foote R. H. (1996). "Sodium chloride, osmolyte, and osmolarity effects on blastocyst formation in bovine embryos produced by *in vitro* fertilization (IVF) and cultured in simple serum-free media." Journal of Assisted Reproduction and Genetics **13**: 562 - 568.
- Long, D., Stone H. A., et al. (1999). "Electroosmotic flows created by surface defects in capillary electrophoresis." Journal of Colloid and Interface Science **212**(2): 338 - 349.
- Lovell-Badge, R. (2001). "The future for stem cell research." Nature **414**: 88 - 91.
- MacMicheal, G. (1986). "The adverse effects of UV and short-wavelength visible radiation on tissue culture." American Biotechnology Laboratory **4**: 30 - 31.
- Mala, G. M. and Li D. (1999). "Flow characteristics of water in microtubes." International Journal of Heat and Fluid Flow **20**(2): 142 - 148.
- Manz, A., Miyahara Y., et al. (1990). "Design of an open-tubular column liquid chromatograph using silicon chip technology." Sensors and Actuators B **1**(249 - 255).
- Marsh, R. F. (1994). "Symposium on risk assessment of the possible occurrence of bovine spongiform encephalopathy in the United States." Journal of the American Veterinary Medical Association **204**: 70 - 73.
- Mastroianni, L. J. and Jones R. (1965). "Oxygen tension in the rabbit fallopian tube." Journal of Reproduction and Fertility **9**: 99 - 102.
- Matsumoto, H. and Colgate J. E. (1990). Preliminary investigation of micropumping based on electrical control of interfacial tension. Micro-Electro-Mechanical-Systems, 1990, Napa Valley, IEEE.

- Maurer, H. R. (1992). Towards serum-free, chemically defined media for mammalian cell culture. Animal Cell Culture: A Practical Approach. R. I. Freshney. Oxford, Oxford University Press: 15 - 46.
- McKiernan, S. H. and Bavister B. D. (1990). "Environmental variables influencing *in vitro* development of hamster 2-cell embryos to the blastocyst stage." Biology of Reproduction **43**(3): 404 - 413.
- McLimans, W. F. (1972). The gaseous environment of the mammalian cell in culture. Growth, Nutrition and Metabolism of Cells in Culture. G. H. Rothblat and V. J. Cristofalo. New York, Academic Press. **1**: 137 - 170.
- Meyvantsson, I. and Beebe D. J. (2008). "Cell culture models in microfluidic systems." Annual Review of Analytical Chemistry **1**: 423 - 449.
- Migun, N. P. and Prokhorenko P. P. (1987). "Measurement of the viscosity of polar liquids in microcapillaries." Colloid Journal of the USSR **49**: 894 - 897.
- Miyazaki, S., Kawai T., et al. (1991). "A piezoelectric pump driven by a flexural progressive wave." Proceeding of IEEE Micro-Electro-Mechanical-Systems: 283 - 288.
- Moffatt, H. K. (1964). "Viscous and resistive eddies near a sharp corner." Journal of Fluid Mechanics **18**: 1 - 18.
- Muntz, E. P. (1989). "Rarefied gas dynamics." Annual Review Of Fluid Mechanics **21**: 387 - 417.
- Nguyen, N. and Wereley S. T. (2006). Fundamentals and Applications of Microfluidics. Norwood, Artech House.
- Noda, Y., Matsumoto H., et al. (1991). "Involvement of superoxide radicals in the mouse two-cell block." Molecular Reproduction and Development **28**(4): 356 - 360.
- O' Shea, K. S. (1999). "Embryonic stem cell models of development." The Anatomical Record (New Anat.) **257**: 32 - 41.
- Olds, D. and VanDemark N. L. (1957). "Composition of luminal fluids in bovine female genitalia." Fertility and Sterility **8**: 345 - 354.
- Olivennes, F., Hazout A., et al. (1994). "Four indications for embryo transfer at the blastocyst stage." Human Reproduction **9**(12): 2367 - 2373.
- Olivier, L. A. and Truskey G. A. (1993). "A numerical analysis of forces exerted by laminar flow on spreading cells in a parallel plate flow chamber assay." Biotechnology and Bioengineering **42**(8): 963 - 973.
- Oran, E. S., Oh C. K., et al. (1998). "Direct simulation Monte Carlo: recent advances and applications." Annual Review of Fluid Mechanics **30**: 403 - 441.
- Pabon, J. E., Findley W. E., et al. (1989). "The toxic effect of short exposures to the atmospheric oxygen concentration on early mouse embryonic development." Fertility and Sterility **51**: 896 - 900.
- Paria, B. C. and Dey S. K. (1990). Preimplantation embryo development *in vitro*: cooperative interactions among embryos and role of growth factors. Proceedings of the National Academy of Sciences.
- Park, J., Berthiaume F., et al. (2005). "Microfabricated grooved substrates as platforms for bioartificial liver reactors." Biotechnology and Bioengineering **90**(5): 632-644.
- Park, J., Toner M., et al. (2006). "Microchannel bioreactors for bioartificial liver support." Microfluidics and Nanofluidics **2**(6): 525 - 535.
- Patankar, S. V. and Spalding D. B. (1972). "A calculation procedure for heat, mass and momentum transfer in three-dimensional parabolic flows." International Journal of Heat Mass Transfer **15**: 1787 - 1806.

- Patzer II, J. F. (2004). "Oxygen consumption in a hollow fiber bioartificial liver - revisited." Artificial Organs **28**(1): 83 - 98.
- Pera, M. F., Reubinoff B., et al. (2000). "Human embryonic stem cells." Journal of Cell Science **113**: 5 - 10.
- Pereira, D. C., Dode M. A., et al. (2005). "Evaluation of different culture systems on the *in vitro* production of bovine embryos." Theriogenology **63**(4): 1131 - 1141.
- Perera, E. L. and Rao H. V. (1990). Flow modeling of a micron-sized fluid dispenser. MME 90, Berlin, Technical Digest.
- Pfhaler, J., Harley J., et al. (1990). "Liquid transport in micron and submicron channels." Sensors and Actuators **A21 - A23**: 431 - 434.
- Pickering, S. J., Braude P. R., et al. (1990). "Transient cooling to room temperature can cause irreversible disruption of the meiotic spindle in the human oocyte." Fertility and Sterility **54**(1): 102 - 108.
- Pincus, G. (1941). "The control of ovum growth." Science **93**: 438.
- Pincus, G. and Werthessen N. T. (1938). "The comparative behavior of mammalian eggs *in vivo* and *in vitro* III: Factors controlling the growth of the rabbit blastocyst." Journal of Experimental Zoology **78**(1): 1 - 18.
- Pinyopummintr, T. and Bavister B. D. (1995). "Minimum energy substrate requirements for early cleavage stages of bovine embryo development *in vitro*." Theriogenology **43**: 299.
- Pong, K. C., Ho C. M., et al. (1994). "Non-linear pressure distribution in uniform microchannels." Application of Microfabrication to Fluid Mechanics **197**: 51 - 56.
- Pruitt, J. A., Forrest D. W., et al. (1991). "Viability and ultrastructure of equine embryos following culture in a static or dynamic system." Journal of Reproduction and Fertility, Supplement **44**: 405 - 410.
- Purcell, E. M. (1977). "Life at low Reynolds number." American Journal of Physics **45**(1): 3 - 11.
- Quinn, P. (1995). "Enhanced results in mouse and human embryo culture using a modified human tubal fluid medium lacking glucose and phosphate." Journal of Assisted Reproduction and Genetics **12**(2): 97 - 105.
- Quinn, P. and Harlow G. M. (1978). "The effect of oxygen on the development of preimplantation mouse embryos *in vitro*." Journal of Experimental Zoology **206**(1): 73 - 80.
- Rappolee, D. A. (2007). "Impact of transient stress and stress enzymes on development." Developmental Biology **304**(1): 1 - 8.
- Rasmussen, A., Mavriplis C., et al. (2001). "Simulation and optimization of a microfluidic flow sensor." Sensors and Actuators A: Physical **88**(2): 121 - 132.
- Raty, S., Walters E. M., et al. (2004). "Embryonic development in the mouse is enhanced via microchannel culture." Lab on a Chip **4**(186-190).
- Richardson, L. F. (1910). "The approximate arithmetical solution by finite differences of physical problems including differential equations, with an application to the stresses in a masonry dam." Philosophical Transactions of the Royal Society of London, Series A **210**: 307 - 357.
- Rivera, R. M. and Hansen P. J. (2001). "Development of cultured bovine embryos after exposure to high temperatures in the physiological range." Reproduction **121**(1): 107 - 115.
- Rizzino, A. (1987). Defining the roles of growth factors during early mammalian development. The Mammalian Preimplantation Embryo: Regulation of Growth and Differentiation *In Vitro*. B. D. Bavister. New York, Plenum Press: 151 - 174.

- Roach, L. S., Song H., et al. (2005). "Controlling nonspecific protein adsorption in a plug-based microfluidic system by controlling interfacial chemistry using fluorinated-phase surfactants." Analytical Chemistry **77**(3): 785 - 796.
- Roh, S., Choi Y. J., et al. (2008). "A novel microtube culture system that enhances the *in vitro* development of parthenogenetic murine embryos." Theriogenology **69**(2): 262 - 267.
- Rousseau, J. P. and Menezo Y. (1993). Role of the female genital tract in the transport and survival of gametes and the fertilized egg. Reproduction in Mammals and Man. C. Thibault, M. C. Levasseur and R. H. F. Hunter. Paris Ellipses: 369 - 386.
- Rowlinson, J. S. and Widom B. (2002). Molecular Theory of Capillarity, Courier Dover Publications.
- Sakkas, D. and Trounson A. O. (1990). "Coculture of mouse embryos with oviduct and uterine cells prepared from mice at different days of pseudopregnancy." Journal of Reproduction and Fertility **90**(1): 109 - 118.
- Sakkas, D., Urner F., et al. (1993). "Effects of glucose and fructose on fertilization, cleavage, and viability of mouse embryos *in vitro*." Biology of Reproduction **49**: 1288 - 1292.
- Saville, D. A. (1977). "Electrokinetics effects with small particles." Annual Review of Fluid Mechanics **9**: 321 - 337.
- Sawada, H., Yamazaki K., et al. (1990). "Trypsin-like hatching protease from mouse embryos: evidence for the presence in culture medium and its enzymatic properties." Journal of Experimental Zoology **254**(1): 83 - 87.
- Schaaf, S. A. and Chambre P. L. (1961). Flow of Rarefied Gases. Princeton, Princeton University Press.
- Scholtes, M. C. W. and Zeilmaker G. H. (1996). "A prospective, randomized study of embryo transfer results after 3 or 5 days of embryo culture *in vitro* fertilization." Fertility and Sterility **65**: 1245 - 1248.
- Schumacher, A. and Fischer B. (1988). "Influence of visible light and room temperature on cell proliferation in preimplantation rabbit embryos." Journal of Reproduction and Fertility **84**(1): 197 - 204.
- Shankar, P. N. and Deshpande M. D. (2000). "Fluid mechanics in the driven cavity." Annual Review of Fluid Mechanics **32**: 93 - 136.
- Shen, C. and Floryan J. M. (1985). "Low Reynolds number flow over cavities." Physics Fluids **28**(11): 3191-3202.
- Sherbahn, R., Frasor J., et al. (1996). "Comparison of mouse embryo development in open and microdrop co-culture systems." Human Reproduction **11**(10): 2223 - 2229.
- Sherman, F. S. (1990). Viscous Flow. New York, McGraw-Hill.
- Spiga, M. and Morini G. L. (1994). "A symmetric solution for velocity profile in laminar flow through rectangular ducts." International Communications in Heat and Mass Transfer **21**(4): 469 - 475.
- Stone, H. A. and Kim S. (2001). "Microfluidics: basic issues, applications, and challenges." American Institute of Chemical Engineers Journal **47**(6): 1250 - 1254.
- Stone, H. A., Stroock A. D., et al. (2004). "Engineering flows in a small devices: microfluidics towards a lab-on-a-chip." Annual Review of Fluid Mechanics **36**: 381 - 411.

- Streffer, C., Van Beuningen D., et al. (1980). "Kinetics of cell proliferation in the preimplantation mouse embryo *in vivo* and *in vitro*." Cell & Tissue Kinetics **13**: 135-143.
- Stroock, A. D., Dertinger S. K. W., et al. (2002). "Chaotic mixer for microchannels." Science **295**(5555): 647 - 651.
- Suh, R. S., Phadke N., et al. (2003). "Rethinking gamete/embryo isolation and culture with microfluidics." Human Reproduction Update **9**(5): 451-461.
- Suh, R. S., Zhu X., et al. (2006). "IVF within microfluidic channels requires lower total numbers and lower concentrations of sperm." Human Reproduction **21**(2): 477 - 483.
- Swart, N. R. and Nathan A. (1992). "Flow-rate microsensor modeling and optimization using SPICE." Sensors and Actuators A: Physical **34**: 109 - 122.
- Taka, M., Iwayama H., et al. (2005). "Effect of the Well of the Well (WOW) system on *in vitro* culture for porcine embryos after intracytoplasmic sperm injection." Journal of Reproduction and Development **51**(4): 533 - 537.
- Tan, Y. C., Fisher J. S., et al. (2004). "Design of microfluidic channel geometries for the control of droplet volume, chemical concentration, and sorting." Lab on a Chip **4**(4): 292 - 298.
- Thompson, J. G. (2007). "Culture without petri-dish." Theriogenology **67**(1): 16 - 20.
- Thompson, J. G., Simpson A. C., et al. (1990). "Effect of oxygen concentration on *in vitro* development of preimplantation sheep and cattle embryos." Journal of Reproduction and Fertility **89**(2): 573 - 578.
- Thomson, J. A., Itskovitz-Eldor J., et al. (1998). "Embryonic stem cell lines derived from human blastocysts." Science **282**(1145 - 1147).
- Thouas, G. A., Jones G. M., et al. (2003). "The 'GO' system - a novel method of microculture for *in vitro* development of mouse zygotes to the blastocyst stage." Reproduction **126**: 161-169.
- Tiren, J., Tenez L., et al. (1989). "A batch-fabricated non-reverse valve with cantilever beam manufactured by micromachining of silicon." Sensors and Actuators **18**(389 - 396).
- Tosun, I. (2007). Modeling in Transport Phenomena: A Conceptual Approach, Elsevier B V.
- Umaoka, Y., Noda Y., et al. (1992). "Effect of oxygen toxicity on early development of mouse embryos." Molecular Reproduction and Development **31**(1): 28 - 33.
- Utada, A. S., Lorenceau E., et al. (2005). "Monodisperse double emulsions generated from a microcapillary device." Science **308**(5721): 537 - 541.
- Vajita, G., Holm P., et al. (1997). "The submarine incubation system, a new tool for *in vitro* embryo culture: a technique report." Theriogenology **48**: 1379 - 1385.
- Vajita, G., Peura T. T., et al. (2000). "New method for culture of zona-included or zona-free embryos: the well of the well (WOW) system." Molecular Reproduction and Development **55**: 256-264.
- Vajta, G., Lewis I. M., et al. (2001). "Somatic cell cloning without micromanipulators." Cloning **3**(2): 89 - 95.
- van de Pol, F. C. M., Breedveld P. C., et al. (1990). Bond-graph modeling of an electro-thermal-pneumatic micropump. MME 90, Berlin, Technical Digest.
- van den Berg, H. R., Seldam C. A., et al. (1993). "Compressible laminar flow in a capillary." Journal of Fluid Mechanics **246**: 1 - 20.
- Van Langendonck, A., Demylle D., et al. (2001). "Comparison of G1.2/G2.2 and Sydney IVF cleavage/blastocyst sequential media for the culture of human

- embryos: a prospective, randomized, comparative study." Fertility and Sterility **76**(5): 1023 - 1031.
- van Oudheusden, B. W. (1992). "Silicon thermal flow sensors." Sensors and Actuators A: Physical **30**: 5 - 26.
- Van Winkle, L. J., Haghghat N., et al. (1990). "Glycine protects preimplantation mouse conceptuses from a detrimental effect on development of the inorganic ions in oviductal fluid." Journal of Experimental Zoology **253**: 215 - 219.
- Versteeg, H. K. and Malalasekera W. (2007). An Introduction to Computational Fluid Dynamics: The Finite Volume Method. New York, Pearson Education Ltd.
- Walters, E. M., Beebe D. J., et al. (2001). "*In vitro* maturation of pig oocytes in polydimethylsiloxane (PDMS) and silicon microfluidic devices." Theriogenology **55**(1): 497.
- Walters, E. M., Clark S. G., et al. (2004). Mammalian embryo culture in a microfluidic devices. Germ Cell Protocols. H. Schatten. New Jersey, Humana Press. **2**: 375 - 381.
- Walters, E. M., Clark S. G., et al. (2003). "Production of life piglets following *in vitro* embryo culture in microfluidic environment." Theriogenology **59**(1): 353.
- Wells, K. D. and Powell A. M. (2000). "Blastomeres from somatic cell nuclear transfer embryos are not allocated randomly in chimeric blastocysts." Cloning **2**(1): 9 - 22.
- Wheeler, M. B., Clark S. G., et al. (2004). "Developments in *in vitro* technologies for swine embryo production." Reproduction, Fertility, and Development **16**: 15 - 25.
- Wheeler, M. B., Walters E. M., et al. (2007). "Toward culture of single gametes: the development of microfluidic platforms for assisted reproduction." Theriogenology **68S**: 178 - 189.
- White, F. M. (2003). Fluid Mechanics. Dubuque, McGraw-Hill.
- Whitten, W. K. (1956). "Culture of tubal mouse ova." Nature **177**: 96.
- Whitten, W. K. (1971). Nutrient requirements for the culture of preimplantation embryos *in vitro*. Advances in the Biosciences. G. Raspe. New York, Pergamon Press. **6**: 129 - 141.
- Wilding, P., Pfahler J., et al. (1994). "Manipulation and flow of biological fluids in straight channels micromachined in silicon." Clinical Chemistry **40**(1): 43 - 47.
- Wiley, L. M., Yanami S., et al. (1986). "Effect of potassium concentration, type of protein supplement and embryo density on mouse preimplantation development *in vitro*." Fertility and Sterility **45**: 111 - 119.
- Wilson, J. M., Zalesky D. D., et al. (1992). "Hormone secretion by preimplantation embryos in a dynamic *in vitro* culture system." Biology of Reproduction **46**(2): 295 - 300.
- Wood, C. and Trounson A. O. (1999). Historical perspectives of IVF. Handbook of In Vitro Fertilization. A. O. Trounson and D. K. Gardner. New York, CRC Press: 1 - 14.
- Wright, R. W. J. and O' Fallon J. (1987). Growth of domesticated animal embryos *in vitro*. The Mammalian Preimplantation Embryo: Regulation of Growth and Differentiation In Vitro. B. D. Bavister. New York, Plenum Press: 251 - 271.
- Xie, Y., Wang F., et al. (2006). "Shear stress induced preimplantation embryo death that is delayed by the zona pellucida and associated with stress-activated protein kinase-mediated apoptosis." Biology of Reproduction **75**: 45-55.
- Young, A. M., Gray M. L., et al. (1993). A microfabricated flow chamber for optical measurements in fluids. Proceeding of MEMS 1993, Fort Lauderdale.

- Zeng, Y., Lee T. S., et al. (2006). "Mass transport and shear stress in a microchannel bioreactor: numerical simulation and dynamic similarity." Journal of Biomechanical Engineering **128**: 185 - 193.
- Zengerle, R. and Richter M. (1994). "Simulation of microfluid systems." journal of Micromechanics and Microengineering **4**: 192 - 204.
- Zeringue, H. C., Wheeler M. B., et al. (2004). "A microfluidic method for removal of the zona pellucida from mammalian embryos." Lab on a Chip **5**: 108 - 110.
- Zhao, B., Viernes N. O., et al. (2002). "Control and applications of immiscible liquids in microchannels." Journal of the American Chemical Society **124**(19): 5284 - 5285.
- Zhong, W., Xie Y., et al. (2007). "Use of hyperosmolar stress to measure stress-activated protein kinase activation and function in human HTR cells and mouse trophoblast stem cells." Reproductive Sciences **14**(6): 534 - 547.